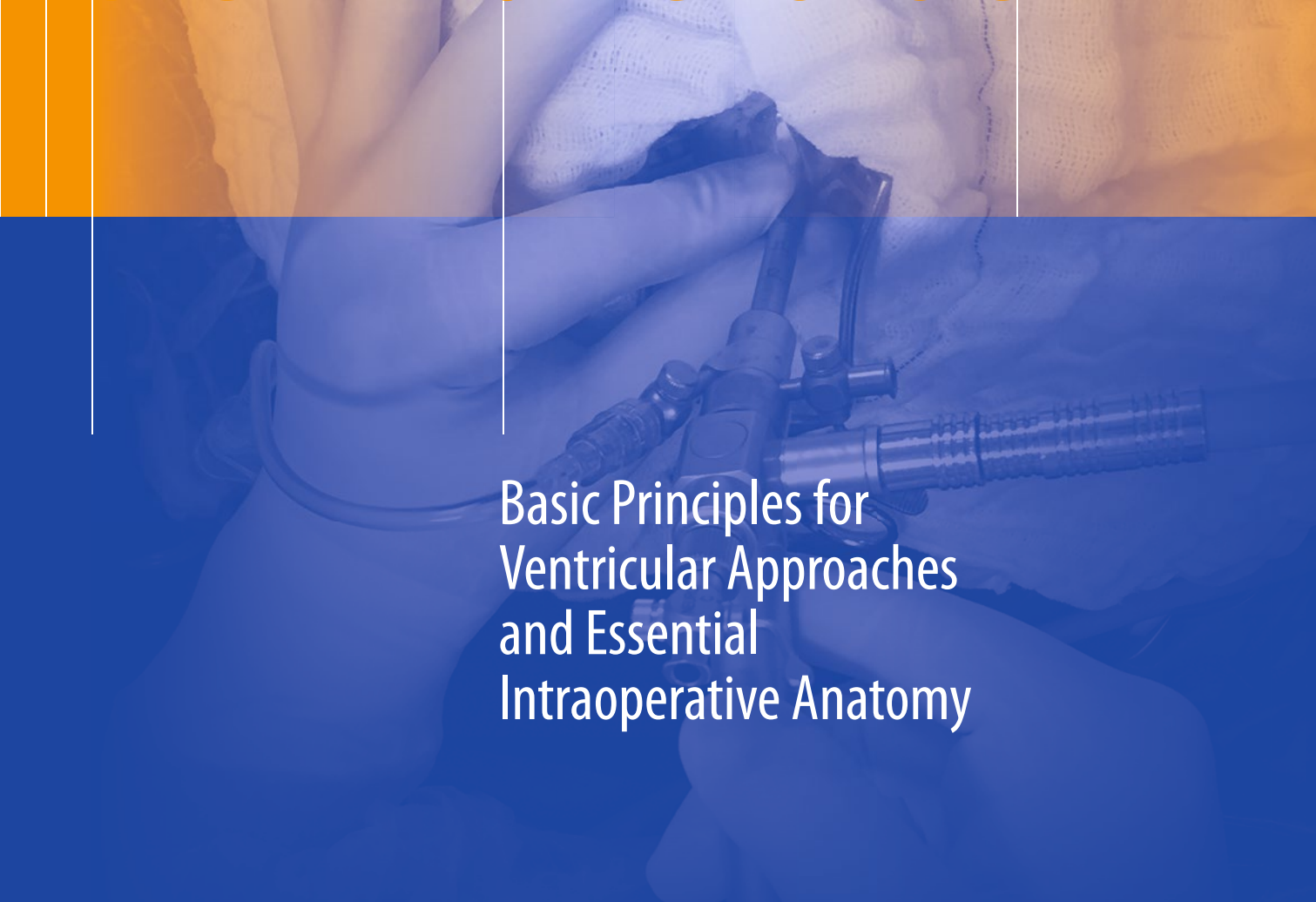


Roberto Alexandre Dezena

# Atlas of Endoscopic Neurosurgery of the Third Ventricle



Basic Principles for  
Ventricular Approaches  
and Essential  
Intraoperative Anatomy

 Springer

---

# Atlas of Endoscopic Neurosurgery of the Third Ventricle

---

Roberto Alexandre Dezena

# Atlas of Endoscopic Neurosurgery of the Third Ventricle

Basic Principles for Ventricular Approaches  
and Essential Intraoperative Anatomy

Roberto Alexandre Dezena, MD, PhD  
Division of Neurosurgery  
Federal University of Triângulo Mineiro  
Uberaba, Minas Gerais, Brazil

ISBN 978-3-319-50067-6      ISBN 978-3-319-50068-3 (eBook)  
DOI 10.1007/978-3-319-50068-3

Library of Congress Control Number: 2017934340

© Springer International Publishing AG 2017

This work is subject to copyright. All rights are reserved by the Publisher, whether the whole or part of the material is concerned, specifically the rights of translation, reprinting, reuse of illustrations, recitation, broadcasting, reproduction on microfilms or in any other physical way, and transmission or information storage and retrieval, electronic adaptation, computer software, or by similar or dissimilar methodology now known or hereafter developed.

The use of general descriptive names, registered names, trademarks, service marks, etc. in this publication does not imply, even in the absence of a specific statement, that such names are exempt from the relevant protective laws and regulations and therefore free for general use.

The publisher, the authors and the editors are safe to assume that the advice and information in this book are believed to be true and accurate at the date of publication. Neither the publisher nor the authors or the editors give a warranty, express or implied, with respect to the material contained herein or for any errors or omissions that may have been made.

Printed on acid-free paper

This Springer imprint is published by Springer Nature  
The registered company is Springer International Publishing AG  
The registered company address is: Gewerbestrasse 11, 6330 Cham, Switzerland

*To the two fathers of Neurosurgery, giants to whom  
all current neurosurgical practice is beholden:  
Professor Harvey Williams Cushing and Professor  
Mahmut Gazi Yaşargil.*

---

## Foreword

A much-needed Atlas of Neuroendoscopy is here! That was my first thought when I received a copy of the manuscript of the present atlas. It is hard to believe the speed with which the practice of neuroendoscopy for the brain and skull base has advanced in the past two decades. Endoscopic approaches to the third ventricle remain as the most basic and essential approaches for the beginning endoscopic neurosurgeon. An excellent understanding of the third ventricular anatomy is a basic requirement prior to the performance of the most basic neuroendoscopic procedures, such as endoscopic third ventriculostomy (ETV).

This well-designed atlas comprises seven rich chapters. The first chapter focuses on the historical, morphological, and physiological aspects of the ventricular system, while the second chapter details the general principles of endoscopic neurosurgery, including historical evolution, basic endoscopic techniques, and procedural indications. The third chapter gives the reader a detailed description of the techniques for entry into the third and lateral ventricles, while the fourth chapter provides a thorough endoscopic anatomy of the anterior, middle, and posterior segments of the third ventricle. The last three chapters enrich the reader's appetite with a more complex neuroendoscopic assessment of the interpeduncular and prepontine cisterns, as well as outlining clinical applications in cases of suprasellar arachnoid cyst and hydranencephaly.

I congratulate Dr. Roberto Dezena, an outstanding Brazilian neurosurgeon, on this excellent effort to advance the education of neurosurgeons and neurosurgical students worldwide in the field of ventricular neuroendoscopy. This meticulous effort of collecting a large number of intraoperative endoscopic images from a personal clinical series required significant hard work and dedication to the field of neuroendoscopy. The main recent advances in the field of hydrocephalus and intraventricular pathologies relate to modern radiological investigations and modern management via minimally invasive endoscopic approaches, since shunts are no longer the exclusive treatment for a patient with hydrocephalus. The evolution of neuroendoscopic techniques to treat hydrocephalus and intraventricular tumors, cysts, and infections has led to significant improvements in the quality of life of millions of patients worldwide, as well as reducing the significant morbidity and mortality rates associated with shunting alone. This evolution in the field requires excellent anatomical and procedural endoscopic resources for the practicing neurosurgeon, such as those provided by the contribution of this remarkable neuroendoscopic atlas. This remarkable multimedia book reflects the technological advances in endoscopic equipment and instrumentation achieved in the past two decades. This atlas is a must-have resource for neurosurgeons who are early or advanced in their endoscopic experience, pediatric neurosurgeons, and all physicians involved in the care of patients with intracranial and intraventricular disease.

Division of Pediatric Neurosurgery  
Saint Louis University School of Medicine  
Saint Louis, MO, USA

Samer K. Elbabaa

---

## Preface



A medical book is not created by chance. It is created, most often, as the result of living and experiences. On the other hand, it may result from the need for a simple, practical and easily accessible work. According to this reasoning, this book was not designed specifically for the luminaries of world neuroendoscopy, whose enormous expertise goes far beyond the contents of this work. It was, rather, intended for those who wish to take the first steps in endoscopic neurosurgery, such as general neurosurgeons, young neurosurgeons, neurosurgical residents, medical students, and professionals in related fields, such as neurologists, neuroscientists, and health professionals in general who are curious about the subject. Despite the title of the book, it looks at more than just the third ventricle. Rather, it deals with the principal ventricular locations and their surroundings, which the neuroendoscopist must know thoroughly. Of all these sites, the third ventricle should undoubtedly be the center of attention, given its strategic position in the center of the ventricular system. For a comprehensive but concise description of the structures, the book was divided into two parts. Part **I** presents basic general concepts of the ventricular system and the neuroendoscopic ventricular technique in two chapters. Part **II**, comprising five chapters, is the atlas itself. In Part **I**, Chap. 1 deals specifically with the cerebral ventricles, the ventricular neuroendoscopy battlefield, emphasizing the historical aspects of their description, their classic anatomy, and the complex mechanism of the cerebrospinal fluid circulation, which is not yet fully elucidated. In Chap. 2, also in Part **I**, the neuroendoscopic technique is presented, from its historical evolutionary aspects to concepts, techniques, and current indications for ventricular approaches. Part **II** presents ventricular endoscopic anatomy through properly labeled intraoperative images. In a different way of viewing the usual ventricular anatomy, the anatomical descriptions follow a logical sequence, from the entry of the neuroendoscope into the skull, through the lateral ventricle and its portions, to the third ventricle and its recesses, until the neuroendoscope reaches the opening in the floor of the third ventricle and the membrane of Liliequist, with the view of the main structures within the interpeduncular and prepontine cisterns. Part **II** also presents endoscopic anatomical aspects inside the suprasellar arachnoid cyst, as well as the endoscopic anatomical aspects of a disease in which there is no brain itself, much less ventricles, called hydranencephaly. All intraoperative endoscopic images, as well as all additional imaging

examinations for the illustrative cases presented, are from our series of patients, all operated at the Clinics Hospital of the Federal University of Triângulo Mineiro in Uberaba, Minas Gerais, Brazil, which is the main site of our neuroendoscopic practice and general neurosurgery.

A special thanks to all the members of my team, especially the surgical instrumentalists responsible not only for the preparation of the operating field and the important intraoperative assistance, but also for recording the surgeries on media. Without such recordings, this work would not have been possible. Far from being the final word on the subject, since new concepts and theories arise in the literature every day, our humble contribution to this fascinating and challenging field of neurosurgery comes to a close.

Uberaba, Minas Gerais, Brazil

Roberto Alexandre Dezena



---

# Contents

## Part I Basic Principles for Ventricular Approaches

<b>1 The Ventricular System</b> .....	3
1.1 Historical Aspects .....	3
1.2 Morphological Aspects .....	20
1.3 Physiological Aspects .....	25
References .....	33
<b>2 General Principles of Endoscopic Neurosurgery</b> .....	35
2.1 Historical Evolution .....	35
2.1.1 Pioneers .....	35
2.1.2 Ostracism of Neuroendoscopy .....	40
2.1.3 Rebirth .....	41
2.2 Basic Techniques for Ventricular Approaches .....	42
2.3 Main Ventricular Procedures and their Indications .....	53
2.3.1 Endoscopic Third Ventriculostomy (ETV) .....	53
2.3.2 Choroid Plexus Coagulation (CPC) .....	57
2.3.3 Septostomy .....	59
2.3.4 Aqueductoplasty .....	60
2.3.5 Complex Hydrocephalus .....	60
2.3.6 Intracranial Arachnoid Cysts .....	61
2.3.7 Biopsies and Tumor Resections .....	61
References .....	61

## Part II Essential Intraoperative Anatomy

<b>3 Entering the Third Ventricle: The Lateral Ventricle</b> .....	69
3.1 Introduction .....	69
3.2 Entering the Ventricular System .....	70
3.3 Right Lateral Ventricle: Foramen of Monro Region .....	74
3.4 Right Lateral Ventricle: Body .....	79
3.5 Right Lateral Ventricle: Foramen of Monro Region .....	84
3.6 Left Lateral Ventricle: Foramen of Monro Region .....	87
3.7 Right Lateral Ventricle: Foramen of Monro Region .....	89
3.8 Right Lateral Ventricle: Body .....	91
3.9 Right Lateral Ventricle: Foramen of Monro Region .....	93
3.10 Right Lateral Ventricle: Septum Pellucidum .....	99
3.11 Left Lateral Ventricle: Septum Pellucidum .....	102
3.12 Right Lateral Ventricle: Septum Pellucidum .....	103
3.13 Right/Left Lateral Ventricle: Septum Pellucidum .....	104
3.14 Left Lateral Ventricle: Septum Pellucidum .....	106
3.15 Left/Right Lateral Ventricle: Septum Pellucidum .....	109
3.16 Left Lateral Ventricle: Septum Pellucidum .....	110
3.17 Right Lateral Ventricle: Frontal Horn .....	111

3.18	Right Lateral Ventricle: Atrium . . . . .	113
3.19	Left Lateral Ventricle: Atrium . . . . .	116
3.20	Right Lateral Ventricle: Atrium . . . . .	118
	References. . . . .	119
<b>4</b>	<b>Inside the Third Ventricle . . . . .</b>	<b>121</b>
4.1	Introduction . . . . .	121
4.2	Third Ventricle: General Vision of the Floor . . . . .	123
4.3	Third Ventricle: Anterior Segment . . . . .	126
4.4	Third Ventricle: Middle Segment. . . . .	168
4.5	Third Ventricle: Posterior Segment . . . . .	181
	References. . . . .	208
<b>5</b>	<b>Beyond the Third Ventricle: Inside the Interpeduncular and Prepontine Cisterns . . . . .</b>	<b>209</b>
5.1	Introduction . . . . .	209
5.2	Interpeduncular and Prepontine Cisterns. . . . .	213
5.3	Illustrative Case: Racemose Neurocysticercosis. . . . .	229
	References. . . . .	236
<b>6</b>	<b>Beyond the Third Ventricle: Suprasellar Arachnoid Cyst . . . . .</b>	<b>237</b>
6.1	Introduction . . . . .	237
6.2	Suprasellar Arachnoid Cyst . . . . .	239
6.2.1	Typical MRI Aspect . . . . .	239
6.2.2	Intraoperative Images. . . . .	240
	References. . . . .	256
<b>7</b>	<b>Beyond the Third Ventricle: Hydranencephaly . . . . .</b>	<b>257</b>
7.1	Introduction . . . . .	257
7.2	Hydranencephaly . . . . .	258
7.2.1	Typical Aspect on Imaging Examinations . . . . .	258
7.2.2	Intraoperative Images. . . . .	259
	References. . . . .	265
	<b>Index. . . . .</b>	<b>267</b>

**Basic Principles for Ventricular Approaches**

## 1.1 Historical Aspects

The first description of the human ventricular system was made in the third century BC by the Greek anatomists Erasistratus (ca. 304 BC–ca. 250 BC) and Herophilus (ca. 335 BC–ca. 280 BC), considered the first anatomists in history (Fig. 1.1). They were founders of the famous School of Medicine of Alexandria and both were allowed to perform dissections and vivisection on humans [1]. Erasistratus considered atoms as the essential elements of the human body, and considered that the atoms were vitalized by external air (*pneuma*), which circulated through the nerves. He described the heart valves and the sigmoid colon, and also suspected that the heart was not the center of the emotions, but that it worked like a pump. He was one of the first to distinguish veins from arteries, and he also believed that the arteries contained air and carried the vital spirit (*pneumazooticon*) from the heart. This idea went against the prevailing belief at the time, that of body humors, suggested by Hippocrates. Additionally, Erasistratus is considered to be the first heart arrhythmologist, studying the rhythm of the heart. It is said that he was appointed royal physician after curing Antiochus I Soter, a Seleucid king, son of Seleucus I Nicator. By measuring the heart palpitations of Antiochus, Erasistratus observed the reactions of the ailing man. He noted that when Antiochus' young and beautiful stepmother, Stratonice, visited him, he had palpitations. Erasistratus concluded that it was the love of Antiochus for her that afflicted him, and so they were allowed to marry [2] (Fig. 1.2).

Herophilus studied the brain in detail, recognizing this organ as the center of the nervous system and intelligence. He described seven pairs of cranial nerves. He also distinguished blood vessels and nerves, including distinguishing the motor nerves from the sensory nerves. Other objects of his study were the eyes, liver, pancreas, salivary glands, digestive system, and genitals. He was one of Hippocrates' scholars and wrote a treatise on the Hippocratic method. Erasistratus and Herophilus both had a particular interest in brain anatomy and, from the first human dissections known

in history, described in the brain four “small stomachs” or “cells”, and their communications with each other. At that time, it was believed that the function of these cavities was to convert the vital spirit (*pneumazooticon*), contained in the blood and coming from the heart, into animal spirit (*pneumapsychikon*), giving rise to thoughts and emotions [3]. It was Herophilus who described and defined the rearmost brain cavity (the fourth ventricle). This region was regarded as the command center of thoughts and emotions, and he compared its posterior wall to the reed pens that were used in Alexandria at the time, and thus emerged the name *calamus scriptorius* or *calamus Herophili* [4].

Claudius Galenus (ca. 129 – ca. 217), or simply Galen (Fig. 1.3), was one of the most important doctors of ancient times. Born in Pergamon, an ancient Greek city (now in Turkey), he traveled extensively throughout the Roman Empire, studying medicine. In 157, Galen returned to



**Fig. 1.1** Woodcut depicting ancient herbalists and scholars of medicinal lore, including the Alexandrian physicians Herophilus and Erasistratus. *Spiegel der Arzney*, woodcut, Lorenz Phryesen (1532)

**Fig. 1.2** Erasistratus, *in red*, shown discovering the cause of Antiochus' disease. Antiochus and Stratonice, oil on canvas, Jacques-Louis David (1774), École Nationale des Beaux-Arts, Paris, France



**Fig. 1.3** Claudius Galenus (ca. 129 – ca. 217). Engraving, Georg Paul Busch (eighteenth century)

Pergamon, where he reached the position of physician for the High Priest's gladiators, and he became one of the richest and most influential men in all of Asia. He spent 4 years in that position and provided very important observations about anatomy and surgery. He reported the wounds of the gladiators he treated as “windows into the body”. Needing to always keep gladiators healthy, as well as treat their injuries, he also highlighted the importance of diet, hygiene, preventive medicine, and exercise. He provided detailed knowledge about general and brain anatomy, which, unfortunately, came from dissections of monkeys or oxen, a fact which, curiously, was never mentioned in his works. Galen described the ventricles in considerable detail, as four cavities and their connections, two anterior, and two posterior (the third and fourth ventricles). He believed that the ventricles were responsible for storing the animal spirit (*pneumapsychikon*), which was regarded as the active ingredient for the brain and nerves. Although it was believed at the time that the ventricles, particularly the anterior ventricle, were the source of *pneumapsychikon*, Galen argued that the soul and the most important cognitive functions were located in the periventricular brain parenchyma. Such considerations are derived from his clinical observations at the gladiator's school in Pergamon. He noted that when a traumatic injury affected the ventricles, death did not occur, even if sensitivity and strength were lost. Imagination, reason, and memory were regarded as the three constituents of the intellect, and it was thought that they could be affected separately. No illustrations of Galen's anatomical observations exist, as he encouraged his students to seek knowledge by handling structures and not by making illustrations [5, 6].

The cerebroventricular doctrine of the time of Galen was followed by the development of the Cell Doctrine, a curious blending of classical Greek medical concepts with Christian

ideologies. In the fourth century AD, the Byzantine physician Poseidon reconfigured the theories of Galen, probably being the first to report concepts of brain localization, stating that anterior brain injuries affect the imagination, medial brain injuries affect reason, and posterior regions, memory [4, 6]. At the same time, church officials, particularly Nemesius, Bishop of Emesa (ca. 390) and St. Augustine (354–430), sought to conceptualize the non-material nature of the soul. Little is known about Nemesius beyond the fact that he was a bishop, and that he innovatively attributed imagination to the connection between the cavity located in the frontal lobe and the five senses. The work attributed to him, *De Natura Hominis*, exerted a significant influence during the scholastic period, although many authors believe the work was written by St. Gregory of Nyssa. In fact, in many ways, the work has ideas that are similar to the thought of the great Nicene doctor. It is a book currently studied in Catholic theology, and is a remarkable work showing the concern of the Bishop of Emesa with the accuracy of the concepts. His way of accepting or rejecting the doctrine of the ancients reveals a person with great knowledge of secular authors. *De Natura Hominis* also contributes to the doctrine of the ventricular localization of mental functions. In fact, a doctrine was created, based on the Alexandrian and Galenic concepts, adapted to Catholic thought. An analogy was made with the Holy Trinity; hence, the division of the brain cavities into

three cells. The Cell Doctrine remained in force throughout the Middle Ages. What are known today as the lateral ventricles were considered to be a single cavity, the first cell of which, in its anterior part, received external impulses and other impulses from the rest of the body, characterizing the reception of common sense (*sensus communis*). From this region, imagination (*imaginativa*) and abstractions (*fantasia*) were created, in the posterior part of the first cell. The second cell (now known as the third ventricle), or medial cell, was the site of the cognitive processes, such as reason (*ratio*), judgment (*aestimativa*), and thought (*cogitativa*). The function of the posterior cell (now known as the fourth ventricle) was changed from a galenic motor concept to the source of memory (*memorativa*) [6–8] (Fig. 1.4).

Albertus Magnus (ca. 1193–1280) (Fig. 1.5), also within Catholic thought, reinforced Cell Doctrine theory and believed that the brain functions were mediated by a system of ventricles or paired chambers. The front ventricles (*sensus communis*) were associated with the processing of the five senses. Images formed therein passed to the medial ventricles, the seat of reason (*ratio*) and thought (*cogitativa*), and the posterior ventricle, the seat of memory (*memorativa*) [9, 10]. These concepts remained as dogma from the Dark Ages to the Renaissance, when they began to be seriously questioned, as a result of more accurate anatomical descriptions. Interestingly, at the time there were only non-illustrated descriptions of the

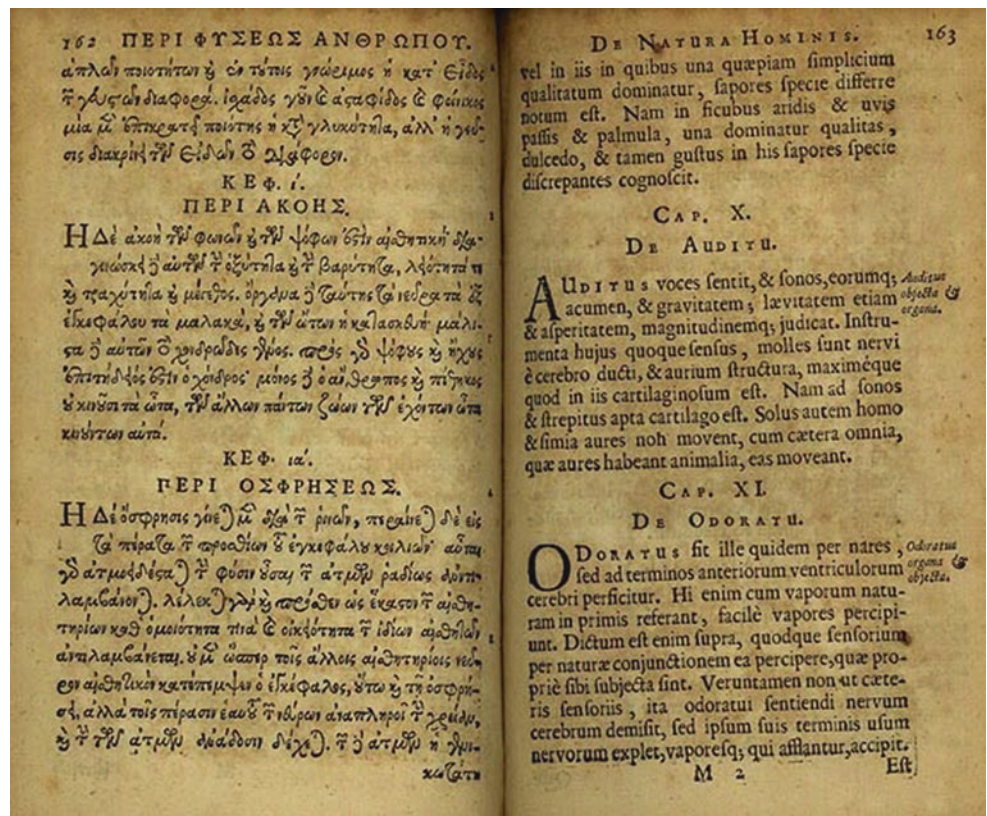


Fig. 1.4 *De natura hominis*. Oxford; 1671



**Fig. 1.5** Albertus Magnus (ca. 1193–1280). Fresco, Tommaso da Modena (1352), Dominican monastery, San Nicolò, Treviso, Italy

Cell Doctrine. The first known drawing of the brain illustrated a text from around 1250, from Salerno, by an unknown author (Fig. 1.6). The drawing is a full-body design with a representation of the thoracic and abdominal cavities, in addition to representations of the blood vessel systems [11, 12].

Still in the Dark Ages, it is worth highlighting Mondino de Luzzi (ca. 1270–1326). He was the first physician to offi-



**Fig. 1.6** Anatomy of the brain and surrounding vessels. Drawing illustrating a text originating in Salerno around 1250, by an unknown artist. Although somewhat simplistically and stylistically rendered, this illustration represents the first known historical attempt at drawing the gyral-sulcal pattern of the cortex

cially receive authorization to perform dissections at the University of Bologna. His masterpiece, *Anathomia Mundini*, was completed in 1316. It was the first book in medical history devoted entirely to the structure and functioning of the human body, and was used for teaching anatomy for more than 200 years. Mondino personally carried out several dissections on human cadavers, but he also made use of a servant, called a barber, working under his orders (Fig. 1.7). With such work, many questions were raised about the works of Galen, the dogmas of the time. As a result, Mondino is considered the “restorer of anatomy.” The editions of *Anathomia Mundini* up to 1478 were only handwritten, but were printed from then on. This because of the invention of the printing press by Johannes Gutenberg (ca. 1398–1468) has occurred in the 1430s, with the first incunable, the Gutenberg Bible, being ready around 1455 [9, 10]. In the Middle Ages, books had practically no illustrations, and so *Anathomia Mundini* did not have anatomical figures until the edition of 1521 [13–15] (Figs. 1.8, 1.9, and 1.10).



**Fig. 1.7** Title page of *Anathomia Mundini*, edition of 1493, depicting a barber surgeon and a physician (probably Mondino) preparing an anatomical dissection. The work was essentially a dissection manual and had great longevity, with approximately 30 manuscripts and editions being available between the fourteenth and sixteenth centuries. Woodcut, Martin Pollich (1493)



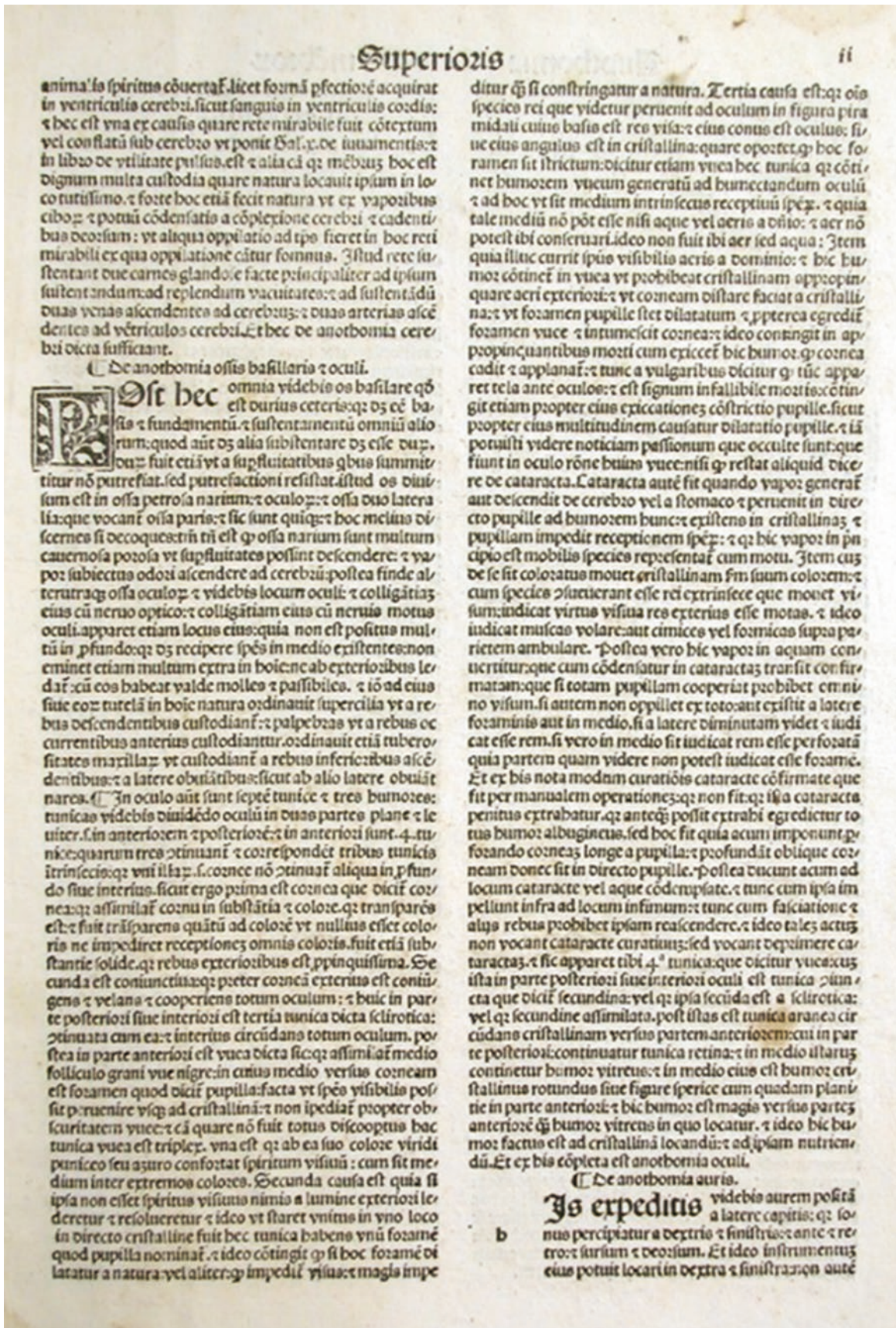
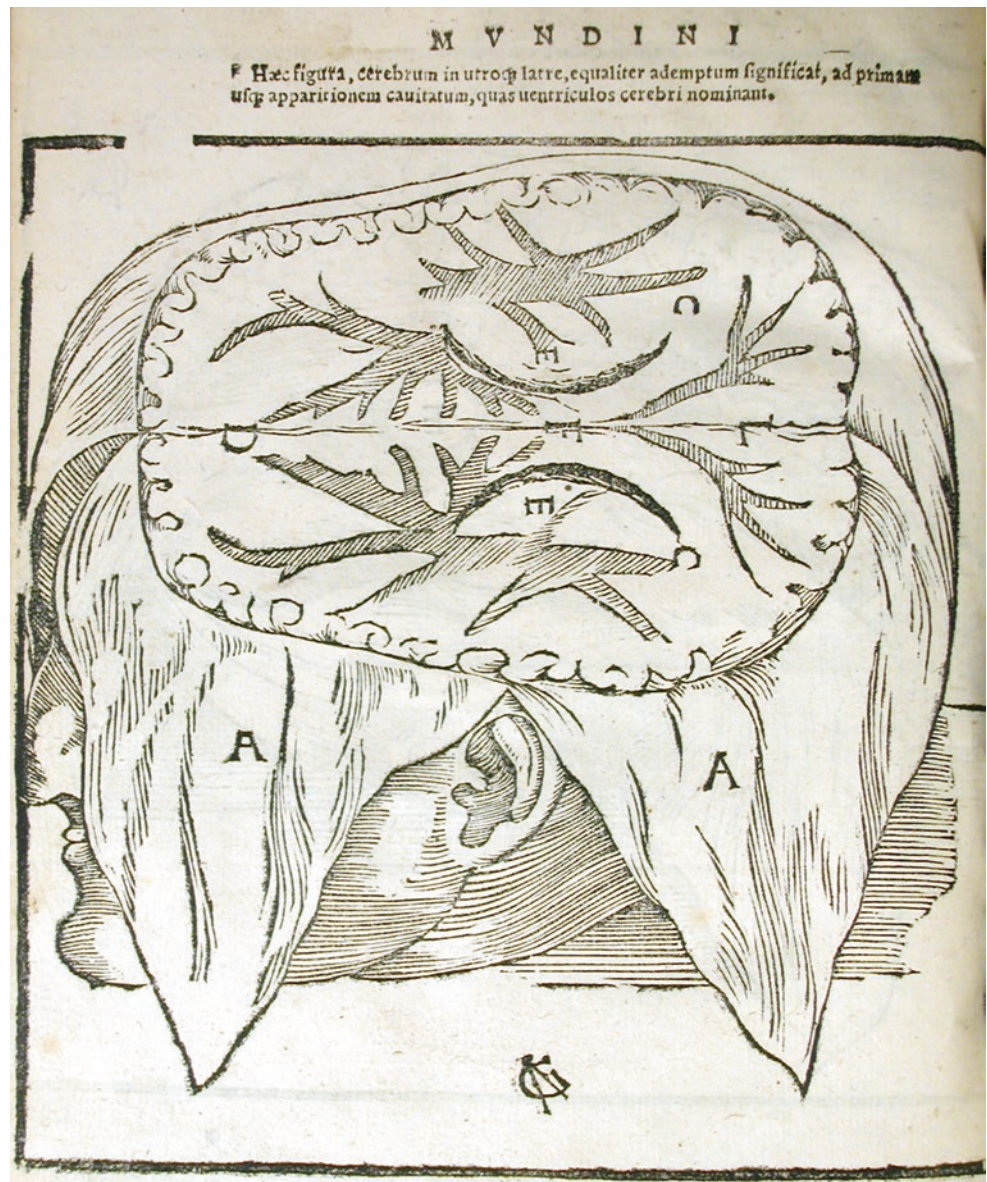


Fig. 1.8 Anatomia Mundini. Edition of 1507 without anatomical figures. Venice; 1507 (Image courtesy of History of Science Collections, University of Oklahoma Libraries)

**Fig. 1.9** *Anathomia Mundini*. Illustrated edition of 1541. Interestingly, this shows *inevitabile fatum* as a common destiny for all humankind (Image courtesy of History of Science Collections, University of Oklahoma Libraries)



**Fig. 1.10** *Anathomia Mundini*. Illustrated edition of 1541. It is possible to see some sketches of the lateral ventricles (Image courtesy of History of Science Collections, University of Oklahoma Libraries)



Guido da Vigevano (ca. 1280 – ca. 1349), great inventor, physician, and student of Mondino, also performed dissections on cadavers, and his manuscript, *Anathomia*, was published in 1345, showing an innovation at the time: the presence of anatomical illustrations [16, 17]. The work demonstrates, for the first time, in six plates, images of the head, brain, and spine. These images, although schematic and very rudimentary, were typical of medieval times, due to the lack of perspective in the drawings (Figs. 1.11 and 1.12). They can be considered as the first neuroanatomical drawings in history, and were the basis for the development of anatomical science in the Renaissance, during which time the ultimate conjunction between science and art took place, reaching its peak with the phenomenal *Fabrica* of Vesalius. [16–18].

Leonardo da Vinci (1452–1519) was the first person to combine the experience of an artist with a profound understanding of anatomy. From the newly introduced technique of the perspective derived from Filippo Brunelleschi (1377–1446), he outlined anatomical figures with extreme precision. Leonardo was a pupil of Andrea del Verrocchio (1435–1488), in Florence, the cradle of the Renaissance, where the perspective technique had been established. Although his work with brain illustrations did not have much influence on his contemporaries, Leonardo brilliantly united art and science, with masterly application of the perspective technique. Around 1487, Leonardo began to record his personal ideas and experiences with anatomy. In his nocturnal dissections, he found his way between the traditional scholasticism and the precise designs made from the direct visu-



**Fig. 1.11** Plate XI from *Anathomia* of Guido da Vigevano, showing trephination of the head by means of a scalpel and a hammer (Reprinted from Wickersheimer et al. [17])

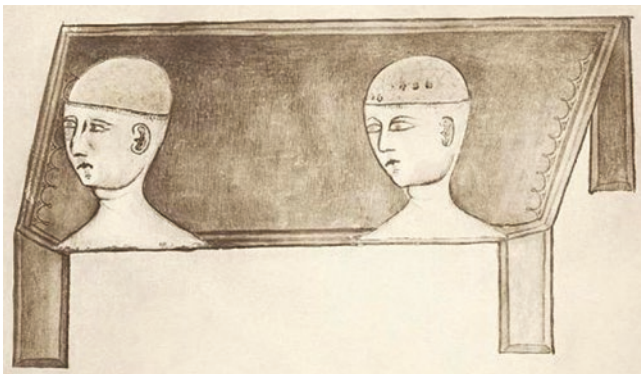


**Fig. 1.12** Plate XIV from *Anathomia* of Guido da Vigevano, showing the internal meningeal layer (“*vocatur pia mater, cerebrum cooperiens*”) (Reprinted from Wickersheimer et al. [17])

alization of anatomical parts. However, his first famous drawing of the brain was still based on the Cell Doctrine (Fig. 1.13). Only in the period between 1504 and 1510, during which Leonardo had his first experiences with ventricu-



**Fig. 1.13** “The Layers of the Scalp Compared with an Onion” (ca. 1490–1492). Still relying on the Cell Doctrine theory, Leonardo drew the brain in pen and ink according to the accepted notion of three cells, while the rest of the head was drawn realistically [23]

lar wax injection, in animals such as oxen, or even in corpses, was it possible to view the ventricles as truly as possible (Fig. 1.14). Thus came about the first ventricular images in true perspective (Fig. 1.15) [19–22].

Despite this evolution in ventricular concepts shown by Leonardo at this time of transition in the Renaissance, there were still authors who blindly defended the Cell Doctrine (Figs. 1.16, 1.17, and 1.18).

Other contemporary brain anatomists, such as Jacopo Berengario da Carpi (ca. 1460–1530) and Johannes Eichmann, also known as Johannes Dryander, or simply Dryander (1500–1560), succeeded Leonardo, and the work of these authors together provided a growing realism in graphic representation of the brain. The great precision of the illustrations was noted, arising from personal participation in dissections and due to the improvement in cadaverous fixation techniques [29]. Although the drawings of these two artists are not necessarily completely precise (the two artists are contradictory to some extent, since they still use some illustrations from the Cell Doctrine), such works solidified the decline, initiated by Leonardo, of the medieval concepts (Figs. 1.19, 1.20, and 1.21). In addition, these publications and illustrations laid the foundation for Vesalius to develop *Fabrica*. There is evidence that Dryander and Vesalius had contact with each other’s work. In the translation of

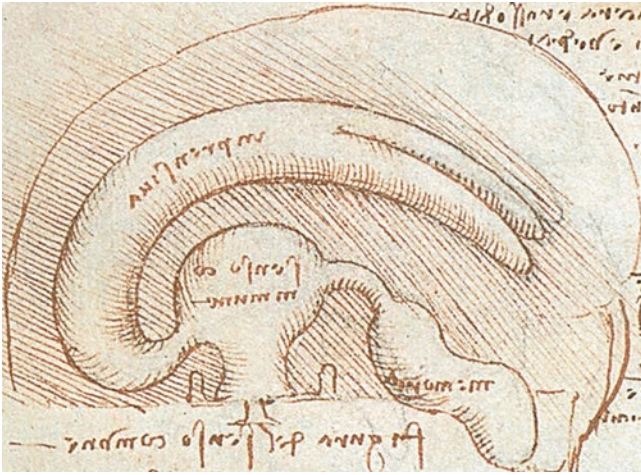


**Fig. 1.14** “The brain injected to demonstrate the shape of the cerebral ventricles” (ca. 1508–1510). By dissecting human cadavers and performing experiments with animals, Leonardo brought realism to his anatomical drawings in pen and ink. This picture comes from the wax-injected brain of an ox [24, 25]

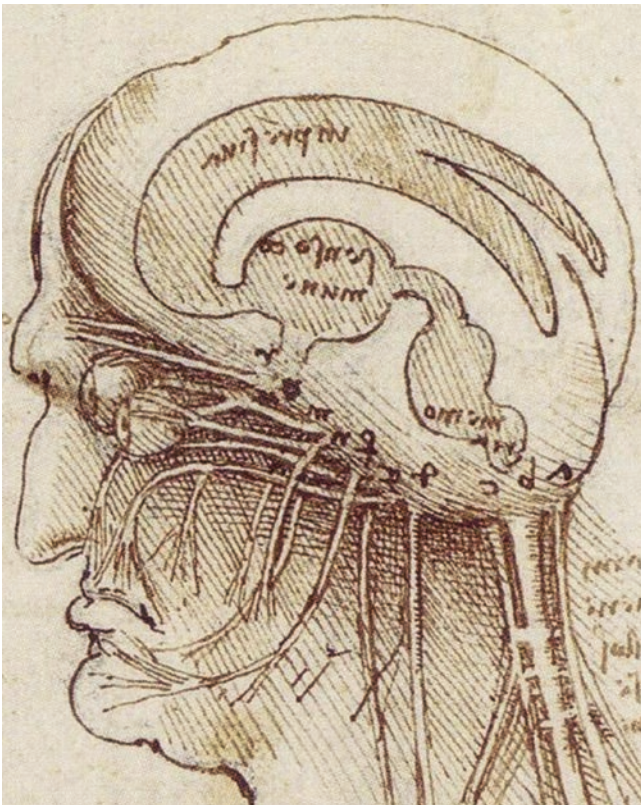


**Fig. 1.15** “Study of brain physiology” (ca. 1508). Drawing in pen and ink by Leonardo after his study of ox brain injections. This rendering of the human brain, ventricles, visual pathways, and skull base reveals Leonardo’s dissection experience and his break from traditional scholasticism, at least as far as personal experience and depiction are concerned [24, 25]



**Fig. 1.16** Illustration of the brain from Albertus of Orlamünde, Dominican (Reprinted from Albertus of Orlamünde, Dominican [26])



**Fig. 1.17** The ten layers of the head, the cerebral ventricles as three cells, and cranial nerves (Reprinted from Hundt [27])

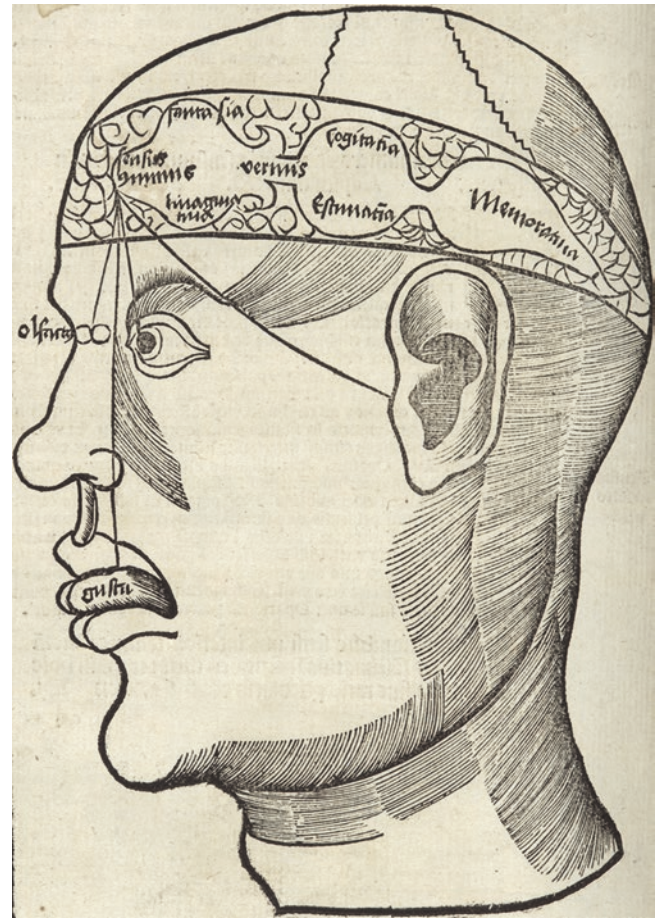


**Fig. 1.18** Representation of the senses and the faculties inside, according to the Cell Doctrine (Reprinted from Reisch [28])



**Fig. 1.19** Illustration of ventricular system by Berengario da Carpi, an Italian surgeon and physician, who refashioned the fourteenth-century anatomical treatise of Mondino de Luzzi for print publication. The illustrations give little anatomical detail, but visually represent the sense of wonder that attends the opening of the body (Reprinted from Carpi [31])

*Anathomia Mundini* in 1542, done by Dryander, it is possible that he copied parts of the text of Vesalius of 1538, *Tabulae Sex*, angering Vesalius [30].

In 1543, the principal benchmark in anatomical history emerged: *De humani corporis fabrica libri septem* or *De humani corporis fabrica*, or simply *Fabrica* (Fig. 1.22), by the Belgian Andreas Vesalius (1514–1564), considered the “father of modern anatomy” [34]. He graduated in medicine from the University of Padua in Italy and in 1538 he published his first work: *Tabulae Sex*, a set of six anatomical drawings made by himself. Before Vesalius, very little had been discovered about anatomy and physiology since ancient times, when the findings were based on the dissection of animals. Vesalius, on the contrary, based his knowledge on human dissections of the bodies of executed criminals and victims of the plague. Vesalius was of humble origin, but after the publication of the *Fabrica*, he became very impor-

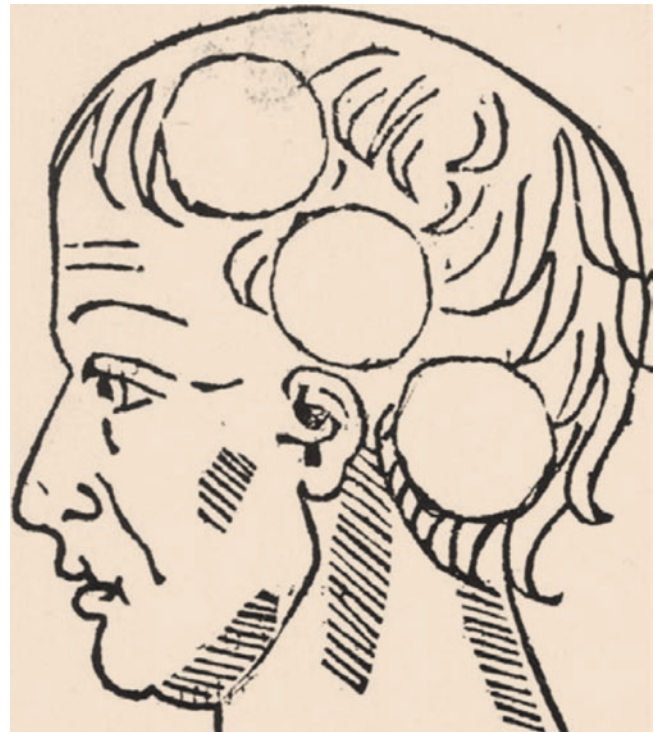


**Fig. 1.20** Picture from Berengario da Carpi, still depicting the Cell Doctrine. This is the first edition of the separate treatise on head injuries and their neurosurgical treatment. In 1517 Berengario was called to attend to Lorenzo de Medici, who had suffered a gunshot wound and an occipital skull fracture in a battle. This illustrated monograph was written as a result of the assignment and was dedicated to Lorenzo (Reprinted from Carpi [32])

tant. In 1546, he was appointed court physician of the Holy Roman Emperor Charles V and remained at his service until his abdication in 1556, thereafter serving Philip II, king of Spain. *Fabrica* is considered one of the most influential scientific books of all time, and stands out for its illustrations, some of the finest woodcuts ever made. Vesalius, with *Fabrica*, questioned a large part of the Galenic theories. To print the work, he spared no expense. He hired the best artists, including the German-born Italian painter Jan Stephan van Calcar (ca. 1499 –ca. 1546), a disciple of the Venetian painter Tiziano Vecelli (ca. 1488–1576), who made the prints in the first two parts of the work, as well as the great printer Johannes Oporinus (1507–1568), from Basel, to prepare the pictures to be printed. Vesalius ended up going to Basel to personally supervise the work. This work is a magnificent example of the best production of books in the Renaissance, with 17 full-page drawings, and several illustrations with text. Consisting of about 700 fine print pages, the book is divided into seven parts or “books” giving a complete overview of the human body. Book VII describes the brain and also presents fantastic ventricular images (Fig. 1.23) [35, 36]. Regarding this last part of his work, Vesalius said at the time:

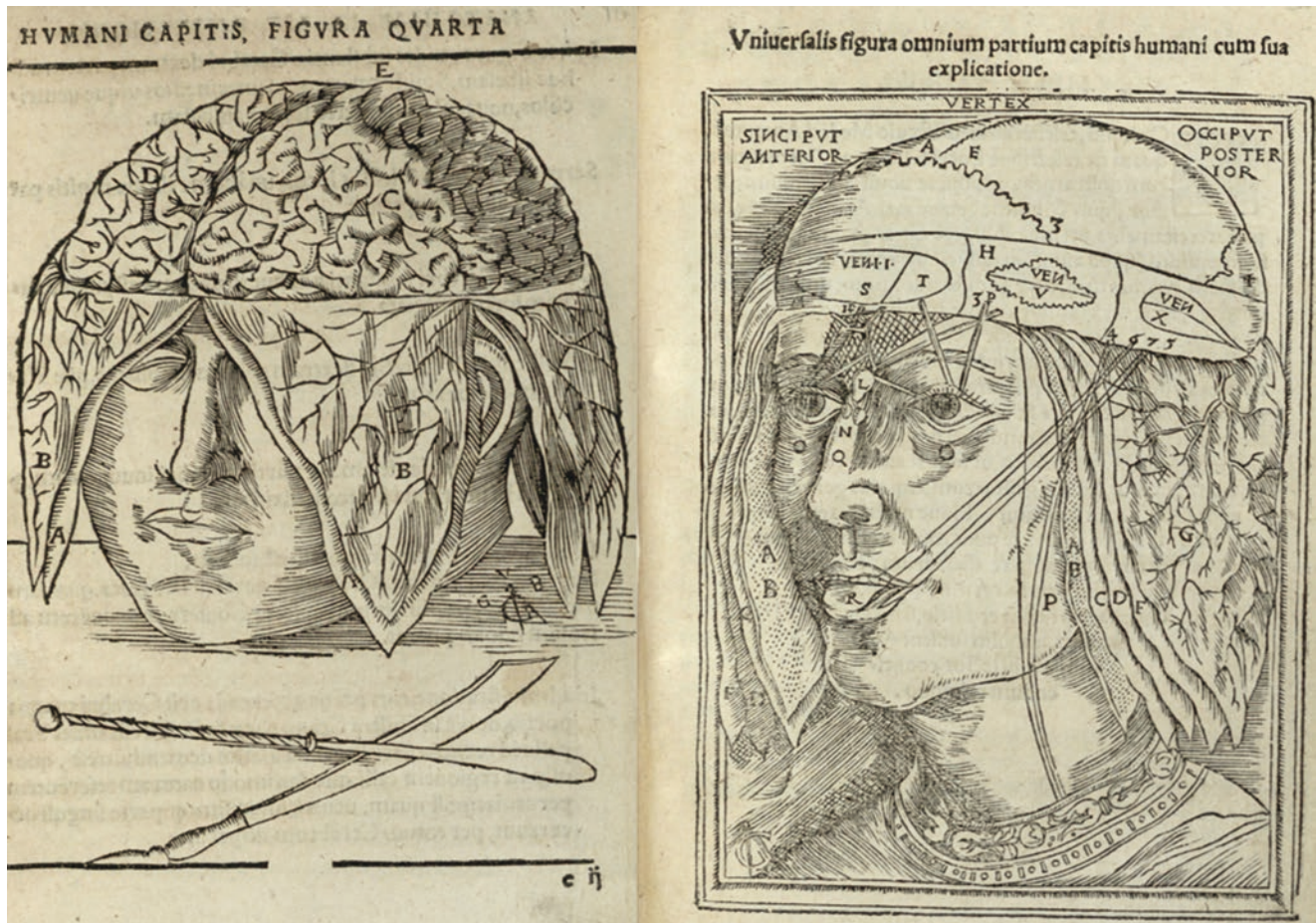


**Fig. 1.21** Evidence of conflicting contemporaneous renderings by Johann Dryander during the transition from the medieval Cell Doctrine to the modern view of the brain (Reprinted from Dryander [33])

“We have resected all the portions of the dural and the thin membranes which occurred in previous figures. Then we have removed in the sequence of dissection the right and left portions of the brain so that the cerebral ventricles now begin to come into view. First, we made a long incision along the right side of the corpus callosum where the sinus denoted by one of the M’s exists, which was led into the right cerebral ventricle. Next we removed the right part of the brain lying above the section where we cut the skull in a circular fashion with a saw. When we had finished the same on the left side, we placed here the left part of the brain so as to show, to some extent, the upper aspect of the left ventricle, while the corpus callosum still remained in the head”. [4]

After Da Vinci and Vesalius, various other authors focused their attention on smaller structures in the ventricular system, such as the union between the third and fourth ventricles, the cerebral aqueduct. Although initially described by Galen, it was better characterized during the Renaissance, particularly by Da Vinci, Berengario, and Vesalius, the most accurate, of course, being Vesalius [37]. In fact, one of the tutors of Vesalius, Jacques Dubois (1478–1555), also known as *Jacobus Sylvius* in Latin, was a famous French anatomist and fanatical

follower of Galen, and had already carried out a detailed description of the aqueduct in his *Isagoge*, published in 1555. However, Vesalius, curiously, does not mention this description in his work. In 1663, a Dutch anatomist named Franz de le Boë (1614–1672) (Fig. 1.24) or, coincidentally, *Franciscus Sylvius*, in its Latinized form, also described the same structure in his *Disputationes*, published in 1663, and it is likely that the term ‘aqueduct of Sylvius’ is a reference to the latter, who also described the lateral fissure of the brain [38].

Despite the precise descriptions of the ventricular cavity made during the Renaissance, there was controversy over its true content. Vesalius, although having made detailed descriptions, still believed in the concept of antiquity that the ventricles were filled with air during inspiration, and that they contained the animal spirit (*pneumapsychikon*). This idea remained quite controversial at the time and divided different authors a great deal, and only after the discovery of cerebrospinal fluid (CSF) was such discussion put to an end. This discovery was made in 1764 by the Italian Domenico Felice Antonio Cotugno (1736–1822) (Fig. 1.25) who,



**Fig. 1.22** The frontispiece of *De humani corporis fabrica*, in its first edition of 1543, printed by Johannes Oporinus, from Basel [34] (Image courtesy of History of Science Collections, University of Oklahoma Libraries)





**Fig. 1.23** The lateral ventricles from *Fabrica*, 1543 [34] (Image courtesy of History of Science Collections, University of Oklahoma Libraries)



**Fig. 1.25** This marble monument of Domenico Cotugno was made in 1961 by the Italian sculptor Giuseppe Pellegrini and can be seen in Piazza Cavallotti, city of Ruvo di Puglia, the hometown of Cotugno



**Fig. 1.24** Portrait of Franz de le Boë, or *Franciscus Sylvius*, and his wife. Oil on oak, Frans van Mieris, the Elder (1671)

besides giving a detailed description of the lumbosacral pathway, also described the possible continuity between the ventricles and the subarachnoid space. This finding of continuity was later confirmed by the French neurologist and experimental physiologist François Jean Magendie (1783–1855) (Fig. 1.26), at the medial region of the fourth ventricle, now known as the foramen of Magendie or median aperture of the fourth ventricle. Magendie, among other contributions, introduced strychnine and opium in the practice of medicine, distinguished sensory and motor functions of the spinal nerves, and introduced the systematic use of laboratory animals in medical research [5, 39, 40].

The description of the interventricular foramen took place in 1783, and is credited to the Scottish physician Alexander Monro secundus (1733–1817) [5] (Fig. 1.27). Monro secundus provided detailed descriptions and illustrations of communication between the lateral ventricles and the third ventricle, now known as the foramen of Monro or the interventricular foramen, and also innovatively described anatomical changes related to hydrocephalus

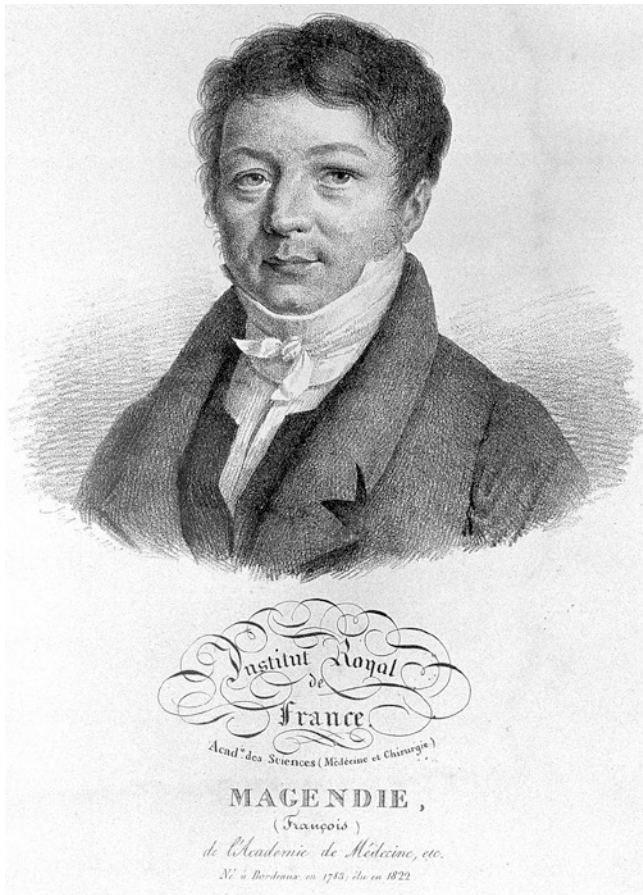


**Fig. 1.26** François Jean Magendie (1783–1855). Lithograph, Julien Leopold Boilly (nineteenth century)

lus. Monro also helped to establish what is now known as the Monro-Kellie doctrine of intracranial hypertension [41, 42]. Following the descriptions of the ventricular details, the Czech anatomist Vincent Alexander Bochdalek (1801–1883) discovered the lateral recesses in 1849, but mistakenly thought they were blind extensions of the fourth ventricle, whereas they are actually communications with the subarachnoid space. This finding was made by the German anatomist Hubert von Luschka (1820–1875) (Fig. 1.28) in 1855, at the University of Tübingen. Such communications were known as lateral apertures of the fourth ventricle, or simply, foramen of Luschka [43]. von Luschka also confirmed the presence of the foramen of Magendie. His findings, though much questioned by his contempo-



**Fig. 1.27** Alexander Monro secundus (1733–1817). Colored stipple engraving, James Heath, after Henry Raeburn (1800)

raries, were later confirmed by many anatomists, including Key and Retzius in 1875 [44, 45].

Without a doubt, the main descriptions of the ventricles and CSF circulation terminate with the work of Axel Key (1832–1901) and Magnus Gustaf Retzius (1842–1919). In their work, which earned Retzius a seat in histology at the Karolinska Institute, they injected colored gelatin into corpses and showed that the gelatin flowed through the arachnoid granulations or villi, or Pacchionian granulations, to the superior sagittal sinus. The colored gelatin was also evident in the cervical lymph nodes [46]. This work presents beautiful images and shows extreme precision in the presentation of ventricular and subarachnoid space anatomy (Figs. 1.29 and 1.30).



**Fig. 1.28** Hubert von Luschka (1820–1875). Oil on canvas, M. Müller-Schüppel (1896) (Image courtesy of Universitätsbibliothek Tübingen Portraitsammlung)



**Fig. 1.29** Precise description of the ventricular system and the sub-arachnoid space (in blue) (Reprinted from Key and Retzius [46])



**Fig. 1.30** Detail of the arachnoid granulations arising from the sub-arachnoid space (in blue) (Reprinted from Key and Retzius [46])

## 1.2 Morphological Aspects

Knowledge of the morphological aspects, anatomical in particular, of the ventricles is of paramount importance for the success of ventricular endoscopy. It is vitally important to have a thorough understanding of the lateral and third ventricles, the sites of most ventricular endoscopic procedures. During the embryonic period, the ventricular system appears in the fourth week, after neural tube closure, at which time the three primitive vesicles are formed: the prosencephalic, mesencephalic, and rhombencephalic, from rostral to caudal. In the fifth week of gestation, the prosencephalon gives rise to the telencephalon (brain hemispheres) and diencephalon. The mesencephalon remains unchanged, and the rhombencephalon gives rise to the metencephalon (pons and cerebellum) and medulla oblongata. Due to these changes, cavities are formed inside these vesicles, communicating with the lumen of the neural tube, and these vesicles are the beginnings of the future ventricles. The cavity of the telencephalon gives rise to the lateral ventricles. The third ventricle comes from the cavity of the diencephalon, and the fourth ventricle comes from the cavity of the rhombencephalon. The lumen of the mesencephalon connects the third and the fourth ventricles, becoming increasingly narrow, constituting the cerebral aqueduct of Sylvius. During this phase, ventricular expansion takes place from caudal to rostral, and is proportionally greater than the brain development [5, 47]. The exact position and spatial conformation of the ventricular system is genetically controlled. This information comes from studies on animals, mostly on chicken and zebrafish embryos. One of these gene controllers is the ventral neural indicator gene, Sonic Hedgehog (Shh), the products of which are secreted by the notochord. Early brain-notochord separation may result from loss of Shh expression, resulting in ventricular collapse of the surrounding tissue [5, 48]. Anatomically, the ventricular system is divided into four chambers that communicate with each other: the right and left lateral ventricles, and the third ventricle and fourth ventricle. The lateral ventricles are C-shaped cavities, situated deep in each cerebral hemisphere. Supposedly, this form is related to the embryonic expansion of the frontal, temporal, and occipital lobes, with the consequent downward and anterior displacement of the temporal lobe (Figs. 1.31 and 1.32).

For the main endoscopic ventricular procedures, detailed knowledge of the anatomy of the lateral ventricles and the third ventricle is crucial. Each lateral ventricle presents a frontal horn (anterior), body, atrium, occipital horn (posterior), and temporal horn (inferior), and each of these parts has a roof; a floor; and anterior, medial, and lateral walls [49]. The body is in the parietal lobe and extends from the posterior limit of the interventricular foramen of Monro to the point where the septum pellucidum disappears, and the corpus callosum and the fornix are found. The lateral wall is formed by the body of the caudate nucleus superiorly

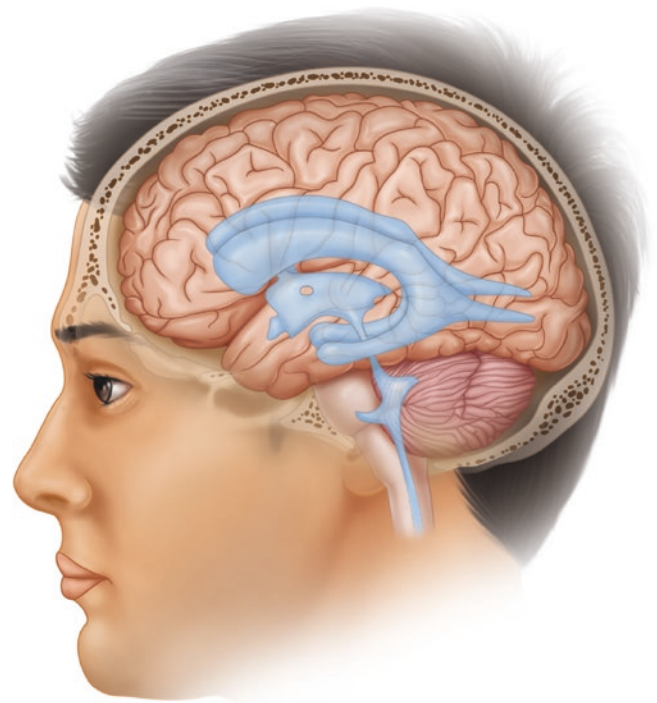


**Fig. 1.31** General aspect and topographic relationship of the ventricular system and the encephalon and head



**Fig. 1.32** Topographic relationship of the ventricular system with the diencephalon, the brainstem, and the cerebellum

and the thalamus inferiorly, separated by the striothalamic sulcus, a cleft in which the stria terminalis and the superior thalamostriate vein run. The medial wall is formed by the

septum pellucidum superiorly and the body of the fornix inferiorly. The floor is formed by the thalamus and the roof by the body of the corpus callosum [49–53]. The body of the lateral ventricle extends posteriorly and continues along the atrium. The atrium communicates with the body anteriorly, and is connected above and below to the thalamus, anteriorly with the temporal horn and subsequently with the occipital horn. The atrium and the occipital horn form a triangular cavity, with the apex in the occipital lobe, and the base anteriorly, connected to the pulvinar of the thalamus. The pulvinar and the crus of the fornix form the anterior wall of the atrium. The roof is formed by the body, splenium, and tapetum of the corpus callosum, and the floor is formed by the collateral trigone, which is a triangular area overlying the end of the collateral sulcus. The medial wall is formed by an upper prominence called the bulb of the corpus callosum, and a lower prominence called the calcar avis, overlying the deepest part of the calcarine sulcus. The anterior portion of the lateral wall is formed by the caudate nucleus and the posterior portion by fibers from the tapetum of the corpus callosum [52–54]. The occipital horn directs posteromedially from the atrium toward the occipital lobe to form a diamond-shaped cavity. Its medial wall is formed by the bulb of the corpus callosum superiorly and the calcar avis inferiorly. The roof and lateral wall are formed by the tapetum of the corpus callosum, overlapped laterally by the optical radiation and the inferior longitudinal fasciculus. The floor is formed by the collateral trigone [49, 52, 53]. The temporal horn is the larger part of the lateral ventricle, extending down and posteromedially around the pulvinar, then anteriorly wrapping around the medial portion of the temporal lobe to end about 2.5 cm from the temporal pole, just behind the amygdala, which is its anterior wall. The floor is formed by the hippocampus and laterally by the collateral eminence, a prominence that overlies the collateral sulcus. The medial portion of the roof is formed by the infe-

rior surface of the thalamus and the tail of the caudate nucleus, separated by the striothalamic sulcus. The lateral portion is formed by the tapetum of the corpus callosum, which also turns inferiorly to form the lateral portion of the temporal horn. The medial wall is formed by the choroidal fissure, a narrow cleft located between the inferolateral part of the thalamus and the fimbria of the fornix [49, 50, 52, 53]. The frontal horn extends anteriorly from the foramen of Monro into the frontal lobe. It has an approximately triangular shape in a coronal section. Its medial wall is formed by the septum pellucidum, separating the frontal horn on both sides, and the columns of the fornix. The anterior wall and the roof are formed by the genu of the corpus callosum and the lateral wall is formed by the head of the caudate nucleus, and its narrow floor by the rostrum of the corpus callosum [49, 50, 52, 53] (Table 1.1 and Fig. 1.33). The third ventricle is a narrow midline cavity located at the center of the ventricular system. It communicates with the lateral ventricles through the foramen of Monro on its anterosuperior aspect, and with the cerebral aqueduct on its posteroinferior aspect. The roof of the third ventricle forms a gentle upward arch, extending from the foramen of Monro anteriorly to the suprapineal recess posteriorly. The roof has four layers [5]: one neural layer, the uppermost layer, is formed by the body of the fornix anteriorly, and by the crus of the fornix and the hippocampal commissure posteriorly. The septum pellucidum is attached to the upper surface of the body of the fornix. Below the neural layer, there are two thin membranous layers of tela choroidea, and a layer of blood vessels (medial posterior choroidal artery and internal cerebral vein) between these two layers. The anterior wall of the third ventricle is formed, from superior to inferior, by the diverging columns of the fornix, the foramen of Monro, the transversely orientated anterior commissure, the lamina terminalis, the optic recess, and the optic chiasm. The anterior half of the floor is formed by diencephalic structures, and

**Table 1.1** Regions and limits of the lateral ventricle

Lateral ventricle	Roof	Floor	Anterior wall	Medial wall	Lateral wall
Frontal horn	Genu of the corpus callosum	Rostrum of the corpus callosum	Genu of the corpus callosum	Septum pellucidum Columns of the fornix	Head of the caudate nucleus
Body	Body of the corpus callosum	Thalamus		Septum pellucidum Body of the fornix	Body of the caudate nucleus Thalamus
Atrium	Body, splenium, and tapetum of the corpus callosum	Collateral trigone	Crus of the fornix Pulvinar of the thalamus	Bulb of the corpus callosum Calcar avis	Tail of the caudate nucleus Tapetum of the corpus callosum
Occipital horn	Tapetum of the corpus callosum	Collateral trigone		Bulb of the corpus callosum Calcar avis	Tapetum of the corpus callosum
Temporal horn	Thalamus Tail of the caudate nucleus Tapetum of the corpus callosum	Hippocampus Collateral eminence	Amygdala	Choroidal fissure	Tapetum of the corpus callosum

the posterior half is formed by mesencephalic structures [5, 49, 50]. The structures forming the floor include, from anterior to posterior, the optic chiasm, the infundibular recess, the tuber cinereum, the mammillary bodies, the posterior perforated substance, and the tegmentum of the mesencephalon, located above the medial aspect of the cerebral peduncles. The lateral walls are formed by the thalamus, hypothalamus,

and the columns of the fornix. The posterior wall is formed, from above to below, by the suprapineal recess, the Habenular commissure, the pineal body and its recess, the posterior commissure, and the cerebral aqueduct [49, 50] (Table 1.2 and Fig. 1.33). Anatomic correlations with computerized tomography (CT) scan and magnetic resonance imaging (MRI) are shown in Figs. 1.34 and 1.35.

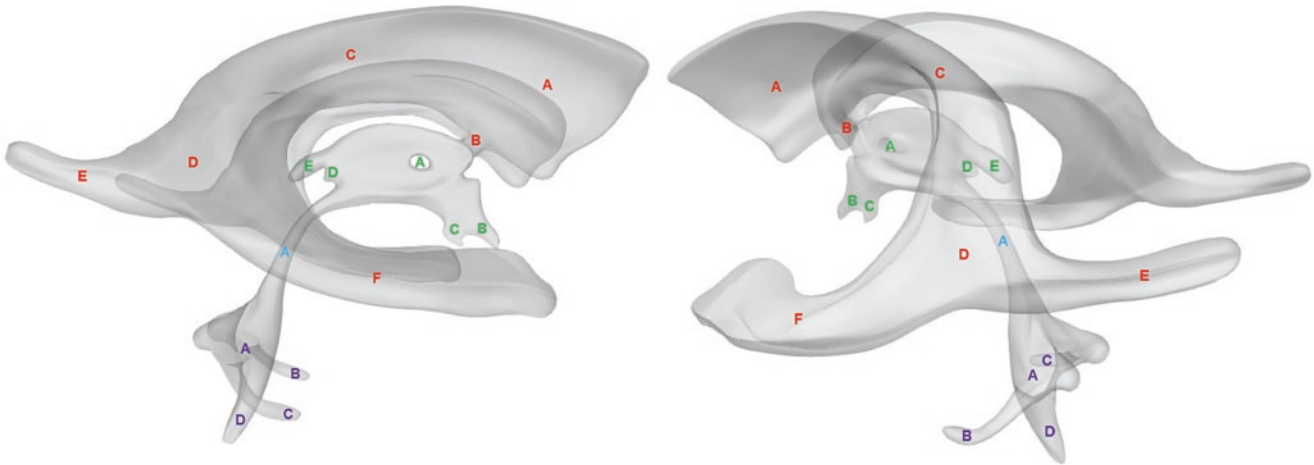


**Fig. 1.33** The ventricular system in right lateral view (superior) and left posterolateral view (inferior). Lateral ventricle (in red): frontal horn (A), foramen of Monro (B), body (C), atrium (D), occipital horn (E), temporal horn (F). Third ventricle (in green): interthalamic adhesion (A), optic recess (B), infundibular recess (C), pineal recess (D), suprapineal

recess (E). Cerebral aqueduct (in blue) (A). Fourth ventricle (in purple): fourth ventricle (A); left lateral recess and left lateral aperture of Luschka (B), right lateral recess and right lateral aperture of Luschka (C), median aperture of Magendie (D)

**Table 1.2** Regions and limits of the third ventricle

Roof	Floor	Anterior wall	Posterior wall	Lateral wall
Body and crus of the fornix, hippocampal commissure Tela choroidea and vessels (medial posterior choroidal artery and internal cerebral vein)	Optic chiasm Infundibular recess Tuber cinereum Mammillary bodies Posterior perforated substance Tegmentum of the mesencephalon	Columns of the fornix Foramen of Monro Anterior commissure Lamina terminalis Optic recess Optic chiasm	Suprapineal recess Habenular commissure Pineal body and pineal recess Posterior commissure Cerebral aqueduct	Thalamus Hypothalamus Columns of the fornix

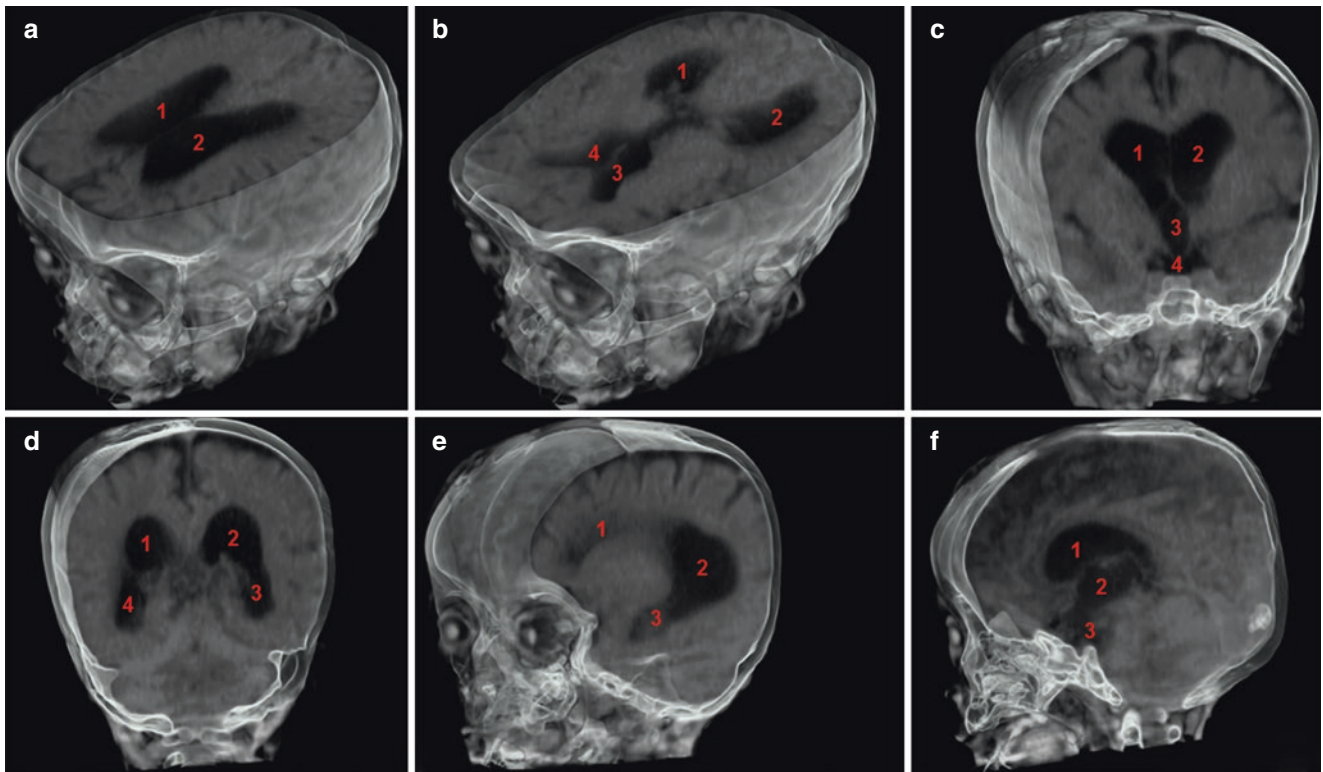


**Fig. 1.34** The ventricular system view on three-dimensional (3D) computerized tomography (CT) scan. **(a)** (axial): right lateral ventricle (1), left lateral ventricle (2). **(b)** (axial): right atrium (1), left atrium (2), left frontal horn (3), right frontal horn (4). **(c)** (coronal): right lateral ventricle (1), left lateral ventricle (2), third ventricle (3), interpeduncu-

lar cistern (4). **(d)** (coronal): right atrium (1), left atrium (2), left temporal horn (3), right temporal horn (4). **(e)** (sagittal): left frontal horn (1), left atrium (2), left temporal horn (3). **(f)** (sagittal): right lateral ventricle (1), third ventricle (2), interpeduncular cistern (3)



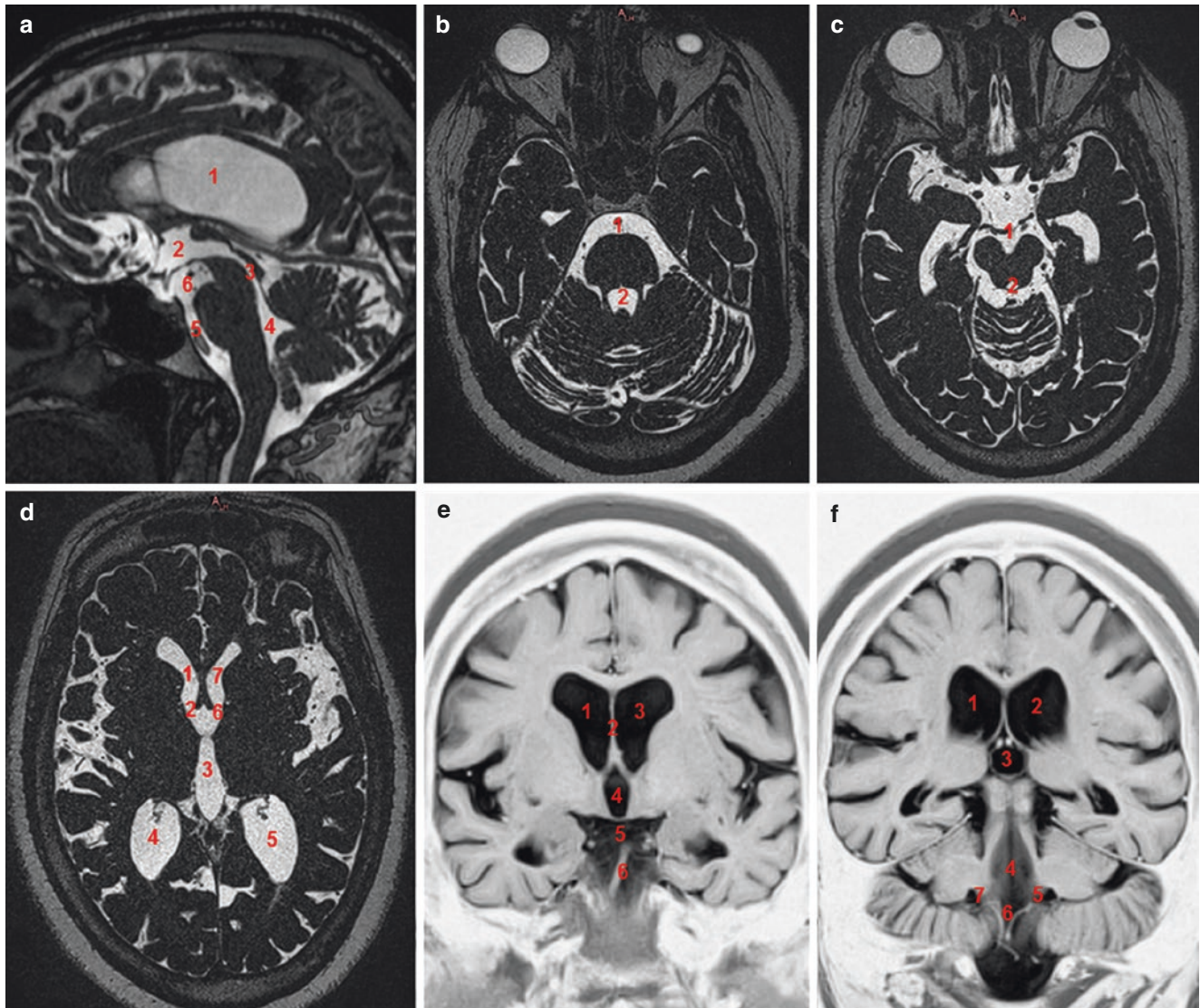


**Fig. 1.35** The ventricular system view on magnetic resonance imaging (MRI). (a) (sagittal T2-weighted): lateral ventricle (1), third ventricle (2), cerebral aqueduct (3), fourth ventricle (4), preoptine cistern (5), interpeduncular cistern (6). (b) (axial T2-weighted): preoptine cistern (1), fourth ventricle (2). (c) (axial T2-weighted): interpeduncular cistern (1), cerebral aqueduct (2). (d) (axial T2-weighted): right frontal horn (1), right interventricular foramen (2), third ventricle (3), right

atrium (4), left atrium (5). (e) (coronal inversion recovery): right frontal horn (1), septum pellucidum (2), left frontal horn (3), third ventricle (4), interpeduncular cistern (5), preoptine cistern (6). (f) (coronal inversion recovery): right frontal horn (1), left frontal horn (2), third ventricle (3), fourth ventricle (4), left lateral recess and left lateral aperture of Luschka (5), median aperture of Magendie (6), right lateral recess and right lateral aperture of Luschka (7)

### 1.3 Physiological Aspects

The first citations regarding cerebral fluid content are from the writings of ancient Egypt, particularly the medical text known as the papyrus of Edwin Smith, from 1700 BC [55]. Throughout ancient times, and during the Middle Ages, it was believed that the ventricular content was not a liquid, but air. During the Renaissance, this idea began to be questioned [35]. This discussion came to an end only after the discovery of CSF by Contugno in the eighteenth century. Thus, the understanding of the production and circulation of the CSF has undergone a major evolution over time [56] (Fig. 1.36). It is assumed that most CSF that circulates within the ventricles comes from the choroid plexus, but this is controversial [57]. Other CSF production sites, such as the brain parenchyma, are currently described (Table 1.3) as contributing to the total amount of circulating CSF [57, 58]. The rate of CSF formation in humans is 0.3–0.4 ml/min, with the total volume of CSF being approximately 90–150 ml in adults [59]. Also, it was traditionally assumed that CSF flows from the lateral and third ventricles, areas with higher concentrations of choroid plexus, reaching the fourth ventricle via the cerebral aqueduct and finally the subarachnoid space through

the apertures of Magendie and Luschka, by being absorbed into the venous blood at the arachnoid granulation level (Figs. 1.37, 1.38, and 1.39). This classic concept, the third circulation model, emerging mainly from animal experiments, is also questioned today [57, 60].

In addition to the mechanical function of damping, reducing apparent brain weight, today it is known that the CSF is also rich in nutrients, including amino acids, vitamins, minerals, proteins, and ions with varying concentrations depending on the stage of development [61]. A number of functions have been assigned to the CSF over the years, from the mechanical protection function, the path for metabolite flow, and neuroendocrine communication [62, 63]. Currently, there is much scientific evidence that the CSF also plays an important role in the development and embryonic organization of the central nervous system, acting as a neuronal guide [64, 65]. The ventricles are lined by ependyma, a single-layer tissue of ciliated cells called ependymocytes that are directly in contact with the CSF [66]. The impetus for the CSF circulation results from macro-scale phenomena, such as the pulsation of the choroid plexus and the movement of the ventricular wall – both induced by cardiac systole – and micro-scale phenomena,

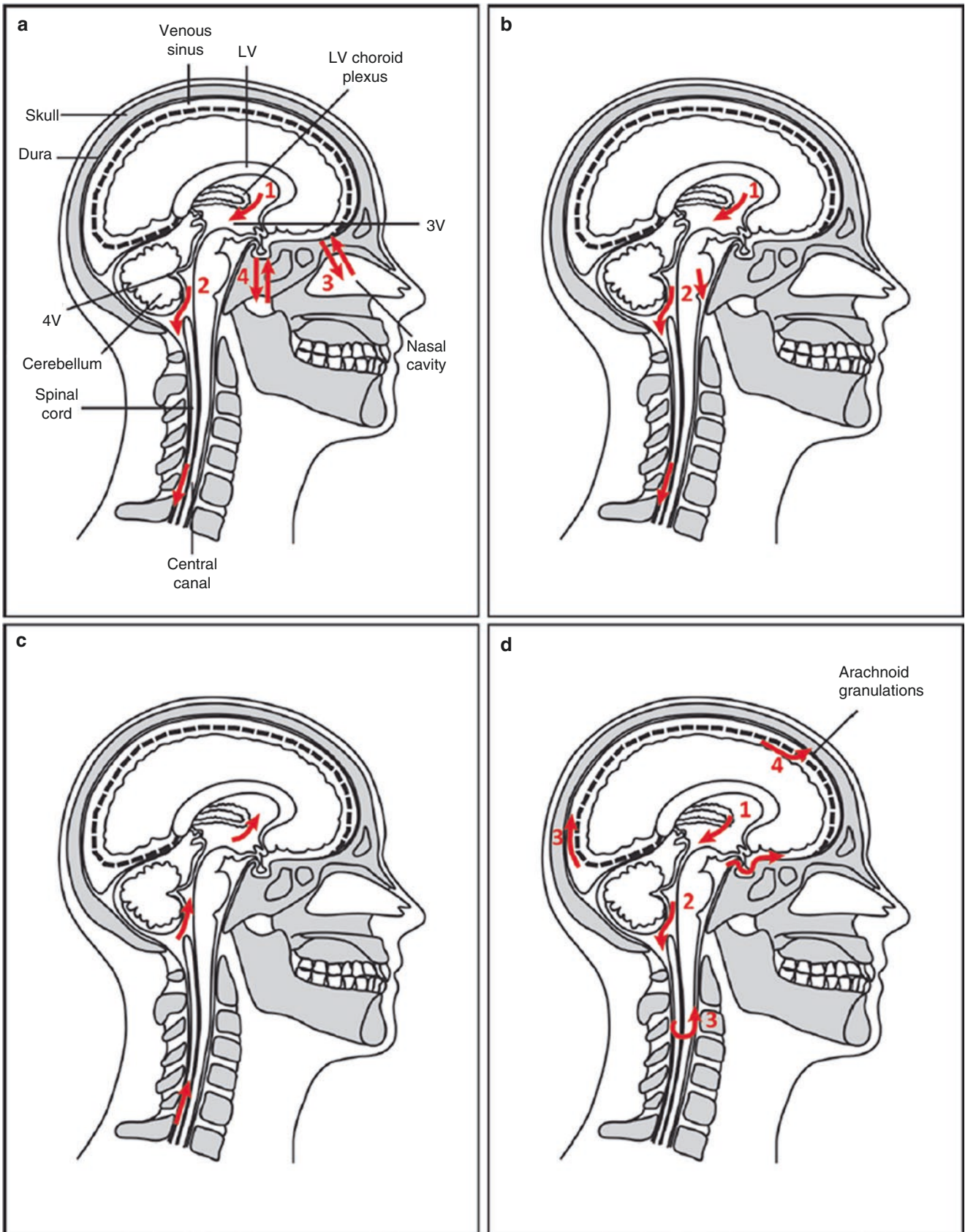


**Table 1.3** Production sites and absorption routes of CSF

Production sites
Choroid plexus
Extra-choroidal sites
1. Ventricular ependyma
2. Subarachnoid space
3. Pia-arachnoid capillary
4. Brain parenchyma
Absorption routes
Arachnoid villi → superior sagittal sinus
Extra-arachnoid villus sites
1. Ventricular ependyma → subependymal vein
2. Leptomeninges → cortical vein
3. Pia-arachnoid capillary → venous system
4. Choroid plexus → deep venous system
5. Perineural space → lymphatic channel

Reprinted from Oi and Di Rocco [58], with permission

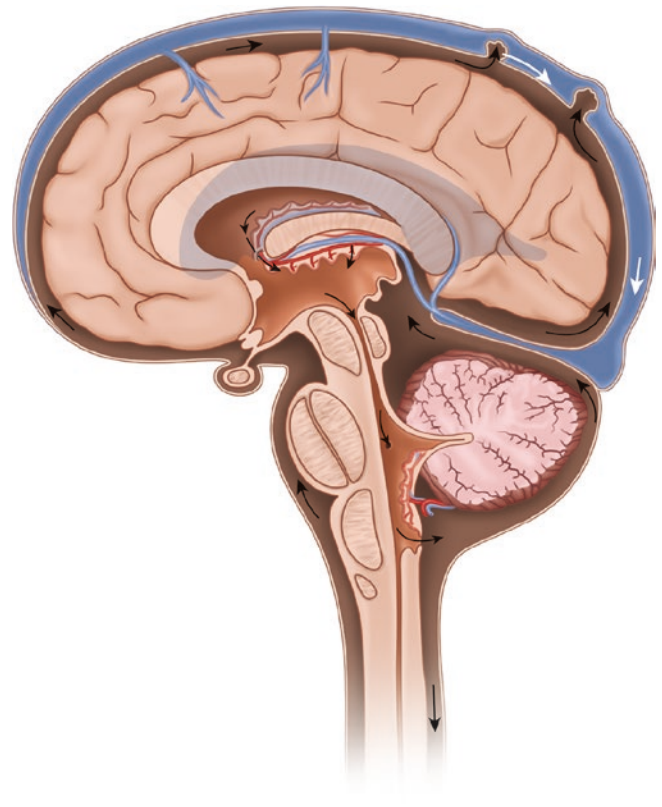


**Fig. 1.37** Traditional third circulation model of CSF pathway. CSF is produced by the choroid plexuses, from where it moves from the lateral ventricles into the third and fourth ventricles. It then flows across the surface of the brain and down the spinal canal (moving from the back to front of the canal). CSF is then reabsorbed by the arachnoid granulations back into the bloodstream

**Fig. 1.36** Evolution of the understanding of CSF production and its pathway in relation to brain spaces. **(a)** Galenic concept of the CSF pathway. In his writings, Galen describes a lateral ventricular choroidal origin (1) and exit through the fourth ventricle to the spinal canal (2). He also, erroneously, describes movement of the fluid across the cribriform plate into the nasal cavity (3) and across the infundibulum to the palate (4). **(b)** CSF pathway, from Albrecht von Haller (1708–1777), who correctly stated the origin of CSF from the ventricles (1), with exit from the fourth ventricle (2) and down the spinal canal for venous absorption. This early description was essentially correct. **(c)** The concept of the CSF pathway from François Magendie (1783–1855) was exactly oppo-

site to the system described by both von Haller and Galen. **(d)** Modern description of the CSF pathway – the third circulation model. CSF is produced by the choroid plexuses (1), from where it moves from the lateral ventricles into the third and fourth ventricles (2). It then flows across the surface of the brain (3) and down the spinal canal (moving from the back to the front (3) of the canal). CSF is then reabsorbed by the arachnoid granulations (4) back into the bloodstream. The arachnoid granulations are projections from the arachnoid layer of the meninges that connect with veins via the venous sinus. Absorption into lymphatics also occurs (not shown). Abbreviations: 3V third ventricle, 4V fourth ventricle, LV lateral ventricle (Reprinted from Liddelow [56])

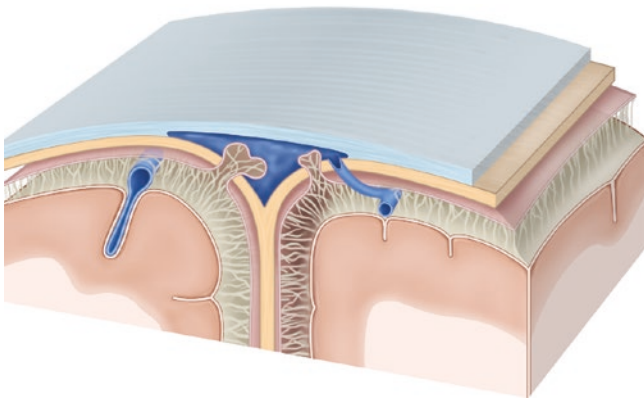


**Fig. 1.38** Traditional third circulation model of CSF pathway ending in the arachnoid granulation, and later flowing toward the superior sagittal sinus



**Fig. 1.39** Arachnoid granulation in detail. In fact, arachnoid granulation is an expansion, through the dura, of the subarachnoid space to the venous system

such as the ciliary beat of ependymocytes [67] (Figs. 1.40, 1.41, and 1.42). This ciliary movement occurs periodically, generating a CSF flow in the vicinity of the ventricular wall [68]. It is proposed that this flow induced by the ciliary beat eliminates small debris from the ventricular wall, and has the effect of diluting substances, particularly in the third ventricle – the supposed intraventricular neuroendocrine communication phenomenon [69]. Possible genetic mutations affecting the ciliary movement may be associated

with hydrocephalus [70–72]. Today the CSF flow is believed to also serve as a signpost for neuronal migration during embryogenesis, keeping in mind that progenitor cells are born below the ependymal layer in the lateral ventricles, later migrating to distant sites, such as the olfactory bulb, where they differentiate into neurons and astroglia [65, 73–75]. Conversely, deficiency in ciliary motility can change the CSF flow [76] and the migration of neuroblasts [65], and such results suggest a strong interrelationship between neuronal migration and the CSF circulatory dynamics near the ventricular wall [67].

Currently, the unidirectional nature of the CSF flow is being questioned, and the CSF flow is also considered to be a location for the dilution and diffusion of substances [57]. The concept of the third circulation has been accepted since the work of Cushing in the decade of the 1920s, suggesting that CSF flows through the ventricles, cisterns, and subarachnoid space and is reabsorbed into the blood through the arachnoid granulation [77–79]. Historically, it was always held that the absorption of CSF into the circulating blood is really more notable in the arachnoid granulation [80–82]. This notion is based on the first experiments performed by Key and Retzius, with the injection of colored gelatin into human cadavers in 1875. In fact, the distribution of the dye was noted throughout the CSF system, as was its passage to the arachnoid granulation in the direction of the venous sinuses [46]. However, their results were questioned because the gelatin was injected at a pressure of 60 mmHg, which could have caused a rupture in the arachnoid granulation [83]. Since then, other means of CSF absorption have been suggested. The arachnoid granulation has a developmental mechanism in humans that is comparable to that in other animals lower on the phylogenetic scale [58] (Fig. 1.43). During pregnancy, the human fetus has practically no arachnoid granulation, comparable to findings in the mouse. From birth, the arachnoid granulations begin to develop, and are equivalent in size to those of a rat and a rabbit. After 1 year of age, the arachnoid granulations develop greatly, gradually reaching a size similar to those in a cat, a sheep, and a horse; finally, at school age, the size is similar to that in the monkey. In the period of the immature brain, the predominant CSF absorption mechanism is not in the arachnoid granulation, but in a minor pathway (Fig. 1.44). With growth, there is a maturation of this mechanism, through the arachnoid granulation, which becomes increasingly important [58] (Fig. 1.45). Currently, although controversial, much importance has been attributed to the CSF circulation around the blood vessels penetrating from the subarachnoid space towards the Virchow-Robin space (Figs. 1.46, 1.47 and 1.48). This space accompanies vessels deep in the brain parenchyma and is involved in a significant exchange between CSF and the interstitial fluid [57]. This circulation not only provides the cleaning of molecules from the brain, but also provides interaction with the immune system. In this important exchange,

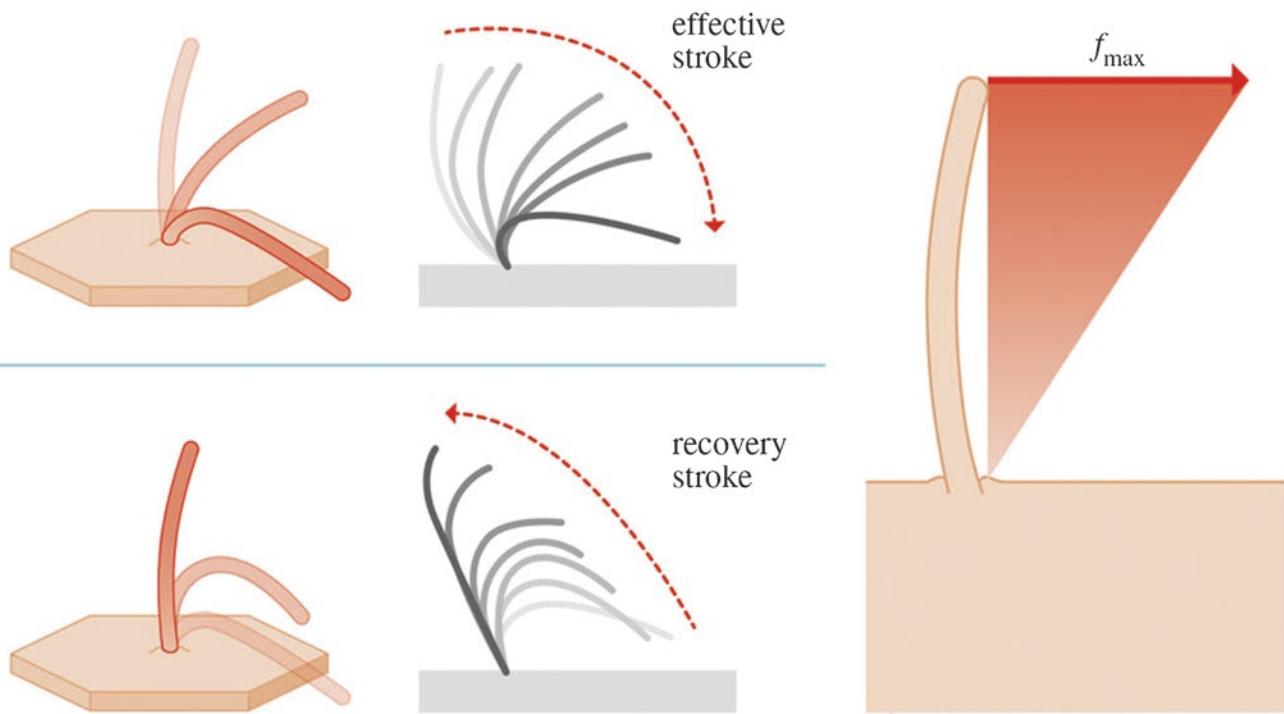


**Fig. 1.40** Schematic of a beating ependymal cilium. The beating motion consists of an effective and a recovery stroke. The action of the cilium is accounted for via body forces acting on the CSF. The  $f_{max}$

(maximum force density) is determined empirically by matching the induced fluid velocity to experimental measurements (Reprinted from Siyahhan et al. [67])

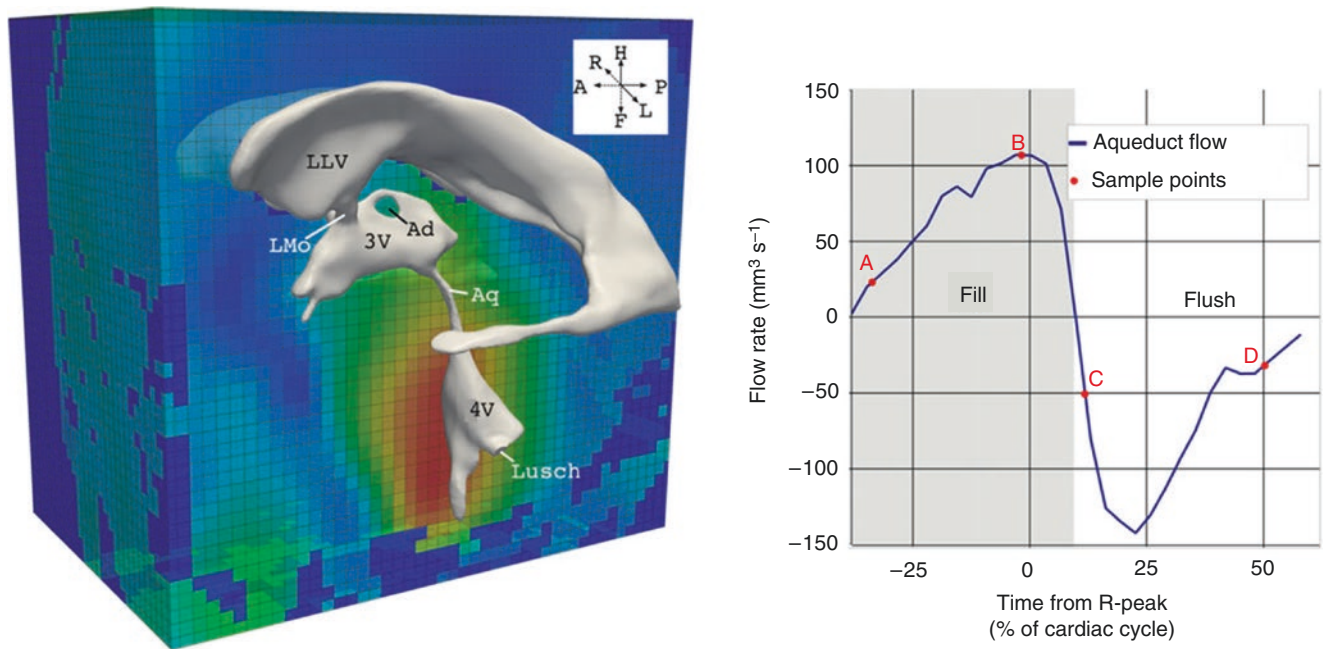


**Fig. 1.41** In vivo data obtained with magnetic resonance imaging (MRI). On the right the ventricular geometry extracted from anatomical MRI images is overlaid on the MRI displacement field. On the left, the CSF flow rate through the aqueduct is reconstructed from the two-dimensional phase contrast gradient echo sequence, and the four sample points (A–D). Note that the electrocardiogram R-peak is used to define the start of the cardiac cycle. Points A and B are in the fill period

where the flow through the aqueduct is oriented in the cranial direction, whereas points C and D correspond to the flush period where the CSF flow is in the caudal direction. Abbreviations: LLV left lateral ventricle, LMO left foramen of Monro, Ad interthalamic adhesion, 3V third ventricle, Aq cerebral aqueduct, 4V fourth ventricle, Lusch foramen of Luschka (Reprinted from Siyahhan et al. [67])

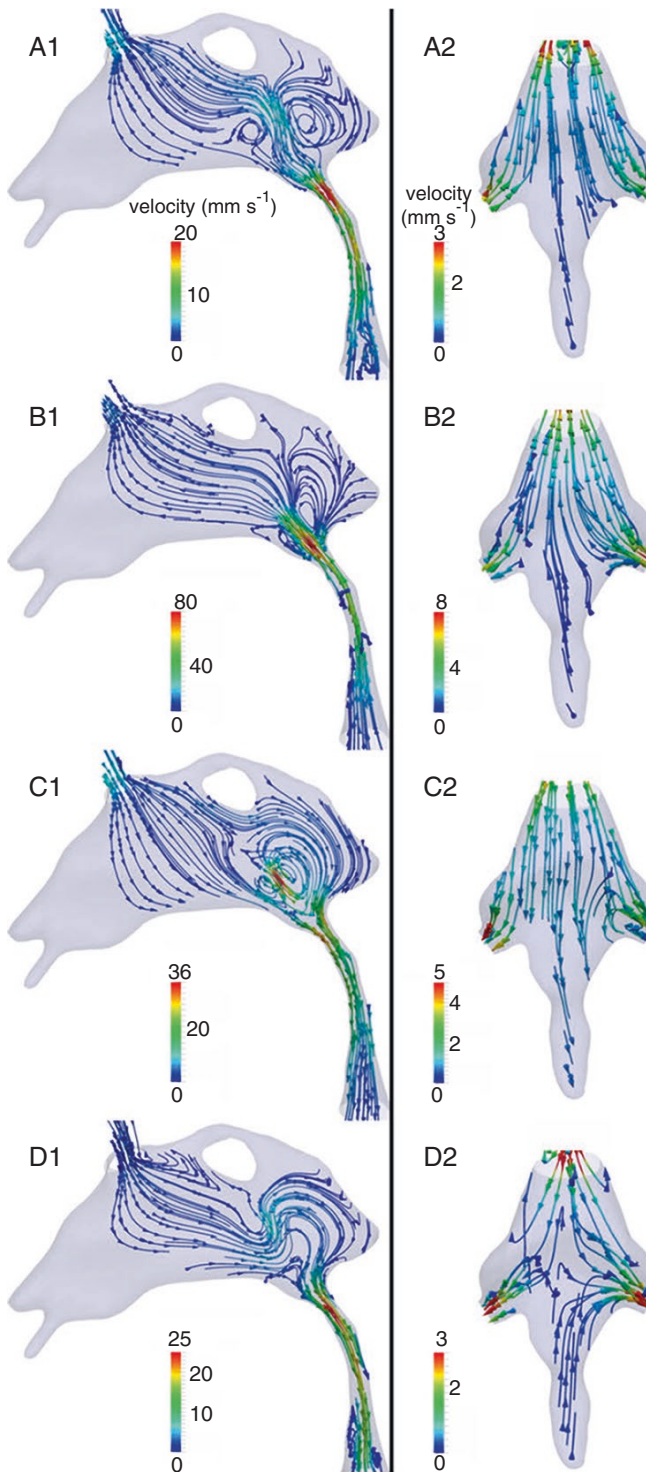


**Fig. 1.42** Flow characteristics in the third ventricle and cerebral aqueduct (A1–D1), and in the fourth ventricle (A2–D2). Streamlines are derived with respect to the global coordinate system and are color-coded by velocity magnitude. Time points A through D correspond to the instants marked in Fig. 1.41 (Reprinted from Siyahhan et al. [67])

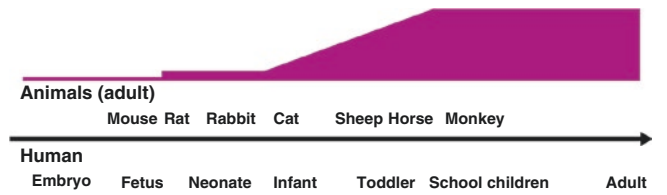


**Fig. 1.43** Ontogenesis of arachnoid granulation in humans compared with other animals (Reprinted from Oi and Di Rocco [58], with permission)

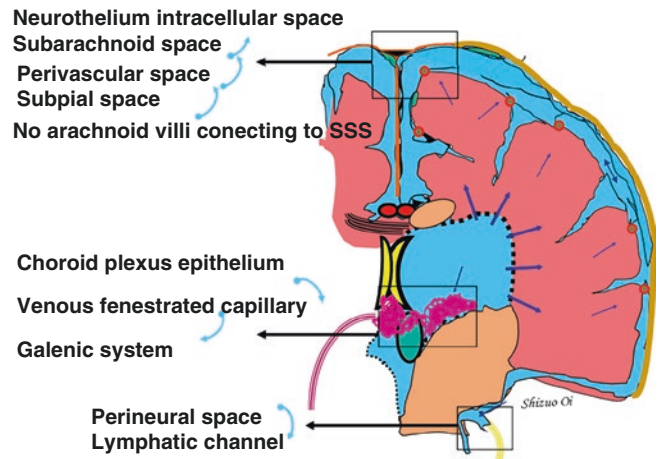


**Fig. 1.44** Minor CSF pathway in immature brain (Reprinted from Oi and Di Rocco [58], with permission)

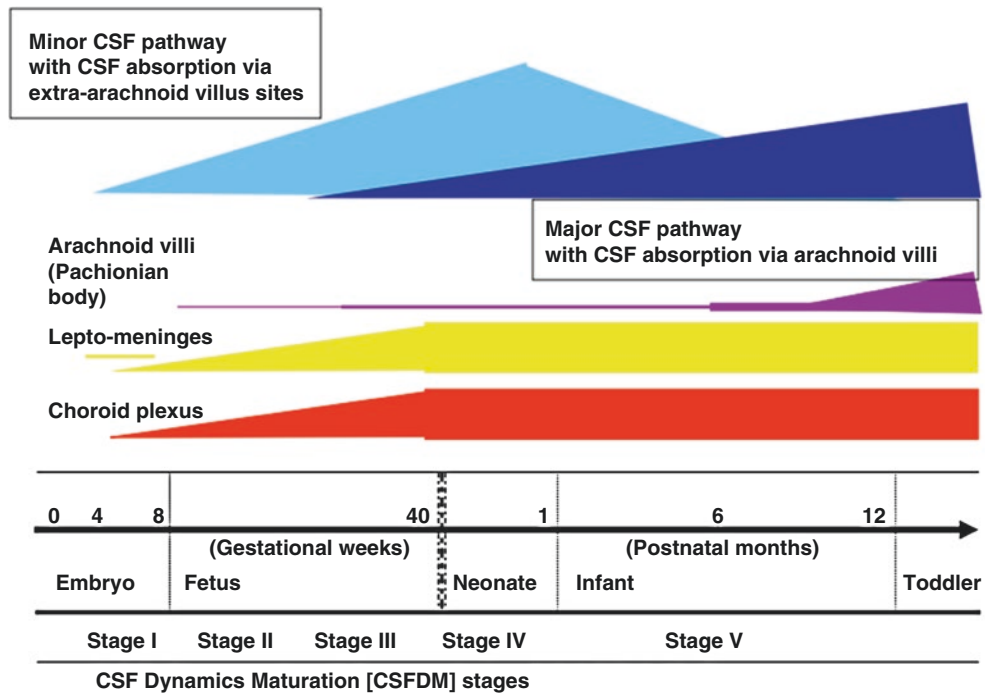


**Fig. 1.45** CSF dynamics maturation (CSFDM) stages I–V in the human (Reprinted from Oi and Di Rocco [58], with permission)

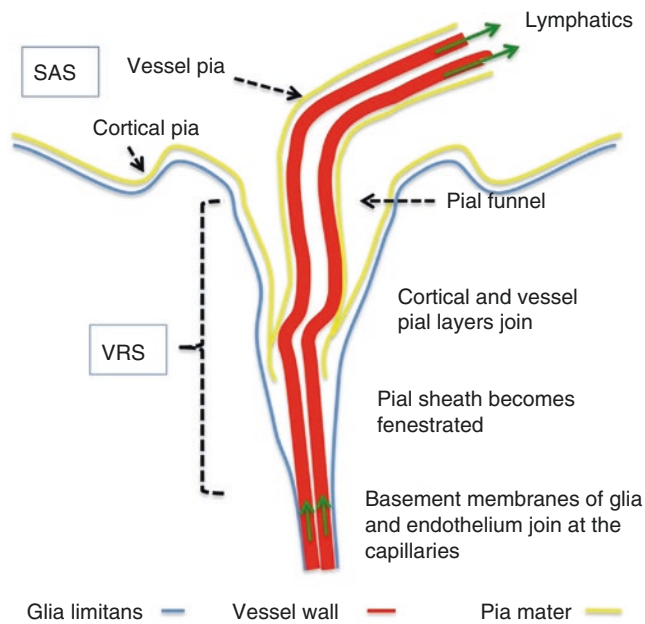


**Fig. 1.46** Morphology of the Virchow-Robin space (VRS). Delineated by the basal membranes of the glia, pia, and endothelium, the VRS consists of the space surrounding vessels that penetrate into the parenchyma. The VRS is obliterated at the capillaries where the basement membranes of the glia and endothelium join. The complex pial architecture may be understood as an invagination of both cortical and vessel pia into the VRS. The pial funnel is not a regular finding. The pial sheath around arteries extends into the VRS, but becomes more fenestrated and eventually disappears at the precapillary section of the vessel. Unlike arteries (as shown in this figure), veins do not possess a pial sheath inside the VRS. Interstitial fluid may drain by way of an intramural pathway along the basement membranes of capillaries and arterioles into the lymphatics at the base of the skull (green arrows). It should be noted that the figure does not depict the recently suggested periarterial flow from the subarachnoid space into the parenchyma and an outward flow into the cervical lymphatics along the veins. Also, it is still a matter of debate whether the VRS, extending between the outer basement membrane of the vessel and the glia, represents a fluid-filled open space. Abbreviations: VRS Virchow-Robin space, SAS subarachnoid space (Reprinted from Brinker et al. [59])



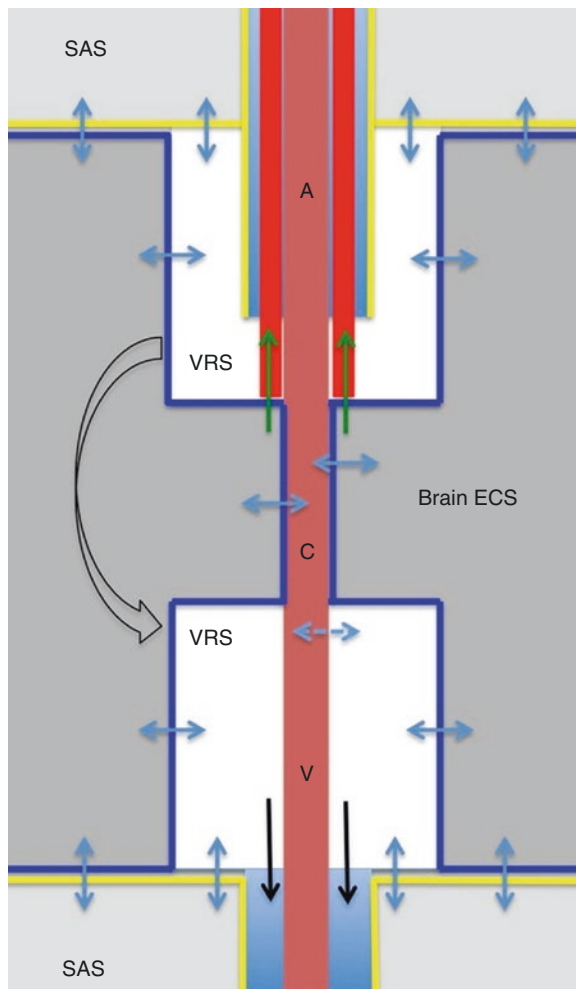


**Fig. 1.47** Diagram representing fluid movements in the Virchow-Robin space (VRS). The complex anatomical structure of the VRS allows a bidirectional fluid exchange between the VRS and both the brain extracellular space (ECS) and the subarachnoid CSF space (blue arrows). Glial (blue lines) and pial (yellow lines) cell membranes enclose the VRS and control fluid exchange. Note that it is a matter of debate whether the VRS represents an open fluid-filled space. Both experimental and clinical evidence indicate the existence of a pathway along the basement membranes of capillaries, arterioles, and arteries for the drainage of interstitial fluid (ISF) and solutes into the lymphatic system (red lines and green arrows). It is unclear whether the subpial perivascular spaces around arteries and veins (light blue) serve as additional drainage pathways. Also, the proposed glymphatic pathway connecting the arterial and venous VRS with the venous perivascular space (black arrows) is still a matter of debate. Abbreviations: VRS Virchow-Robin space, SAS subarachnoid space, A artery, C capillary, V vein (Reprinted from Brinker et al. [59])

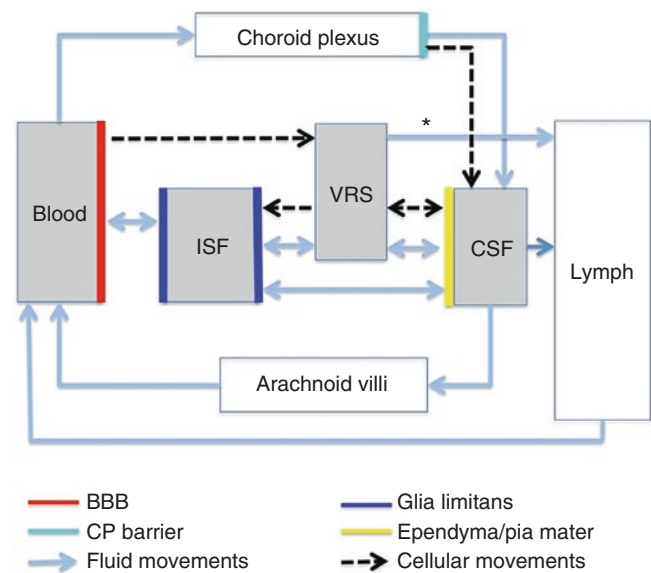


**Fig. 1.48** Diagram of the current understanding of the CSF circulation. This diagram summarizes fluid and cellular movements across the different barriers of the brain compartments (blood, ISF, VRS, CSF space comprising the cerebral ventricles, basal cisterns, and cortical subarachnoid space). Aquaporins and other transporters control the fluid exchange at the glial, endothelial, and choroid plexus barrier. At the glial, endothelial, and pial barrier, bidirectional flow may generate either a net in- or outflux, providing fluid exchange rates, which surpass the net CSF production rate by far. The choroid plexus is the only direct connection between the blood and the CSF compartment. Major portions of brain water are drained into the cervical lymphatics from the VRS (including its capillary section) via intramural arterial pathways (asterisks) and from the CSF space (via the perineural subarachnoid space of the cranial nerves). The capillary and venular endothelium may contribute to brain water absorption. Blood-borne inflammatory cells may enter the brain via VRS venules or via the choroid plexus. Fluid movements at the barriers are driven by osmotic and hydrostatic gradients or by active transporter processes. Fluid movements into and out of the VRS depend on respiratory and cardiac pressure pulsations. Abbreviations: ISF interstitial fluid VRS Virchow-Robin space, BBB blood-brain barrier, CP choroid plexus (Reprinted from Brinker et al. [59])

physiological functions may be activated, such as the regeneration of the brain during sleep [59]. Currently, in regard to CSF absorption, the importance of aquaporin 4 (AQP4) is also cited. AQP4 is a membrane transport protein, present in the central nervous system, particularly in the membrane of the astrocytic feet and the basolateral membranes of ependymal cells. It has also been noted that there are no tight junctions between the cells of the pia mater and the ependyma, so water and other substances pass freely between the cerebral parenchyma and subarachnoid space [57].

## References

- Von Staden H. Herophilus: the art of medicine in early Alexandria. New York: Cambridge University Press; 1989.
- Dobson JF. Erasistratus. *Proc R Soc Med.* 1927;20:825–32.
- Longrigg J. Anatomy in Alexandria in the third century BC. *Br J Hist Sci.* 1988;21:455–88. doi:10.1017/S000708740002536X.
- Tascioglu AO, Tascioglu AB. Ventricular anatomy: illustrations and concepts from antiquity to Renaissance. *Neuroanatomy.* 2005;4:57–63.
- Mortazavi MM, Adeeb N, Griessenauer CJ, Sheikh H, Shahidi S, Tubbs RI, et al. The ventricular system of the brain: a comprehensive review of its history, anatomy, histology, embryology, and surgical considerations. *Childs Nerv Syst.* 2014;30:19–35. doi:10.1007/s00381-013-2321-3.
- Gross CG. Brain, vision, memory: tales in the history of neuroscience. Cambridge: MIT Press; 1998.
- Telfer W. Cyril of Jerusalem and Nemesius of Emesa. Philadelphia: Westminster Press; 1955.
- Corner GW. Anatomical texts of the earlier middle ages: a study in the transmission of cultures. Carnegie Institute of Washington: Washington; 1927.
- Woolam DMH. Concepts of the brain and its functions in classical antiquity. In: Poynter FNL, editor. The history and philosophy of knowledge of the brain and its function. Springfield: Thomas; 1958. p. 48–75.
- Singer CJ. A short history of anatomy from the Greeks to Harvey. 2nd ed. New York: Dover Publications; 1957.
- Sudhoff K. Ein Beitrag zur Geschichte der Anatomie im Mittelalter: speziell der anatomischen Graphik nach Handschriften des 9. bis 15. Leipzig: JA Barth, Studien zur Geschichte der Medizin, hft 4; 1908. p.11–23.
- Clarke E, Dewhurst K. An illustrated history of brain function. Berkeley: University of California Press; 1972.
- Luzzi M. Anatomia. L. Cappelli: Bologna; 1930.
- Herrlinger R. History of medical illustrations from antiquity to AD 1600. London: Ditman; 1970.
- Roberts KB, Tomlinson JDW. The fabrics of the body: European traditions of anatomical illustrations. New York: Clarendon Press; 1992.
- Lucy WA. Anatomical illustrations before Vesalius. *J Morphol.* 1911;22:945–88.
- Wickersheimer E. L'Anatomie de Guido de Vigevano, médecin de la reine Jeanne de Bourgogne (1345). *Archiv für Geschichte der Medizin.* 1913;7:1–25.
- Di Ieva A, Tschabitscher M, Prada F, Gaetani P, Aimar E, Pisano P, et al. The neuroanatomical plates of Guido da Vigevano. *Neurosurg Focus.* 2007;23:E15. doi:10.3171/foc.2007.23.1.15.
- Cavalcanti DD, Feindel W, Goodrich JT, Dagi TF, Prestigiacomo CJ, Preul MC. Anatomy, technology, art, and culture: toward a realistic perspective of the brain. *Neurosurg Focus.* 2009;27:E2. doi:10.3171/2009.7.
- Keele KD. Leonardo da Vinci's influence on Renaissance anatomy. *Med Hist.* 1964;8:360–70.
- McMurrich JP. Leonardo da Vinci the anatomist. Baltimore: Williams and Wilkins; 1930.
- Clayton M. Leonardo da Vinci: the anatomy of man. Boston: Little, Brown and Company; 1992.
- Vinci L, Vangensten OCL, Fonahn A, Hopstock H. Quaderni di anatomia. Jacob Dubwad: Christiania; 1911-1916.
- Ariès P. The hour of our death. New York: Knopf; 1981.
- Peccatori S, Zuffi S. Piero della Francesca. London: Dorling Kindersley; 1999.
- Albertus of Orlamünde, Dominican (fl. late 13th c.). *Philosophia pauperum.* Venice: Georgium de Arriubenis; 1496.
- Hundt M. *Antropologium de hominis dignitate, natura et proprietatibus, de elementis, partibus et membris humani corporis.* Leipzig: Wolfgang Stöckel; 1501.
- Reisch G. *Margarita philosophica.* Freiburg: Schott; 1503.
- Goodrich JT. A millennium review of skull base surgery. *Childs Nerv Syst.* 2000;16:669–85. doi:10.1007/s003810000322.
- Hanigan WC, Ragen W, Foster R. Dryander of Marburg and the first textbook of neuroanatomy. *Neurosurgery.* 1990;26:489–98.
- Carpi JB. *Isagogae breves, perlucidae ac uberrimae, in anatomiam humani corporis a communi medicorum academia usitatam.* Bologna: Benedictus Hectoris; 1523.
- Carpi JB. *Tractatus de fractura calve sive cranei.* Bologna: Hieronymus de Benedictis; 1518.
- Dryander J. *Anatomia Capitis Humani.* Marburg: Eucharius Cervicornus Agrippina; 1536.
- Vesalius A. *De humani corporis fabrica libri septem.* Basel: Johannes Oporinus; 1543.
- O'Malley CD. *Andreas Vesalius of Brussels, 1514–1564.* Berkeley: University of California Press; 1964.
- Saunders JB, O'Malley CD. *The anatomical drawings of Andreas Vesalius.* New York: Bonanza Books; 1982.
- Longatti P, Fiorindi A, Perin A, Martinuzzi A. Endoscopic anatomy of the cerebral aqueduct. *Neurosurgery.* 2007;61:1–5. doi:10.1227/01.neu.0000289705.64931.0c.
- Santos ARL, Fratzoglou M, Perneczky A. A historical mistake: the aqueduct of Sylvius. *Neurosurg Rev.* 2004;27:224–5. doi:10.1007/s10143-004-0334-9.
- Rogers L. The foramen of Magendie. *J Anat.* 1931;65:457–67.
- Tubbs RS, Loukas M, Shoja MM, Shokouhi G, Oakes WJ. François Magendie (1783–1855) and his contributions to the foundations of neuroscience and neurosurgery. *J Neurosurg.* 2008;108:1038–42. doi:10.3171/JNS/2008/108/5/1038.
- Monro A. *Observations on the structure and function of the nervous system.* Edinburgh: William Creech; 1783.
- Tubbs RS, Oakes P, Maran IS, Salib C, Loukas M. The foramen of Monro: a review of its anatomy, history, pathology, and surgery. *Childs Nerv Syst.* 2014;30:1645–9. doi:10.1007/s00381-014-2512-6.
- Von Luschka H. *Die Adergeflechte des menschlichen Gehirnes: eine Monographie.* Berlin: Georg Reimer; 1855.
- Sharifi M, Ungier E, Ciszek B, Krajewski P. Microsurgical anatomy of the foramen of Luschka in the cerebellopontine angle, and its vascular supply. *Surg Radiol Anat.* 2009;31:431–7. doi:10.1007/s00276-009-0464-4.
- Tubbs RS, Vahedi P, Loukas M, Shoja MM, Cohen-Gadol AA. Hubert von Luschka (1820–1875): his life, discoveries, and contributions to our understanding of the nervous system. *J Neurosurg.* 2011;114:268–72. doi:10.3171/2010.8.JNS10683.
- Key A, Retzius MG. *Studien in der Anatomie des Nervensystems und des Bindegewebes.* Stockholm: Samson and Wallin; 1875.
- Sadler TW. *Langman's medical embryology.* Philadelphia: Lippincott Williams and Wilkins; 2006.
- Lowery LA. *Mechanisms of brain ventricle development.* Cambridge: Massachusetts Institute of Technology; 2008.

49. Rhoton Jr AL. The lateral and third ventricles. *Neurosurgery*. 2002;51:S207–71.
50. Standring S. *Gray's anatomy: the anatomical basis of clinical practice*. Edinburgh: Churchill Livingstone; 2008.
51. Snell RS. *Clinical neuroanatomy*. Philadelphia: Wolters Kluwer / Lippincott Williams and Wilkins; 2010.
52. Timurkaynak E, Rhoton Jr AL, Barry M. Microsurgical anatomy and operative approaches to the lateral ventricles. *Neurosurgery*. 1986;19:685–723.
53. Le Gars D, Lejeune JP, Peltier J. Surgical anatomy and surgical approaches to the lateral ventricles. *Adv Tech Stand Neurosurg*. 2009;34:147–87.
54. Kawashima M, Li X, Rhoton Jr AL, Ulm AJ, Oka H, Fujii K. Surgical approaches to the atrium of the lateral ventricle: microsurgical anatomy. *Surg Neurol*. 2006;65:436–45. doi:[10.1016/j.surneu.2005.09.033](https://doi.org/10.1016/j.surneu.2005.09.033).
55. Breadsted J. *The Edwin Smith surgical papyrus*. Chicago: University of Chicago Press; 1930.
56. Liddelow SA. Fluids and barriers of the CNS: a historical viewpoint. *Fluids Barriers CNS*. 2011;8:2. doi:[10.1186/2045-8118-8-2](https://doi.org/10.1186/2045-8118-8-2).
57. Miyajima M, Arai H. Evaluation of the production and absorption of cerebrospinal fluid. *Neurol Med Chir*. 2015;55:647–56. doi:[10.2176/nmc.ra.2015-0003](https://doi.org/10.2176/nmc.ra.2015-0003).
58. Oi S, Di Rocco C. Proposal of “evolution theory in cerebrospinal fluid dynamics” and minor pathway hydrocephalus in developing immature brain. *Childs Nerv Syst*. 2006;22:662–9. doi:[10.1007/s00381-005-0020-4](https://doi.org/10.1007/s00381-005-0020-4).
59. Brinker T, Stopa E, Morrison J, Klinge P. A new look at cerebrospinal fluid circulation. *Fluids Barriers CNS*. 2014;11:10. doi:[10.1186/2045-8118-11-10](https://doi.org/10.1186/2045-8118-11-10).
60. Hassin GB. The cerebrospinal fluid pathways (a critical note). *J Neuropathol Exp Neurol*. 1947;6:172–6.
61. Davson H. *Physiology of the cerebrospinal fluid*. London: J. and A. Churchill Ltd; 1967.
62. Davson H, Segal MB. *Physiology of the CSF and blood–brain barriers*. 1st ed. New York: CRC Press; 1996.
63. Rodriguez EM, Blazquez JL, Guerra M. The design of barriers in the hypothalamus allows the median eminence and the arcuate nucleus to enjoy private milieus: the former opens to the portal blood and the latter to the cerebrospinal fluid. *Peptides*. 2010;31:757–76. doi:[10.1016/j.peptides.2010.01.003](https://doi.org/10.1016/j.peptides.2010.01.003).
64. Lehtinen MK, Walsh CA. Neurogenesis at the brain–cerebrospinal fluid interface. *Annu Rev Cell Dev Biol*. 2011;27:653–79. doi:[10.1146/annurevcellbio-092910-154026](https://doi.org/10.1146/annurevcellbio-092910-154026).
65. Sawamoto K, Wichterle H, Gonzalez-Perez O, Cholfin JA, Yamada M, Spassky N, et al. New neurons follow the flow of cerebrospinal fluid in the adult brain. *Science*. 2006;311:629–32. doi:[10.1126/science.1119133](https://doi.org/10.1126/science.1119133).
66. Del Bigio MR. The ependyma: a protective barrier between brain and cerebrospinal fluid. *Glia*. 1995;14:1–13. doi:[10.1002/glia.440140102](https://doi.org/10.1002/glia.440140102).
67. Siyahhan B, Knobloch V, de Zélicourt D, Asgari M, Schmid Daners M, Poulikakos D, et al. Flow induced by ependymal cilia dominates near-wall cerebrospinal fluid dynamics in the lateral ventricles. *J R Soc Interface*. 2014;11:20131189. doi:[10.1098/rsif.2013.1189](https://doi.org/10.1098/rsif.2013.1189).
68. Lechtreck KF, Delmotte P, Robinson ML, Sanderson MJ, Witman GB. Mutations in *hyd1n* impair ciliary motility in mice. *J Cell Biol*. 2008;180:633–43. doi:[10.1083/jcb.200710162](https://doi.org/10.1083/jcb.200710162).
69. Roth Y, Kimhi Y, Edery H, Aharonson E, Priel Z. Ciliary motility in brain ventricular system and trachea of hamsters. *Brain Res*. 1985;330:291–7. doi:[10.1016/0006-8993\(85\)90688-2](https://doi.org/10.1016/0006-8993(85)90688-2).
70. Ibanez-Tallon I, Pagenstecher A, Fliegau M, Olbrich H, Kispert A, Ketelsen UP, et al. Dysfunction of axonemal dynein heavy chain *Mdnah5* inhibits ependymal flow and reveals a novel mechanism for hydrocephalus formation. *Hum Mol Genet*. 2004;13:2133–41. doi:[10.1093/hmg/ddh219](https://doi.org/10.1093/hmg/ddh219).
71. Tissir F, Qu Y, Montcouquiol M, Zhou L, Komatsu K, Shi D, et al. Lack of *cadherins Celsr2* and *Celsr3* impairs ependymal ciliogenesis, leading to fatal hydrocephalus. *Nat Neurosci*. 2010;13:700–7. doi:[10.1038/nn.2555](https://doi.org/10.1038/nn.2555).
72. Lee L. Riding the wave of ependymal cilia: genetic susceptibility to hydrocephalus in primary ciliary dyskinesia. *J Neurosci Res*. 2013;91:1117–32. doi:[10.1002/jnr.23238](https://doi.org/10.1002/jnr.23238).
73. Benner EJ, Luciano D, Jo R, Abdi K, Paez-Gonzalez P, Sheng H, et al. Post-injury protective astrogenesis from SVZ niche is controlled by Notch modulator *Thbs4*. *Nature*. 2013;497:369–73. doi:[10.1038/nature12069](https://doi.org/10.1038/nature12069).
74. Curtis MA, Benner EJ, Kam M, Nannmark U, Anderson MF, Axell MZ, Wikkelso C, et al. Human neuroblasts migrate to the olfactory bulb via a lateral ventricular extension. *Science*. 2007;315:1243–9. doi:[10.1126/science.1136281](https://doi.org/10.1126/science.1136281).
75. Suzuki SO, Goldman JE. Multiple cell populations in the early postnatal subventricular zone take distinct migratory pathways: a dynamic study of glial and neuronal progenitor migration. *J Neurosci*. 2003;23:4240–50.
76. Banizs B, Pike MM, Millican CL, Ferguson WB, Komlosi P, Sheetz J, et al. Dysfunctional cilia lead to altered ependyma and choroid plexus function, and result in the formation of hydrocephalus. *Development*. 2005;132:5329–39. doi:[10.1242/dev.02153](https://doi.org/10.1242/dev.02153).
77. Cushing H. *Studies in intracranial physiology and surgery. The third circulation. The hypophysis. The gliomas*. London: Oxford University Press; 1926.
78. Black PM. Harvey Cushing at the Peter Bent Brigham hospital. *Neurosurgery*. 1999;45:990–1001.
79. Milhorat TH. The third circulation revisited. *J Neurosurg*. 1975;42:628–45.
80. Davson H. Formation and drainage of the cerebrospinal fluid. *Sci Basis Med Annu Rev*. 1966;238–59.
81. Davson H, Domer FR, Hollingsworth JR. The mechanism of drainage of the cerebrospinal fluid. *Brain*. 1973;96:329–36.
82. Johanson CE, Duncan 3rd JA, Klinge PM, Brinker T, Stopa EG, Silverberg GD. Multiplicity of cerebrospinal fluid functions: new challenges in health and disease. *Cerebrospinal Fluid Res*. 2008;5:10. doi:[10.1186/1743-8454-5-10](https://doi.org/10.1186/1743-8454-5-10).
83. Weed LH. *Studies on cerebro-spinal fluid. No. II: the theories of drainage of cerebro-spinal fluid with an analysis of the methods of investigation*. *J Med Res*. 1914;31:21–49.

## 2.1 Historical Evolution

### 2.1.1 Pioneers

The first neuroendoscopic procedure reported in the literature was conducted by Victor Darwin Lespinasse (1878–1946) (Fig. 2.1) in 1910 [1]. Lespinasse, a urologist from Chicago, was also famous for being a pioneer and a defender of testicular transplantation. The neuroendoscopic procedure he reported consisted of bilateral choroid plexus coagulation, making use of a small cystoscope. In this first experiment, two children were treated; one died in the immediate postoperative period, while the other lived on for another 5 years. Lespinasse did not officially record this adventure in the scientific literature, he merely introduced the method to the local medical society and mentioned it in his application, in 1913, to the American College of Surgeons, in which he cited the “destruction of the choroid plexus for internal hydrocephalus” among his surgical areas of interest. He would later tell his daughter Victoire, an obstetrician also from Chicago, that this pioneer procedure was “an intern’s stunt” [2].

The great pioneer of neuroendoscopy was Walter Edward Dandy (1886–1946) (Fig. 2.2), from Johns Hopkins

School of Medicine, in Baltimore. He is considered to be the father of pediatric neurosurgery and also neuroendoscopy, because of the great knowledge of ventricular anatomy he acquired from his ventriculography studies, a technique that permitted visualization of the ventricular system for the first time (Fig. 2.3). Dandy said, with respect to ventriculography:

“All of the injections have been made in children varying from 6 months to 12 years of age. Invariably, the lateral ventricle has been sharply outlined in the radiogram. In two instances, the third ventricle and the foramen of Monro were visible. In none, however, have we observed the fourth ventricle or the aqueduct of Sylvius. The practical value from pneumoventriculography is expected principally from the shadows of the lateral ventricles” [3].

In 1922, Dandy published the first endoscopic observations of the ventricles through the use of an endoscope illuminated by an external light reflection in a mirror, coining the term “ventriculscopy” [4] (Fig. 2.4), in which he said:

“It was possible to see practically the entire extent of the lateral ventricle, the foramen of Monro, the septum pellucidum with numerous perforations in it, and the entire extent of the choroid plexus ...” [5].

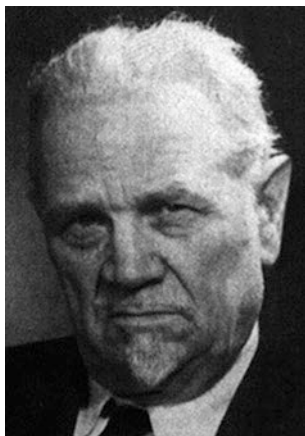


**Fig. 2.1** Victor Darwin Lespinasse (1878–1946)



**Fig. 2.2** Walter Edward Dandy (1886–1946)

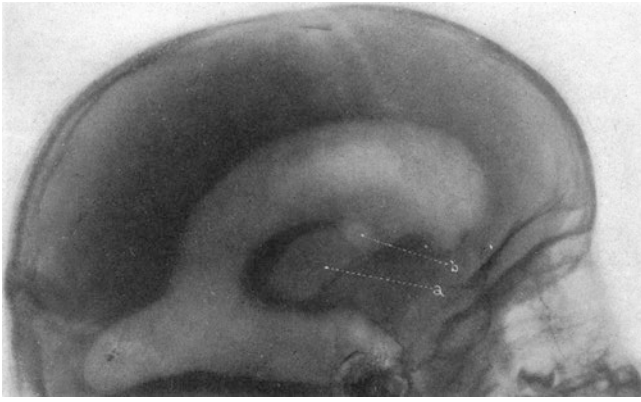


**Fig. 2.3** From the initial studies of Dandy, pneumoventriculography in a 3-year-old child with tuberculous meningitis. It is possible to see “the third ventricle (*a*) and probably the foramen of Monro (*b*)” according to his own words (Reprinted from Dandy [3])

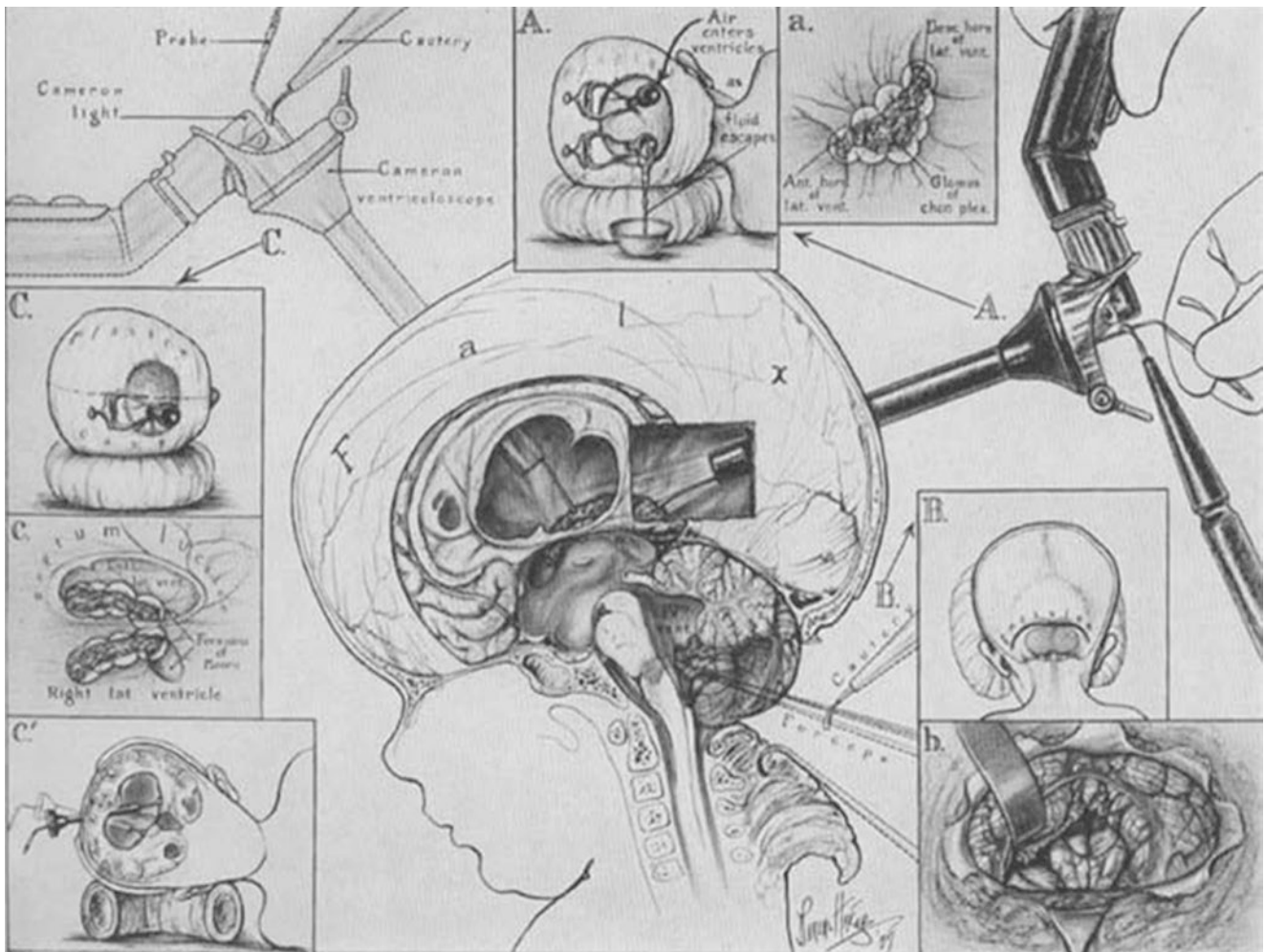


**Fig. 2.4** Publication of 1922 by Dandy, after his first endoscopic observations (Reprinted from Dandy [5])

However, despite the good visualization achieved with “ventriculoscopy”, resection of the choroid plexus, a common technique at the time, was not possible with the use of the ventriculoscope. Dandy also stated:

“The remarkable visualization of the ventricular system provided by the ventriculoscope did not surpass the images produced by the more routine pneumoventriculography” [6].

He continued with his endoscopic experiences, and in 1923, using a small cystoscope, he performed resection of the choroid plexus in two patients [7], followed by others in the following years, and he achieved results similar to those of a craniotomy [8] (Fig. 2.5). After years of enthusiasm, at the end of his brilliant career, Dandy said, of ventriculoscopy:

“Its usefulness is probably restricted to infants and young children, and to those tumors which are accidentally disclosed during choroid plexectomies rather than tumors, however small, that are causing obstruction to the ventricular channels” [9].

In Germany, the pioneer of neuroendoscopy was Erwin Payr (1871–1946), professor of neurosurgery at the University of Leipzig. He was known for the use of venous grafts for draining cerebrospinal fluid (CSF) from the ventricles to the superior sagittal sinus and jugular vein [10]. Payr presented the tools, preliminary tests, and the technical feasibility of “*Enzephaloskopie*” to Leipzig Medical Society in 1919 [2]. William Jason Mixter (1888–1958) (Fig. 2.6), chief of the Neurosurgical Service of Massachusetts General Hospital, in Boston, from 1933 to 1946, performed the first

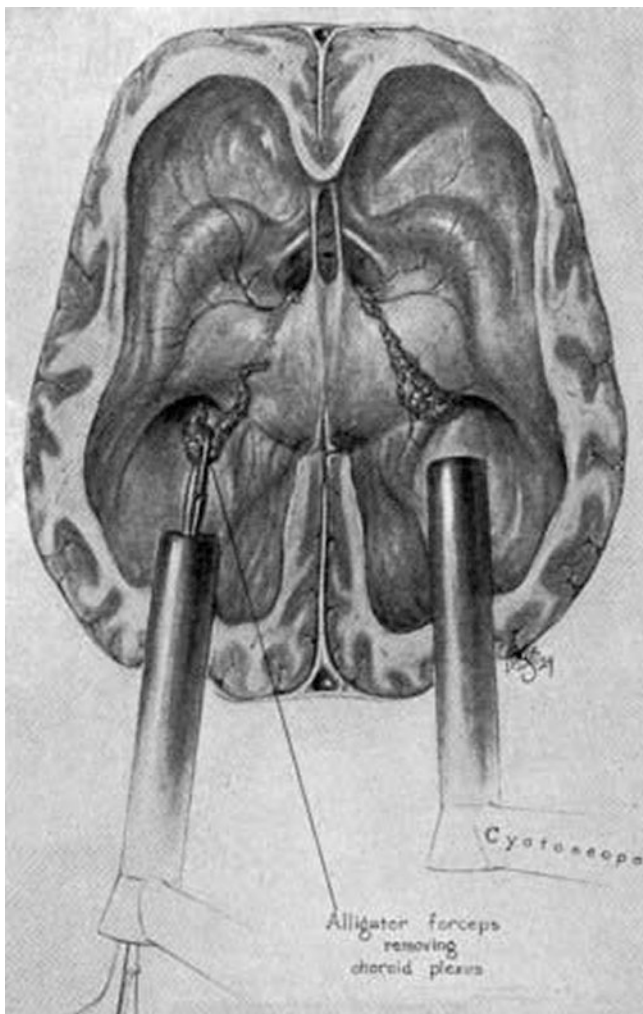


**Fig. 2.5** Description of Dandy’s technique for removal of the choroid plexus of the lateral ventricles using two Kelly cystoscopes (Reprinted from Dandy [9])



**Fig. 2.6** William Jason Mixter (1888–1958)

endoscopic third ventriculostomy (ETV) in 1923. He was also famous for being the pioneer in recognizing the relationship between herniated intervertebral discs and radicular syndromes, and published the report of the first successful discectomy, in 1934 [11]. This is still a topic for debate, because, interestingly, another pioneer of neuroen-

doscopy, Dandy, published a surgical report of “loose cartilage from intervertebral disk simulating a tumor of the spinal cord” in 1929 [12]. Fay and Grant, from Philadelphia, reported the first images of dilated infant ventricles via a cystoscope coupled with a camera in 1923 (Fig. 2.7). The exposure time for the acquisition of these images was up to 75 s

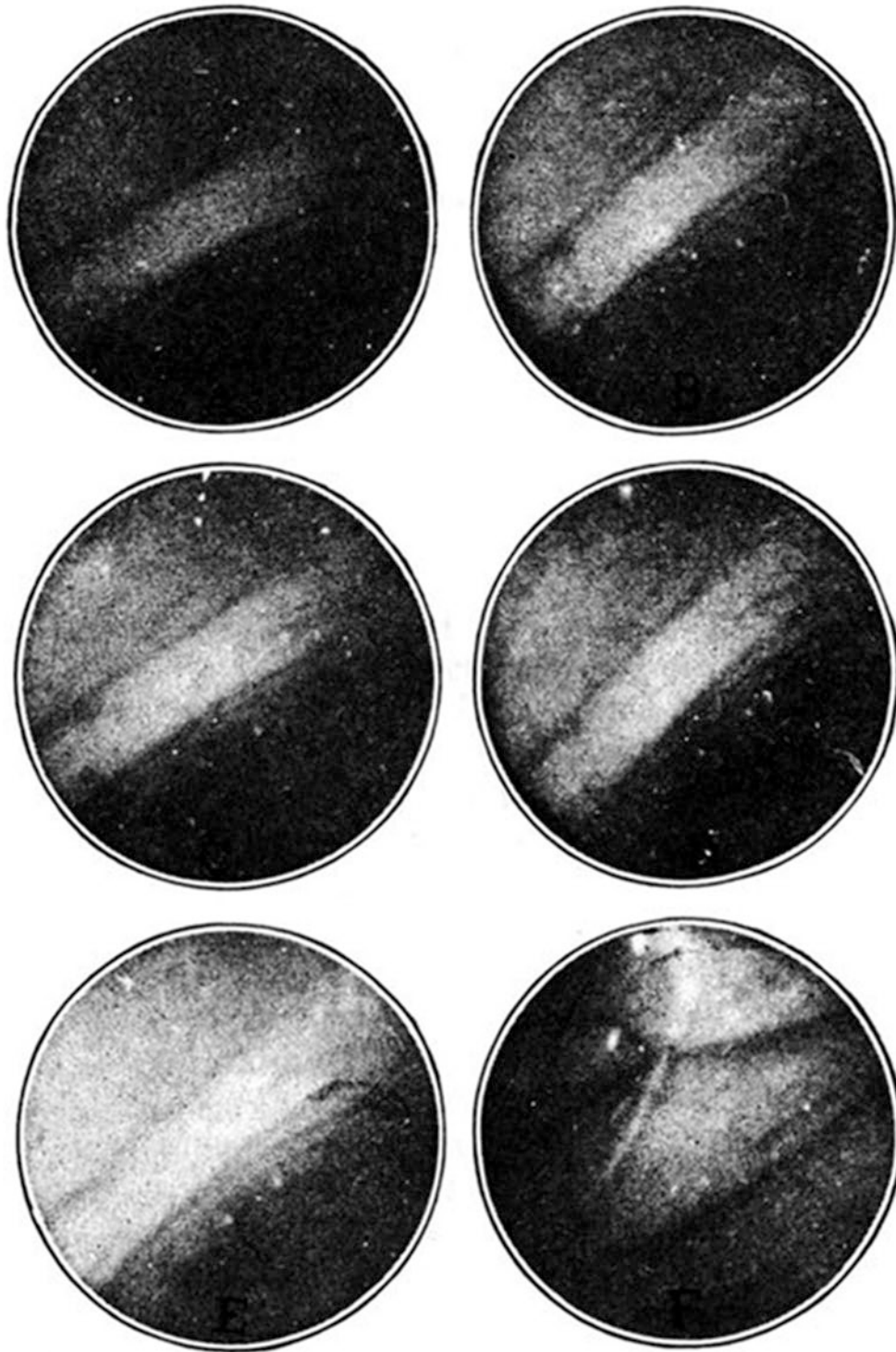


**Fig. 2.7** The first register of ventricular endoscopic images. The exposure time for the acquisition of these images was up to 75 s (Reprinted from Fay and Grant [13])

[13]. Also in 1923, Johannes Allwill Max Volkmann (1889–1982), professor at the University Surgical Clinic in Halle, Germany, published his first experiences with “*Enzephalskopie*”. After some tests on cadavers, the first ventricular inspection was carried out on a 3-year-old child with hydrocephalus. In the beginning an infant cystoscope was used, but then an “*Enzephalskop*” was designed that was lighter and easier to handle. It had a 22-cm sheath with a 6-mm outer diameter (OD), along with two irrigation holes. The optics were introduced inside the sheath, allowing rotation once inside the ventricle [14, 15].

In 1934, Tracy Jackson Putnam (1894–1975) (Fig. 2.8), a great neurologist and neurosurgeon from New York

Neurological Institute at Columbia University, was aiming to carry out a plectomy again, the procedure introduced by Dandy years earlier. For the procedure, Putnam described a new instrument called a “ventriculoscope,” for the purpose of cauterizing the choroid plexus in children with communicating hydrocephalus [16, 17]. This instrument had a length of 10 cm with a 6-mm OD (small model) or a length of 11 cm with a 7-mm OD (large model). With such equipment, bilateral choroid plexus coagulation was carried out in seven children with hydrocephalus, with “encouraging” results [18]. John Edwin Scarff (1898–1978) (Fig. 2.9) was the head of the Department of Neurological Surgery at Columbia University, New York, in 1935 [19]. In 1936, he published



**Fig. 2.8** Tracy Jackson Putnam (1894–1975)



**Fig. 2.9** John Edwin Scarff (1898–1978)



his first experience with an endoscopic plexectomy using a new apparatus [20]. His ventriculoscope, very similar to a cystoscope, was 10 cm long with a 6-mm OD (small model) or 18 cm long with a 7-mm OD (large model). The equipment permitted continuous irrigation in order to maintain constant intraventricular pressure and prevent ventricular collapse. This fact was, presumably, the cause of the bad initial results reported by Dandy, who stated in 1918:

Following the escape of the fluid, the thin brain walls collapse. ... The mechanical kinking of the larger vascular trunks by angulations of the enfolding brain must have a pronounced effect upon the circulation [21].

In Scarff's system a movable coagulation probe was also included, allowing a large range of movement, making it possible to coagulate a large area of the choroid plexus. Through the same channel, another mobile probe was also created, with the purpose of perforating the floor of the third ventricle. Scarff published a report of a series of 19 patients in 1951, 15 of whom had a good outcome with a permanent reduction in intracranial pressure; 3 did not benefit from the intervention and 1 patient died [4, 22, 23].

### 2.1.2 Ostracism of Neuroendoscopy

The decades of the 1950s and 1960s represented a period of ostracism of the practice of neuroendoscopy. This was due to the advent of ventricular shunts, the development of microsurgery, and above all, the technological limitations of

the time [24]. In 1949, Frank Nulsen and Eugene Spitz performed the first surgery to install a shunt for hydrocephalus [25], and also, in the decade following the introduction of microsurgical techniques, there were extraordinary advances, contributing to the temporary overlooking of neuroendoscopy. The microscope provided the neurosurgeon precisely what neuroendoscopy did not provide: adequate lighting, magnification, and the ability to access deep structures without incurring adjacent brain damage. In the 1960s, despite the stagnation in neuroendoscopy, there were major technological advances that allowed the resurgence of endoscopic techniques [26]. These advances correspond to the invention of a system of lenses with a variable refractive index by Harold Horace Hopkins (1918–1994) (Fig. 2.10), the invention of charged-couple devices (CCDs), and improvements in fiber optic technology [27]. Of these, undoubtedly, the technology of Hopkins deserves to be highlighted; it consisted of a system composed of a glass tube with thin lenses made of air, a rod-lens system (Fig. 2.11) [28]. This system is the basis of current rigid neuroendoscopy, and is the technology purchased by Karl Storz [29]. The Hopkins system, incredibly, increased the field of view, color rendition, and resolution by approximately 10 times compared with previous endoscopes, and it is perhaps for this reason that Hopkins has been nominated twice for the Nobel Prize in Physics [30]. Charged-couple devices (CCD) are small semiconductor sensors that capture images formed by an integrated circuit containing an array of coupled capacitors. Their unique ability to convert optical signals into electrical impulses, approximately 10 times more sensitive to light than photo-

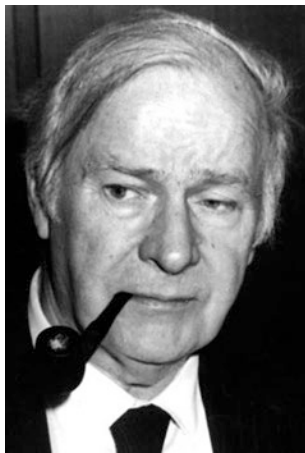


**Fig. 2.10** Harold Horace Hopkins (1918–1994)

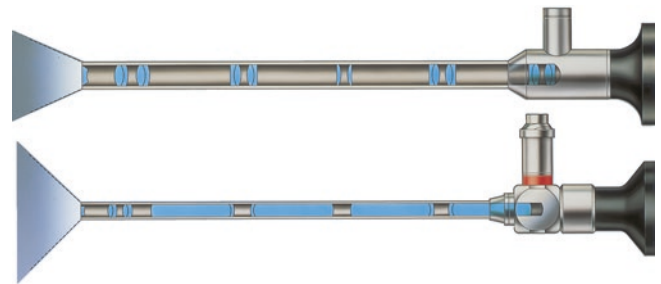


**Fig. 2.11** Standard endoscope (*above*) and Hopkins rod-lens system (*below*). The glass rods in the Hopkins telescope provide a larger image, greater light transmission, and clarity of vision improved by approximately 10 times compared with previous endoscopes (Image courtesy of Karl Storz, Tuttlingen, Germany)

graphic film, has made them vital to the miniaturization of the equipment, making it lighter to handle [27, 31]. Also, advances in fiber optic technology allowed for the use of powerful light sources that could be placed distally and transmitted with increasing efficiency to the structures of interest. These extraordinary advances in optics, which minimized the loss of reflected light and improved video capture methods, have led to a revival of neuroendoscopy and a great interest in the method in the past 20 years [24].

### 2.1.3 Rebirth

The revival of neuroendoscopy occurred only thanks to technological development. In this phase, the contribution of Gerard Guiot (1912–1998), from Paris, is primarily highlighted [32, 33]. His contribution was made thanks to the innovation introduced by Fourestier and Vulmière, from the Optical Institute of Paris. The innovation consisted of the installation of the light source not at the distal end of the endoscope, but at the proximal end, on the outside, in a separate optical apparatus. Thus, it was possible to regulate the light intensity from the outside. With this innovation, the light intensity was improved, allowing photos and video recordings, and above all, safer handling of instruments in the ventricular environment [2]. This innovation was first used by Guiot in 1962, at the Foch Hospital in Paris, in a patient with

a cystic tumor bilaterally occluding the foramen of Monro. The endoscopic procedure was performed with a tumor puncture and a third ventriculostomy. Two months after the endoscopic procedure, the tumor was completely removed under a microsurgical approach, and it was possible to show the third ventricle floor with the patent ventriculostomy. The patient had a favorable progression, and returned to work 2 months after the microsurgical procedure. A second neuroendoscopic procedure was also carried out in 1962, on a 3-month-old child with obstructive hydrocephalus; a third ventriculostomy was performed, with good patient progression [2]. Another great achievement of this revival period occurred in 1973. Takanori Fukushima, from Tokyo, was the first to use a flexible endoscope. This “ventriculofiberscope” had a diameter of 4 mm, a flexible end, and a working channel. With this equipment 37 procedures were performed, which included biopsies, septostomies, and ventriculostomies [34, 35]. Other achievements also in this phase included the development of the first endoscopy system based on the Hopkins optic system, by Griffith, from Bristol in the United Kingdom. This device had an OD sheath of 4.5 mm, and plexectomies, aqueductoplasties, and biopsies were performed with it [36, 37]. Also, in 1977, Apuzzo and colleagues, from Los Angeles, published a pioneer work on the application of the Hopkins system to several neurosurgical procedures. As an innovation, the work introduced optics with angles from 70° to 120° in cranial, spinal, and transfenoidal surgeries [28].

## 2.2 Basic Techniques for Ventricular Approaches

Neuroendoscopy has attracted great attention in the past two decades due to the technological development of optical systems, cameras, and monitors, providing great safety and elegance for the procedures. With such advances, the endoscope has been definitively added to the modern equipment arsenal of the neurosurgeon. The neuroendoscope, when compared with the surgical microscope, provides a completely different view, with advantages and disadvantages (Fig. 2.12). Current systems of rigid endoscopy with the Hopkins rod-lens system (Karl Storz, Tuttlingen, Germany), those most used worldwide, provide a field of view resulting in an excellent panoramic vision (wide angle), and even lesions not located directly in front of the endoscope can be easily recognized. There are also flexible endoscopy systems, based on a bundle of optical fibers which – despite allowing for broad angulation for viewing inside the ventricle – do not have the same image resolution, which is lower than that of rigid endoscopy [38, 39]. As a result of the aspect of a panoramic view and greater ease in identifying intraventricular structures, the orientation during endoscopic navigation is extremely safe. This feature is important, because in neuroendoscopy, the surgeon works in a narrow and deep corridor. Endoscopes with angled optics permit “looking around the corner” or behind vascular structures, which is a very positive feature of microsurgeries that are controlled and assisted by neuroendoscopy [38, 39]. The vast majority of ventricular endoscopic procedures may be performed with non-angled systems. The use of endoscopes allows viewing of the neurosurgical target with impeccable lighting, even in a very deep field. Another important advantage of the endoscope over the

microscope is the excellent depth of field, so there is no need to adjust the focus during the procedure, a feature which is required with the use of the microscope, particularly at high magnifications. Obviously, the endoscope also has its limitations. The most striking is the lack of stereoscopic vision. The view provided by the endoscope is a “fish eye” view, which is a kind of pseudo three-dimensional (3D) view. This aspect is partly influenced by a phenomenon called parallax, a term derived from astronomy, which is the impression that objects displayed closer to the endoscope move more than more distant objects, and this contributes to the pseudo 3D effect [38, 39]. Intraventricular navigation in the absence of a stereoscopic view is compensated by training. Training should be started mainly on the simplest cases, using non-angled optics. The lack of image resolution is another disadvantage of the endoscope compared with the microscope, which has objective lenses with a larger diameter. Another reason for the good resolution of the microscope is that the surgeon is looking directly through the lens system and the human retina is the sensor that captures the images. With the endoscope, on the other hand, this sensor is the CCD located on the head of the camera coupled to the optics. Even with the recent introduction of high-definition cameras, which generate images of 1080 lines and 2 million pixels, this image is still not comparable to the power of resolution of the human retina [39]. Currently, cerebral endoscopy can be classified in terms of endoscopic neurosurgery, endoscope-controlled microneurosurgery, and endoscope-assisted microneurosurgery [38, 40]. Endoscopic neurosurgery or ventricular neuroendoscopy (“channel endoscopy”) basically consists of the use of the neuroendoscope in the ventricular cavity, with the instruments being employed through a working channel in the endoscope itself. The neuroendoscope is used to navigate in

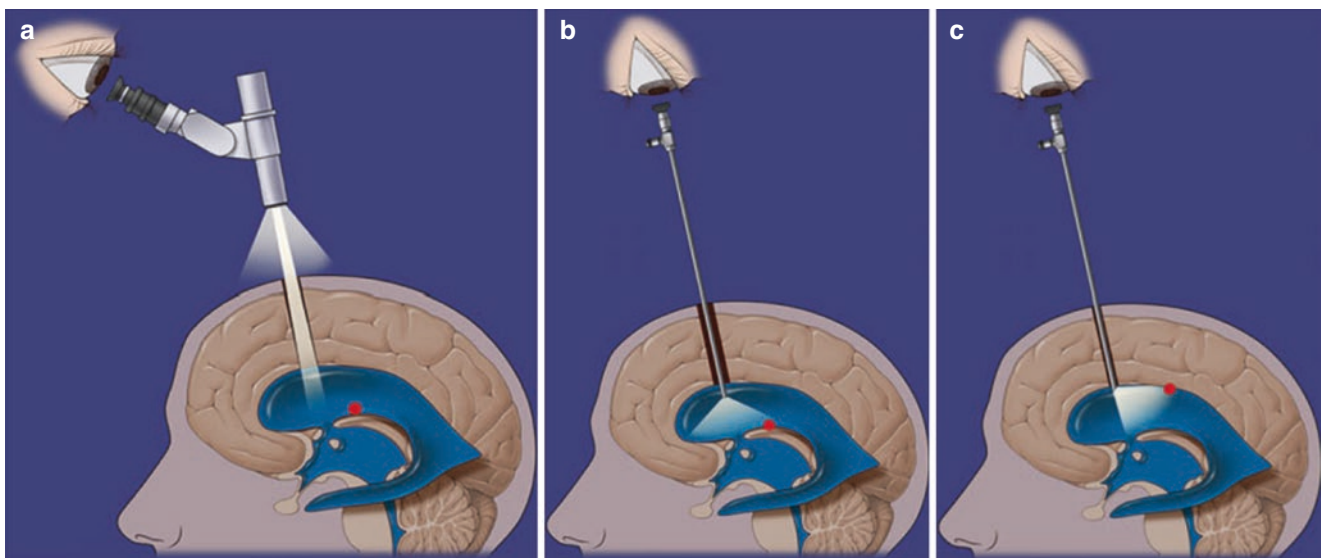


**Fig. 2.12** Comparison of microscopic view (a) and non-angled (b) and angled (c) endoscopic views (Reprinted from Schroeder [38], with permission)

the ventricular liquid medium, so the blood is the worst enemy, given the difficulty in viewing the structures. Because of this, continuous ventricular irrigation with warmed saline through a channel of the endoscope is mandatory. Endoscope-controlled microneurosurgery basically consists of the resection of hypophyseal tumors, skull base tumors, and tumors in other cranial locations done exclusively with the endoscope. Endoscope-assisted microneurosurgery consists of the use of the neuroendoscope alongside the surgical microscope, in the same operation, whether for the removal of tumors or in vascular surgeries [38–40]. The general indications for endoscopic neurosurgery are obstructions in cerebrospinal fluid (CSF) circulation pathways, arachnoid and intraparenchymal cysts, and intraventricular lesions [41–44]. The most common techniques for restoring CSF movement include: endoscopic third ventriculostomy (ETV), septostomy, foraminoplasty, aqueductoplasty with or without a stent, cyst fenestrations in general, and tumor removals [45–51]. The most common cranial point for ventricular neuroendoscopy is Kocher's point, located in the frontal region, about 2 cm anterior to the coronal suture and 2 cm lateral to the midline. All the images for this atlas were obtained from this point, with small variations, in centimeters, according to the presence or absence of a patent fontanelle (in children), the ventricular anatomy, and the type of disease being treated. Other points of ventricular access are described both for endoscopic procedures themselves, and for ventricular punctures in general [52] (Figs. 2.13, 2.14, and 2.15). In adults and older children, the skull opening is done through a burr hole, and in newborns, the fontanelle can be used as a natural portal for the introduction of the endoscope (Figs. 2.16, 2.17, 2.18, 2.19 and 2.20). In newborns, the approach can also be performed by a minicraniotomy [53] (Fig. 2.21). Before the beginning of the surgery itself it is very important to check the position of the monitor for good visualization and for the comfort of the surgeon, mainly in more time-consuming procedures (Figs. 2.22 and 2.23). In adults and older children the opening of the skull can be performed with a high-rotation drill followed by a cross fashion dural opening (Figs. 2.24 and 2.25). In newborns the fontanelle is a physiological way and the dura is opened in linear fashion, allowing watertight closure at the end (Figs. 2.26 and 2.27). In endoscopic neurosurgery, the endoscope itself is the only ventricular visualization tool, and the tools are introduced into the surgical field through working channels that are part of each system. Currently several types of neuroendoscopes are available. Compact and small-size systems, such as the Oi HandyPro and Gaab systems (Karl Storz, Tuttlingen, Germany) allow more free movements inside the ventricle, as well as providing excellent image quality (Figs. 2.28 and 2.29). The endoscope can be inserted into the ventricular system through a trocar inside a sheath (Fig. 2.30), but some surgeons prefer a peel-away sheath. After the ventricular puncture is done, the trocar is removed, and in its

place the optic is inserted, which is nothing more than the endoscope itself. At this point, it is possible to navigate the ventricle by maneuvering the optic with the dominant hand and holding the sheath at its entry into the skull with the non-dominant hand, in order to avoid inadvertent introduction of the system into the ventricle (Fig. 2.31). Some neuroendoscopists prefer to make use of an articulated arm in order to keep the endoscope in place and have both hands free to manipulate instruments through the working channels. Another alternative is that the neuroendoscopist can perform the navigation with both hands, as described above, and a second neuroendoscopist can manipulate the instruments through the working channel without concern for the navigation [54]. In this case, some systems allow the use of instruments in two work channels simultaneously, resulting in a bimanual dissection, although with coaxial movement, and obviously not as elegant as a microsurgical dissection [55]. A third alternative, which is the preference of this author, is a frameless free-hand technique [56], wherein the ventricular navigation through the endoscope is performed with the non-dominant hand and instruments are used through the working channel with the dominant hand. Among the various types of rigid endoscopy systems applicable to ventricular procedures, the first in which this technique has been described is the Oi HandyPro [56, 57] (Fig. 2.32). The Gaab system, although it was not designed specifically for this technique, allows the use of the free-hand technique due to its compact size (Figs. 2.33, 2.34, and 2.35). All images in this book were obtained with these two systems. It is possible for the neuroendoscopist to perform the procedures in a sitting or standing position, depending on the duration of the surgery (Figs. 2.36 and 2.37). At the end of the procedure, in adults and older children, biological glue is sufficient to seal the corticotomy, and closure of the scalp with planes is sufficient. On the other hand, in newborns, dural watertight closure (polypropylene or silk) and biological glue is mandatory (Figs. 2.38, 2.39, 2.40, and 2.41). When performing minicraniotomy [53], dural closure is also necessary, as well as bone fixation (Fig. 2.42). The scalp is closed layer by layer, in watertight fashion. In adults, the skin is closed with mononylon in separate points (Fig. 2.43), with the same skin closure used for children, although in babies an absorbable suture can be a good option for the skin. The ability to capture and archive neuroendoscopic videos, images, and patient data easily and securely during procedures ensures that detailed and accurate records of the diagnosis and treatment are achieved. These records also provide a valuable knowledge base for training, education, publication, and sharing scientific information with colleagues. The AIDA (Advanced Image and Data Acquisition) system (Karl Storz, Tuttlingen, Germany) offers a solution for the recording of patient data and full high-definition (HD) videos and still images. An intuitive interface and user-friendly front panel supports fast and uncomplicated handling (Fig. 2.44).

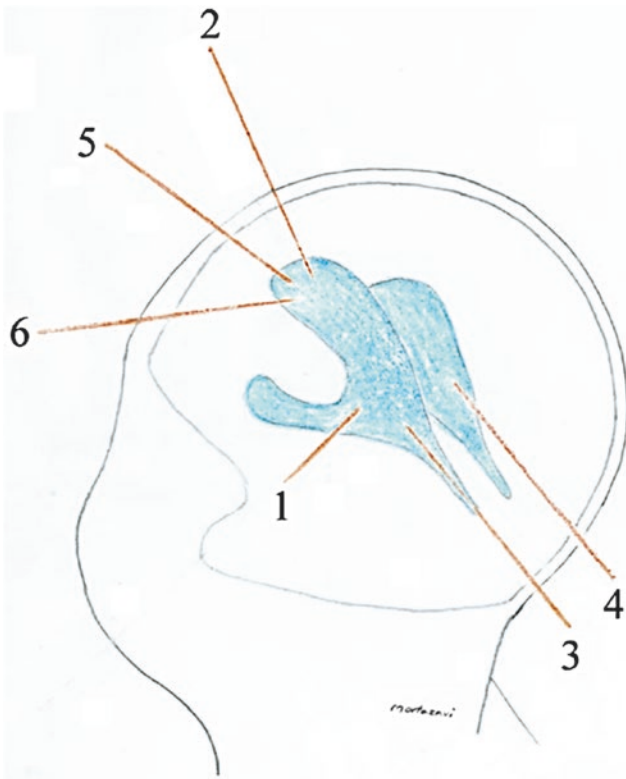


**Fig. 2.13** Schematic illustration of all the extra-calvarial ventricular access points: Keen (1), Kocher (2), Dandy (3), Frazier (4), Kaufman (5), and Tubbs (6) (Reprinted from Mortazavi et al. [52], with permission)



**Fig. 2.15** Kocher's point in a 2-year-old child



**Fig. 2.14** Kocher's point in an adult

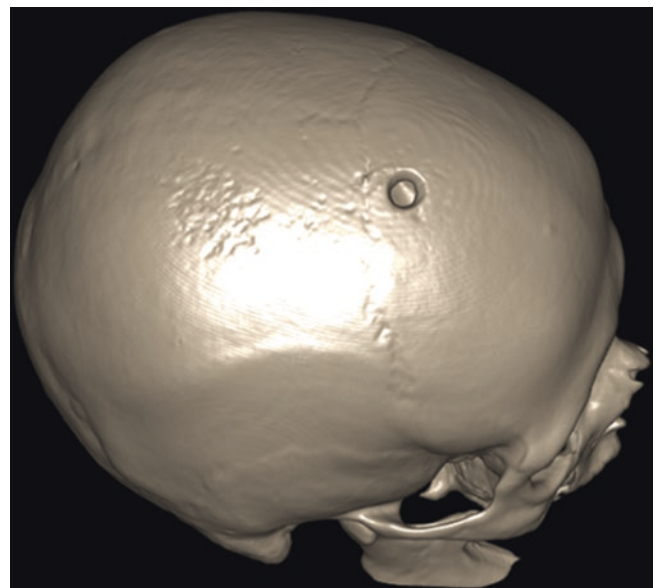


**Fig. 2.16** Three-dimensional (3D) computerized tomography (CT) scan depicting the burr hole at Kocher's point in an adult

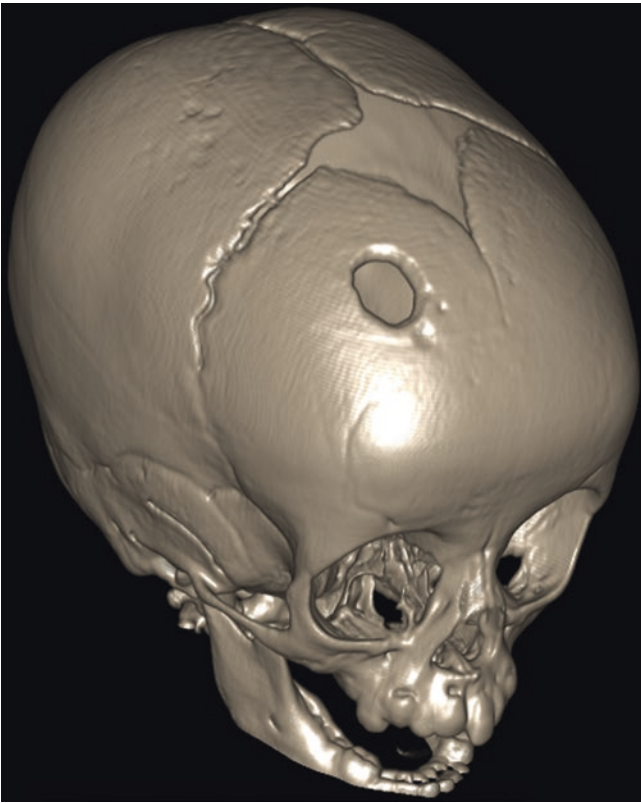


**Fig. 2.17** 3D CT scan depicting the burr hole more anterior to the traditional reference of Kocher's point, in a 2-year-old child with reduced fontanelle



**Fig. 2.19** Detail of the transfontanelle approach in a patient with complex hydrocephalus, after several external ventricular drainages



**Fig. 2.18** Detail of the transfontanelle approach



**Fig. 2.20** 3D CT scan showing detail of the postoperative linear incision in the transfontanelle approach

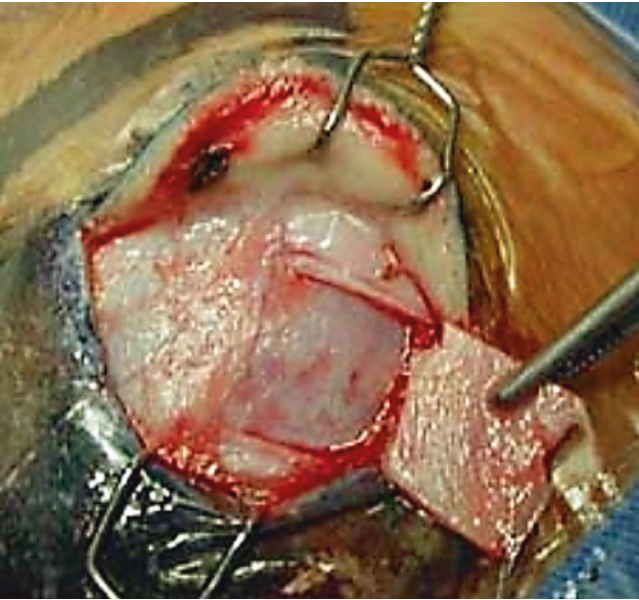


**Fig. 2.21** Approach by minicraniotomy (Reprinted from Costa Val [53], with permission)



**Fig. 2.22** Position of the neuroendoscopy tower

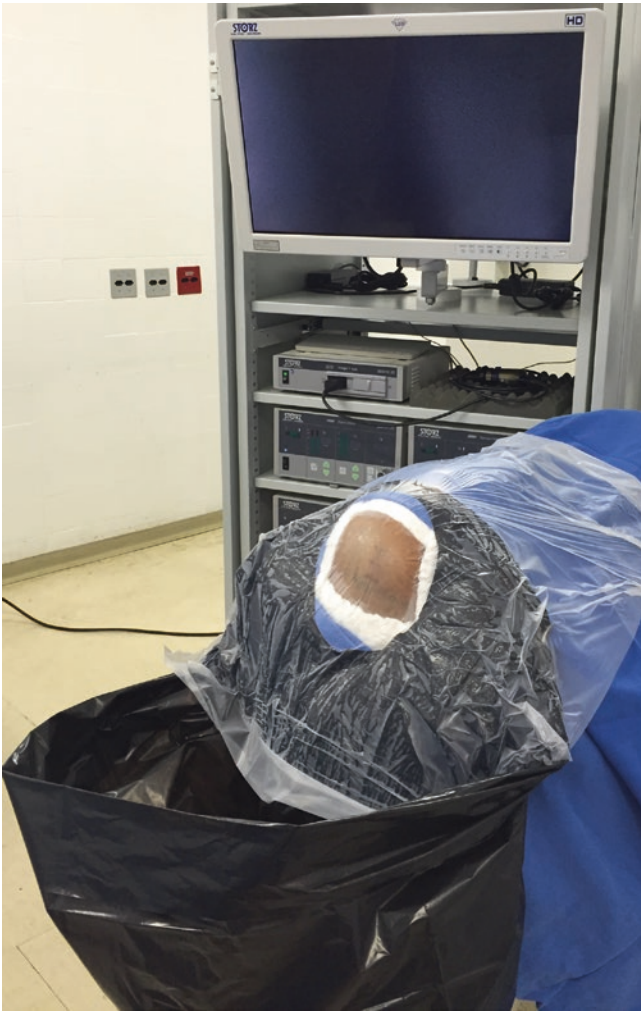


**Fig. 2.23** Position of the neuroendoscopy tower and ready surgical field. Because of the continuous irrigation a waterproof bag is very useful

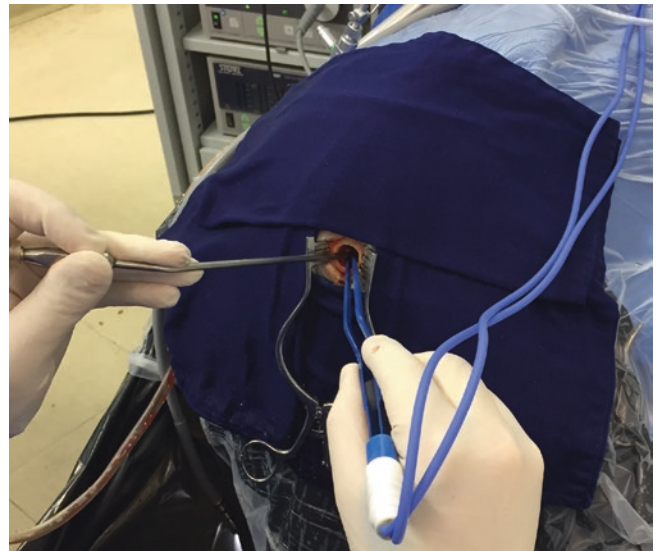


**Fig. 2.25** Bipolar coagulation before the dural opening, performed in cross fashion, in an adult

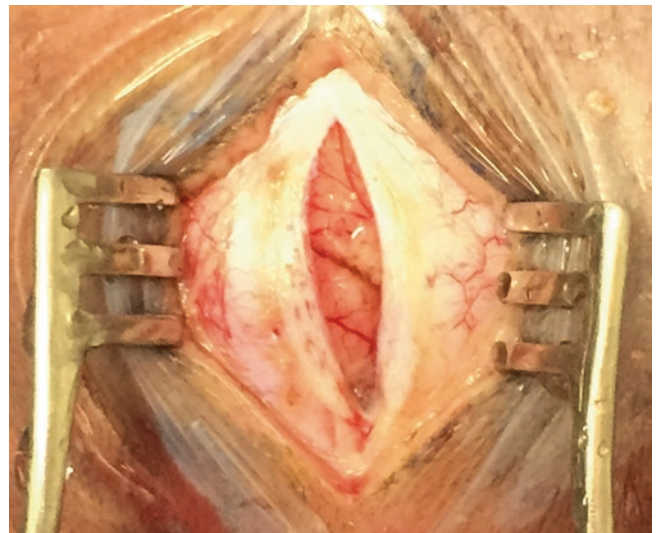


**Fig. 2.26** Dural opening performed in a linear fashion in a newborn

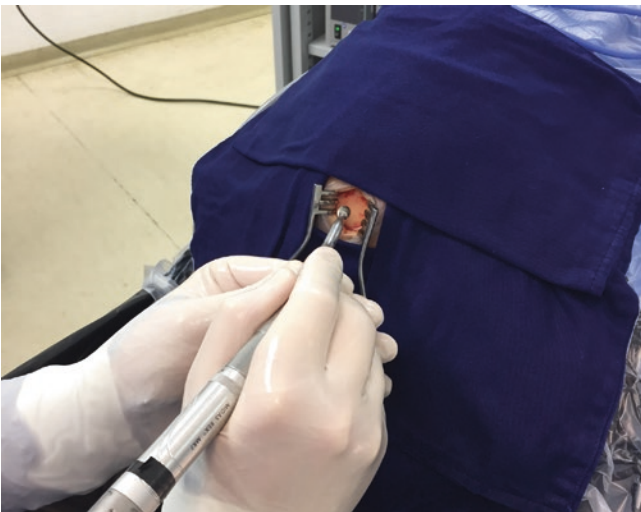


**Fig. 2.24** Skull opening with a high-rotation drill in an adult



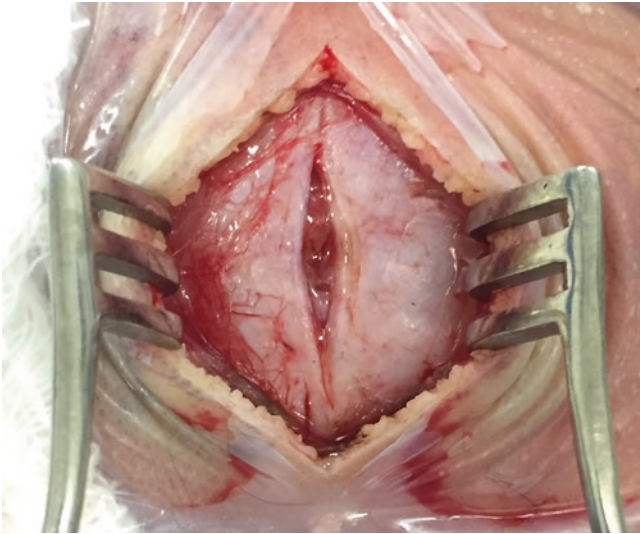


**Fig. 2.27** Corticotomy with bipolar coagulation avoiding the dural edge to allow closure after the procedure

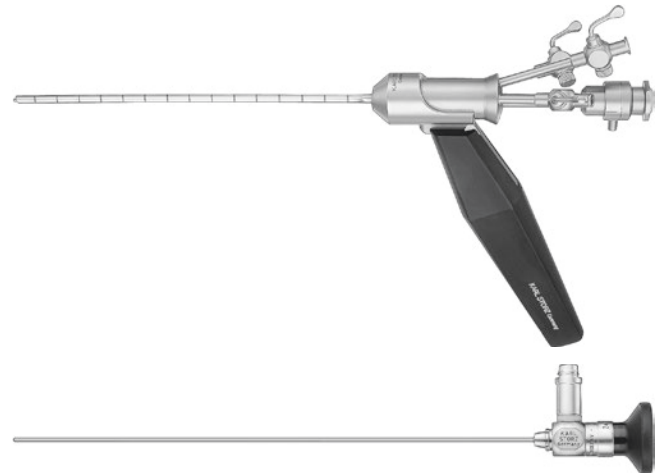


**Fig. 2.28** Oi HandyPro system, with removable handle, including operating sheath handle (three work channels), mandrel, and wide-angle straightforward telescope 0° (enlarged view, diameter 2 mm, length 26 cm). Instruments (diameter 1.3 mm, working length 30 cm), including scissors (single-action jaws), biopsy forceps (double-action jaws), grasping forceps (double-action jaws), unipolar coagulation electrode, and bipolar coagulation electrode (Images courtesy of Karl Storz, Tuttlingen, Germany)



**Fig. 2.29** Gaab system, including wide-angle straightforward telescope 6°, with working channel diameter 3 mm, length 15 cm. Operating sheath, graduated, outer diameter 6.5 mm, working length 13 cm, with lateral stopcock and catheter port and obturator. Instruments, including grasping forceps (single-action jaws, diameter 2.7 mm, working length 30 cm), biopsy forceps (single-action jaws, diameter 2.7 mm, working length 30 cm), scissors (pointed, single-action jaws, diameter 2.7 mm, working length 30 cm), scissors (pointed, slightly curved, double-action jaws, diameter 1.7 mm, working length 30 cm), biopsy forceps (double-action jaws, diameter 1.7 mm, working length 30 cm), forceps for ventriculostomy (diameter 1.7 mm, working length 30 cm), bipolar forceps (with flat jaws, size 2.4 mm, working length 24 cm), bipolar coagulation electrode (diameter 1.7 mm, working length 30 cm), unipolar coagulation electrode (semiflexible, diameter 1.7 mm, working length 30 cm), suction catheter (flexible, for single use, diameter 2.5 mm, working length 45 cm), irrigation tube, and holding system (Images courtesy of Karl Storz, Tuttlingen, Germany)

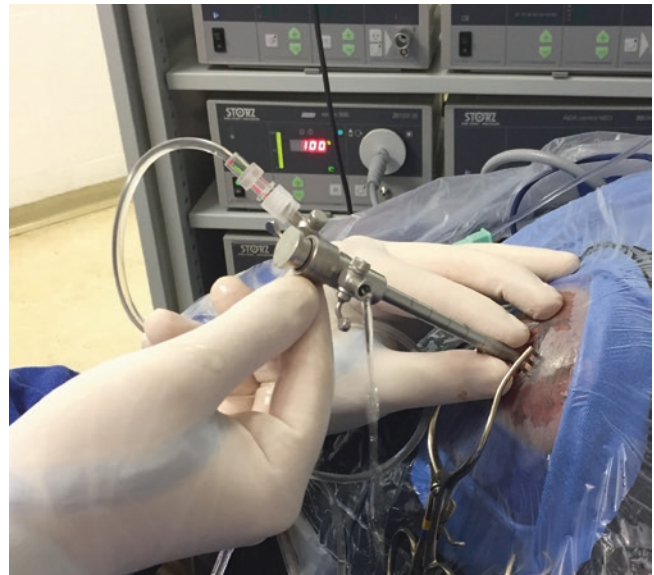


**Fig. 2.30** Ventricular puncture under irrigation with Gaab system operation sheath. During the procedure it is very important to maintain continuous irrigation to avoid ventricular collapse. It is mandatory to have the passive exit always open to avoid intraventricular hypertension

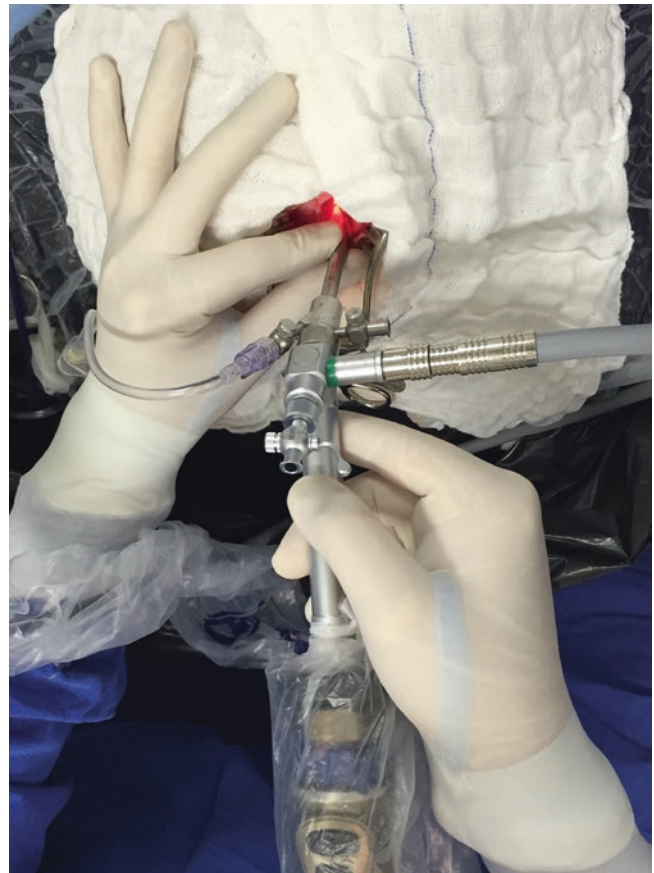


**Fig. 2.31** Ventricular navigation and inspection with the Gaab system



**Fig. 2.32** Oi HandyPro frameless free-hand system

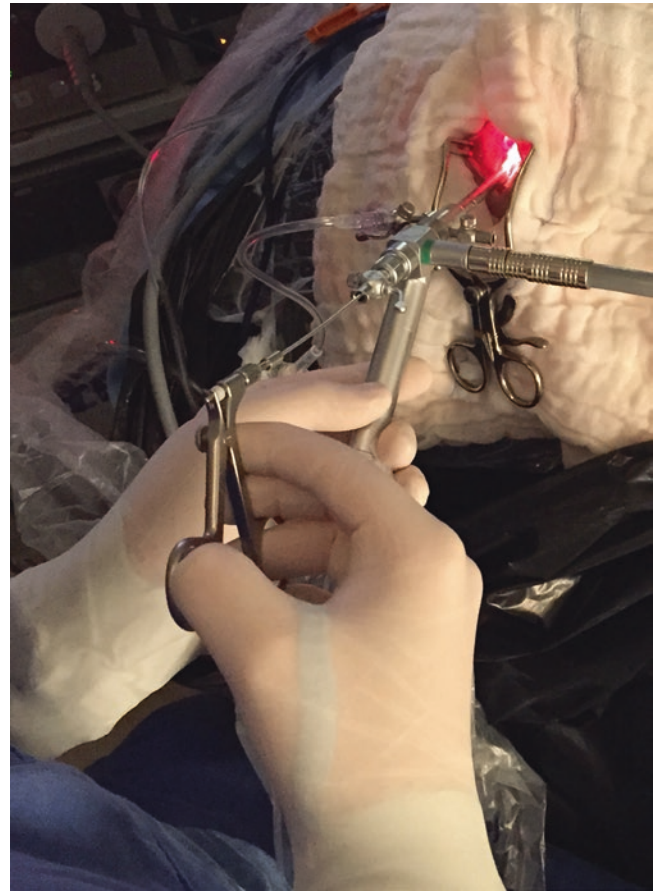


**Fig. 2.33** Free-hand technique with the Gaab system, holding the neuroendoscope with the non-dominant hand and handling the instrument (grasping forceps) with the dominant hand



**Fig. 2.34** Free-hand technique with the Gaab system, holding the neuroendoscope with the non-dominant hand and handling the instrument (scissors) with the dominant hand

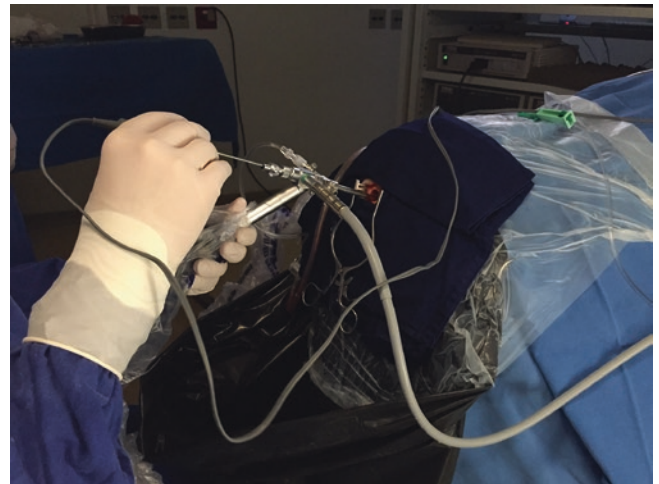


**Fig. 2.35** Free-hand technique with the Gaab system, holding the neuroendoscope with the non-dominant hand and handling the instrument (bipolar coagulation electrode) with the dominant hand



**Fig. 2.36** Performing the surgery in the sitting position

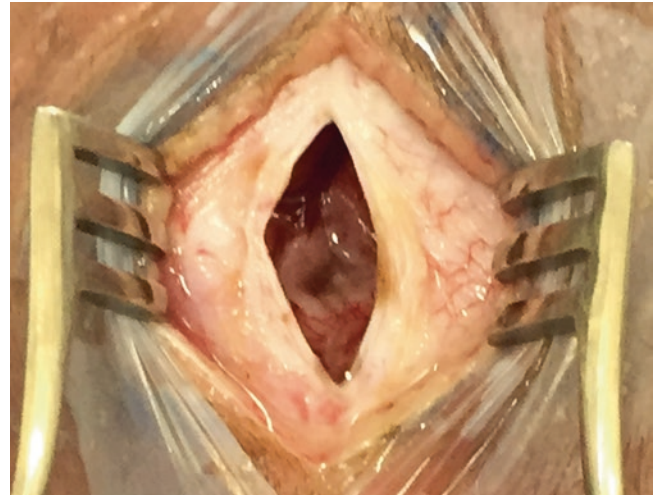


**Fig. 2.38** Aspect of dural opening at the end of the procedure. There is evident brain shift



**Fig. 2.37** Performing the surgery in the standing position

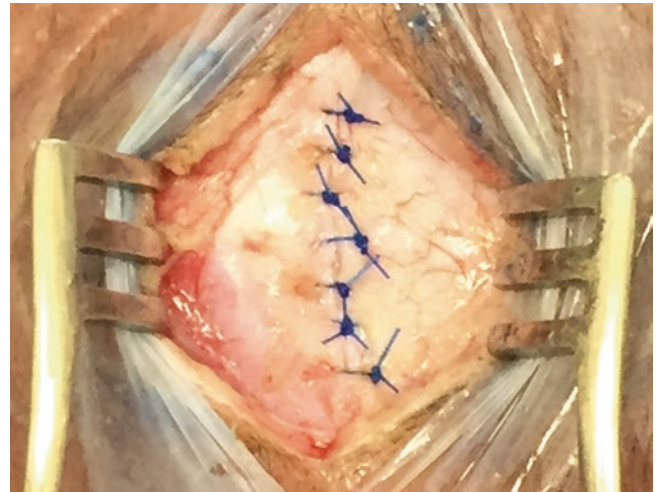


**Fig. 2.39** Polypropylene watertight dural closure

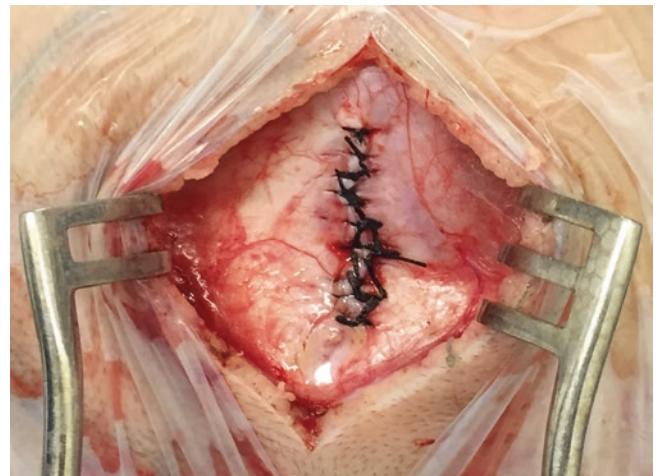


**Fig. 2.40** Silk watertight dural closure

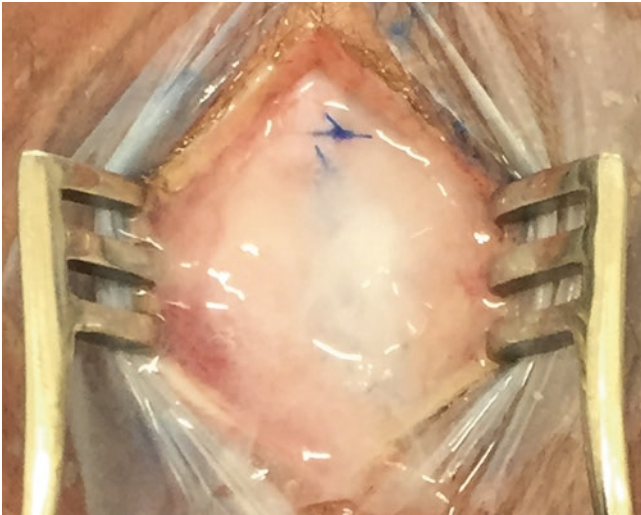


**Fig. 2.41** Biological glue over suture



**Fig. 2.43** Mononylon separate point skin closure

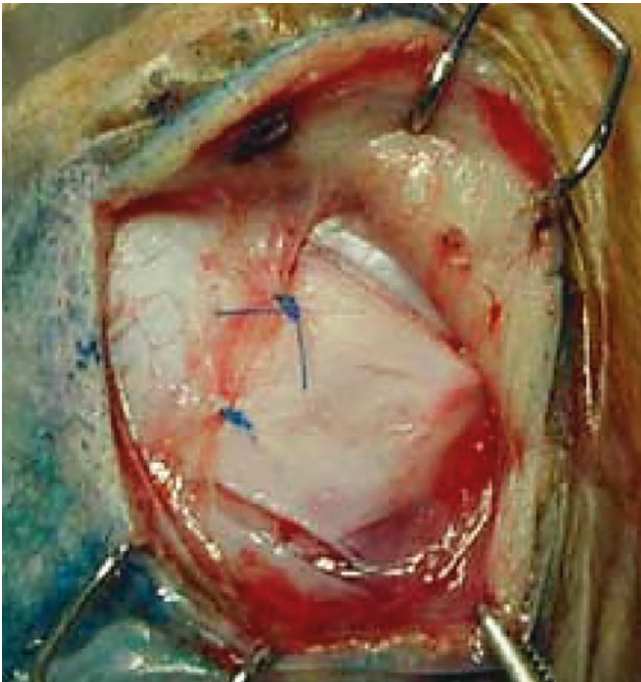


**Fig. 2.42** After a minicraniotomy, the osteoplastic flap returns to its place, attached with the pericranium aid, after watertight dural closure (Reprinted from Costa Val [53], with permission)



**Fig. 2.44** AIDA (Advanced Image and Data Acquisition) system. A solution for the recording of patient data, full high-definition (HD) videos, and images (Image courtesy of Karl Storz, Tuttlingen, Germany)

## 2.3 Main Ventricular Procedures and their Indications

### 2.3.1 Endoscopic Third Ventriculostomy (ETV)

ETV is the most often performed endoscopic procedure, and therefore it is the one most studied in the neuroendoscopic literature worldwide. The technique is based on the creation of an alternative exit route for draining CSF from the ventricular system into the subarachnoid space. In this technique a fenestration is performed in the third ventricle floor and in the membrane of Lilliequist just below it, allowing the CSF to flow out to the interpeduncular and prepontine cisterns. The main indication for ETV is for obstructive hydrocephalus, and such obstruction may be located anywhere from the middle and posterior portion of the third ventricle to the median and lateral openings of the fourth ventricle. Moreover, patency of the subarachnoid space and preservation of CSF absorption at the arachnoid granulations level are necessary conditions. Magnetic resonance imaging (MRI) is the gold standard for the indication of this procedure, because it allows the topographic identification of the obstruction. The sagittal T2-weighted sequence is the most suitable for such analysis. On the other hand, there is no additional examination able to accurately assess the cisternal circulation and CSF absorption. Therefore, if, in association with the intraventricular obstruction mechanism, there is some pathological condition interfering with CSF circulation in the subarachnoid space or CSF absorption, the successful outcome of ETV can be questioned [48]. Other relevant information provided by MRI is the space below the third ventricle floor, particularly the gap between the clivus and the basilar artery in the interpeduncular cistern (Figs. 2.45 and 2.46). This data allows the third ventricle floor to be opened safely [58]. The lack of space is not an absolute contraindication to carrying out fenestration, but doing so requires a learning curve. The ETV technique involves inserting the endoscope through the frontal approach at Kocher's point, typically situated 2 cm in front of the coronal suture and 2 cm lateral to the midline. This is not an absolute point, because small variations can be made, especially in the pediatric age group, taking into account the position of the fontanelle, which is a physiological portal, and ventricular size, always avoiding penetration in eloquent areas [59]. The right side is usually chosen, but the side on which the frontal horn is larger may be used. Penetrating the lateral ventricle, access to the third ventricle is achieved through the foramen of Monro. Soon after, the structures of the floor of the third ventricle can be identified; arranged in the anteroposterior direction, these are: optic chiasm, tuber cinereum with the infundibular recess, and the mammillary bodies. Fenestration in the tuber cinereum is

done at the midpoint between the infundibulum and the mammillary bodies and may vary in some cases depending on the position of the bifurcation of the basilar artery, sometimes seen due to transparency through the tuber cinereum. This fenestration is usually performed with bipolar coagulation, or sometimes by using the tip of a non-activated bipolar electrode, serving as a blunt instrument. For such fenestration at an experimental level, a type of water jet has been conceived [60], and also laser can be an option [61]. After fenestration, the stoma is generally expanded by using a 3F or 4F Fogarty balloon catheter, or any other suitable instrument. Opening of the membrane of Lilliequist, located just below the third ventricle floor, is of great importance. In cases of delayed closure, repeating ETV before considering a shunt implant is recommended [62]. After the fenestration, the endoscope can be inserted inside the interpeduncular cistern to expand the stoma and see if the subarachnoid space is patent. Technical details may vary between neuroendoscopists, from using a Fogarty catheter balloon, to grasping forceps, to using a double balloon catheter in the form of an eight, especially developed for ETV [63]. The overall success rate of the ETV procedure is around 75%, but this depends on the etiology of the hydrocephalus and, above all, on the age of the patient [64]. In adults with obstructive hydrocephalus, the chance of success is very high. Also, in normal-pressure hydrocephalus when there is an obstructive component present, the results are favorable [65]. In children, taking into consideration the etiology, the best results are seen in hydrocephalus secondary to aqueductal stenosis, and in tumors in the posterior portion of the third ventricle or in the posterior fossa. Spennato et al. reviewed the literature and found an average success rate of 68% in patients with aqueduct stenosis [66]. Sainte-Rose et al. carried out a comparative study of the performance of ETV in children with posterior fossa tumors. When the endoscopic procedure was performed before the approach to the tumor, the chance of long-term development of hydrocephalus was only 6.6% [67]. On the other hand, in cases in which external ventricular drainage or simple resection of the tumor was done in attempts to restore the CSF circulation, the rate of hydrocephalus requiring further treatment was 26.8%. Although this was not a prospective, randomized study, the authors concluded that ETV was superior to any other approach in the management of hydrocephalus secondary to posterior fossa tumors [67]. O'Brien et al. [68] analyzed 170 cases of primary pediatric ETV; that is, ETV used as the first treatment for hydrocephalus of different etiologies. These authors reported a success rate of around 70%. However, when they analyzed patients with hydrocephalus secondary to intraventricular hemorrhage or meningitis, the success rate was just 27% or 0%, respectively, once again confirming the significance of the obstructive etiology. These authors also analyzed 63 cases where ETV

was performed in the presence of dysfunction (mechanical or infectious) of a ventriculoperitoneal shunt. The success rate was 78%, showing that although the shunt was present and there was possible lower CSF circulation in the subarachnoid space previously, these factors would not be a hindrance for an ETV operation [68]. Concerning etiology, pediatric ETV has a high failure rate in children with previous shunts and in those with postinfectious hydrocephalus [69]. If, on one hand, the etiology in children is well defined as a prognostic factor for the success of ETV, the age is also an important factor to be considered. Today it is known that the earlier the procedure is performed, the greater the chance of failure, due to the immaturity of the ventricular system and also due to the existence of alternative pathways for different CSF drainage compared with those in adults. It has been considered that age of less than 2 years would be a factor for poor prognosis. Later, studies emerged that advocated avoiding ETV alone in children under 1 year of age, which seems to be the most reasonable recommendation in the current literature [70]. In a study by Koch-Wiewrodt and Wagner [71], in a series of 28 children who underwent ETV before 1 year of age, when comparing the average age of those with a successful procedure with the age of those whose procedure failed, there was no statistically significant difference. However, when considering the chance of failure month by month, these authors noticed an increasing trend

in the success rate after age 2–4 months. This observation was also noted in patients with aqueduct stenosis in the cases found in the literature of the time [71]. Other small series are in favor of ETV at any age [72, 73]. Given this controversy, there is now the possibility of predicting the success of ETV in pediatric patients using a scale, the ETV Success Score (ETVSS). The scale takes into account the age, etiology, and the presence or absence of a previous shunt, and the points assigned to each parameter are summed. The higher the sum, the greater the chance of success [74, 75]. Another way to predict success in pediatric patients is through artificial neural networks (ANN) [76]. An association between ETV and choroid plexus coagulation seems to be a promising technique for patients under 1 year of age, as discussed in Sect. 2.3.2 (Choroid Plexus Coagulation [CPC]). Like any surgical procedure, ETV is not without complications. A literature review shows the overall complication rate is between 5% and 15%, the permanent morbidity is less than 3%, and mortality is less than 1% [77]. Of course, when analyzing the number of complications in the literature, one should take into account the limitations and the learning curve of each individual neurosurgeon. To assess patient outcomes, apart from clinical evolution, postoperative imaging such as CT or MRI is important to evaluate the success of the ETV (Figs. 2.47, 2.48, 2.49, 2.50, and 2.51).

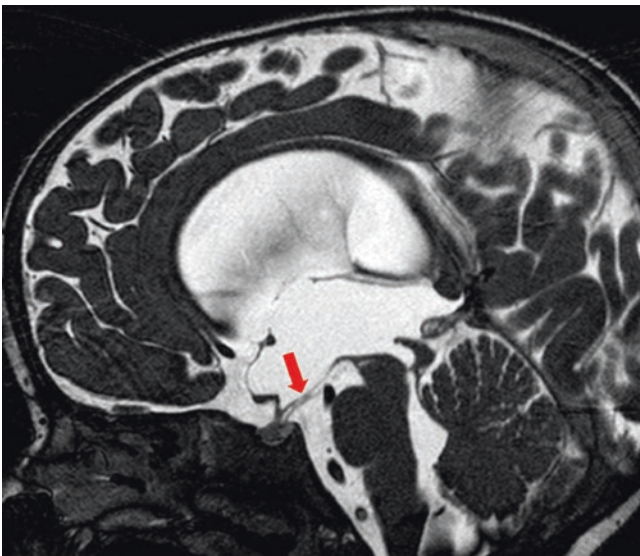


**Fig. 2.45** Sagittal T2-weighted MRI showing obstructive hydrocephalus due to aqueductal obstruction. Note the presence of an adequate space between the clivus and the top of the basilar artery (*red arrow*). This allows to perform a safe ETV

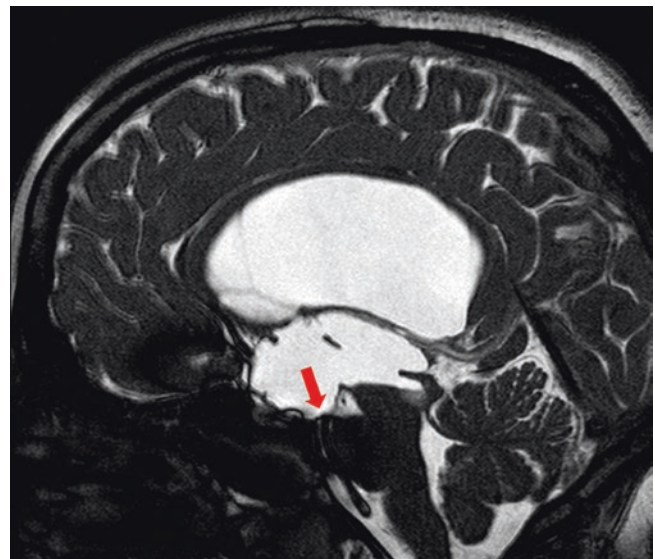


**Fig. 2.46** Sagittal T2-weighted MRI showing obstructive hydrocephalus due to pineal tumor obstruction. There is no space between the clivus and the top of the basilar artery (*red arrow*). Before the neurosurgeon can perform a safe ETV, a learning curve is necessary



**Fig. 2.47** Axial CT scan showing presence of air inside the lateral ventricle after ETV. This is a common finding

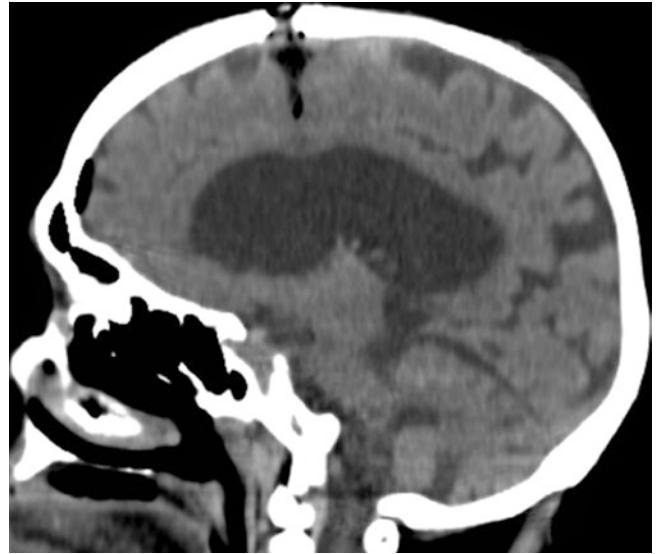


**Fig. 2.49** Sagittal CT scan showing habitual neuroendoscope trajectory

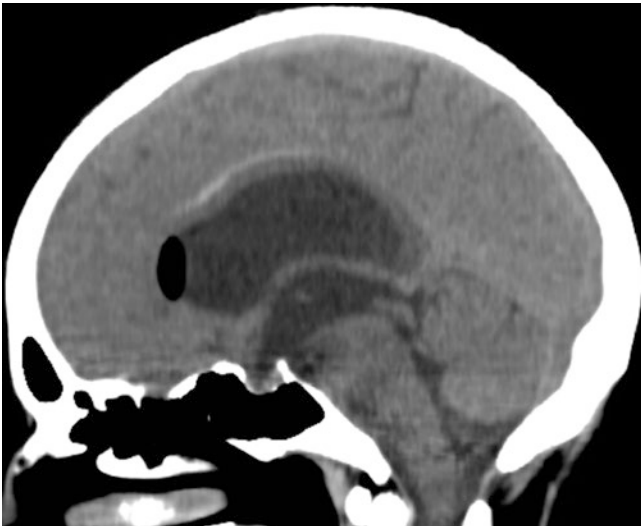


**Fig. 2.48** Sagittal CT scan showing the presence of air inside the lateral ventricle after ETV. This is a common finding

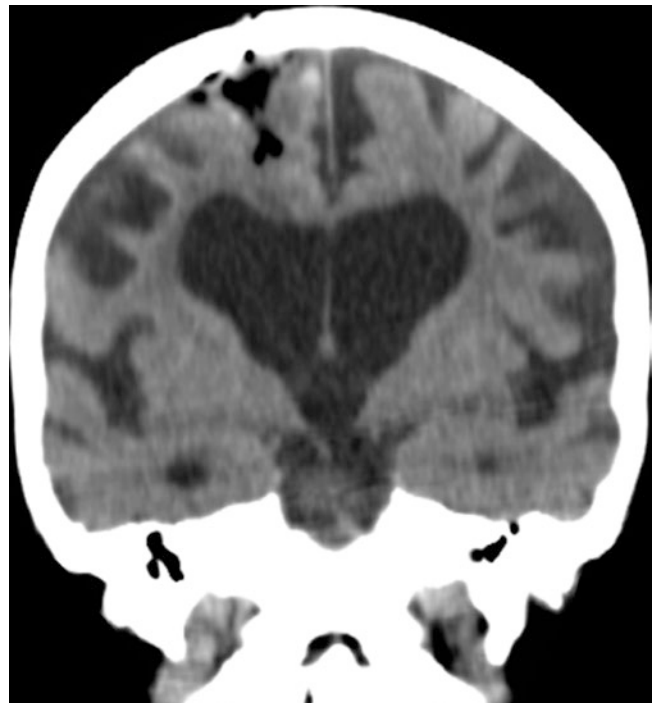


**Fig. 2.50** Coronal CT scan showing habitual neuroendoscope trajectory



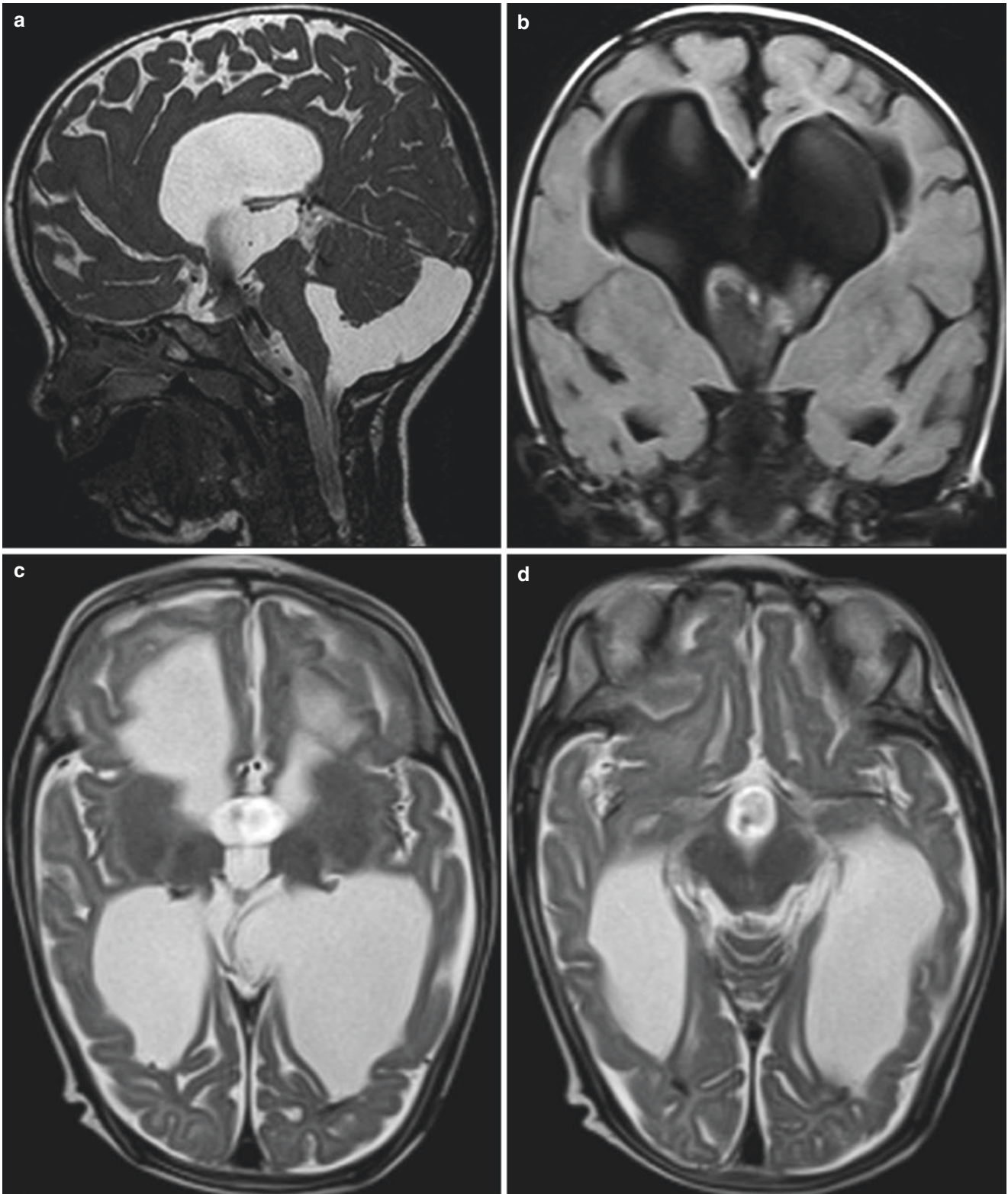


**Fig. 2.51** MRI sequences showing CSF flow artifact after a successful ETV. Sagittal T2-weighted (a); coronal flair (b); axial T2-weighted, with flow inside the third ventricle (c); and inside interpeduncular cistern (d)

### 2.3.2 Choroid Plexus Coagulation (CPC) [78–80]

Faivre, in 1854, and Luschka, in 1855, were the first researchers to suggest that the choroid plexus is the source of CSF [81, 82]. Cushing supported this hypothesis through intraoperative observations [83]. Extrachoroidal fluid production was suggested by Weed, in 1914, from animal studies [82]. Dandy, in 1918, demonstrated, in an animal study, that unilateral hydrocephalus was produced when the fourth ventricle was blocked, together with the access through the foramen of Monro to the contralateral plexectomized lateral ventricle [21, 84]. Furthermore, in the same year, he also demonstrated, in an animal study, that CSF was produced by the choroid plexus. Based on this result, he performed choroid plexus extirpation by open surgery in four infants with communicating hydrocephalus. In this series, one infant with moderate hydrocephalus and myelomeningocele was well at 10 months follow-up, and the other three infants, with severe hydrocephalus, died within 4 weeks after the operation [21, 84]. Later, in 1932, Dandy also used a rigid Kelly cystoscope to inspect the lateral ventricles in two hydrocephalic children [84, 85]. CPC was attempted in one case, as described in detail in 1938 [84, 86]. The technique of CPC was first described by Putnam in 1934 [18, 84]. In subsequent years, besides CPC, other surgical treatments of hydrocephalus were introduced, including ETV and extrathecal CSF shunts. In a review, there were 95 cases of CPC from 1934 to 1957. The mean mortality rate was 15%, while the mean success rate was 60%, with an average follow-up period of 8 years. On the other hand, there were 1087 cases of various kinds of CSF shunts, including 230 ventriculoperitoneal shunts (VPSs). The mean mortality rate was 10%, and the mean initial success rate was 60%, with an average follow-up time of 2 years [84]. The results of these reviews showed a shift from CPC to CSF shunts, perhaps due to poor and limited technology. However, the late complication rate for CSF shunts was 57% [84, 87]. Scarff, in 1970, published the first large series of CPC cases, his own series of 39 children treated during a 23-year period, with a 67% success rate [88]. Milhorat, in 1974, reported his series of 12 patients who underwent choroid plexectomy. Of the 11 survivors, 8 (72%) failed and required a further shunt [89]. After this report, and a report that CPC in rhesus monkeys reduced CSF production by only 40%, the use of CPC declined in favor of the use of CSF shunts [84]. In the neuroendoscopic literature from the 1980s to 2004, the success rate of CPC was between 30% and 52% [36, 90, 91]. In small series, two out of three cases were successful [84, 92]. Griffith, in 1986, gave a detailed account of endoscopic intracranial neurosurgery, through a report of the results of 71 patients treated by CPC with or without CSF shunt, from 1972 to 1982 [93]. The selection criteria were infants with hydrocephalus who had progressively enlarging

head circumference with grossly dilated ventricles and absent superficial CSF space on CT scans. Behavioral changes were also considered. In this series, 30% of the patients were not shunt-dependent. The success rates were 54%, 58%, and 22% for groups with myelomeningocele, and those with communicating and obstructive hydrocephalus, respectively. The same author, in 1990, further reported the results of 32 childhood hydrocephalus cases treated by CPC between 1985 and 1988 with CT scan examinations. Eighteen patients were under the age of 6 months. Patient selection was the same as that in his previous report. In addition, all patients showed marked ventricular dilatation on a preoperative CT scan [90]. In contrast to his previous series, in this series, Griffith added postoperative perfusion of the ventricular system with artificial CSF to clear the postcoagulation blood and protein released into the CSF. The average follow-up time ranged from 1 to 4 years. Fifty-two percent of the patients were shunt-independent. All those who required VPS, except for one patient, showed that requirement within an interval of  $\leq 12$  weeks. Among the successful group, most of the patients showed a head circumference similar to the preoperative size [84]. Pople and Ettles, in 1995, reviewed the results of CPC in 116 children with hydrocephalus operated from 1973 to 1993 [91]. The mean age was 2 years and the overall hydrocephalus control rate was 49.5%. In the children with communicating hydrocephalus, there was a slow to moderate rate of increase in head circumference, and the long-term control rate was 64%. On the other hand, in the patients who presented with tense fontanelles and rapidly progressing hydrocephalus, only 35% achieved long-term control without CSF shunts, and the authors suggested that the main indication for CPC in infants was mildly progressive communicating hydrocephalus. In these patients, it seemed that the balance between the production and absorption of CSF could be restored by only a small reduction in outflow from the choroid plexus of the lateral ventricle. In contrast, CPC was not recommended for rapidly progressive hydrocephalus with acutely raised intracranial pressure [84, 91, 94]. These first experiences were quite controversial, perhaps because of technological limitations [78–80]. In the late 1990s to early 2000s, due to the advances in neurosurgical technology, the mortality rate in isolated CPC has decreased, but the key issue for its decline in clinical practice is its relative lack of efficacy [84]. The Uganda series reported by Dr. Benjamin Warf, investigated the beneficial effect of ETV associated with CPC for the first time, again arousing interest in this technique. It was concluded that the ETV/CPC procedure was superior to ETV alone in infants younger than 1 year of age, particularly among those with non-postinfectious hydrocephalus and myelomeningocele, but longer follow-up with neurocognitive assessment was necessary [95]. Warf published his first results from ETV/CPC for children in Africa in 2005 [95]. The long-term outcome and neuro-

cognitive outcome were reported in 2008 [96] and 2009 [97], respectively. These reports highlighted the fact that shunt dependency in children with hydrocephalus is more dangerous in developing countries than in developed countries because of the limitations in accessing competent centers in the event of shunt malfunction or infection [95]. Warf and Campbell, in 2008 [96], reported the long-term result of ETV/CPC for East African infants with hydrocephalus related to myelomeningocele. Among the 338 infants whose myelomeningocele was repaired prior to 6 months of age, 258 patients (66%) who had been followed-up for >6 months required treatment for hydrocephalus. There were 93 patients (mean age, 3 months) who had completed ETV/CPC with >1 month follow-up. A success (shunt-independent) rate of 76% was achieved. This success rate was higher in ETV/CPC patients than in those with ETV alone for infants aged 6 months or younger with hydrocephalus in association with myelomeningocele, as reported in the literature [98, 99]. In 2009, Warf et al. [97] reported the neurocognitive outcome and ventricular volume in children with myelomeningocele treated for hydrocephalus in Uganda. The modified Bayley Scales of Infant Development (BSID-III) and the frontal/occipital horn ratio (FOR) were used to compare three groups of patients with myelomeningocele. For the modified BSID-III, there was a statistically significant difference between the treatment groups with VPS and those with ETV/CPC. For the ventricular size, the FOR was 0.7, 0.65, and 0.62 for the VPS, ETV/CPC, and the treatment-not required group, respectively, without a statistically significant difference between the groups. The authors suggested that future research is needed to compare outcomes by using a larger control group of children treated primarily with VPS [97]. Even so, Warf et al. have applied ETV/CPC to encephalocele, with a success rate of 85% [100], and in obstructive hydrocephalus due to aqueductal stenosis, they have achieved a success rate of 81.9% in patients treated by ETV/CPC [101]. Dandy-Walker complex is another condition that is treatable by ETV/CPC, according to Warf's African series [102]. Also, a larger series of this disease treated by neuroendoscopy in the Uganda scenario was reported, and this technique should be strongly considered as the primary management in place of the traditional standard of creating shunt dependence. For this disease, the success rate was 74% for Dandy-Walker malformation, 73% for Dandy-Walker variant, and 100% for mega cisterna magna. Eighty-eight percent of the patients were younger than 12 months and 95% had an open aqueduct at the time of the ETV/CPC. None required posterior fossa shunting in a mean follow-up of 24.2 months [102]. From the same Warf's African series, the use of ETV/CPC in communicating hydrocephalus was a

viable option [103]. ETV/CPC was significantly more successful than ETV alone in treating congenital idiopathic hydrocephalus of infancy. In this study with 64 infants (mean/median age, 6.1/5.0 months), 16 consecutive patients were treated by ETV alone, and the subsequent 48 by ETV/CPC (mean/median follow-up 34.4/36.0 months). ETV was successful in 20% and ETV/CPC in 72.4% at 4 years ( $p < 0.0002$ , log rank test;  $p = 0.0006$ , Gehan-Breslow-Wilcoxon test; hazard ratio 6.9, 95% confidence interval [CI] 2.5–19.3). It was assumed that the primary effect of ETV, as a pulsation absorber, and of CPC, as a pulsation reducer, may be to reduce the net force of the intraventricular pulsations that produce ventricular expansion. On the other hand, ETV alone may be less successful for infants because of their greater brain compliance. Nevertheless, this technique appears to have a higher long-term success rate and a lower infection rate than primary shunt placement and should be considered an effective primary treatment option for congenital idiopathic hydrocephalus [103]. A new predictor of ETV/CPC success arose from the Uganda series: the CCHU (CURE Children's Hospital of Uganda) ETV Success Score. This model allows clinicians to accurately identify children with a good chance of successful outcome with ETV, taking into account the unique characteristics and circumstances of the Ugandan population [104].

An early North American multicenter experience with ETV/CPC in infants demonstrates that the procedure has reasonable safety in selected cases. The degree of CPC achieved might be associated with a surgeon's learning curve and this appears to affect success, suggesting that surgeon training might improve results [105]. Of note, both the ETV Success Score and the CCHU ETV Success Score predicted success following ETV/CPC in a single-center North American cohort of patients [106]. For complex or multiloculated hydrocephalus, choroid plexus coagulation or its resection in conjunction with multiple septal fenestration and CSF shunt is a good option to control hydrocephalus. In a review of their series of 93 cases of multiloculated hydrocephalus, Zuccaro and Ramos [107] reported that choroid plexus coagulation and its resection was performed in 14 cases (8 by endoscopy and 6 by craniotomy). In another review, Zhu and DiRocco concluded that, because of the variable success rate, each patient must be studied individually [84]. Initial experience with ETV/CPC for post-hemorrhagic hydrocephalus of prematurity has revealed the importance of the prepontine cistern status and the predictive value of fast imaging employing steady-state acquisition (FIESTA) MRI imaging [108]. In premature infants with intraventricular hemorrhage (IVH) and hydrocephalus, ETV/CPC is a safe initial procedure that obviates the need for a CSF shunt in selected

patients. Even though the success rate is low (37%), the lower rate of complications in comparison with shunt treatment may justify this procedure in the initial management of hydrocephalus. As several of the studied factors have been shown to influence the outcome, patient selection based on these observations might increase the success rate [109]. Besides the combined ETV/CPC technique, nowadays there are new indications for isolated CPC, such as in extreme hydrocephalus and hydranencephaly [92, 110, 111] (see Chap. 7). Avoidance of a CSF shunt is desirable in these conditions, due to the thinness and fragility of the scalp, as well as the common presence of infected scalp ulcers at the parietal bosses. In 2004, Morota and Fujiyama described a unilateral transmural approach technique for bilateral CPC, in which they used a flexible neuroendoscope for three infants with IVH related to hydrocephalus. Two of the patients were shunt-independent. The authors suggested that the characteristics of favorable candidates for CPC were severely advanced hydrocephalus, such as hydranencephalic hydrocephalus, slow progressive hydrocephalus, and lack of/or thinned-out septum pellucidum to make the bilateral endoscopic access possible [92]. Malheiros et al., in 2010, in a series of 17 patients, carried out CPC in 9 patients; the procedure successfully controlled excessive head circumference and signs of increased intracranial pressure in 8 of these patients (88.8%). One endoscopic procedure in a hydranencephalic child failed after 7 months, resulting in VPS placement. There were no complications related to this method of treatment. The authors concluded that CPC is an acceptable alternative to VPS for the treatment of hydranencephaly and near hydranencephaly, because it is a single, definitive, safe, effective, and economical treatment that may avoid the complications of shunting [110]. In another recent study, in severe congenital hydrocephalus and hydranencephaly, CPC stabilized macrocephaly in approximately 40% of the infants who had the procedure, and was considered as an alternative to VPS placement. Patients were followed for 30–608 days (median, 120 days). Of the 30 evaluable patients, CPC was considered to have been successful in 13 (43.3%), including 8 of 20 patients with severe hydrocephalus and 5 of 10 with hydranencephaly. CPC failure was evident from increased head circumference in 14 (82%) of the 17 failed patients and from CSF leakage in 3. Of the 17 failures, 13 occurred within 3 months of surgery. Six patients died: 3 whose CPC procedures were failures, 2 whose CPC was successful, and 1 postoperatively. Of the 17 patients in whom CPC failed, 10 subsequently underwent VPS insertion. This African study concluded that isolated CPC stabilizes macrocephaly and can be considered as an alternative to CSF shunt placement [111]. Figure 2.52 shows a postoperative aspect after CPC in an infant.

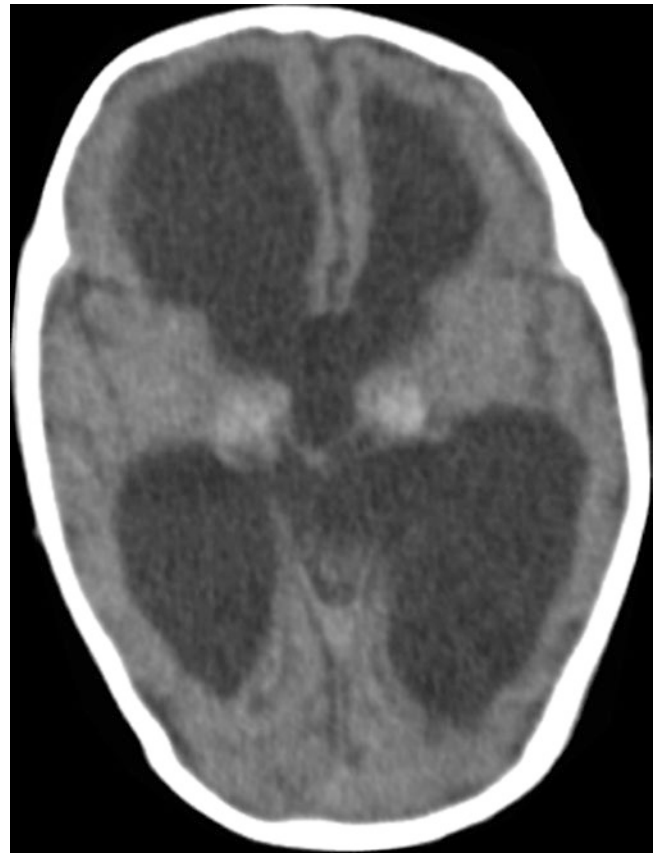


**Fig. 2.52** Axial CT scan depicting choroid plexus region in lateral ventricles after coagulation

### 2.3.3 Septostomy

Endoscopic septostomy is the fenestration of the septum pellucidum, allowing communication between the two lateral ventricles. Its main indication is related to the asymmetric dilatation of the lateral ventricles, classified as complex hydrocephalus. This condition can be observed when there is obstruction of the foramen of Monro, due to inflammatory, congenital, or tumoral causes, with dilatation of the corresponding lateral ventricle. Another very common situation is, in a patient with CSF shunt, that obstruction of the foramen of Monro occurs at the side in which the ventricular catheter is inserted. The result is the isolation of this ventricle, and the shunt drains only this cavity, which becomes small. The remaining ventricular cavities would once again become dilated; in particular, the contralateral ventricle. When one lateral ventricle communicates with the opposite side by septostomy, the CSF will drain through the contralateral foramen of Monro, and the ventricular catheter will drain all the ventricles again. Septostomy is simpler and less risky than foraminoplasty of Monro in a patient with a

CSF shunt, because in such a case, there would be a risk of creating a fornix lesion in any attempt to dilate the fornix, or there may even be damage to the venous angle. Septostomy may also be indicated in a patient in whom there is obstruction of the two foramina of Monro and there is a need for hydrocephalus treatment with a shunt system. The intention is to avoid the insertion of two systems. The septostomy technique is to approach the lateral ventricle, and with a monopolar or bipolar coagulation electrode, to make a large opening in the septum pellucidum. Once the septum pellucidum has shifted to the smaller side of the ventricle, after penetration using a traditional 2-cm burr hole lateral to the median line, the viewing angle is not adequate and the fenestration is technically more difficult. To overcome this difficulty, placing the burr hole more laterally than normal, around 6 cm, is recommended. This has the advantage of enabling the surgeon to work in a larger cavity, but there is a risk of injury to the caudate nucleus and the contralateral thalamus. On the other hand, when a ventricle is approached with a shunt catheter from the opposite side, CSF drainage is not accompanied by septum displacement. Penetrating the usual distance from the midline is recommended, but on the smaller side of the ventricle, so there will be less difficulty in fenestrating the septum, and also a smaller chance of damaging the contralateral ventricular wall [47]. Another attractive option is to approach the ventricle through a parieto-occipital opening on the dilated ventricle side. By following the body of the ventricle, the most anterior and broadest portion of the septum is reached, at a more perpendicular angle to the septum than that created with the parasagittal frontal approach [112]. In some cases, neuronavigation and biportal access may be required in complicated cases of postmeningitis hydrocephalus, because the larger the stoma, the greater the chance of success, especially in children under 2 years old [113].

### 2.3.4 Aqueductoplasty

Endoscopic aqueductoplasty consists of opening the cerebral aqueduct in a patient in whom the aqueduct is congenitally stenotic, stenotic after some inflammatory process, or stenotic because of tumor compression. In this situation, triventricular dilation takes place. Over the years, different technical variations have been used, such as Fogarty balloon catheters, flexible endoscopy passing through the narrowed aqueduct, and stents. Regardless of these variations, endoscopic aqueductoplasty is an effective procedure with relatively low morbidity, and in general, with a patient at an advanced age at the time of surgery, congenital etiology and the use of a stent are predictors of a good outcome [114]. The

combination of a miniature intracatheter endoscope and a prepared ventricular catheter enables careful and elegant aqueductal stenting [115]. Another technique consists of a suboccipital approach, as low as possible, slightly paramedian (to avoid the occipital sinus), transcerebellar, or, more rarely, through the cisterna magna and the opening of the foramen of Magendie. Once inside the fourth ventricle, the endoscope should continue cranially until the aqueductal obstruction is viewed. Through a monopolar bipolar electrode, used only as a rigid instrument, the stenosis can be perforated [116].

### 2.3.5 Complex Hydrocephalus

Complex hydrocephalus, also called multiloculated hydrocephalus, is associated in most cases with a prior infectious ventricular condition or intraventricular hemorrhage, which occurs most commonly, but not exclusively, in the first year of life. In this condition, septations are formed within the ventricular system and/or there are obstruction of the natural CSF pathways, such as the foramen of Monro, cerebral aqueduct, and exit openings of the fourth ventricle. Arachnoiditis and/or obstruction at the arachnoid granulations level may be associated with the condition. Therefore, because of the impairment of the subarachnoid CSF circulation and absorption, the vast majority of patients need a shunt system. In the pre-endoscopic era, the ventricles were compartmentalized, and the solution was the insertion of bilateral systems, with or without Y connections, between the ventricular catheters and the distal component of the shunt. This procedure increased the incidence of mechanical and infectious complications. Neuroendoscopy, in patients with complex hydrocephalus, aims to open several septations, which may be associated with aqueductoplasty and septostomy. Once all cavities are communicating, a single shunt system will be sufficient for CSF drainage. A patient with this condition may or may not already have a shunt system. In the former case, the surgery is limited to the communication of the cavities. In the latter, after the opening of the septations by the neuroendoscope is complete, the introduction of the ventricular catheter is done parallel to the endoscope trocar and its tip is placed under an endoscopic view at the location that is considered most appropriate. Supernumerary holes can be made along the catheter, which generally passes through more than one cavity. Technically, the opening of the septations is similar to septostomy. The wall of the septum is coagulated with a monopolar or bipolar electrode and the perforation is made. It is believed that the wider and the larger the number of openings, the less chance there is of them closing [112].

### 2.3.6 Intracranial Arachnoid Cysts

Arachnoid cysts are congenital malformations related to a defect in the arachnoid, where the CSF is trapped and may increase over time, coming to exert a mass effect and impair the ventricular CSF circulation. Classically, arachnoid cysts were always treated with shunt systems for the peritoneum. However, there were some problems with this modality, such as the technical difficulty of inserting the proximal catheter and/or the mechanical and infectious complications that could occur, as with any shunt device. Another therapeutic option is microsurgery for fenestration of the cyst and communication to an arachnoid cistern, although this has the disadvantage of being a larger procedure. In arachnoid cysts with possible associated hydrocephalus, neuroendoscopic treatment consists of opening the cyst wall, connecting it to a cistern (cystocisternostomy) or a ventricular cavity (cystoventriculostomy), and restoring the CSF circulation. The opening of the cyst wall can be done with a monopolar or bipolar electrode, followed by dilatation with a Fogarty balloon catheter. Microscissors and grasping forceps can also be used for fenestrating the membrane and further enlargement of the fenestration, or even removal of part of the cyst wall. Within the scope of this book, it is the suprasellar arachnoid cyst that has almost always presented itself in association with hydrocephalus. A particular case of suprasellar arachnoid cyst treatment consists of approaching the ventricular system through Kocher's point. Once inside the lateral ventricle, it is possible to see the top of the cyst occupying the dilated foramen of Monro. The cyst is coagulated and fenestrated (ventriculocystostomy), and once inside the cyst cavity, it is possible to see its base behind the dorsum sellae, where fenestrations are made alongside the basilar artery region (cystocisternostomy). Data from the literature show that the success rate is higher (92%) with both upper and lower openings (ventriculocystocisternostomy) than with ventriculocystostomy (84%) [117] (see Chap. 6).

### 2.3.7 Biopsies and Tumor Resections

Intraventricular or paraventricular lesions touching the wall of the cavity have many differential diagnoses, and can be treated conservatively or by surgical resection, depending on the diagnosis. Thus, making the diagnosis is crucial. Performing a biopsy through a craniotomy can be disadvantageous, because it involves complex surgery and entails some risk in a condition that is sometimes clinically manageable. Against this background, stereotactic biopsy has emerged as an effective method for diagnosis. An endoscopic biopsy has the same benefits as the stereotactic technique, in

addition to the advantage of being able to treat hydrocephalus by ETV, which is generally associated with these conditions. The biopsy is performed with biopsy forceps that pass through the working channel of the endoscope. As many fragments are necessary to make a diagnosis, it is important to remove specimens both from the surface and from deeper parts of the lesion. If there is bleeding, this may be overcome by irrigation with warmed saline or by bipolar or monopolar coagulation. The positive results of endoscopic biopsies range from 82.8% to 94.7%. The complication rate is around 3.4–6.0% and mortality is 0–3.4% [118–120]. A recent systematic review and meta-analysis of a total of 2069 biopsies, which has added significantly to the current neuroendoscopic literature, shows that neuroendoscopic biopsies were performed concurrently with at least one other procedure in 82.7% of cases. The combined diagnostic yield in 28 studies reporting 1995 biopsies was 87.9%, the combined major morbidity from 17 studies reporting 592 biopsies was 3.1%, the combined mortality of 22 studies reporting 991 biopsies was 2.2%, and no significant differences were found in the diagnostic yield when comparing studies using rigid versus flexible endoscopes exclusively [121, 122]. With the progressive growth of endoscopic techniques, interest in intraventricular tumor resection through this less invasive method has emerged. Although there are no absolute conditions for the procedure to succeed, the ideal condition is for the injury to be poorly vascularized, have a soft consistency, be up to 2 cm in diameter, and have ventricular dilatation. A lesion that perfectly fits these conditions is the colloid cyst of the third ventricle. Several authors have reported excellent results, with lower morbidity, using the endoscopic resection technique, although the recurrence rate seems to be higher than that with microsurgery [123, 124]. The parallelism of the instruments makes handling them difficult. Their smaller diameter, and bleeding that clouds the view, requiring frequent irrigation, still make the endoscopic resection technique very limited. Currently, there is already an endoscope model that allows the use of an ultrasonic aspirator inside it, increasing the efficiency of the resection [125]. It is possible that the development of new instruments may increase the potential of this technique in the resection of intraepithelial and paraventricular lesions.

## References

1. Davis L. Neurological surgery. Philadelphia: Lea & Febiger; 1936.
2. Decq P, Schroeder HW, Fritsch M, Cappabianca P. A history of ventricular neuroendoscopy. *World Neurosurg.* 2013;79:S14. e1–6. doi:10.1016/j.wneu.2012.02.034.
3. Dandy WE. Ventriculography following the injection of air into the cerebral ventricles. *Ann Surg.* 1918;68:5–11.

4. Hellwig D, Grotenhuis JA, Tirakotai W, Riegel T, Schulte DM, Bauer BL. Endoscopic third ventriculostomy for obstructive hydrocephalus. *Neurosurg Rev.* 2005;28:1–34. doi:10.3171/2009.4.
5. Dandy WE. Cerebral ventriculostomy. *Bull Johns Hopkins Hosp.* 1922;33:189–90.
6. Hsu W, Li KW, Bookland M, Jallo GI. Keyhole to the brain: Walter Dandy and neuroendoscopy. *J Neurosurg Pediatr.* 2009;3:439–42. doi:10.3171/2009.1.
7. Goodrich JT. Reprint of “The operative treatment of communicating hydrocephalus” by Walter E. Dandy, MD. 1938. *Childs Nerv Syst.* 2000;16:545–50.
8. Abbott R. History of neuroendoscopy. *Neurosurg Clin N Am.* 2004;15:1–7.
9. Dandy WE. *Surgery of the Brain.* W. F. Prior Company: Hagerstown; 1945.
10. Payr E. Drainage of the cerebral ventricles by means of free transplantation of blood vessels: remarks about hydrocephalus [in German]. *Arch Klin Chir.* 1908;87:801–85.
11. Parisien RC, Ball PA. William Jason Mixter (1880–1958). Ushering in the dynasty of the disc. *Spine (Phila Pa 1976).* 1998;1:2363–6.
12. Weinstein JS, Burchiel KJ. Dandy’s disc. *Neurosurgery.* 2009;65:201–5.
13. Fay T, Grant FC. Ventriculostomy and intraventricular photography in internal hydrocephalus. Report of case. *JAMA.* 1923;80:461–3. doi:10.1001/jama.1923.02640340017007.
14. Volkmann J. The endoscope [in German]. *Sonderabdruck Zentralbl Chirug.* 1924;23:1233–4.
15. Volkmann J. About attempts at direct visual inspection of the brain chambers (endoscopy) [in German]. *Münchener Med Wochenschr.* 1923;46:1382.
16. Putnam TJ. Results of treatment of hydrocephalus by endoscopic coagulation of choroid plexus. *Arch Pediatr.* 1935;52:676–85.
17. Putnam TJ. Surgical treatment of infantile hydrocephalus. *Surg Gynecol Obstet.* 1943;76:171–8.
18. Putnam TJ. Treatment of hydrocephalus by endoscopic coagulation of choroid plexuses: description of a new instrument and preliminary report of results. *N Engl J Med.* 1934;210:1373–6.
19. Scarff JE. Third ventriculostomy as the rational treatment of obstructive hydrocephalus. *J Pediatr.* 1935;6:870–1.
20. Scarff JE. Endoscopic treatment of hydrocephalus: description of a ventriculoscope and preliminary report of cases. *Arch Neurol Psychiatry.* 1936;38:853–61. doi:10.1001/archneurpsyc.1936.02260040163011.
21. Dandy WE. Extirpation of the choroids plexus of the lateral ventricles in communicating hydrocephalus. *Ann Surg.* 1918;68:569–79.
22. Scarff JE. Nonobstructive hydrocephalus: Treatment by endoscopic cauterization of choroid plexus. Long term results. *J Neurosurg.* 1952;9:164–76.
23. Scarff JE. Treatment of nonobstructive (communicating) hydrocephalus by cauterization of the choroid plexuses. Long term follow-up study. *Acta Psychiatr Neurol Scand.* 1959;34:354–74. doi:10.1111/j.1600-0447.1959.tb07585.x.
24. Abd-El-Barr MM, Cohen AR. The origin and evolution of neuroendoscopy. *Childs Nerv Syst.* 2013;29:727–37. doi:10.1007/s00381-013-2055-2.
25. Nulsen FE, Spitz EB. Treatment of hydrocephalus by direct shunt from ventricle to jugular vein. *Surg Forum.* 1951;399–403
26. Li KW, Nelson C, Suk I, Jallo GI. Neuroendoscopy: past, present, and future. *Neurosurg Focus.* 2005;19:E1. doi:10.3171/foc.2005.19.6.2.
27. Zada G, Liu C, Apuzzo ML. “Through the looking glass”: optical physics, issues, and the evolution of neuroendoscopy. *World Neurosurg.* 2012;77:92–102. doi:10.1016/j.wneu.2013.02.001.
28. Apuzzo ML, Heifetz MD, Weiss MH, Kurze T. Neurosurgical endoscopy using the side-viewing telescope. Technical note. *J Neurosurg.* 1977;46:398–400. doi:10.3171/jns.1977.46.3.0398.
29. Liu CY, Wang MY, Apuzzo ML. The physics of image formation in the neuroendoscope. *Childs Nerv Syst.* 2004;20:777–82. doi:10.1007/s00381-004-0930-6.
30. Bhatt J, Jones A, Foley S, Shah Z, Malone P, Fawcett D, et al. Harold Horace Hopkins: a short biography. *BJU Int.* 2010;106:1425–8.
31. Liu JK, Das K, Weiss MH, Laws Jr ER, Couldwell WT. The history and evolution of transsphenoidal surgery. *J Neurosurg.* 2001;95:1083–96. doi:10.3171/jns.2001.95.6.1083.
32. Comoy C. Cerebral ventriculostomy [in French]. Paris: Thèse de médecine; 1963.
33. Guiot G, et al. Endoscopic intracranial explorations [in French]. *Presse Med.* 1963;71:23–7.
34. Fukushima T, Ishijima B, Hirakawa K, Nakamura N, Sano K. Ventriculofiberscope: a new technique for endoscopic diagnosis and operation. *J Neurosurg.* 1973;38:251–6.
35. Fukushima T, Schramm J. Clinical trial of endoscopy of the spinal canal: a memorandum [in German]. *Neurochir Stuttg.* 1975; 18:199–203.
36. Griffith HB. Endoneurosurgery: endoscopic intracranial surgery. *Proc R Soc Lond B.* 1977;195:261–8.
37. Griffith HB. Technique of fontanelle and persutural ventriculostomy and endoscopic ventricular surgery in infants. *Child Brain.* 1975;1:359–3.
38. Schroeder HWS. Current status and future developments of neuroendoscopically assisted neurosurgery. In: Sgouros S, editor. *Neuroendoscopy.* Berlin Heidelberg: Springer-Verlag; 2014. p. 65–80. doi:10.1007/978-3-642-39085-2\_6.
39. Schroeder HW, Nehlsen M. Value of high-definition imaging in neuroendoscopy. *Neurosurg Rev.* 2009;32:303–8. doi:10.1007/s10143-009-0200-x.
40. Hopf NJ, Perneczky A. Endoscopic neurosurgery and endoscope-assisted microneurosurgery for the treatment of intracranial cysts. *Neurosurgery.* 1998;43:1330–6.
41. Gaab MR, Schroeder HW. Neuroendoscopic approach to intraventricular lesions. *Neurosurg Focus.* 1999;6:e5.
42. Schroeder HW, Gaab MR. Endoscopic resection of colloid cysts. *Neurosurgery.* 2002;51:1441–4.
43. Schroeder HW, Gaab MR, Niendorf WR. Indications for endoscopic neurosurgery in children. *Childs Nerv Syst.* 1996;12:485–6.
44. Schroeder HW, Gaab MR, Niendorf WR. Neuroendoscopic approach to arachnoid cysts. *J Neurosurg.* 1996;85:293–8. doi:10.3171/jns.1996.85.2.0293.
45. Gaab MR, Schroeder HW. Neuroendoscopic approach to intraventricular lesions. *J Neurosurg.* 1998;88:496–505. doi:10.3171/jns.1998.88.3.0496.
46. Oertel JM, Baldauf J, Schroeder HW, Gaab MR. Endoscopic options in children: experience with 134 procedures. *J Neurosurg Pediatr.* 2009;3:81–9. doi:10.3171/2008.11.PEDS0887.
47. Oertel JM, Schroeder HW, Gaab MR. Endoscopic stomy of the septum pellucidum: indications, technique, and results. *Neurosurgery.* 2009;64:482–91. doi:10.1227/01.NEU.0000338944.42411.67.
48. Schroeder HW, Oertel J, Gaab MR. Endoscopic treatment of cerebrospinal fluid pathway obstructions. *Neurosurgery.* 2008;62:1084–92. doi:10.1227/01.neu.0000333774.81563.d8.

49. Schroeder HW, Gaab MR. Endoscopic aqueductoplasty: technique and results. *Neurosurgery*. 1999;45:508–15.
50. Schroeder HW, Gaab MR. Intracranial endoscopy. *Neurosurg Focus*. 1999;6:e1.
51. Schroeder HW, Niendorf WR, Gaab MR. Complications of endoscopic third ventriculostomy. *J Neurosurg*. 2002;96:1032–40. doi:10.3171/jns.2002.96.6.1032.
52. Mortazavi MM, Adeeb N, Griessenauer CJ, Sheikh H, Shahidi S, Tubbs RI, et al. The ventricular system of the brain: a comprehensive review of its history, anatomy, histology, embryology, and surgical considerations. *Childs Nerv Syst*. 2014;30:19–35. doi:10.1007/s00381-013-2321-3.
53. Costa Val JA. Minicraniotomy for endoscopic third ventriculostomy in babes: technical note with a 7-year-segment analysis. *Childs Nerv Syst*. 2009;25:357–9. doi:10.1007/s00381-008-0748-8.
54. Caemaert J, Abdullah J, Calliauw L. A multipurpose cerebral endoscope and reflections on technique and instrumentation in endoscopic neurosurgery. *Acta Neurochir Suppl (Wien)*. 1994;61:49–53.
55. Schroeder HW. A new multipurpose ventriculoscope. *Neurosurgery*. 2008;62:489–91. doi:10.1227/01.neu.0000316017.43668.6c.
56. Oi S, Samii A, Samii M. Frameless free-hand maneuvering of a small-diameter rigid-rod neuroendoscope with a working channel used during high-resolution imaging. Technical note. *J Neurosurg Pediatr*. 2005;102:113–8. doi:10.3171/ped.2005.102.1.0113.
57. Oi S. Frameless free-hand neuroendoscopic surgery – development of the finest rigid-rod neuroendoscope model to cope with the current limitations of neuroendoscopic surgery. *J Neuroendoscopy*. 2010;1:2–11.
58. Chowdhry SA, Cohen AR. Intraventricular neuroendoscopy: complication avoidance and management. *World Neurosurg*. 2013;79:S15.e1–S15.e10. doi:10.1016/j.wneu.2012.02.030.
59. Zador Z, Coope DJ, Kamaly-Asl ID. Comparative analysis of endoscopic third ventriculostomy trajectories in pediatric cases. *J Neurosurg Pediatr*. 2015;16:626–32. doi:10.3171/2015.4.PEDS14430.
60. Oertel J, Gen M, Krauss JK, Zumkeller M, Gaab MR. The use of waterjet dissection in endoscopic neurosurgery. Technical note. *J Neurosurg*. 2006;105:928–31. doi:10.3171/jns.2006.105.6.928.
61. van Beijnum J, Hanlo PW, Fischer K, Majidpour MM, Kortekaas MF, Verdaasdonk RM, et al. Laser-assisted endoscopic third ventriculostomy: long-term results in a series of 202 patients. *Neurosurgery*. 2008;62:437–43. doi:10.1227/01.neu.0000316011.13174.b1.
62. Hellwig D, Giordano M, Kappus C. Redo third ventriculostomy. *World Neurosurg*. 2013;79:S22. doi:10.1016/j.wneu.2012.02.006.e13–20.
63. Guzman R, Pendharkar AV, Zerah M, Sainte-Rose C. Use of the NeuroBalloon catheter for endoscopic third ventriculostomy. *J Neurosurg Pediatr*. 2013;11:302–6. doi:10.3171/2012.10.PEDS11159.
64. Vogel TW, Bahuleyan B, Robinson S, Cohen AR. The role of endoscopic third ventriculostomy in the treatment of hydrocephalus. *J Neurosurg Pediatr*. 2013;12:54–61. doi:10.3171/2013.4.PEDS12481.
65. Eshra MA. Endoscopic third ventriculostomy in idiopathic normal pressure hydrocephalus. *Alexandria J Med*. 2014;50:341–4. doi:10.1016/j.ajme.2013.11.004.
66. Spennato P, Tazi S, Bekaert O, Cinalli G, Decq P. Endoscopic third ventriculostomy for idiopathic stenosis. *World Neurosurg*. 2013;79:S21.e13–20. doi:10.1016/j.wneu.2012.02.007.
67. Sainte-Rose C, Cinalli G, Roux FE, Maixner R, Chumas PD, Mansour M, et al. Management of hydrocephalus in pediatric patients with posterior fossa tumors: the role of endoscopic third ventriculostomy. *J Neurosurg*. 2001;95:791–7. doi:10.3171/jns.2001.95.5.0791.
68. O'Brien DF, Javadpour M, Collins DR, Spennato P, Mallucci CL. Endoscopic third ventriculostomy: an outcome analysis of primary cases and procedures performed after ventriculoperitoneal shunt malfunction. *J Neurosurg*. 2005;103:393–400. doi:10.3171/ped.2005.103.5.0393.
69. Elbabaa SK, Steinmetz M, Ross J, Moon D, Luciano MG. Endoscopic third ventriculostomy for obstructive hydrocephalus in the pediatric population: evaluation of outcome. *Eur J Pediatr Surg*. 2001;11:S52–4.
70. Lam S, Harris D, Rocque BG, Ham SA. Pediatric endoscopic third ventriculostomy: a population-based study. *J Neurosurg Pediatr*. 2014;4:455–64. doi:10.3171/2014.8.PEDS13680.
71. Koch-Wiewrodt D, Wagner W. Success and failure of endoscopic third ventriculostomy in young infants: are there different age distributions? *Childs Nerv Syst*. 2006;22:1537–41. doi:10.1007/s00381-006-0191-7.
72. Gorayeb RP, Cavalheiro S, Zymberg ST. Endoscopic third ventriculostomy in children younger than 1 year of age. *J Neurosurg*. 2004;100:427–9. doi:10.3171/ped.2004.100.5.0427.
73. Fritsch MJ, Kienke S, Ankermann T, Padoin M, Mehdorn M. Endoscopic third ventriculostomy in infants. *J Neurosurg*. 2005;103:50–3. doi:10.3171/ped.2005.103.1.0050.
74. Kulkarni AV, Drake JM, Kestle JR, Mallucci CL, Sgouros S, Constantini S, et al. Predicting who will benefit from endoscopic third ventriculostomy compared with shunt insertion in childhood hydrocephalus using the ETV Success Score. *J Neurosurg Pediatr*. 2010;6:310–5. doi:10.3171/2010.8.PEDS103.
75. Kulkarni AV, Riva-Cambria J, Browd SR. Use of the ETV Success Score to explain the variation in reported endoscopic third ventriculostomy success rates among published case series of childhood hydrocephalus. *J Neurosurg Pediatr*. 2011;7:143–6. doi:10.3171/2010.11.PEDS10296.
76. Azimi P, Mohammadi HR. Predicting endoscopic third ventriculostomy success in childhood hydrocephalus: an artificial neural network analysis. *J Neurosurg Pediatr*. 2014;13:426–32. doi:10.3171/2013.12.PEDS13423.
77. Bouras T, Sgouros S. Complications of endoscopic third ventriculostomy. *World Neurosurg*. 2013;79:S22.e9–S22.e12. doi:10.3171/2011.4.PEDS10503.
78. Dezena RA, Pereira CU, Araújo LP, Ribeiro MP, Oliveira HA. Neuroendoscopic choroid plexus coagulation for pediatric hydrocephalus: review of historical aspects and rebirth. *J Bras Neurocirurg*. 2014;25:30–5.
79. Dezena RA. The rebirth of neuroendoscopic choroid plexus coagulation as treatment of pediatric hydrocephalus. *J Neurol Stroke*. 2014;1:00012.
80. Dezena RA. Neuroendoscopic choroid plexus coagulation in the current pediatric neurosurgery. *J Neurosurg Sci*. 2016;60:287–8.
81. Cserr HF. Physiology of the choroid plexus. *Physiol Rev*. 1971;51:273–311.
82. Weed LH. Studies on cerebro-spinal fluid. No. IV: The dual source of cerebro-spinal fluid. *J Med Res*. 1914;31:93–118.
83. Cushing H. Studies on the cerebrospinal fluid. I Introduction. *J Med Res*. 1914;31:1–19.
84. Zhu X, Di Rocco C. Choroid plexus coagulation for hydrocephalus not due to CSF overproduction: a review. *Childs Nerv Syst*. 2013;29:35–42. doi:10.1007/s00381-012-1960-0.
85. Dandy WE. *The brain*. W. F. Prior Company: Hagerstown; 1932.
86. Dandy WE. The operative treatment of communicating hydrocephalus. *Ann Surg*. 1938;108:194–202.



87. Scarff JE. Evaluation of treatment of hydrocephalus. Results of third ventriculostomy and endoscopic cauterization of choroid plexuses compared with mechanical shunts. *Arch Neurol.* 1966;14:382–91.
88. Scarff JE. The treatment of nonobstructive (communicating) hydrocephalus by endoscopic cauterization of the choroid plexuses. *J Neurosurg.* 1970;33:1–18.
89. Milhorat TH. Failure of choroid plexectomy as treatment for hydrocephalus. *Surg Gynecol Obstet.* 1974;139:505–8.
90. Griffith HB, Jamjoom AB. The treatment of childhood hydrocephalus by choroid plexus coagulation and artificial cerebrospinal fluid perfusion. *Br J Neurosurg.* 1990;4:95–100.
91. Pople IK, Ettles D. The role of endoscopic choroid plexus coagulation in the management of hydrocephalus. *Neurosurgery.* 1995;36:698–701.
92. Morota N, Fujiyama Y. Endoscopic coagulation of choroid plexus as treatment for hydrocephalus: indication and surgical technique. *Childs Nerv Syst.* 2004;20:816–20. doi:10.1007/s00381-004-0936-0.
93. Griffith HB. Endoneurosurgery: endoscopic intracranial surgery. *Adv Tech Stand Neurosurg.* 1986;14:2–24.
94. Phillips MF, Shanno G, Duhaime AC. Treatment of villous hypertrophy of the choroid plexus by endoscopic contact coagulation. *Pediatr Neurosurg.* 1998;28:252–6.
95. Warf BC. Comparison of endoscopic third ventriculostomy alone and combined with choroid plexus cauterization in infants younger than 1 year of age: a prospective study in 550 African children. *J Neurosurg.* 2005;103:475–81. doi:10.3171/ped.2005.103.6.0475.
96. Warf BC, Campbell JW. Combined endoscopic third ventriculostomy and choroid plexus cauterization as primary treatment of hydrocephalus for infants with myelomeningocele: long-term results of a prospective intent-to-treat study in 115 East African infants. *J Neurosurg Pediatr.* 2008;2:310–6. doi:10.3171/PED.2008.2.11.310.
97. Warf B, Ondoma S, Kulkarni A, Donnelly R, Ampeire M, Akona J, et al. Neurocognitive outcome and ventricular volume in children with myelomeningocele treated for hydrocephalus in Uganda. *J Neurosurg Pediatr.* 2009;4:564–70. doi:10.3171/2009.7.PEDS09136.
98. Kadrian D, van Gelder J, Florida D, Jones R, Vonau M, Teo C, et al. Long-term reliability of endoscopic third ventriculostomy. *Neurosurgery.* 2005;56:1271–8.
99. Teo C, Jones R. Management of hydrocephalus by endoscopic third ventriculostomy in patients with myelomeningocele. *Pediatr Neurosurg.* 1996;25:57–63.
100. Warf BC, Stagno V, Mugamba J. Encephalocele in Uganda: ethnic distinctions in lesion location, endoscopic management of hydrocephalus, and survival in 110 consecutive children. *J Neurosurg Pediatr.* 2011;7:88–93. doi:10.3171/2010.9.PEDS10326.
101. Warf BC, Tracy S, Mugamba J. Long-term outcome for endoscopic third ventriculostomy alone or in combination with choroid plexus cauterization for congenital aqueductal stenosis in African infants. *J Neurosurg Pediatr.* 2012;10:108–11. doi:10.3171/2012.4.PEDS1253.
102. Warf BC, Dewan M, Mugamba J. Management of Dandy-Walker complex associated infant hydrocephalus by combined endoscopic third ventriculostomy and choroid plexus cauterization. *J Neurosurg Pediatr.* 2011;8:377–83. doi:10.3171/2011.7.PEDS1198.
103. Warf BC. Congenital idiopathic hydrocephalus of infancy: the results of treatment by endoscopic third ventriculostomy with or without choroid plexus cauterization and suggestions for how it works. *Childs Nerv Syst.* 2013;29:935–40. doi:10.1007/s00381-013-2072-1.
104. Warf BC, Mugamba J, Kulkarni AV. Endoscopic third ventriculostomy in the treatment of childhood hydrocephalus in Uganda: report of a scoring system that predicts success. *J Neurosurg Pediatr.* 2010;5:143–8. doi:10.3171/2009.9.PEDS09196.
105. Kulkarni AV, Riva-Cambrin J, Browd SR, Drake JM, Holubkov R, Kestle JR, et al. Endoscopic third ventriculostomy and choroid plexus cauterization in infants with hydrocephalus: a retrospective Hydrocephalus Clinical Research Network study. *J Neurosurg Pediatr.* 2014;14:224–9. doi:10.3171/2014.6.
106. Weil AG, Fallah A, Chamiraju P, Ragheb J, Bhatia S. Endoscopic third ventriculostomy and choroid plexus cauterization with a rigid neuroendoscope in infants with hydrocephalus. *J Neurosurg Pediatr.* 2015;30:1–11. doi:10.3171/2015.5.PEDS14692.
107. Zuccaro G, Ramos JG. Multiloculated hydrocephalus. *Childs Nerv Syst.* 2011;27:1609–19. doi:10.1007/s00381-011-1528-4.
108. Warf BC, Campbell JW, Riddle E. Initial experience with combined endoscopic third ventriculostomy and choroid plexus cauterization for post-hemorrhagic hydrocephalus of prematurity: the importance of prepontine cistern status and the predictive value of FIESTA MRI imaging. *Childs Nerv Syst.* 2011;7:1063–71. doi:10.1007/s00381-011-1475-0.
109. Chamiraju P, Bhatia S, Sandberg DI, Ragheb J. Endoscopic third ventriculostomy and choroid plexus cauterization in posthemorrhagic hydrocephalus of prematurity. *J Neurosurg Pediatr.* 2014;13:433–9. doi:10.3171/2013.12.PEDS13219.
110. Malheiros JA, Trivelato FP, Oliveira MM, Gusmão S, Cochrane DD, Steinbok P. Endoscopic choroid plexus cauterization versus ventriculoperitoneal shunt for hydranencephaly and near hydranencephaly: a prospective study. *Neurosurgery.* 2010;66:459–64. doi:10.1227/01.NEU.0000365264.99133.CA.
111. Shitsama S, Wittayanakorn N, Okechi H, Albright AL. Choroid plexus coagulation in infants with extreme hydrocephalus or hydranencephaly. *J Neurosurg Pediatr.* 2014;14:55–7. doi:10.3171/2014.3.PEDS13488.
112. Teo C, Kadrian D, Hayhurst C. Endoscopic management of complex hydrocephalus. *World Neurosurg.* 2013;79:S21.e1–7. doi:10.1016/j.wneu.2012.02.015.
113. Hamada H, Hayashi N, Kurimoto M, Umemura K, Hirashima Y, Endo S. Neuroendoscopic septostomy for isolated lateral ventricle. *Neurol Med Chir (Tokyo).* 2003;43:582–7.
114. Fallah A, Wang AC, Weil AG, Ibrahim GM, Mansouri A, Bhatia S. Predictors of outcome following cerebral aqueductoplasty: an individual participant data meta-analysis. *Neurosurgery.* 2016;78:285–96. doi:10.1227/NEU.0000000000001024.
115. Antes S, Salah M, Linsler S, Tschan CA, Breuskin D, Oertel J. Aqueductal stenting with an intra-catheter endoscope – a technical note. *Childs Nerv Syst.* 2016;32:359–63. doi:10.1007/s00381-015-2902-4.
116. Fritsch MJ, Schroeder HW. Endoscopic aqueductoplasty and stenting. *World Neurosurg.* 2013;79:S20. doi:10.1016/j.wneu.2012.02.013.e15–18.
117. Maher CO, Goumnerova L. The effectiveness of ventriculocystocisternostomy for suprasellar arachnoid cysts. *J Neurosurg Pediatr.* 2011;7:64–72. doi:10.3171/2010.10.PEDS10356.
118. Mohanty A, Santosh V, Devi I, Satish S, Biswas A. Efficacy of simultaneous single trajectory endoscopic tumor biopsy and endoscopic cerebrospinal fluid diversion procedures in intra-and paraventricular tumors. *Neurosurg Focus.* 2011;30:E4. doi:10.3171/2011.1.FOCUS10295.
119. Hayashi N, Murai H, Ishihara S, Kitamura T, Miki T, Miwa T, et al. Nationwide investigation of the current status of therapeutic neuroendoscopy for ventricular and paraventricular tumors in Japan. *J Neurosurg.* 2011;115:1147–57. doi:10.3171/2011.7.JNS101976.
120. Constantini S, Mohanty A, Zymberg S, Cavalheiro S, Mallucci C, Hellwig D, et al. Safety and diagnostic accuracy of neuroendoscopic biopsies: an international multicenter study. *J Neurosurg Pediatr.* 2013;11:704–9. doi:10.3171/2013.3.PEDS12416.
121. Somji M, Badhiwala J, McLellan A, Kulkarni AV. Diagnostic yield, morbidity, and mortality of intraventricular neuroendoscopic

- biopsy: systematic review and meta-analysis. *World Neurosurg.* 2016;85:315–24. doi:[10.1016/j.wneu.2015.09.011](https://doi.org/10.1016/j.wneu.2015.09.011).
122. Elbabaa SK. Ventricular neuroendoscopic surgery: lessons learned from the literature. *World Neurosurg.* 2016;88:646–8. doi:[10.1016/j.wneu.2015.11.019](https://doi.org/10.1016/j.wneu.2015.11.019).
123. Boogaarts HD, Decq P, Grotenhuis JA, Le Guérinel C, Niseir R, Jarraya B, et al. Longterm results of the neuroendoscopic management of colloid cysts of the third ventricle: a series of 90 cases. *Neurosurgery.* 2011;68:179–87. doi:[10.1227/NEU.0b013e3181ffae71](https://doi.org/10.1227/NEU.0b013e3181ffae71).
124. Horn EC, Feiz-Erfan I, Bristol RE, Lekovic GP, Goslar PW, Smith KA, et al. Treatment options for third ventricular colloid cysts: comparison of open microsurgical versus endoscopic resection. *Neurosurgery.* 2007;60:613–8. doi:[10.1227/01.NEU.0000255409.61398.EA](https://doi.org/10.1227/01.NEU.0000255409.61398.EA).
125. Oertel J, Krauss JK, Gaab MR. Ultrasonic aspiration in neuroendoscopy: first results with new tool. *J Neurosurg.* 2008;109:908–11. doi:[10.3171/JNS/2008/109/11/0908](https://doi.org/10.3171/JNS/2008/109/11/0908).

---

**Part II**

**Essential Intraoperative Anatomy**

## 3.1 Introduction

The basic condition for good visualization of ventricular structures is ventricular dilatation. Although currently it is possible to perform endoscopic procedures with non-dilated ventricles by neuronavigation techniques [1, 2], the vast majority of procedures are performed with dilated ventricles. Rigid endoscopy systems have a much higher image quality when compared with flexible systems. All pictures presented here were obtained from Karl Storz rigid endoscopy Gaab (6° viewing angle) systems and Oi HandyPro (0° viewing angle) (Karl Storz, Tuttlingen, Germany). The entry point used was Kocher's point, in most cases on the right side, a point from which it is possible to perform the majority of ventricular procedures. This hole is located about 2 cm anterior to the coronal suture and 2 cm lateral to the midline, approximately at the mid-pupillary line [3, 4]. Depending on the condition being treated, these coordinates may vary by centimeters. After entering the lateral ventricle (Figs. 3.1, 3.2, 3.3, 3.4, and 3.5), the first significant anatomical viewing is the foramen of Monro, the gateway to the third ventricle. An important topographic detail is that the choroid plexus always lies in the posterior margin of the foramen, in close contact with the angle formed by the superior thalamostriate vein and the anterior septal vein [3] (Fig. 3.6). In certain cases a foramino-

plasty may be necessary, making use of a Fogarty balloon catheter. Although this procedure is controversial, it can be performed safely and without permanent memory deficit if the structures in this region are properly displayed [5, 6, 7]. The foramen may still be occluded by arachnoid cysts within the lateral ventricles (which are basically treated with fenestrations to reduce their volume [8, 9]), or by tumors such as colloid cysts, which can be completely resected by neuroendoscopy [10]. Other procedures to be performed in this region are septostomy for an isolated lateral ventricle [7], and choroid plexus coagulation, as discussed in Part I. The initial endoscopic viewing angle shown in Fig. 3.7 is intended for visualization of the structures in the body of the lateral ventricle (see Figs. 3.8, 3.9, 3.10, 3.11, 3.12, 3.13, 3.14, 3.15, 3.16, 3.17, 3.18, 3.19, 3.20, 3.21, 3.22, 3.23, 3.24, 3.25, 3.26, 3.27, 3.28, 3.29, 3.30, 3.31, 3.32, 3.33, 3.34, 3.35, 3.36, 3.37, 3.38, 3.39, 3.40, 3.41, 3.42, 3.43, 3.44, 3.45, 3.46, 3.47, 3.48, 3.49, 3.50, 3.51, 3.52, and 3.53). The endoscopic viewing angles for better visualization of the septum pellucidum (Fig. 3.54), frontal horn (Fig. 3.75), and atrium (Fig. 3.80) are shown prior to the following figures in each region (Fig. 3.55, 3.56, 3.57, 3.58, 3.59, 3.60, 3.61, 3.62, 3.63, 3.64, 3.65, 3.66, 3.67, 3.68, 3.69, 3.70, 3.71, 3.72, 3.73, 3.74, 3.76, 3.77, 3.78, 3.79, 3.81, 3.82, 3.83, 3.84, 3.85, 3.86, 3.87, 3.88, and 3.89). Illustrative cases are presented.

### 3.2 Entering the Ventricular System

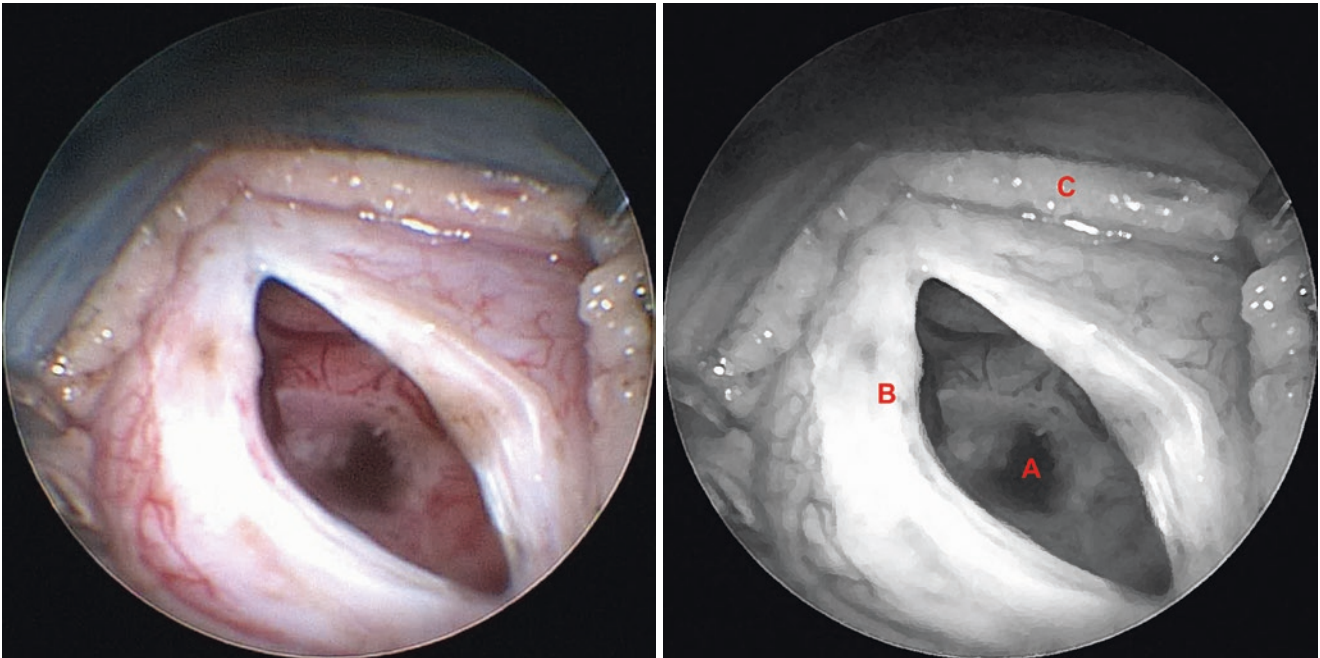


**Fig. 3.1** Transfontanelle standard dural opening in a newborn. (A) Corticotomy, (B) Dura mater, (C) Scalp

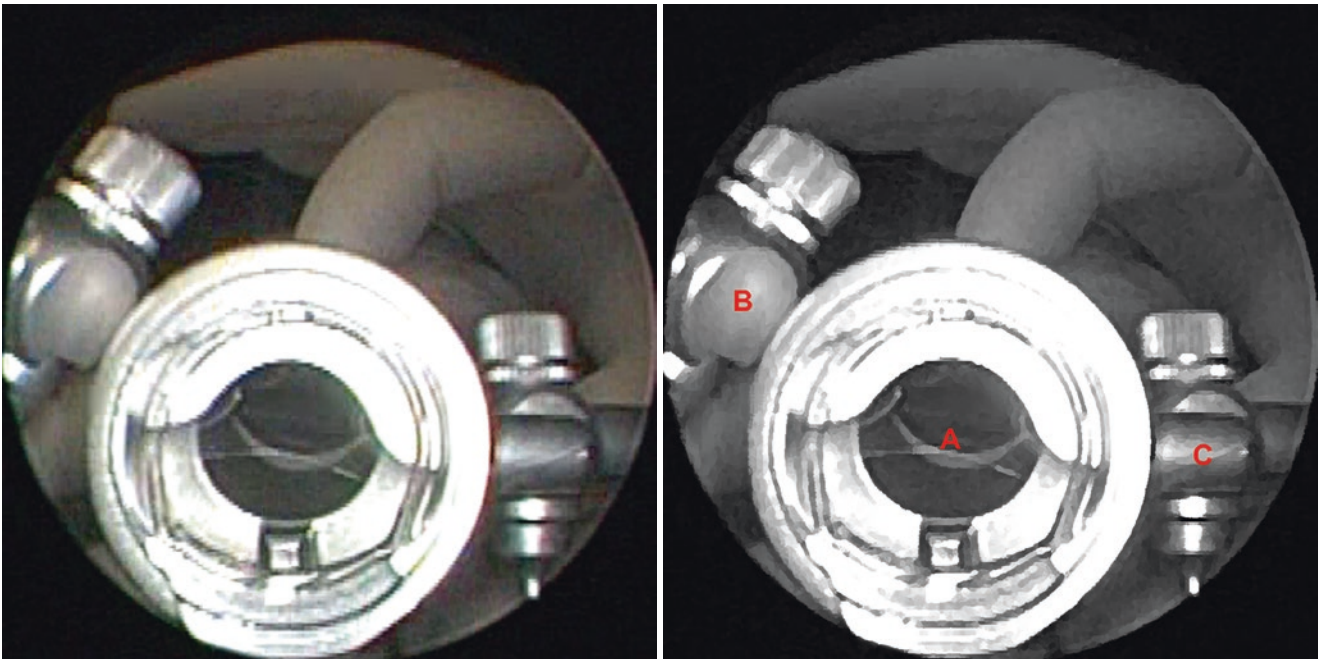


**Fig. 3.2** Gaab system operating sheath. (A) Neuroendoscope optics entrance, (B) Saline solution entrance channel, (C) Saline passive exit channel

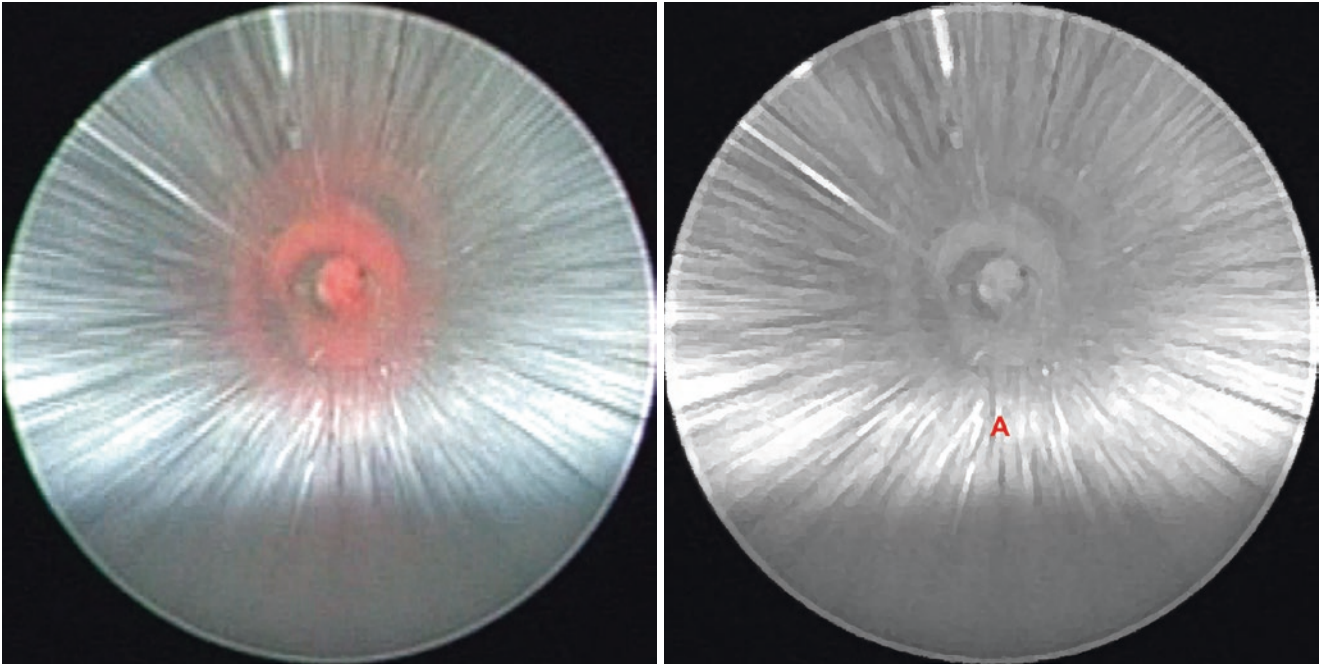


**Fig. 3.3** Inside operating sheath. (A) Inside operating sheath

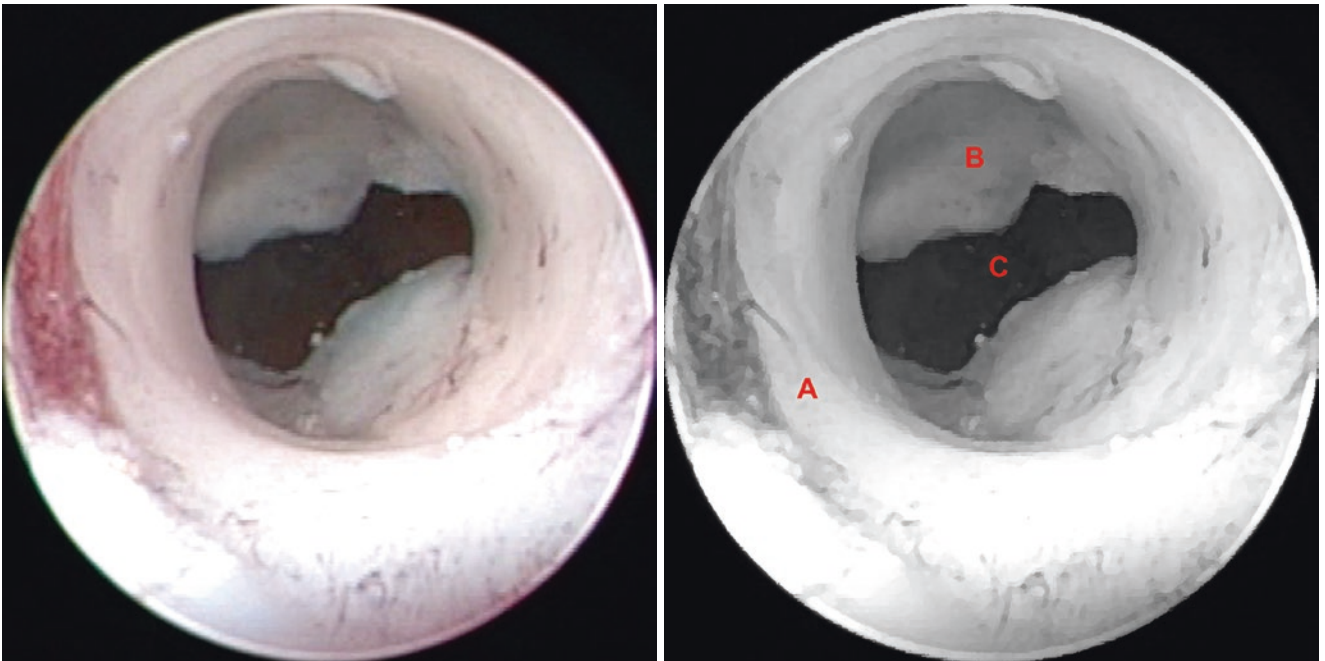


**Fig. 3.4** Cerebral trajectory. (A) Brain, (B) Ependymal layer, (C) Inside the lateral ventricle

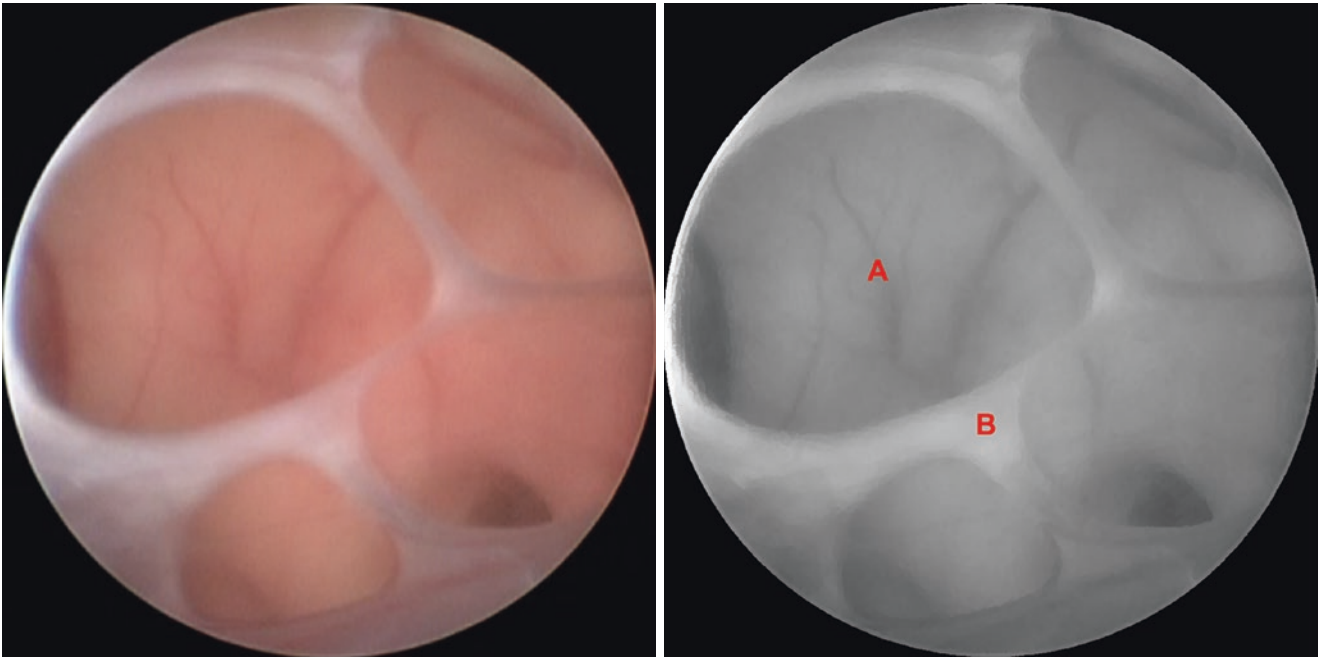


**Fig. 3.5.** Ependymal layer. (A) Inside the lateral ventricle, (B) Fenestrated ependymal layer

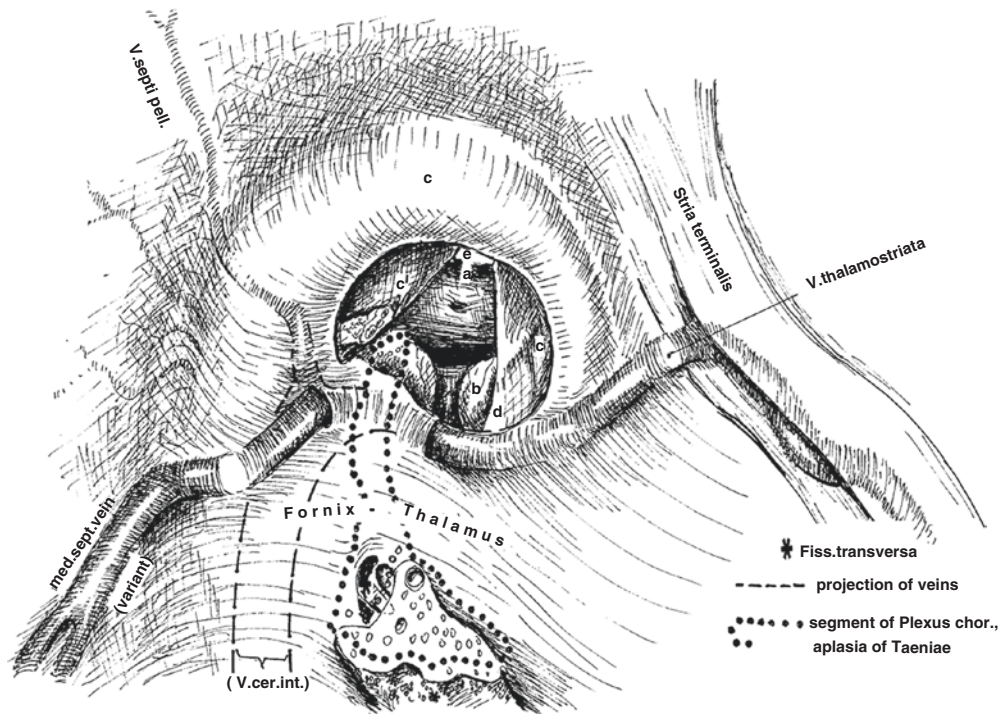


**Fig. 3.6** Foramen of Monro, its adjacent structures, and anterior segment of the third ventricle. Infundibular recess (a), right mammillary body (b), right column of the fornix (c), left column of the fornix (c'), thalamus (d), and optic chiasm (e) (Reprinted from Seeger [11])

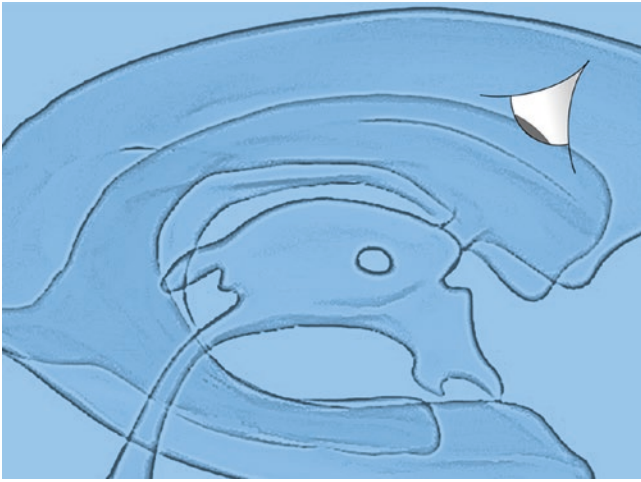


**Fig. 3.7** Direction of the endoscopic vision after entering the right lateral ventricle



### 3.3 Right Lateral Ventricle: Foramen of Monroe Region

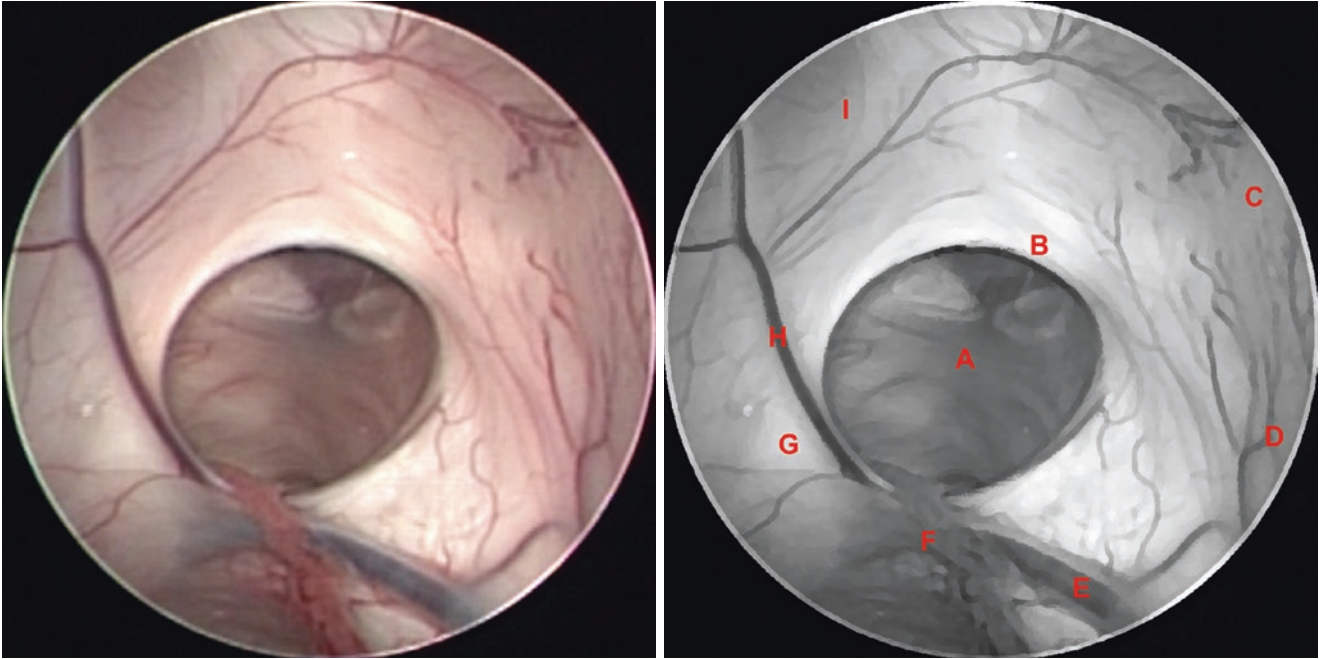


**Fig. 3.8** Normal anatomy. (A) Foramen of Monroe, (B) Column of the fornix, (C) Frontal horn, (D) Head of the caudate nucleus, (E) Superior thalamostriate vein, (F) Choroid plexus, (G) Body of the fornix, (H) Anterior septal vein, (I) Septum pellucidum

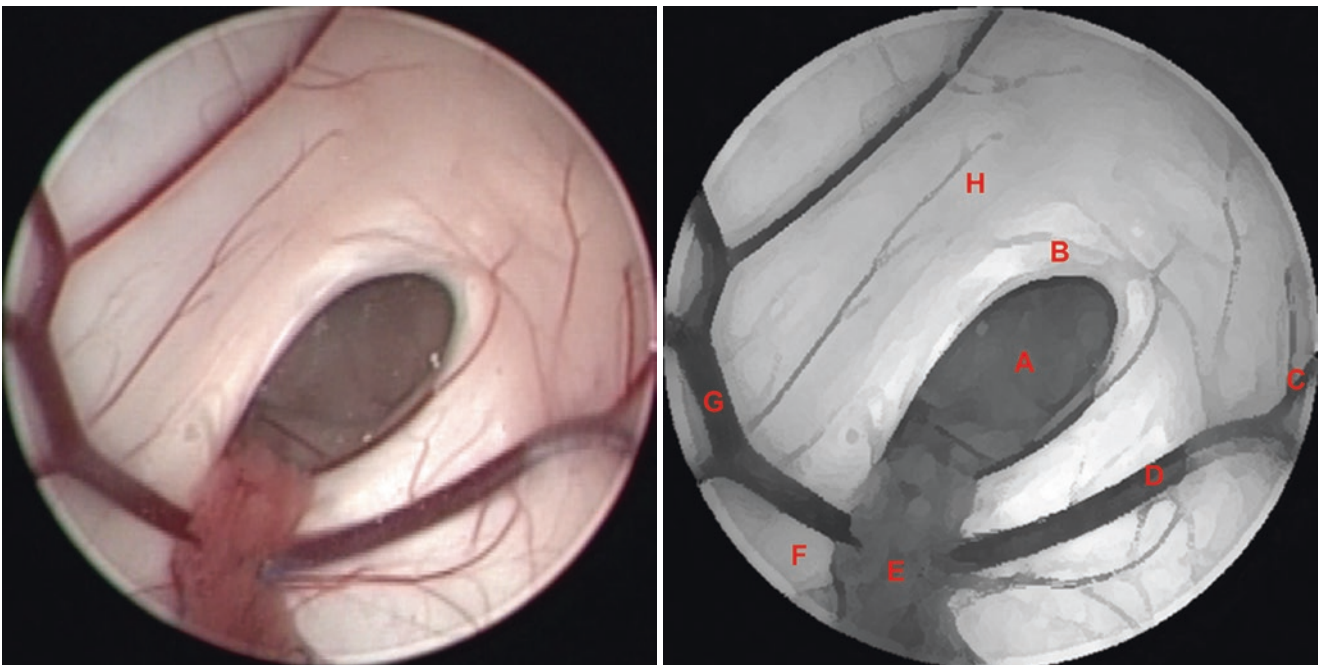


**Fig. 3.9** Normal anatomy. (A) Foramen of Monroe, (B) Column of the fornix, (C) Anterior caudate vein, (D) Superior thalamostriate vein, (E) Choroid plexus, (F) Body of the fornix, (G) Anterior septal vein, (H) Septum pellucidum

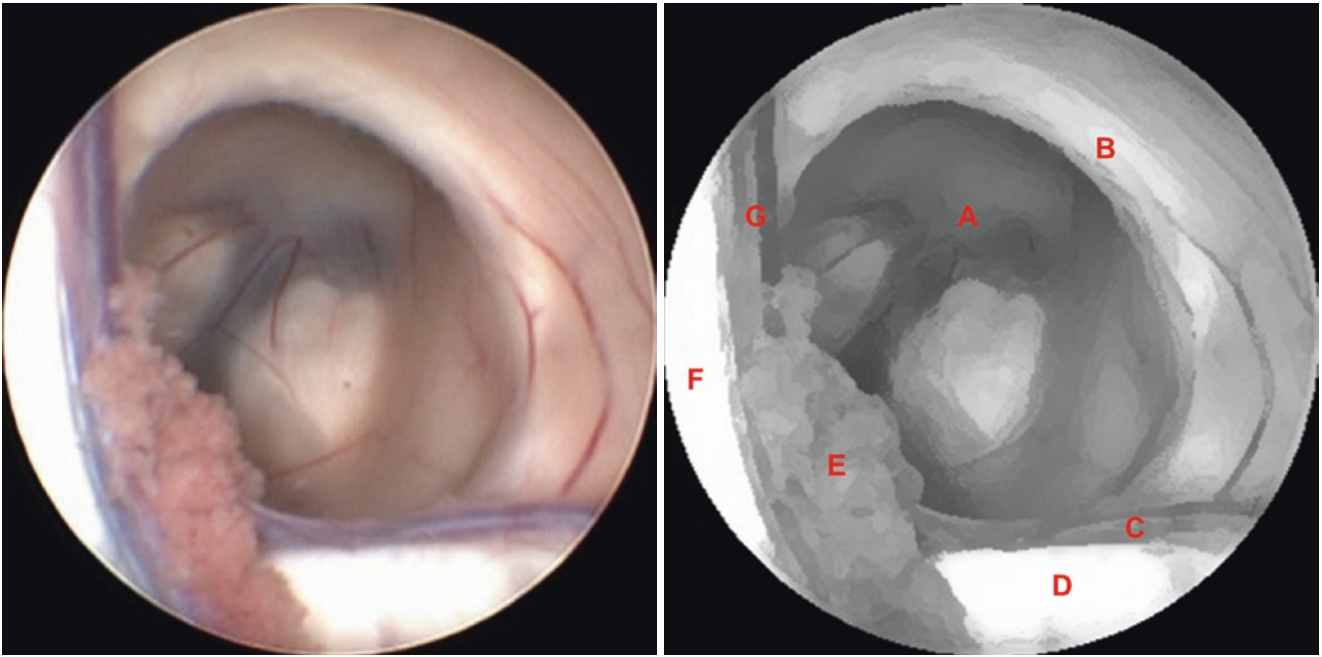


**Fig. 3.10** Normal anatomy. (A) Foramen of Monro, (B) Column of the fornix, (C) Superior thalamostriate vein, (D) Thalamus, (E) Choroid plexus, (F) Body of the fornix, (G) Anterior septal vein

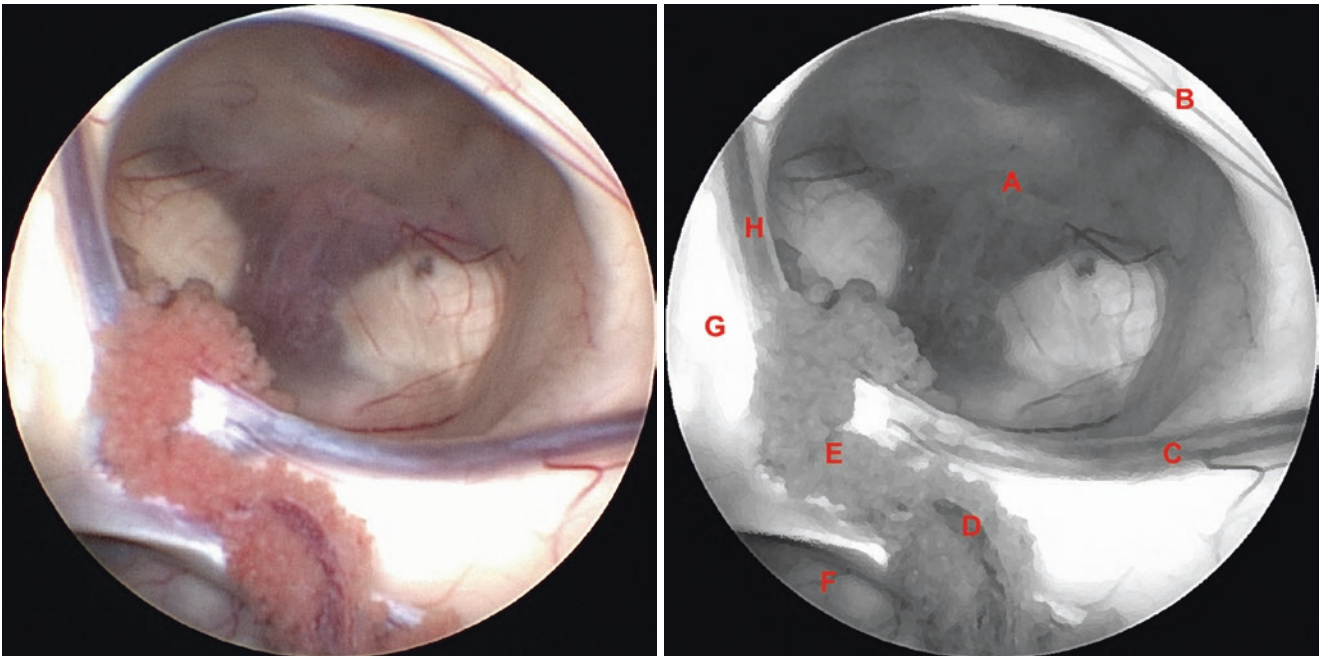


**Fig. 3.11** Normal anatomy. (A) Foramen of Monro, (B) Column of the fornix, (C) Superior thalamostriate vein, (D) Superior choroidal vein, (E) Choroid plexus, (F) Atrium, (G) Body of the fornix, (H) Anterior septal vein

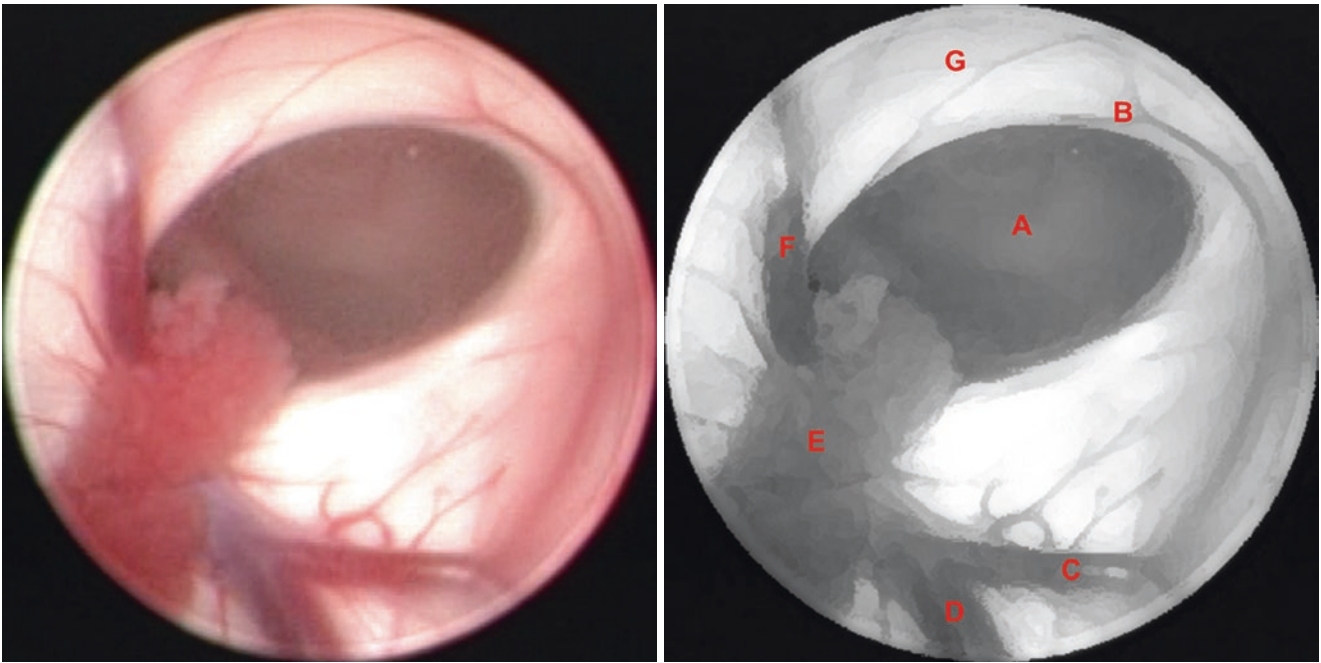


**Fig. 3.12** Normal anatomy. (A) Foramen of Monro, (B) Column of the fornix, (C) Anterior caudate vein, (D) Superior thalamostriate vein, (E) Choroid plexus, (F) Anterior septal vein, (G) Septum pellucidum

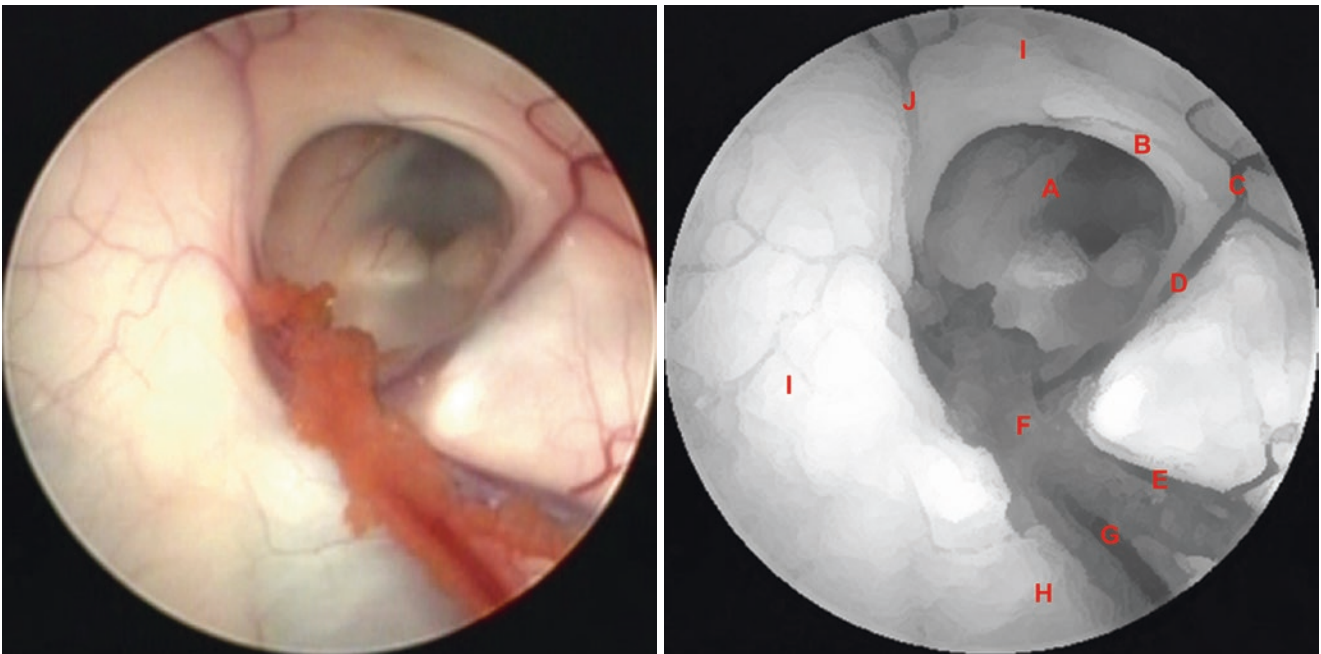


**Fig. 3.13** Normal anatomy. (A) Foramen of Monro, (B) Column of the fornix, (C) Anterior caudate vein, (D) Substitute superior thalamostriate vein [12], (E) Superior thalamostriate vein, (F) Choroid plexus, (G)

Lateral posterior choroidal artery, (H) Thalamus, (I) Septum pellucidum, (J) Anterior septal vein

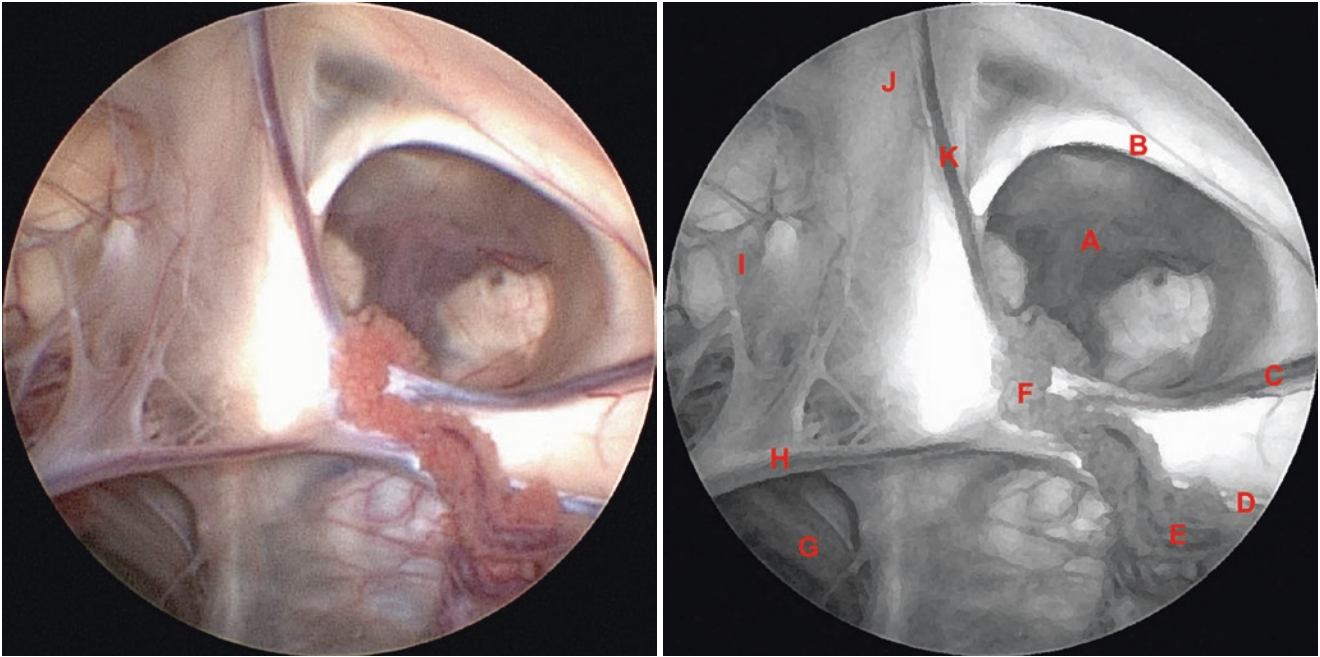


**Fig. 3.14** Normal anatomy. (A) Foramen of Monro, (B) Column of the fornix, (C) Substitute superior thalamostriate vein [12], (D) Superior thalamostriate vein, (E) Superior choroidal vein, (F) Choroid plexus,

(G) Atrium, (H) Posterior septal vein, (I) Spontaneous fenestration in the septum pellucidum, (J) Normal septum pellucidum, (K) Anterior septal vein

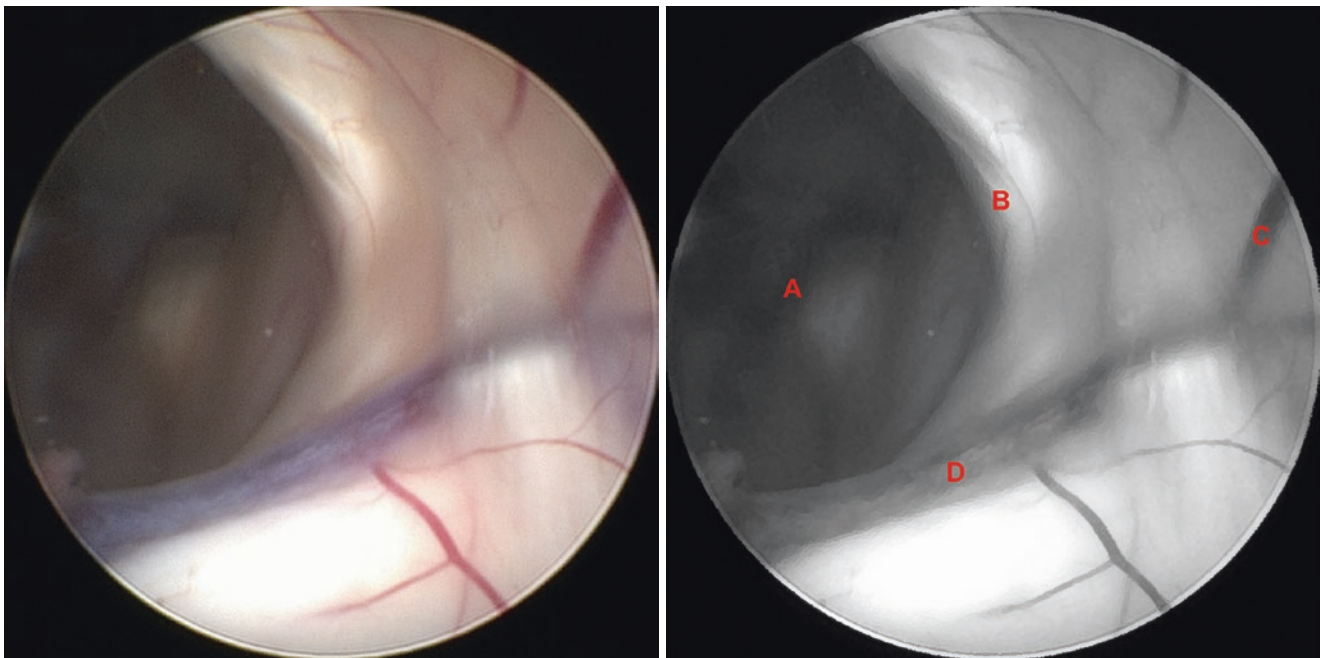


**Fig. 3.15** Normal anatomy. (A) Foramen of Monro, (B) Column of the fornix, (C) Anterior caudate vein, (D) Substitute superior thalamostriate vein [12]

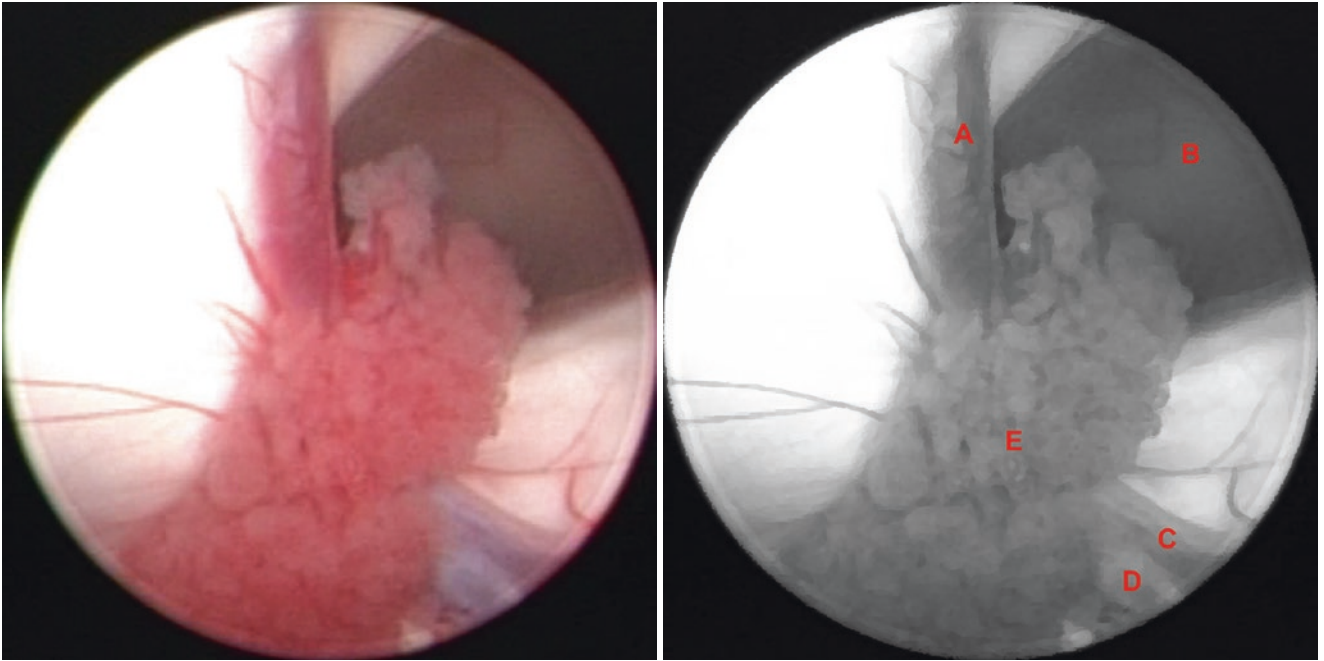


**Fig. 3.16** Normal anatomy. (A) Anterior septal vein, (B) Foramen of Monro, (C) Substitute superior thalamostriate vein [12], (D) Superior thalamostriate vein, (E) Choroid plexus

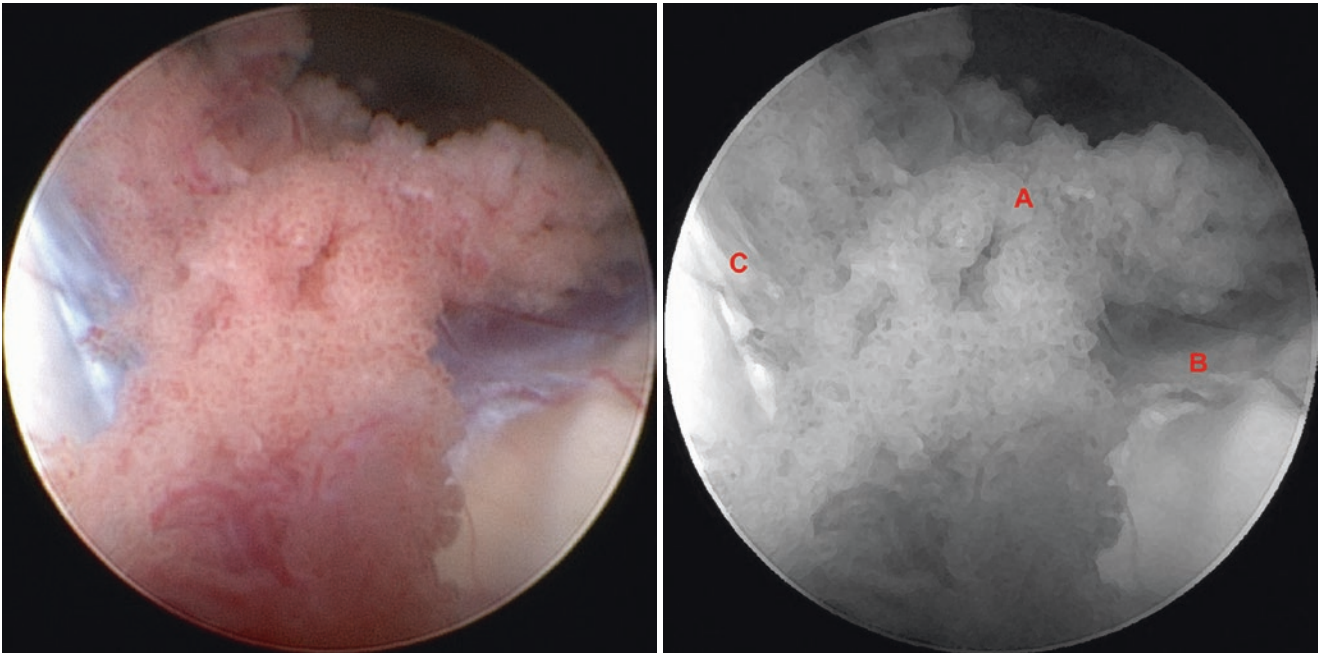


**Fig. 3.17** Normal anatomy. (A) Choroid plexus, (B) Superior thalamostriate vein, (C) Anterior septal vein

### 3.4 Right Lateral Ventricle: Body

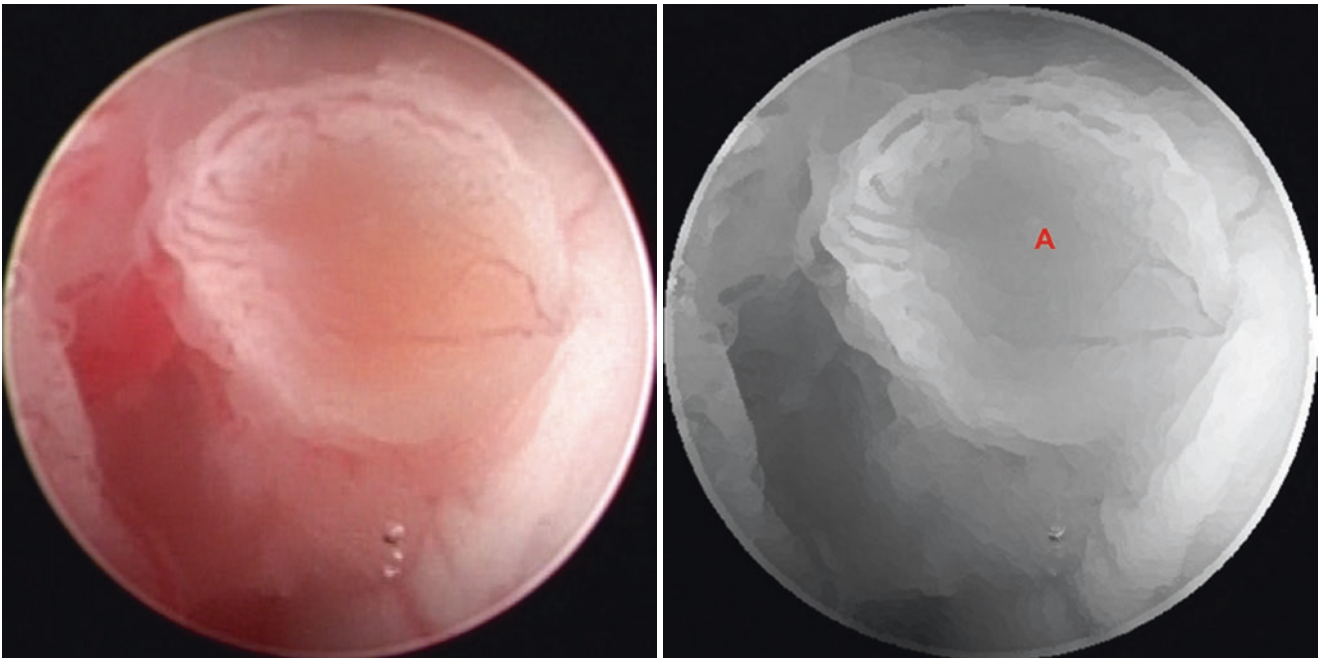


**Fig. 3.18** Normal anatomy. (A) Choroid plexus

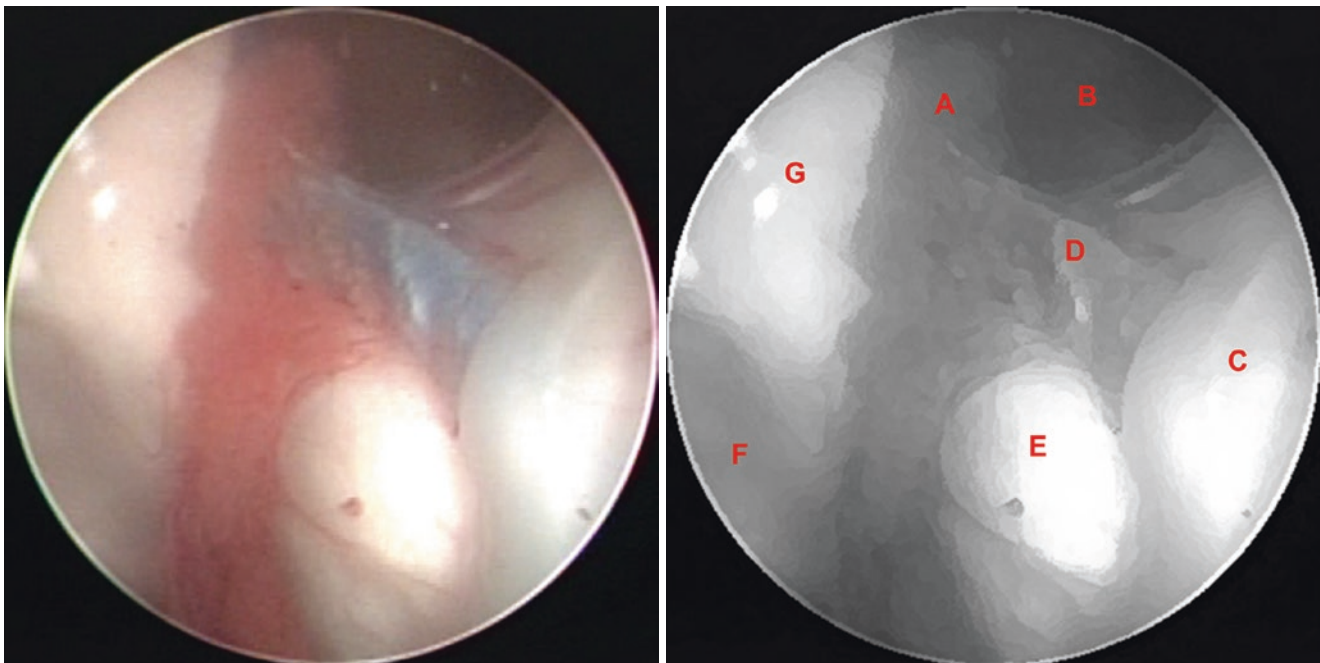


**Fig. 3.19** Normal anatomy. (A) Choroid plexus, (B) Foramen of Monro, (C) Body of the caudate nucleus, (D) Superior thalamostriate vein, (E) Thalamus, (F) Atrium, (G) Body of the fornix

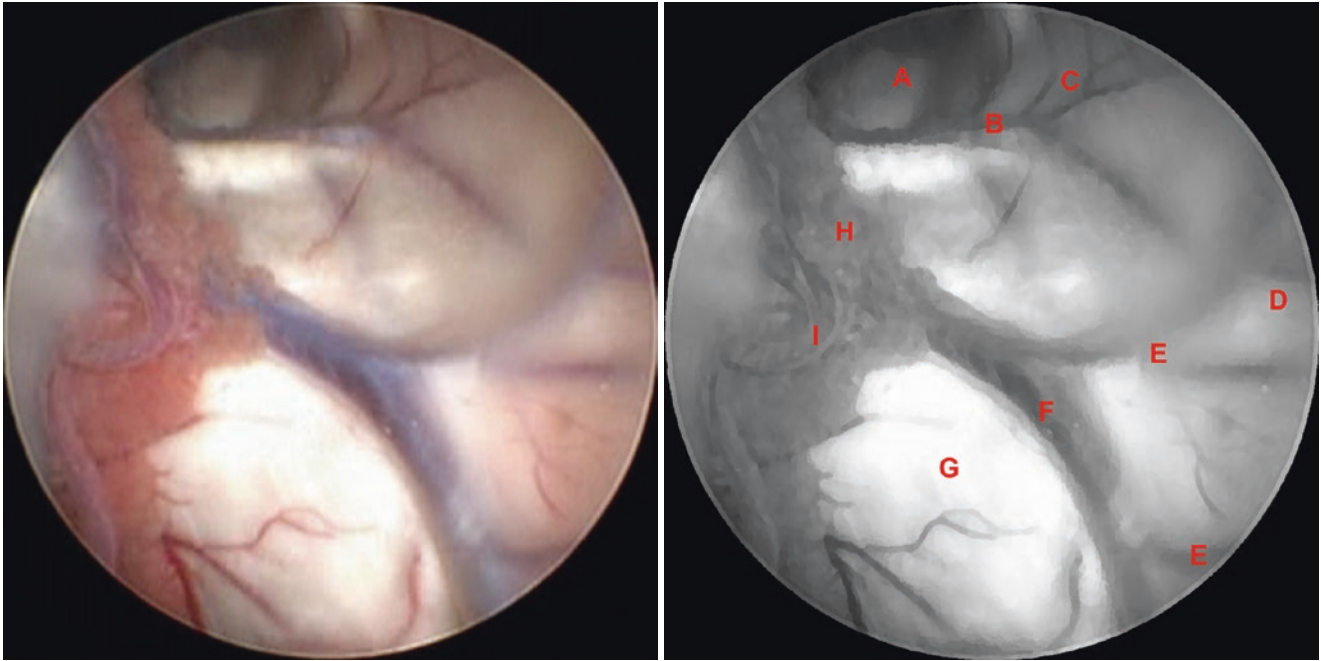


**Fig. 3.20** Normal anatomy. (A) Foramen of Monro, (B) Substitute superior thalamostriate vein [12], (C) Anterior caudate veins, (D) Body of the caudate nucleus, (E) Caudate branches to superior thalamostriate

vein, (F) Superior thalamostriate vein, (G) Thalamus, (H) Choroid plexus, (I) Lateral posterior choroidal artery

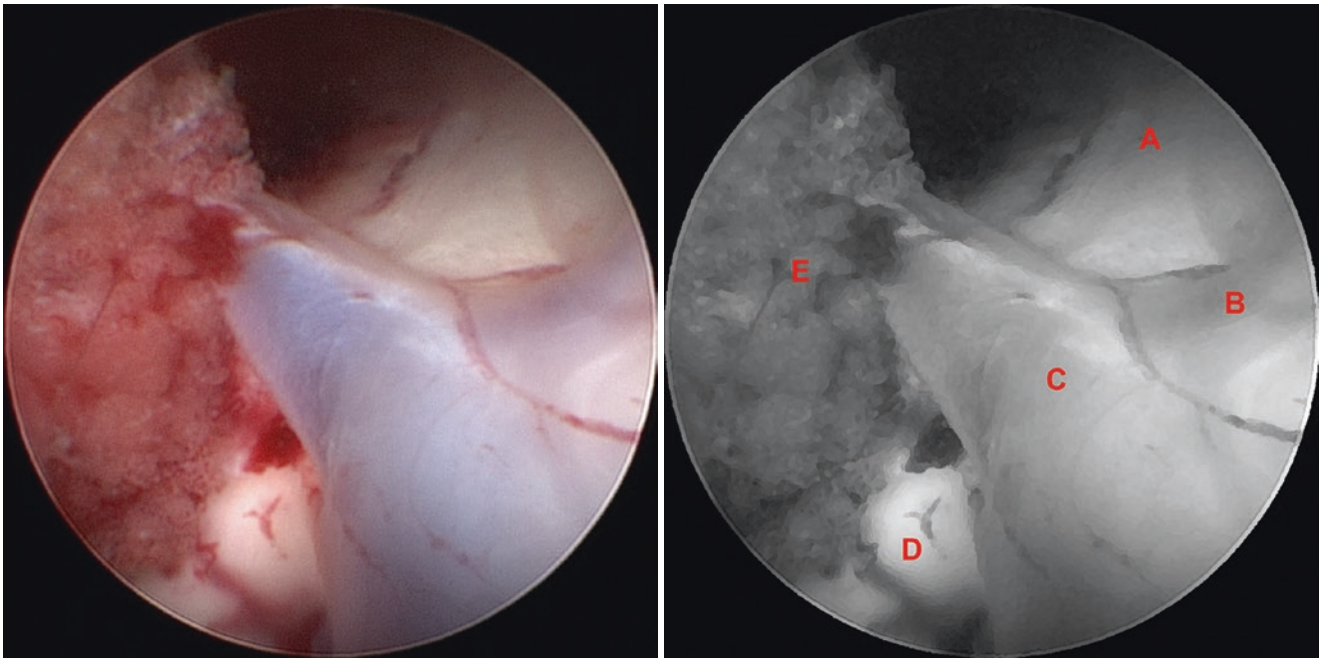


**Fig. 3.21** Normal anatomy. (A) Body of the caudate nucleus, (B) Caudate branch to superior thalamostriate vein, (C) Superior thalamostriate vein, (D) Thalamus, (E) Choroid plexus

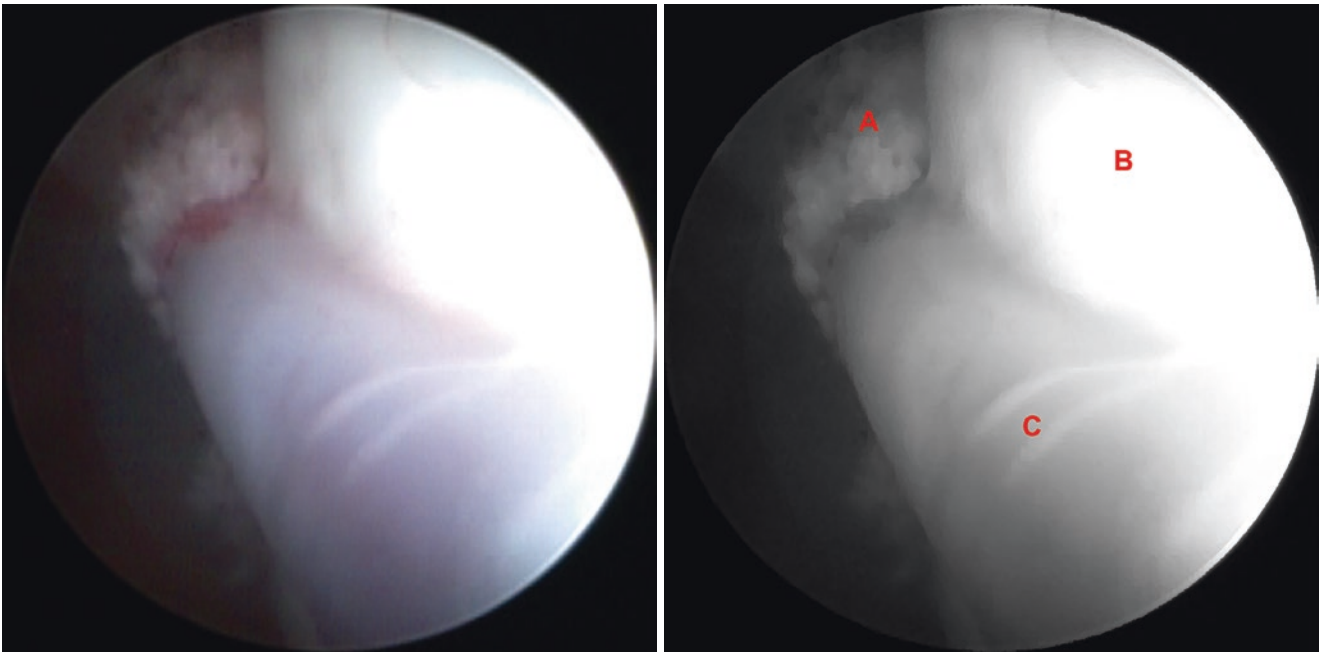


**Fig. 3.22** Normal anatomy. (A) Choroid plexus, (B) Body of the caudate nucleus, (C) Superior thalamostriate vein

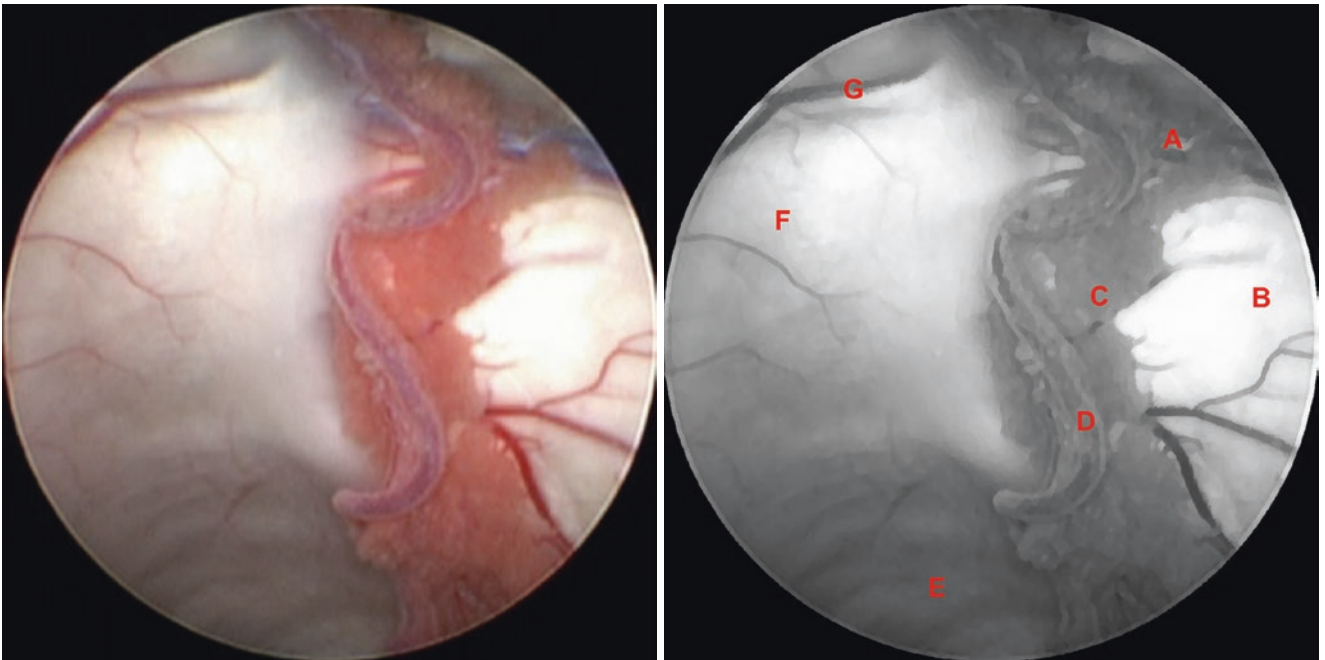


**Fig. 3.23** Normal anatomy. (A) Superior thalamostriate vein, (B) Thalamus, (C) Choroid plexus, (D) Lateral posterior choroidal artery, (E) Atrium, (F) Septum pellucidum, (G) Posterior septal vein



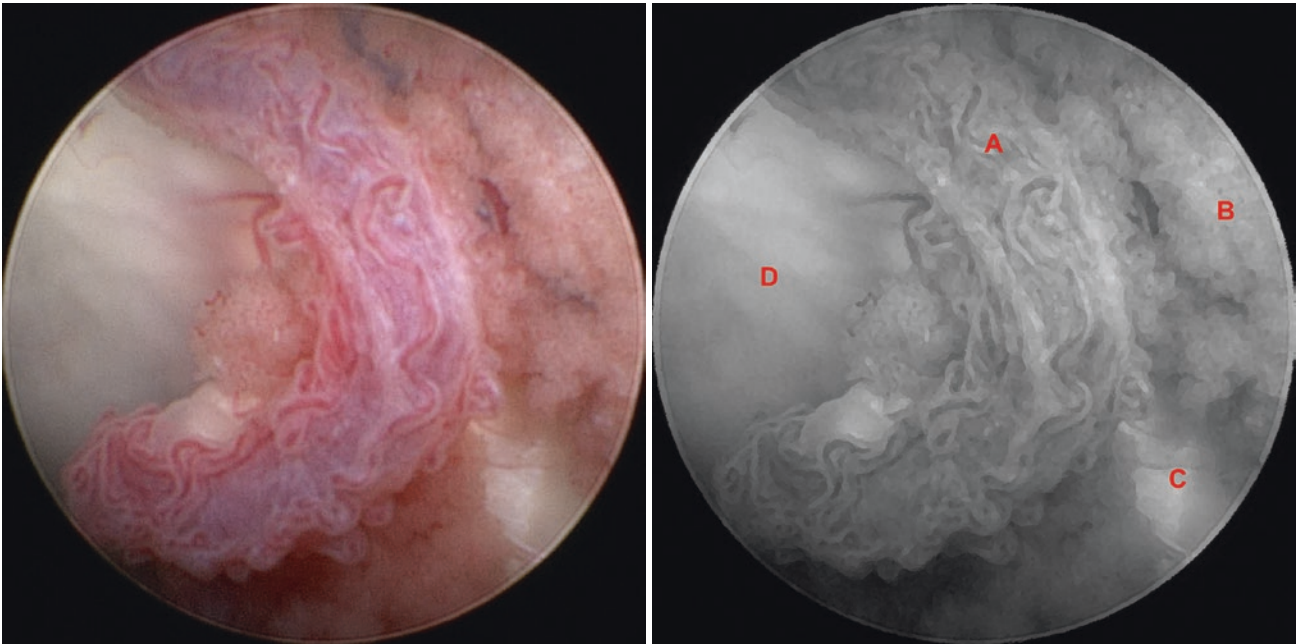


**Fig. 3.24** Normal anatomy. (A) Lateral posterior choroidal artery and vasa vasorum, (B) Choroid plexus, (C) Thalamus, (D) Septum pellucidum

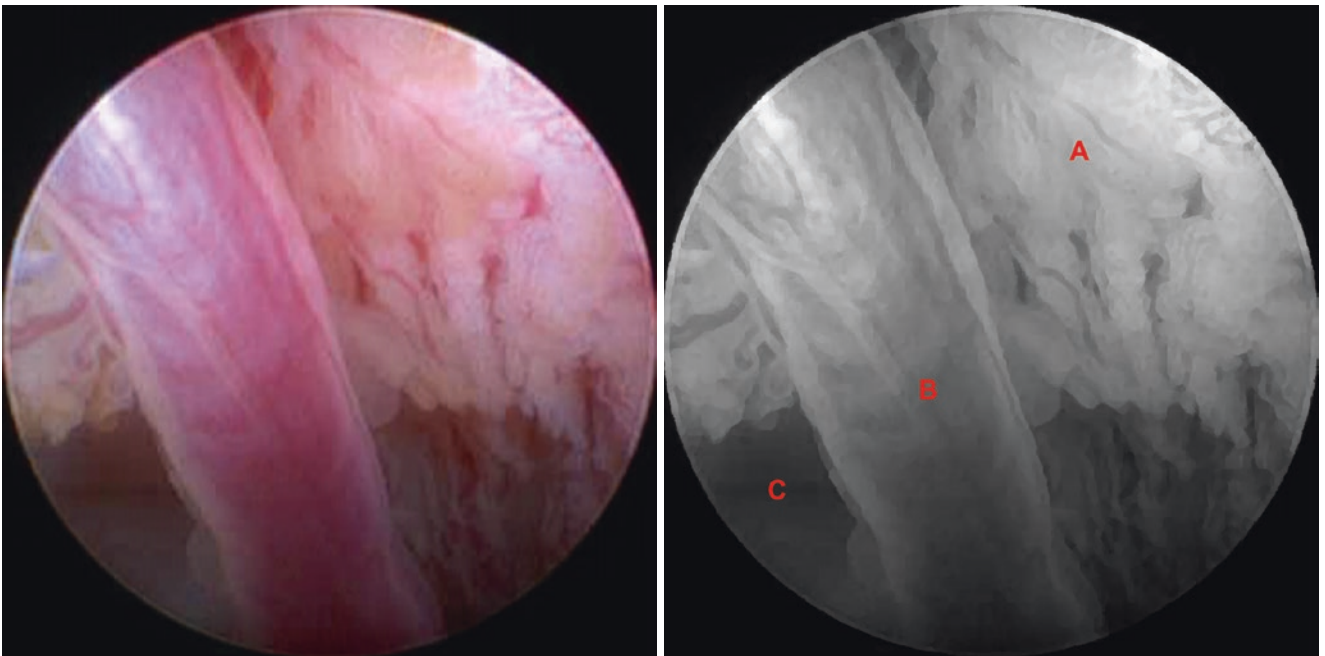


**Fig. 3.25** Normal anatomy. (A) Choroid plexus, (B) Lateral posterior choroidal artery and vasa vasorum, (C) Atrium

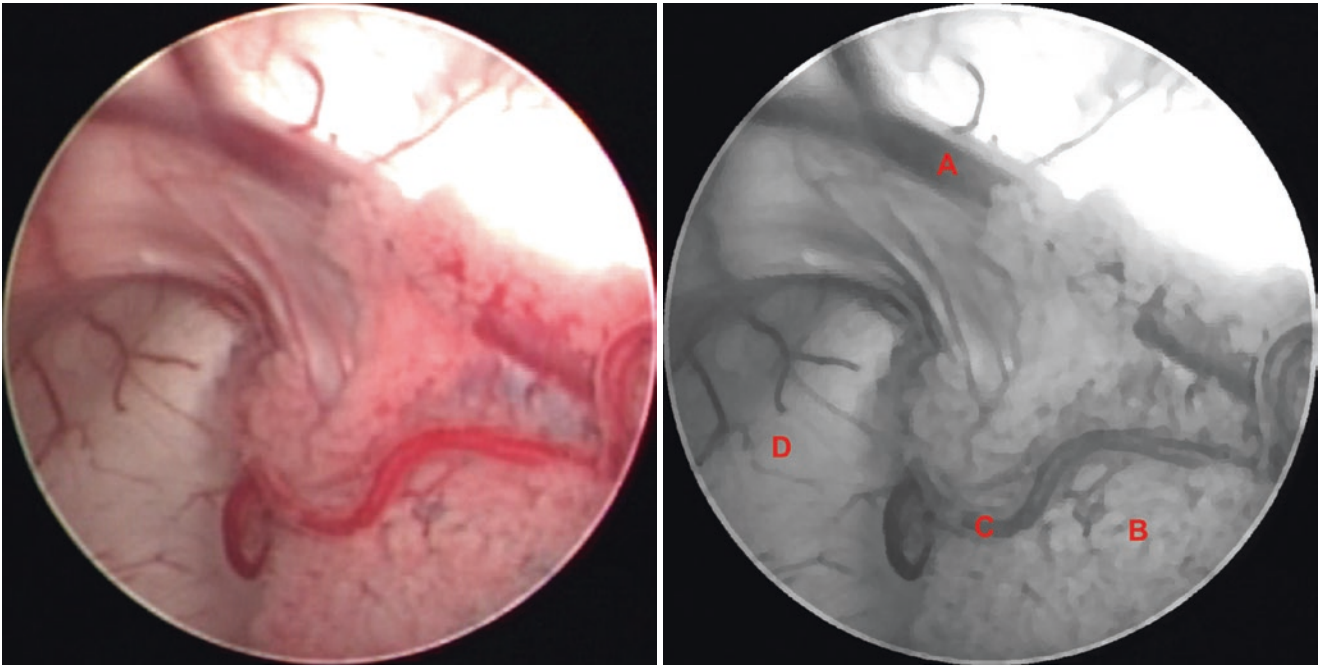


**Fig. 3.26** Normal anatomy. (A) Posterior septal vein, (B) Choroid plexus, (C) Lateral posterior choroidal artery, (D) Atrium

### 3.5 Right Lateral Ventricle: Foramen of Monro Region

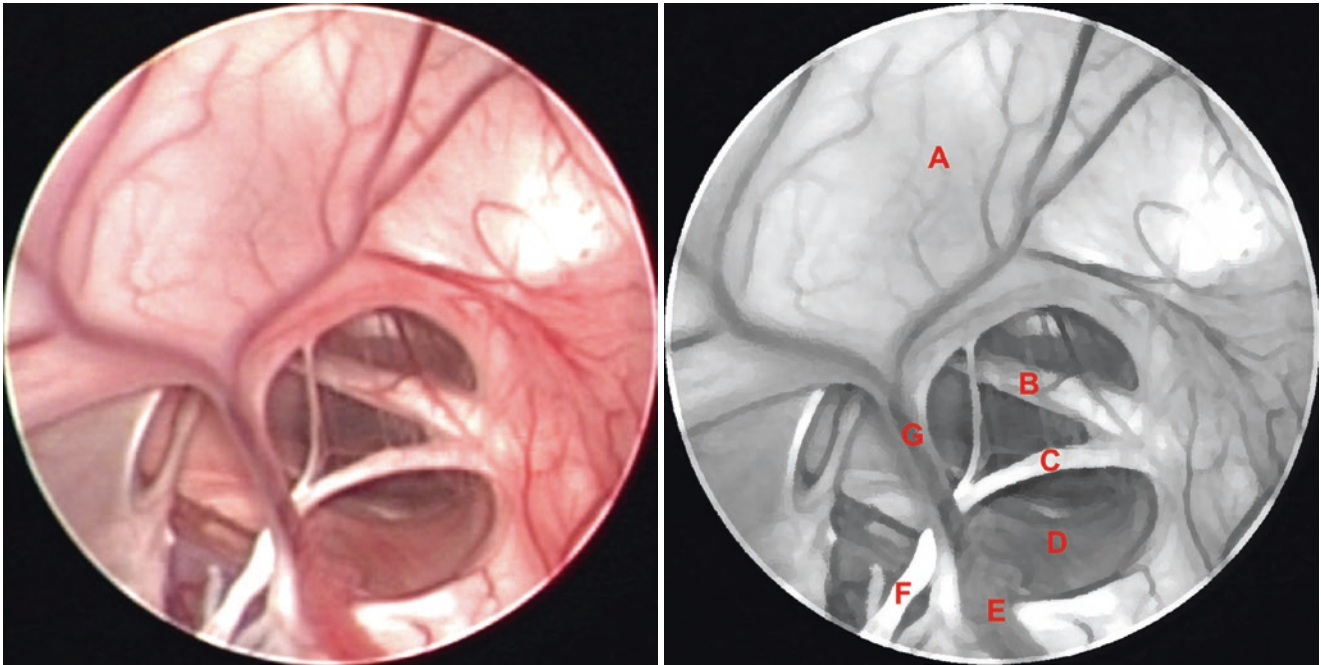


**Fig. 3.27** Abnormal anatomy – untreated chronic hydrocephalus. (A) Septum pellucidum, (B) Interthalamic adhesion seen through spontaneous fenestration at the septum pellucidum, (C) Column of the fornix,

(D) Foramen of Monro, (E) Choroid plexus, (F) Body of the fornix, (G) Anterior septal vein

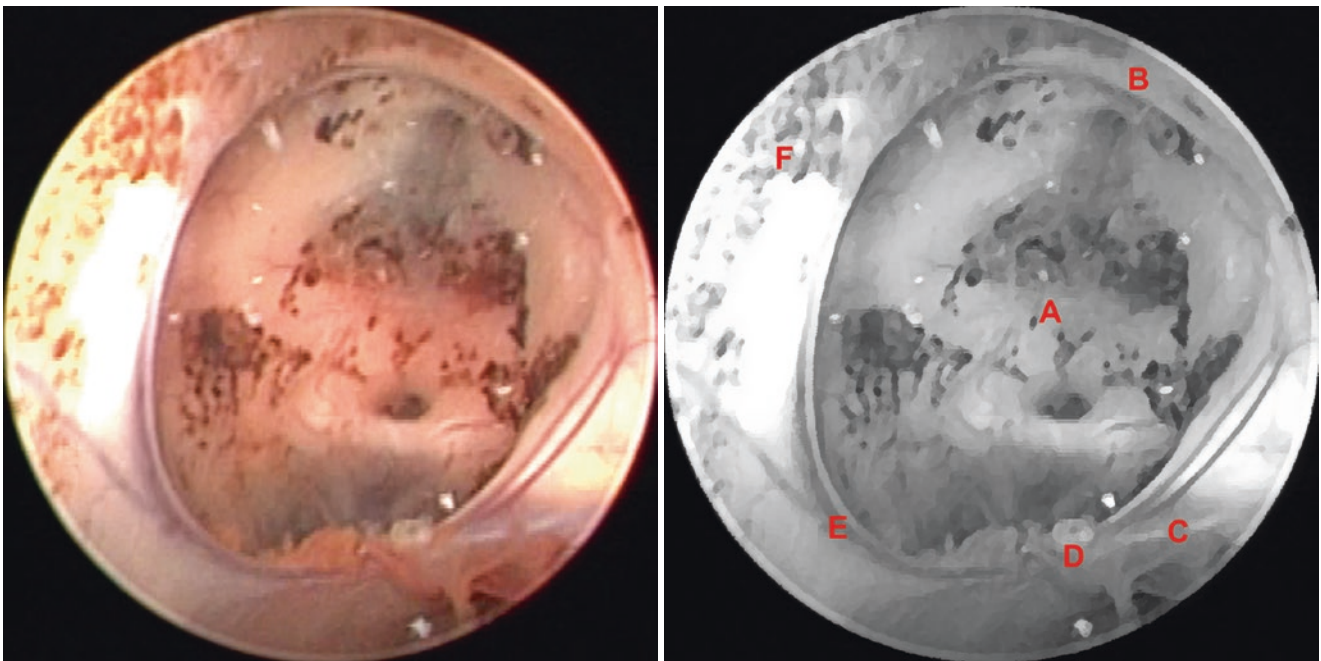


**Fig. 3.28** Abnormal anatomy – late intraventricular hemorrhage. (A) Foramen of Monro, (B) Column of the fornix, (C) Superior thalamostriate vein, (D) Choroid plexus, (E) Anterior septal vein, (F) Septum pellucidum,

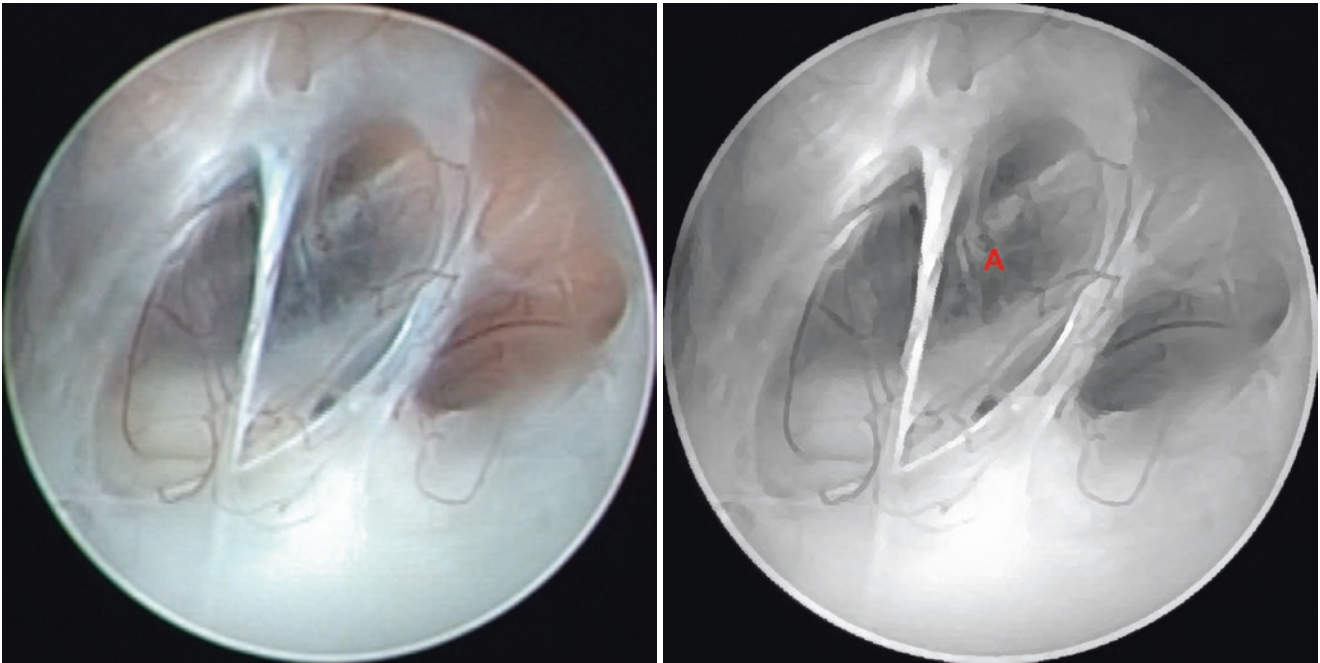


**Fig. 3.29** Abnormal anatomy – congenital membrane over the foramen of Monro. (A) Membrane over foramen of Monro

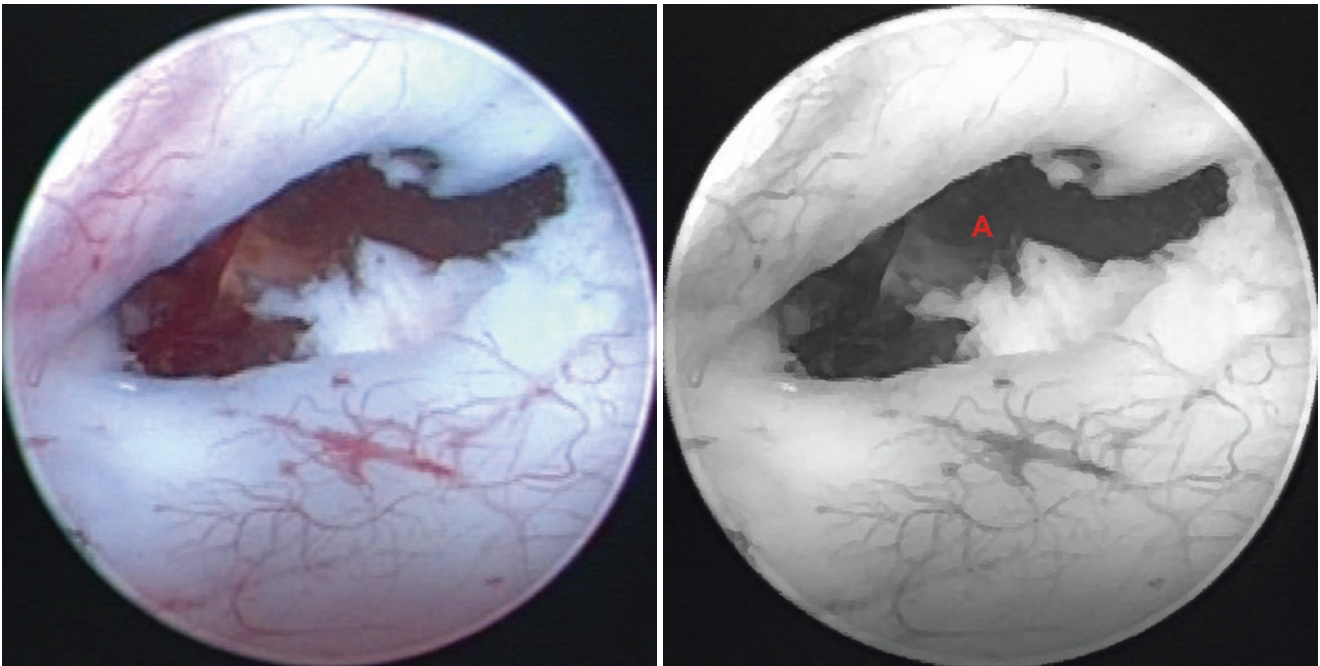


**Fig. 3.30** Abnormal anatomy – postinfectious aspect of the foramen of Monro. (A) Foramen of Monro

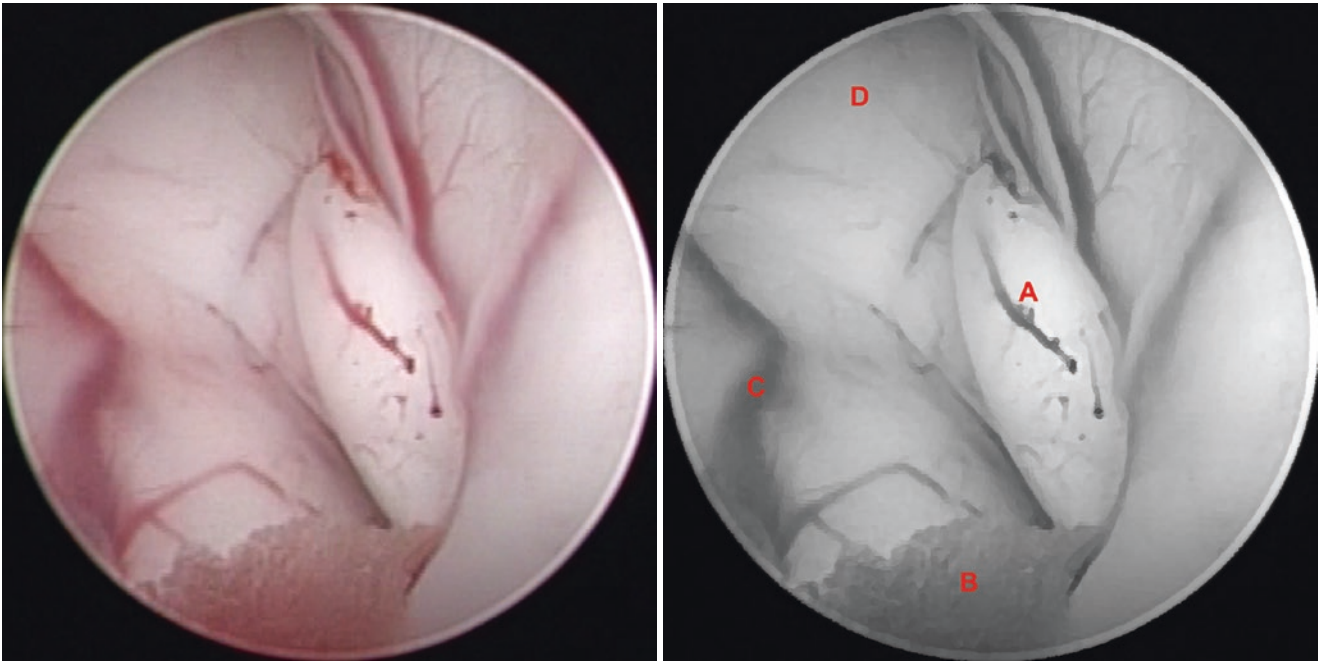


**Fig. 3.31** Abnormal anatomy – postinfectious occlusion of the foramen of Monro. (A) Occluded foramen of Monro, (B) Choroid plexus, (C) Anterior septal vein, (D) Septum pellucidum

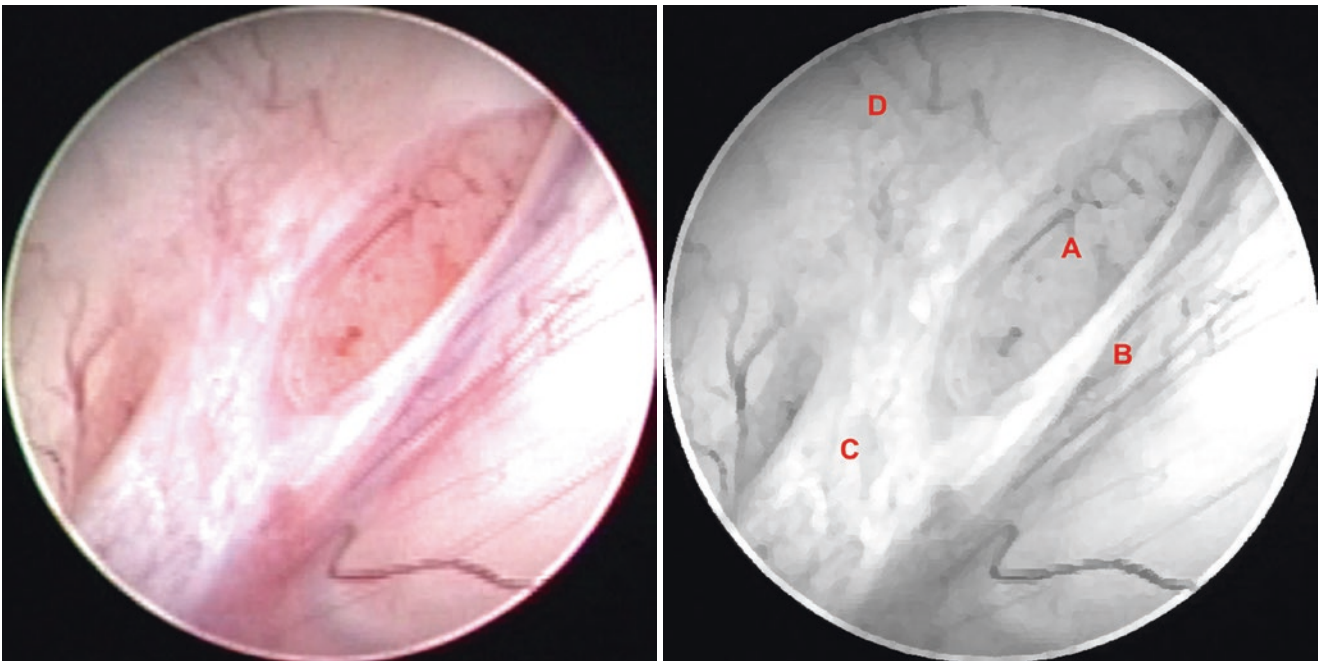


**Fig. 3.32** Abnormal anatomy – postinfectious occlusion of the foramen of Monro. (A) foramen of Monro occluded by the choroid plexus, (B) Superior thalamostriate vein, (C) Chronic inflammatory process, (D) Septum pellucidum

### 3.6 Left Lateral Ventricle: Foramen of Monro Region

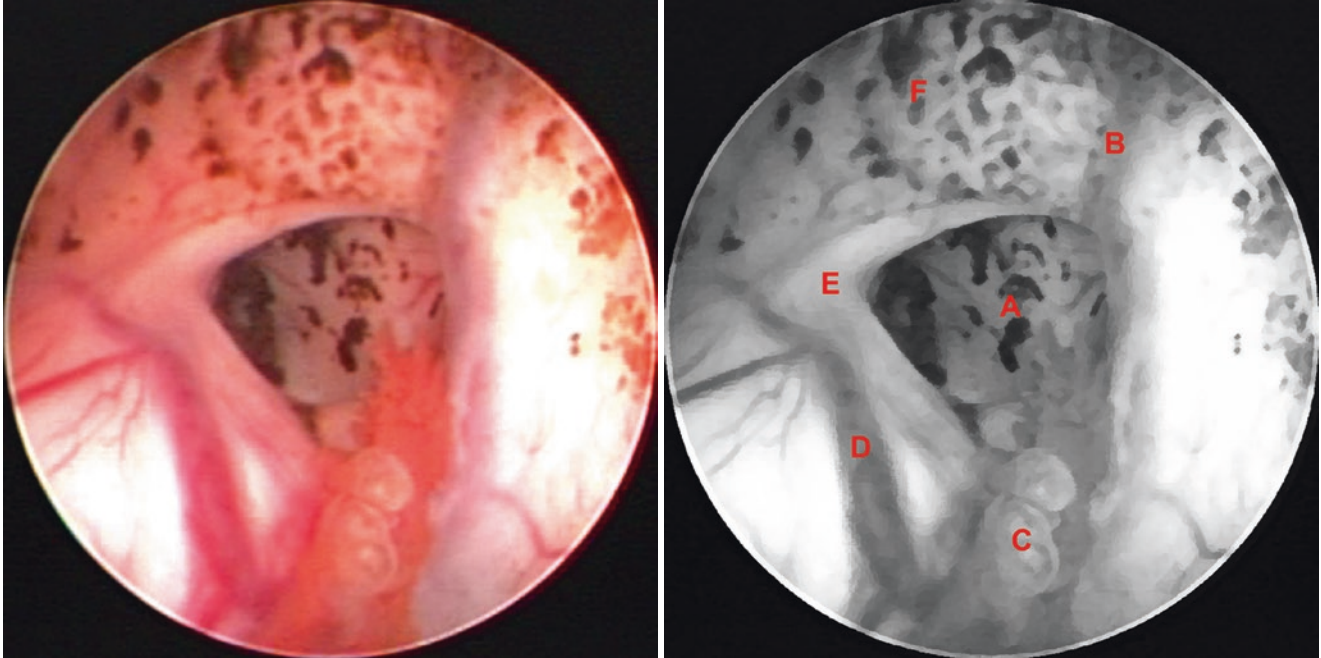


**Fig. 3.33** Surgical procedure – Monro foraminoplasty in a 1-month-old baby. (A) Foramen of Monro, (B) Anterior septal vein, (C) Choroid plexus, (D) Superior thalamostriate vein, (E) Column of the fornix, (F) Septum pellucidum

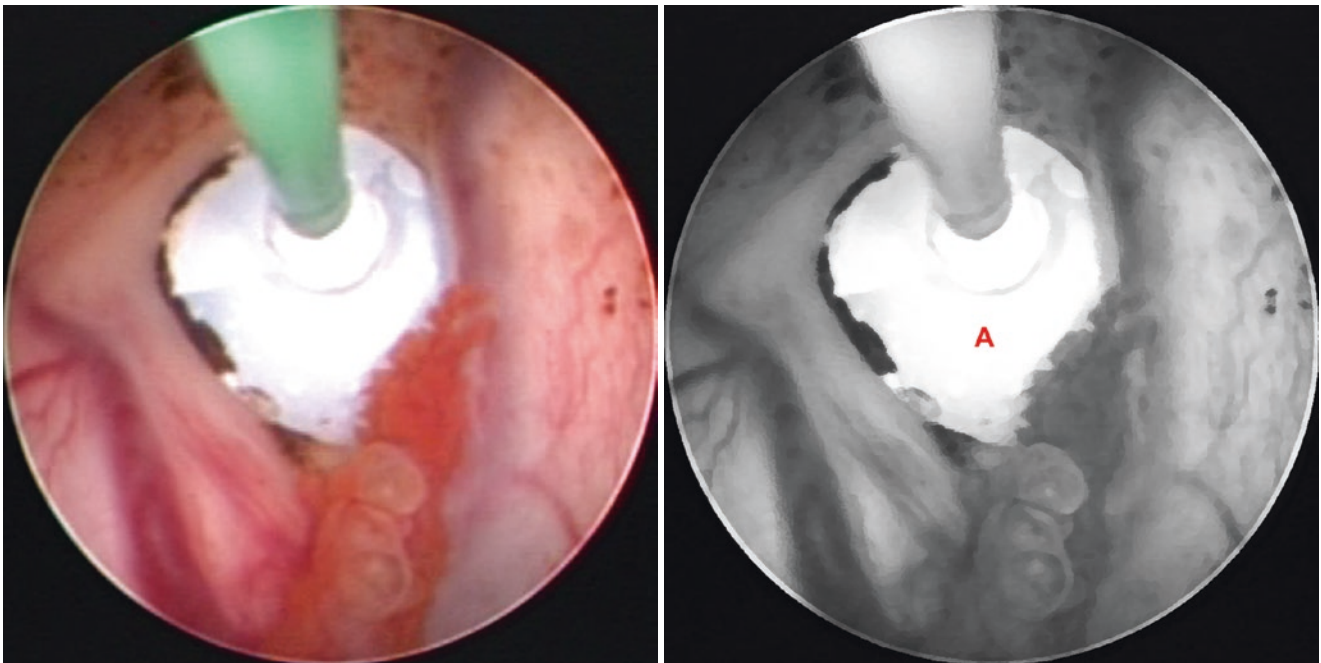


**Fig. 3.34** Surgical procedure – Monro foraminoplasty in a 1-month-old baby. (A) Fogarty balloon catheter

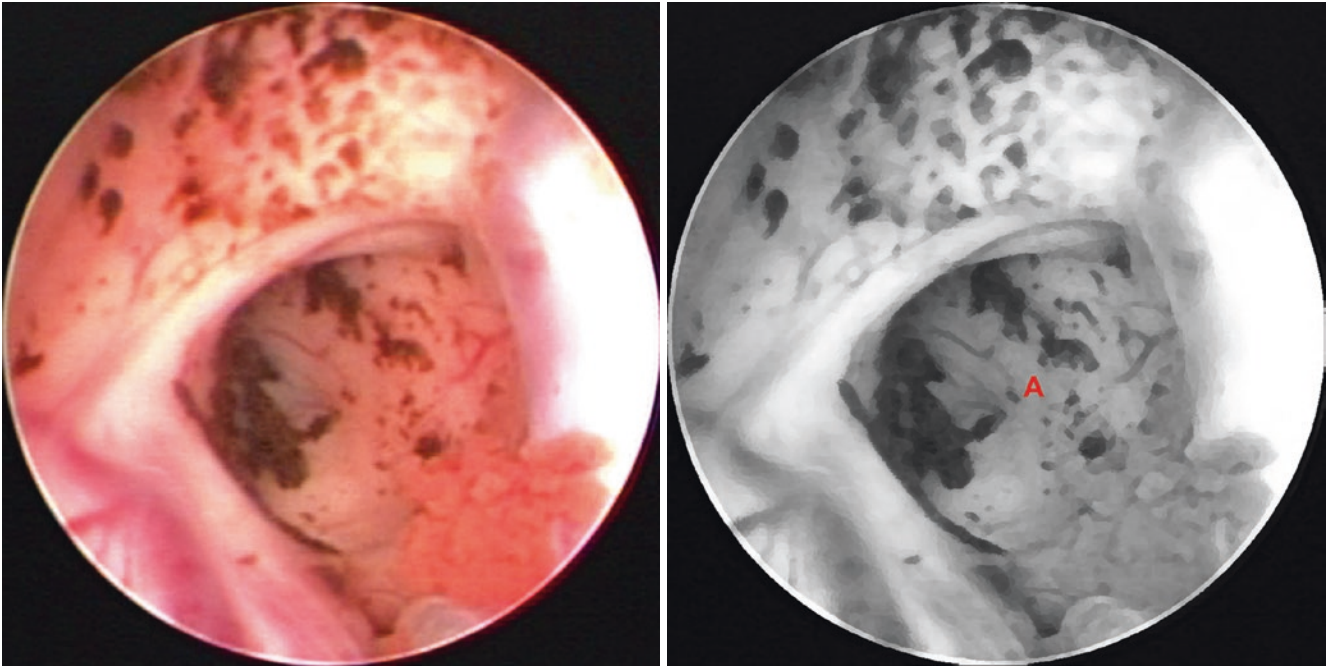


**Fig. 3.35** Surgical procedure – Monro foraminoplasty in a 1-month-old baby. (A) Dilated foramen of Monro

### 3.7 Right Lateral Ventricle: Foramen of Monro Region

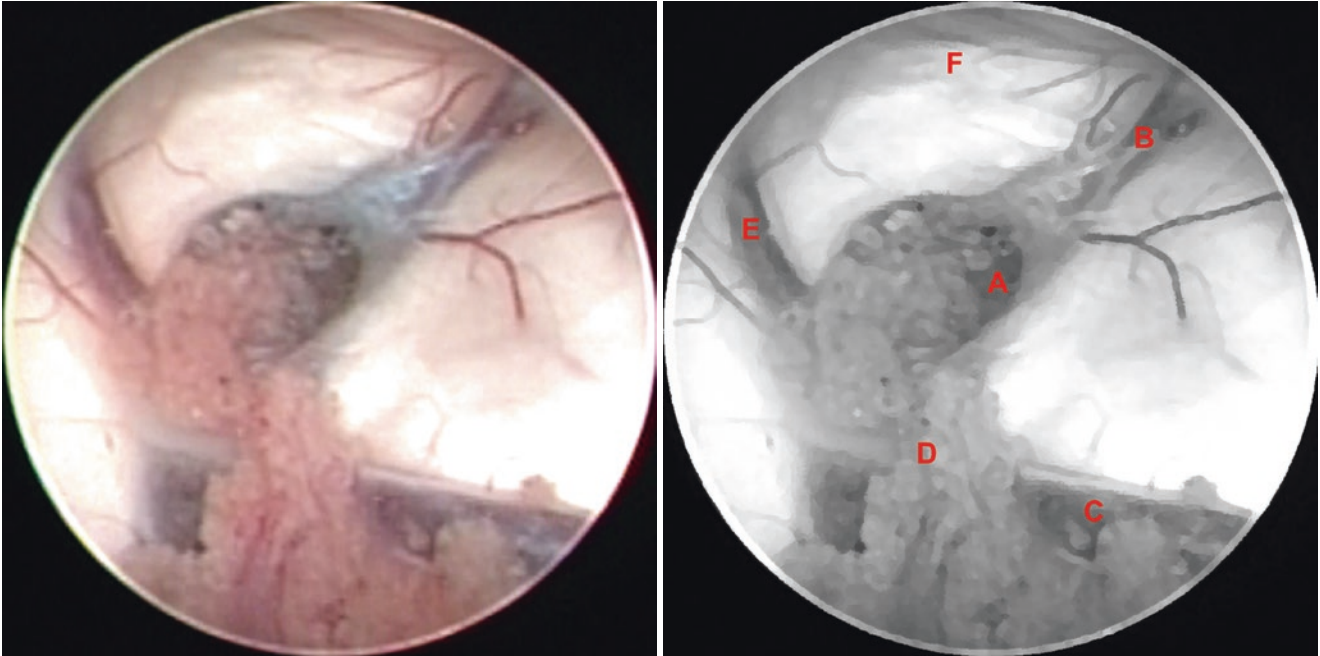


**Fig. 3.36** Surgical procedure – Monro foraminoplasty in an adult. (A) Foramen of Monro, (B) Anterior caudate vein, (C) Superior thalamostriate vein, (D) Choroid plexus, (E) Anterior septal vein, (F) Septum pellucidum

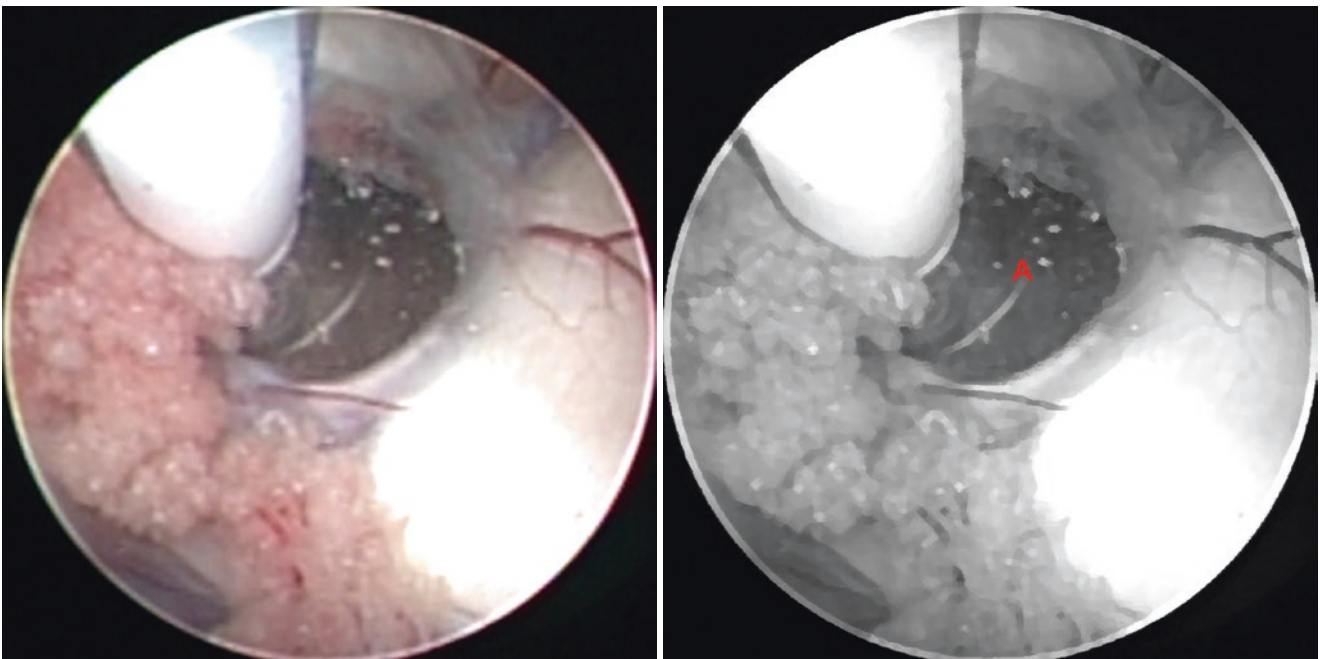


**Fig. 3.37** Surgical procedure – Monro foraminoplasty in an adult. (A) Fogarty balloon catheter



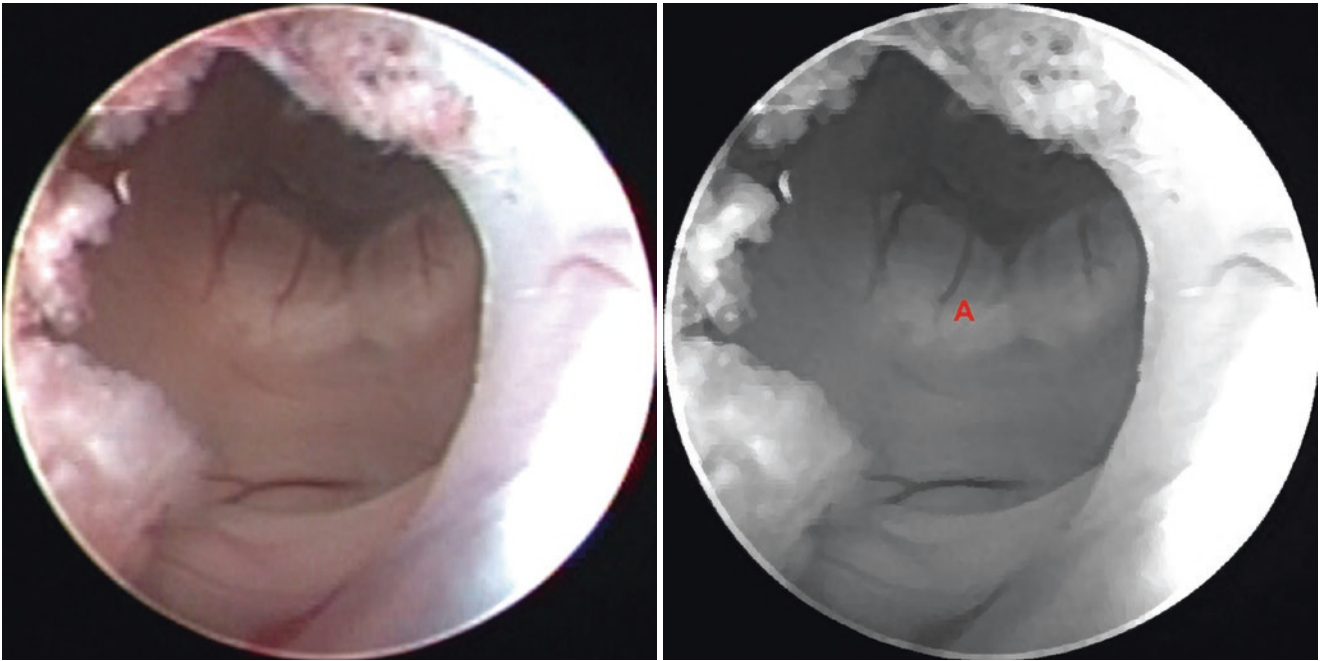


**Fig. 3.38** Surgical procedure – Monro foraminoplasty in an adult. (A) Dilated foramen of Monro

### 3.8 Right Lateral Ventricle: Body

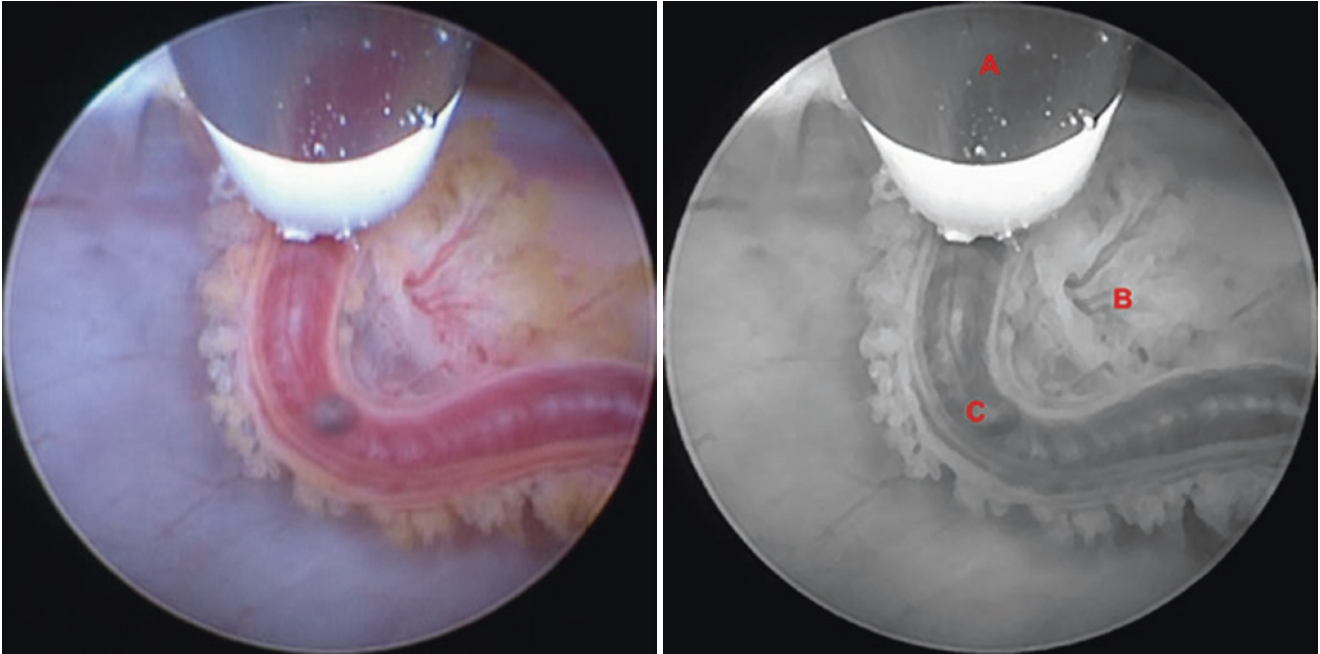


**Fig. 3.39** Surgical procedure – choroid plexus coagulation. (A) Bipolar coagulation electrode, (B) Choroid plexus, (C) Lateral posterior choroidal artery

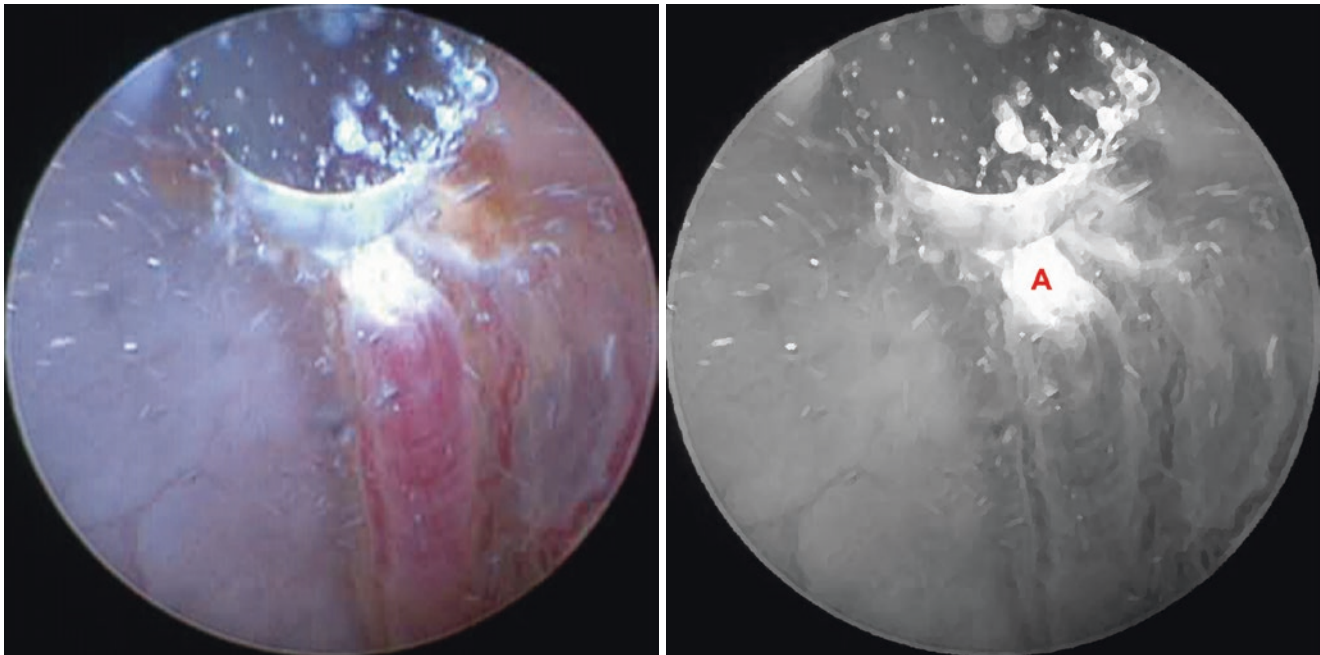


**Fig. 3.40** Surgical procedure – choroid plexus coagulation. (A) Bipolar coagulation of the lateral posterior choroidal artery

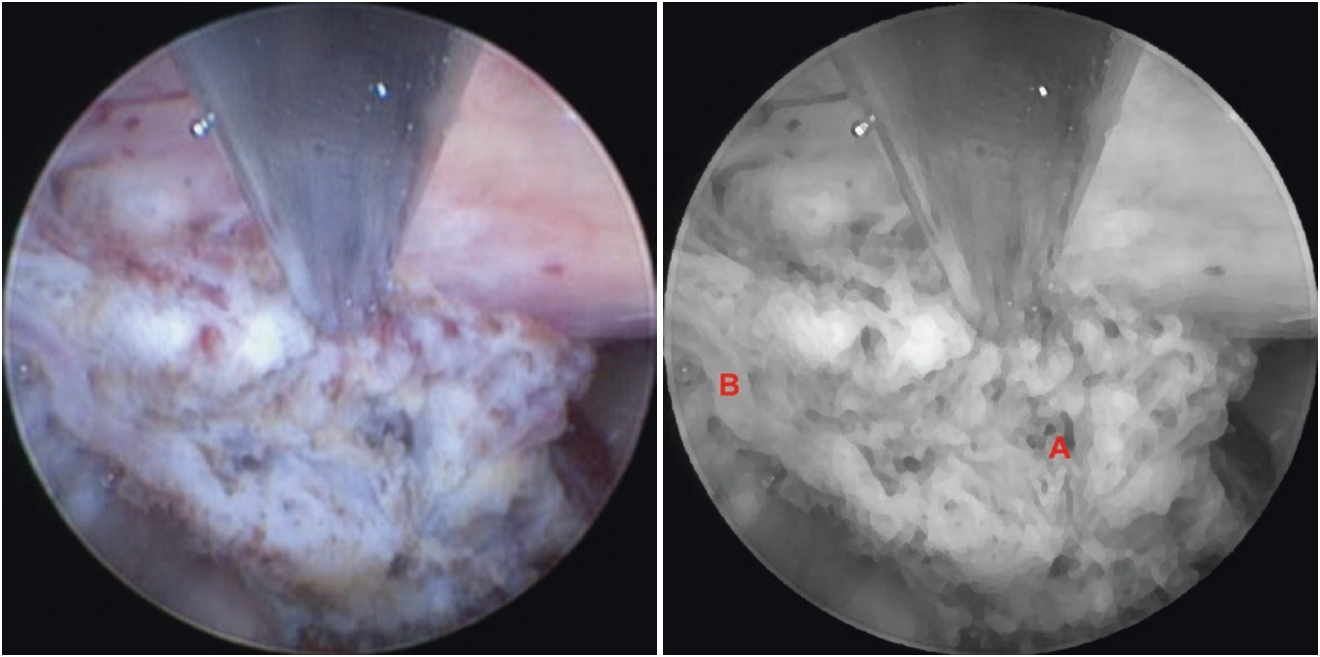


**Fig. 3.41** Surgical procedure – choroid plexus coagulation. (A) Coagulation of the choroid glomus, (B) Coagulated lateral posterior choroidal artery

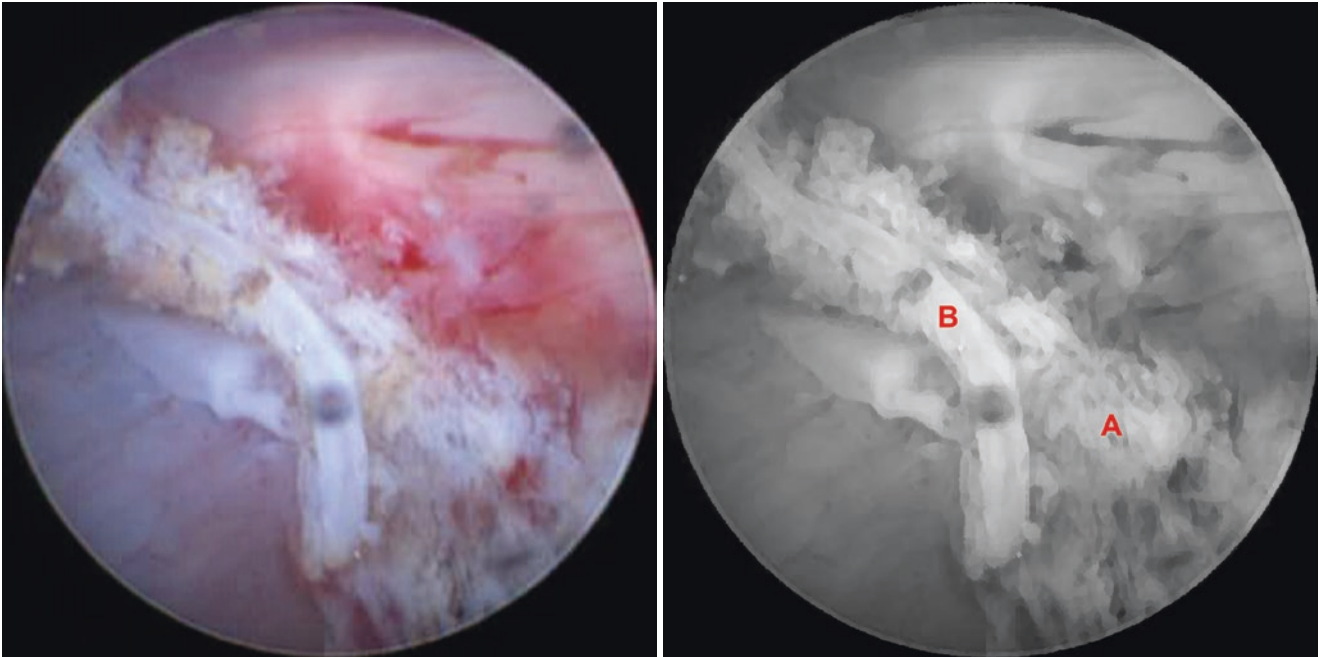


**Fig. 3.42** Surgical procedure – choroid plexus coagulation. (A) Coagulated choroid plexus, (B) Coagulated lateral posterior choroidal artery

### 3.9 Right Lateral Ventricle: Foramen of Monro Region

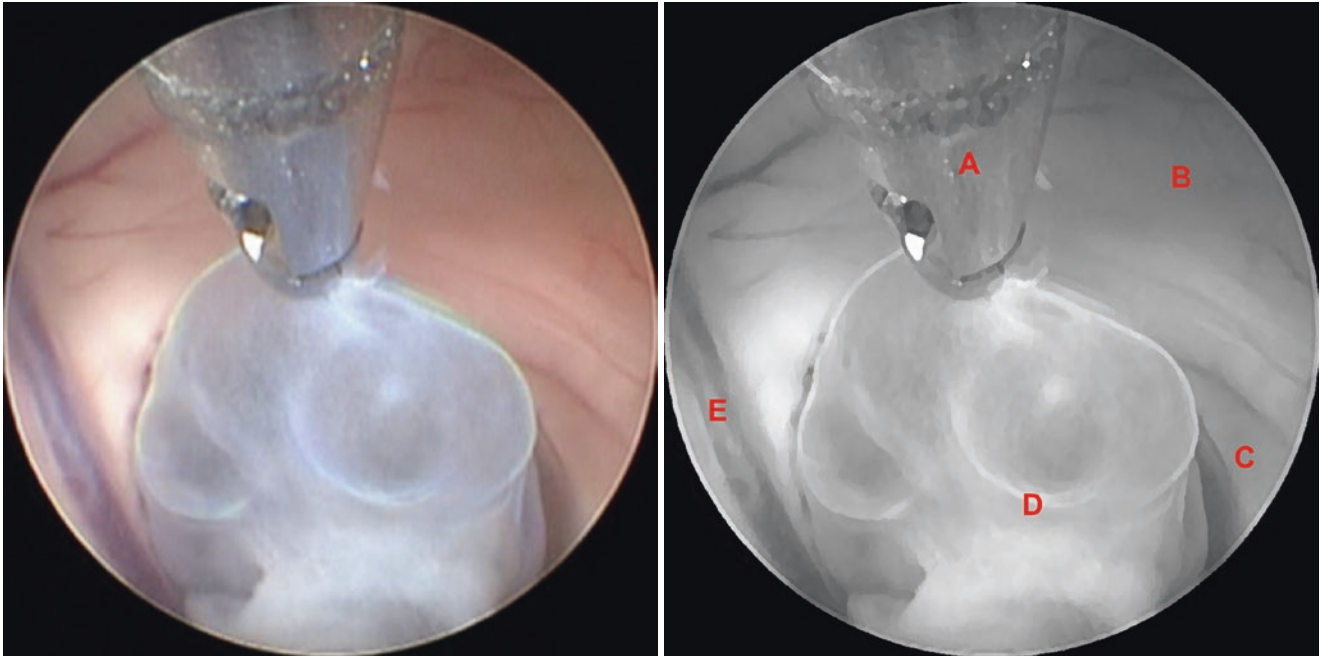


**Fig. 3.43** Surgical procedure – resection of intraventricular racemose neurocysticercosis. (A) Grasping forceps, (B) Septum pellucidum, (C) Column of the fornix, (D) Cyst of racemose neurocysticercosis, (E) Anterior septal vein

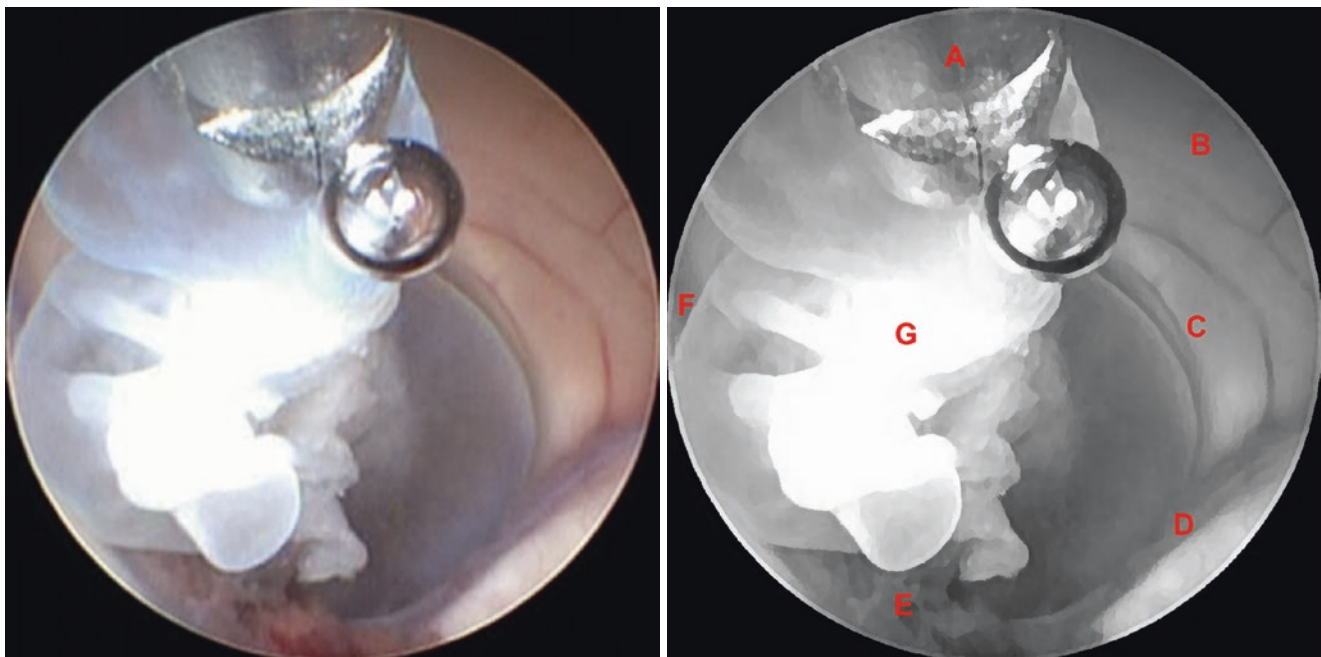


**Fig. 3.44** Surgical procedure – resection of intraventricular racemose neurocysticercosis. (A) Grasping forceps, (B) Septum pellucidum, (C) Column of the fornix, (D) Superior thalamostriate vein, (E) Choroid plexus, (F) Anterior septal vein, (G) Cyst of racemose neurocysticercosis

Illustrative case 1 – fenestration of a giant infra/supratentorial arachnoid cyst.

Clinical data: 8-year-old child, headache.



**Fig. 3.45** Coronal T2-weighted magnetic resonance imaging (MRI) showing an infra/supratentorial arachnoid cyst



**Fig. 3.46** Sagittal T2-weighted MRI showing an infra/supratentorial arachnoid cyst

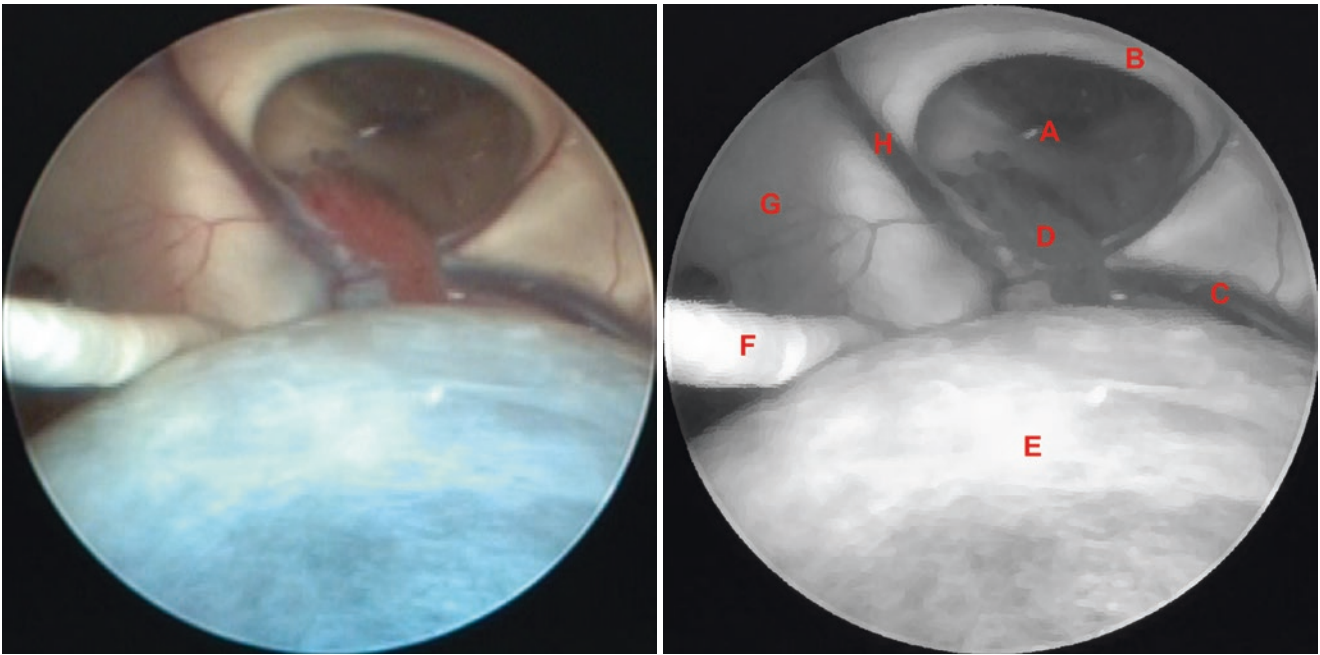


**Fig. 3.47** Illustrative case 1 – fenestration of a giant infra/supratentorial arachnoid cyst. (A) Foramen of Monro, (B) Column of the fornix, (C) Superior thalamostriate vein, (D) Choroid plexus, (E) Giant arach-

noid cyst, (F) Chronic intraventricular adhesion, (G) Septum pellucidum, (H) Anterior septal vein

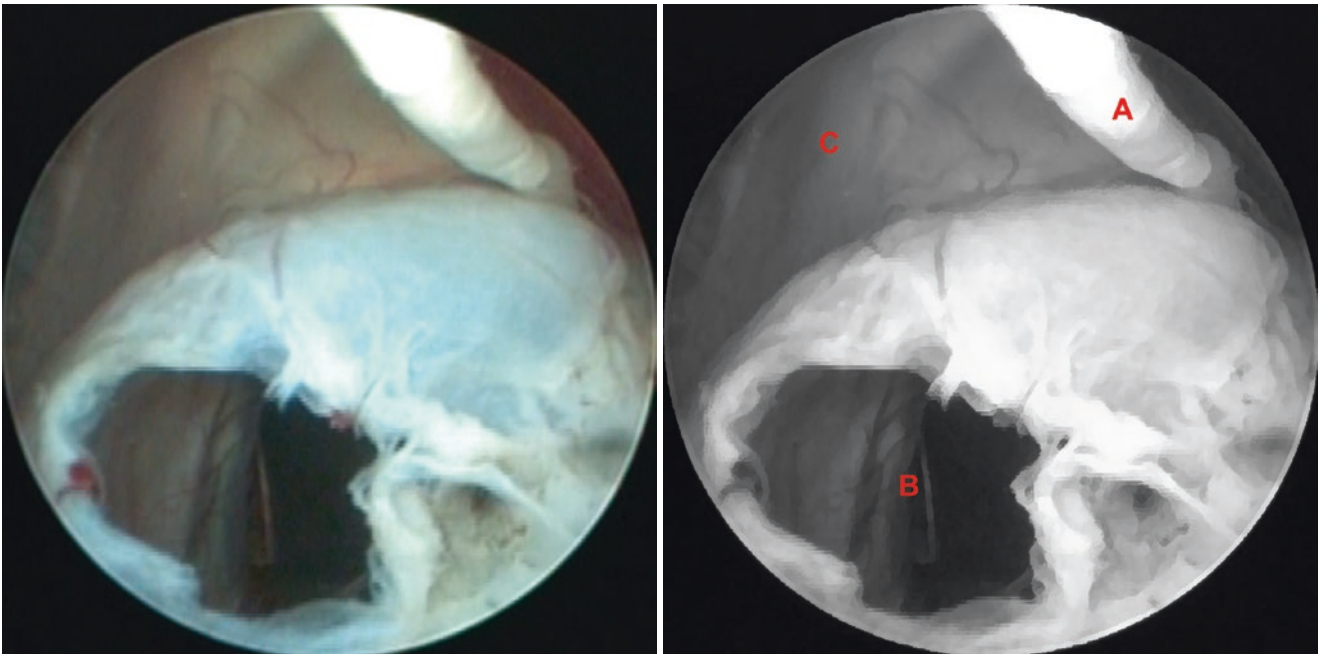


**Fig. 3.48** Illustrative case 1 – fenestration of a giant infra/supratentorial arachnoid cyst. (A) Chronic intraventricular adhesion, (B) Fenestrated cyst, (C) Septum pellucidum

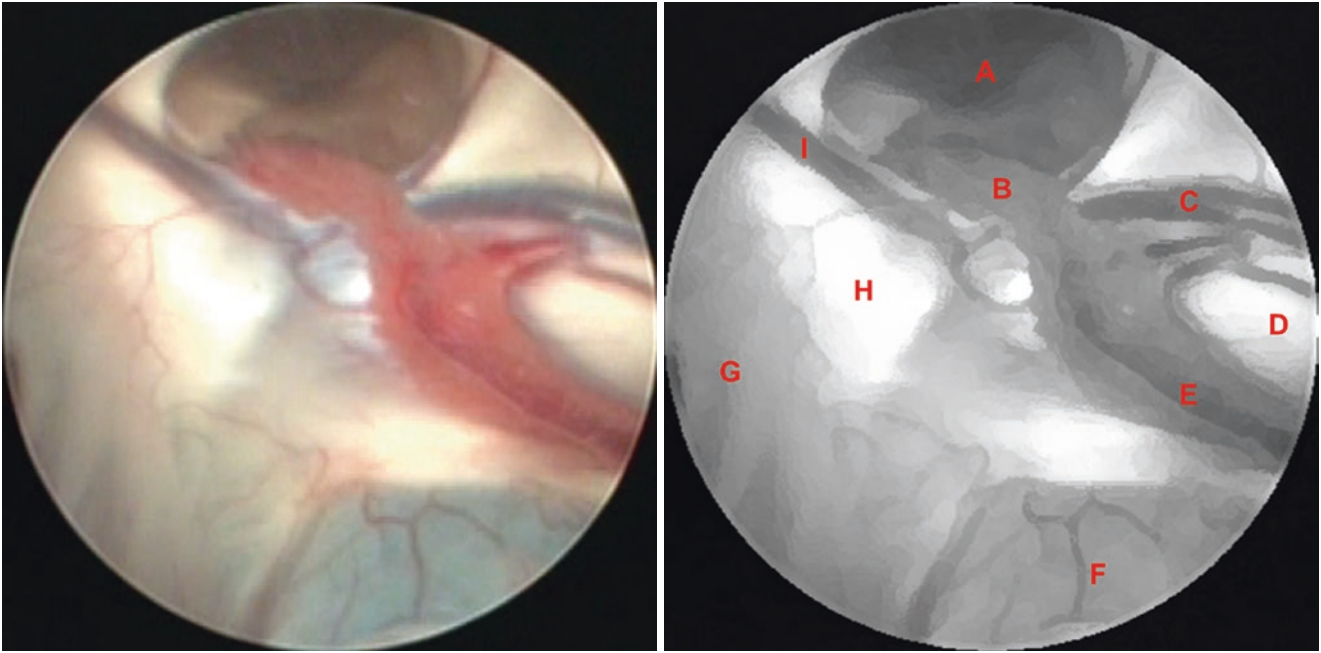


**Fig. 3.49** Illustrative case 1 – fenestration of a giant infra/supratentorial arachnoid cyst. (A) Foramen of Monro, (B) Choroid plexus, (C) Superior thalamostriate vein, (D) Thalamus, (E) Superior choroidal

vein, (F) Reduced arachnoid cyst, (G) Septum pellucidum, (H) Body of the fornix, (I) Anterior septal vein

Illustrative case 2 – colloid cyst.

Clinical data: 56-year-old, headache.

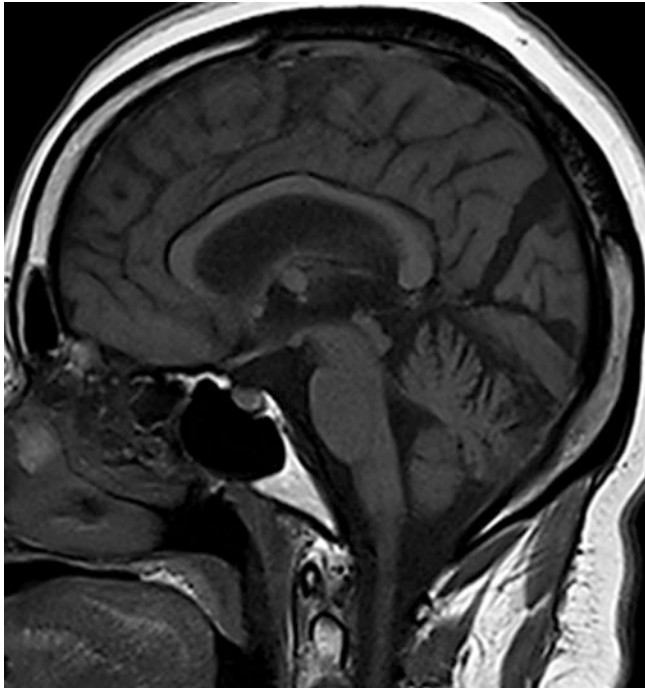


**Fig. 3.50** Sagittal T1-weighted MRI showing a colloid cyst in the third ventricle



**Fig. 3.51** Axial T2-weighted MRI showing a colloid cyst in the third ventricle exactly at the midline

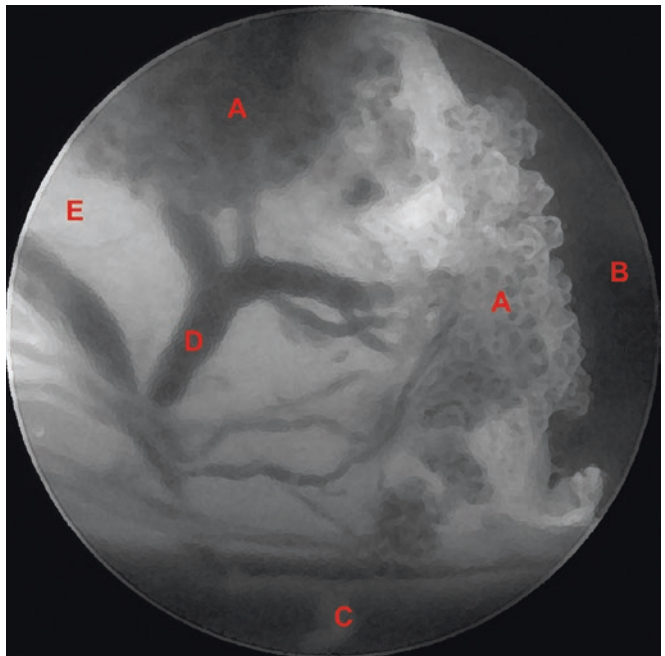
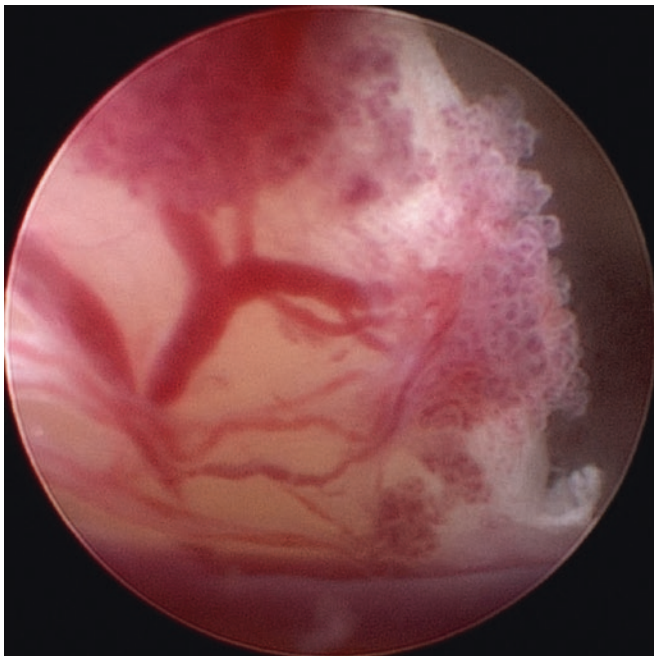


**Fig. 3.52** Illustrative case 2 – colloid cyst. (A) Choroid plexus over colloid cyst, (B) Third ventricle, (C) Superior thalamostriate vein, (D) Tumor vessels, (E) Tumor wall



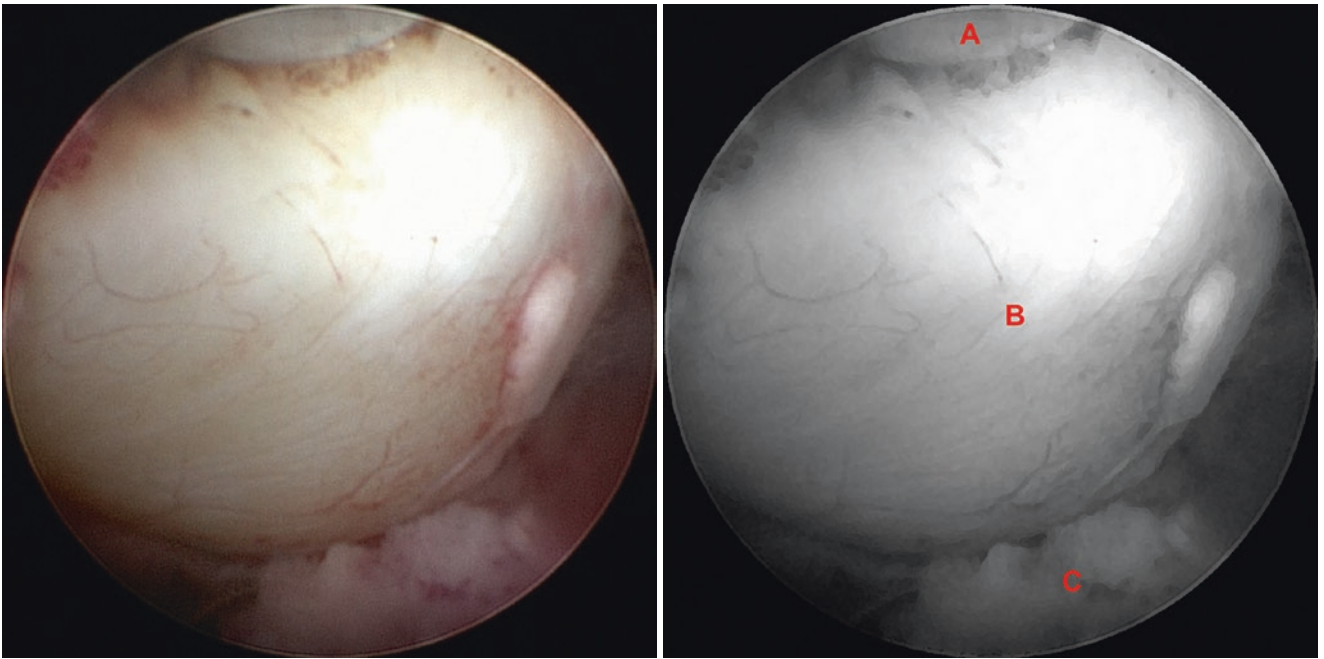


**Fig. 3.53** Illustrative case 2 – colloid cyst. (A) Bipolar coagulation electrode, (B) Tumor wall, (C) Choroid plexus

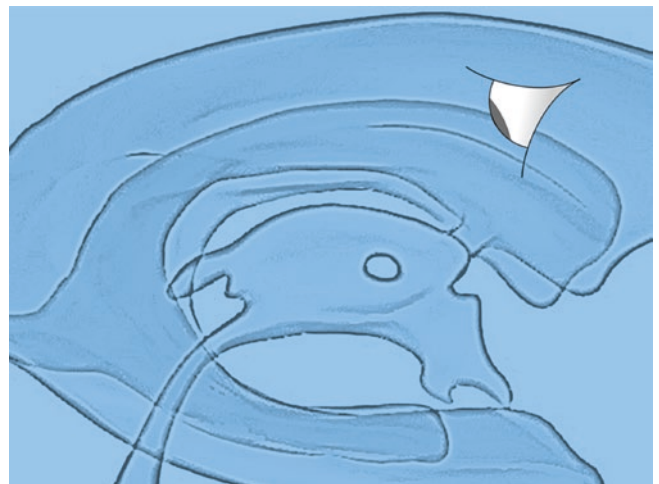


**Fig. 3.54** Direction of the endoscopic vision for the septum pellucidum from the right lateral ventricle

### 3.10 Right Lateral Ventricle: Septum Pellucidum

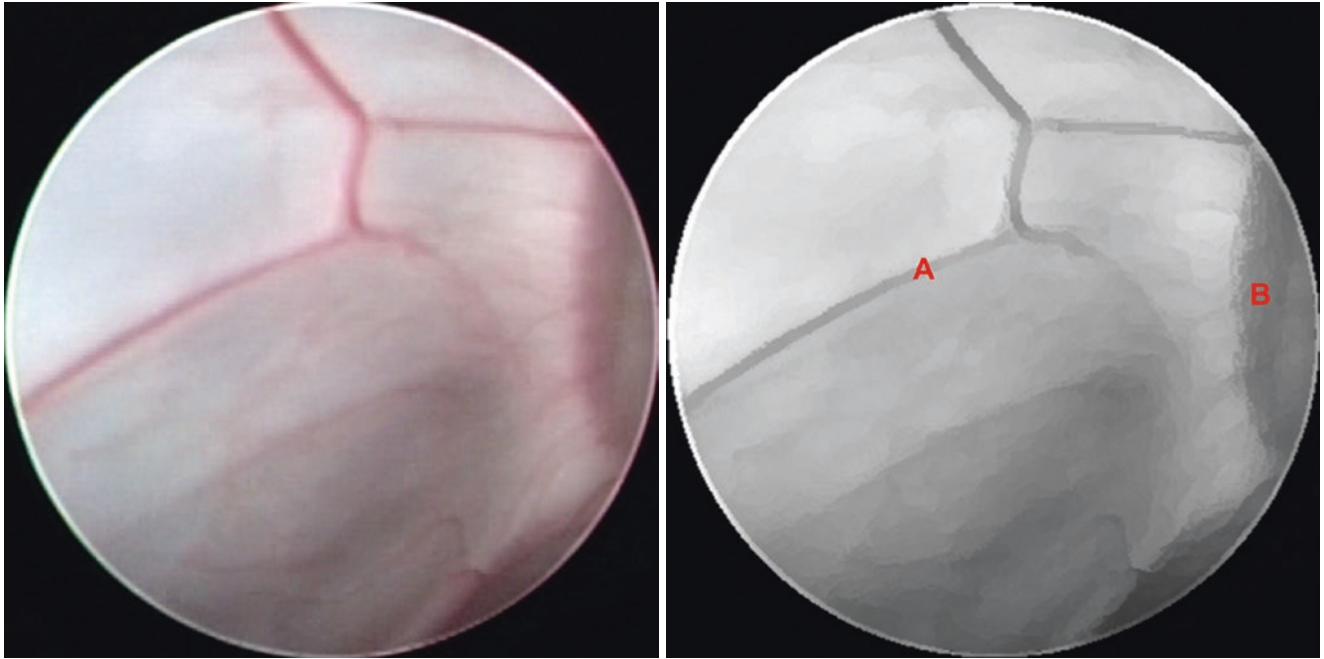


**Fig. 3.55** Normal anatomy. (A) Septal veins, (B) Anterior septal vein

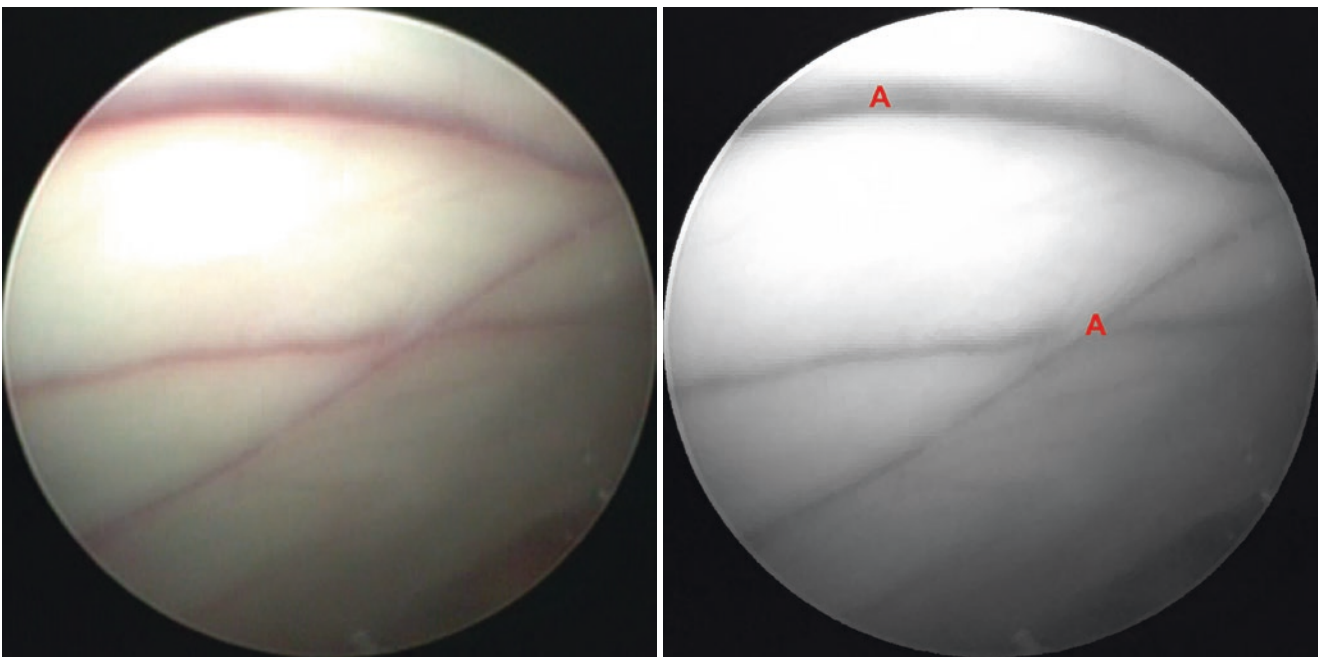


**Fig. 3.56** Normal anatomy. (A) Septal veins

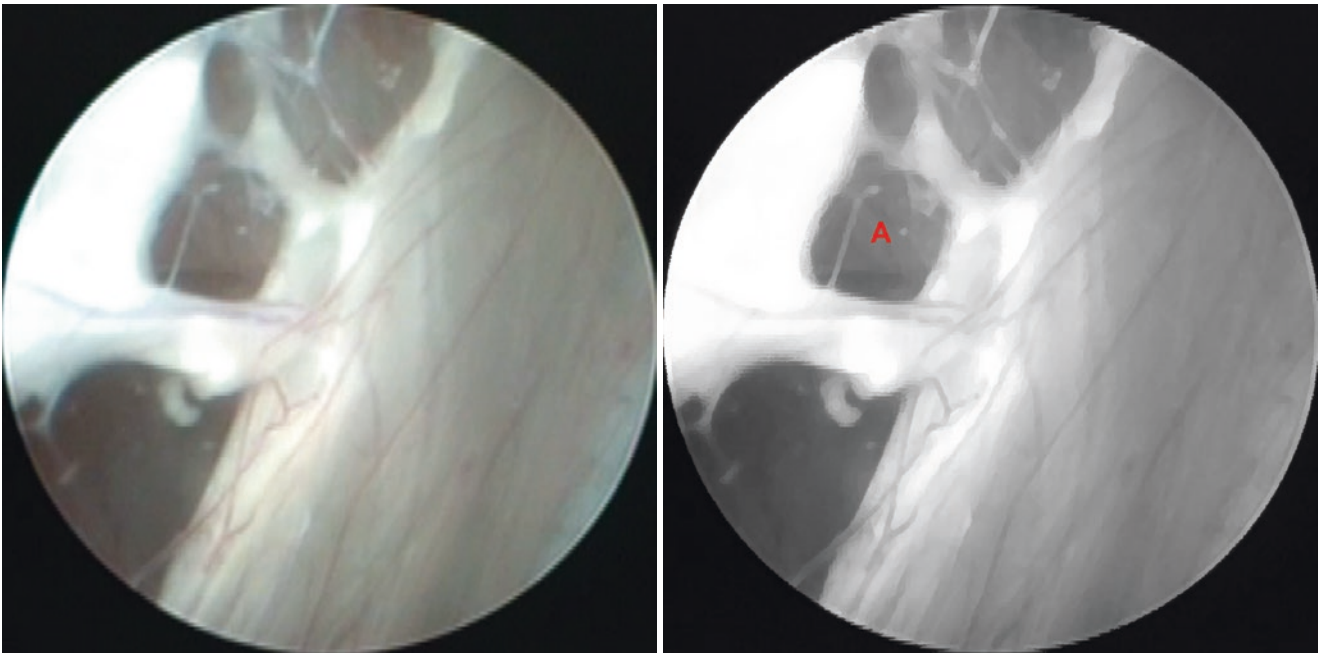


**Fig. 3.57** Abnormal anatomy – chronic hydrocephalus due to an intraventricular arachnoid cyst. (A) Spontaneous fenestration at the septum pellucidum

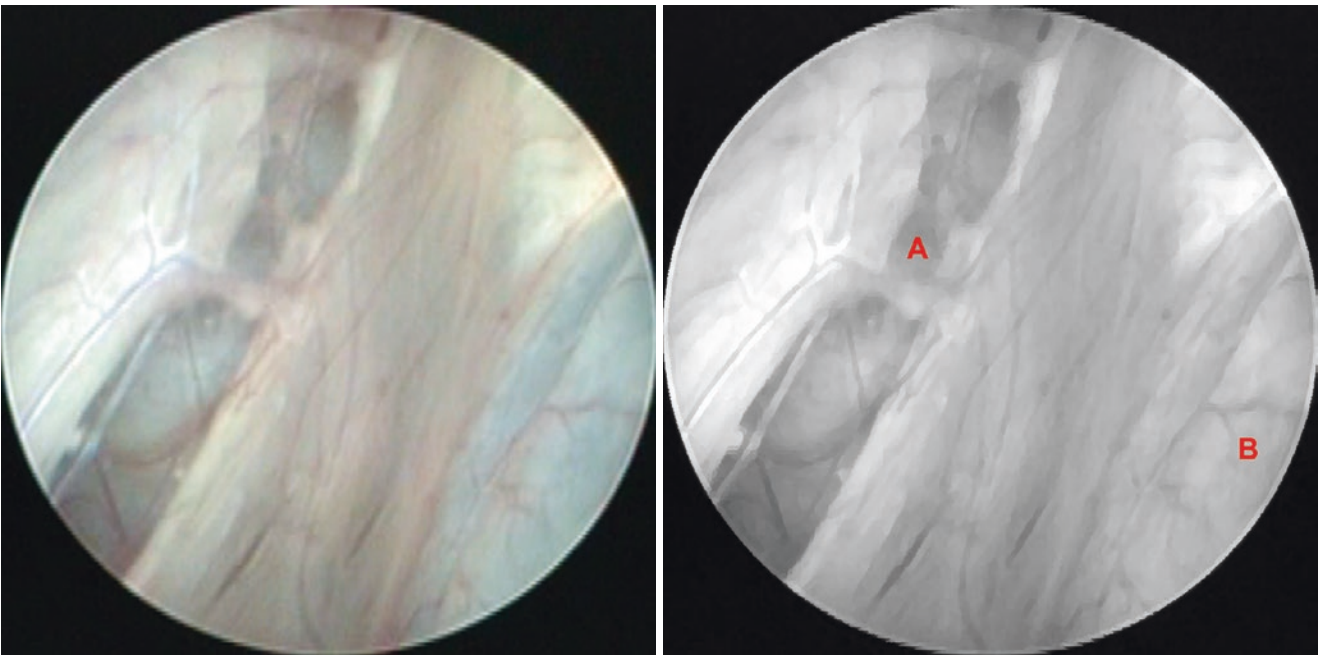


**Fig. 3.58** Abnormal anatomy – chronic hydrocephalus due to an intraventricular arachnoid cyst. (A) Spontaneous fenestration at the septum pellucidum, (B) Arachnoid cyst

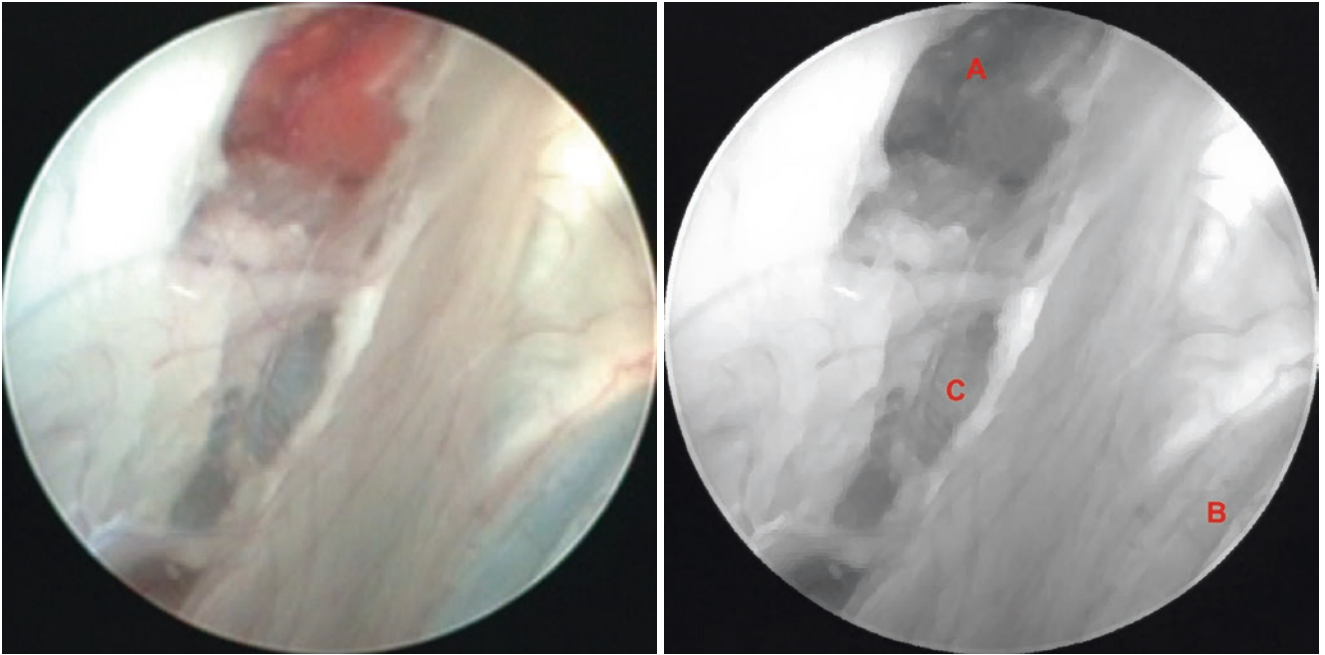


**Fig. 3.59** Abnormal anatomy – chronic hydrocephalus due to an intraventricular arachnoid cyst. (A) Spontaneous fenestration at the septum pellucidum, (B) Right portion of the arachnoid cyst, (C) Left portion of the arachnoid cyst

### 3.11 Left Lateral Ventricle: Septum Pellucidum

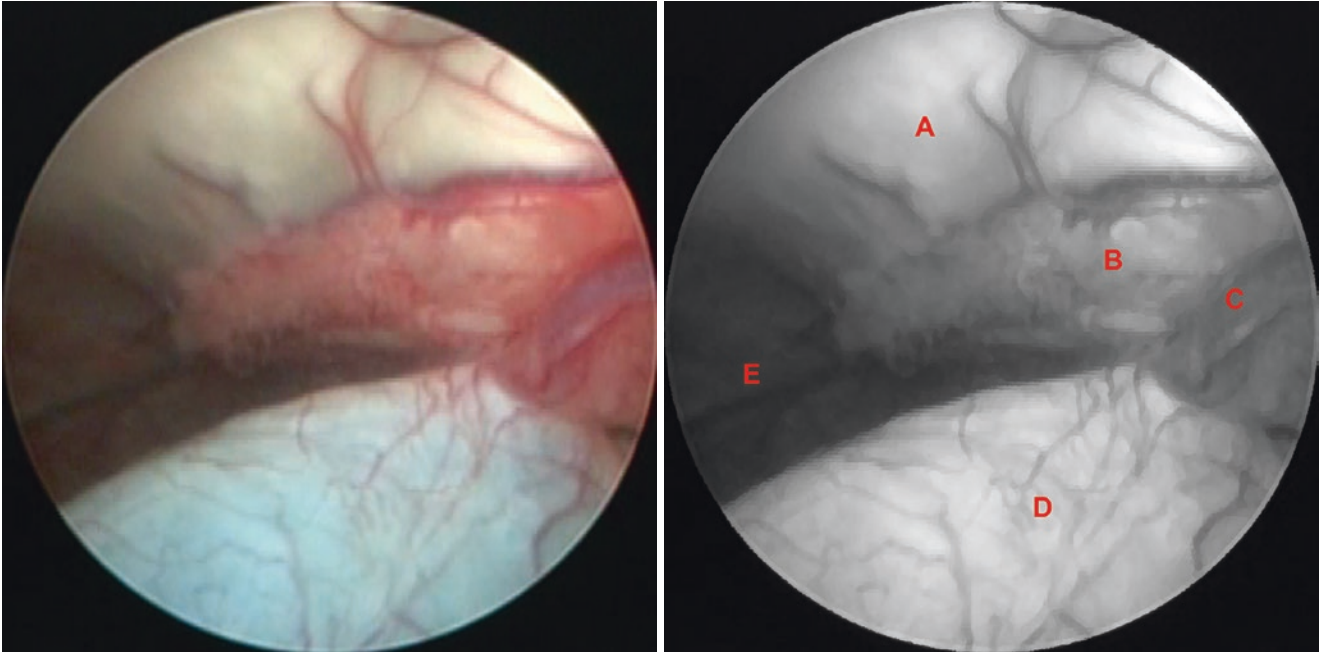


**Fig. 3.60** Abnormal anatomy – chronic hydrocephalus due to an intraventricular arachnoid cyst. (A) Thalamus, (B) Choroid plexus, (C) Superior choroidal vein, (D) Left portion of the arachnoid cyst, (E) Atrium

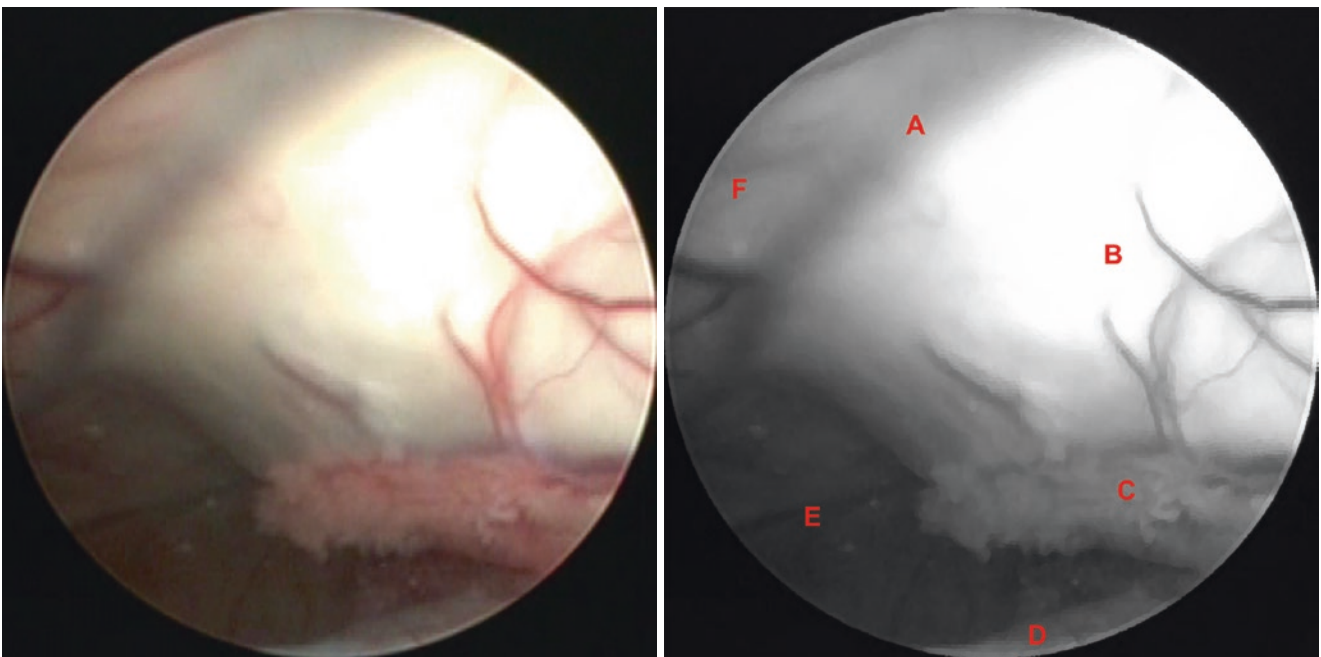


**Fig. 3.61** Abnormal anatomy – chronic hydrocephalus due to an intraventricular arachnoid cyst. (A) Superior thalamostriate vein, (B) Thalamus, (C) Choroid plexus, (D) Left portion of the arachnoid cyst, (E) Atrium, (F) Tail of the caudate nucleus

### 3.12 Right Lateral Ventricle: Septum Pellucidum

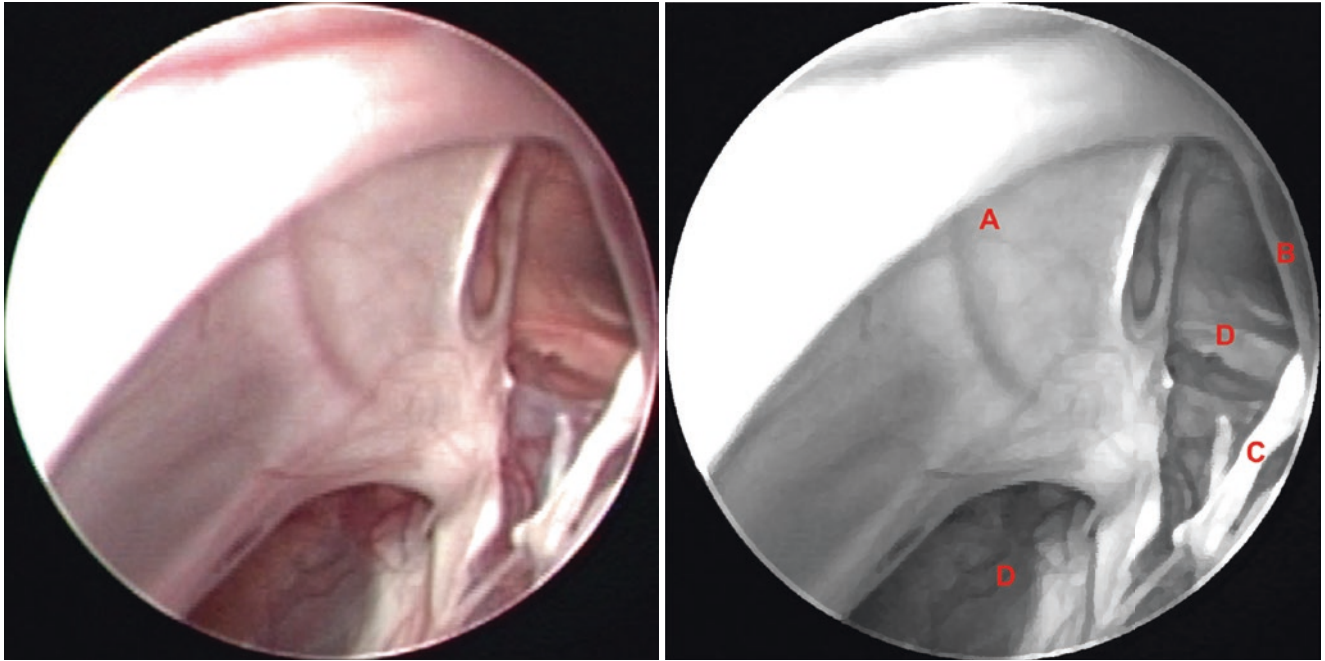


**Fig. 3.62** Abnormal anatomy – chronic hydrocephalus due to infra/supratentorial arachnoid cyst. (A) Septum pellucidum, (B) Anterior septal vein, (C) Body of the fornix, (D) Spontaneous fenestration at the septum pellucidum

### 3.13 Right/Left Lateral Ventricle: Septum Pellucidum

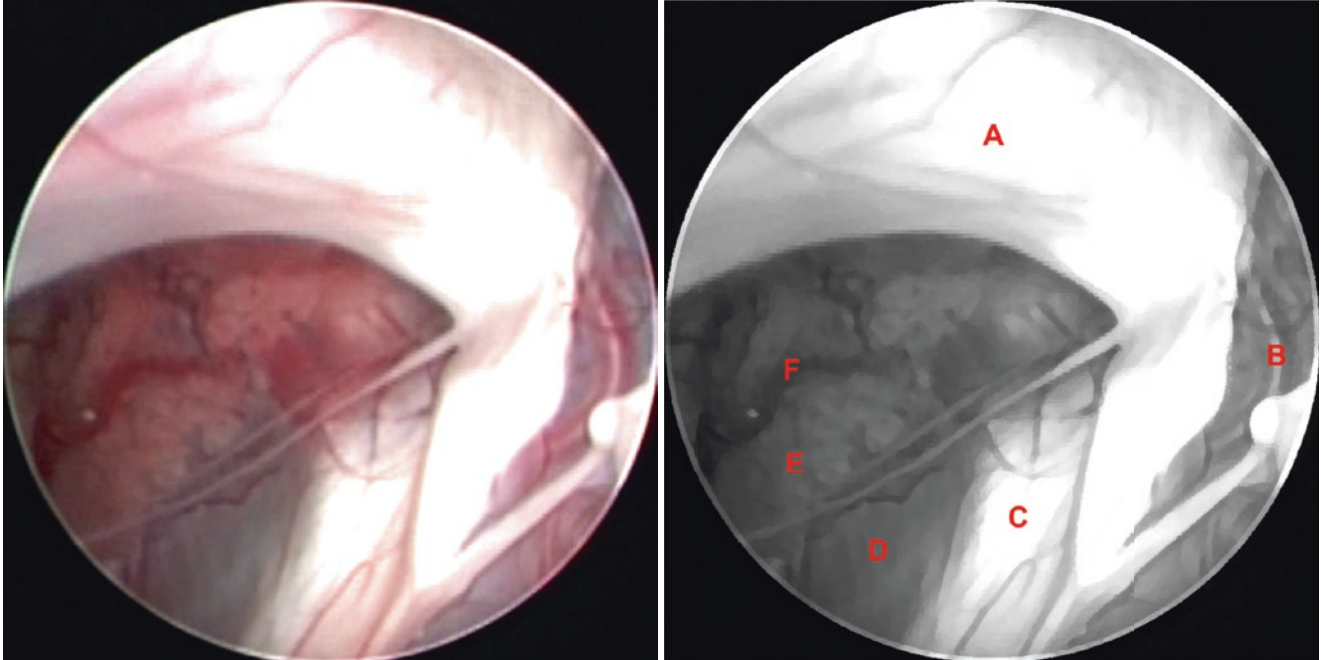


**Fig. 3.63** Abnormal anatomy – chronic hydrocephalus due to infra/supratentorial arachnoid cyst. (A) Septum pellucidum, (B) Right lateral posterior choroidal artery, (C) Left thalamus, (D) Left infratentorial portion of the cyst, (E) Left choroid plexus, (F) Left lateral posterior choroidal artery

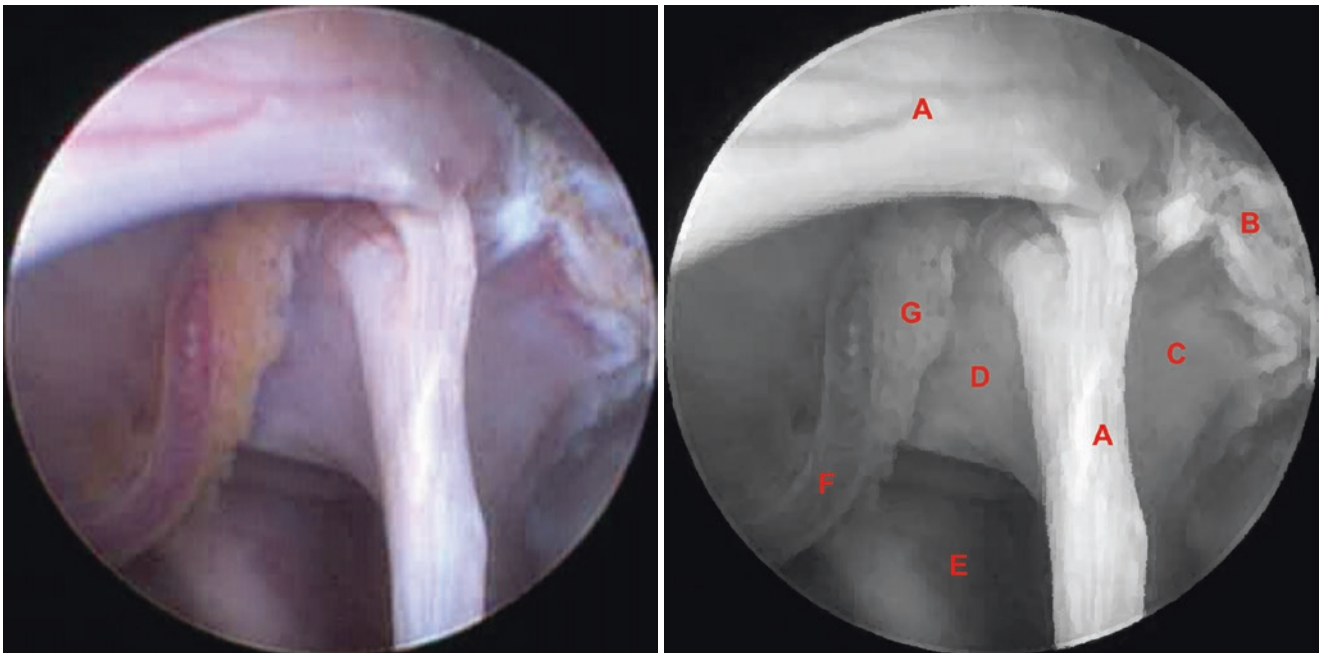


**Fig. 3.64** Surgical procedure – bilateral choroid plexus coagulation through spontaneously fenestrated septum pellucidum. (A) Spontaneously fenestrated septum pellucidum, (B) Right coagulated

choroid plexus, (C) Right pulvinar of the thalamus, (D) Left pulvinar of the thalamus, (E) Left atrium, (F) Left lateral posterior choroidal artery, (G) Left choroid plexus

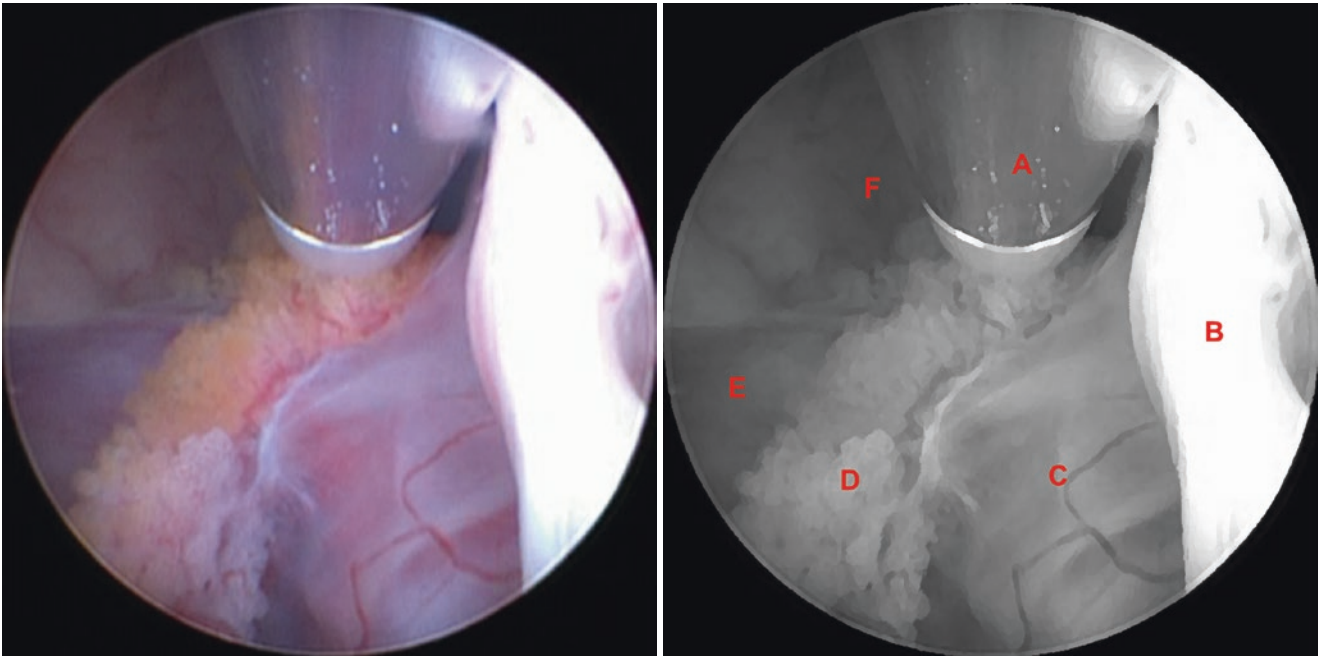


**Fig. 3.65** Surgical procedure – bilateral choroid plexus coagulation through spontaneously fenestrated septum pellucidum. (A) Bipolar coagulation electrode, (B) Spontaneously fenestrated septum pellu-

cidum, (C) Left pulvinar of the thalamus, (D) Left choroid plexus, (E) Left Thalamus, (F) Body of the left lateral ventricle

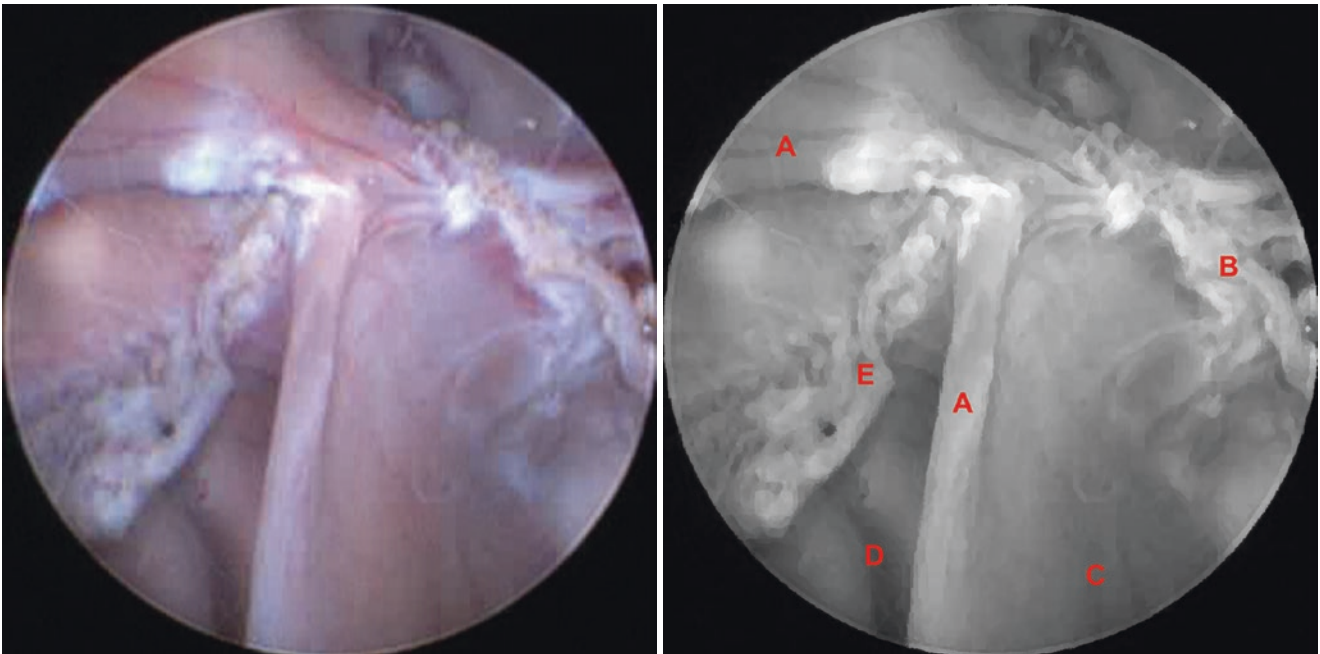


**Fig. 3.66** Surgical procedure – bilateral choroid plexus coagulation through spontaneously fenestrated septum pellucidum. (A) Spontaneously fenestrated septum pellucidum, (B) Coagulated right

choroid plexus, including lateral posterior choroidal artery, (C) Right atrium, (D) Left atrium, (E) Coagulated left choroid plexus, including lateral posterior choroidal artery



### 3.14 Left Lateral Ventricle: Septum Pellucidum

Illustrative case 3 – septostomy from the left side.

Clinical data: 2-year-old child, complex hydrocephalus after meningitis.

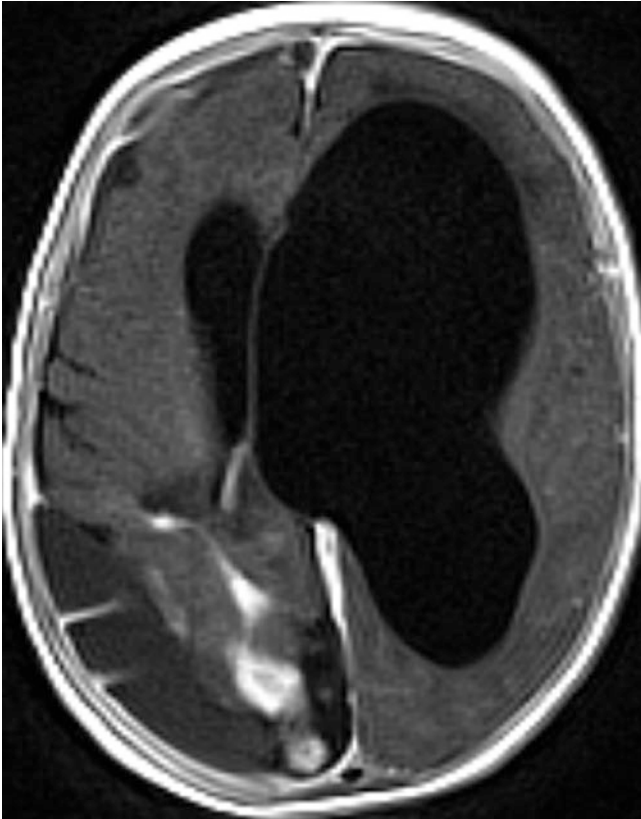


**Fig. 3.67** Gadolinium-enhanced axial T1-weighted MRI showing isolated left lateral ventricle

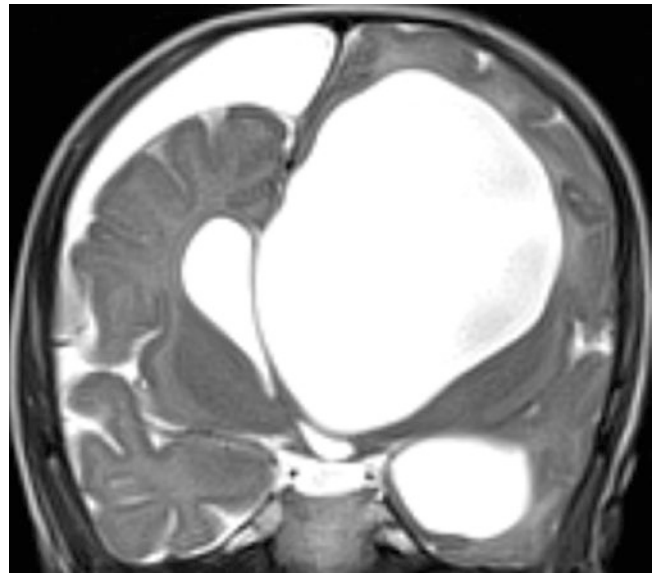


**Fig. 3.68** Coronal T2-weighted MRI showing isolated left lateral ventricle

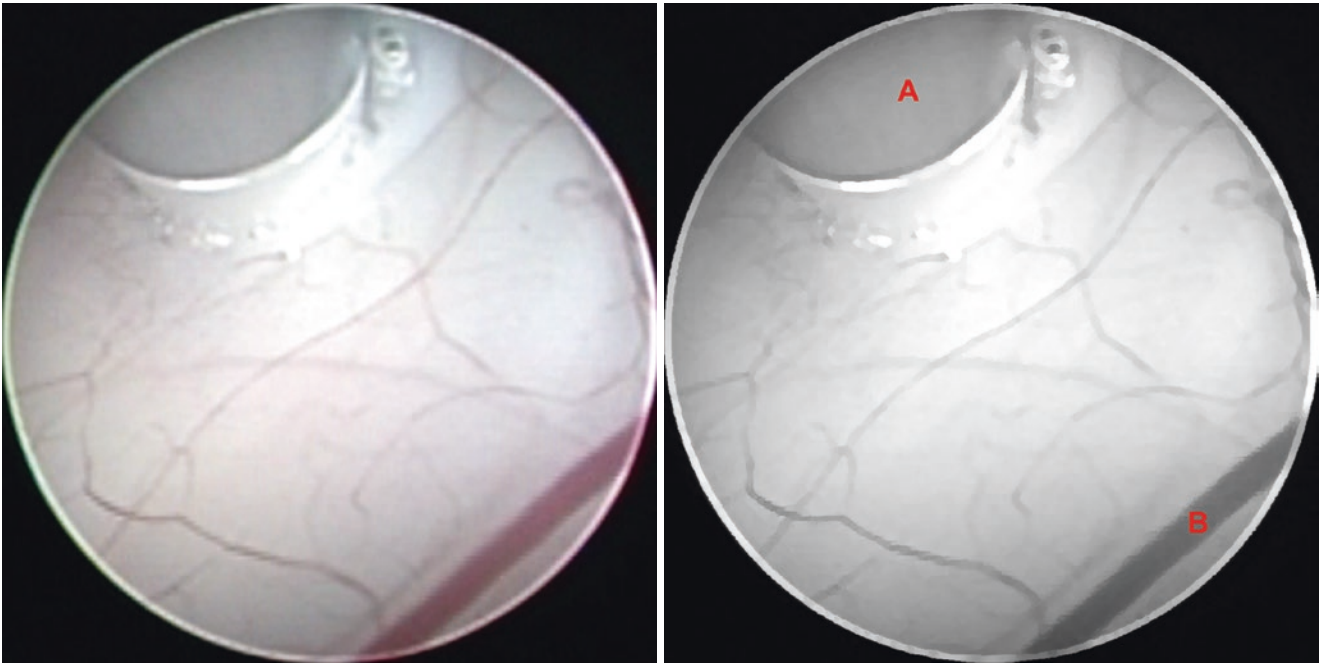


**Fig. 3.69** Illustrative case 3 – septostomy from the left side. (A) Bipolar coagulation electrode, (B) Septal vein

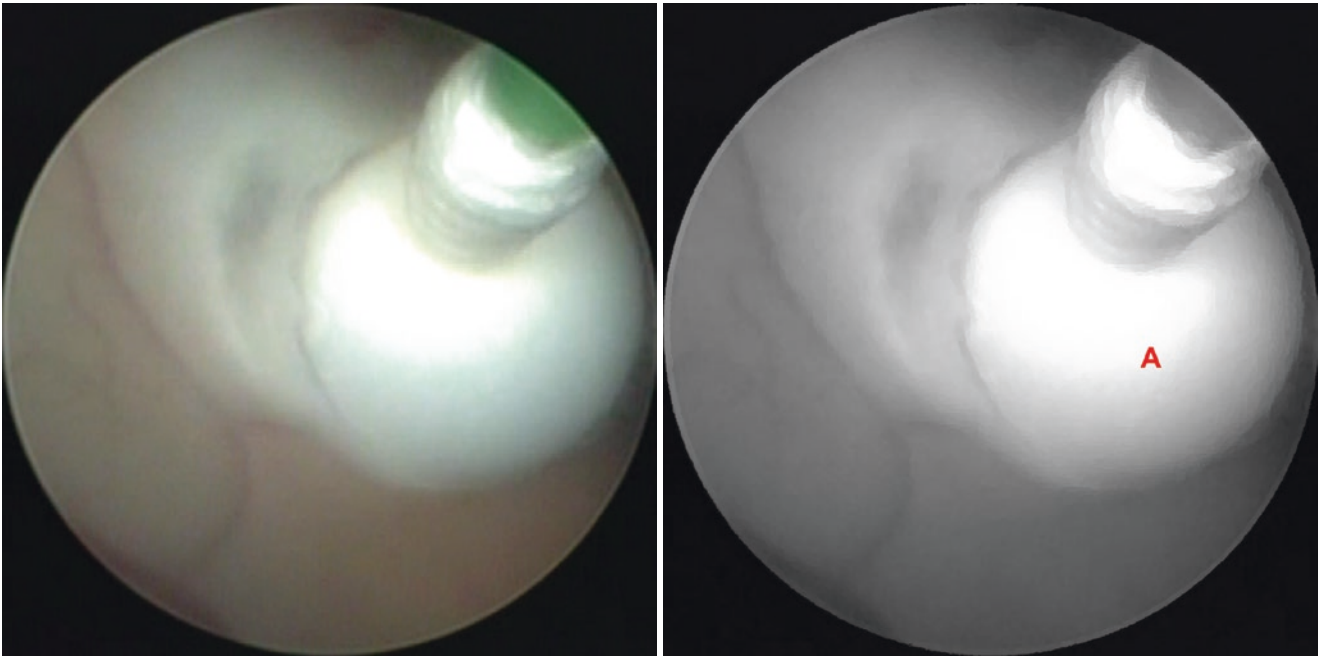


**Fig. 3.70** Illustrative case 3 – septostomy from the left side. (A) Fogarty ballon catheter dilatation

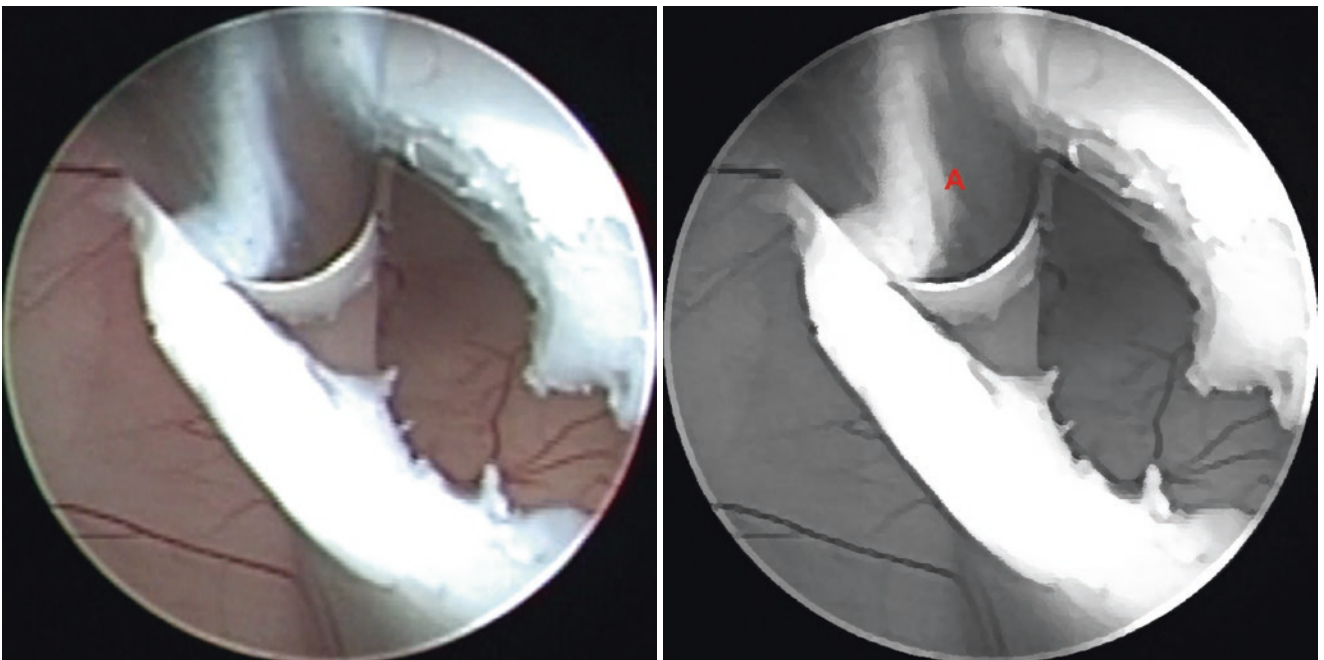


**Fig. 3.71** Illustrative case 3 – septostomy from the left side. (A) Non-activated bipolar coagulation electrode opening the septum pellucidum

### 3.15 Left/Right Lateral Ventricle: Septum Pellucidum

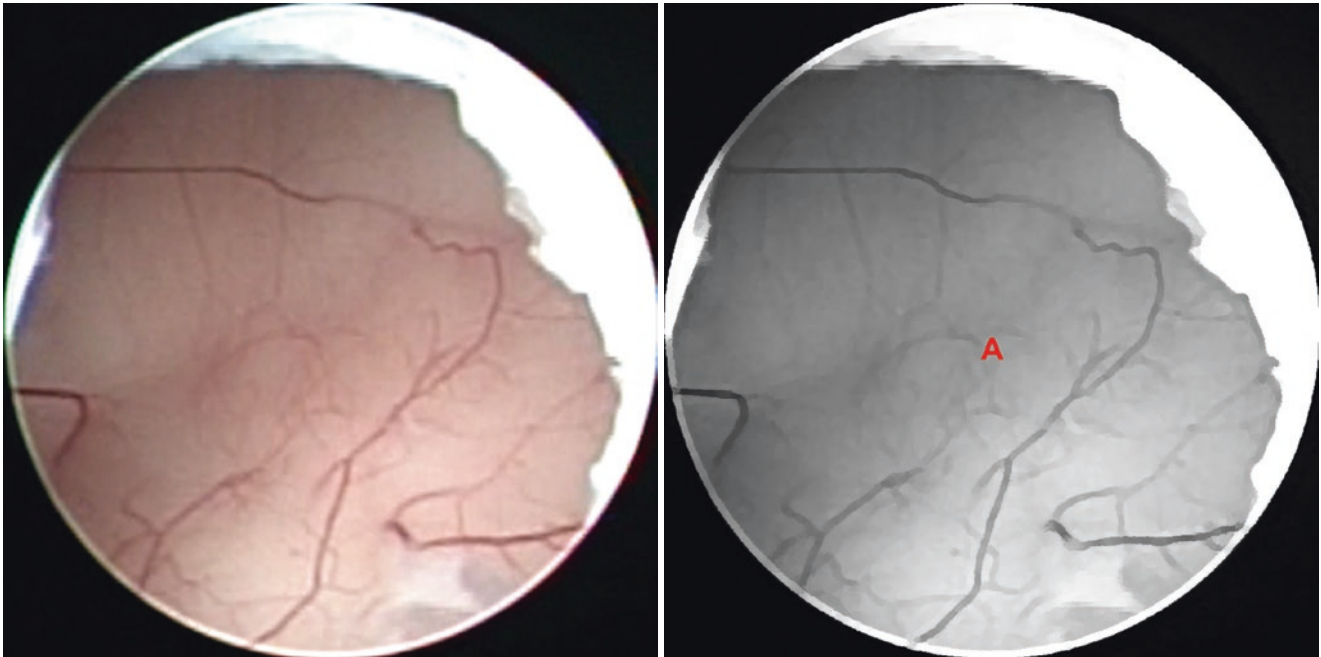


**Fig. 3.72** Illustrative case 3 – septostomy from the left side. (A) Right lateral ventricle through the fenestrated septum pellucidum

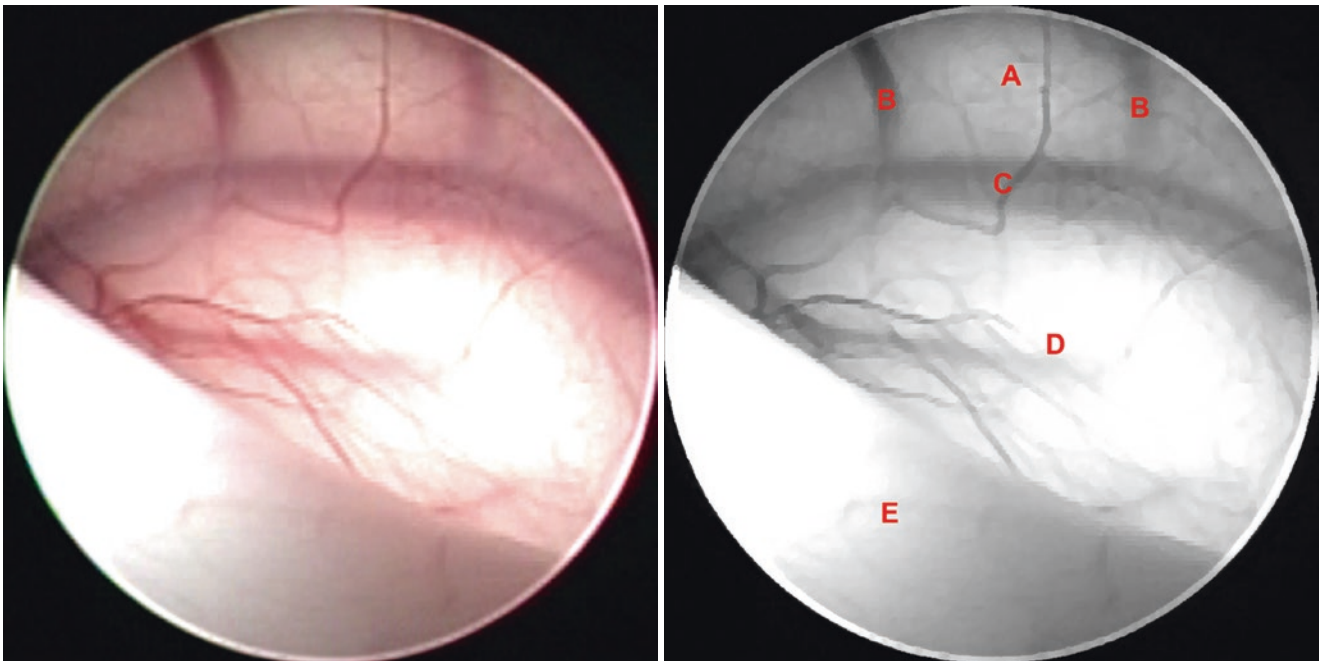


**Fig. 3.73** Illustrative case 3 – septostomy from the left side. (A) Body of the right caudate nucleus, (B) Caudate branches to the right superior thalamostriate vein, (C) Right superior thalamostriate vein, (D) Right thalamus, (E) Fenestrated septum pellucidum

### 3.16 Left Lateral Ventricle: Septum Pellucidum

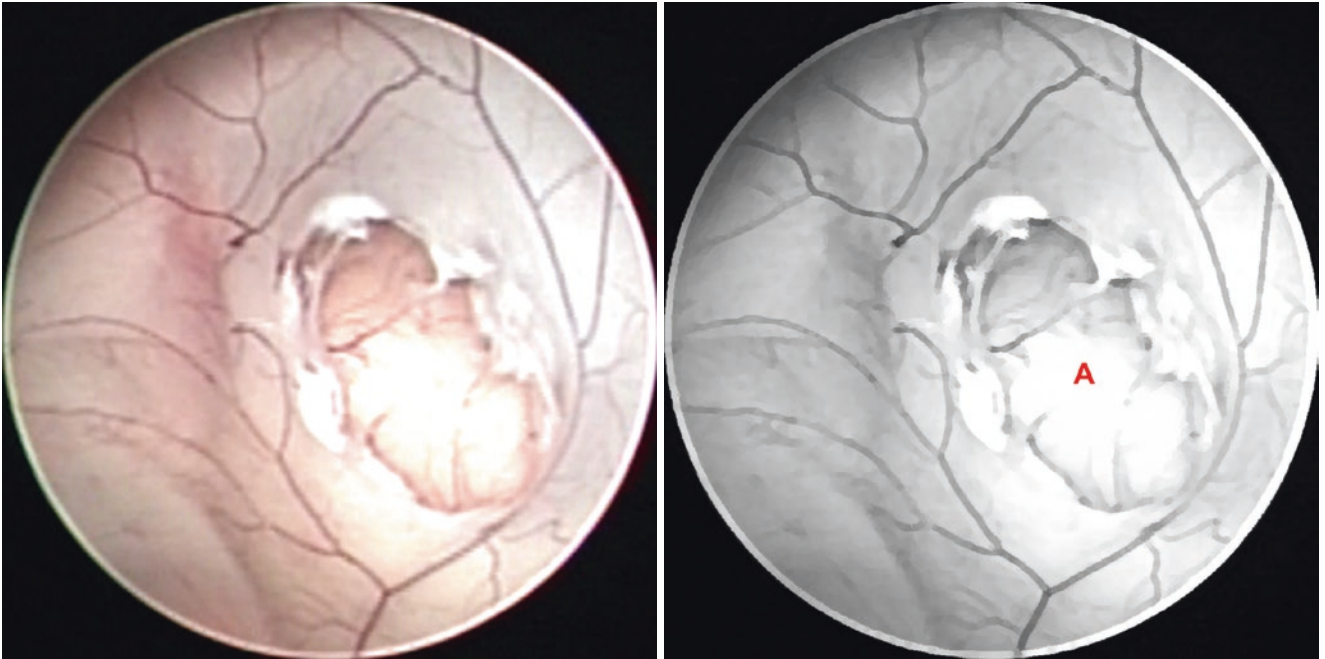


**Fig. 3.74** Illustrative case 3 – septostomy from the left side. (A) Final aspect of the septostomy

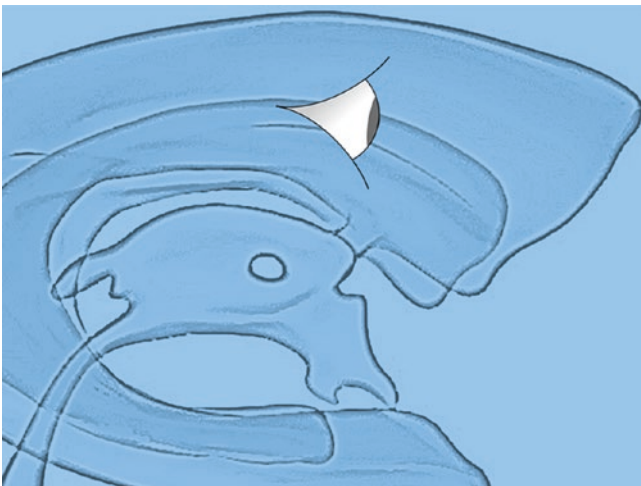


**Fig. 3.75** Direction of the endoscopic vision for the right frontal horn

### 3.17 Right Lateral Ventricle: Frontal Horn

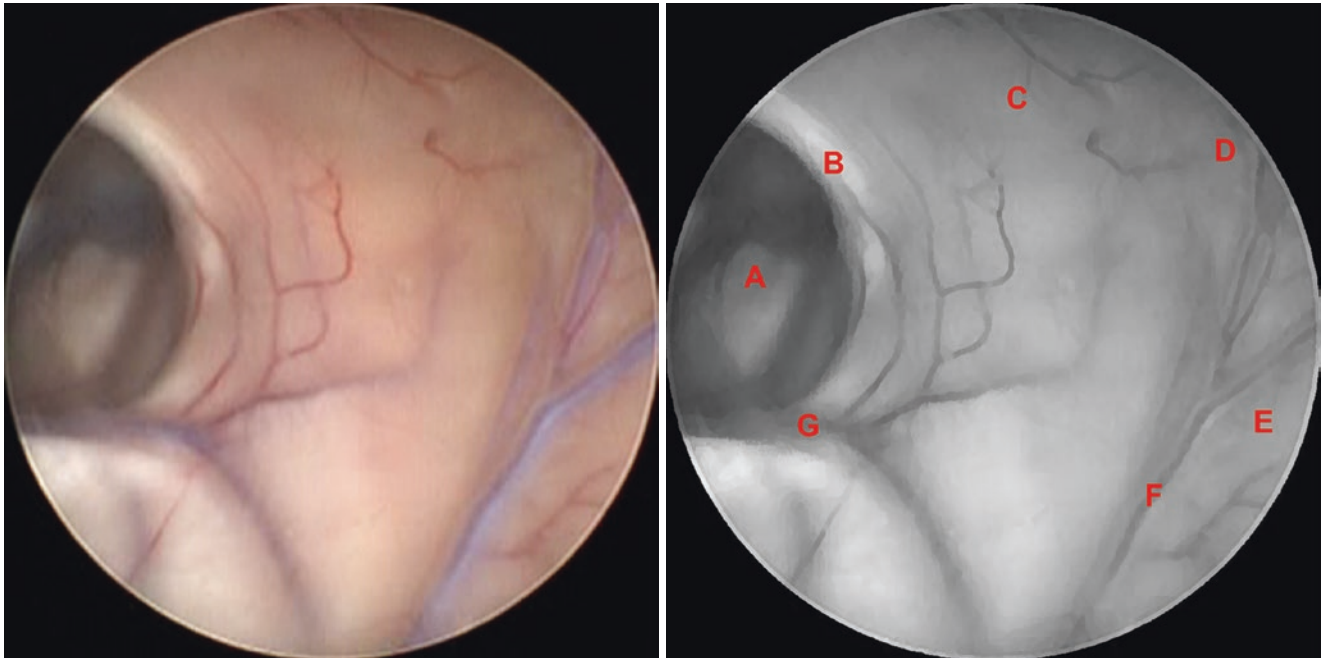


**Fig. 3.76** Normal anatomy. (A) Foramen of Monro, (B) Column of the fornix, (C) Septum pellucidum, (D) Frontal horn, (E) Head of the caudate nucleus, (F) Anterior caudate vein, (G) Substitute superior thalamostriate vein [12]

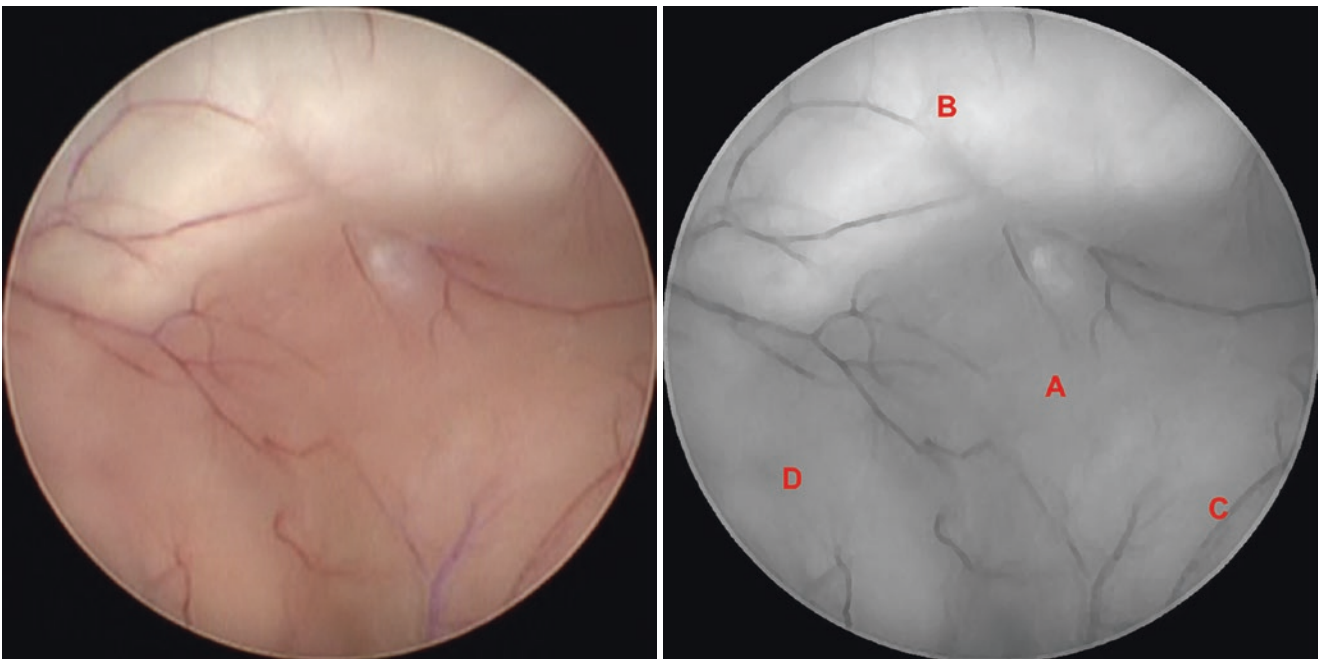


**Fig. 3.77** Normal anatomy. (A) Frontal horn, (B) Genu of the corpus callosum, (C) Head of the caudate nucleus, (D) Septum pellucidum

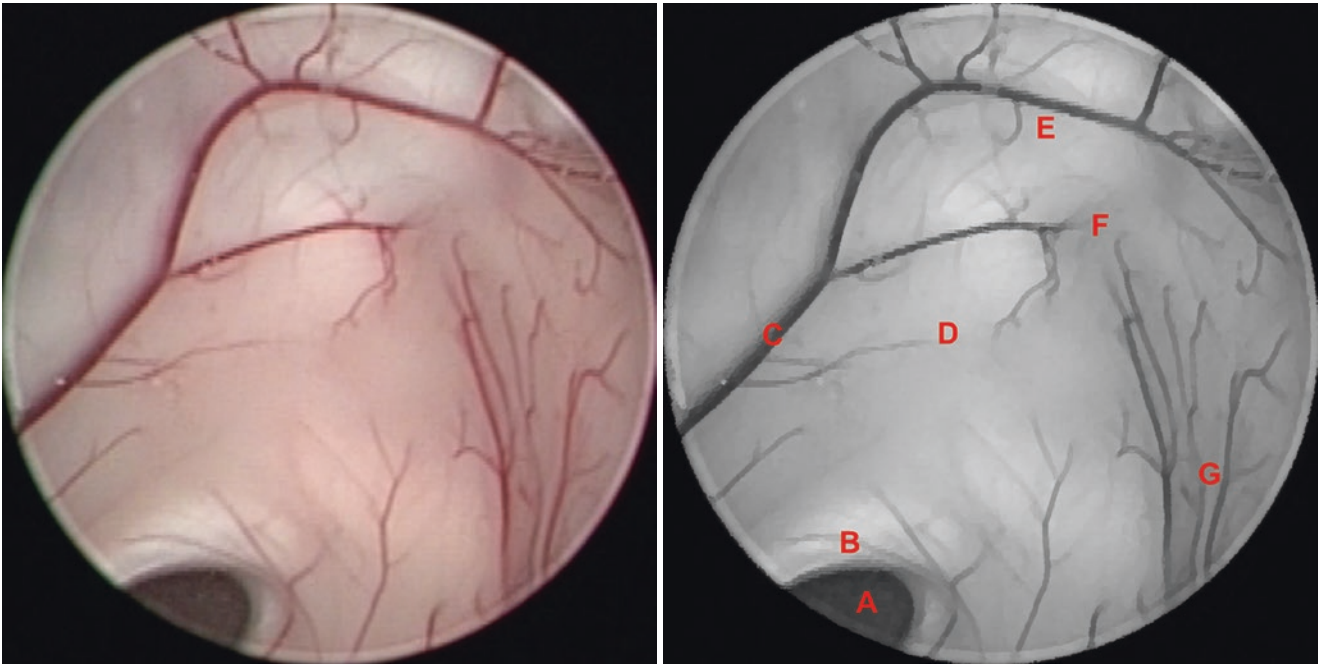


**Fig. 3.78** Normal anatomy. (A) Foramen of Monro, (B) Column of the fornix, (C) Anterior septal vein, (D) Septum pellucidum, (E) Genu of the corpus callosum, (F) Frontal horn, (G) Head of the caudate nucleus

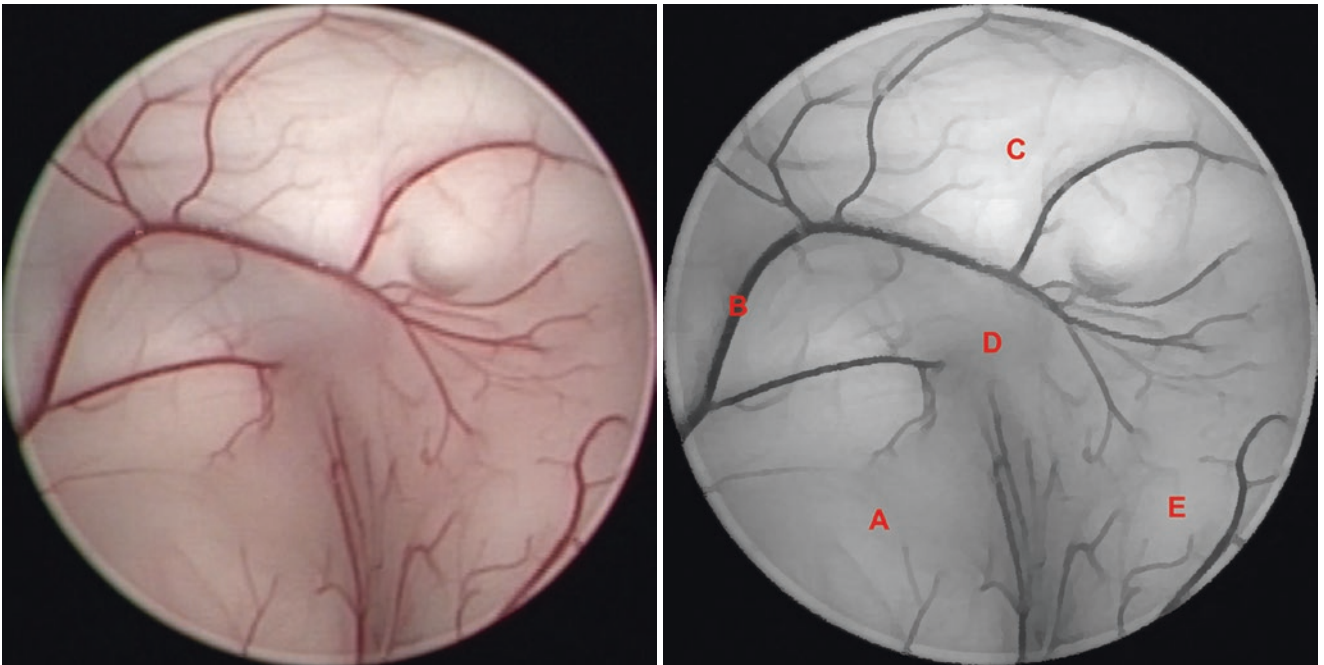


**Fig. 3.79** Normal anatomy. (A) Septum pellucidum, (B) Anterior septal vein, (C) Genu of the corpus callosum, (D) Frontal horn, (E) Head of the caudate nucleus

### 3.18 Right Lateral Ventricle: Atrium

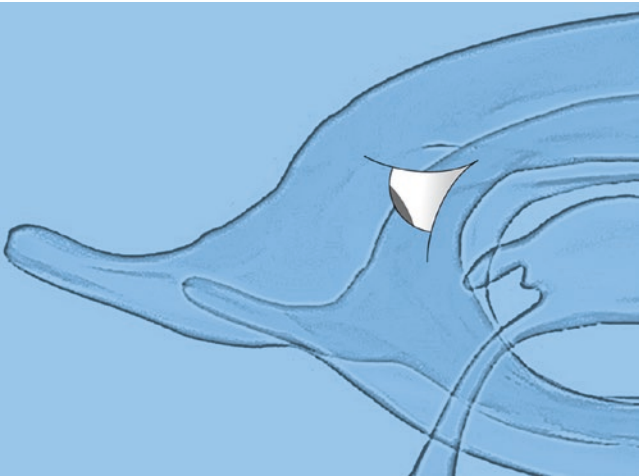


**Fig. 3.80** Direction of the endoscopic vision for the right atrium

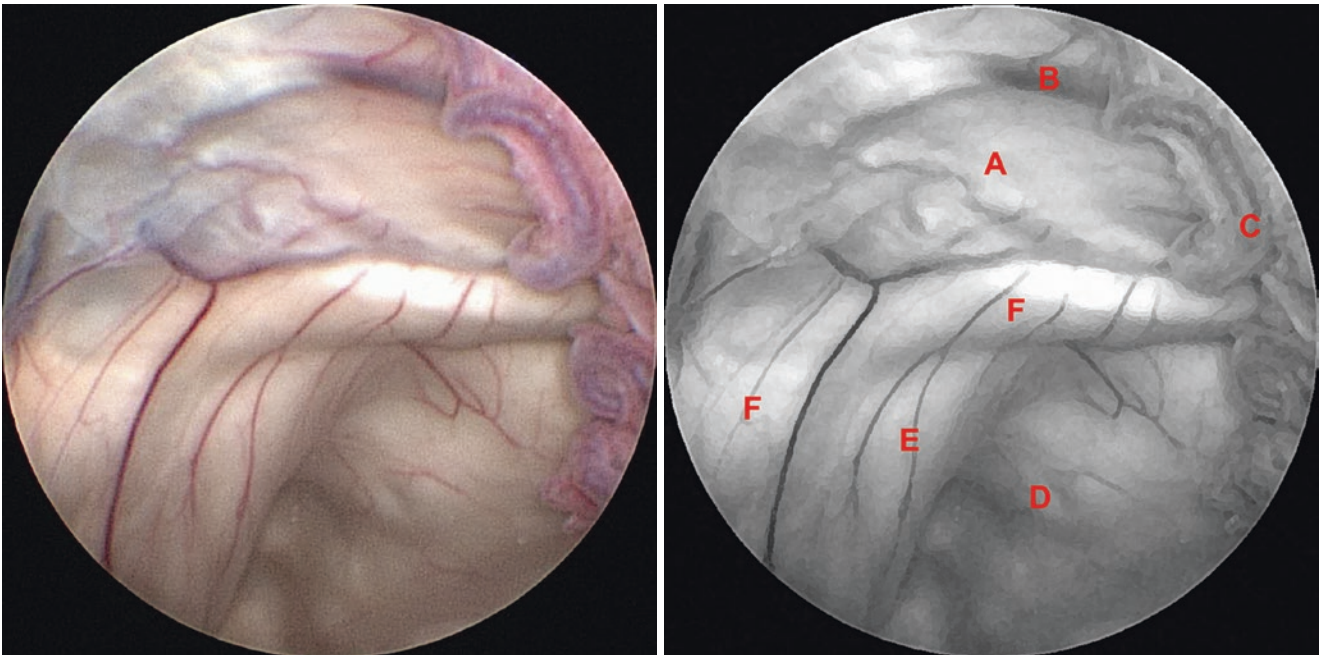


**Fig. 3.81** Normal anatomy. (A) Septum pellucidum, (B) Posterior septal vein, (C) Superior choroidal vein, (D) Collateral eminence, (E) Calcar avis, (F) Bulb of the occipital horn



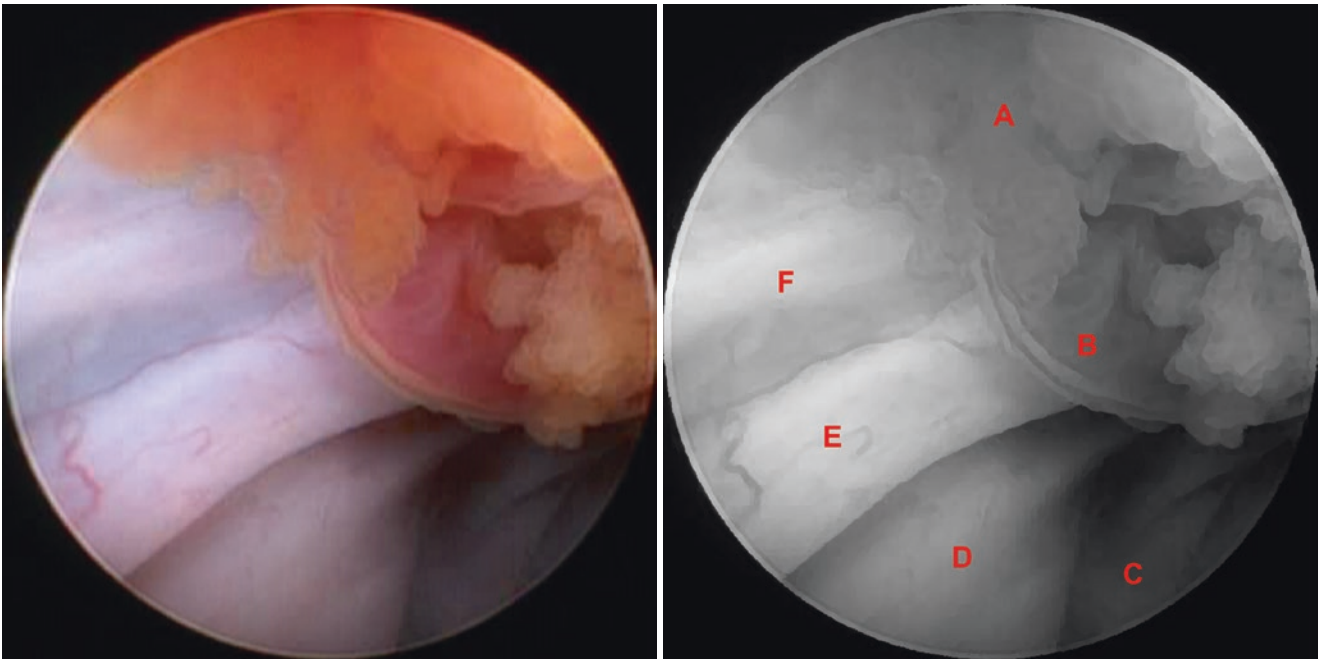


**Fig. 3.82** Normal anatomy. (A) Choroid plexus, (B) Lateral posterior choroidal artery, (C) Collateral eminence, (D) Calcar avis, (E) Bulb of the occipital horn, (F) Septum pellucidum

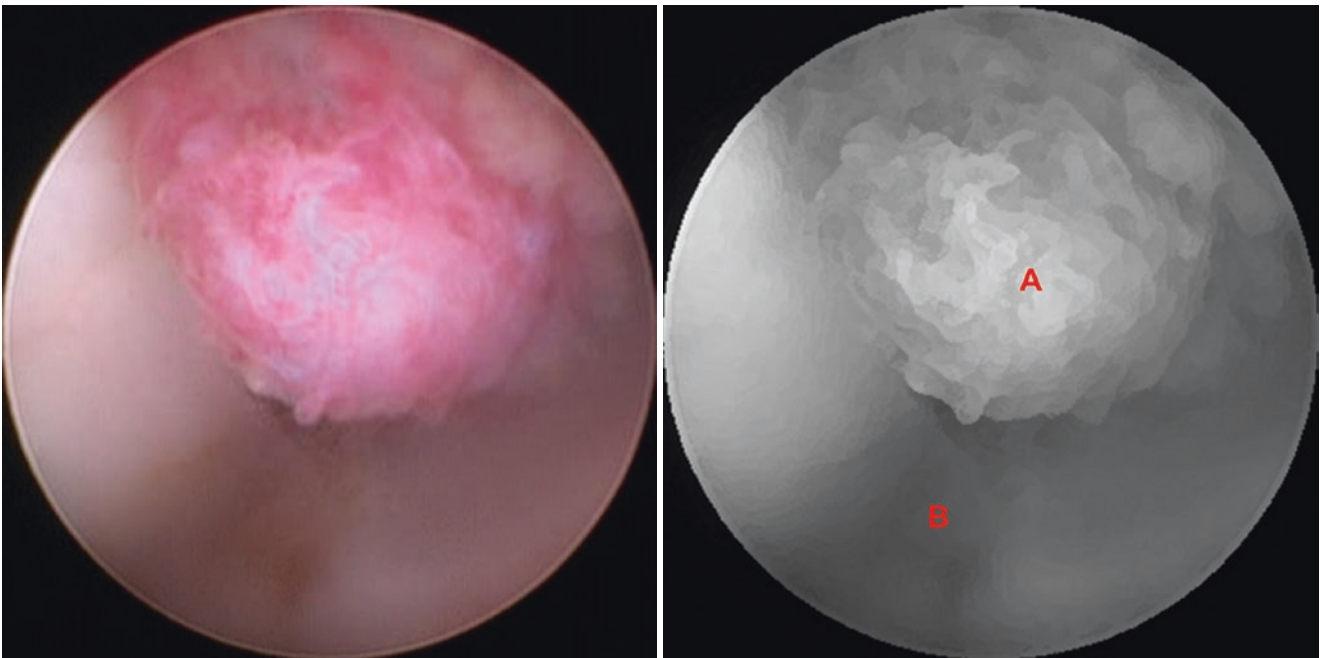


**Fig. 3.83** Normal anatomy. (A) Glomus of the choroid plexus, (B) Atrium

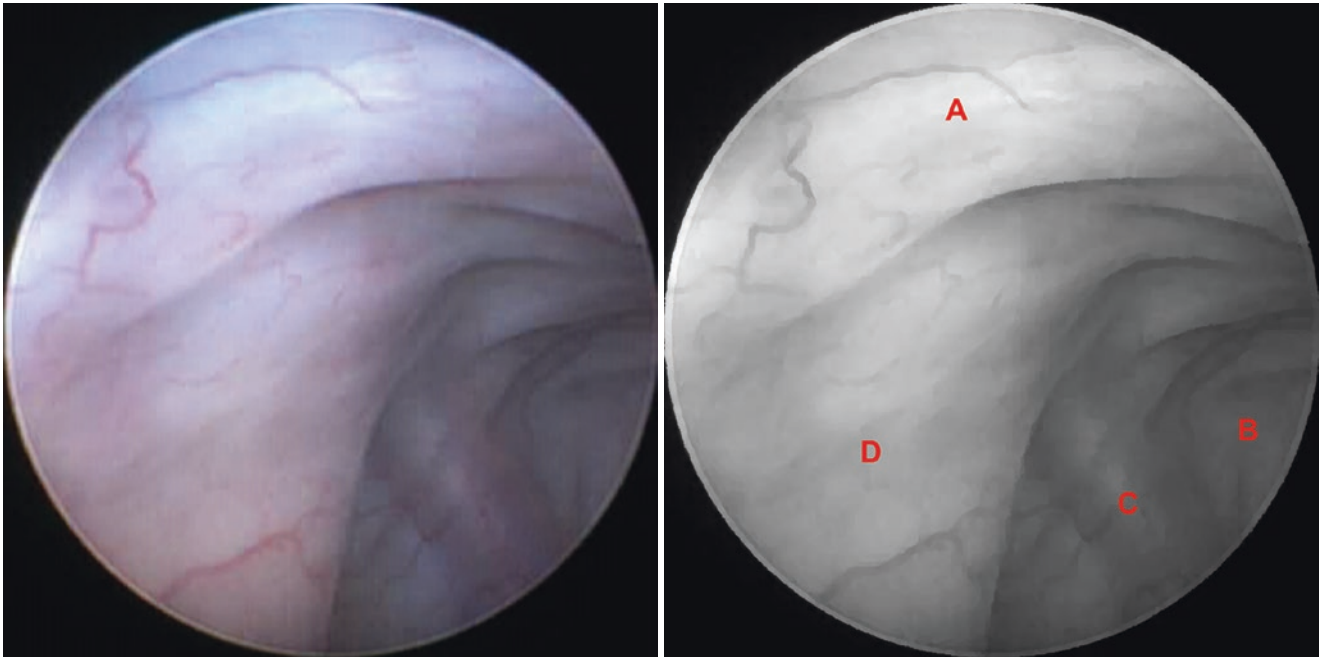


**Fig. 3.84** Normal anatomy. (A) Bulb of the occipital horn, (B) Collateral eminence, (C) Medial atrial vein, (D) Calcar avis

### 3.19 Left Lateral Ventricle: Atrium

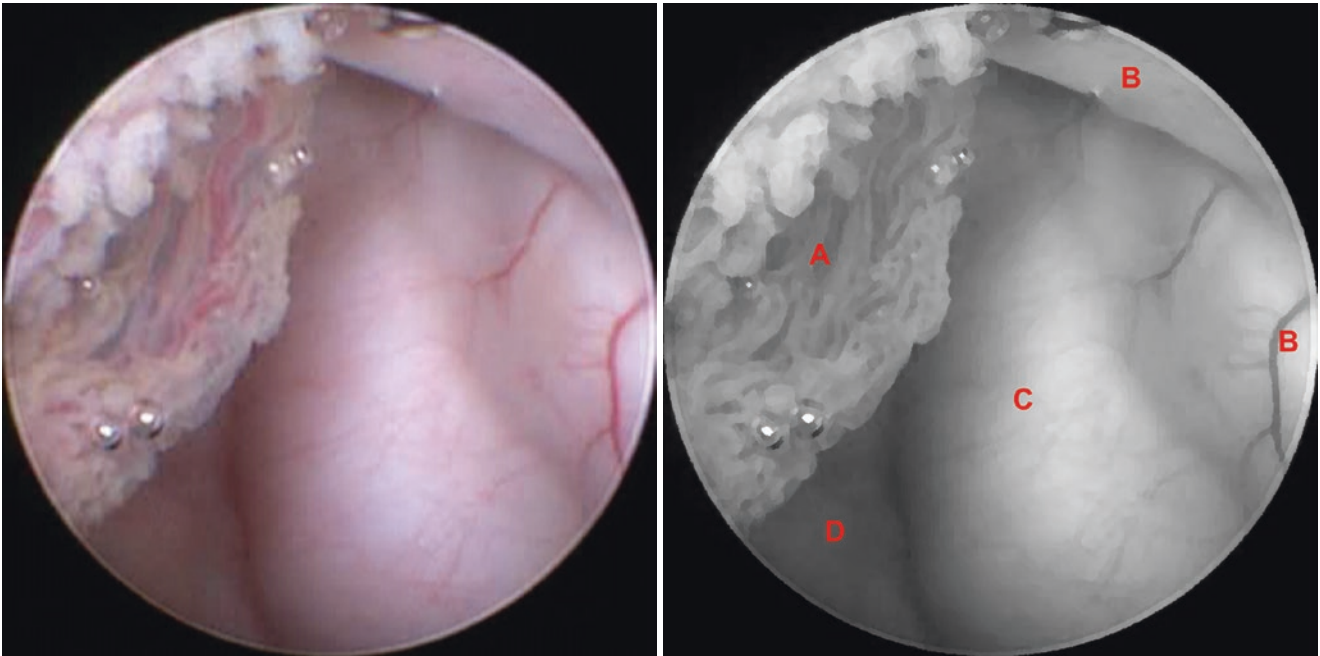


**Fig. 3.85** Normal anatomy. (A) Choroid plexus, (B) Bulb of the occipital horn, (C) Calcar avis, (D) Collateral eminence

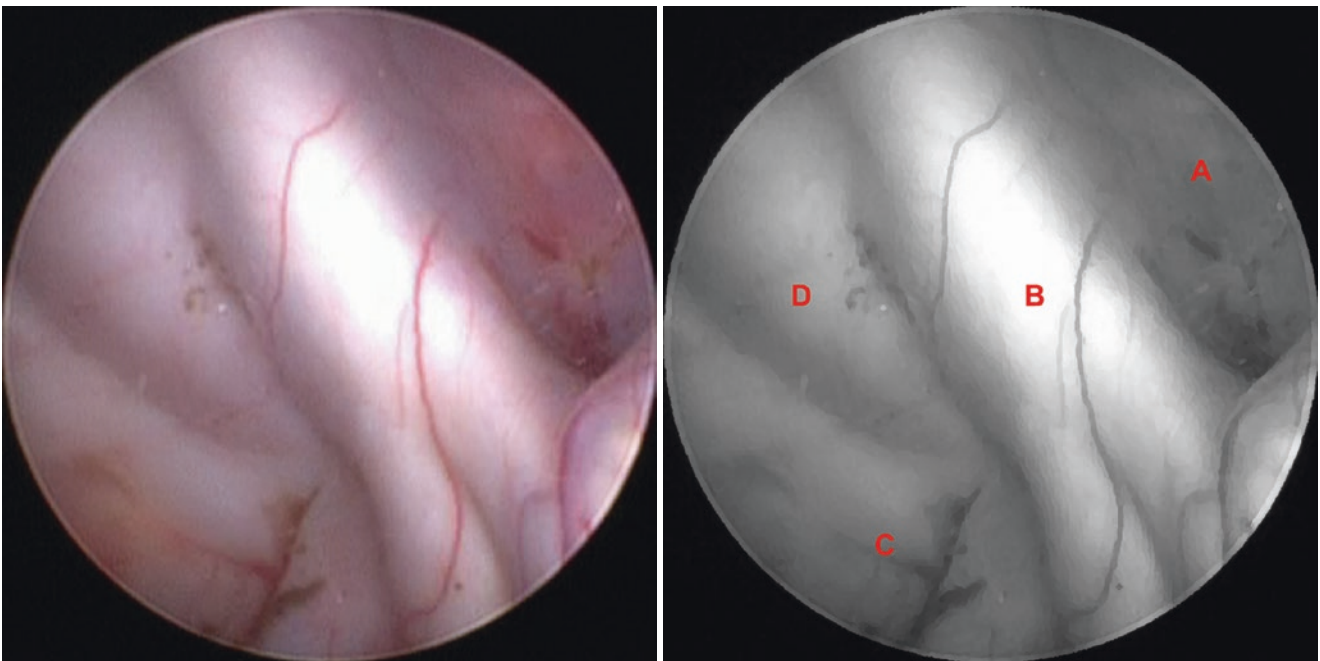


**Fig. 3.86** Normal anatomy. (A) Cerebellar culmen, (B) Bulb of the occipital horn, (C) Collateral eminence, (D) Calcar avis

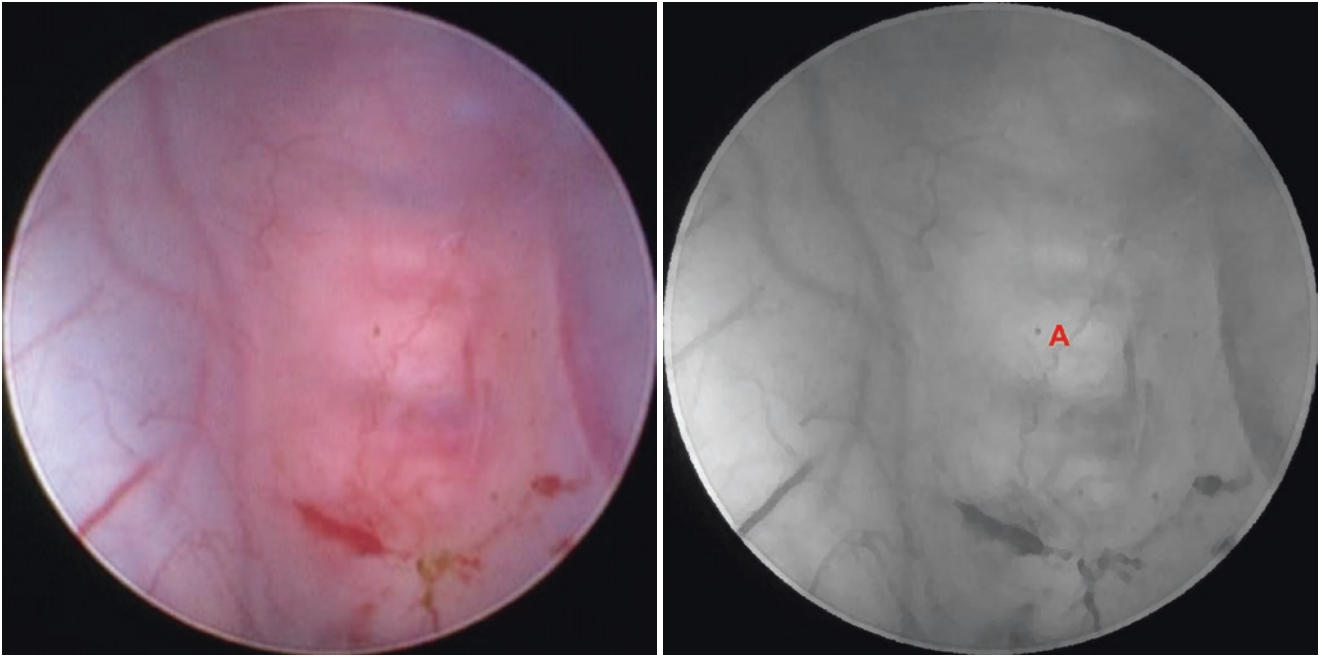


**Fig. 3.87** Normal anatomy. (A) Cerebellar culmen

### 3.20 Right Lateral Ventricle: Atrium

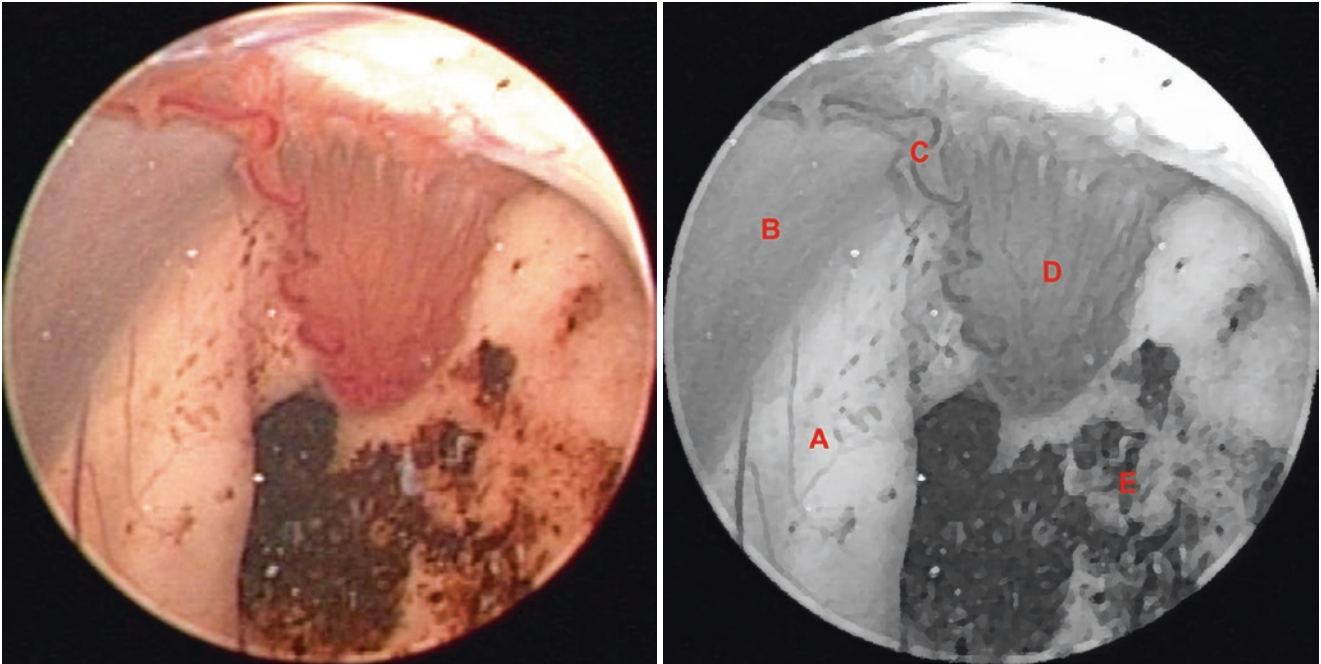


**Fig. 3.88** Abnormal anatomy – late post-hemorrhage aspect. (A) Calcar avis, (B) Bulb of the occipital horn, (C) Lateral posterior choroidal artery, (D) Choroid plexus, (E) Hemorrhage over collateral eminence

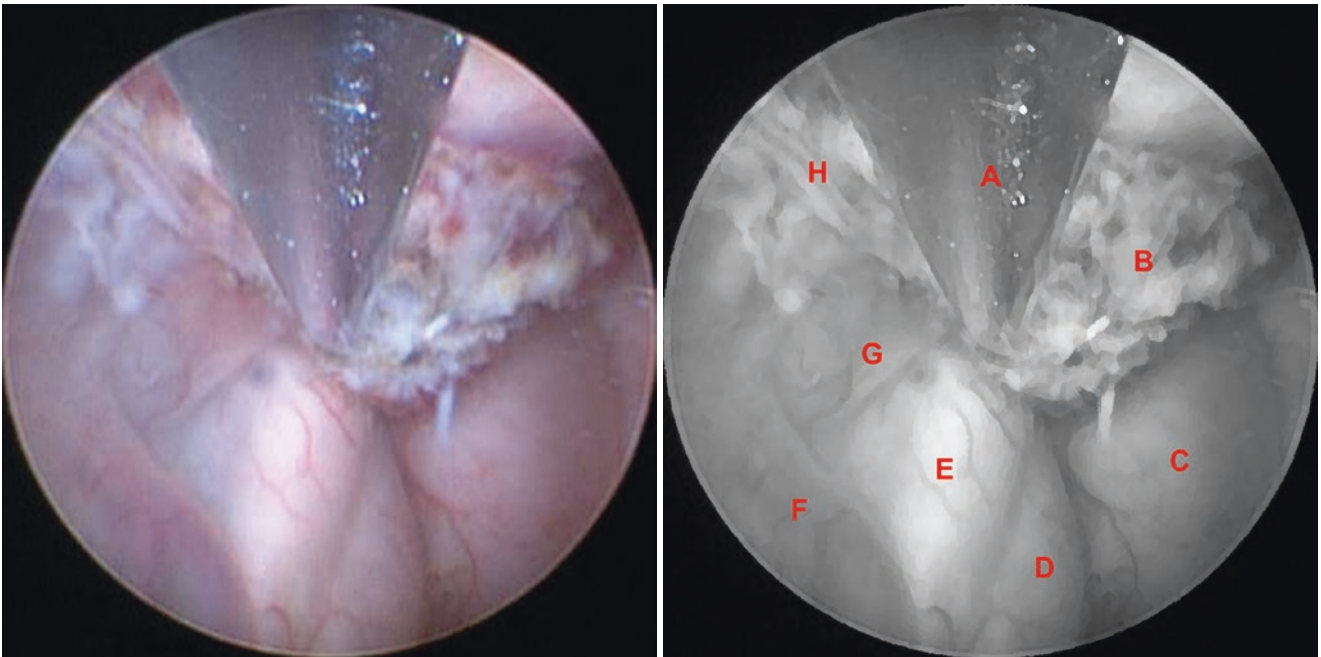


**Fig. 3.89** Surgical procedure – choroid plexus coagulation. (A) Bipolar coagulation electrode, (B) Coagulated choroid plexus, (C) Collateral eminence, (D) Calcar avis, (E) Bulb of the occipital horn, (F) Medial

atrial vein, (G) Septum pellucidum, (H) Coagulated lateral posterior choroidal artery

## References

1. Ashour AM, Elbabaa SK, Caputy AJ, Gragnaniello C. Navigation-guided endoscopic intraventricular injectable tumor model: cadaveric tumor resection model for neurosurgical training. *World Neurosurg.* 2016;pii: S1878–8750:30175–9. doi:[10.1016/j.wneu.2016.04.048](https://doi.org/10.1016/j.wneu.2016.04.048).
2. Fiorella D, Gutman F, Woo H, Arthur A, Aranguren R, Davis R. Minimally invasive evacuation of parenchymal and ventricular hemorrhage using the Apollo system with simultaneous neuronavigation, neuroendoscopy and active monitoring with cone beam CT. *J Neurointerv Surg.* 2015;7:752–7. doi:[10.1136/neurintsurg-2014-011358](https://doi.org/10.1136/neurintsurg-2014-011358).
3. Decq P. Endoscopic anatomy of the ventricles. In: Cinalli G, Sainte-Rose C, Maixner WJ, editors. *Pediatric hydrocephalus*. Milan: Springer; 2005. p. 351–9. doi:[10.1007/978-88-470-2121-1\\_24](https://doi.org/10.1007/978-88-470-2121-1_24).
4. Mapstone TB, Ratcheson RA. Techniques of ventricular puncture. In: Wilkins RH, Rengachary SS, editors. *Neurosurgery*. 2nd ed. New York: McGraw-Hill; 1996. p. 179–83.
5. Krucoff MO, Chinn M, Babington P, Litvack ZN. Controversial neuroendoscopic Monro foraminoplasty in the management of isolated lateral ventricle in an adult. *Interdiscip Neurosurg.* 2015;2:108–10. doi:[10.1016/j.inat.2015.03.004](https://doi.org/10.1016/j.inat.2015.03.004).
6. Sharifi G, Alavi E, Rezaee O, Jahanbakhshi A, Faramarzi F. Neuroendoscopic foraminoplasty for bilateral idiopathic occlusion of foramina of Monro. *Turk Neurosurg.* 2012;22:265–8. doi:[10.5137/1019-5149.JTN.3268-10.2](https://doi.org/10.5137/1019-5149.JTN.3268-10.2).
7. Enchev YP, Oi S. The application of neuroendoscopic techniques in improving altered CSF physiology. In: Sgouros S, editor. *Neuroendoscopy*. Berlin/Heidelberg: Springer; 2014. p. 11–30. doi:[10.1007/978-3-642-39085-2\\_2](https://doi.org/10.1007/978-3-642-39085-2_2).
8. Oertel JM, Baldauf J, Schroeder HW, Gaab MR. Endoscopic cysto-ventriculostomy for treatment of paraxial arachnoid cysts. *J Neurosurg.* 2009;110:792–9. doi:[10.3171/2008.7.JNS0841](https://doi.org/10.3171/2008.7.JNS0841).
9. El-Ghandour NMF. Endoscopic treatment of intraparenchymal arachnoid cysts in children. *J Neurosurg Pediatr.* 2014;14:501–7. doi:[10.3171/2014.7.PEDS13647](https://doi.org/10.3171/2014.7.PEDS13647).
10. Decq P. Neuroendoscopic treatment of colloid cysts. In: Sgouros S, editor. *Neuroendoscopy*. Berlin/Heidelberg: Springer; 2014. p. 127–32. doi:[10.1007/978-3-642-39085-2\\_11](https://doi.org/10.1007/978-3-642-39085-2_11).
11. Seeger W. Endoscopic anatomy of the third ventricle. *Microsurgical and endoscopic approaches*. Wien: Springer; 2006. doi:[10.1007/3-211-31178-5](https://doi.org/10.1007/3-211-31178-5).
12. Lang J. *Clinical anatomy of the head. Neurocranium, orbit and cranio-cervical regions*. Berlin/Heidelberg: Springer; 1983. doi:[10.1007/978-3-642-68242-1](https://doi.org/10.1007/978-3-642-68242-1).

## 4.1 Introduction

Most endoscopic ventricular procedures take place inside the third ventricle, which occupies a strategic area because it is the topographic center of the ventricular system. As a result of the ventricular dilatation required for endoscopic ventricular navigation, the third ventricle can be divided into anterior, middle, and posterior segments, each having several recesses (Fig. 4.1). During the preoperative planning it is important to recognize the anatomy on imaging studies, especially on sagittal T2-weighted magnetic resonance imaging (MRI) (Fig. 4.2). The gateway to the third ventricle is the foramen of Monro, and after the passage of the endoscope through this it is possible to have a panoramic view of the third ventricle segments (Fig. 4.3, 4.4, and 4.5). In the anterior segment the most important area is that between the mammillary bodies and the pituitary infundibulum, the tuber cinereum. This region is the site in which endoscopic third ventriculostomy (ETV) is performed [1, 2]. Before the passage of the endoscope through the foramen of Monro, an overview of this region is possible (Fig. 4.6). The interthalamic adhesion is generally located in the middle segment, although this segment has an extremely variable position in the third ventricle, and there are reports of the existence of a duplicate variant of this structure [3]. The posterior segment is located at the entrance of the cerebral aqueduct. Above this, in sequence from bottom to top, lie the posterior commissure, which has extremely variable size [4, 5, 6]; the pineal recess; and the suprapineal recess, which is in contact with the roof of the third ventricle and contains the choroid plexus. The pineal

gland can be seen through the pineal recess. The view of such posterior segment structures is possible when the skull entry point is more anterior than the Kocher's point; for instance, when aqueductoplasty is performed [7], or when the hydrocephalus is of large proportion, allowing a posterior orientation of the endoscope subsequently.

For the anterior segment, the endoscopic viewing angle is shown in Fig. 4.7, followed by images of this segment (see Figs. 4.8, 4.9, 4.10, 4.11, 4.12, 4.13, 4.14, 4.15, 4.16, 4.17, 4.18, 4.19, 4.20, 4.21, 4.22, 4.23, 4.24, 4.25, 4.26, 4.27, 4.28, 4.29, 4.30, 4.31, 4.32, 4.33, 4.34, 4.35, 4.36, 4.37, 4.38, 4.39, 4.40, 4.41, 4.42, 4.43, 4.44, 4.45, 4.46, 4.47, 4.48, 4.49, 4.50, 4.51, 4.52, 4.53, 4.54, 4.55, 4.56, 4.57, 4.58, 4.59, 4.60, 4.61, 4.62, 4.63, 4.64, 4.65, 4.66, 4.67, 4.68, 4.69, 4.70, 4.71, 4.72, 4.73, 4.74, 4.75, 4.76, 4.77, 4.78, 4.79, 4.80, 4.81, 4.82, 4.83, 4.84, 4.85, 4.86, 4.87, 4.88, 4.89, and 4.90). For the middle segment, the endoscopic viewing angle is shown in Fig. 4.91, followed by images of this segment (see Figs. 4.92, 4.93, 4.94, 4.95, 4.96, 4.97, 4.98, 4.99, 4.100, 4.101, 4.102, 4.103, 4.104, 4.105, 4.106, 4.107, 4.108, 4.109, 4.110, 4.111, 4.112, 4.113, and 4.114). For the posterior segment, the endoscopic viewing angle is shown in Fig. 4.115, followed by images of this segment (see Figs. 4.116, 4.117, 4.118, 4.119, 4.120, 4.121, 4.122, 4.123, 4.124, 4.125, 4.126, 4.127, 4.128, 4.129, 4.130, 4.131, 4.132, 4.133, 4.134, 4.135, 4.136, 4.137, 4.138, 4.139, 4.140, 4.141, 4.142, 4.143, 4.144, 4.145, 4.146, 4.147, 4.148, 4.149, 4.150, 4.151, 4.152, 4.153, 4.154, 4.155, 4.156, 4.157, 4.158, 4.159, 4.160, 4.161, 4.162, 4.163, 4.164, 4.165, and 4.166).

Illustrative cases are presented.

**Fig. 4.1** Regions and recesses of the third ventricle (Reprinted from Seeger [1], with permission)

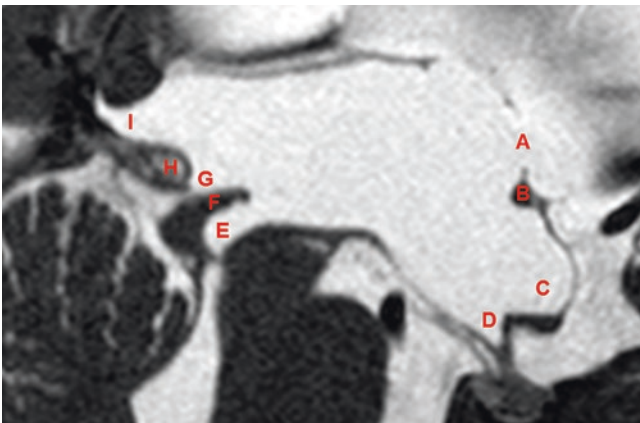
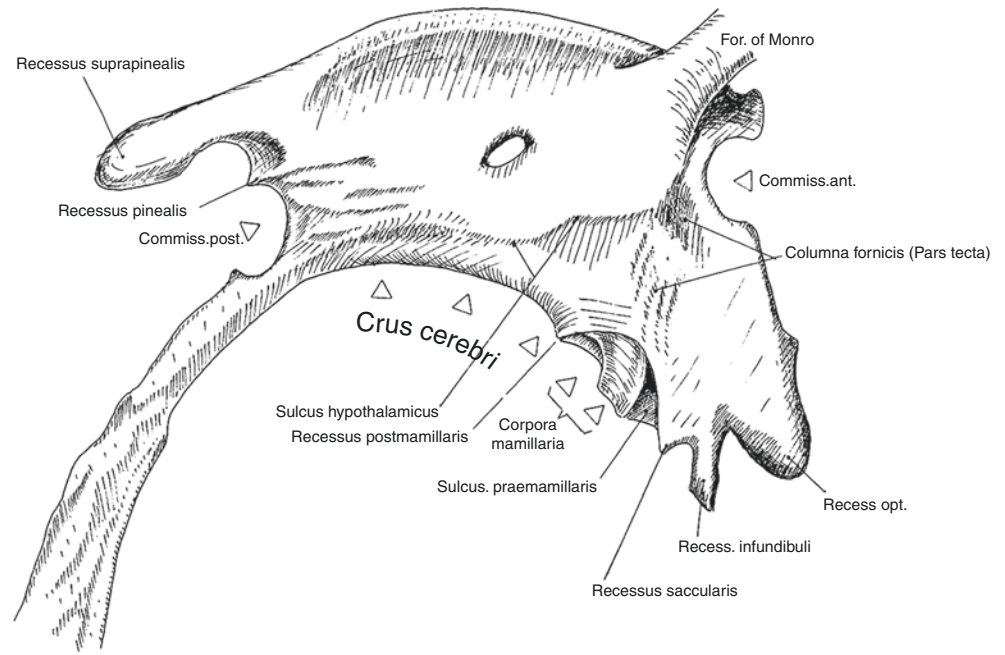


**Fig. 4.2** Sagittal T2-weighted magnetic resonance imaging (MRI) depicting the structures and main recesses of the third ventricle as viewed in Fig. 4.1. Foramen of Monro (A), anterior commissure (B), optic recess (C), infundibular recess (D), cerebral aqueduct entrance (obstructed) (E), posterior commissure (F), pineal recess (G), pineal gland (H), suprapineal recess (I)



## 4.2 Third Ventricle: General Vision of the Floor

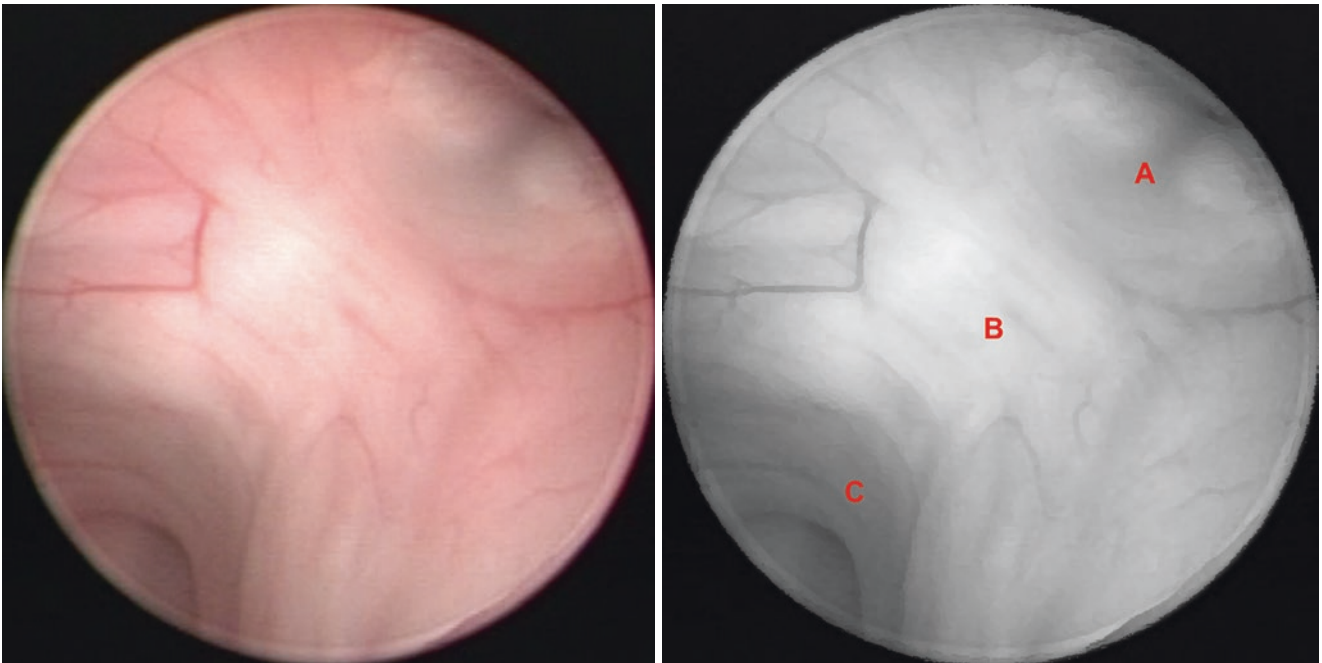


**Fig. 4.3** Normal anatomy. (A) Anterior segment, (B) middle segment, (C) posterior segment

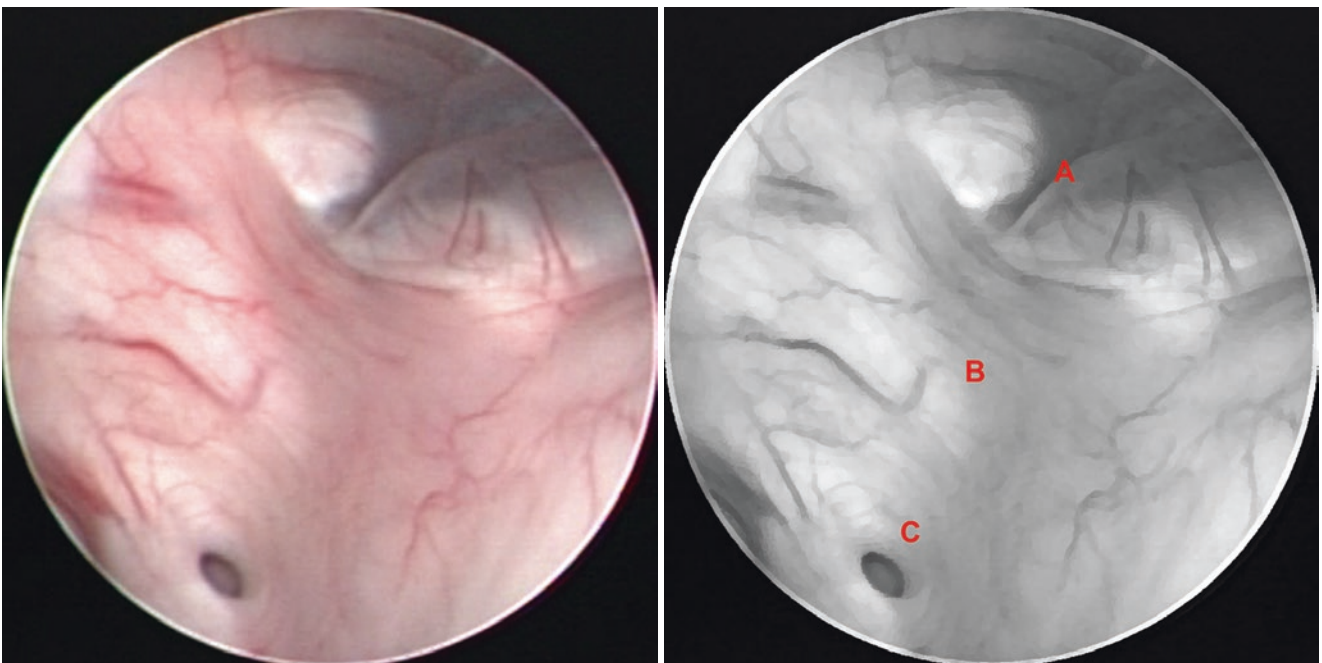


**Fig. 4.4** Normal anatomy. (A) Anterior segment, (B) middle segment, (C) posterior segment

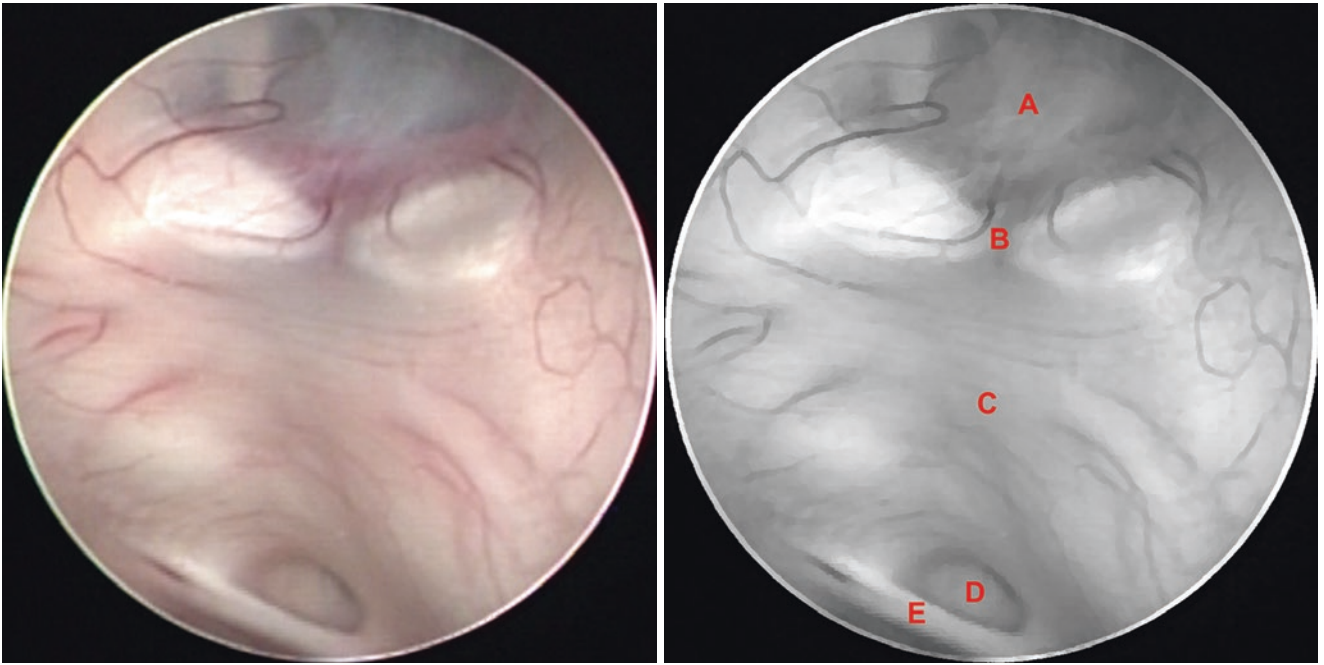


**Fig. 4.5** Normal anatomy. (A) Tuber cinereum, (B) mammillary bodies, (C) middle segment, (D) cerebral aqueduct, (E) posterior commissure

**Fig. 4.6** Vision of the anterior portion of the third ventricle through the foramen of Monro. Anterior commissure (*a*), column of the fornix (*b*), optic chiasm (*c*), infundibular recess (*d*), saccular recess (*e*), premammillary sulcus (*f*), left mammillary body (*g*), hypothalamic sulcus (*h*), thalamus (*i*) (Reprinted from Seeger [1], with permission)

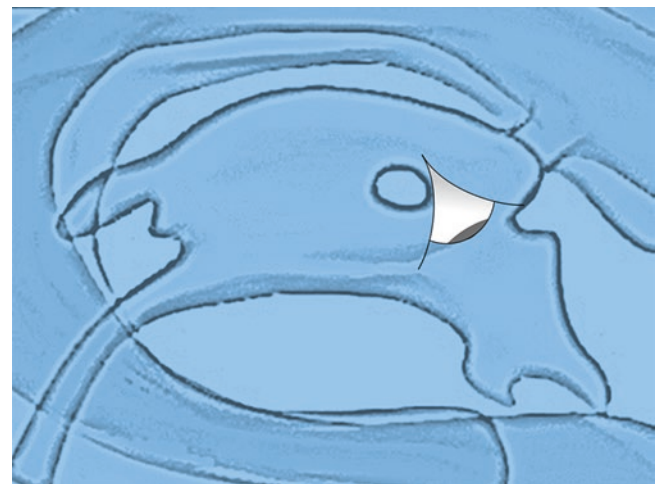
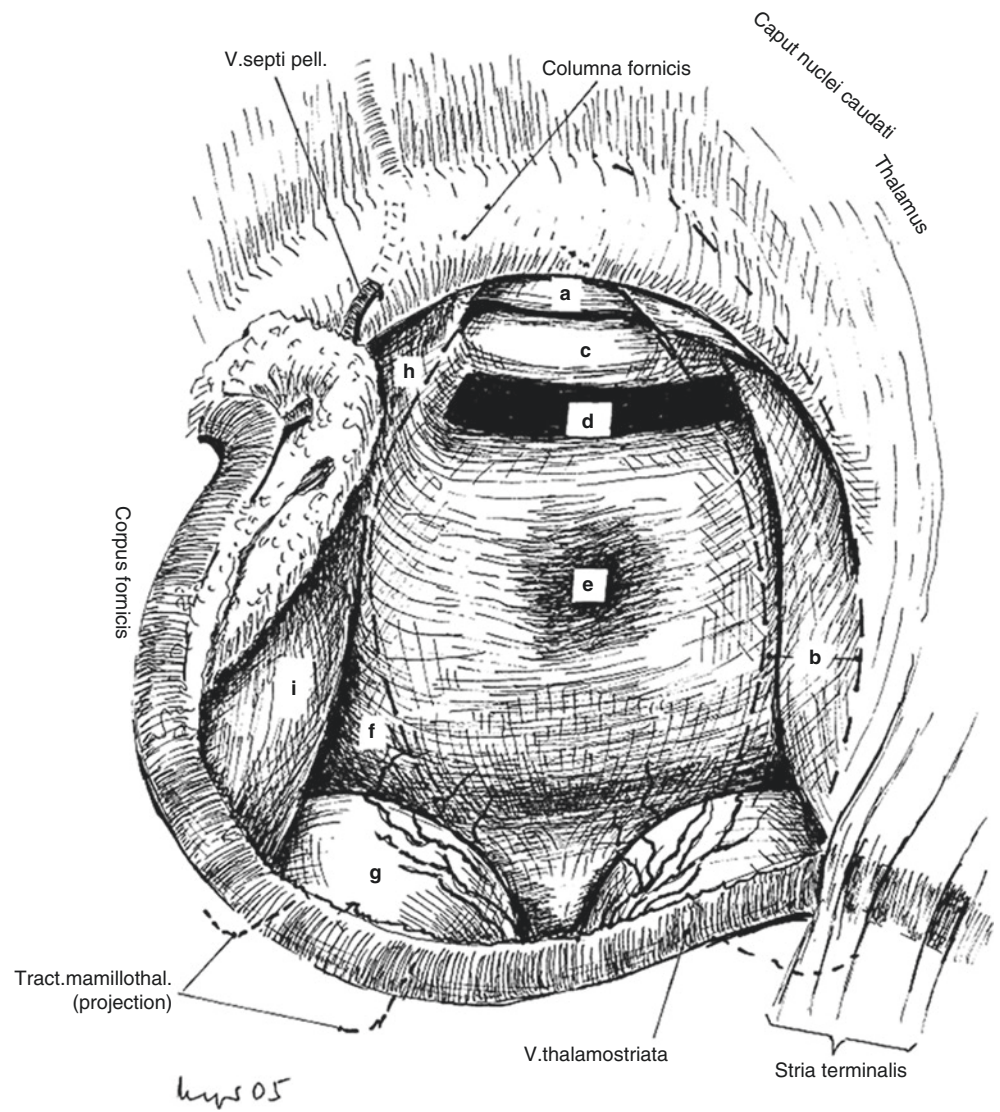


**Fig. 4.7** Direction of the endoscopic vision for the anterior segment of the third ventricle

### 4.3 Third Ventricle: Anterior Segment

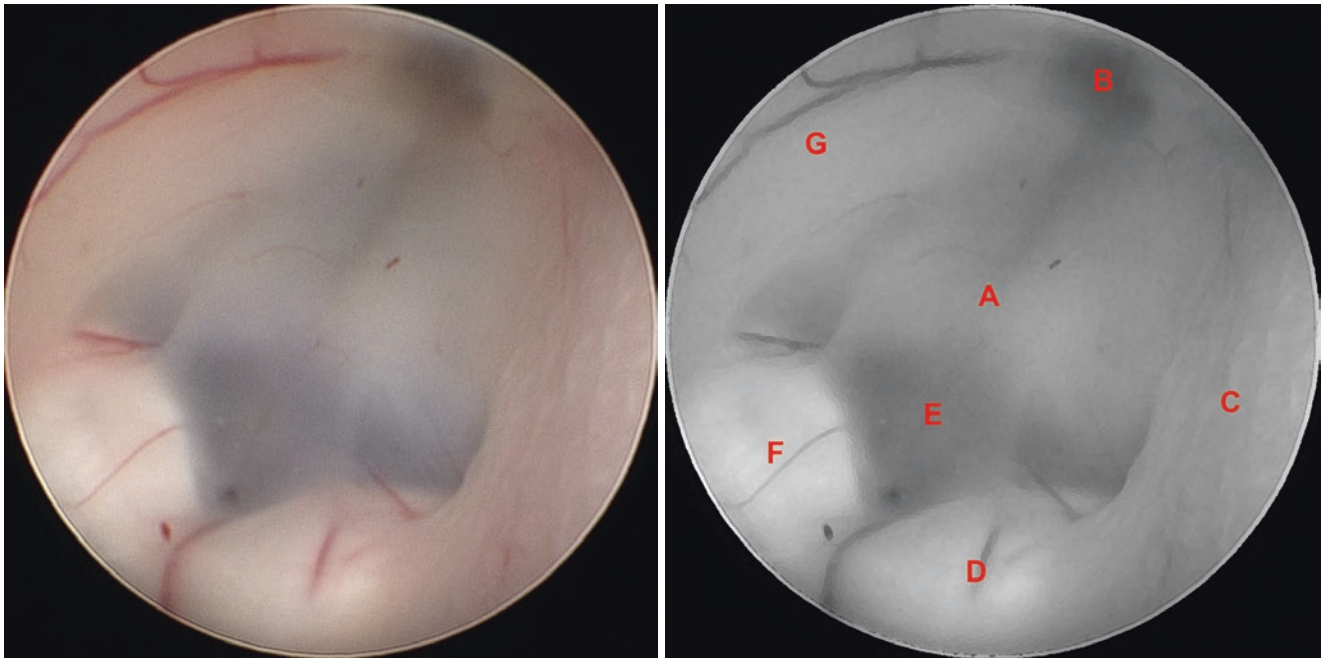


**Fig. 4.8** Normal anatomy. (A) Tuber cinereum, (B) Infundibular recess, (C) Right hypothalamus, (D) Right mammillary body, (E) Premammillary recess, (F) Left mammillary body, (G) Left hypothalamus

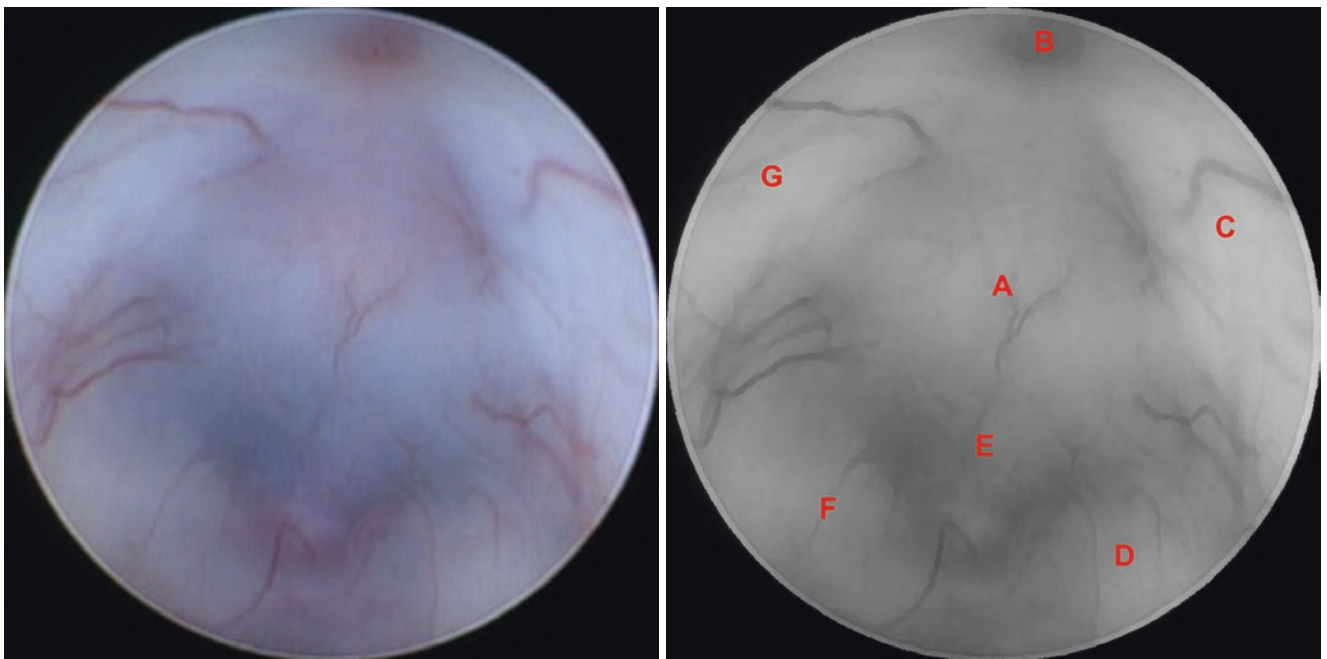


**Fig. 4.9** Normal anatomy. (A) Tuber cinereum, (B) Infundibular recess, (C) Right hypothalamus, (D) Right mammillary body, (E) Premammillary recess, (F) Left mammillary body, (G) Left hypothalamus

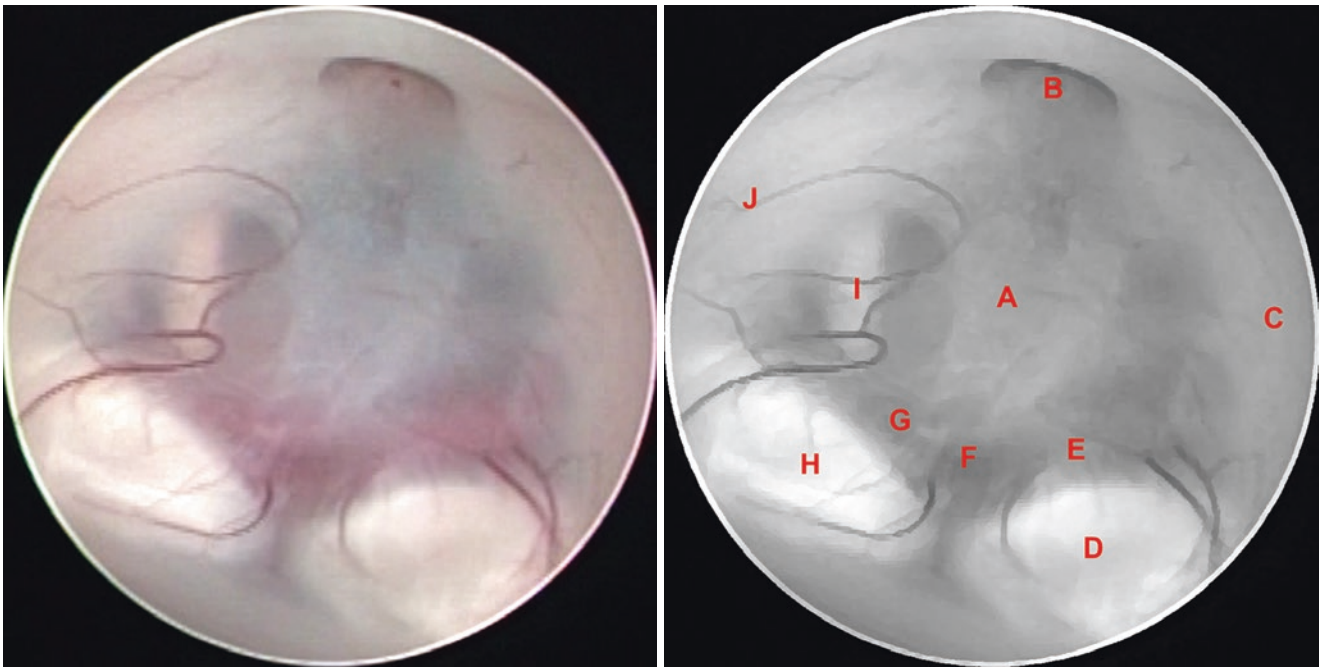


**Fig. 4.10** Normal anatomy. (A) Tuber cinereum, (B) Infundibular recess, (C) Right hypothalamus, (D) Right mammillary body, (E) Right posterior cerebral artery (P1), (F) Bifurcation of the basilar artery, (G)

Left posterior cerebral artery (P1), (H) Left mammillary body, (I) Left oculomotor nerve (CN III), (J) Left hypothalamus

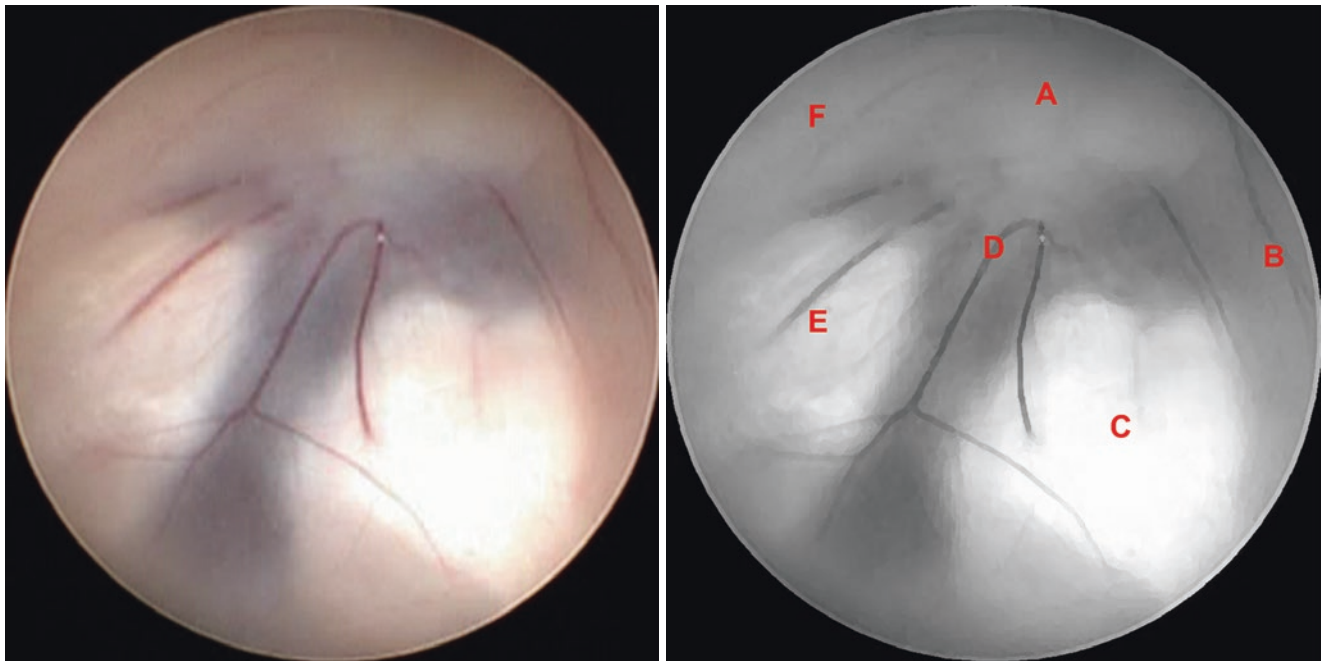


**Fig. 4.11** Normal anatomy. (A) Tuber cinereum, (B) Right hypothalamus, (C) Right mammillary body, (D) Premammillary recess, (E) Left mammillary body, (F) Left hypothalamus

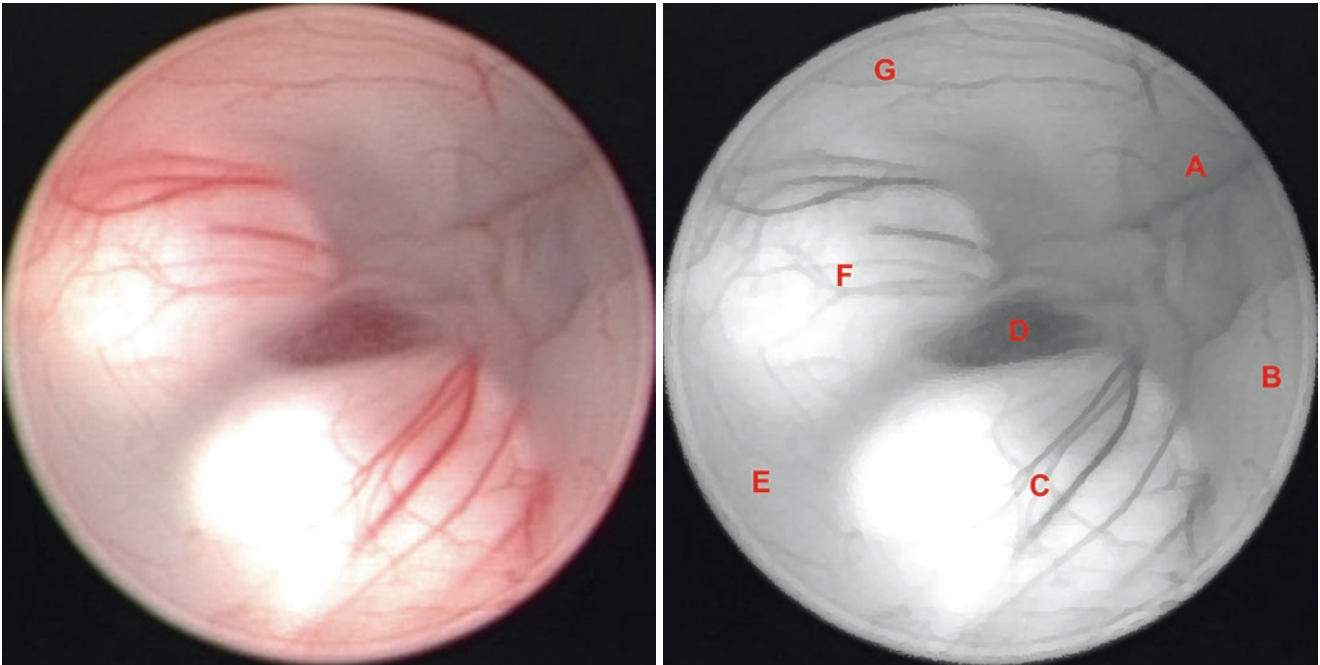


**Fig. 4.12** Normal anatomy. (A) Tuber cinereum, (B) Right hypothalamus, (C) Right mammillary body, (D) Thalamoperforating arteries under premammillary recess, (E) Postmammillary recess, (F) Left mammillary body, (G) Left hypothalamus

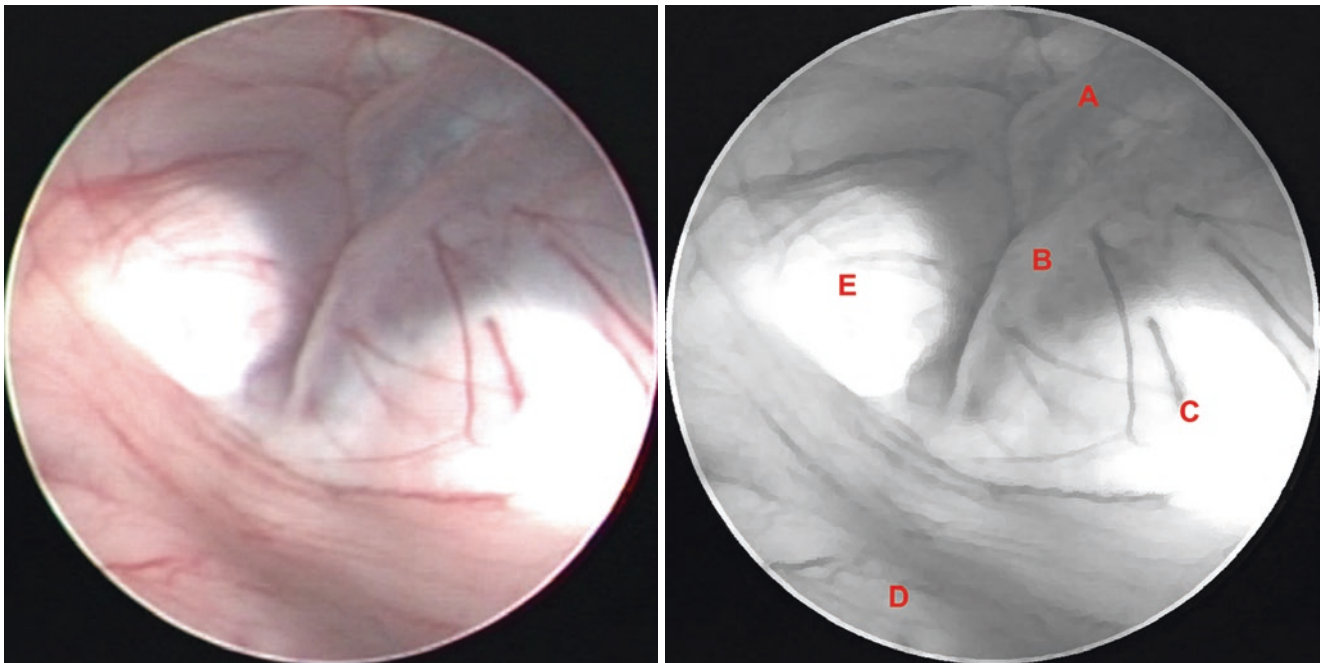


**Fig. 4.13** Normal anatomy. (A) Tuber cinereum, (B) Premammillary recess, (C) Right mammillary body, (D) Postmammillary recess, (E) Left mammillary body

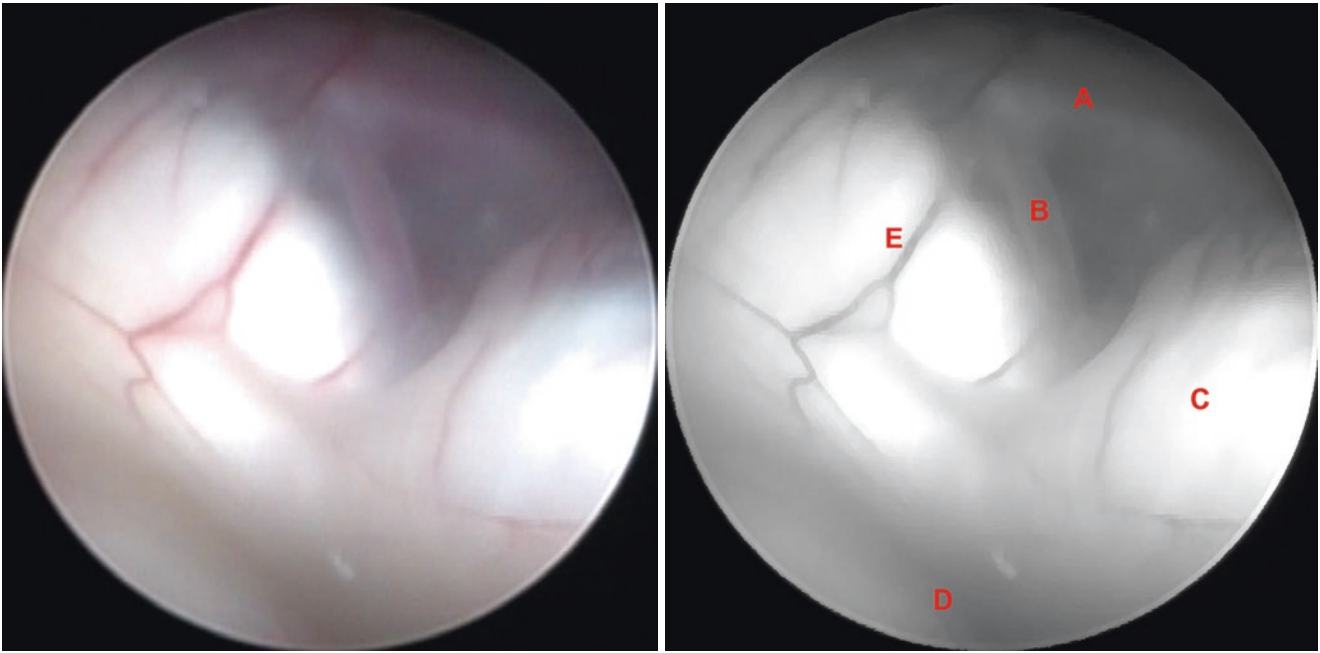


**Fig. 4.14** Normal anatomy. (A) Left posterior cerebral artery (P1), (B) Thalamoperforating artery, (C) Right mammillary body, (D) Postmammillary recess, (E) Left mammillary body

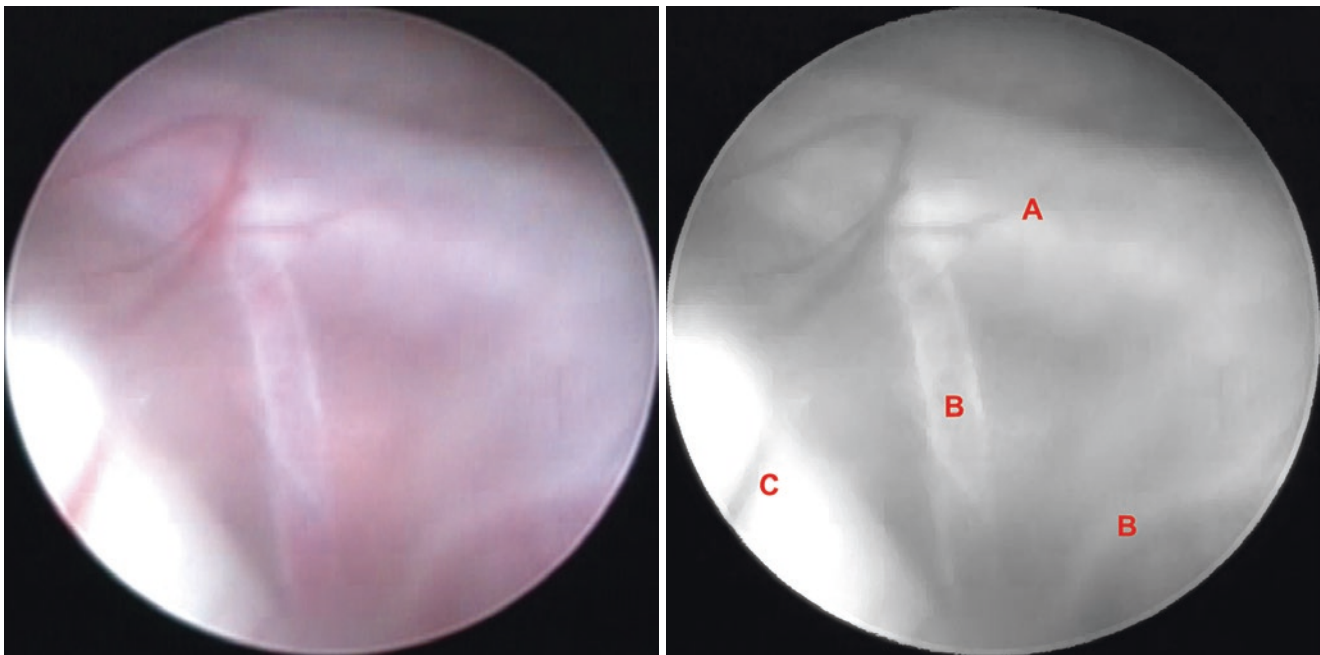


**Fig. 4.15** Normal anatomy. (A) Left posterior cerebral artery (P1), (B) Thalamoperforating arteries, (C) Left mammillary body

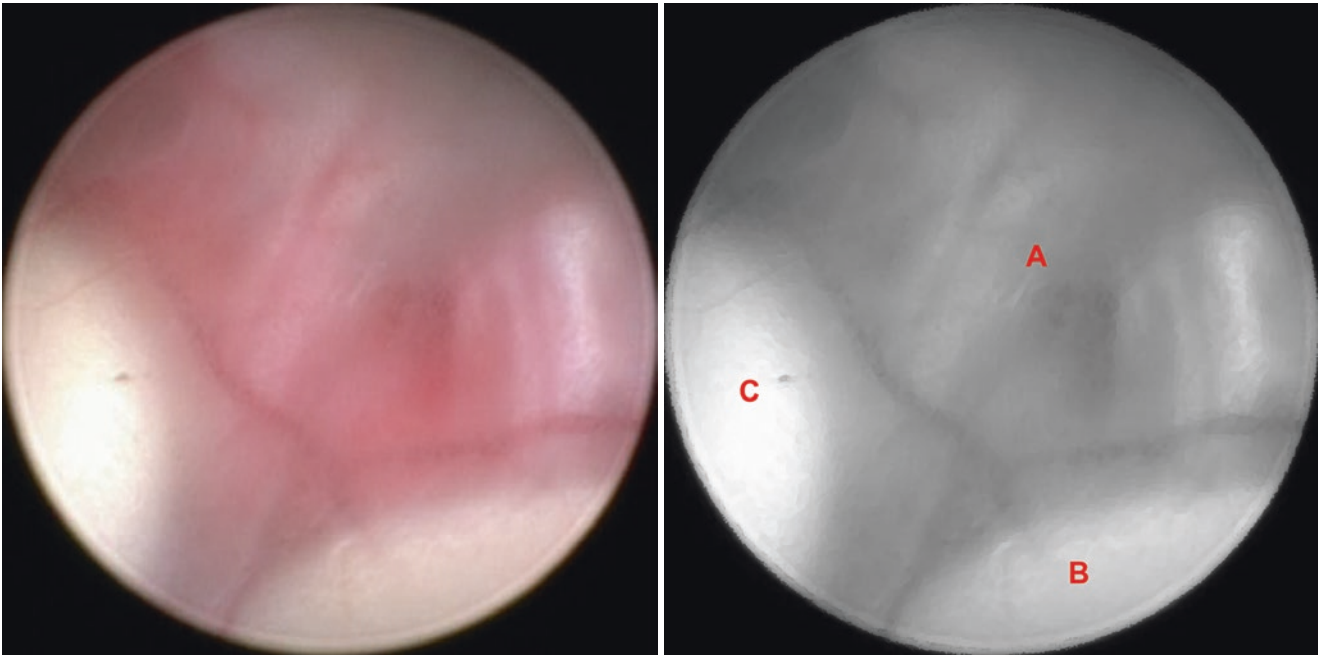


**Fig. 4.16** Normal anatomy. (A) Thalamoperforating arteries under the premammillary recess, (B) Right mammillary body, (C) Left mammillary body

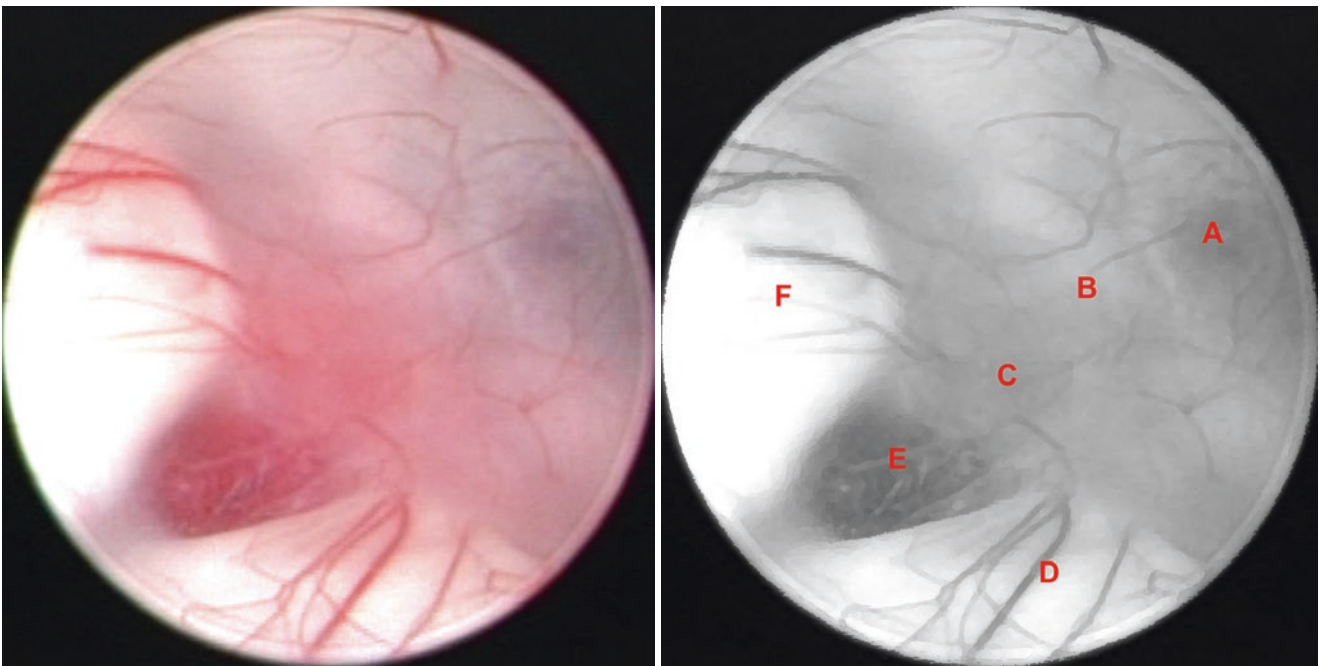


**Fig. 4.17** Normal anatomy. (A) Infundibular recess, (B) Tuber cinereum, (C) Premammillary recess, (D) Right mammillary body, (E) Thalamoperforating arteries under the premammillary recess, (F) Left mammillary body



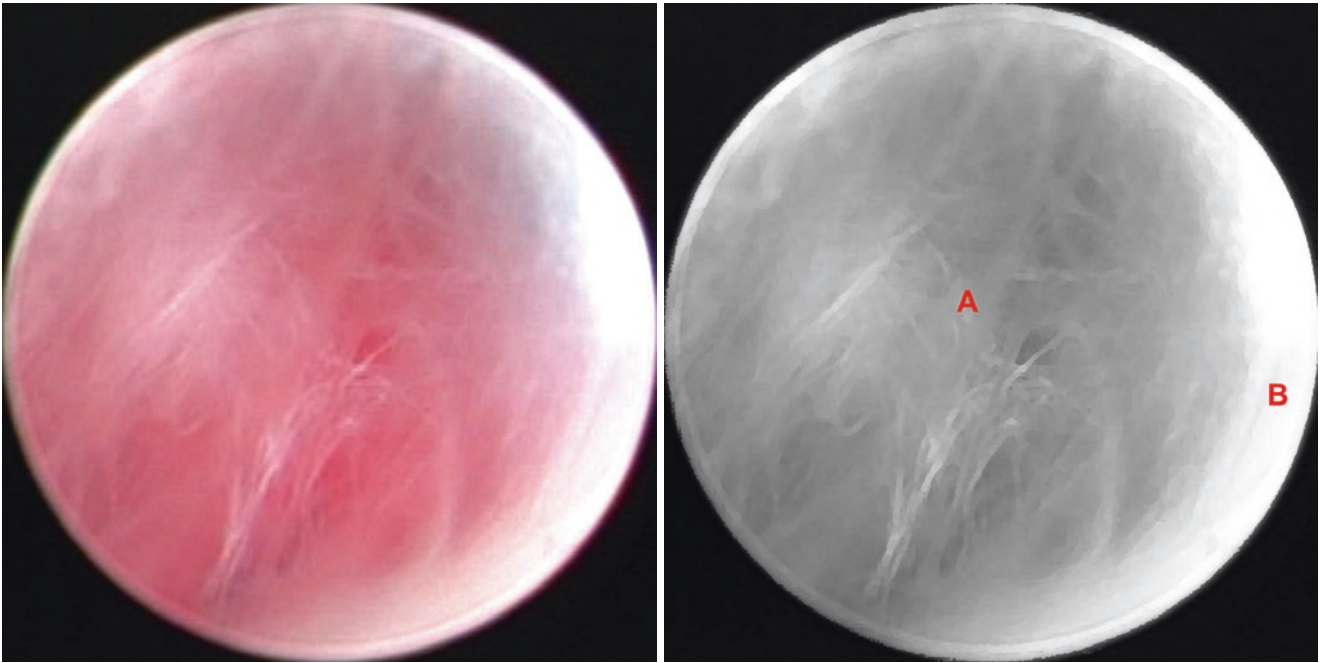


**Fig. 4.18** Normal anatomy. (A) Thalamoperforating arteries under the premammillary recess, (B) Right mammillary body

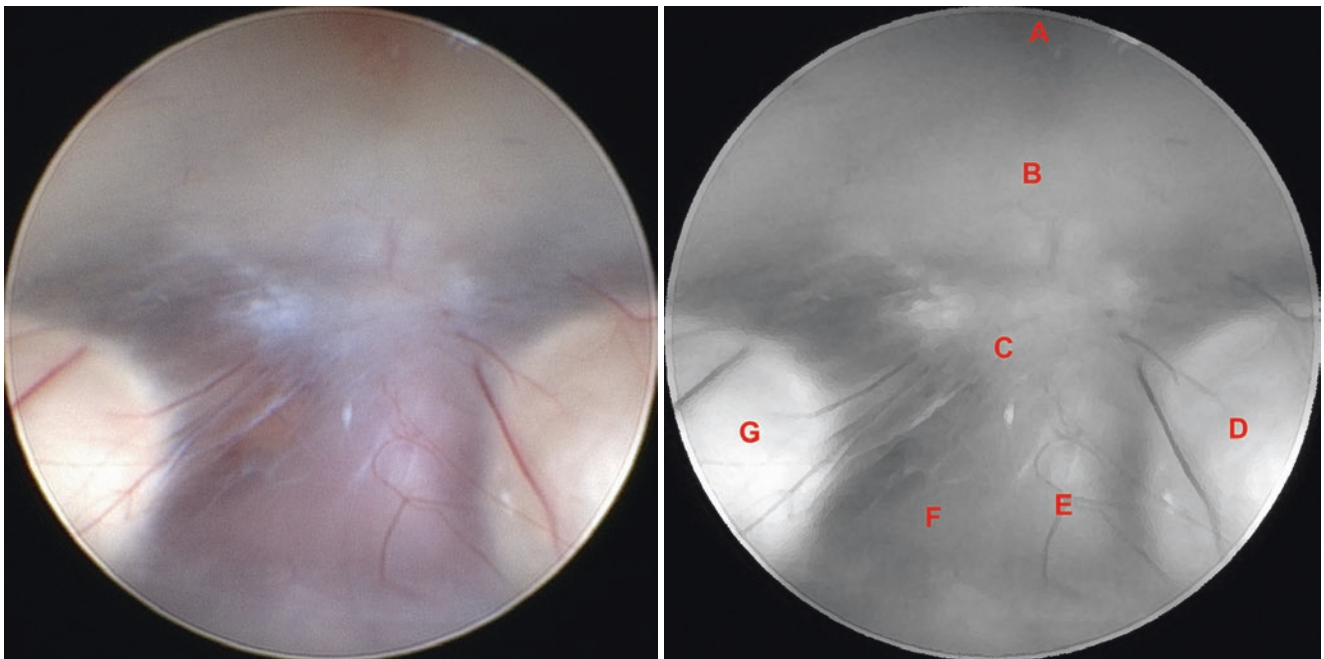


**Fig. 4.19** Normal anatomy. (A) Infundibular recess, (B) Tuber cinereum, (C) Premammillary recess, (D) Right mammillary body, (E) Bifurcation of the basilar artery, (F) Left posterior cerebral artery (P1), (G) Left mammillary body

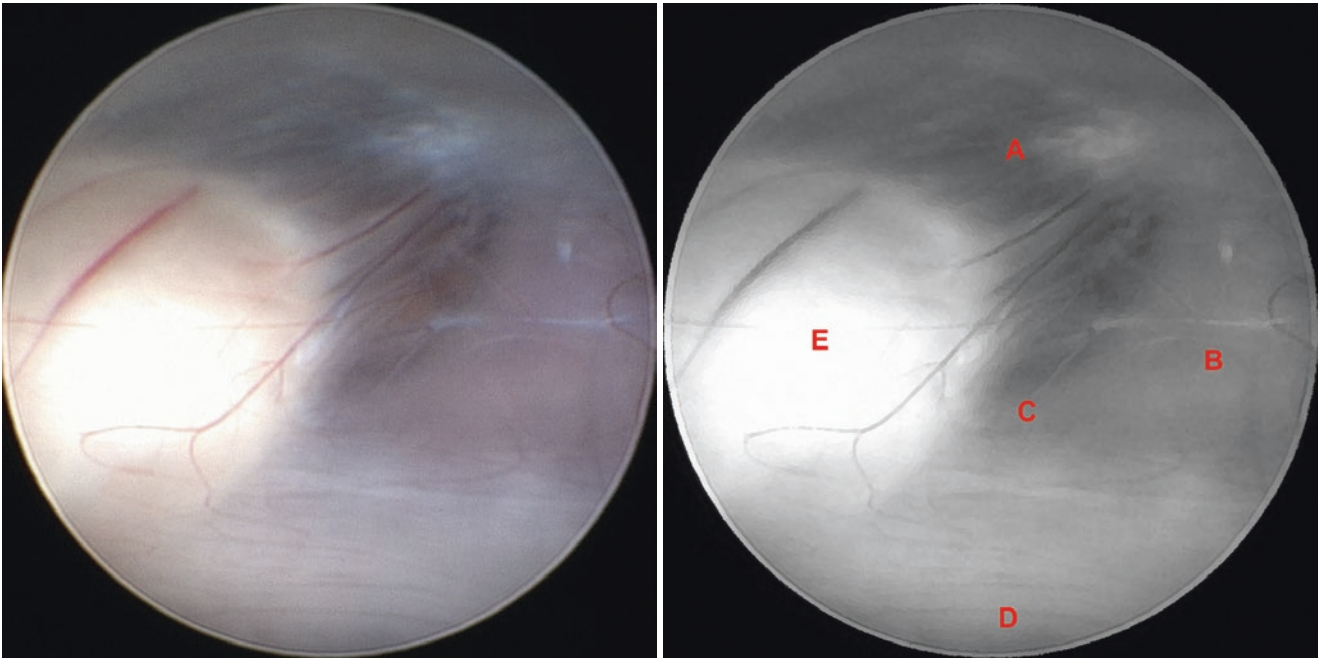


**Fig. 4.20** Normal anatomy. (A) Premammillary recess, (B) Bifurcation of the basilar artery, (C) Left posterior cerebral artery (P1), (D) Postmammillary recess, (E) Left mammillary body

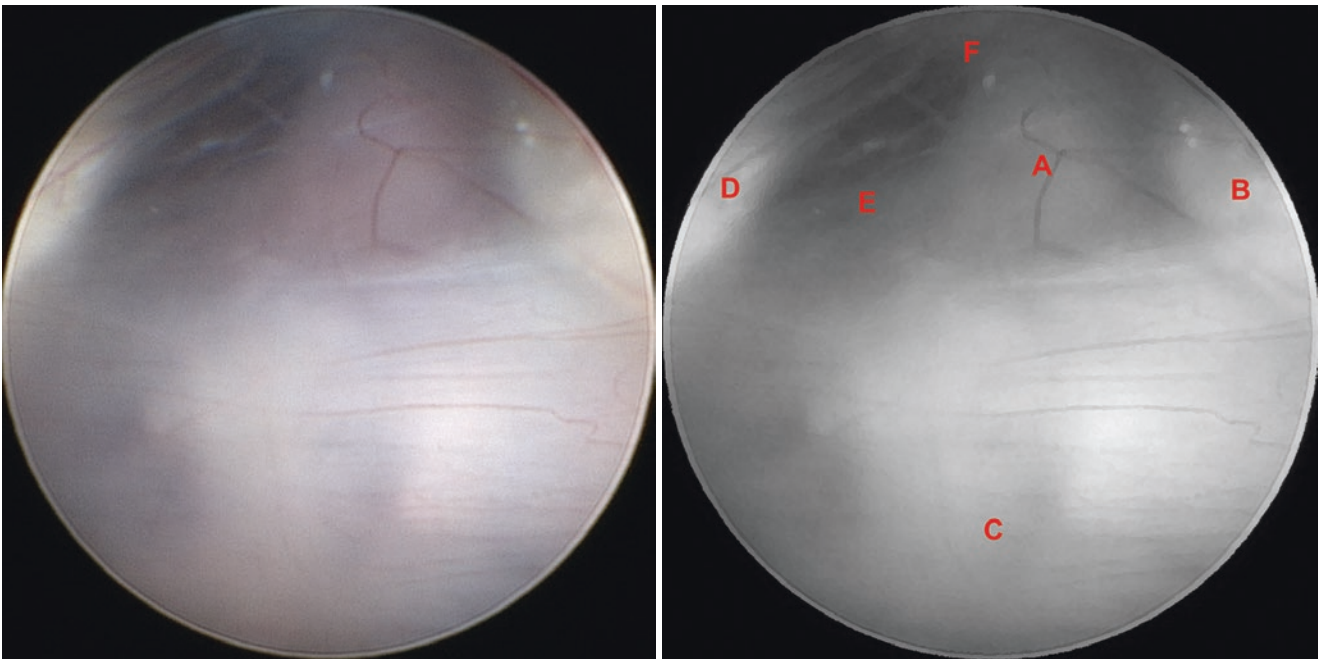


**Fig. 4.21** Normal anatomy. (A) Bifurcation of the basilar artery, (B) Right mammillary body, (C) Postmammillary recess, (D) Left mammillary body, (E) Left posterior cerebral artery (P1), (F) Premammillary recess

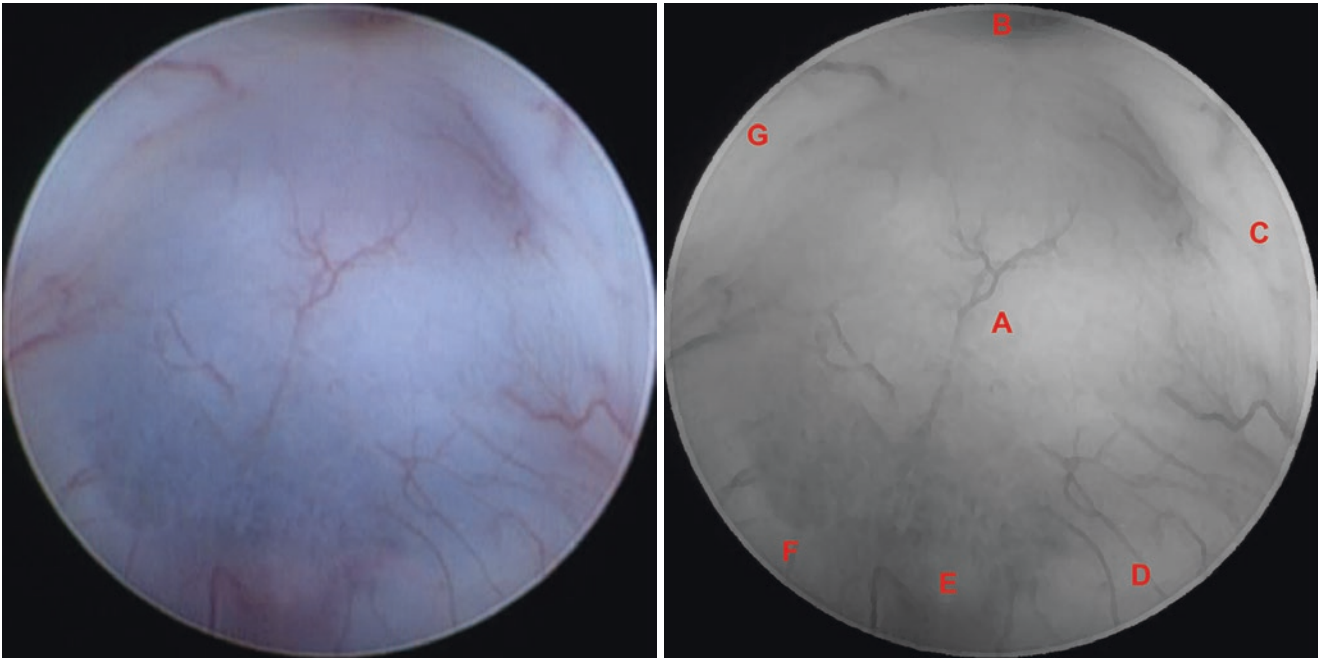


**Fig. 4.22** Normal anatomy. (A) Tuber cinereum, (B) Infundibular recess, (C) Right hypothalamus, (D) Right mammillary body, (E) Bifurcation of the basilar artery under pre-mammillary recess, (F) Left mammillary body, (G) Left hypothalamus

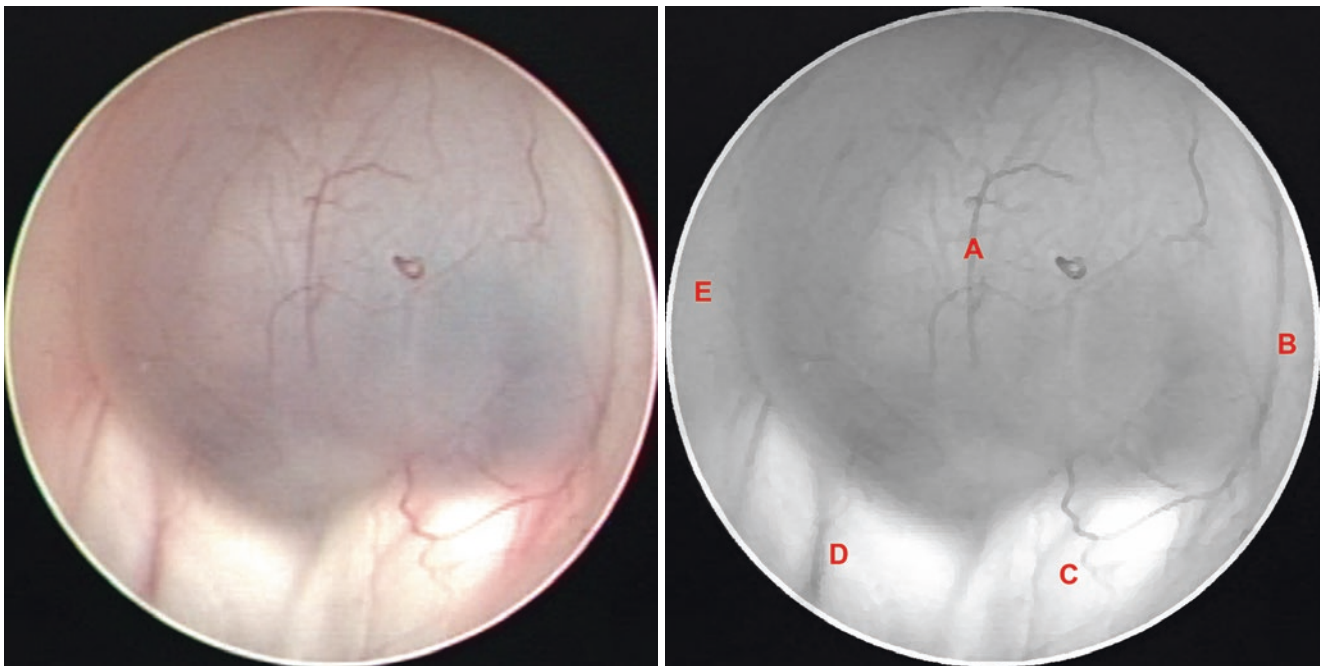


**Fig. 4.23** Normal anatomy. (A) Tuber cinereum, (B) Right hypothalamus, (C) Right mammillary body, (D) Left mammillary body, (E) Left hypothalamus

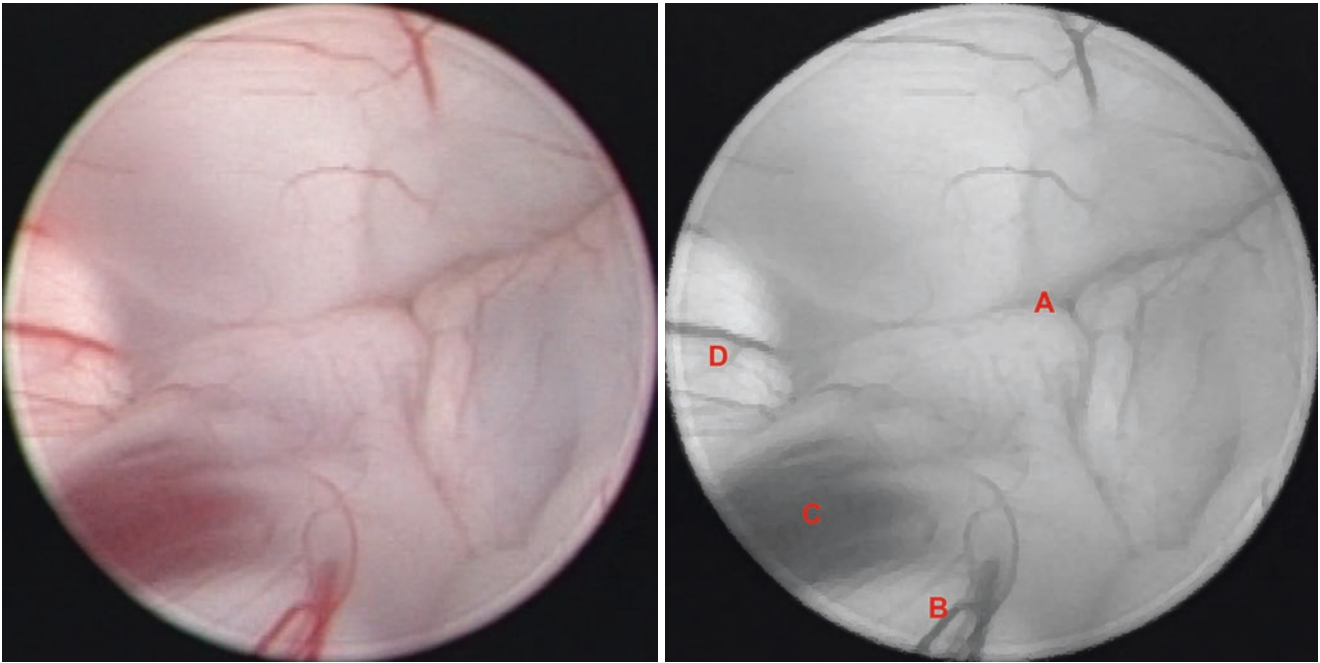


**Fig. 4.24** Normal anatomy. (A) Tuber cinereum, (B) Right mammillary body, (C) Thalamoperforating arteries under premammillary recess, (D) Left mammillary body

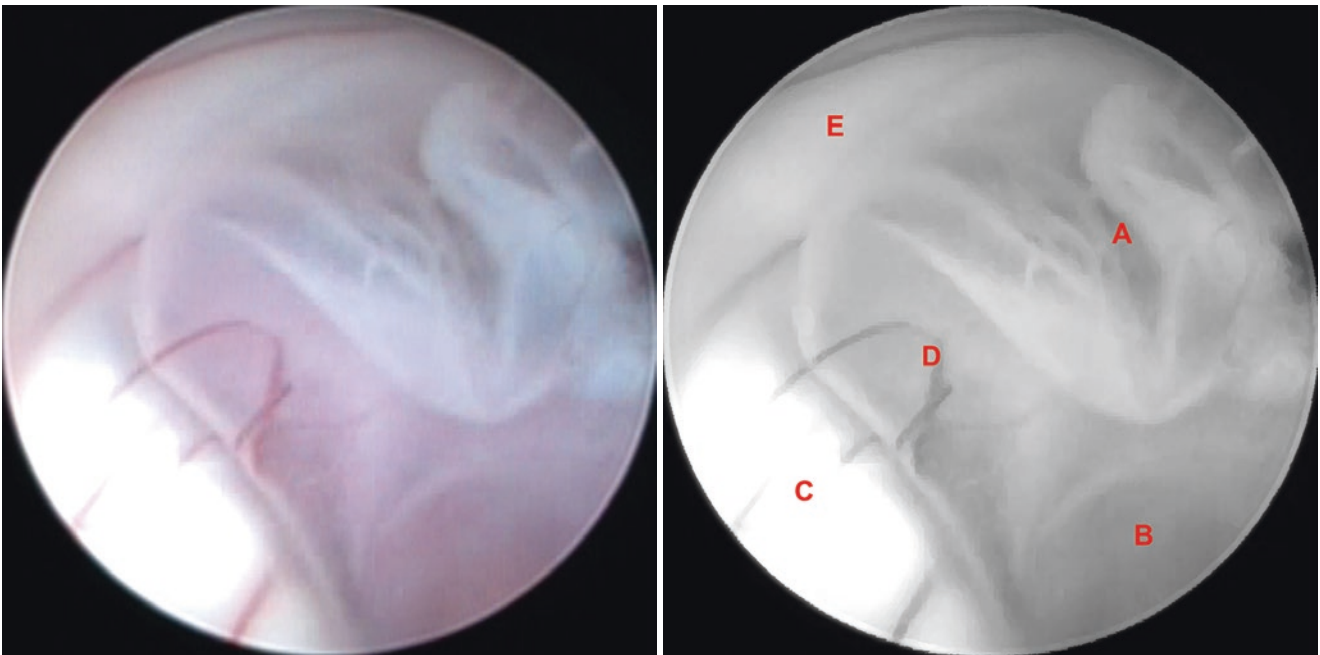


**Fig. 4.25** Normal anatomy. (A) Tuber cinereum, (B) Bifurcation of the basilar artery, (C) Left mammillary body, (D) Left posterior cerebral artery (P1), (E) Left hypothalamus

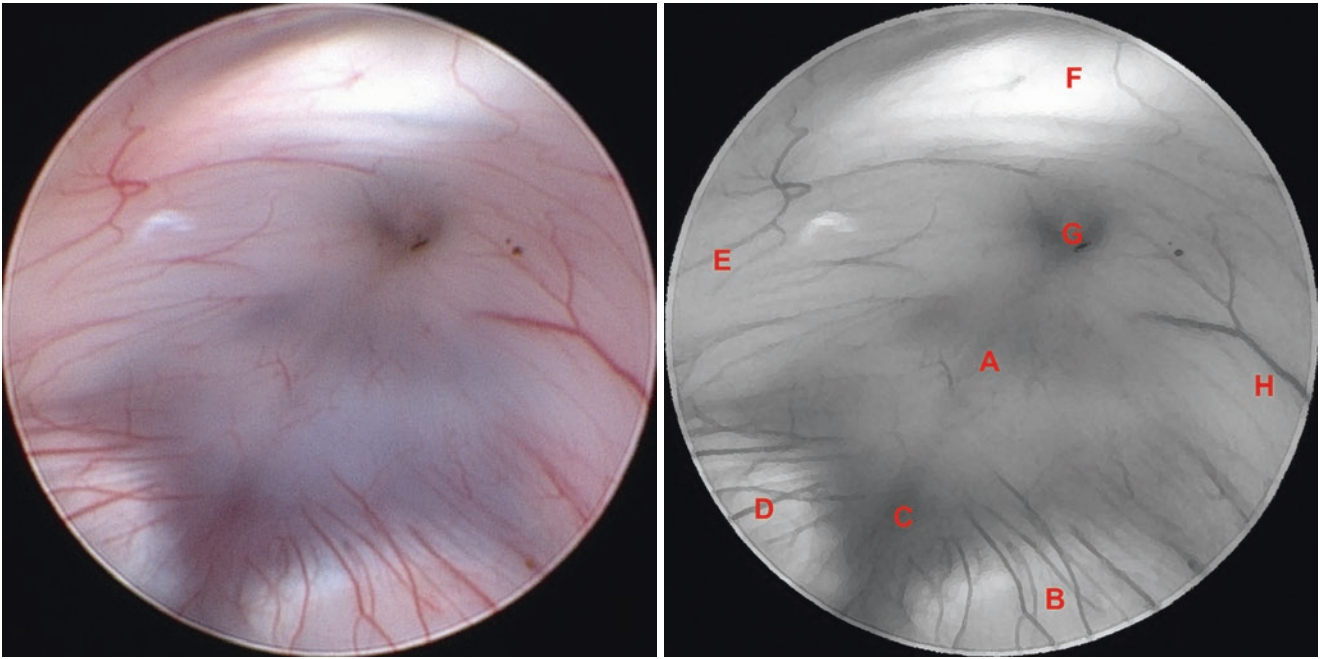


**Fig. 4.26** Normal anatomy. (A) Tuber cinereum, (B) Right mammillary body, (C) Premammillary recess, (D) Left mammillary body, (E) Left hypothalamus, (F) Optic chiasm, (G) Infundibular recess, (H) Right hypothalamus

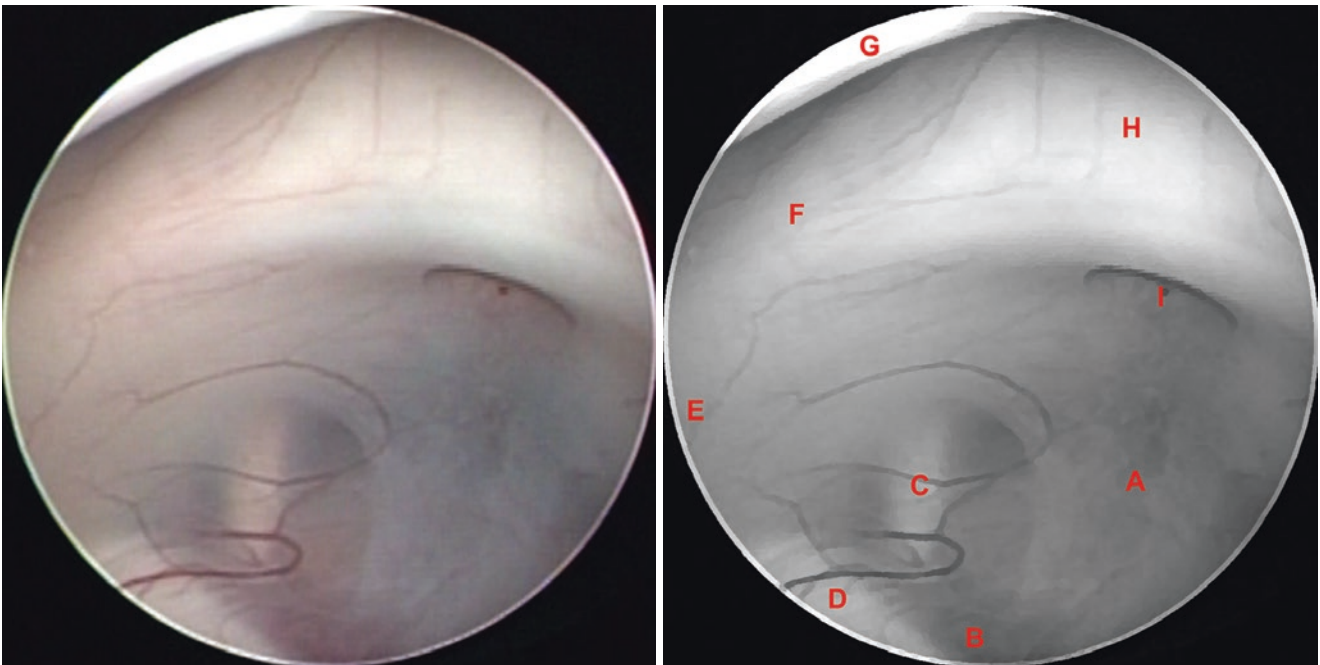


**Fig. 4.27** Normal anatomy. (A) Tuber cinereum, (B) Bifurcation of the basilar artery under premammillary recess, (C) Left oculomotor nerve (CN III), (D) Left mammillary body, (E) Left hypothalamus, (F) Left optic tract, (G) Anterior commissure, (H) Optic chiasm, (I) Infundibular recess

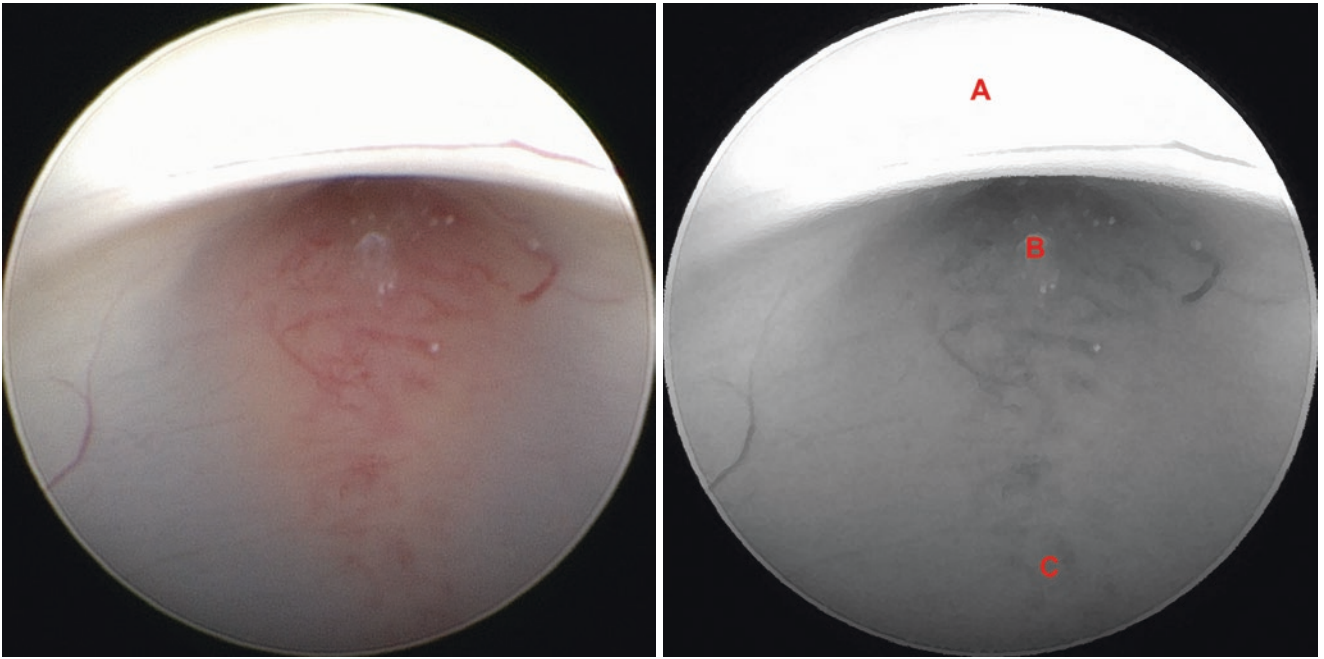


**Fig. 4.28** Normal anatomy. (A) Optic chiasm, (B) Infundibular recess, (C) Tuber cinereum

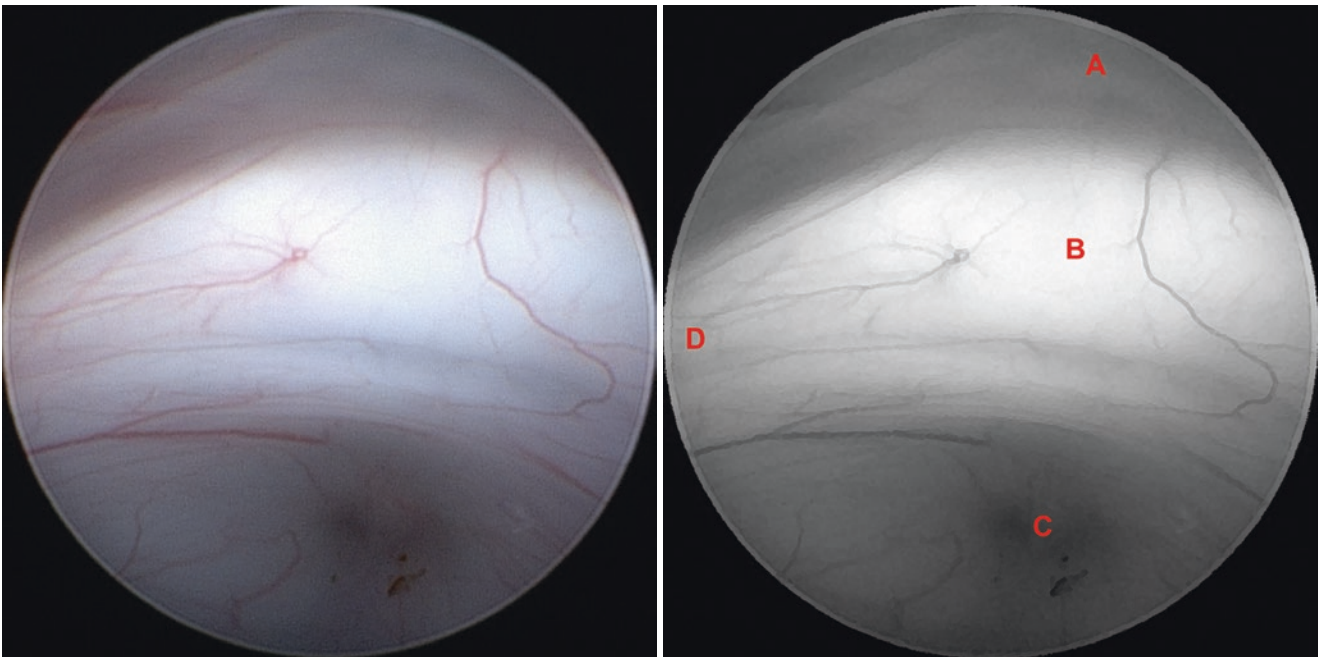


**Fig. 4.29** Normal anatomy. (A) Lamina terminalis, (B) Optic chiasm, (C) Infundibular recess, (D) Left optic tract

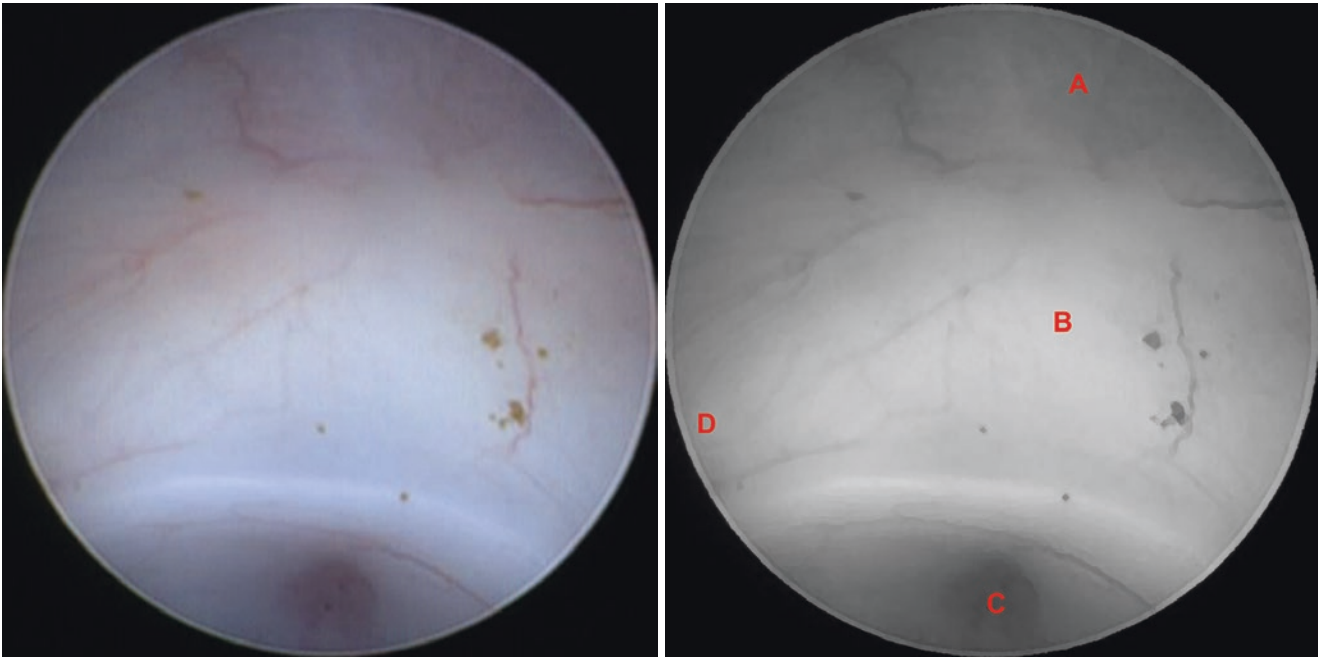


**Fig. 4.30** Normal anatomy. (A) Lamina terminalis, (B) Optic chiasm, (C) Infundibular recess, (D) Left optic tract

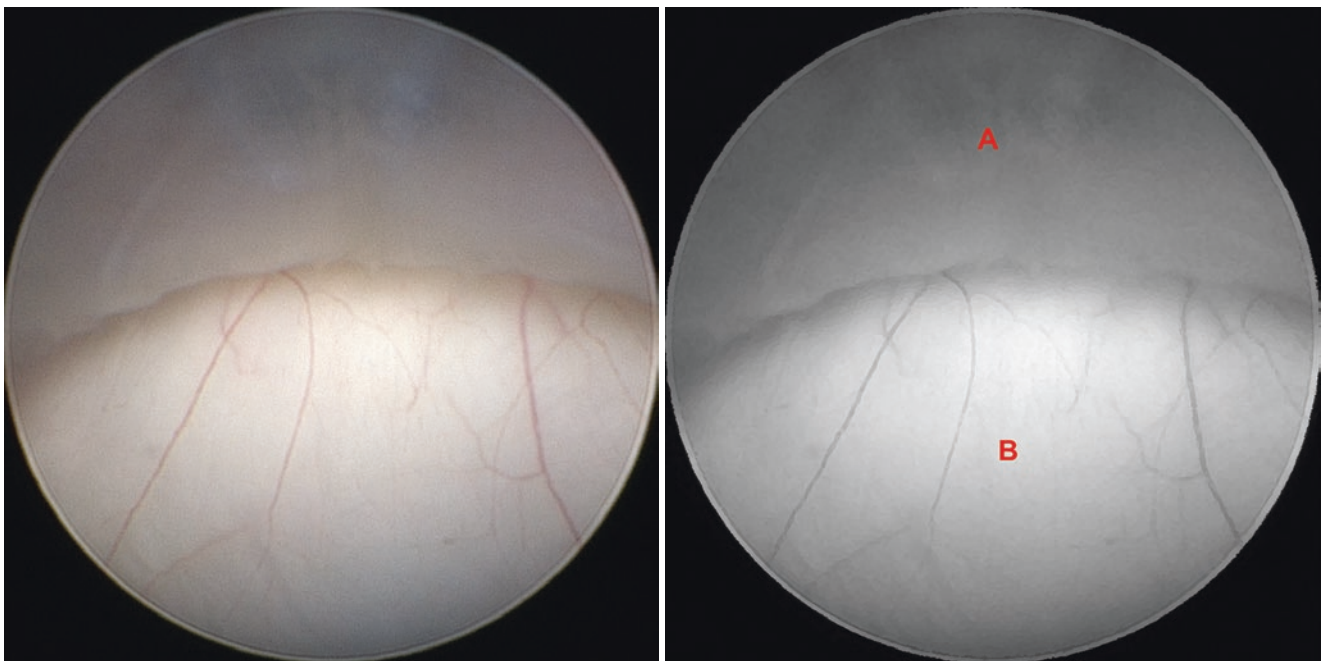


**Fig. 4.31** Normal anatomy. (A) Lamina terminalis, (B) Optic chiasm

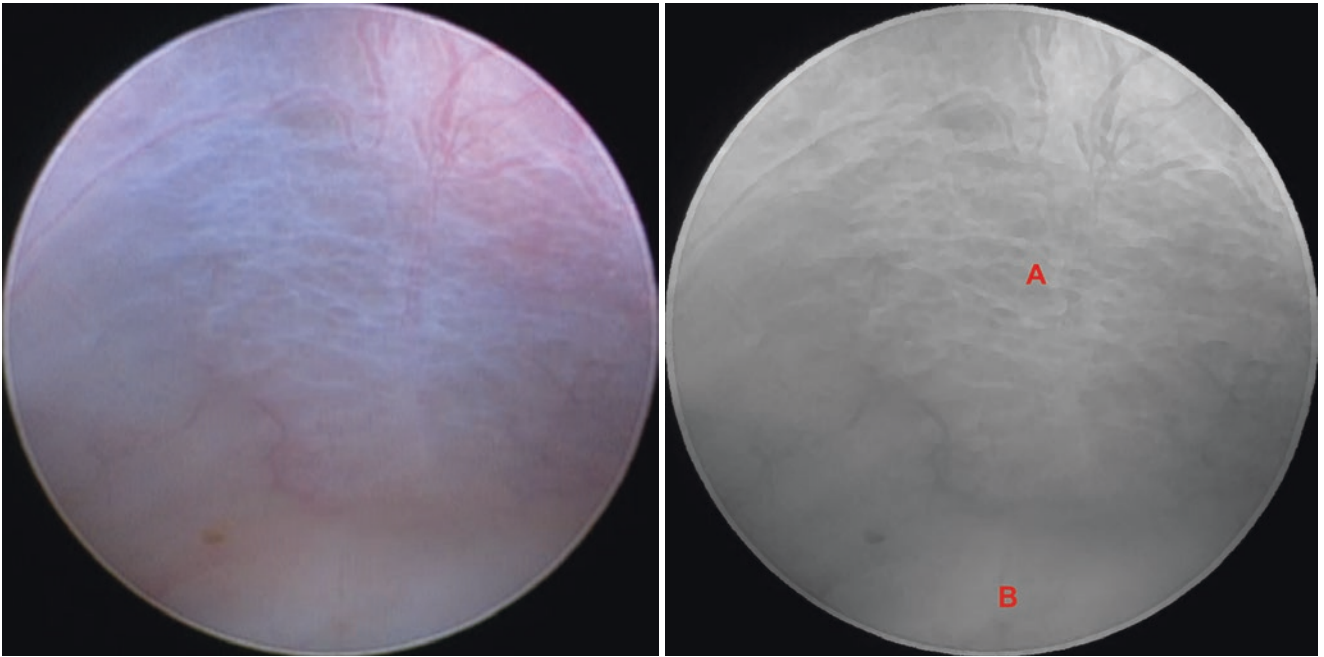


**Fig. 4.32** Normal anatomy. (A) Lamina terminalis, (B) Optic chiasm

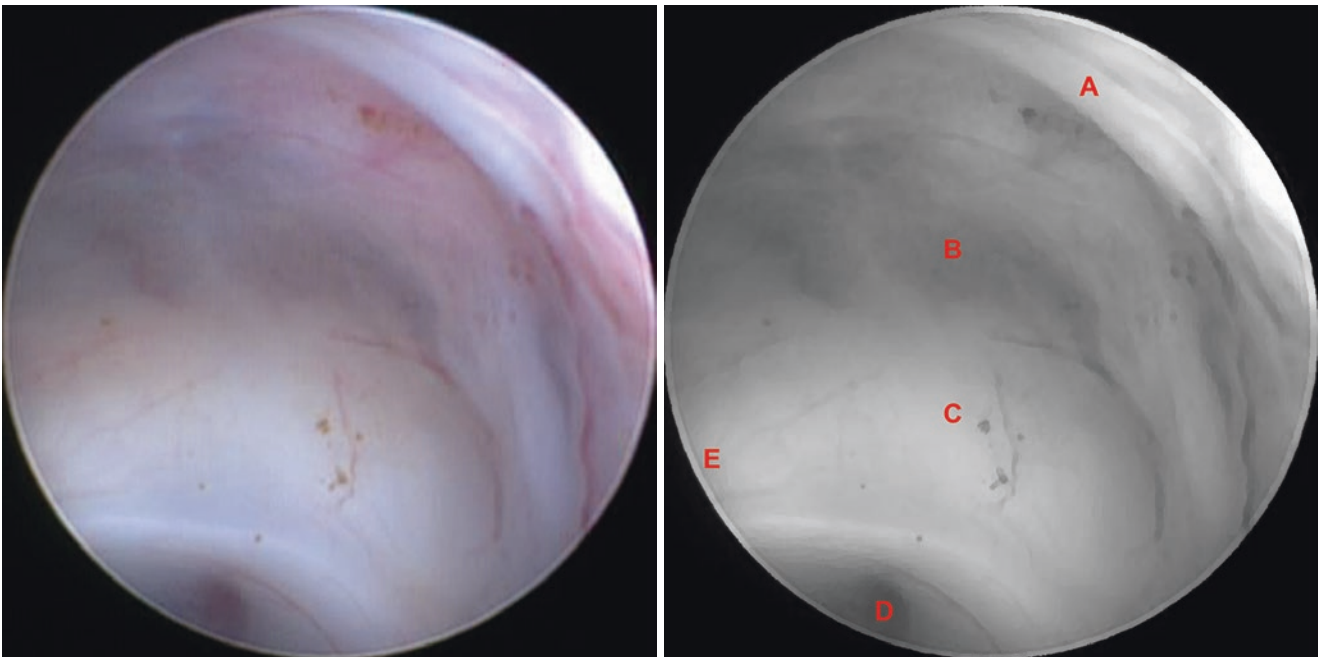


**Fig. 4.33** Normal anatomy. (A) Anterior commissure, (B) Lamina terminalis, (C) Optic chiasm, (D) Infundibular recess, (E) Left optic tract



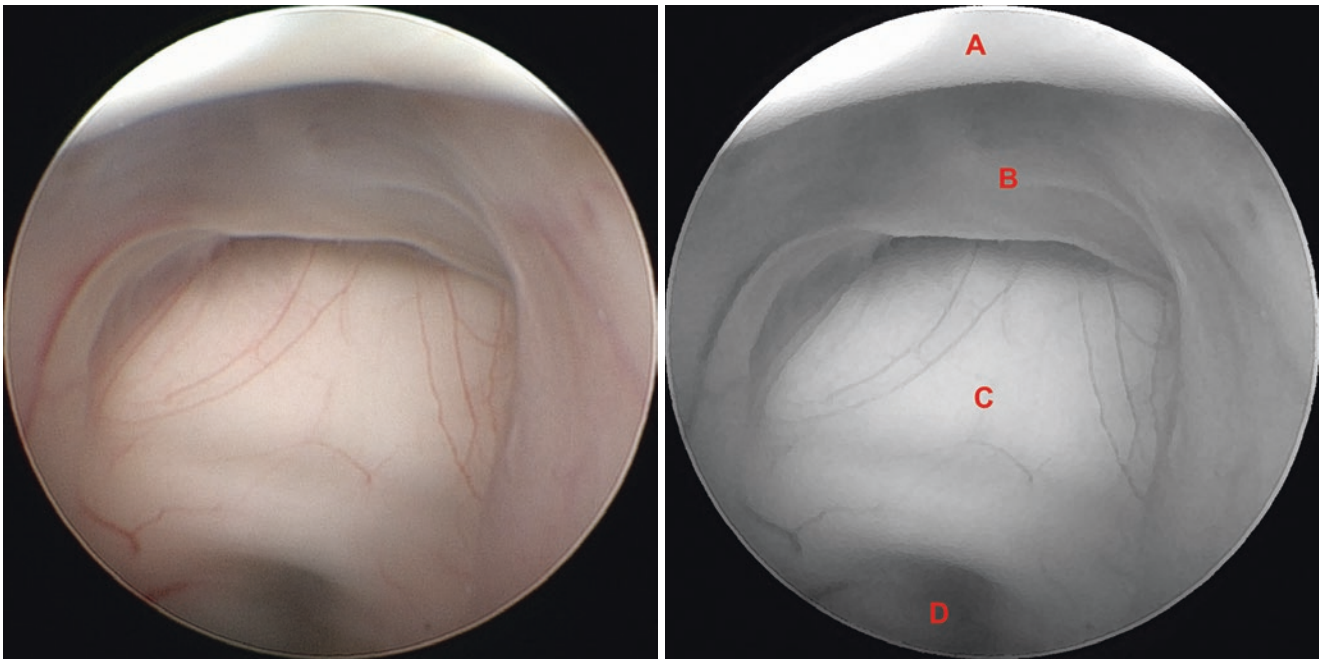


**Fig. 4.34** Normal anatomy. (A) Anterior commissure, (B) Lamina terminalis, (C) Optic chiasm, (D) Infundibular recess

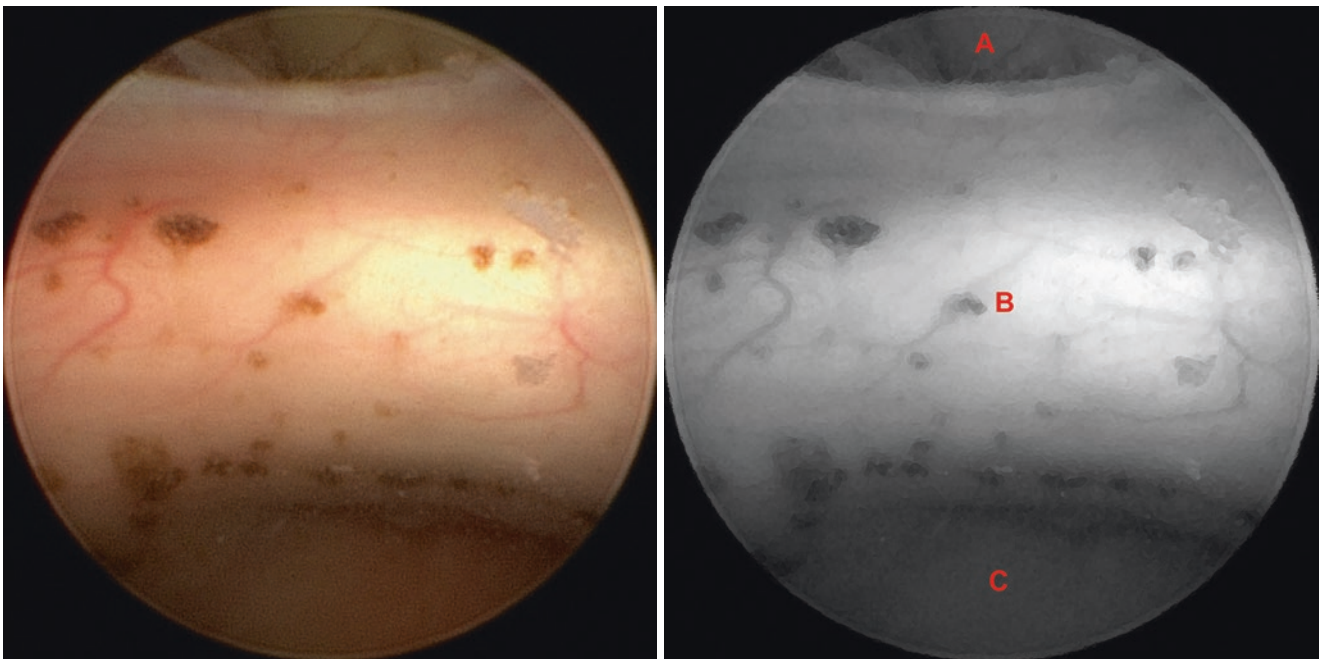


**Fig. 4.35** Abnormal anatomy – chronic hydrocephalus in an adult. (A) Spontaneous opening at the lamina terminalis, (B) Optic chiasm, (C) Infundibular recess

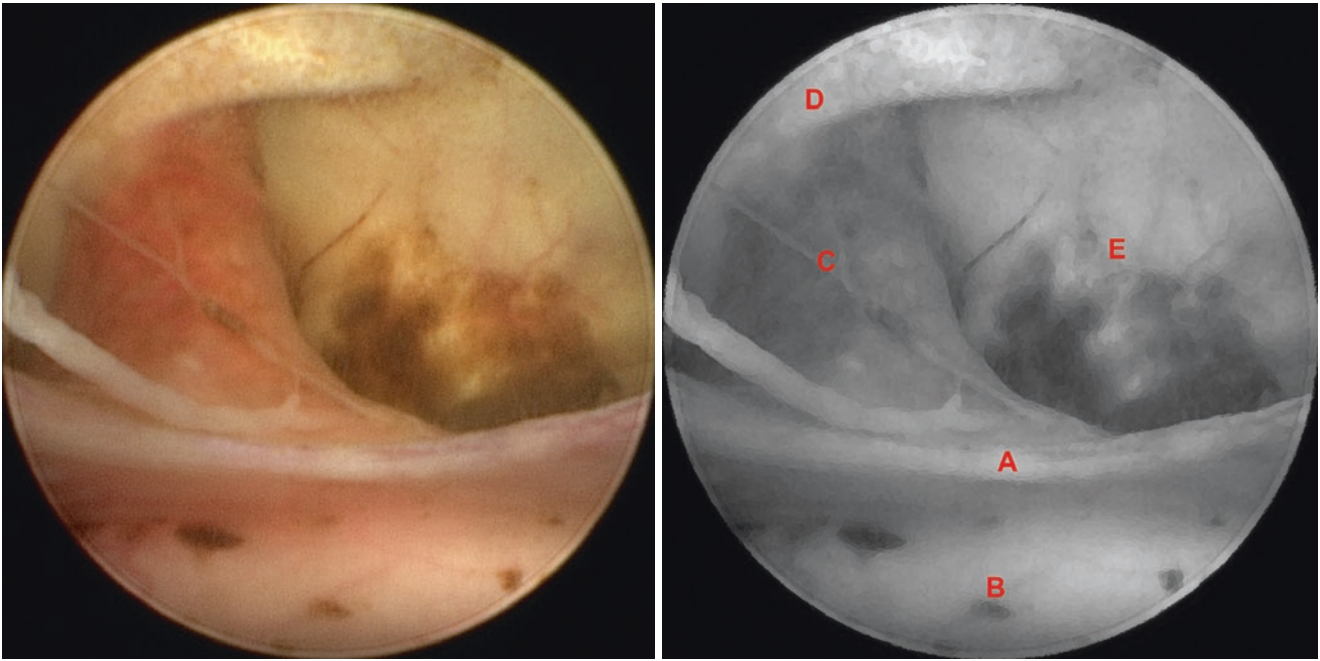


**Fig. 4.36** Abnormal anatomy – chronic hydrocephalus in an adult. (A) Spontaneously fenestrated lamina terminalis, (B) Optic chiasm, (C) Left optic nerve (CN II), (D) Superior portion of the left optic foramen, (E) Frontal skull base

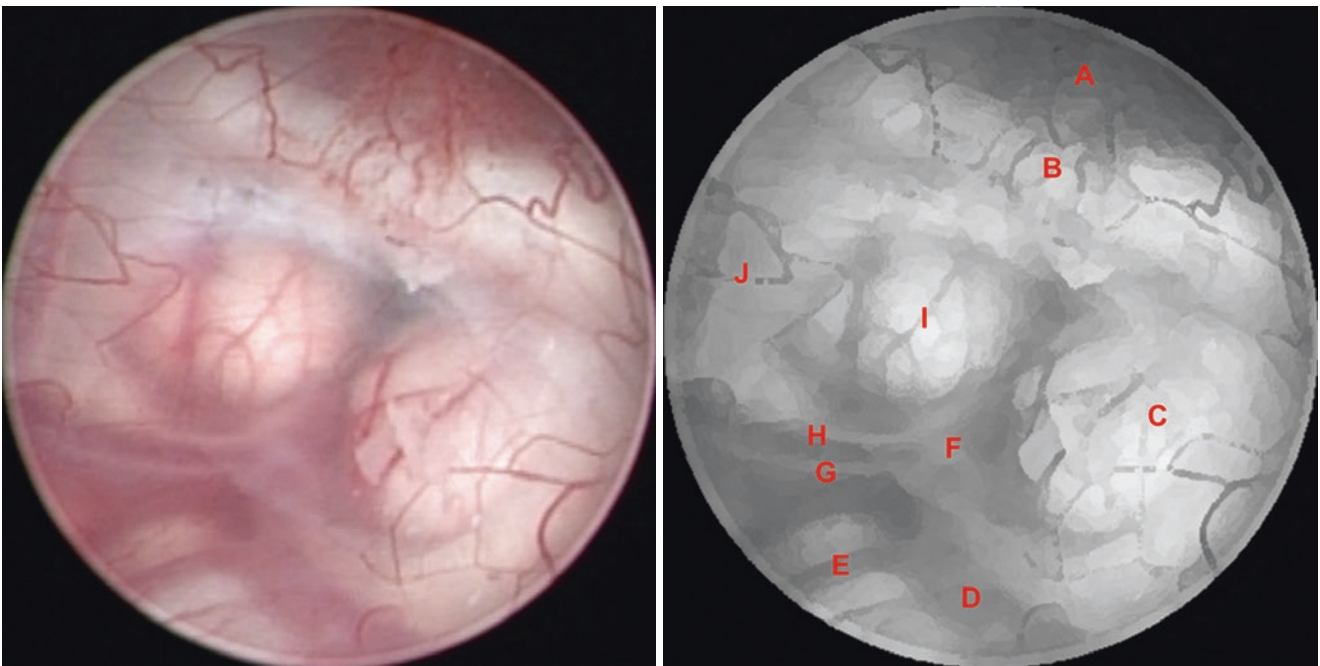


**Fig. 4.37** Normal anatomy. (A) Pituitary gland, (B) Dorsum sellae, (C) Right mammillary body, (D) Right posterior cerebral artery (P1), (E) Thalamoperforating artery, (F) Bifurcation of the basilar artery, (G) Left posterior cerebral artery (P1), (H) Left superior cerebellar artery, (I) Left mammillary body, (J) Left hypothalamus

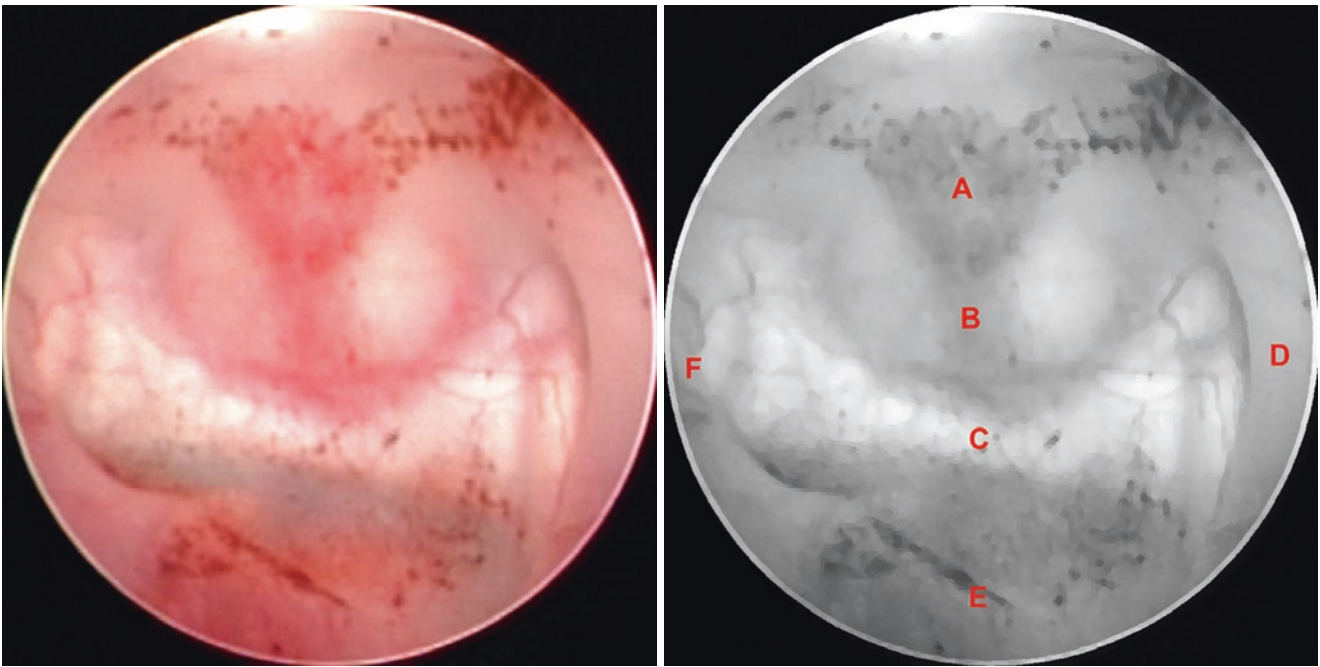


**Fig. 4.38** Normal anatomy. (A) Pituitary stalk, (B) Pituitary gland, (C) Dorsum sellae, (D) Right hypothalamus, (E) Tuber cinereum, (F) Left hypothalamus

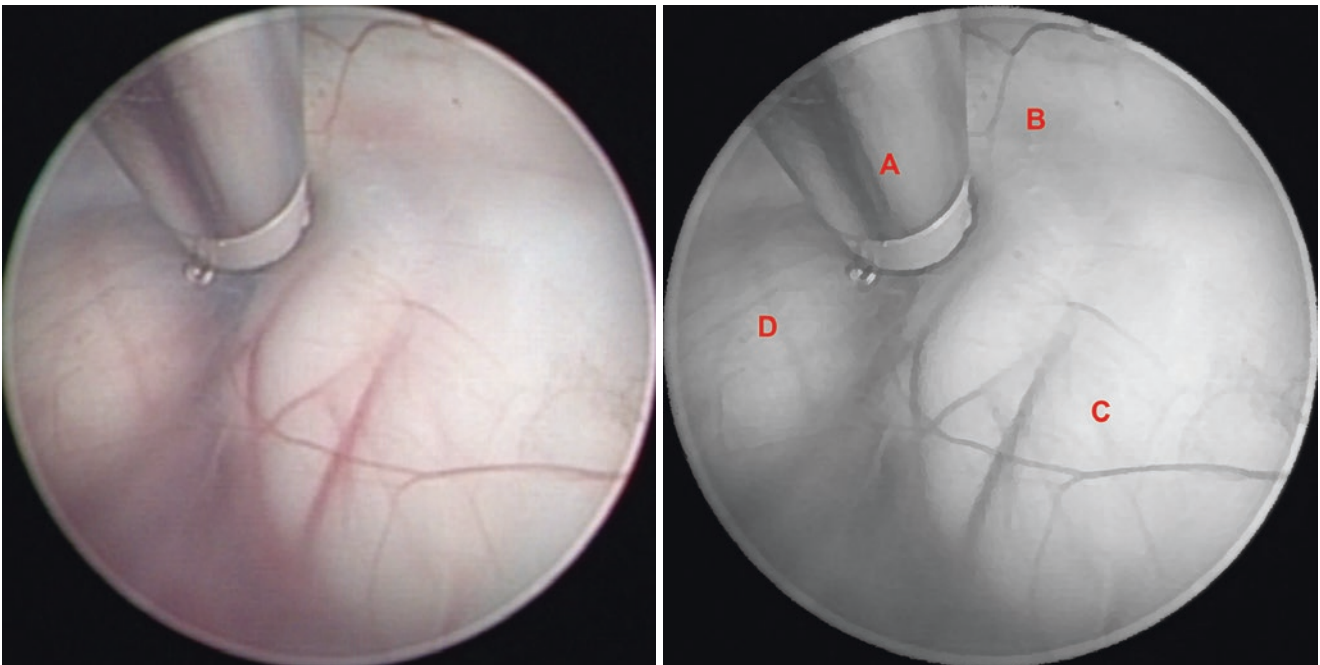


**Fig. 4.39** Surgical procedure – third ventriculostomy. (A) Bipolar coagulation electrode over pre-mammillary recess, (B) Tuber cinereum, (C) Right mammillary body, (D) Left mammillary body

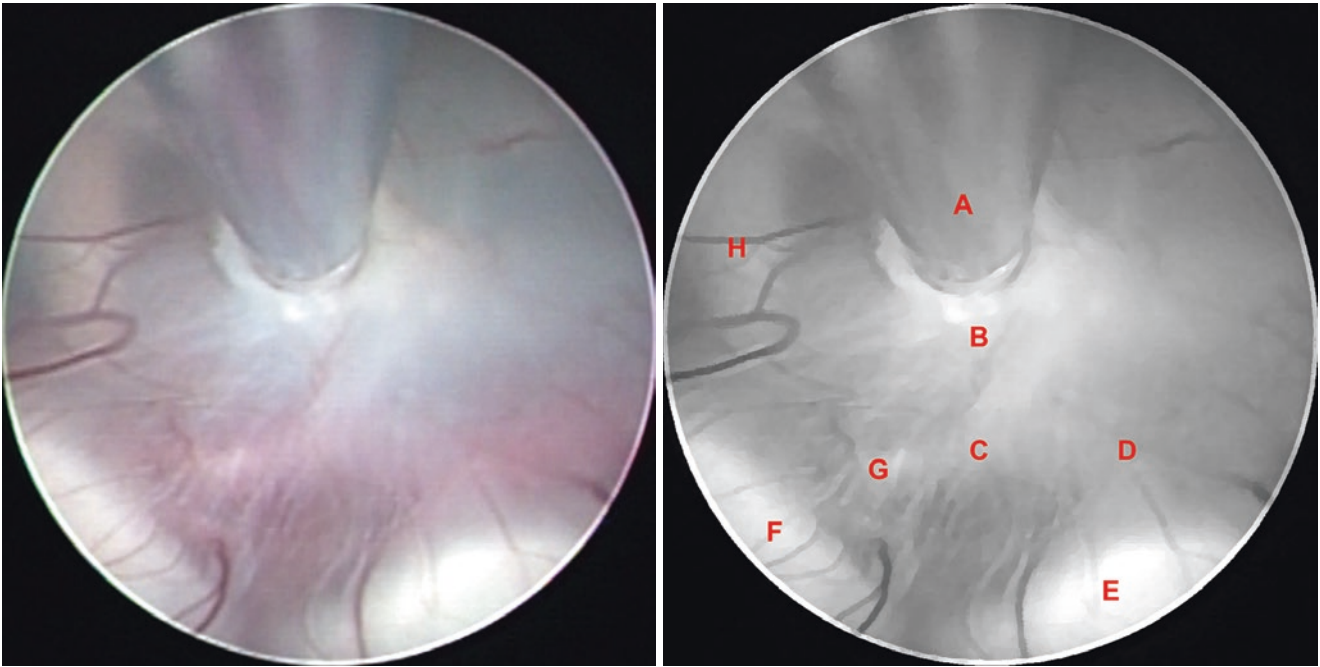


**Fig. 4.40** Surgical procedure – third ventriculostomy. (A) Bipolar coagulation electrode, (B) Tuber cinereum, (C) Bifurcation of the basilar artery, (D) Right posterior cerebral artery (P1), (E) Right mammil-

lary body, (F) Left mammillary body, (G) Left posterior cerebral artery (P1), (H) Left oculomotor nerve (CN III)

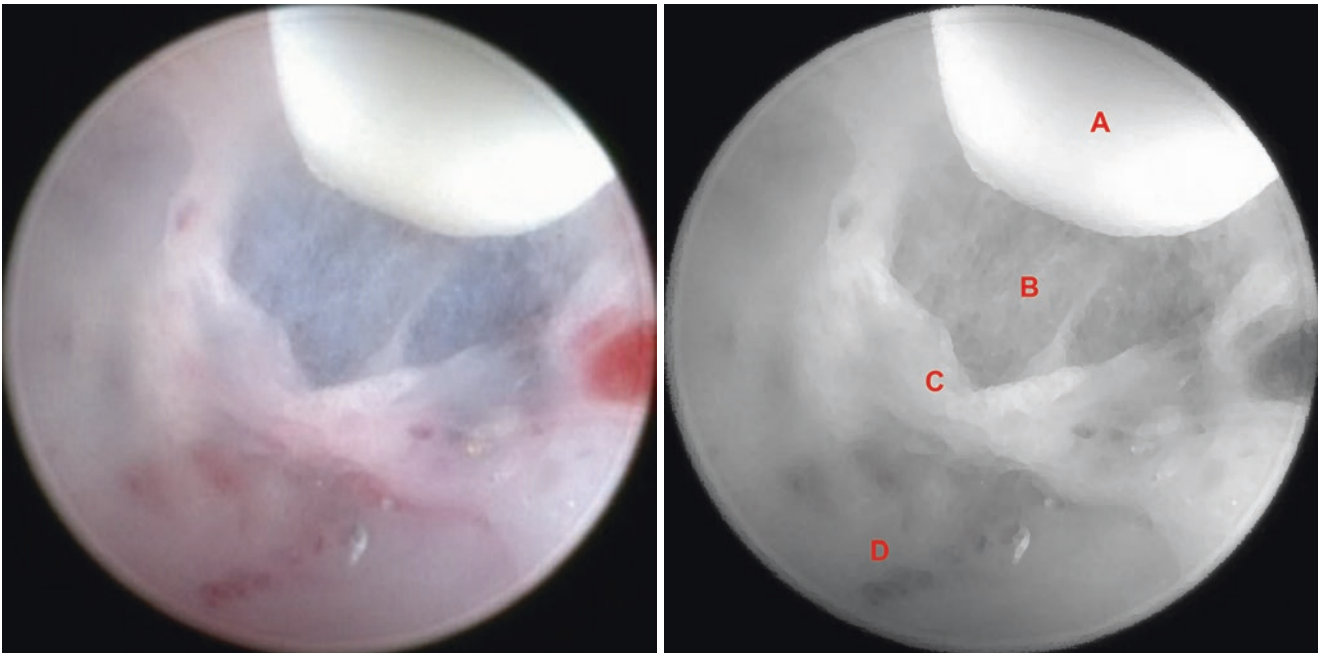


**Fig. 4.41** Surgical procedure – third ventriculostomy. (A) Bipolar coagulation electrode, (B) Membrane of Lilliequist, (C) Coagulated tuber cinereum, (D) Tuber cinereum

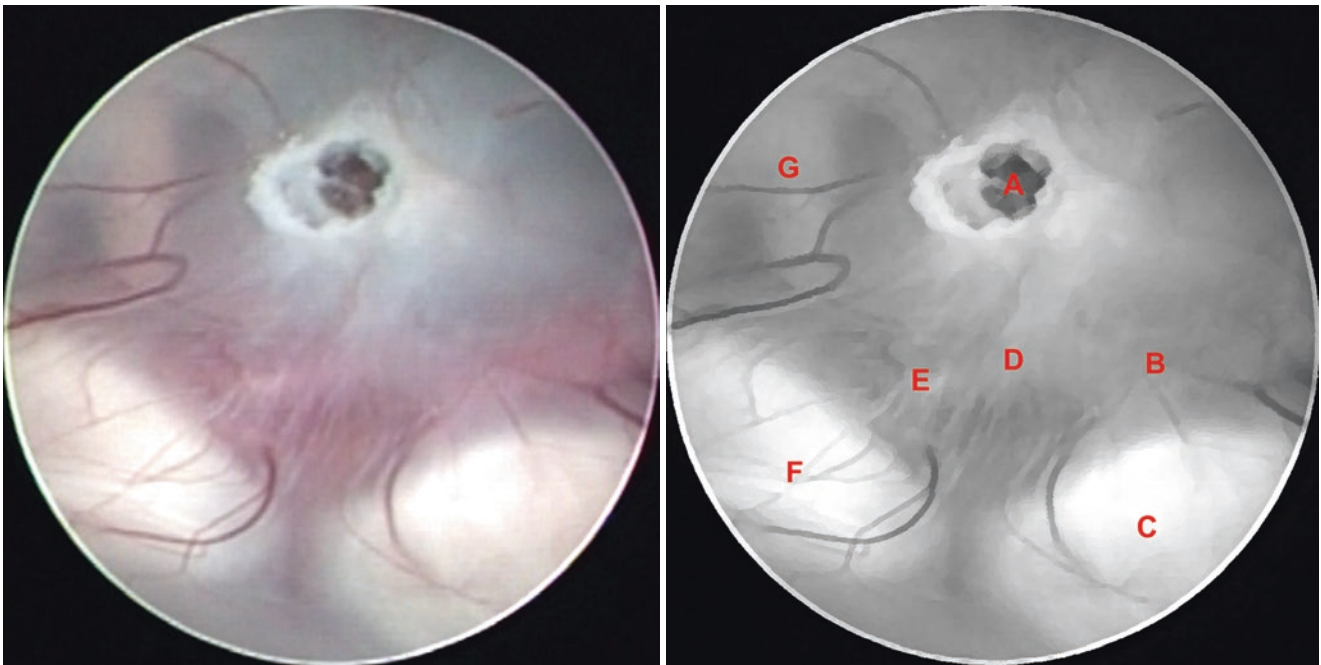


**Fig. 4.42** Surgical procedure – third ventriculostomy. (A) Fenestration at tuber cinereum after coagulation, (B) Right posterior cerebral artery (P1), (C) Right mammillary body, (D) Bifurcation of the basilar artery,

(E) Left posterior cerebral artery (P1), (F) Left mammillary body, (G) Left oculomotor nerve (CN III)

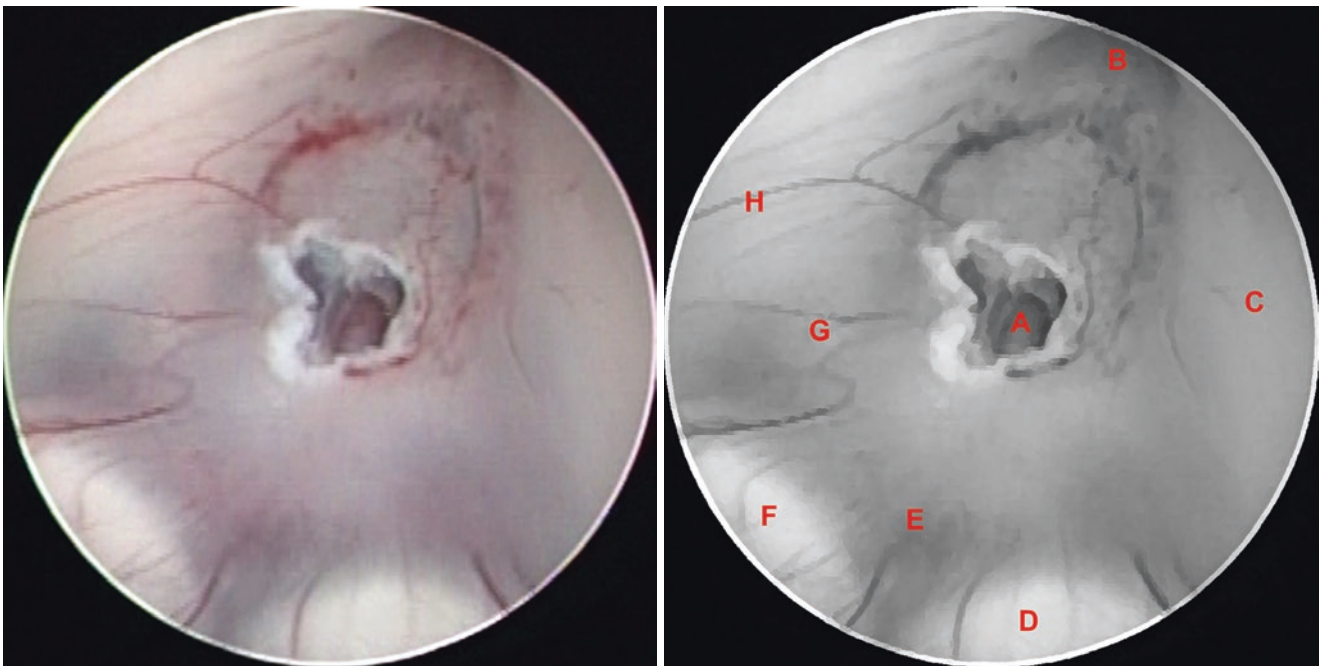


**Fig. 4.43** Surgical procedure – third ventriculostomy. (A) Fenestration at the tuber cinereum and the membrane of Lilliequist after coagulation, (B) Infundibular recess, (C) Right hypothalamus, (D) Right mammil-

lary body, (E) Bifurcation of the basilar artery under pre-mammillary recess, (F) Left mammillary body, (G) Left oculomotor nerve (CN III), (H) Left hypothalamus

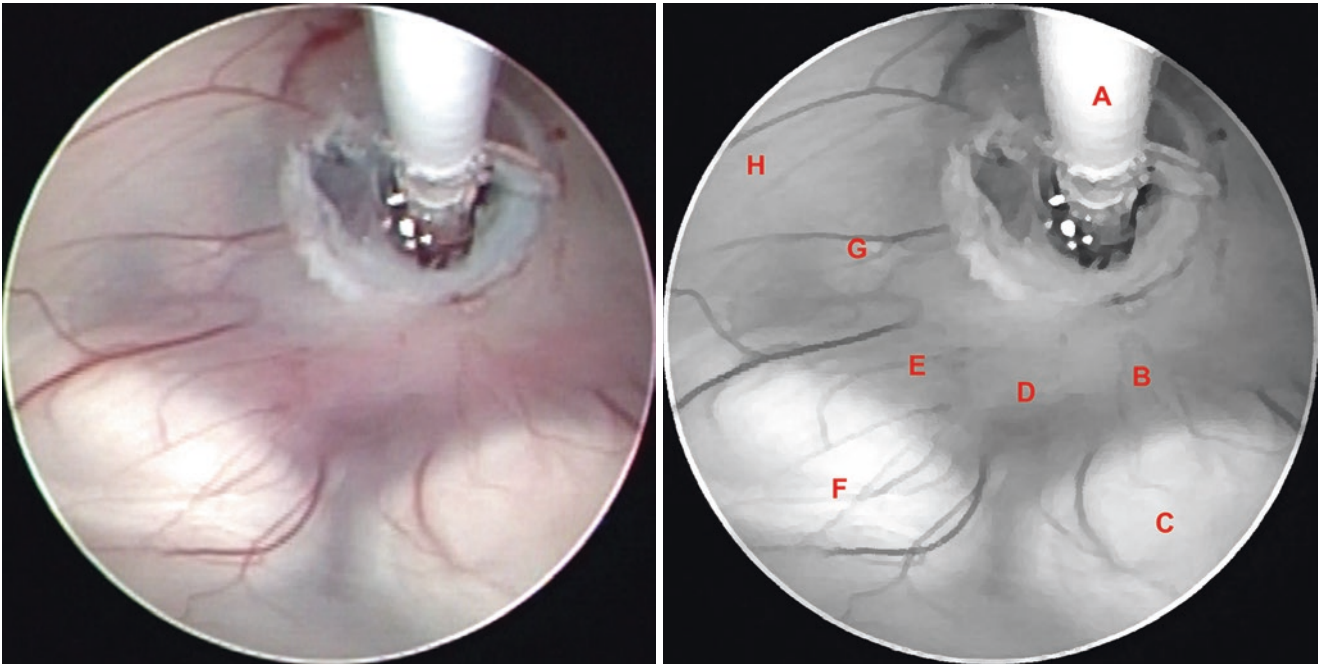


**Fig. 4.44** Surgical procedure – third ventriculostomy. (A) Fogarty balloon catheter dilatation, (B) Right posterior cerebral artery (P1), (C) Right mammillary body, (D) Bifurcation of the basilar artery under pre-

mammillary recess, (E) Left posterior cerebral artery (P1), (F) Left mammillary body, (G) Left oculomotor nerve (CN III), (H) Left hypothalamus

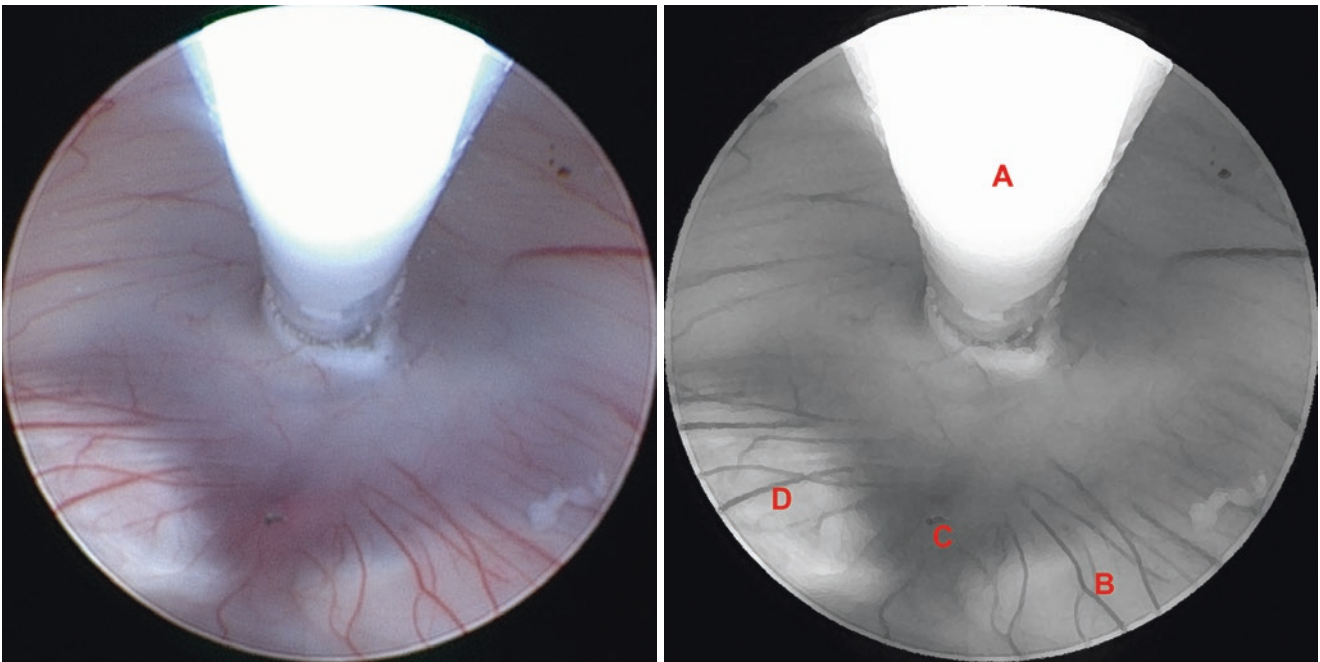


**Fig. 4.45** Surgical procedure – third ventriculostomy. (A) Fogarty balloon catheter dilatation, (B) Right mammillary body, (C) Bifurcation of the basilar artery under pre-mammillary recess, (D) Left mammillary body

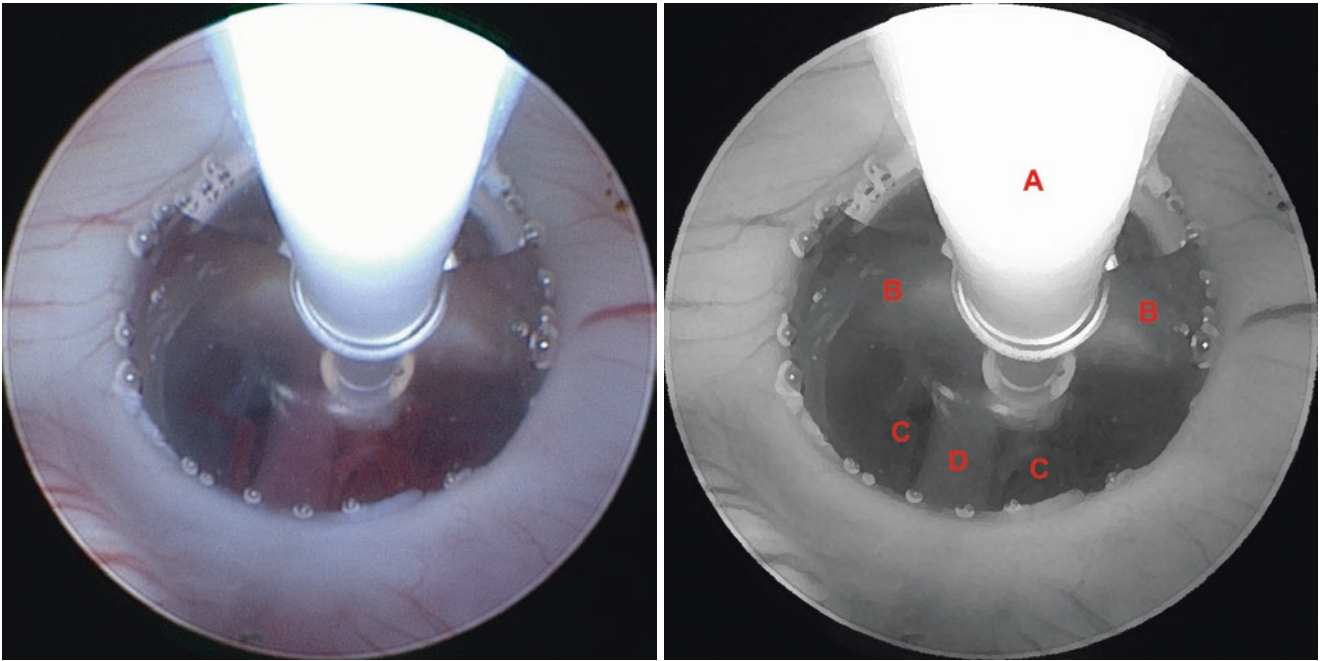


**Fig. 4.46** Surgical procedure – third ventriculostomy. (A) Fogarty balloon catheter dilatation, (B) Dorsum sellae, (C) Pontine branches of the basilar artery, (D) Basilar artery

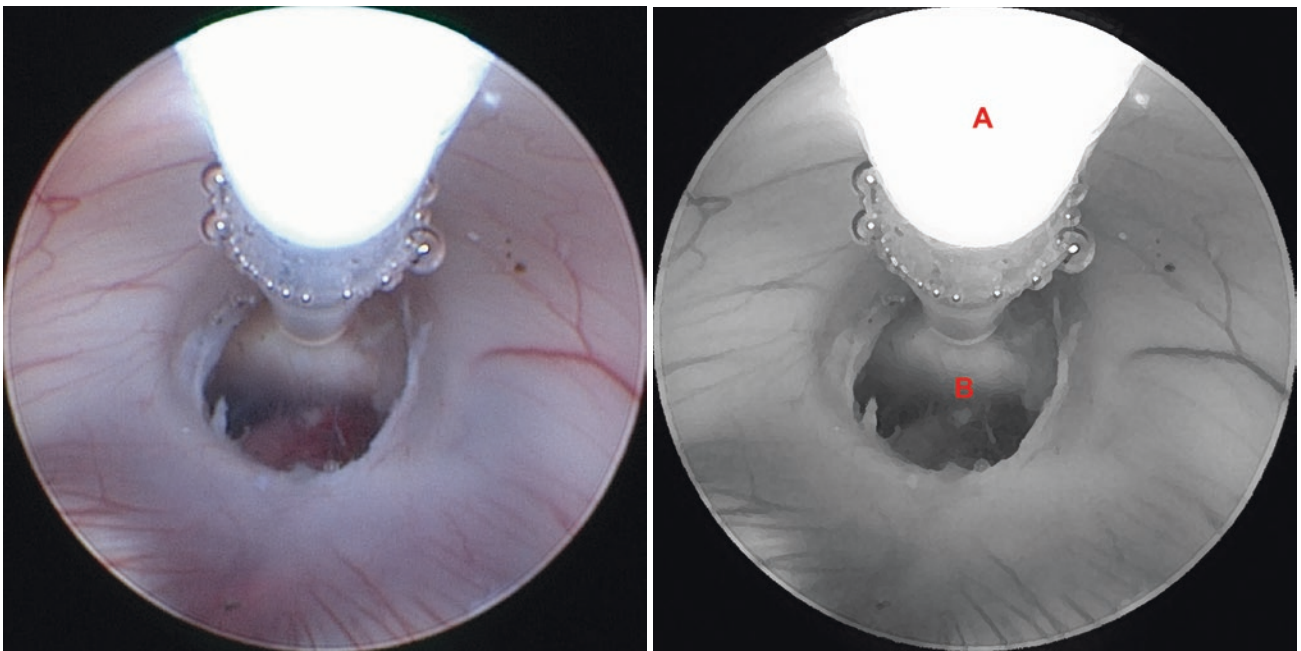


**Fig. 4.47** Surgical procedure – third ventriculostomy. (A) Fogarty balloon catheter, (B) Ventriculostomy

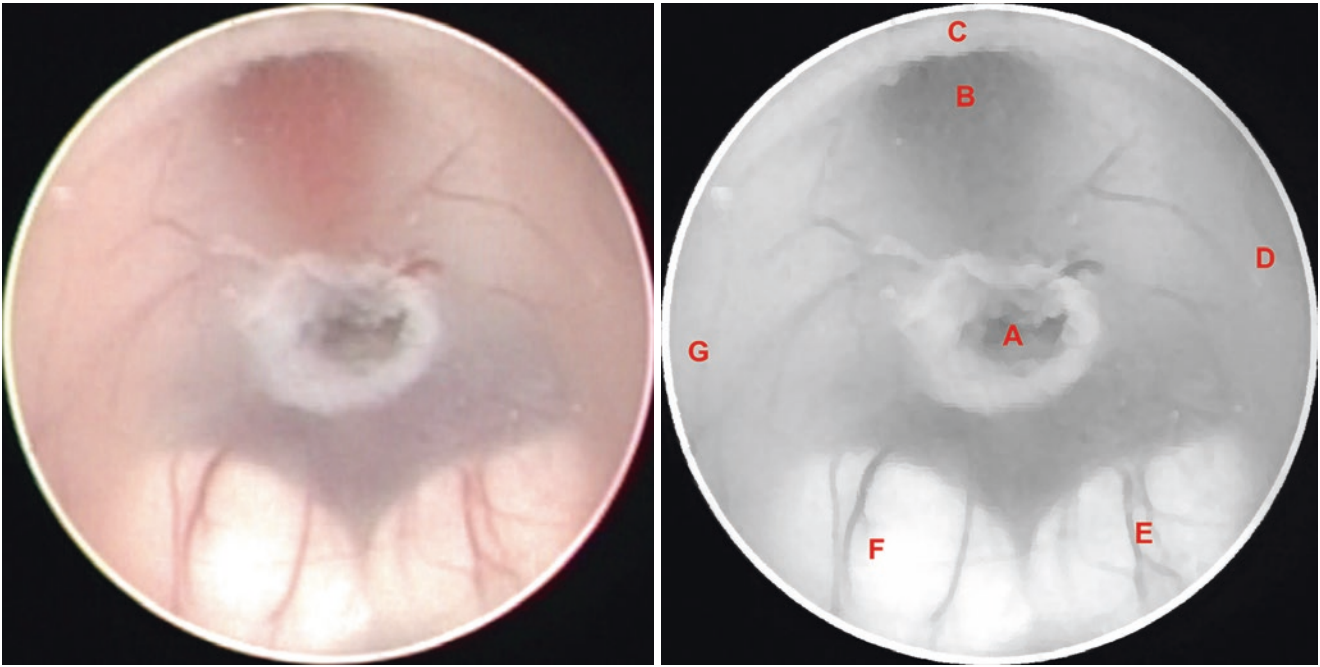


**Fig. 4.48** Surgical procedure – third ventriculostomy. (A) Coagulated tuber cinereum, (B) Infundibular recess, (C) Optic chiasm, (D) Right hypothalamus, (E) Right mammillary body, (F) Left mammillary body, (G) Left hypothalamus

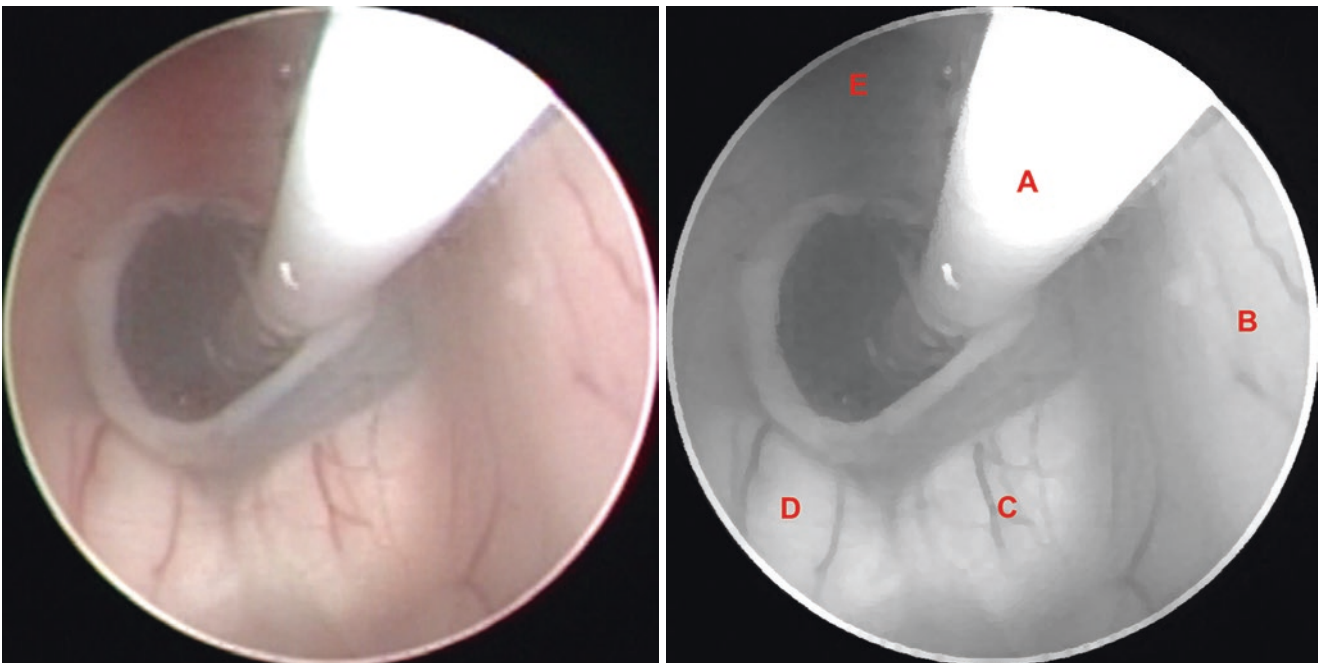


**Fig. 4.49** Surgical procedure – third ventriculostomy. (A) Fogarty balloon catheter, (B) Right hypothalamus, (C) Right mammillary body, (D) Left mammillary body, (E) Infundibular recess



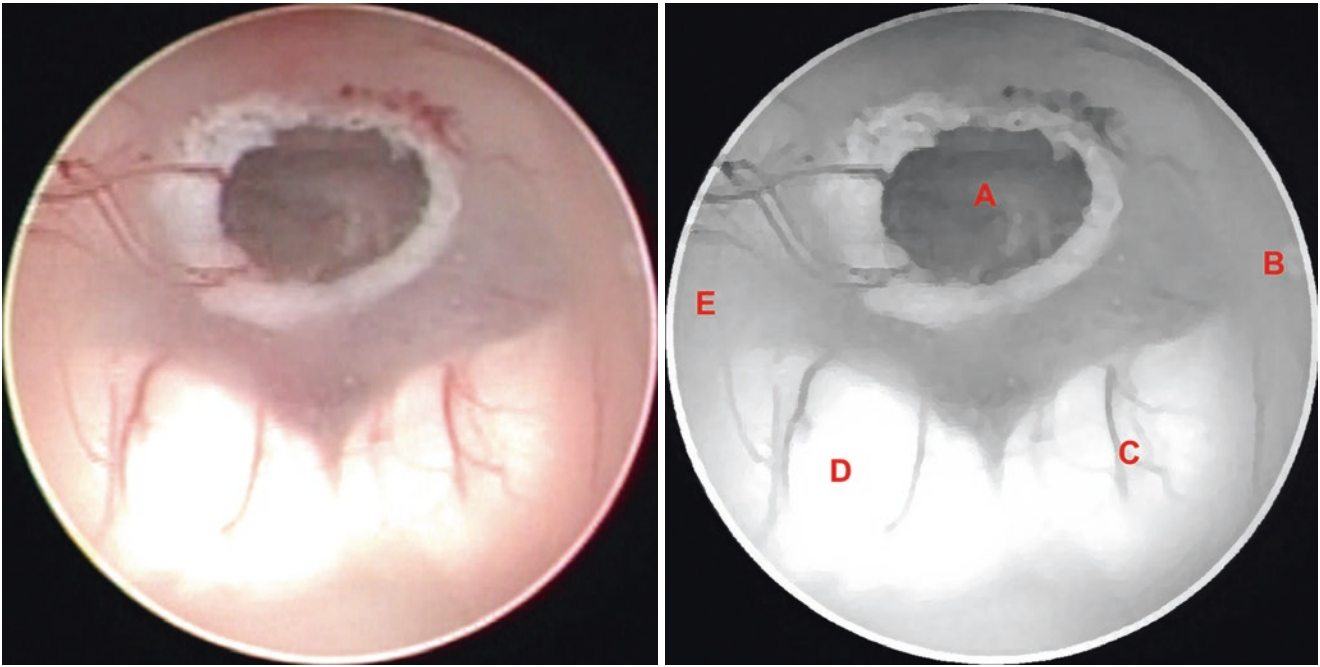


**Fig. 4.50** Surgical procedure – third ventriculostomy. (A) Ventriculostomy, (B) Right hypothalamus, (C) Right mammillary body, (D) Left mammillary body, (E) Left hypothalamus

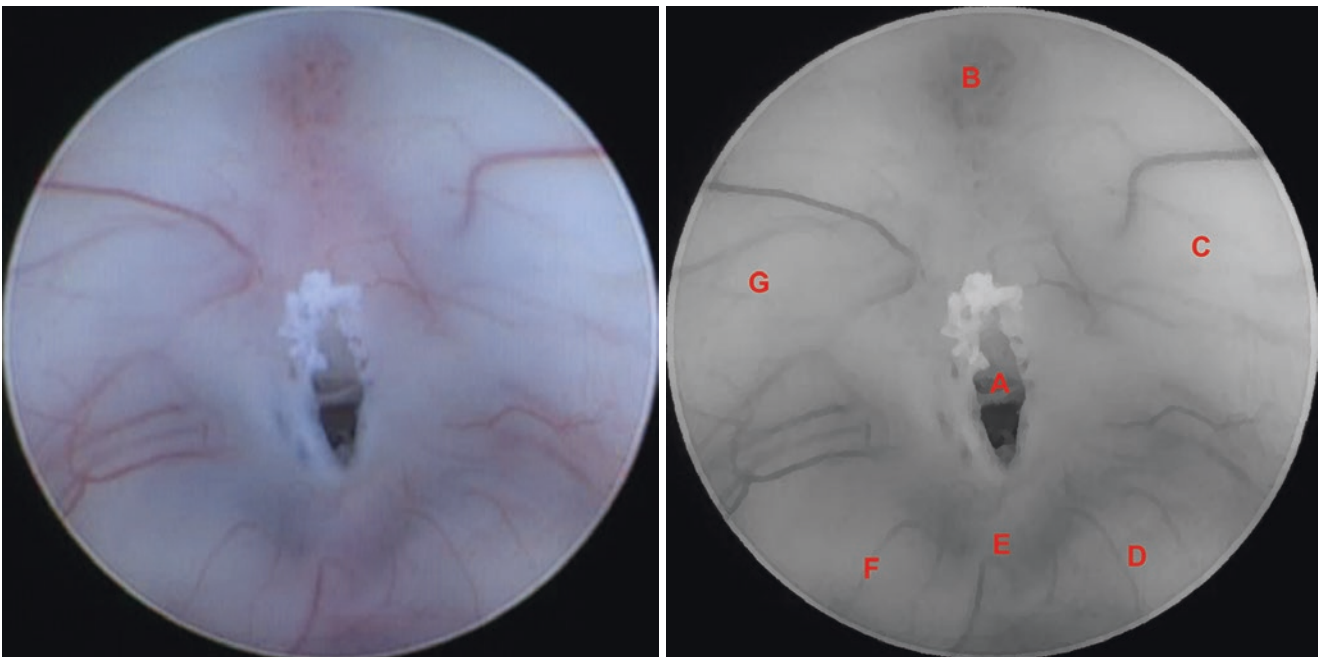


**Fig. 4.51** Surgical procedure – third ventriculostomy. (A) Ventriculostomy, (B) Infundibular recess, (C) Right hypothalamus, (D) Right mammillary body, (E) Basilar artery under pre-mammillary recess, (F) Left mammillary body, (G) Left hypothalamus

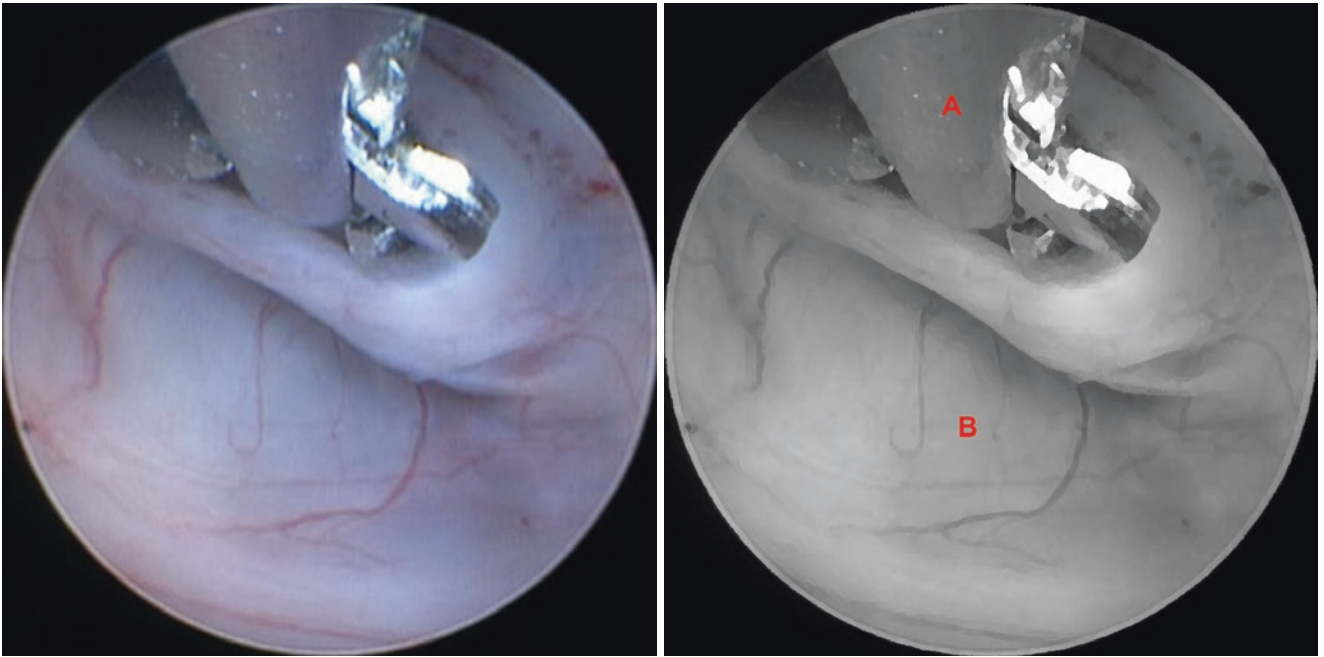


**Fig. 4.52** Surgical procedure – third ventriculostomy. (A) Biopsy forceps dilatation, (B) Tuber cinereum

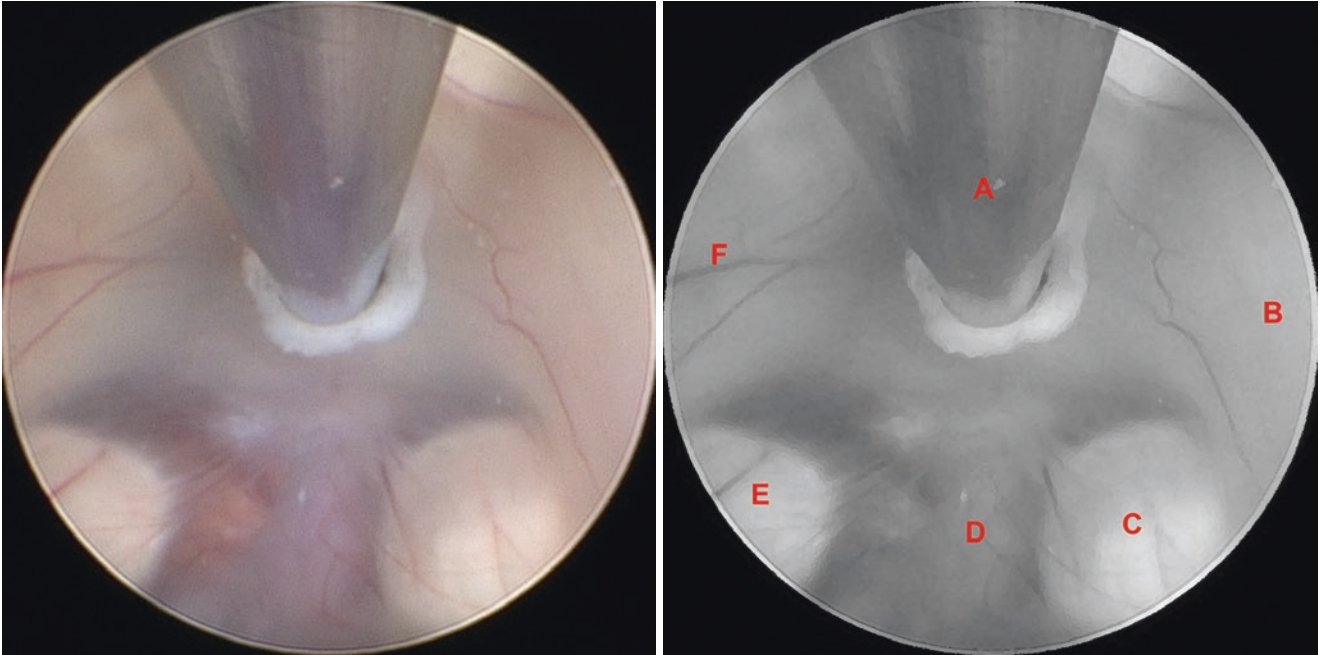


**Fig. 4.53** Surgical procedure – third ventriculostomy. (A) Bipolar coagulation electrode, (B) Right hypothalamus, (C) Right mammillary body, (D) Basilar artery under premammillary recess, (E) Left mammillary body, (F) Left hypothalamus

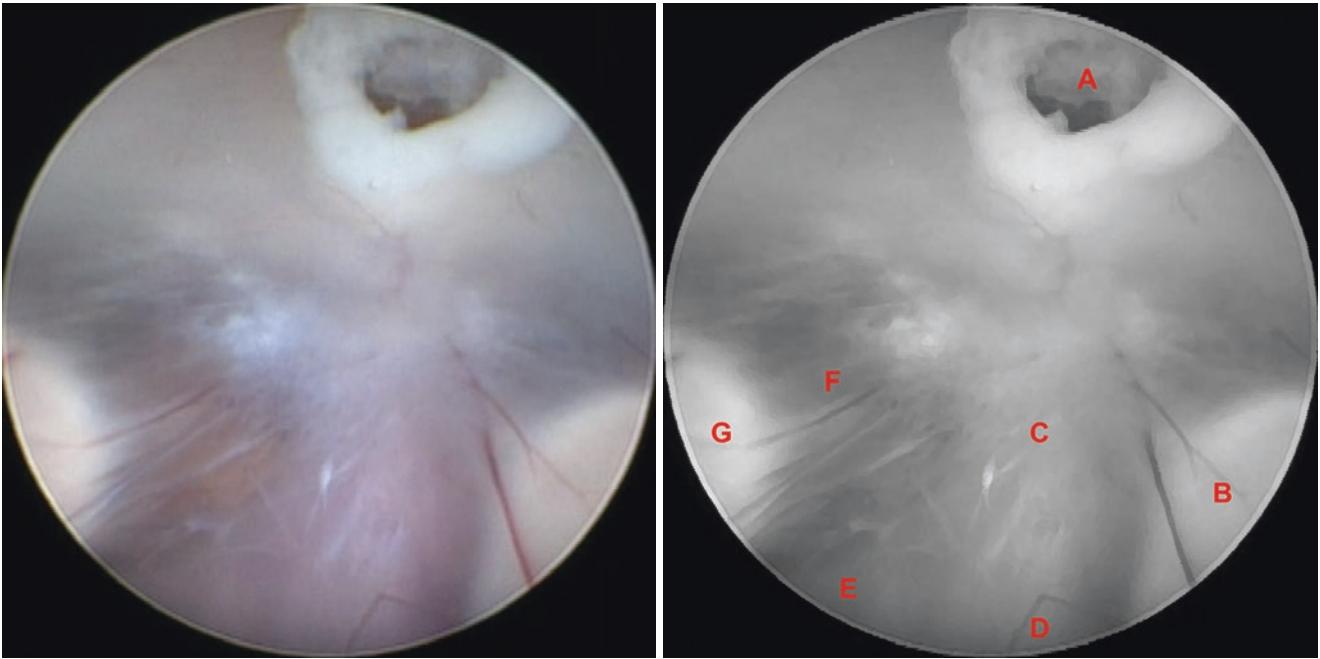


**Fig. 4.54** Surgical procedure – third ventriculostomy. (A) Ventriculostomy, (B) Right mammillary body, (C) Basilar artery under pre-mammillary recess, (D) Right posterior cerebral artery (P1), (E) Left posterior cerebral artery (P1), (F) Pons under thinner portion of the pre-mammillary recess, (G) Left mammillary body

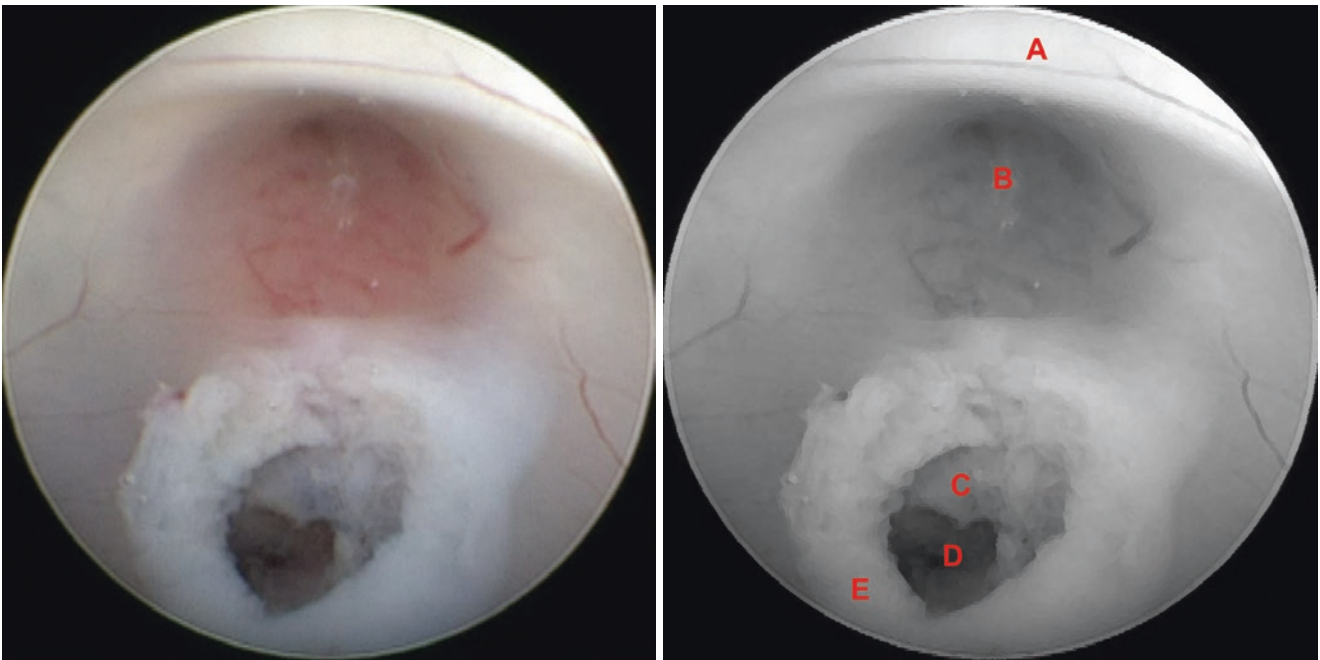


**Fig. 4.55** Surgical procedure – third ventriculostomy. (A) Optic chiasm, (B) Infundibular recess, (C) Fenestrated membrane of Liliequist, (D) Interpeduncular cistern, (E) Coagulated tuber cinereum

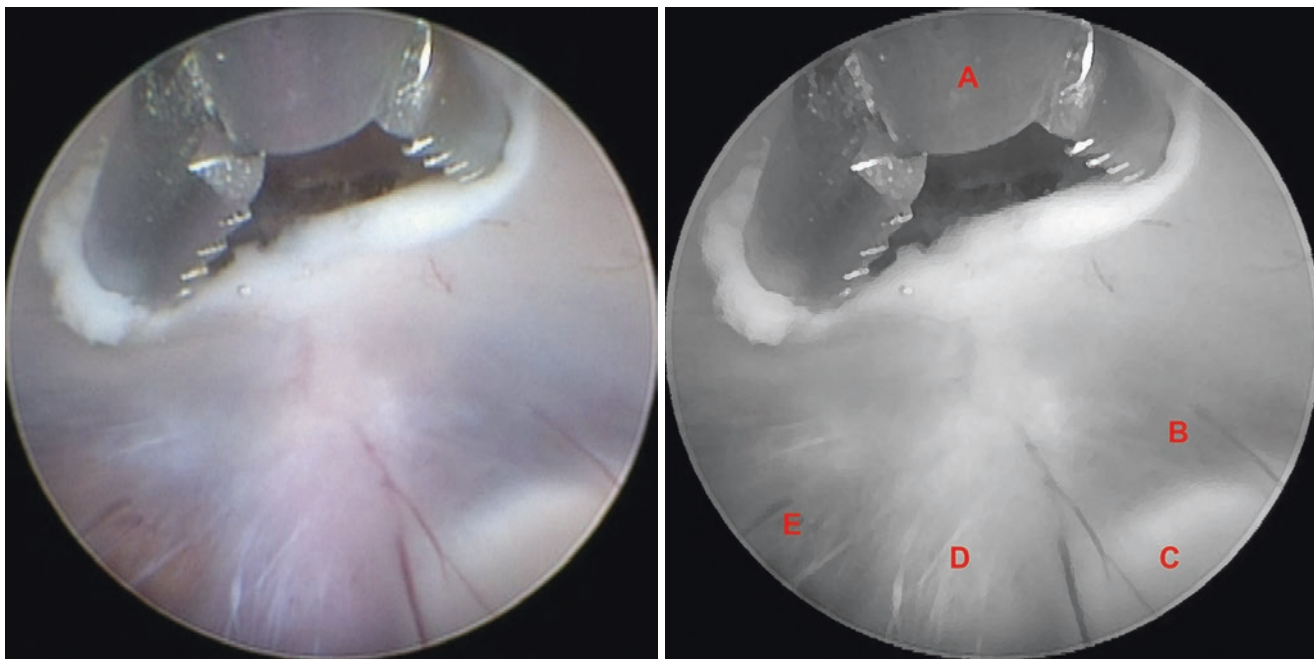


**Fig. 4.56** Surgical procedure – third ventriculostomy. (A) Grasping forceps, (B) Premammillary recess, (C) Right mammillary body, (D) Basilar artery, (E) Pons under thinner portion of the premammillary recess

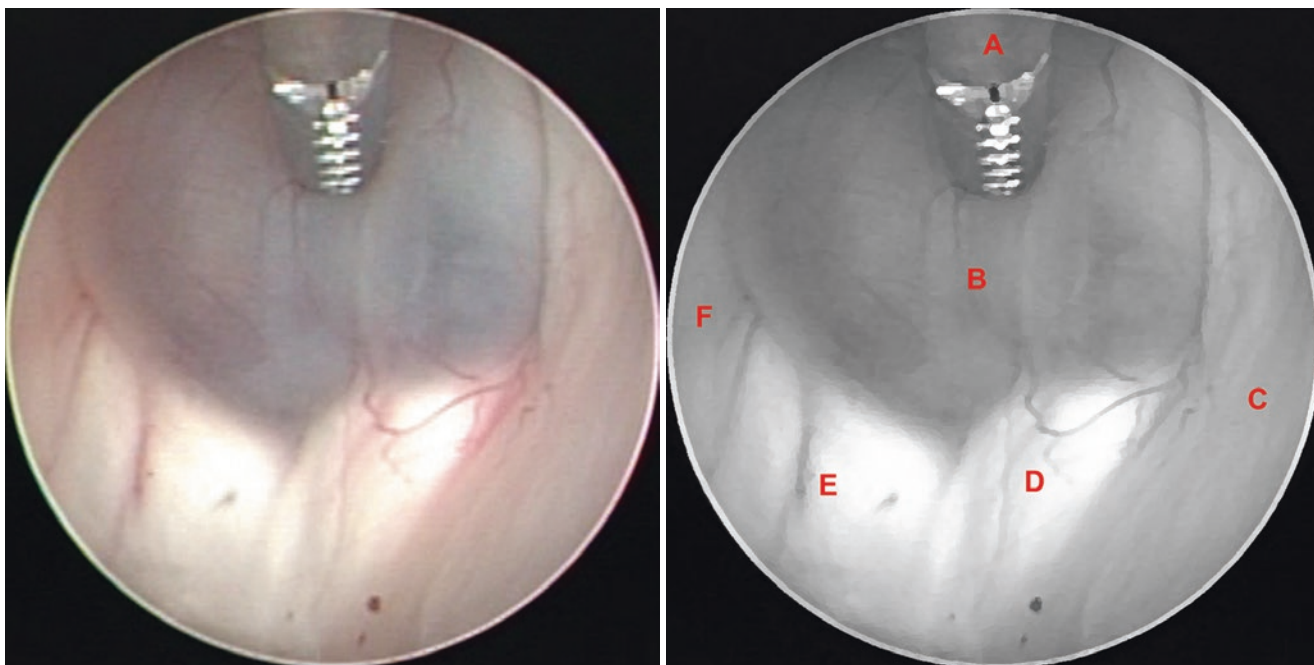


**Fig. 4.57** Surgical procedure – third ventriculostomy. (A) Grasping forceps, (B) Tuber cinereum, (C) Right hypothalamus, (D) Right mammillary body, (E) Left mammillary body, (F) Left hypothalamus

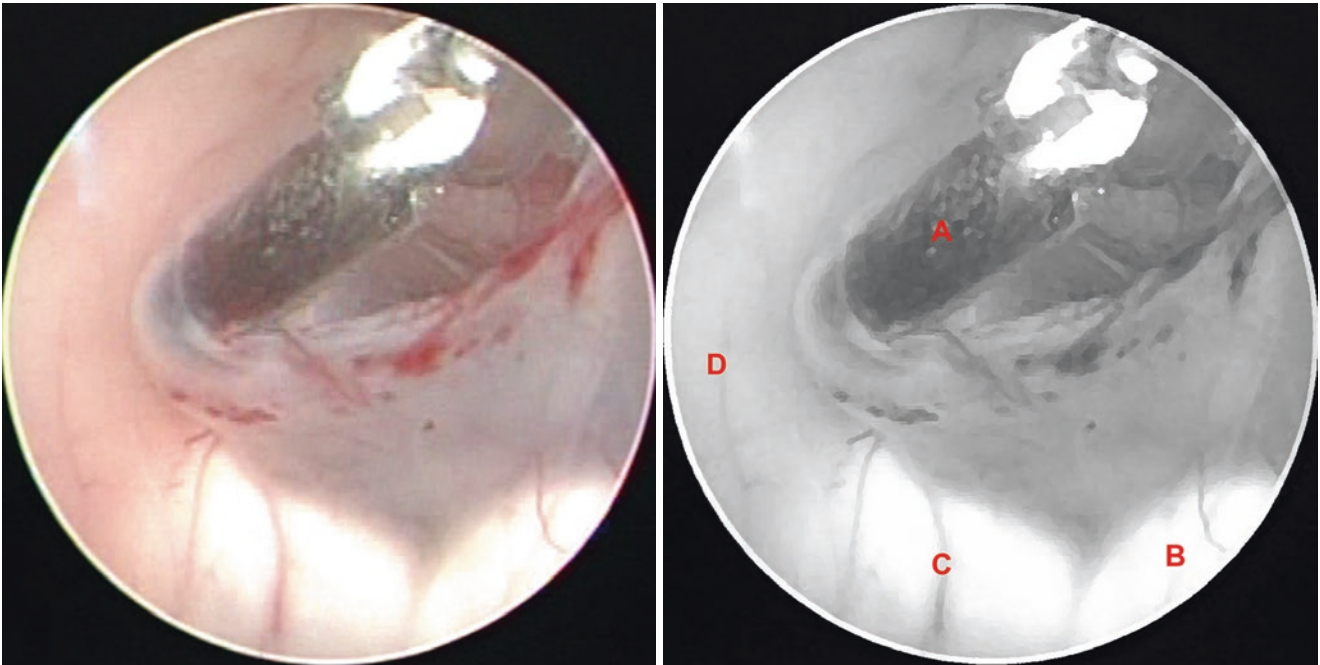


**Fig. 4.58** Surgical procedure – third ventriculostomy. (A) Grasping forceps, (B) Right mammillary body, (C) Left mammillary body, (D) Left hypothalamus

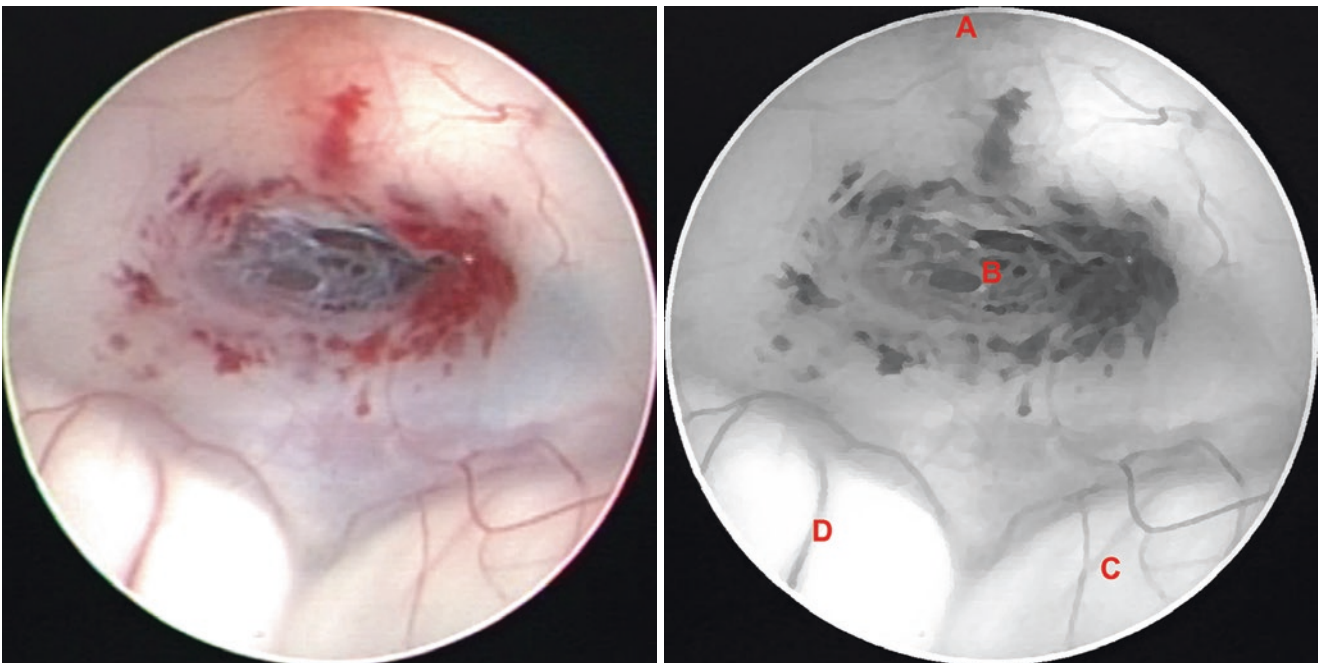


**Fig. 4.59** Surgical procedure – third ventriculostomy. (A) Infundibular recess, (B) Membrane of Liliequist, (C) Right mammillary body, (D) Left mammillary body

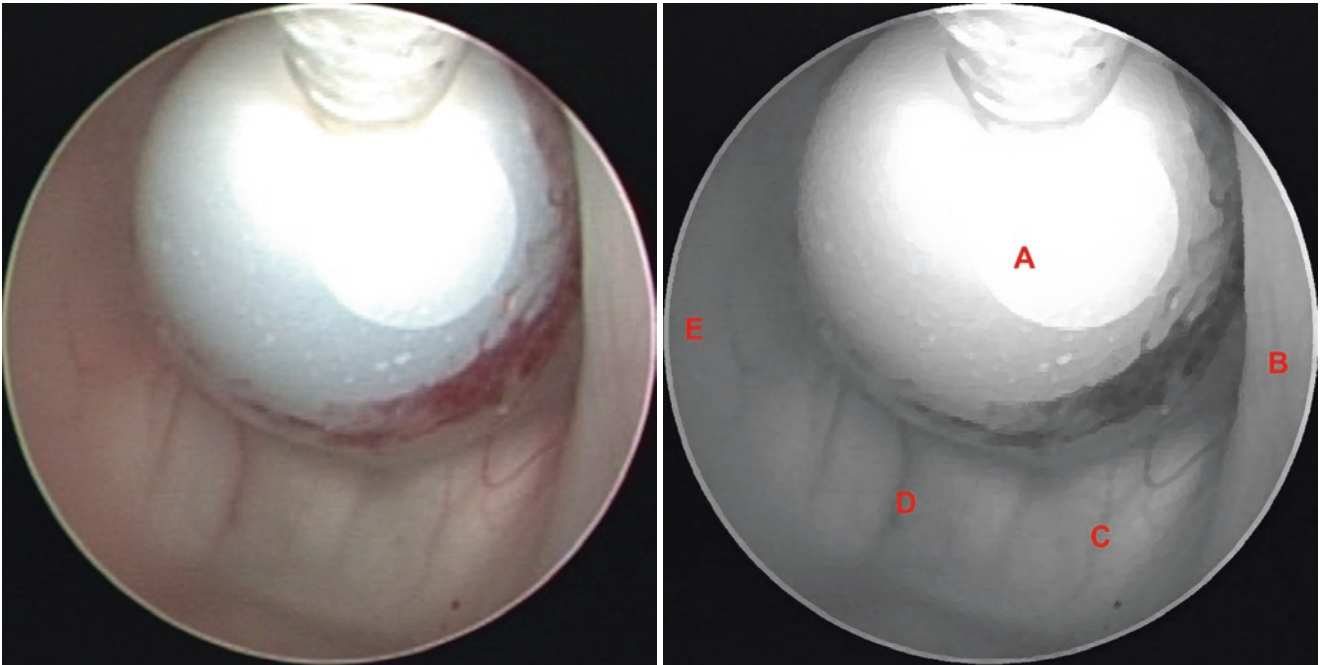


**Fig. 4.60** Surgical procedure – third ventriculostomy. (A) Fogarty balloon catheter dilatation, (B) Right hypothalamus, (C) Right mammillary body, (D) Left mammillary body, (E) Left hypothalamus

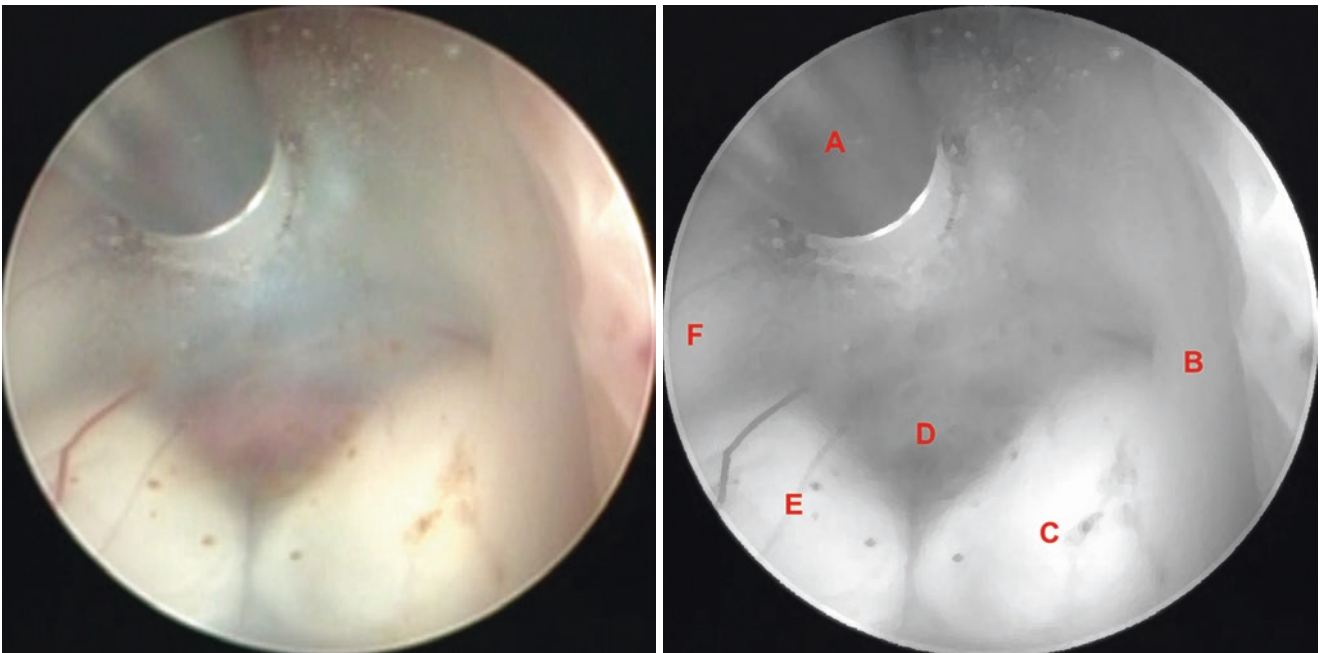


**Fig. 4.61** Surgical procedure – third ventriculostomy. (A) Bipolar coagulation electrode, (B) Right hypothalamus, (C) Right mammillary body, (D) Basilar artery under premammillary recess, (E) Left mammillary body, (F) Left hypothalamus

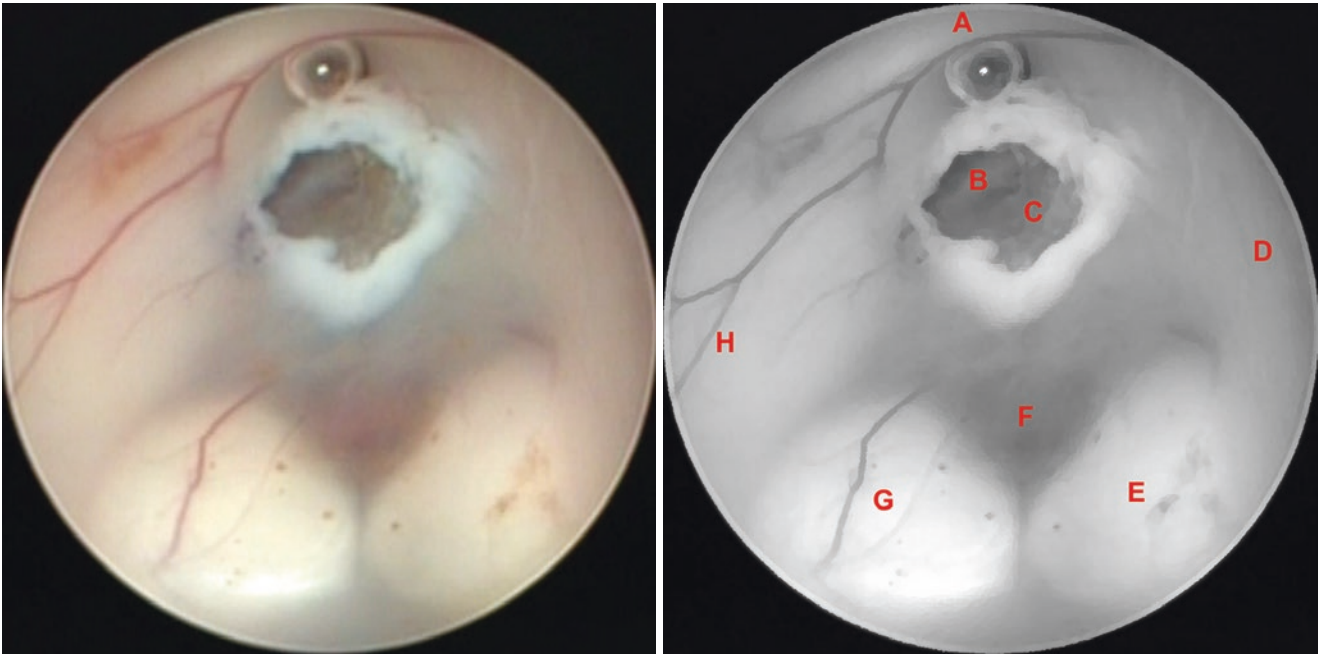


**Fig. 4.62** Surgical procedure – third ventriculostomy. (A) Optic chiasm, (B) Dorsum sellae, (C) Membrane of Liliequist, (D) Right hypothalamus, (E) Right mammillary body, (F) Basilar artery under pre-mammillary recess, (G) Left mammillary body, (H) Left hypothalamus

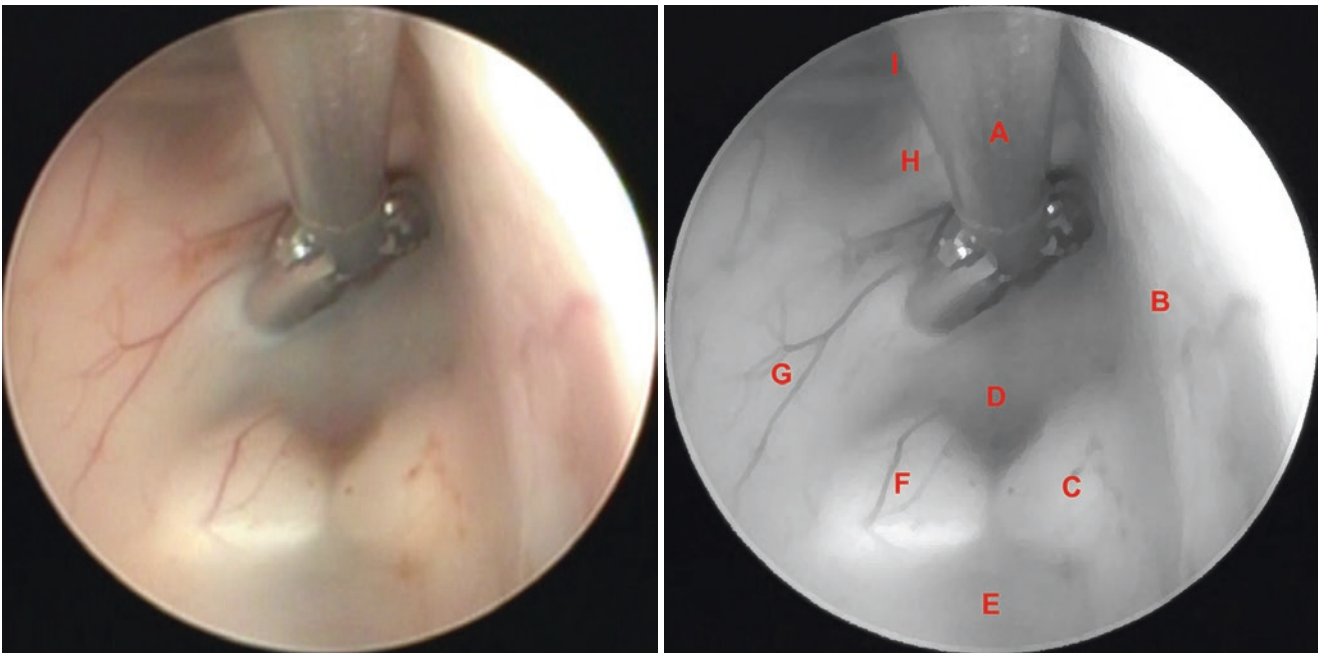


**Fig. 4.63** Surgical procedure – third ventriculostomy. (A) Fenestration of the membrane of Liliequist by biopsy forceps, (B) Right hypothalamus, (C) Right mammillary body, (D) Pre-mammillary recess, (E)

Post-mammillary recess, (F) Left mammillary body, (G) Left hypothalamus, (H) Optic chiasm, (I) Lamina terminalis

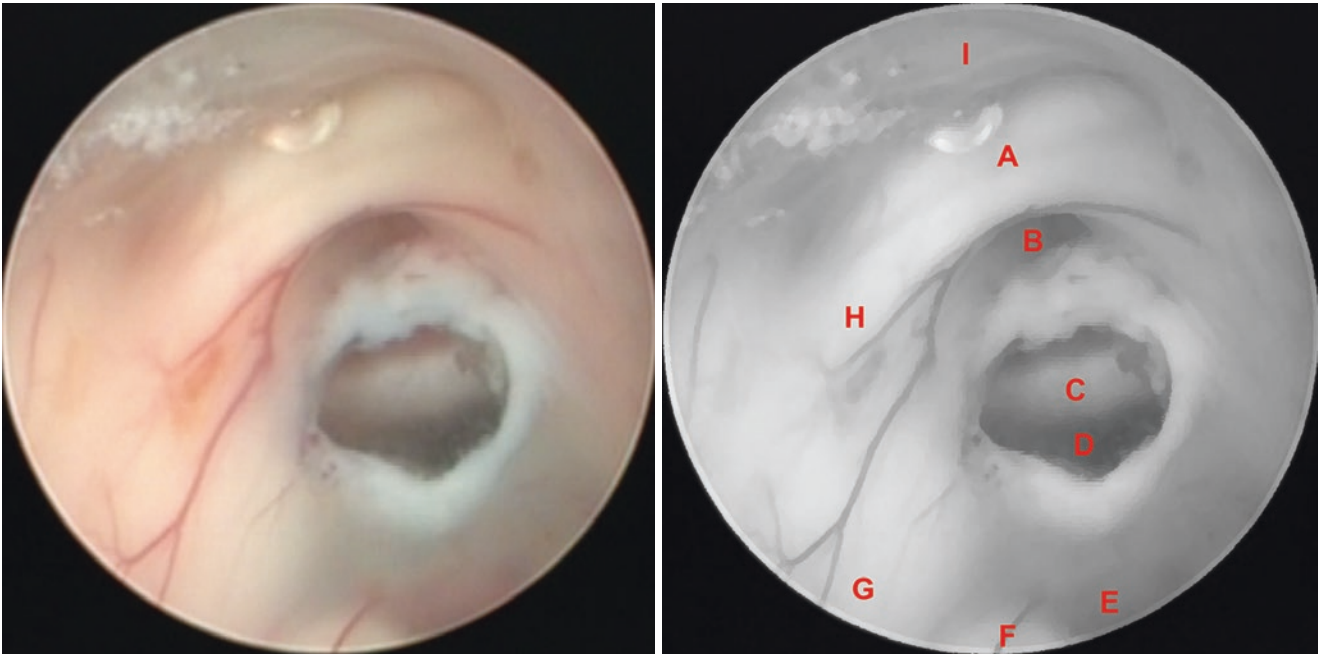


**Fig. 4.64** Surgical procedure – third ventriculostomy. (A) Optic chiasm, (B) Infundibular recess, (C) Dorsum sellae, (D) Interpeduncular cistern, (E) Basilar artery under pre-mammillary membrane, (F) Left

mammillary body, (G) Left hypothalamus, (H) Left optic tract, (I) Lamina terminalis

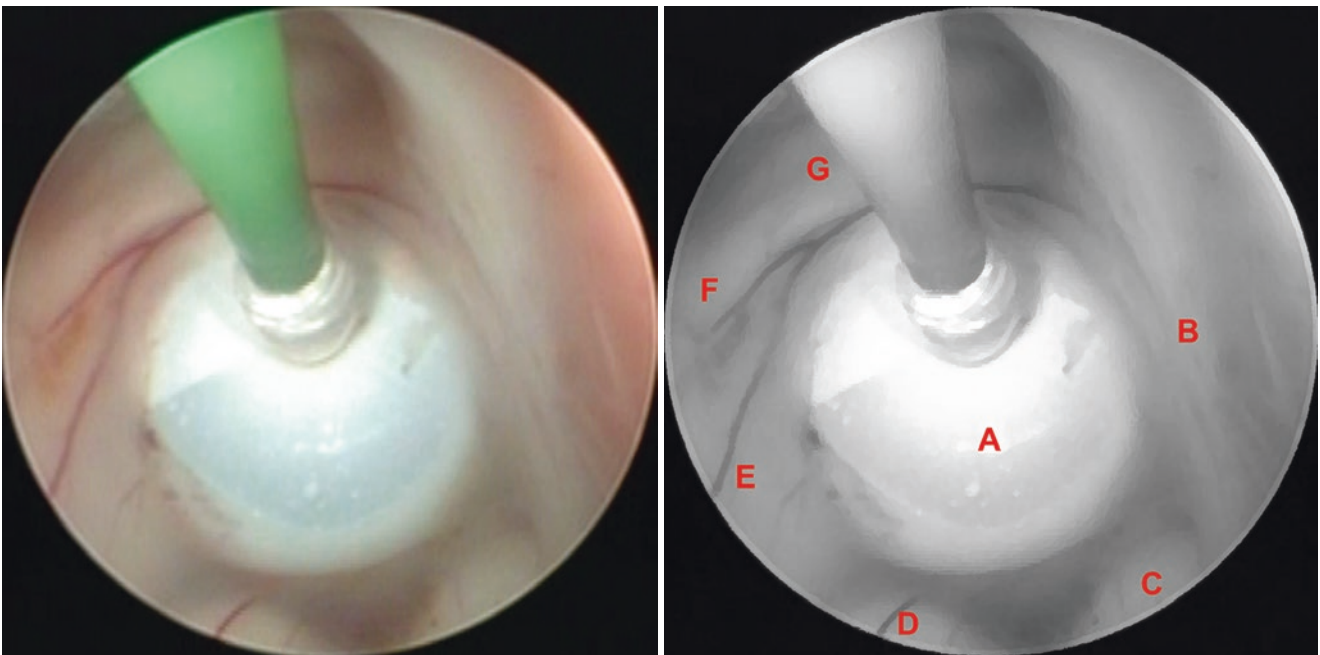


**Fig. 4.65** Surgical procedure – third ventriculostomy. (A) Fogarty balloon catheter, (B) Right hypothalamus, (C) Right mammillary body, (D) Left mammillary body, (E) Left hypothalamus, (F) Left optic tract, (G) Optic chiasm



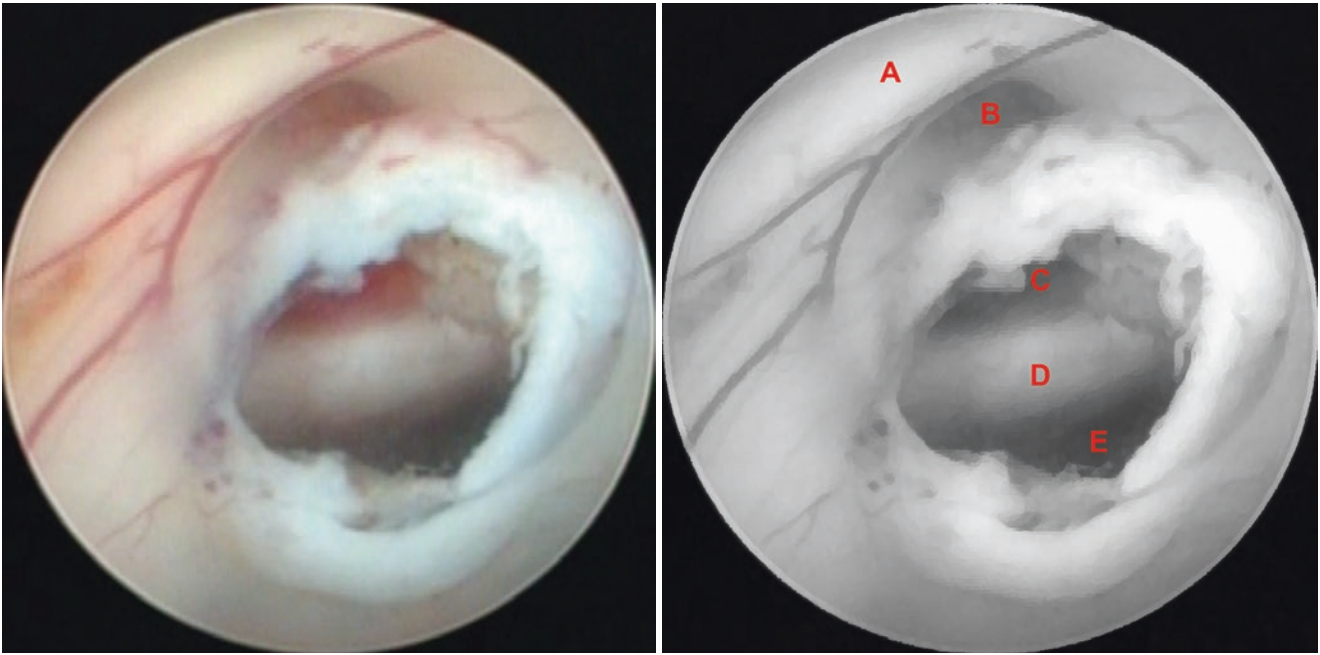


**Fig. 4.66** Surgical procedure – third ventriculostomy. (A) Optic chiasm, (B) Infundibular recess, (C) Pituitary gland, (D) Dorsum sellae, (E) Interpeduncular cistern

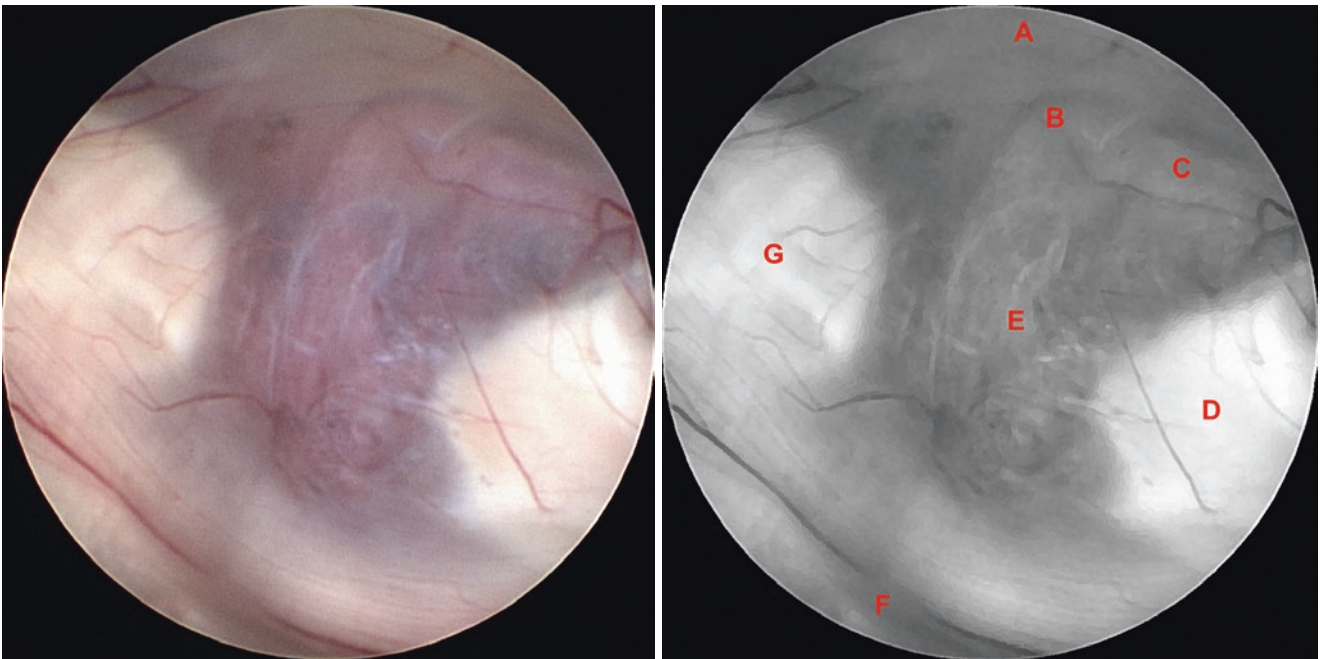


**Fig. 4.67** Surgical procedure – third ventriculostomy. (A) Tuber cinereum, (B) Bifurcation of the basilar artery, (C) Right posterior cerebral artery (P1), (D) Right mammillary body, (E) Thalamoperforating arteries, (F) Postmammillary recess, (G) Left mammillary body

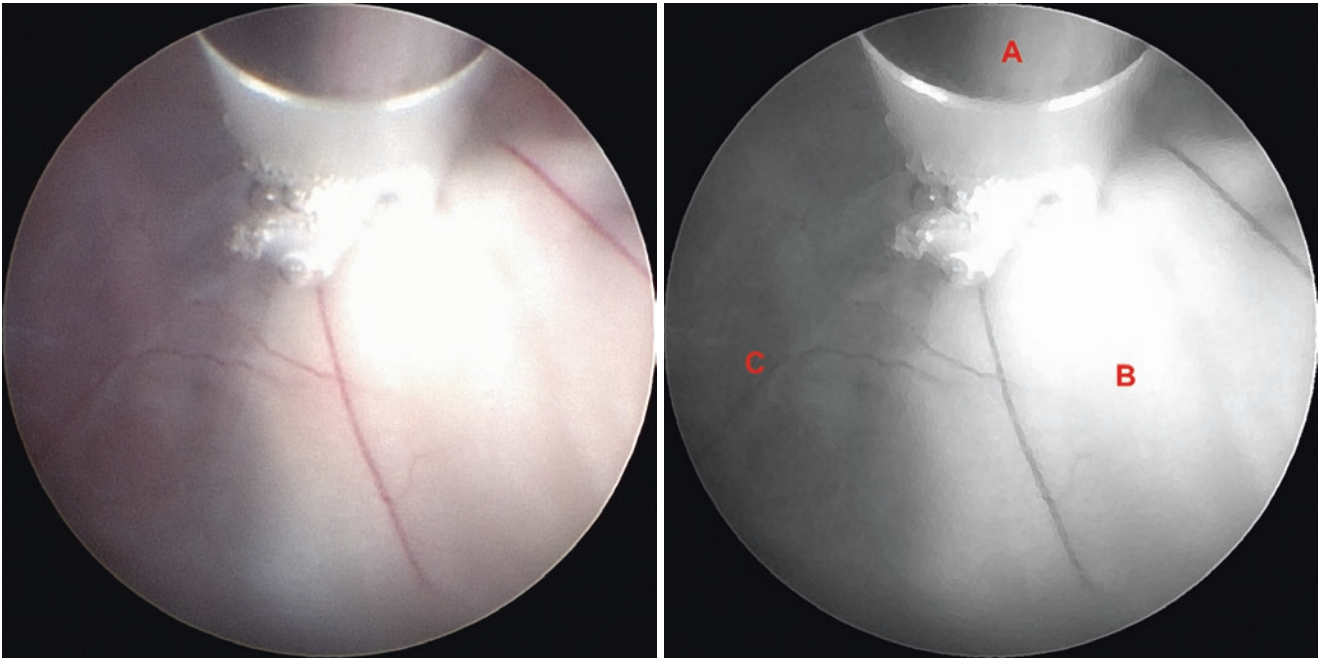


**Fig. 4.68** Surgical procedure – third ventriculostomy. (A) Bipolar coagulation electrode, (B) Right mammillary body, (C) Thalamoperforating arteries

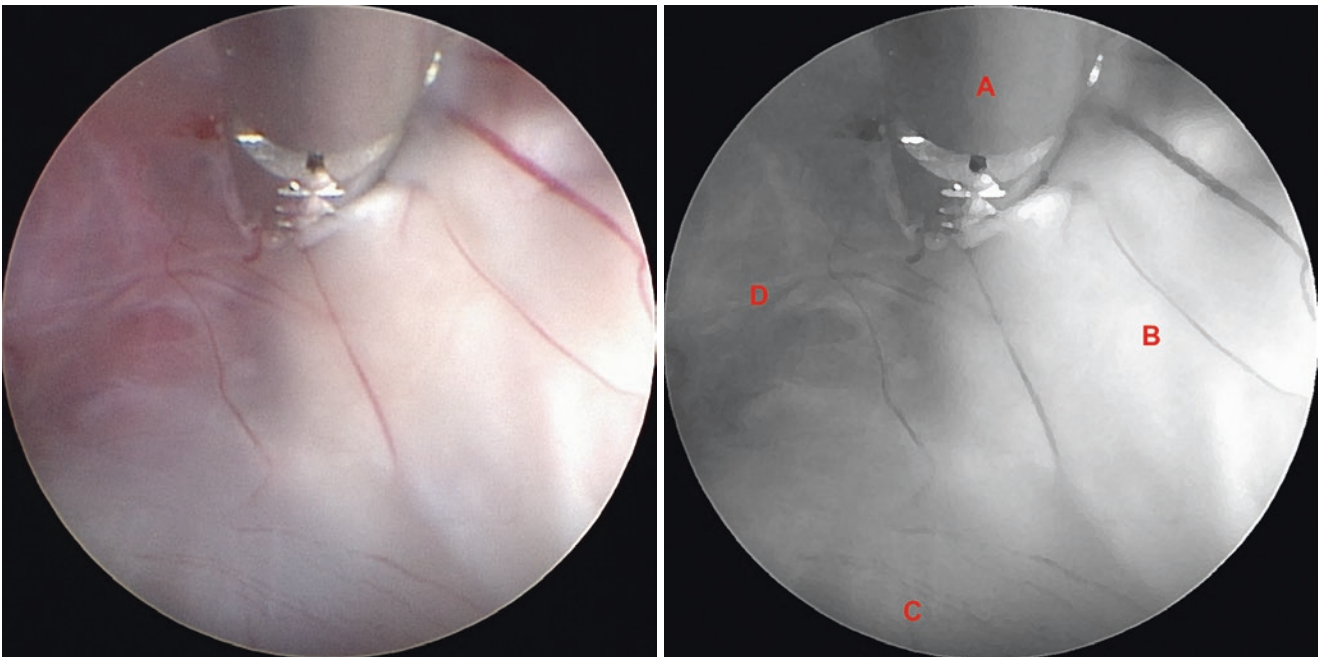


**Fig. 4.69** Surgical procedure – third ventriculostomy. (A) Grasping forceps, (B) Right mammillary body, (C) Postmammillary recess, (D) Thalamoperforating arteries

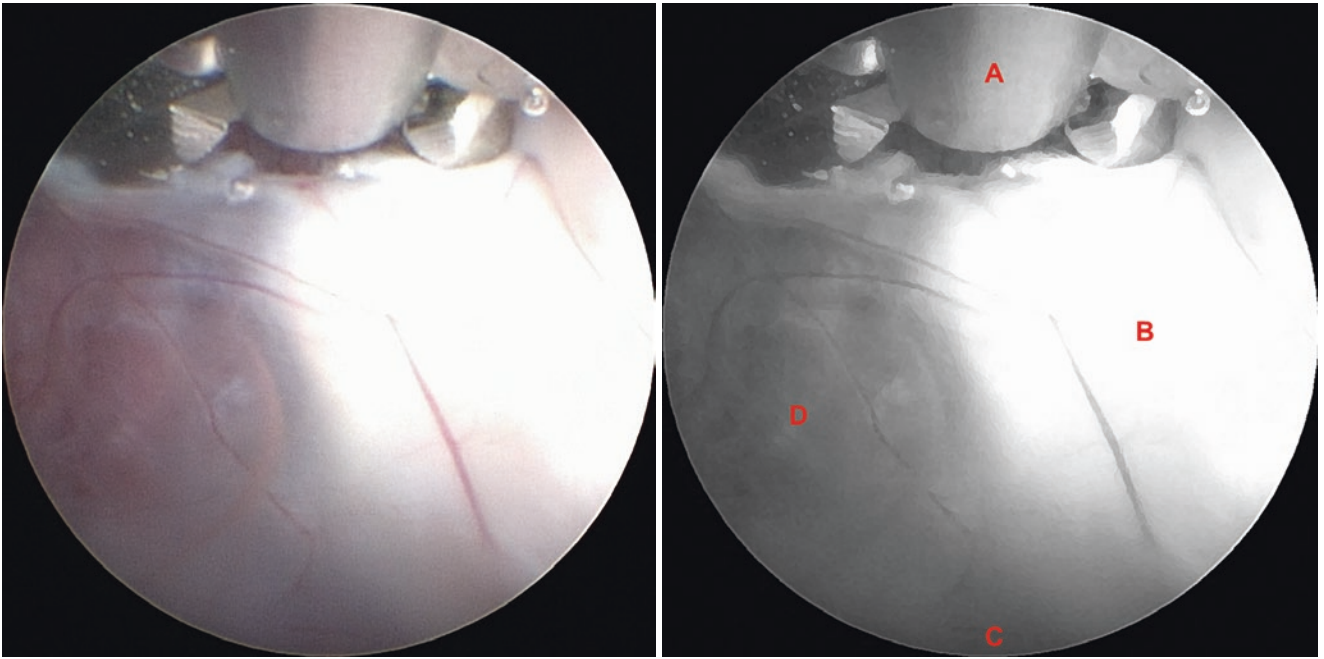


**Fig. 4.70** Surgical procedure – third ventriculostomy. (A) Dilatation with grasping forceps, (B) Right mammillary body, (C) Postmammillary recess, (D) Thalamoperforating arteries

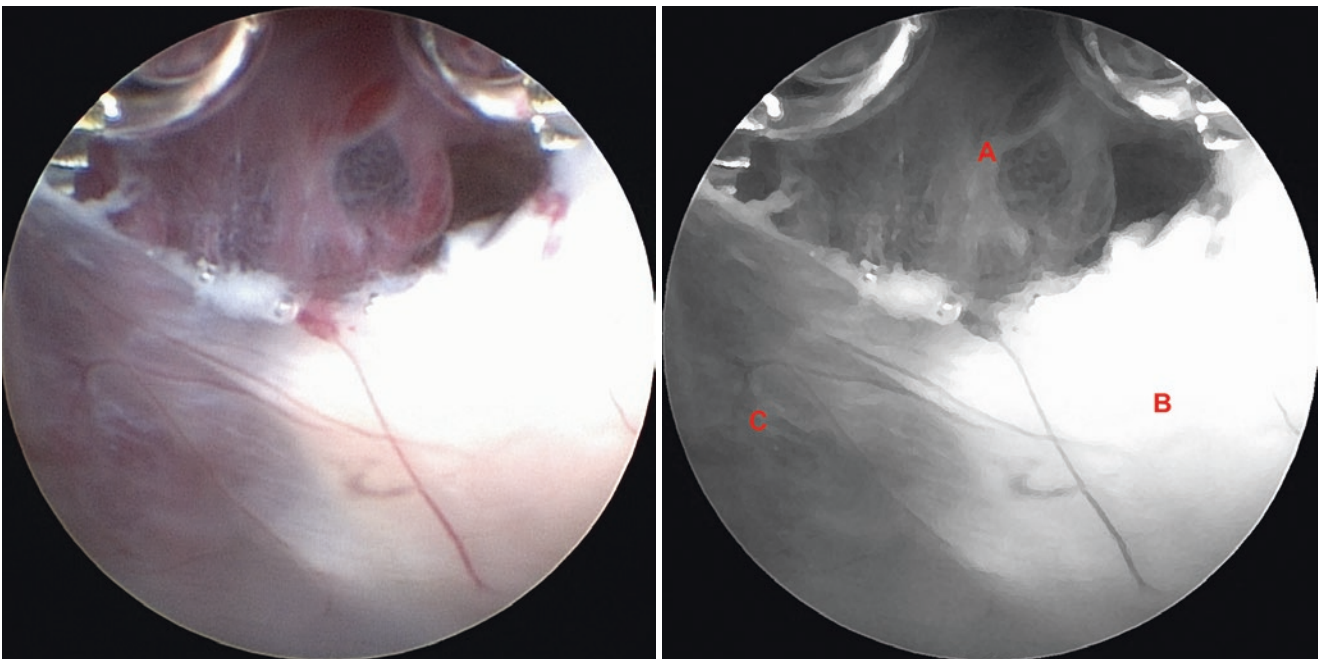


**Fig. 4.71** Surgical procedure – third ventriculostomy. (A) Thalamoperforating arteries under membrane of Lilliequist, (B) Right mammillary body, (C) Premammillary recess

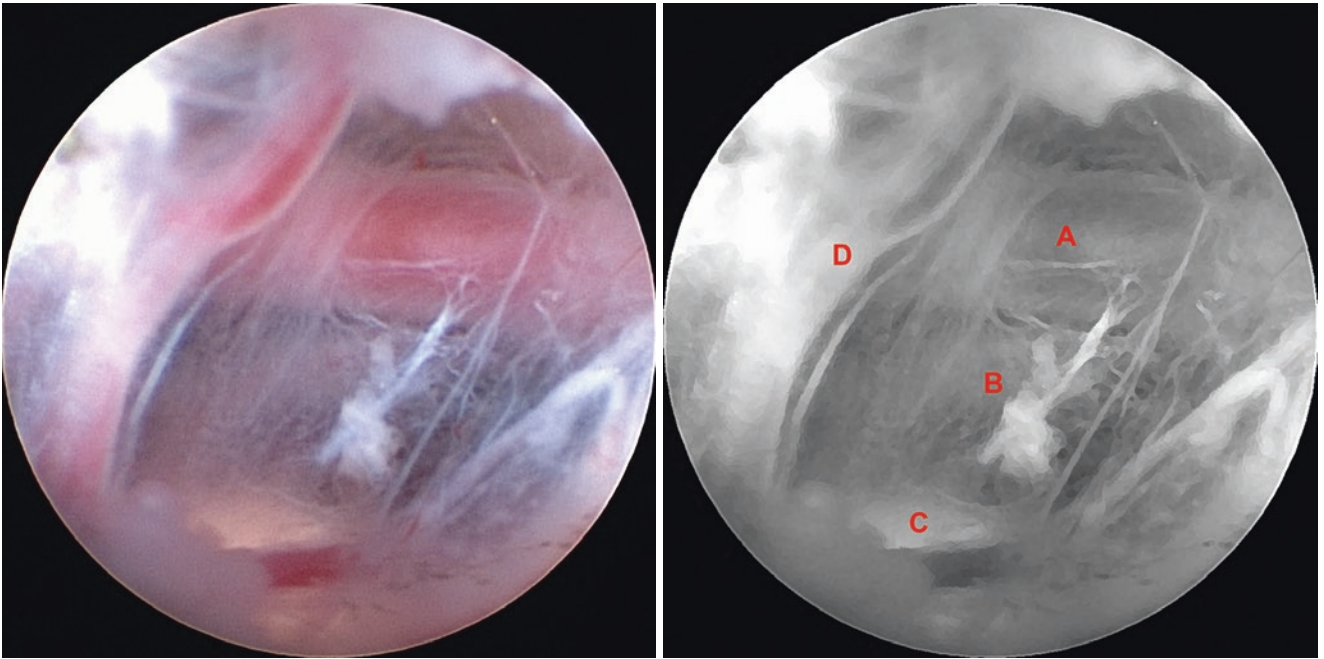


**Fig. 4.72** Surgical procedure – third ventriculostomy. (A) Right posterior cerebral artery (P1), (B) Membrane of Lilliequist, (C) Pons under membrane of Lilliequist, (D) Thalamoperforating artery

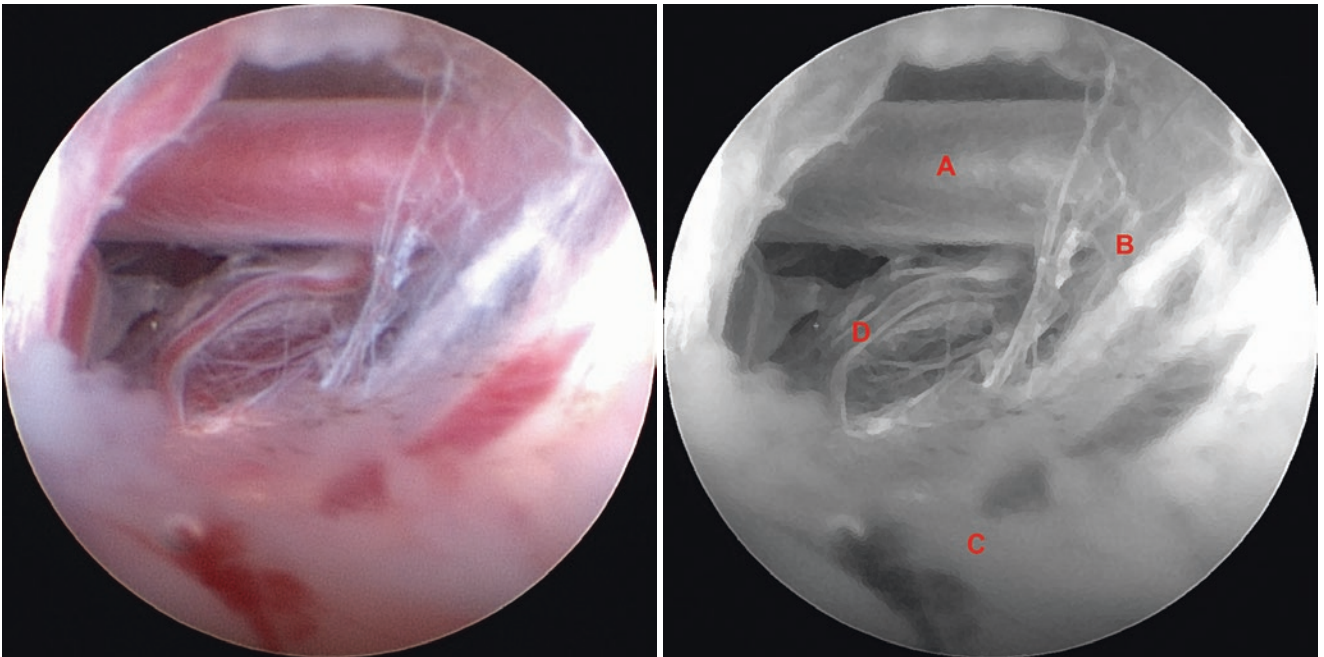


**Fig. 4.73** Surgical procedure – third ventriculostomy. (A) Right posterior cerebral artery (P1), (B) Membrane of Lilliequist, (C) Tuber cinereum, (D) Thalamoperforating artery

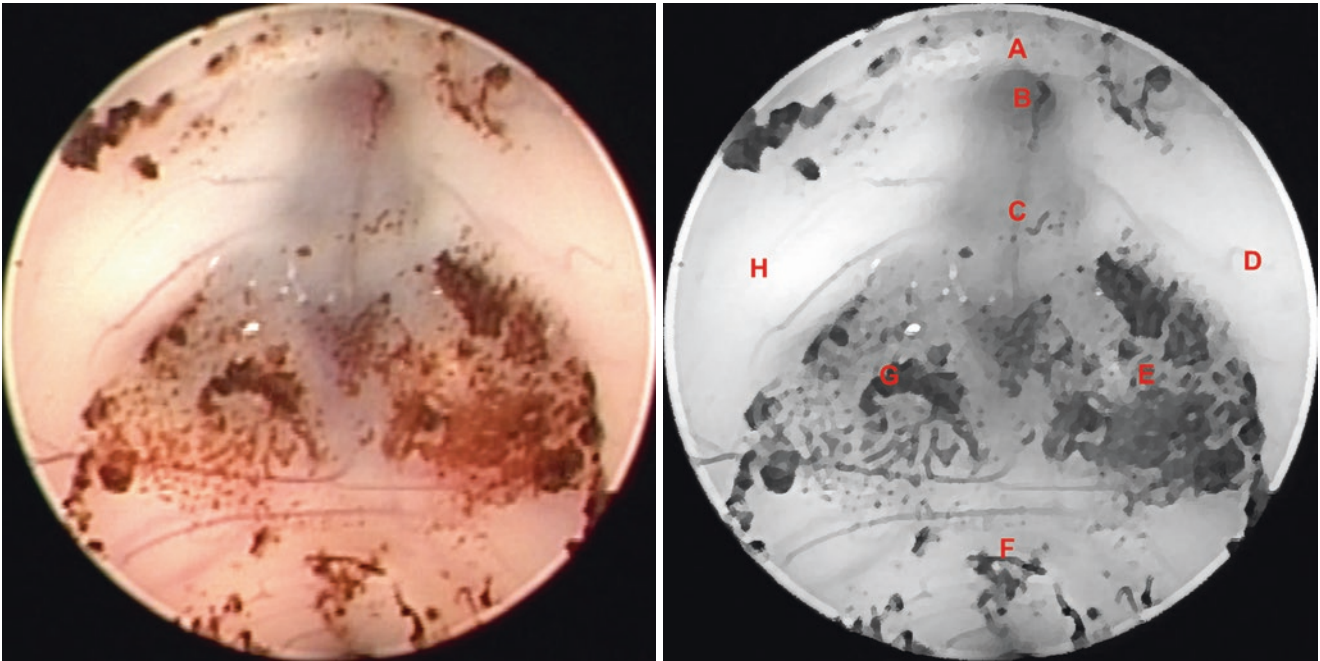


**Fig. 4.74** Surgical procedure – third ventriculostomy. (A) Optic chiasm, (B) Infundibular recess, (C) Tuber cinereum, (D) Right hypothalamus, (E) Right mammillary body under clots, (F) Postmammillary recess, (G) Left mammillary body under clots, (H) Left hypothalamus

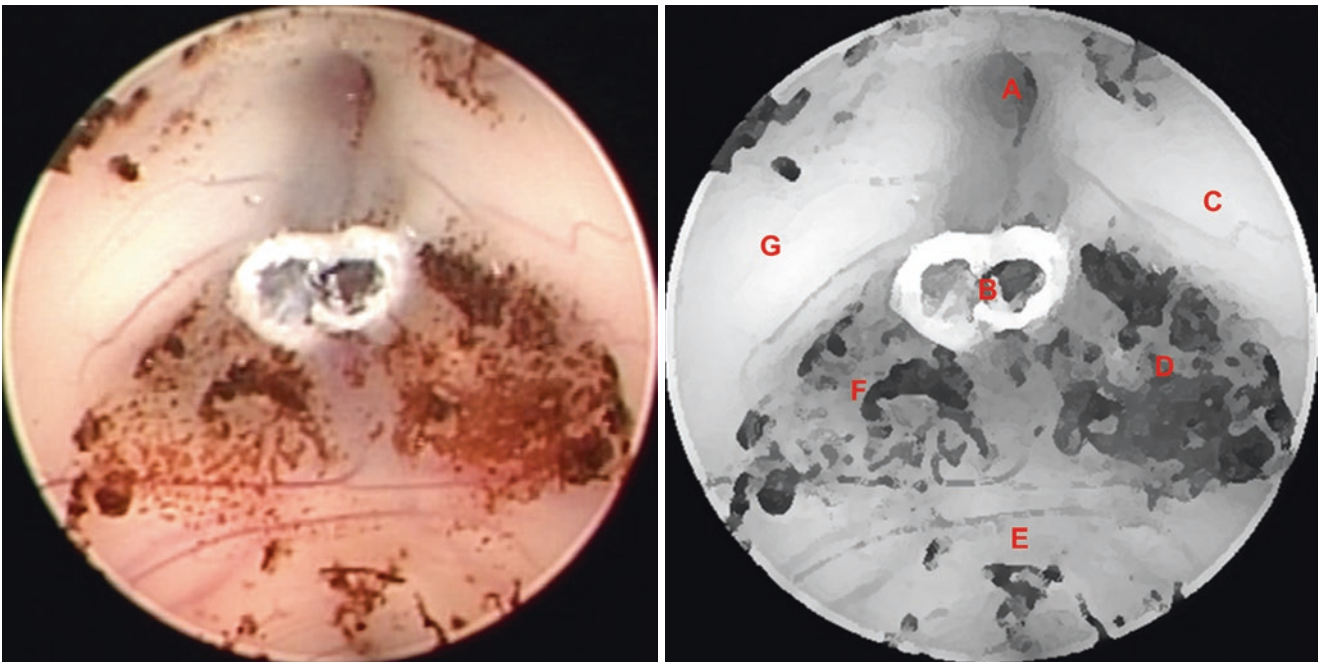


**Fig. 4.75** Surgical procedure – third ventriculostomy. (A) Infundibular recess, (B) Coagulated tuber cinereum, (C) Right hypothalamus, (D) Right mammillary body under clots, (E) Postmammillary recess, (F) Left mammillary body under clots, (G) Left hypothalamus

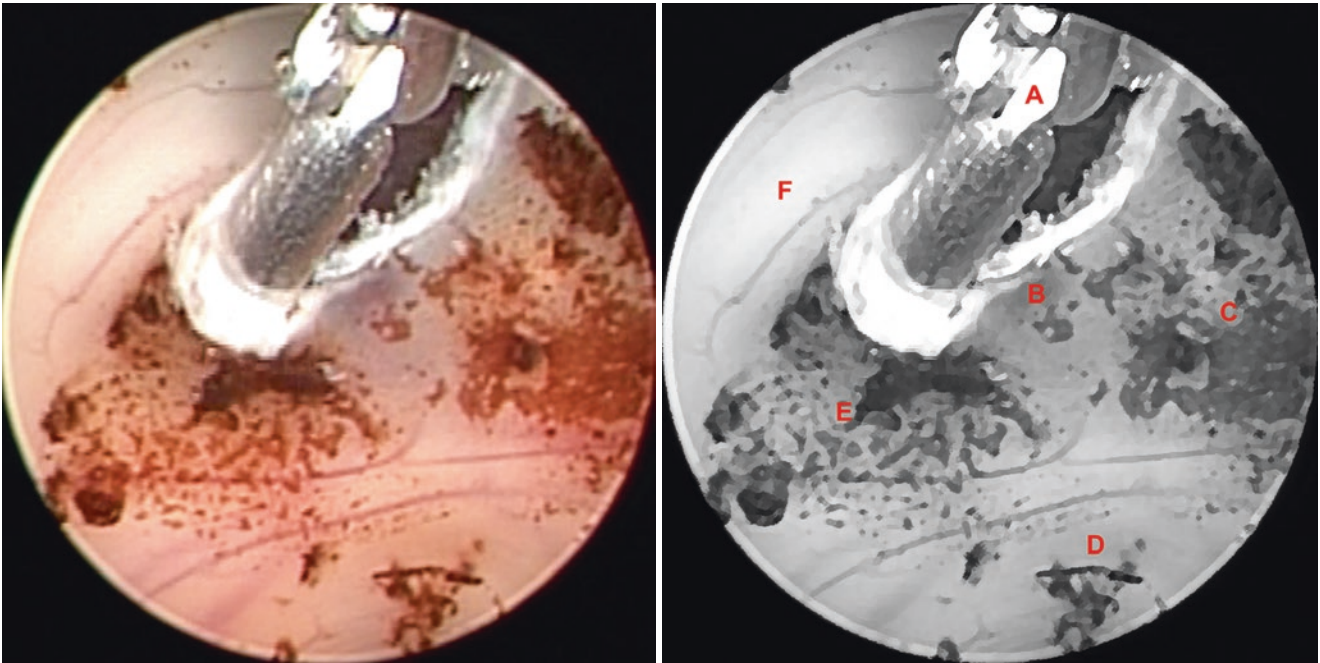


**Fig. 4.76** Surgical procedure – third ventriculostomy. (A) Grasping forceps, (B) Tuber cinereum, (C) Right mammillary body under clots, (D) Postmammillary recess, (E) Left mammillary body under clots, (F) Left hypothalamus

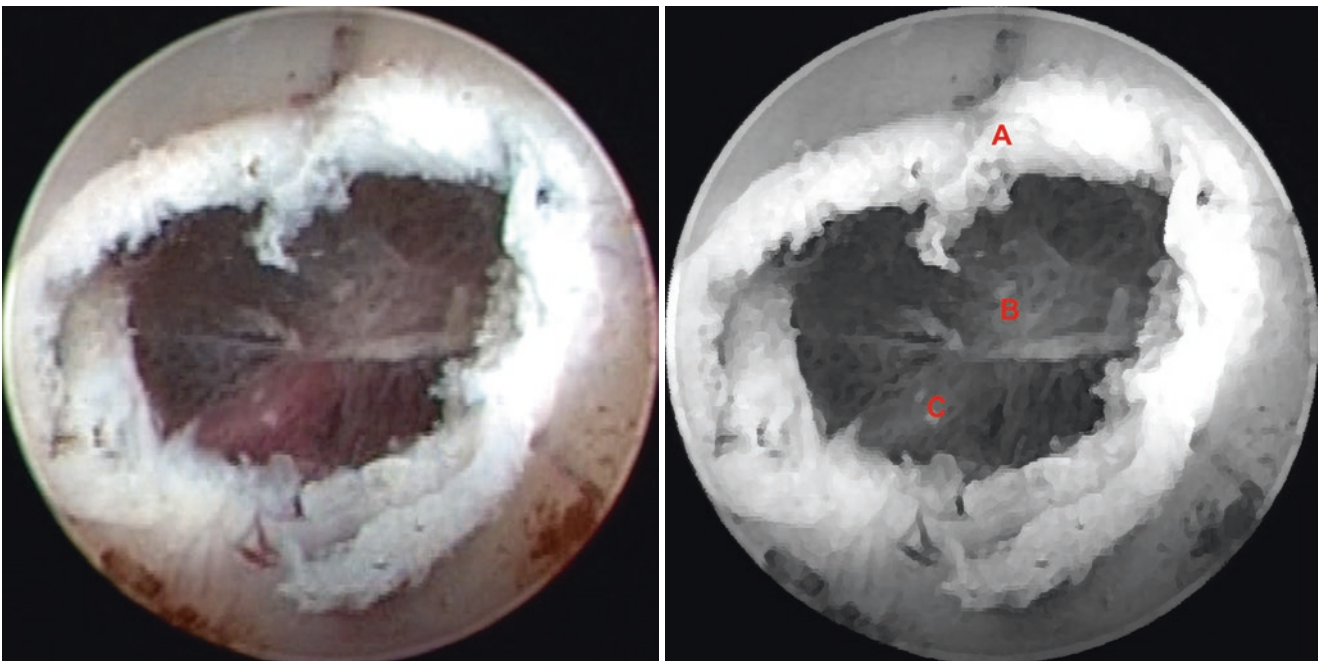


**Fig. 4.77** Surgical procedure – third ventriculostomy. (A) Coagulated tuber cinereum, (B) Membrane of Liliequist, (C) Bifurcation of the basilar artery

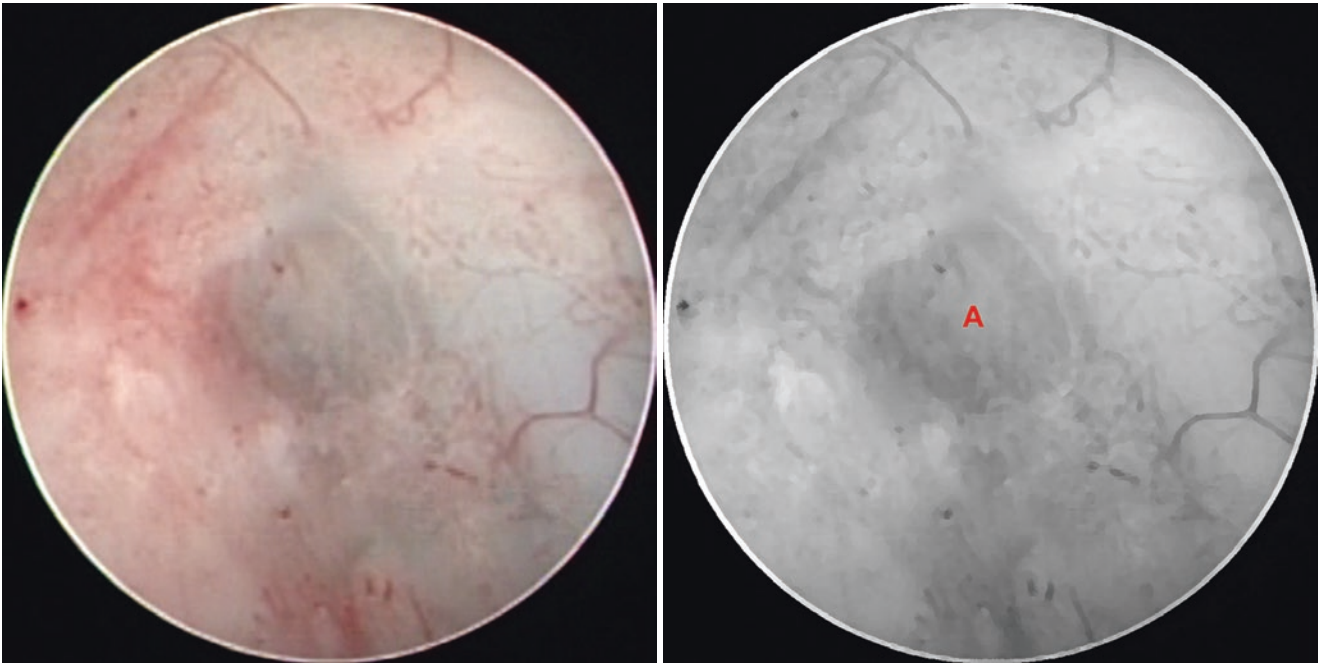


**Fig. 4.78** Surgical procedure – aborted third ventriculostomy due to distorted anatomy. (A) Tuber cinereum

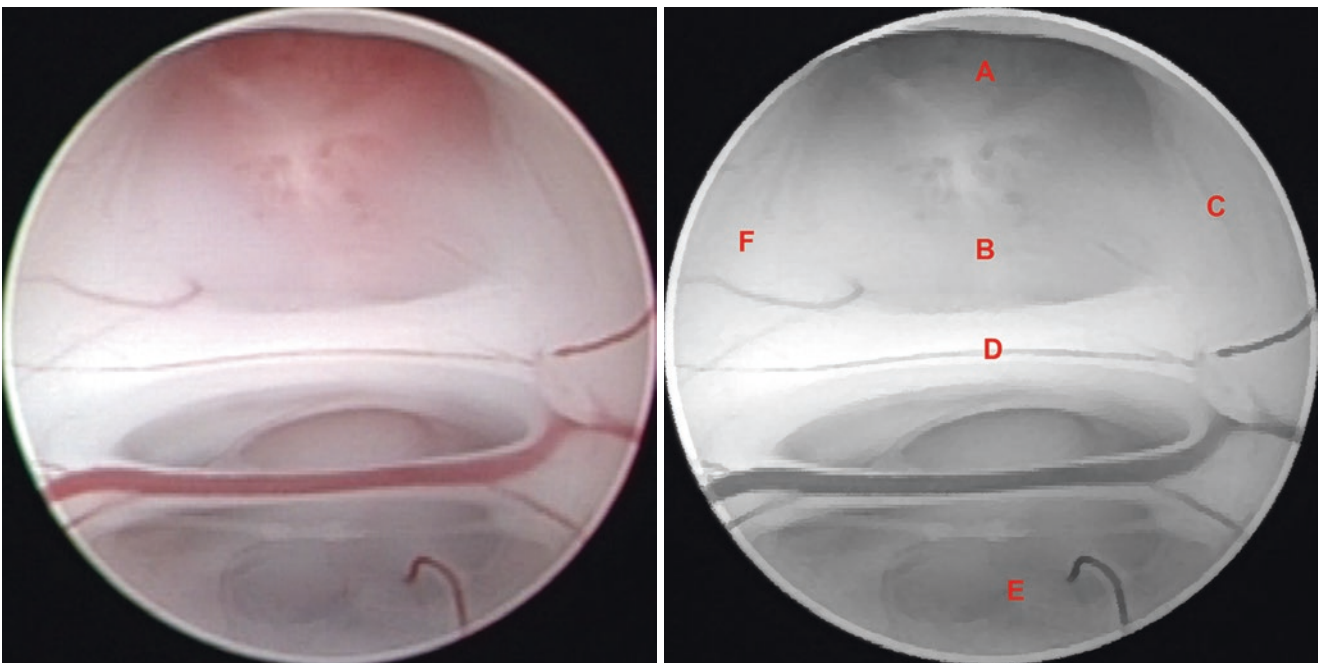


**Fig. 4.79** Surgical procedure – aborted third ventriculostomy due to distorted anatomy. (A) Infundibular recess, (B) Tuber cinereum, (C) Right hypothalamus, (D) Adhesion between mammillary bodies, (E) Postmammillary recess, (F) Left hypothalamus

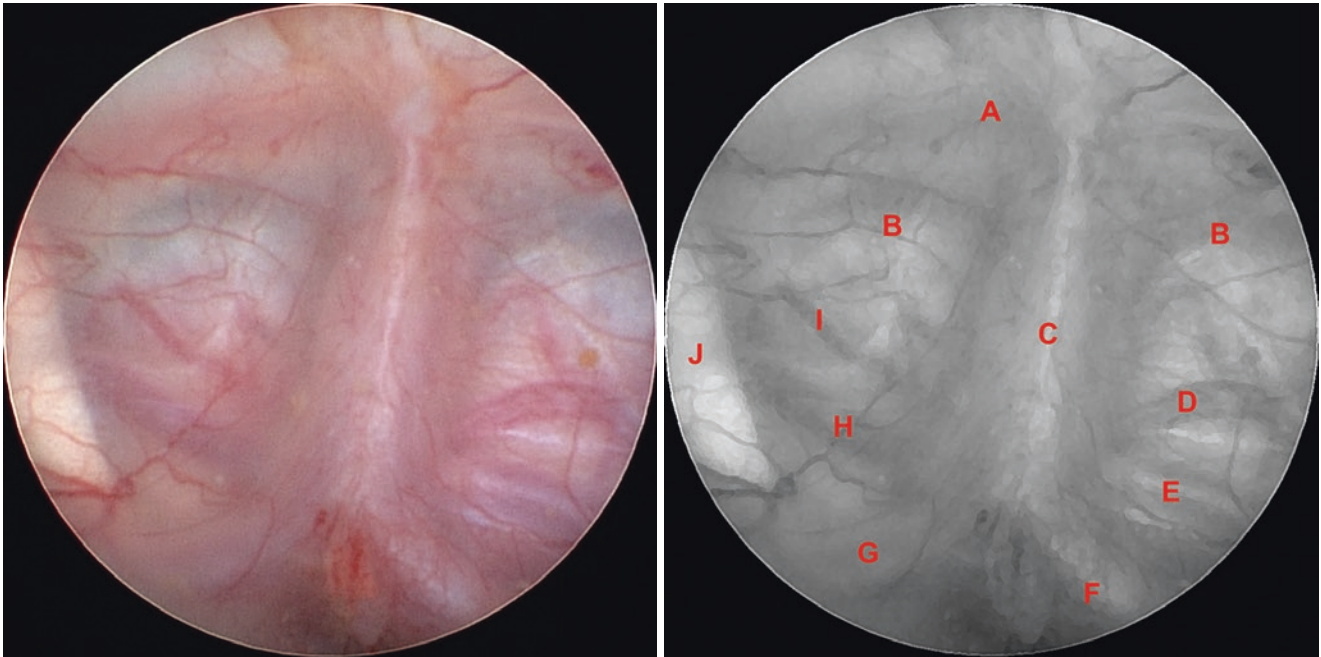


**Fig. 4.80** Illustrative case 1 – third ventriculostomy in a patient with reduced distance between basilar artery and clivus (MRIs of this case are shown in Figs. 4.148 and 4.149). (A) Dorsum sellae, (B) Tuber cinereum, (C) Basilar artery, (D) Right pontine branch of the basilar artery,

(E) Right superior cerebellar artery, (F) Right posterior cerebral artery (P1), (G) Left posterior cerebral artery (P1), (H) Left superior cerebellar artery, (I) Left pontine branch of the basilar artery, (J) Left oculomotor nerve (CN III)

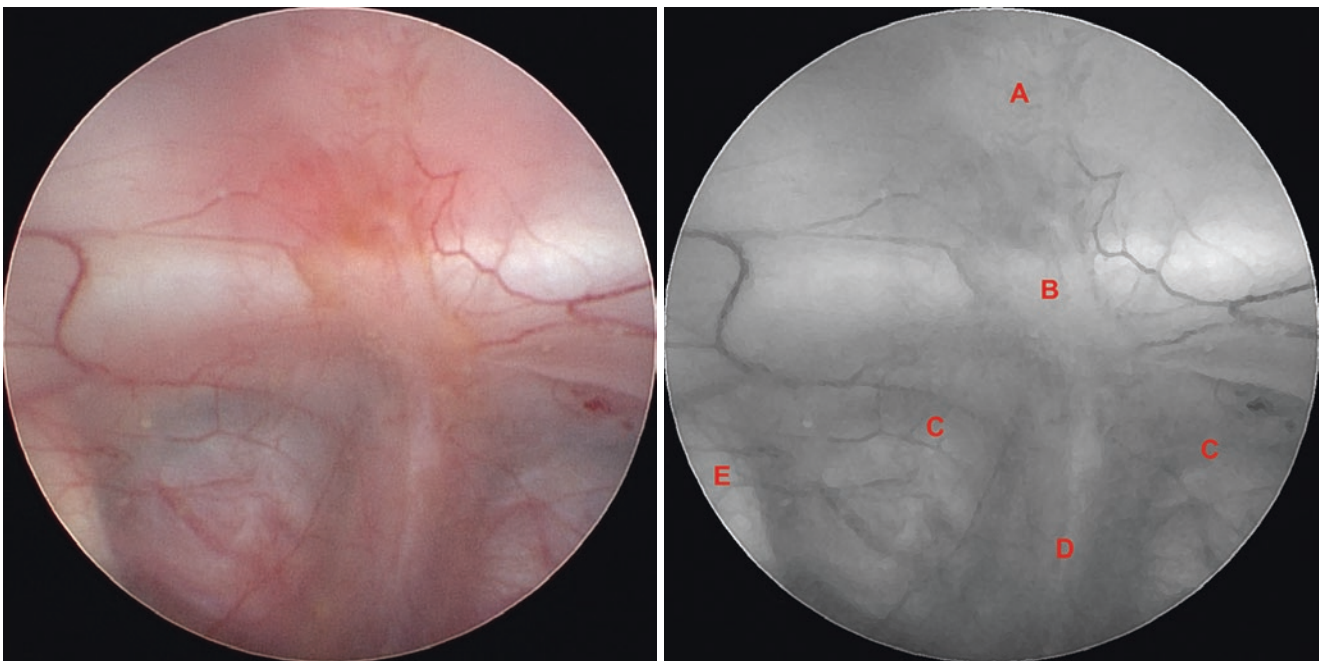


**Fig. 4.81** Illustrative case 1 – third ventriculostomy in a patient with reduced distance between basilar artery and clivus (MRIs of this case are shown in Figs. 4.148 and 4.149). (A) Pituitary gland, (B) Dorsum

sellae, (C) Tuber cinereum, (D) Basilar artery, (E) Left oculomotor nerve (CN III)



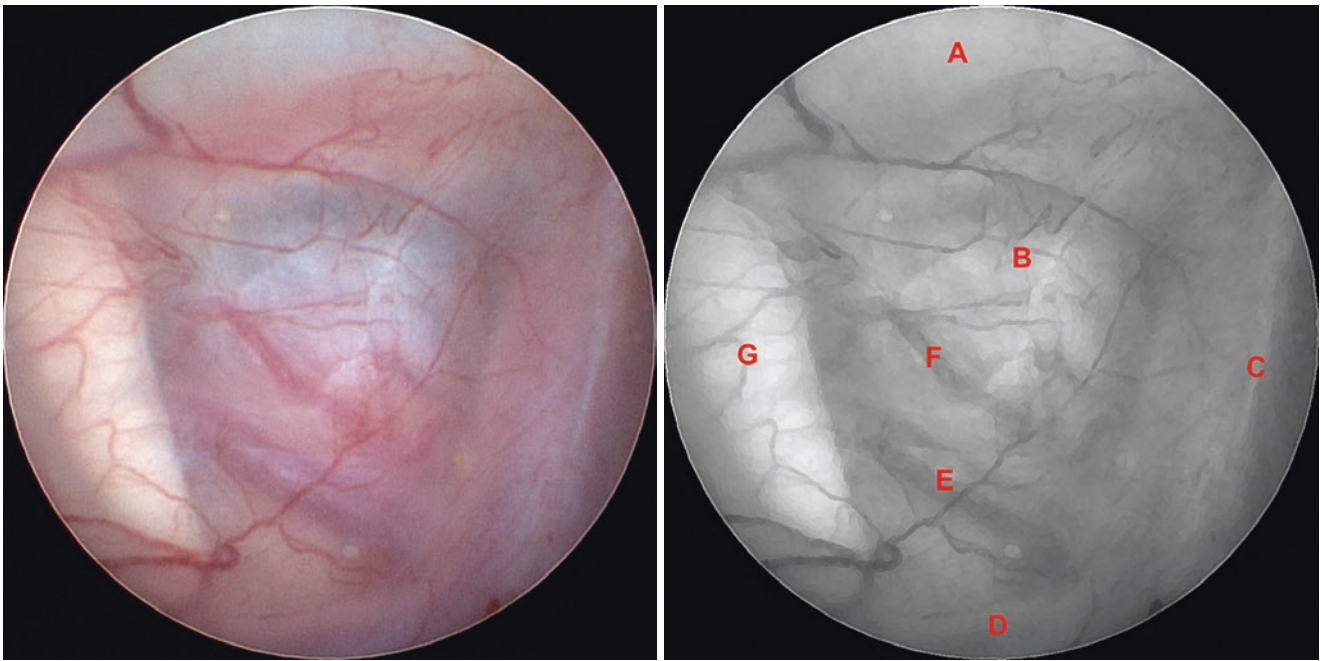


**Fig. 4.82** Illustrative case 1 – third ventriculostomy in a patient with reduced distance between basilar artery and clivus (MRIs of this case are shown in Figs. 4.148 and 4.149). (A) Dorsum sellae, (B) Tuber cine-

reum, (C) Basilar artery, (D) Left posterior cerebral artery (P1), (E) Left superior cerebellar artery, (F) Left pontine branch of the basilar artery, (G) Left oculomotor nerve (CN III)

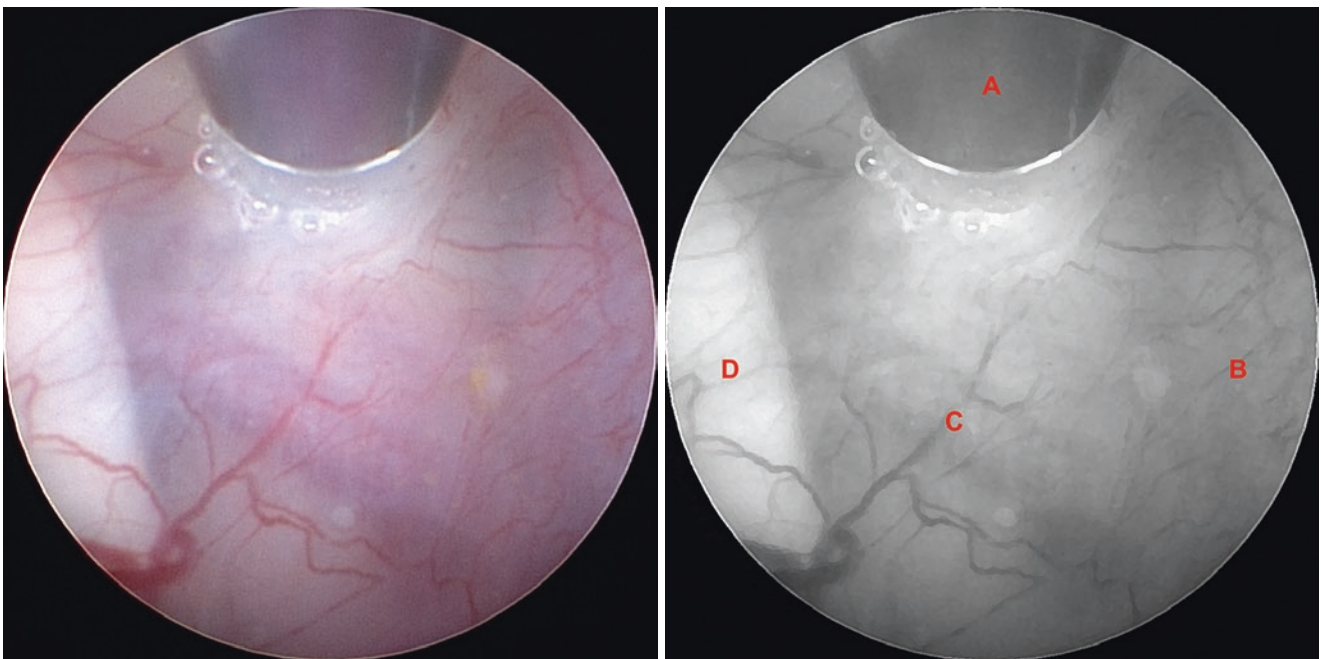


**Fig. 4.83** Illustrative case 1 – third ventriculostomy in a patient with reduced distance between basilar artery and clivus (MRIs of this case are shown in Figs. 4.148 and 4.149). (A) Bipolar coagulation electrode,

(B) Basilar artery, (C) Left pontine branch of the basilar artery, (D) Left oculomotor nerve (CN III)

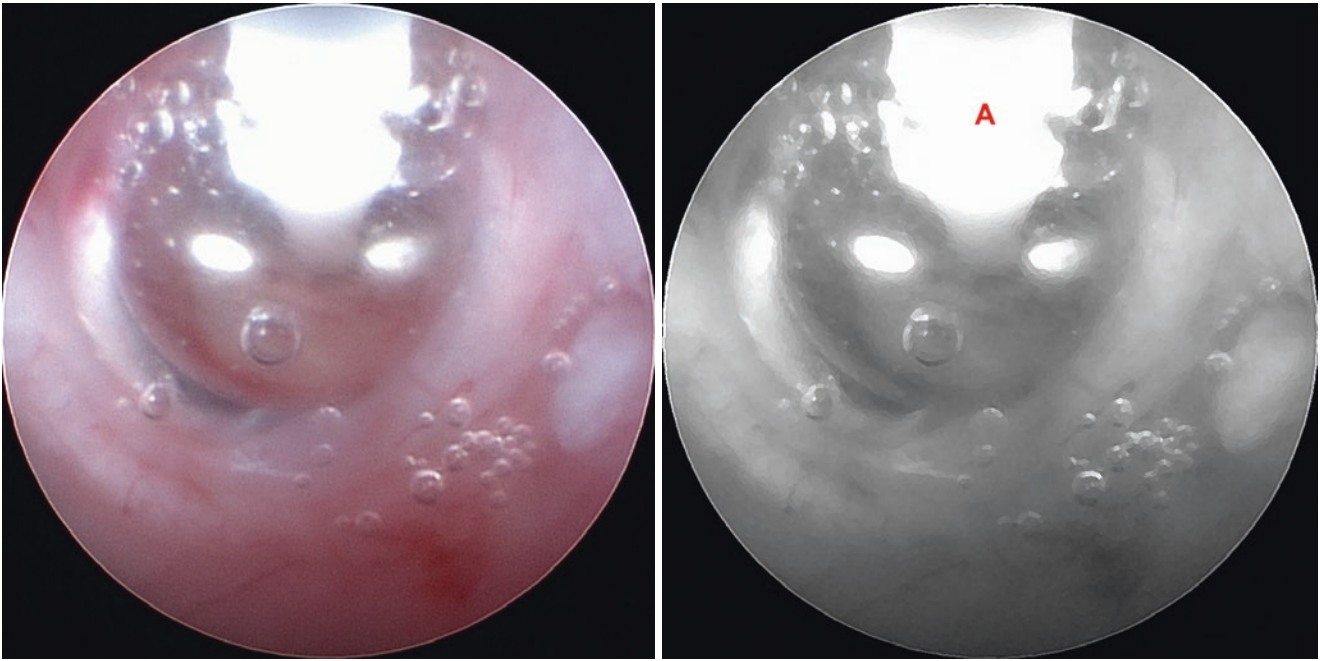


**Fig. 4.84** Illustrative case 1 – third ventriculostomy in a patient with reduced distance between basilar artery and clivus (MRIs of this case are shown in Figs. 4.148 and 4.149). (A) Fogarty balloon catheter

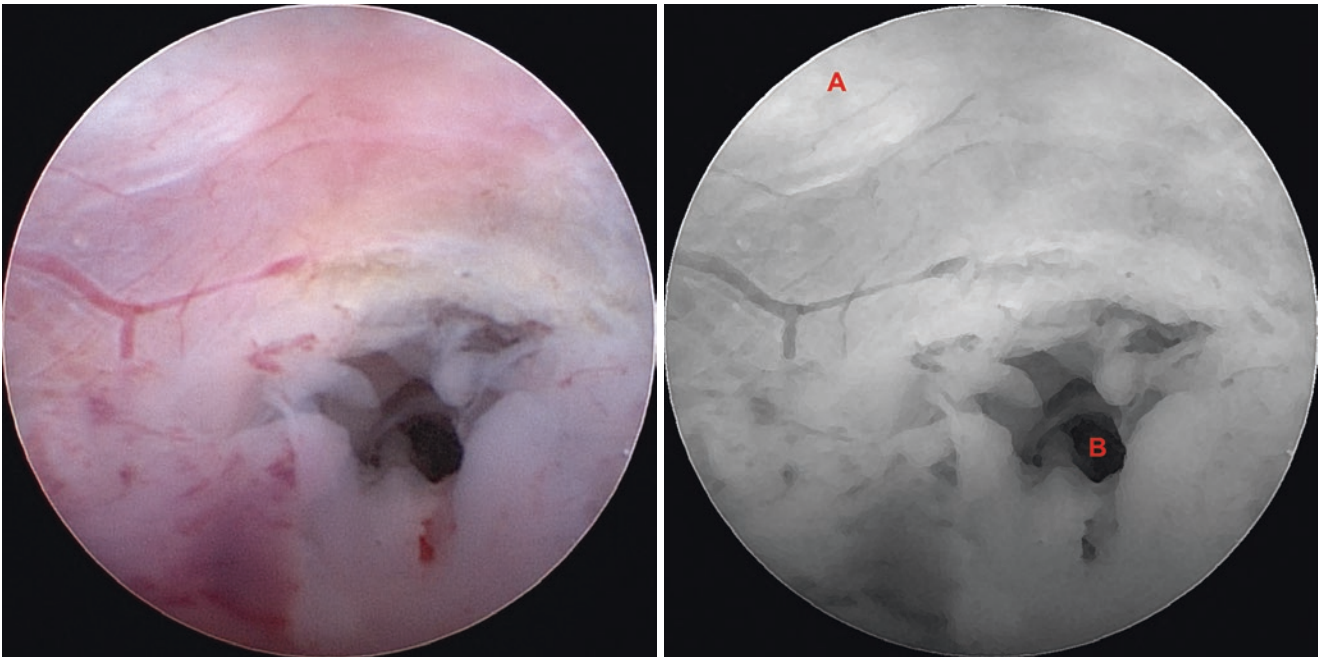


**Fig. 4.85** Illustrative case 1 – third ventriculostomy in a patient with reduced distance between basilar artery and clivus (MRIs of this case are shown in Figs. 4.148 and 4.149). (A) Dorsum sellae, (B) Ventriculostomy

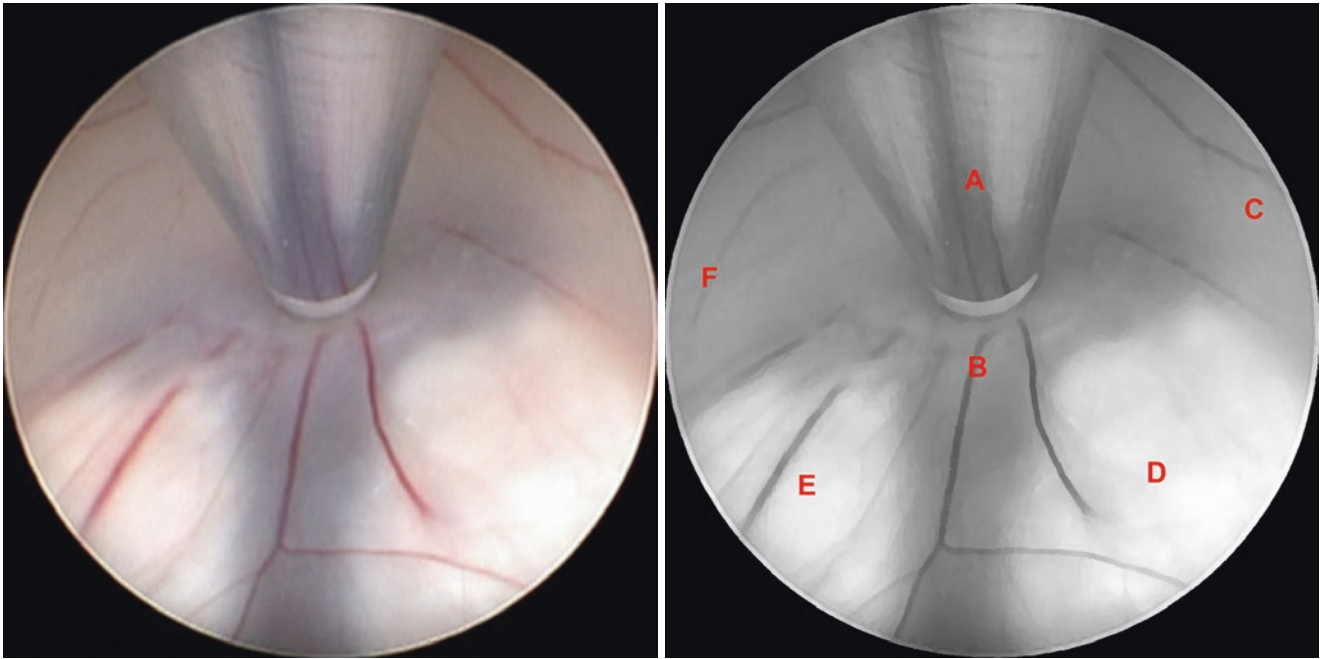


**Fig. 4.86** Illustrative case 2 – removal of racemose cysts of neurocysticercosis by third ventriculostomy (MRIs of this case are shown in Figs. 5.37 and 5.38 in chapter 5). (A) Bipolar coagulation electrode over

the tuber cinereum, (B) Premamillary recess, (C) Right hypothalamus, (D) Right mammillary body, (E) Left mammillary body, (F) Left hypothalamus

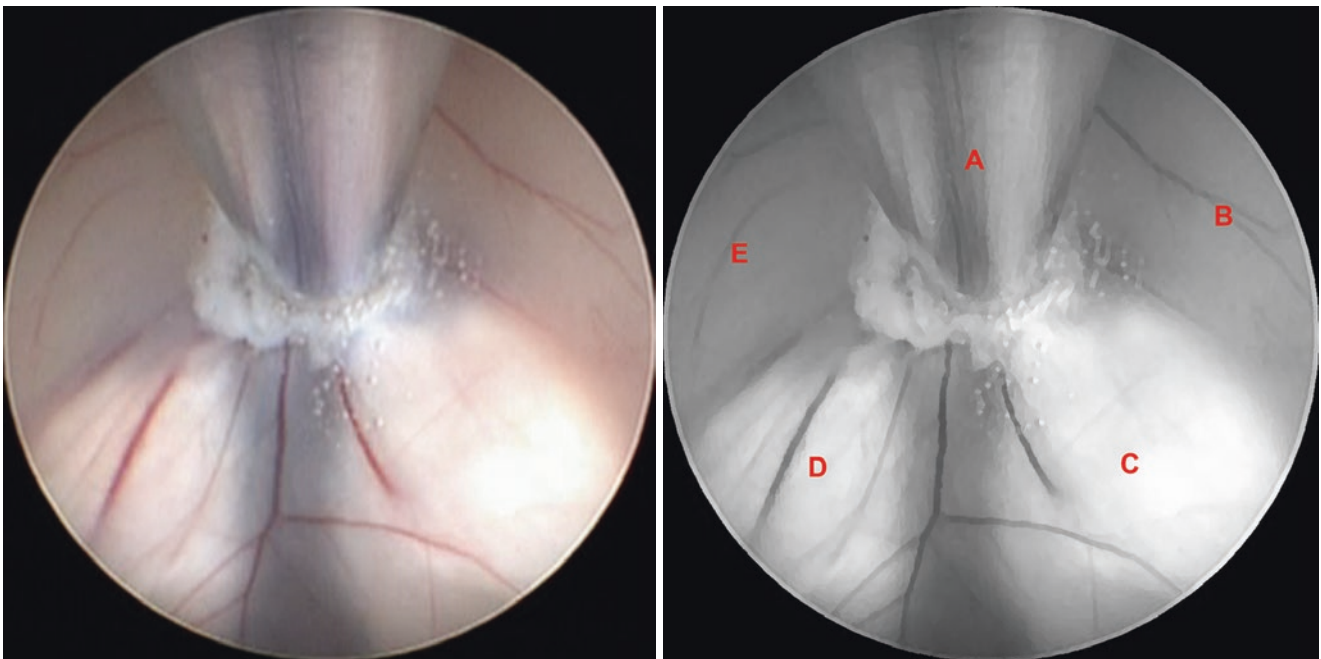


**Fig. 4.87** Illustrative case 2 – removal of racemose cysts of neurocysticercosis by third ventriculostomy (MRIs of this case are shown in Figs. 5.37 and 5.38 in Chap. 5). (A) Bipolar coagulation of the tuber

cinereum, (B) Right hypothalamus, (C) Right mammillary body, (D) Left mammillary body, (E) Left hypothalamus

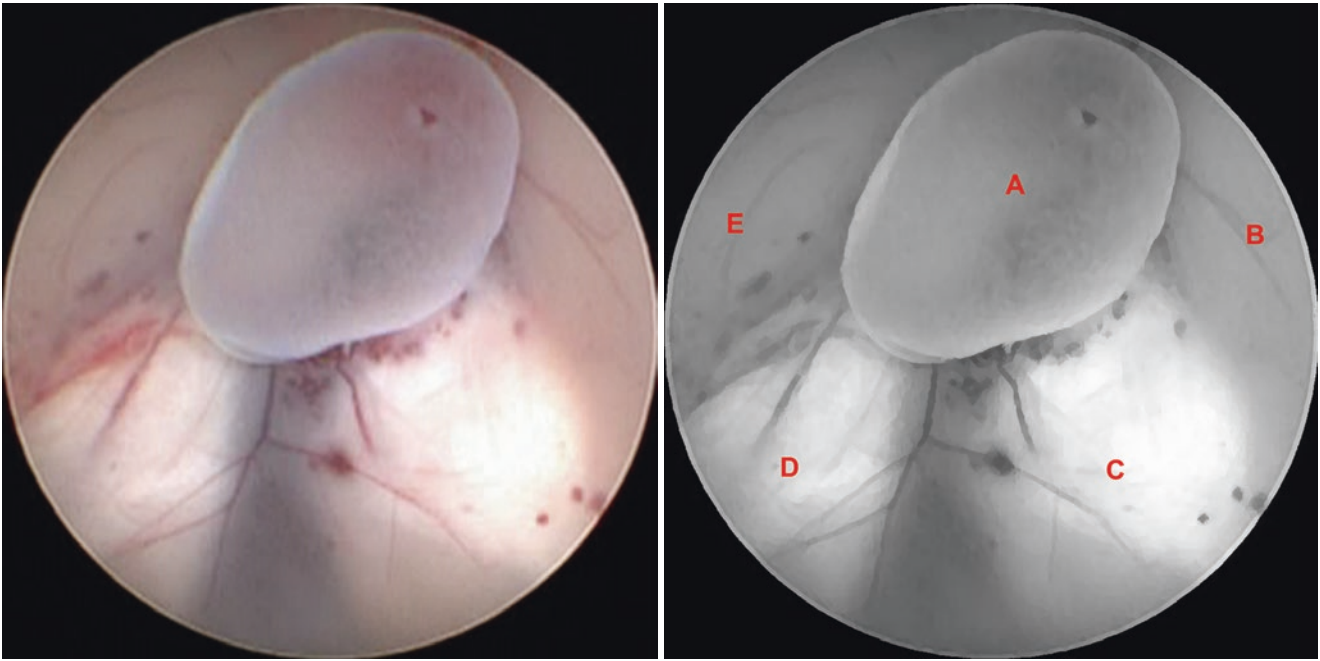


**Fig. 4.88** Illustrative case 2 – removal of racemose cysts of neurocysticercosis by third ventriculostomy (MRIs of this case are shown in Figs. 5.37 and 5.38 in Chap. 5). (A) Racemose cyst, (B) Right hypo-

thalamus, (C) Right mammillary body, (D) Left mammillary body, (E) Left hypothalamus

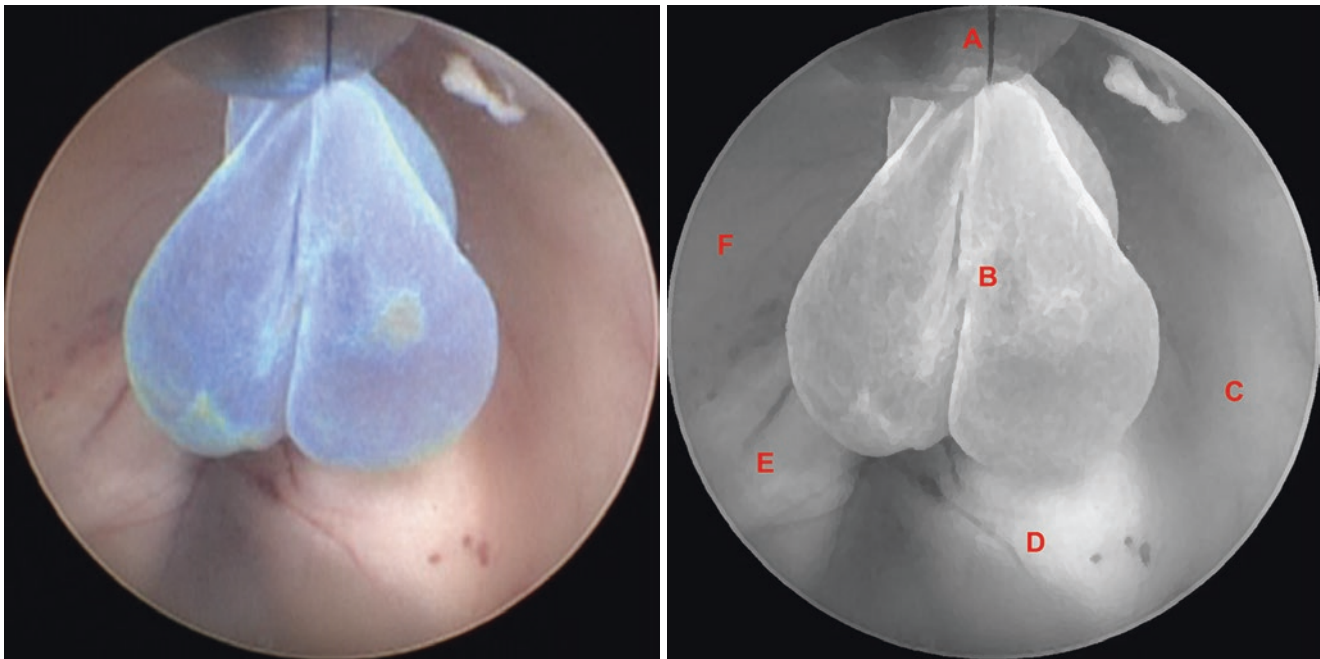


**Fig. 4.89** Illustrative case 2 – removal of racemose cysts of neurocysticercosis by third ventriculostomy (MRIs of this case are shown in Figs. 5.37 and 5.38 in Chap. 5). (A) Biopsy forceps, (B) Racemose cyst,

(C) Right hypothalamus, (D) Right mammillary body, (E) Left mammillary body, (F) Left hypothalamus

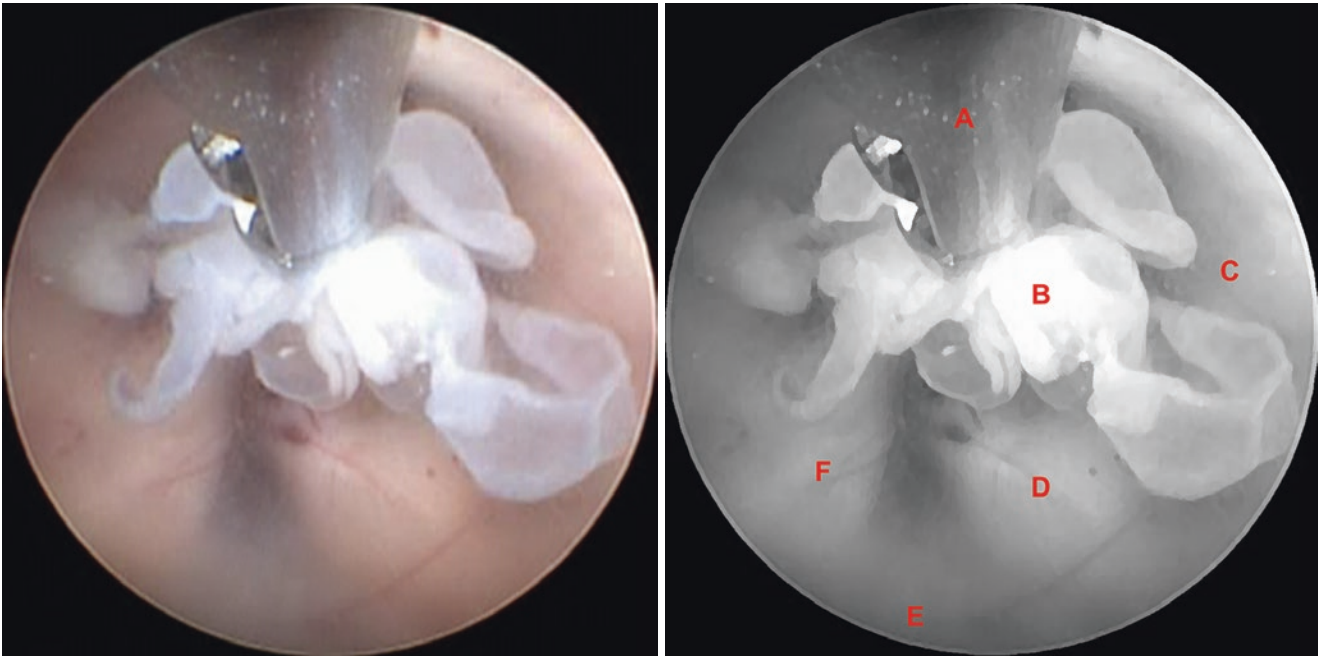


**Fig. 4.90** Illustrative case 2 – removal of racemose cysts of neurocysticercosis by third ventriculostomy (MRIs of this case are shown in Figs. 5.37 and 5.38 in Chap. 5). (A) Biopsy forceps, (B) Racemose cyst,

(C) Right hypothalamus, (D) Right mammillary body, (E) Postmammillary recess, (F) Left mammillary body

#### 4.4 Third Ventricle: Middle Segment

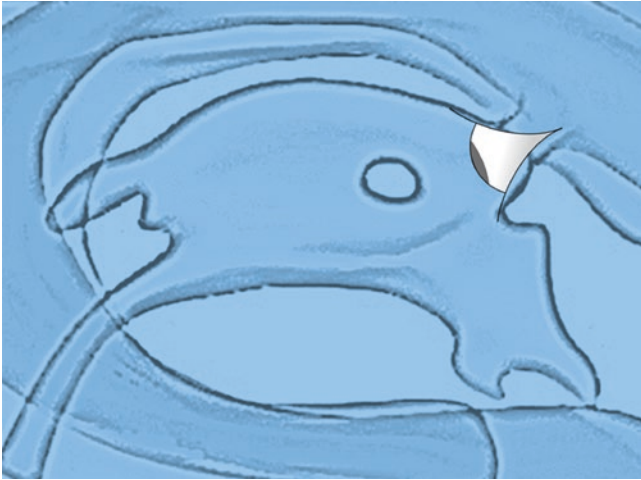


**Fig. 4.91** Direction of the endoscopic vision for the middle segment of the third ventricle

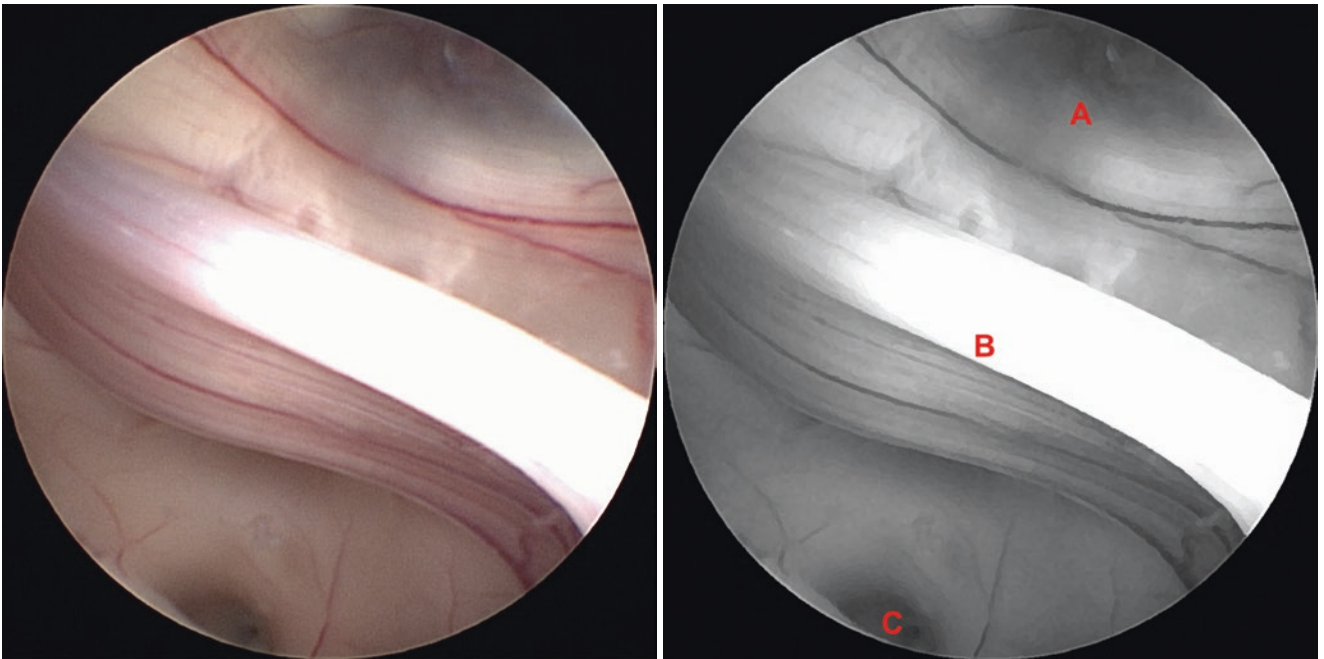


**Fig. 4.92** Normal anatomy. (A) Postmammillary recess, (B) Interthalamic adhesion, (C) Cerebral aqueduct entrance

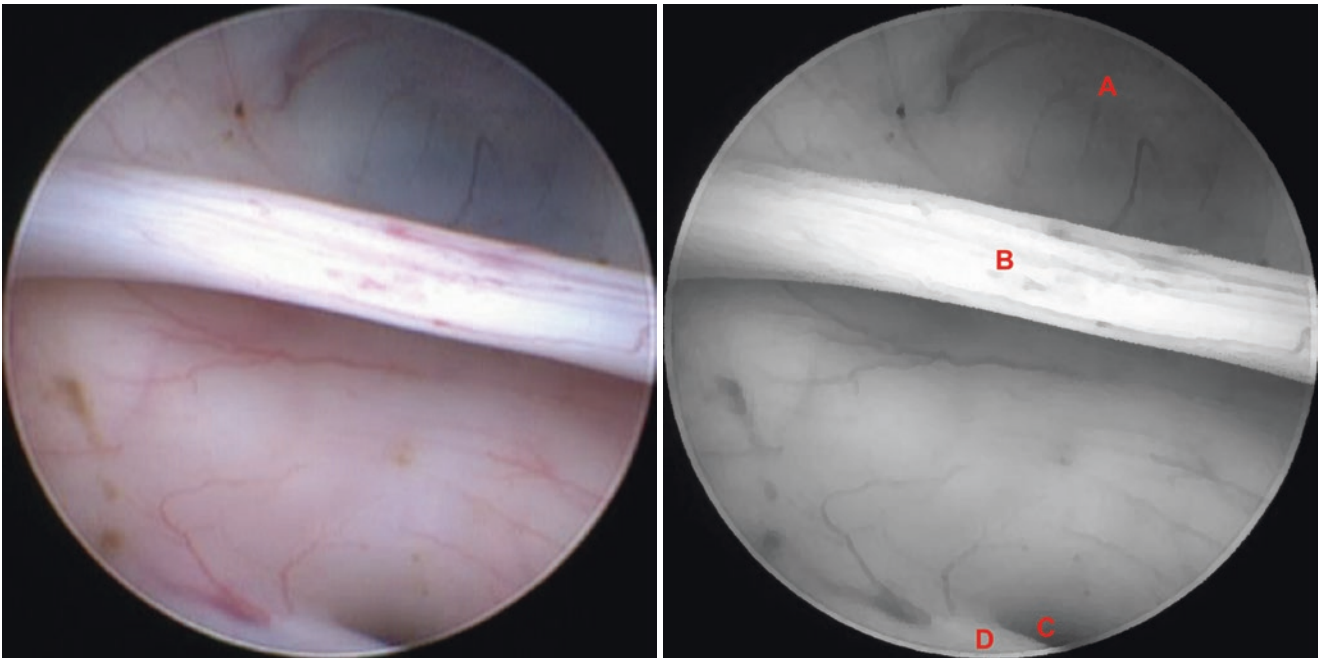


**Fig. 4.93** Normal anatomy. (A) Postmammillary recess, (B) Interthalamic adhesion, (C) Cerebral aqueduct entrance, (D) Posterior commissure

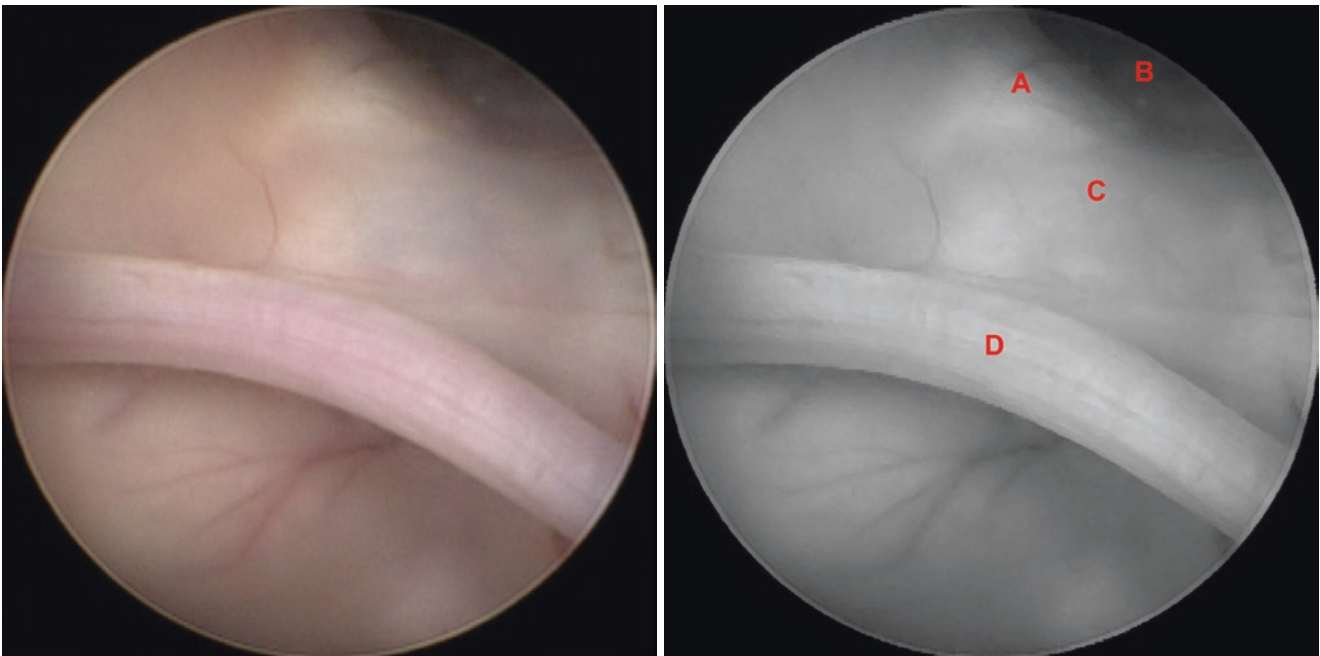


**Fig. 4.94** Normal anatomy. (A) Left mammillary body, (B) Premammillary recess, (C) Postmammillary recess, (D) Interthalamic adhesion

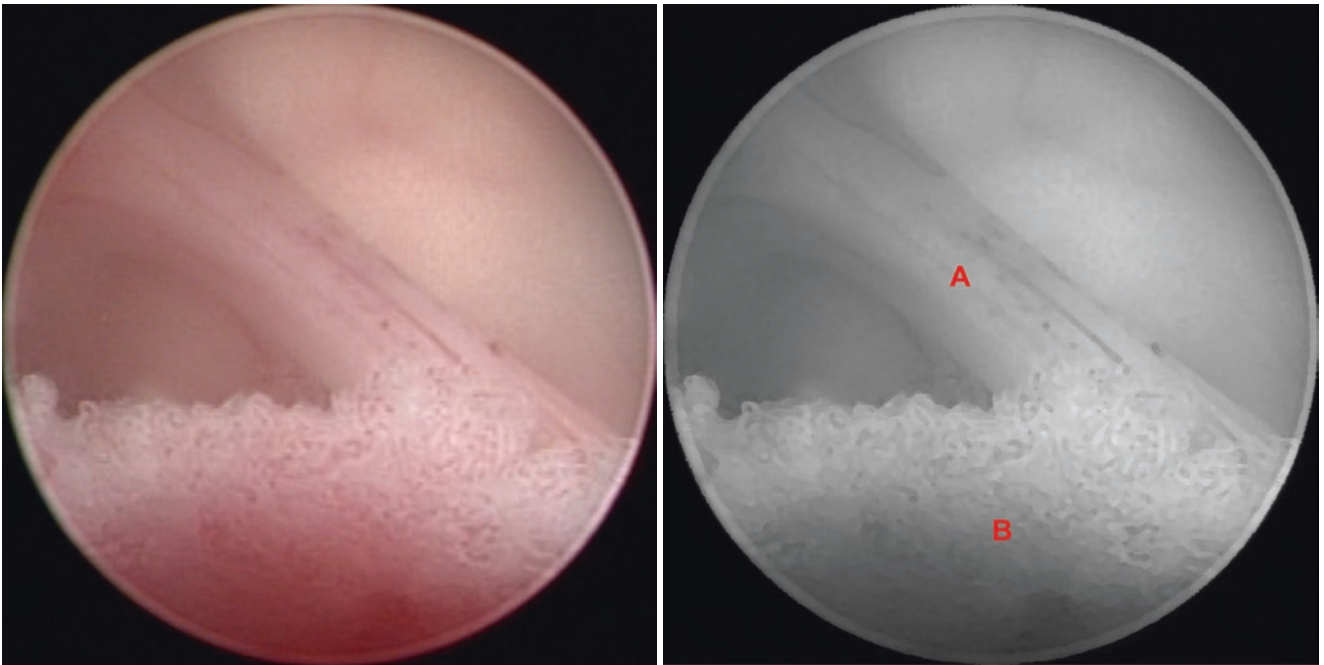


**Fig. 4.95** Normal anatomy. (A) Interthalamic adhesion, (B) Choroid plexus at the right foramen of Monro

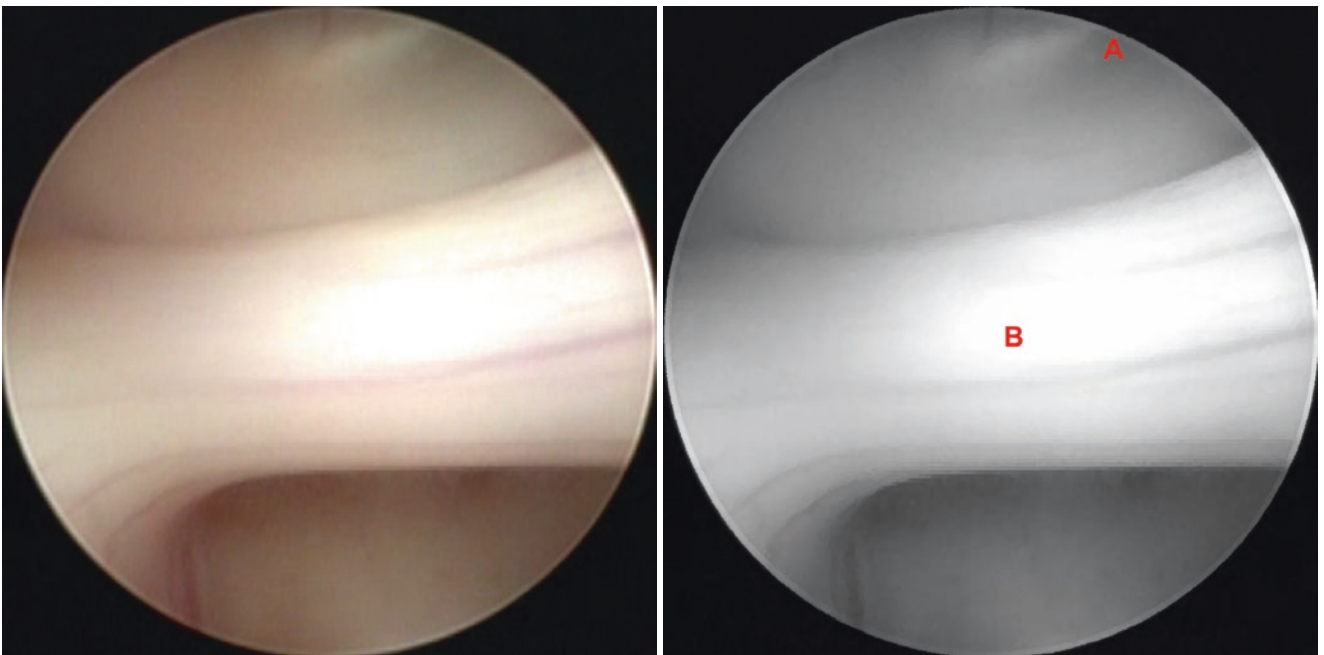


**Fig. 4.96** Normal anatomy. (A) Postmammillary recess, (B) Interthalamic adhesion



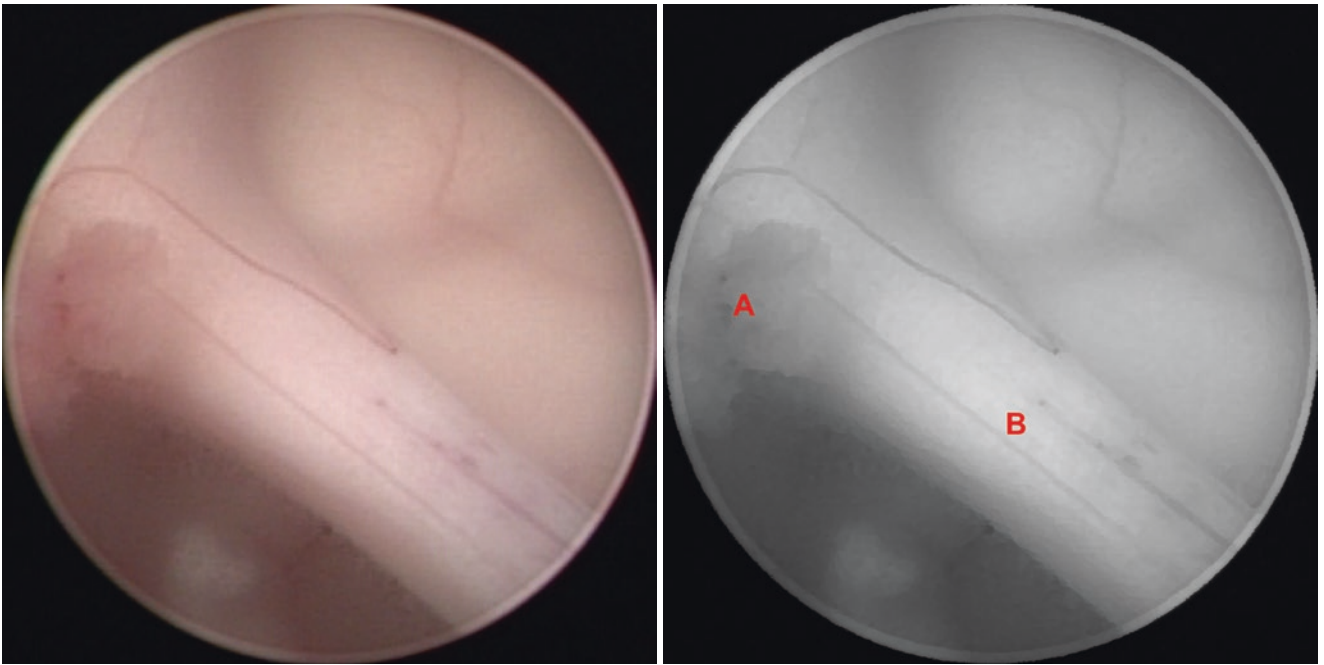


**Fig. 4.97** Normal anatomy. (A) Choroid plexus at the left foramen of Monro, (B) Interthalamic adhesion

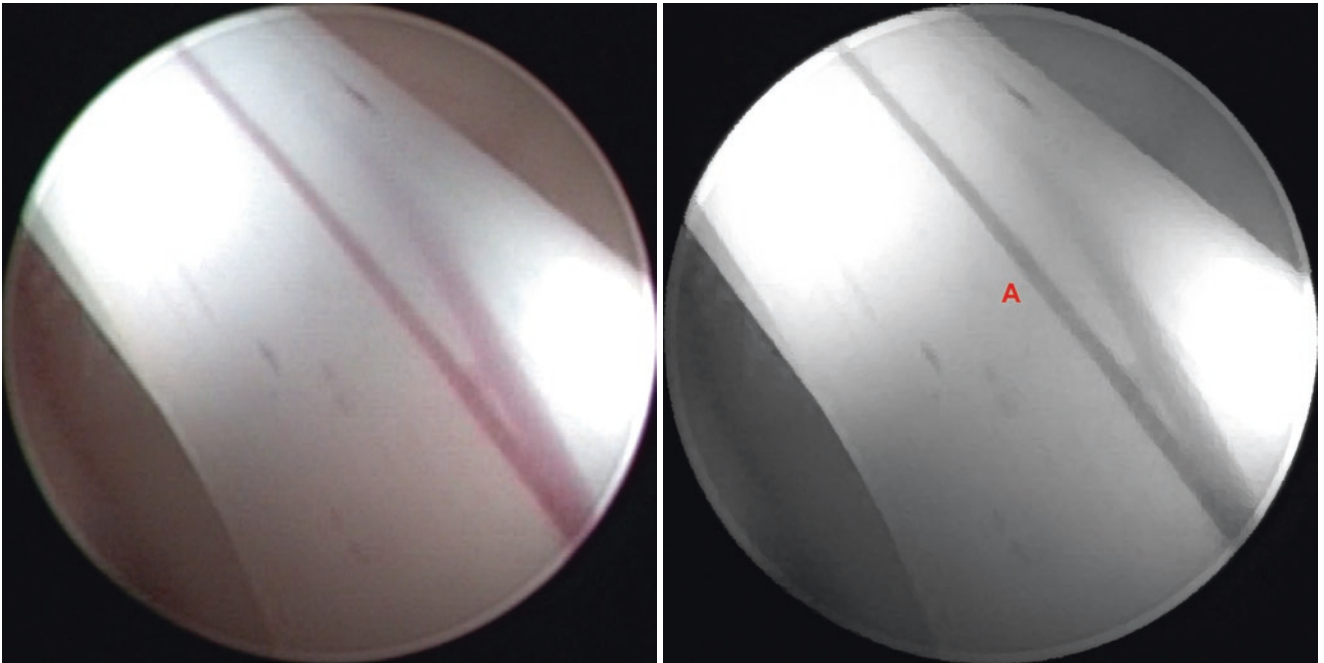


**Fig. 4.98** Normal anatomy. (A) Interthalamic adhesion

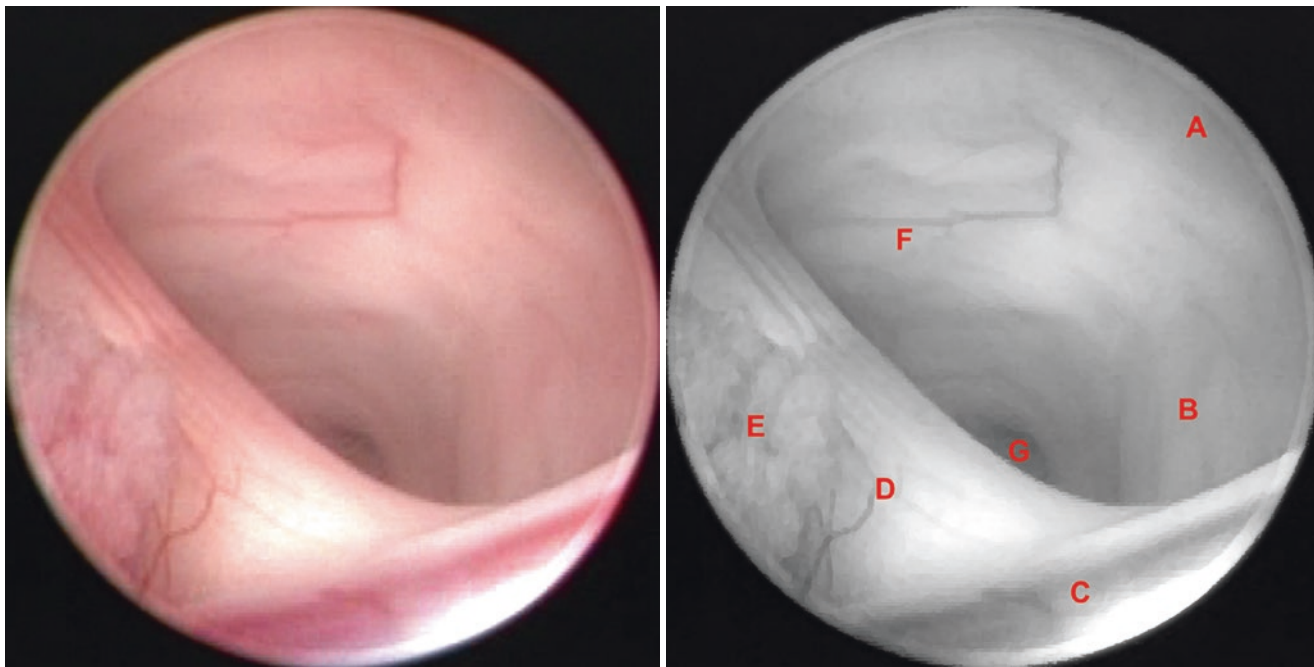


**Fig. 4.99** Normal anatomy. (A) Postmammillary recess, (B) Right thalamus, (C) Right superior thalamostriate vein, (D) Interthalamic adhesion, (E) Choroid plexus at the right foramen of Monro, (F) Left thalamus, (G) Cerebral aqueduct entrance

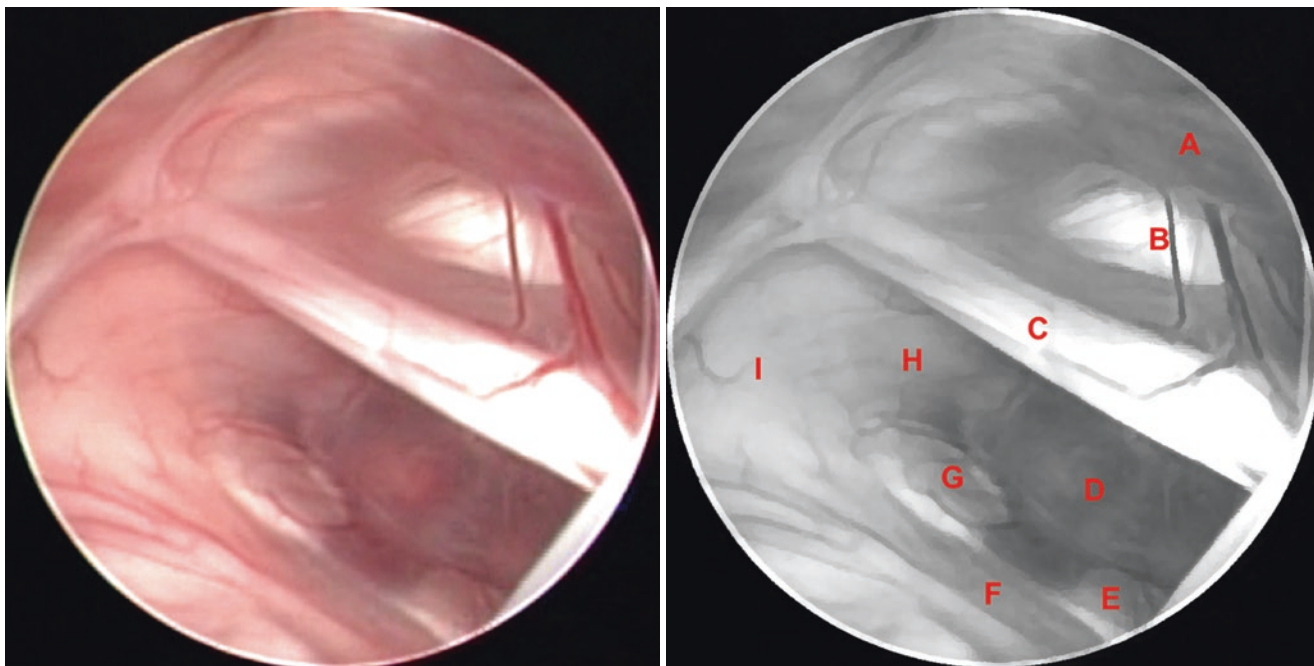


**Fig. 4.100** Normal anatomy. (A) Lamina terminalis, (B) Optic chiasm, (C) Interthalamic adhesion, (D) Tuber cinereum, (E) Right mammillary body, (F) Postmammillary recess, (G) Left mammillary body, (H) Left hypothalamus, (I) Left thalamus

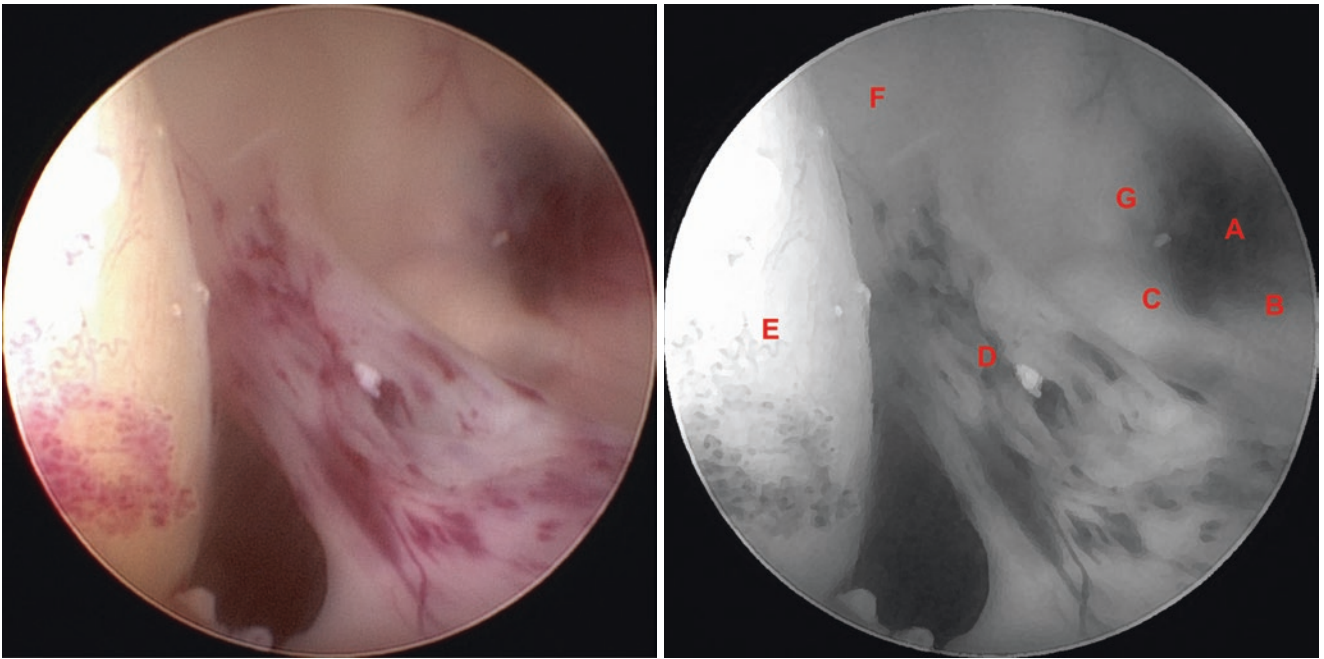


**Fig. 4.101** Abnormal anatomy. (A) Premammillary recess, (B) Right mammillary body, (C) Postmammillary recess, (D) Interthalamic adhesion, (E) Colloid cyst, (F) Left thalamus, (G) Left mammillary body

Illustrative case 3 – endoscopic biopsy of a right thalamic tumor after ETV.

Clinical data: 7-year-old child; headache, ocular deviation.

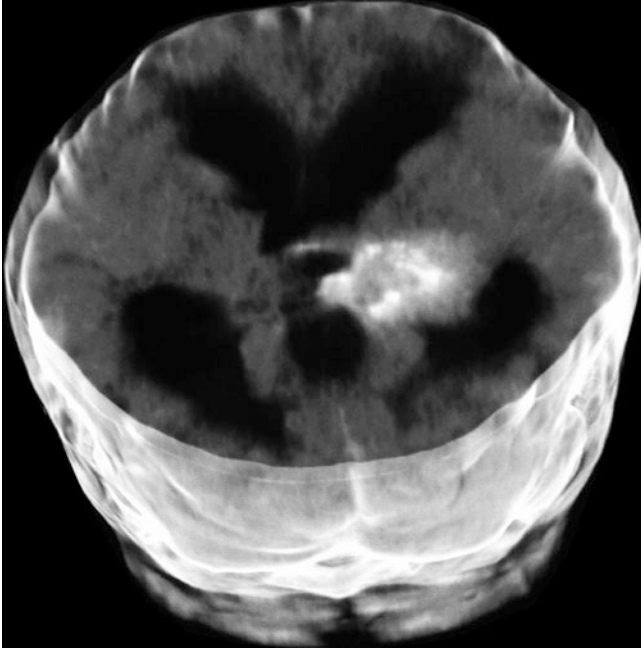


**Fig. 4.102** Three-dimensional (3D) computed tomography (CT) scan showing right thalamic tumor and hydrocephalus

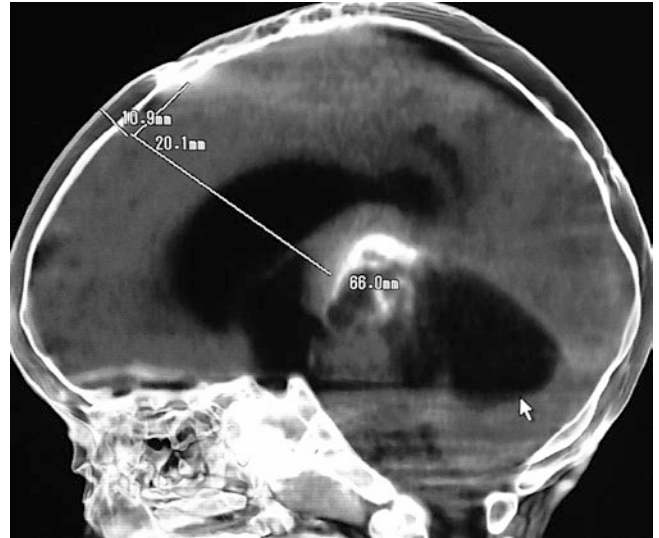


**Fig. 4.103** CT scan showing preoperative planning for endoscopic biopsy after ETV

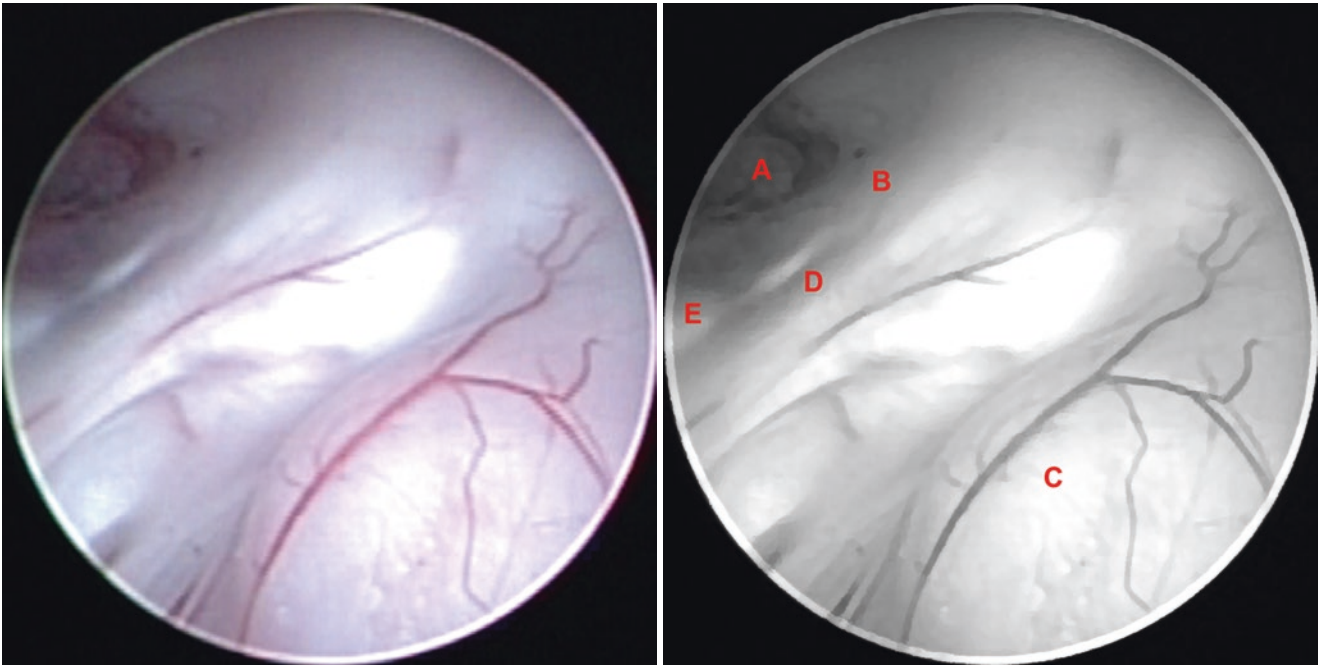


**Fig. 4.104** Illustrative case 3 – endoscopic biopsy of a right thalamic tumor after ETV. (A) Ventriculostomy, (B) Right mammillary body, (C) Tumor, (D) Postmammillary recess, (E) Left mammillary body

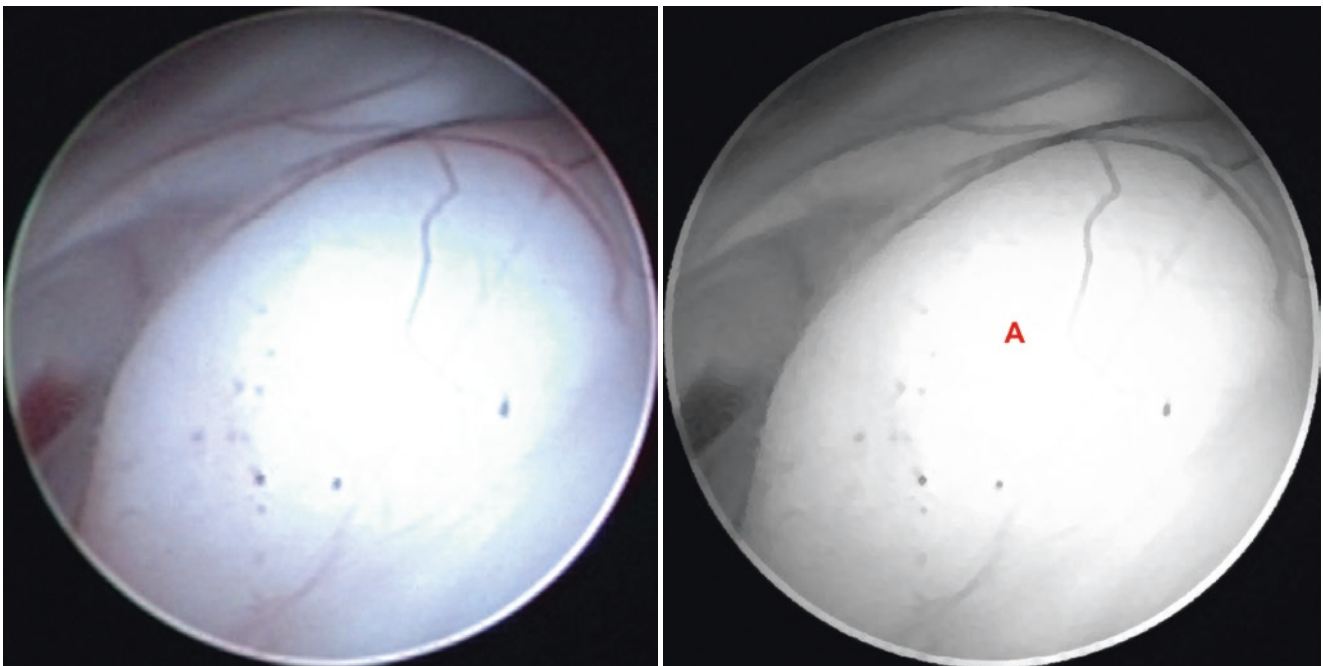


**Fig. 4.105** Illustrative case3 – endoscopic biopsy of a right thalamic tumor after ETV. (A) Tumor

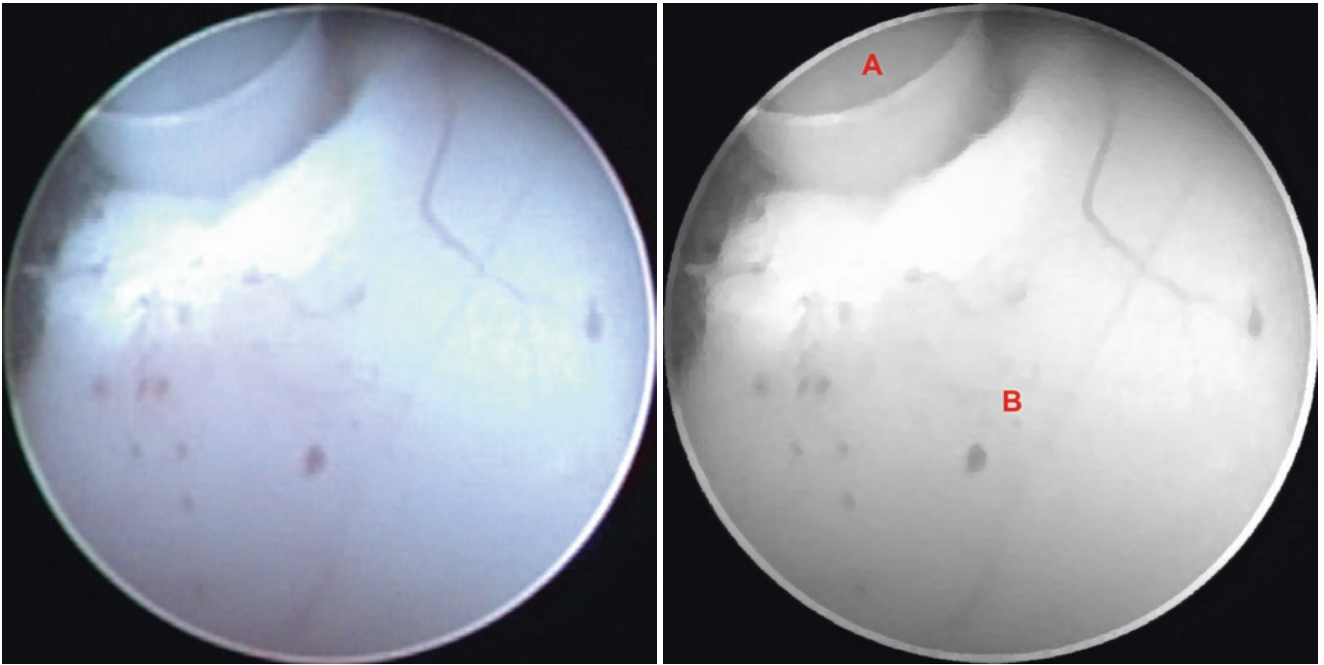


**Fig. 4.106** Illustrative case 3 – endoscopic biopsy of a right thalamic tumor after ETV. (A) Bipolar coagulation electrode, (B) Tumor

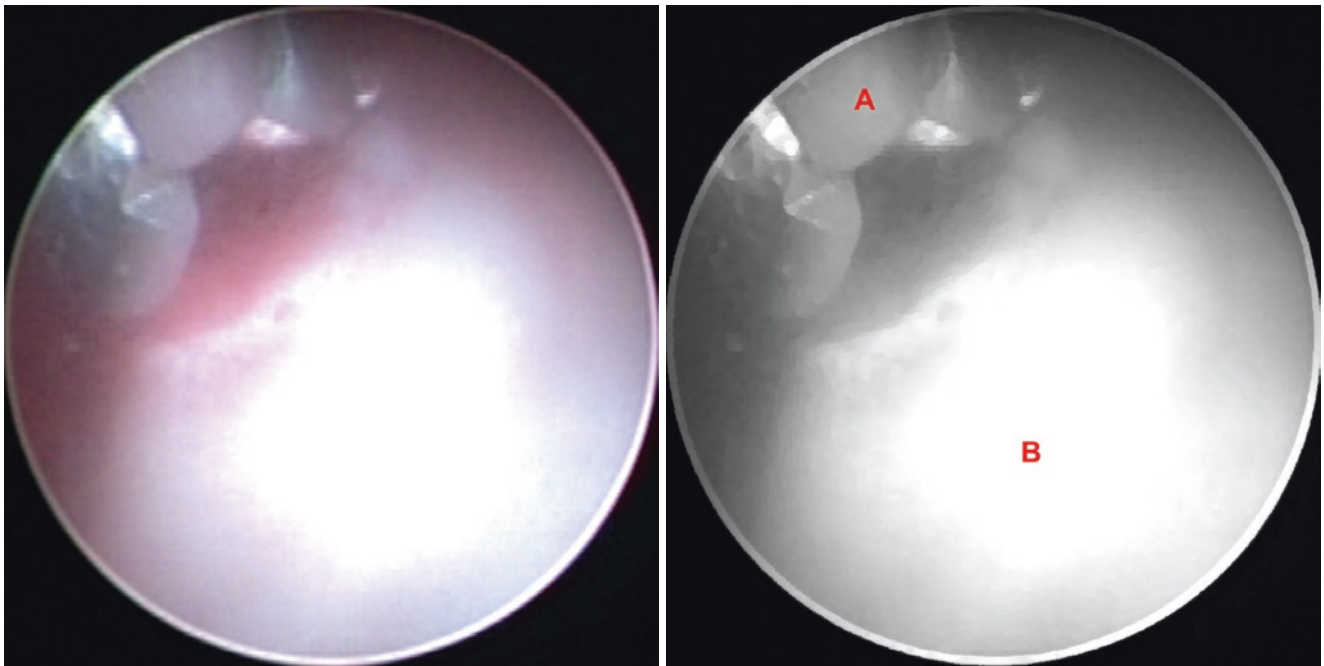


**Fig. 4.107** Illustrative case 3 – endoscopic biopsy of a right thalamic tumor after ETV. (A) Biopsy forceps, (B) Tumor

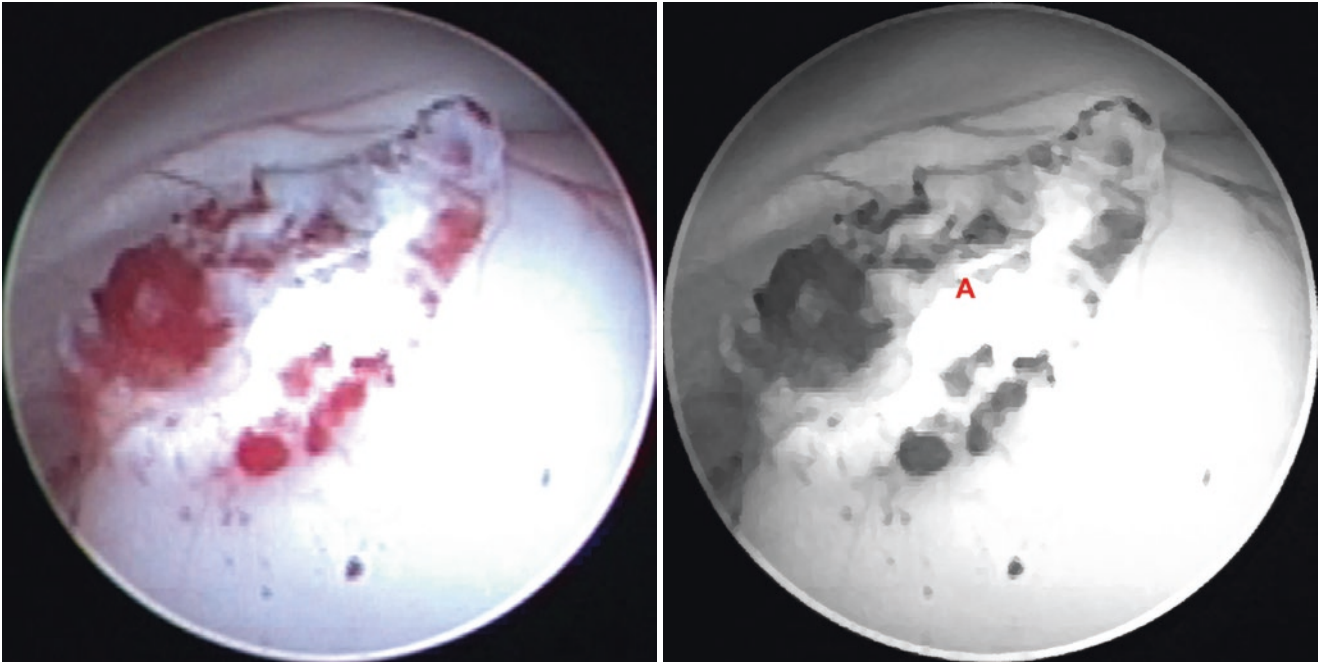


**Fig. 4.108** Illustrative case 3 – endoscopic biopsy of a right thalamic tumor after ETV. (A) Final aspect of the tumor after biopsy

Illustrative case 4 – endoscopic biopsy of an intrinsic brainstem tumor after ETV.

Clinical data: 1-year-old child; ocular deviation.

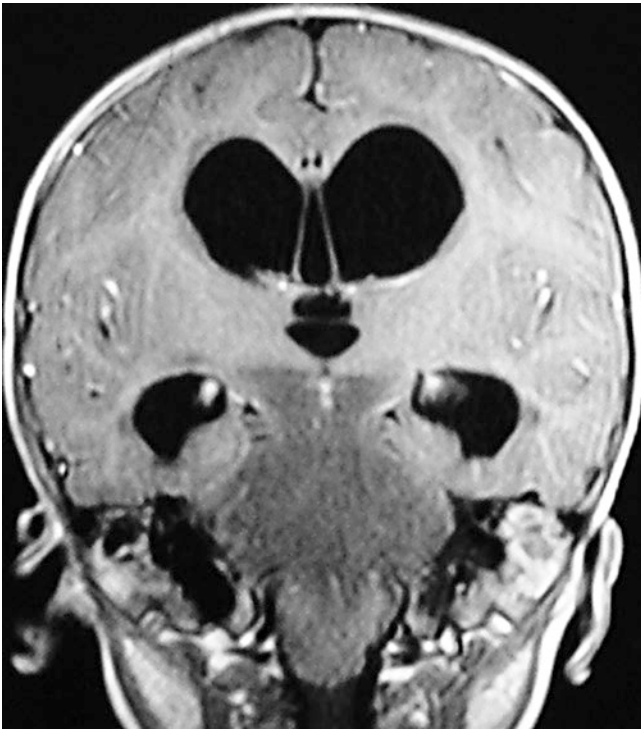


**Fig. 4.109** Gadolinium-enhanced coronal T1-weighted MRI showing an intrinsic brainstem tumor close to the third ventricle floor, and hydrocephalus

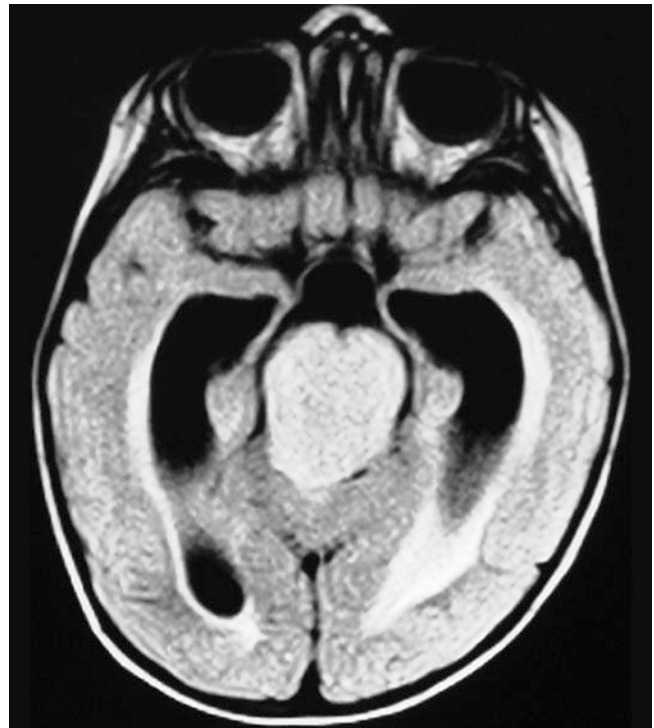


**Fig. 4.110** Axial flair MRI showing a typical aspect of an intrinsic brainstem tumor and hydrocephalus



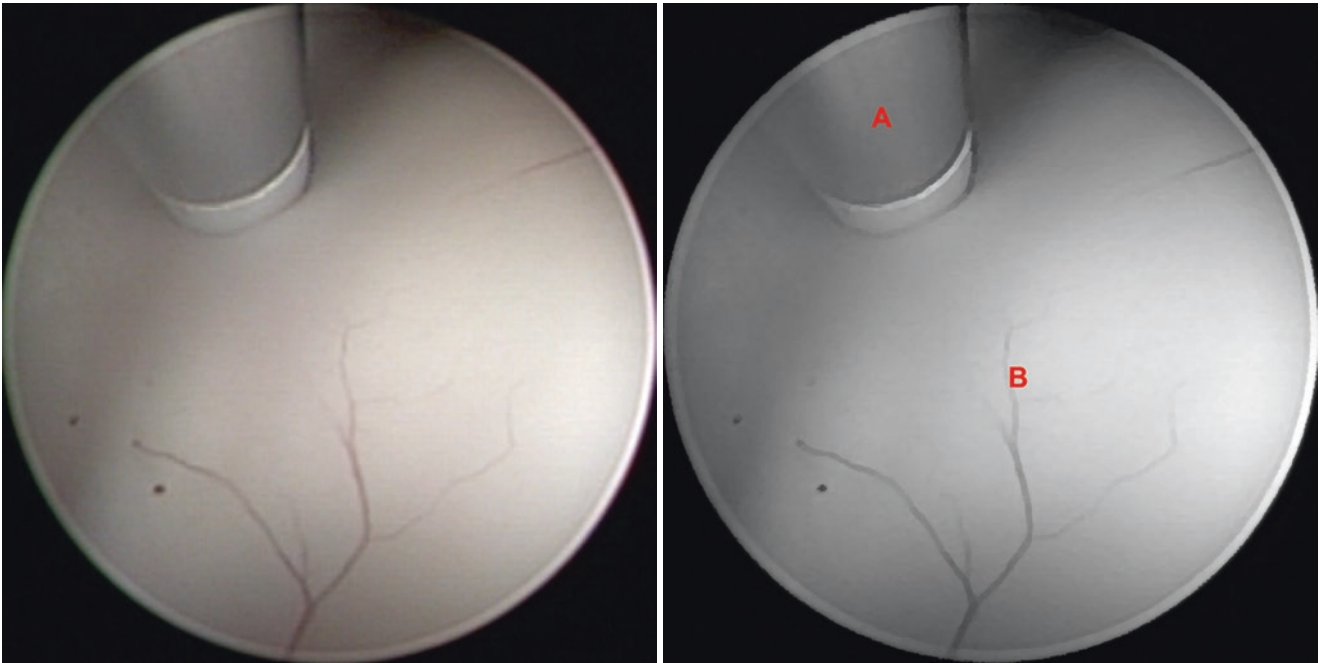


**Fig. 4.111** Illustrative case 4 – endoscopic biopsy of an intrinsic brainstem tumor after ETV. (A) Bipolar coagulation electrode, (B) Third ventricle floor

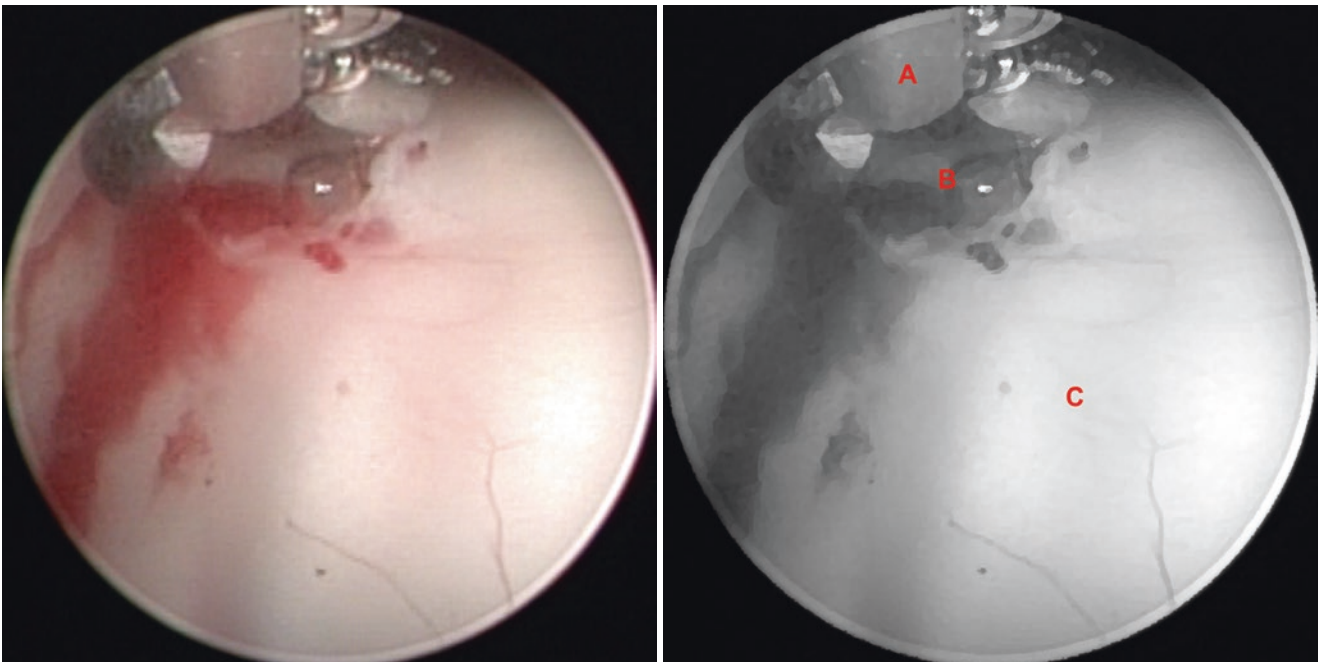


**Fig. 4.112** Illustrative case 4 – endoscopic biopsy of an intrinsic brainstem tumor after ETV. (A) Biopsy forceps, (B) Tumor, (C) Third ventricle floor

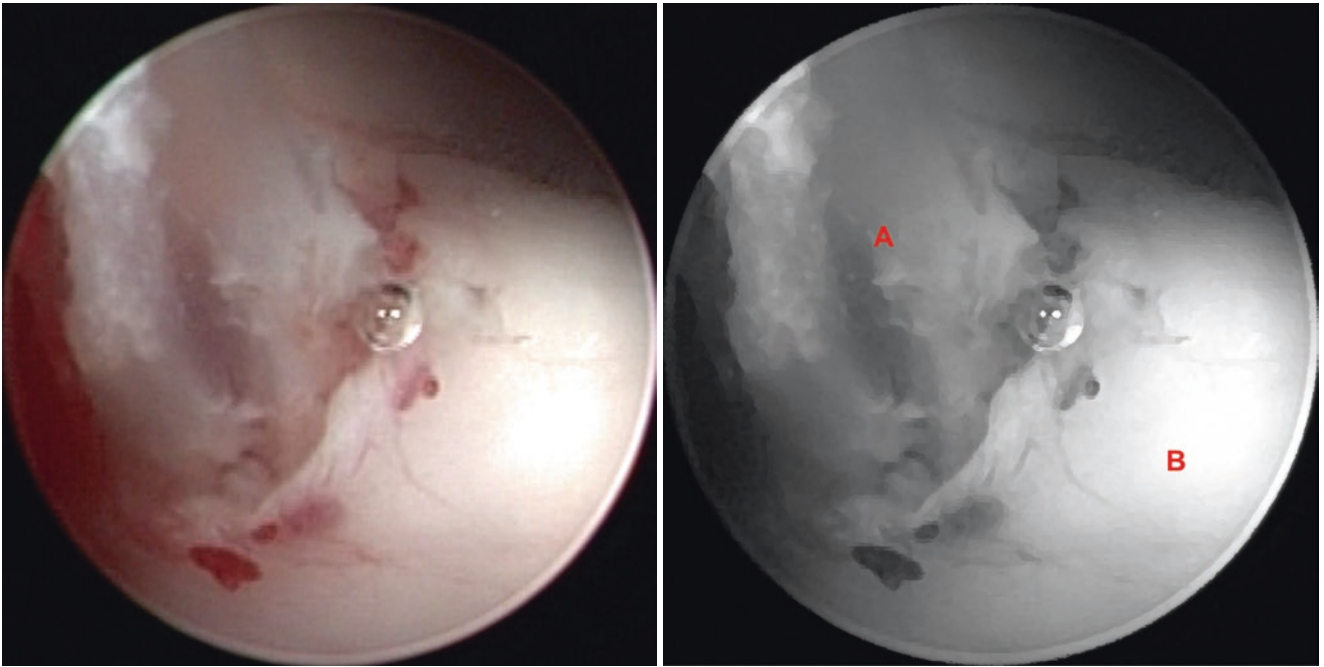


**Fig. 4.113** Illustrative case 4 – endoscopic biopsy of an intrinsic brainstem tumor after ETV. (A) Tumor, (B) Third ventricle floor

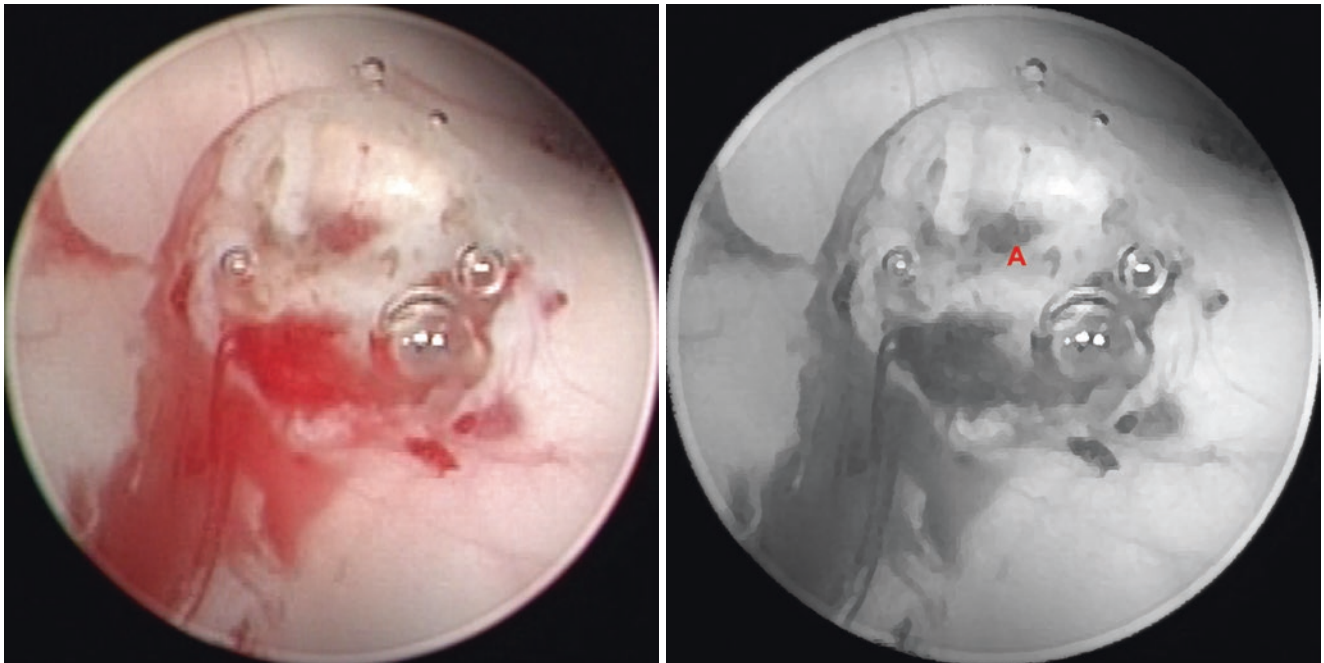


**Fig. 4.114** Illustrative case 4 – endoscopic biopsy of an intrinsic brainstem tumor after ETV. (A) Final aspect of the tumor after biopsy

## 4.5 Third Ventricle: Posterior Segment

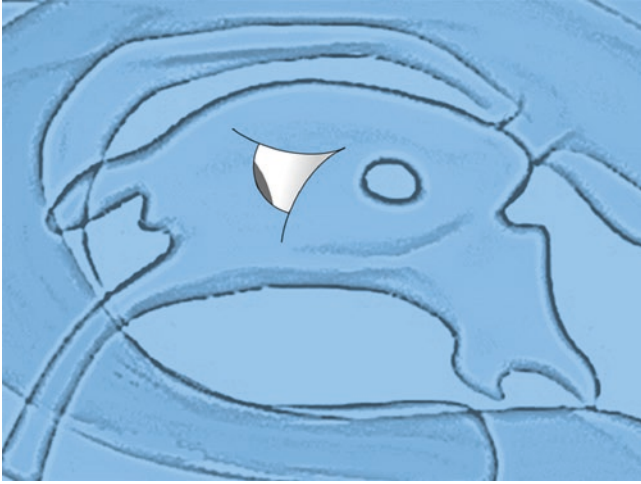


**Fig. 4.115** Direction of the endoscopic vision for the posterior segment of the third ventricle

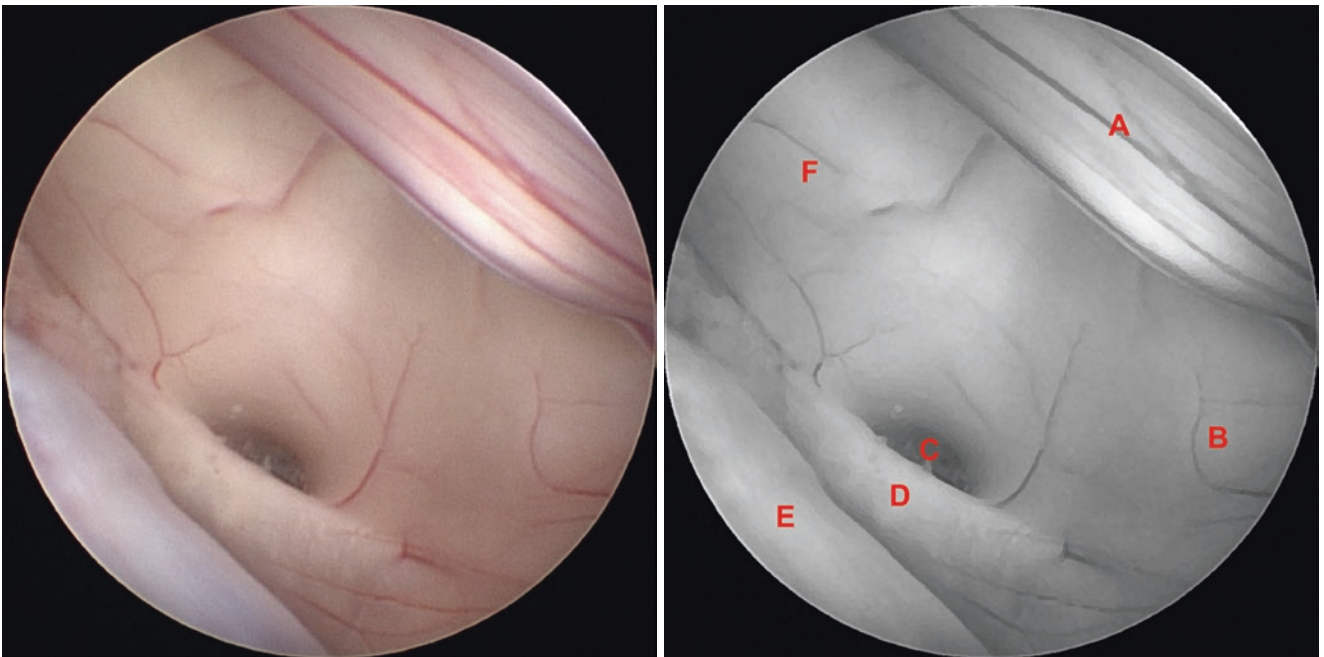


**Fig. 4.116** Normal anatomy. (A) Interthalamic adhesion, (B) Right thalamus, (C) Cerebral aqueduct entrance, (D) Posterior commissure, (E) Roof of the third ventricle, (F) Left thalamus

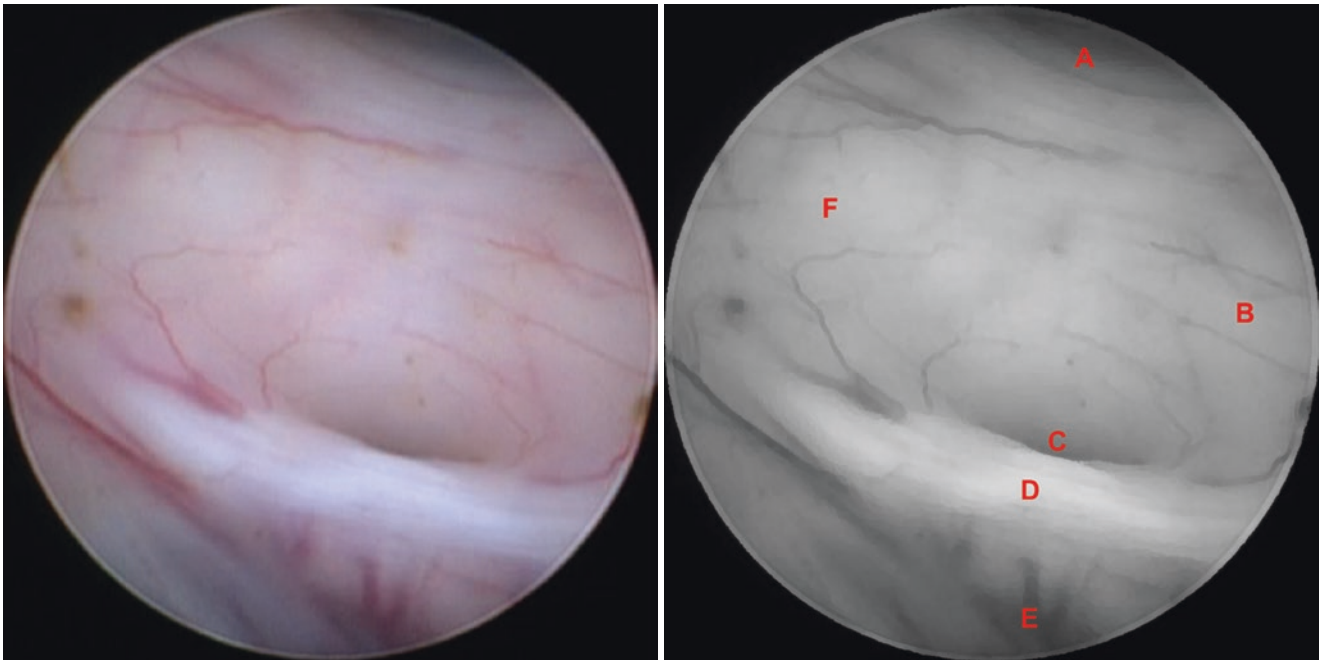


**Fig. 4.117** Normal anatomy. (A) Postmammillary recess, (B) Right thalamus, (C) Cerebral aqueduct entrance, (D) Posterior commissure, (E) Pineal recess, (F) Left thalamus

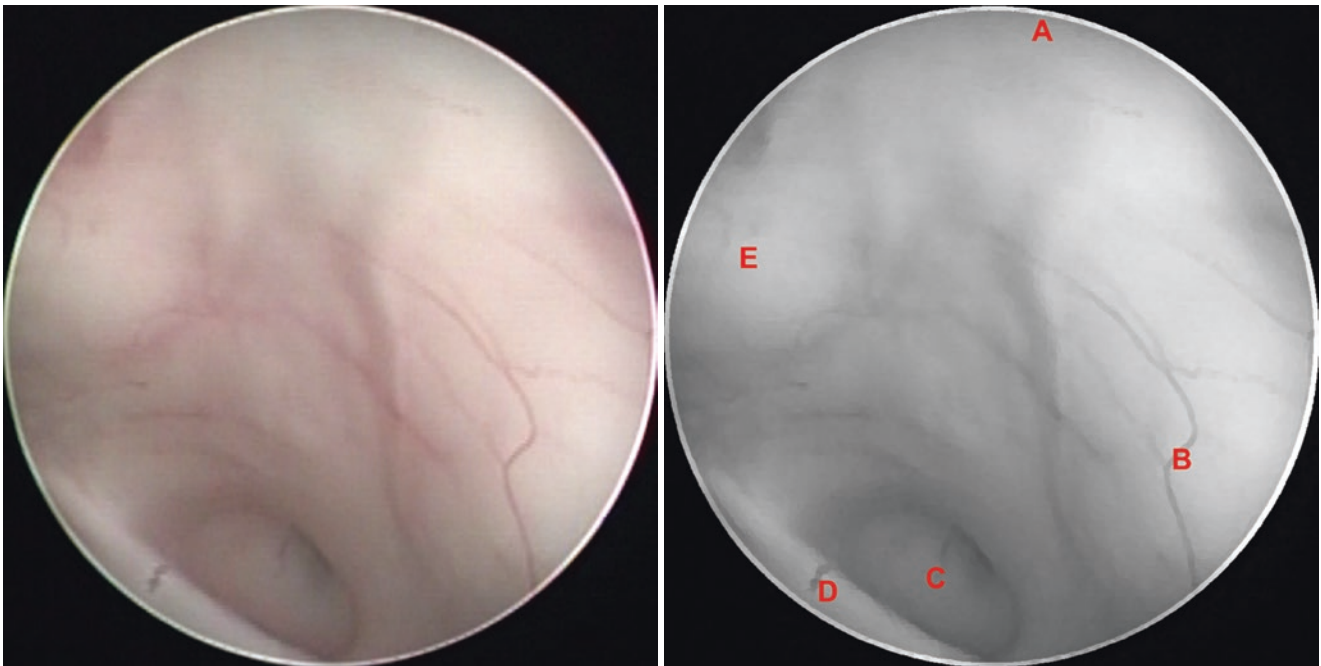


**Fig. 4.118** Normal anatomy. (A) Postmammillary recess, (B) Right thalamus, (C) Cerebral aqueduct entrance, (D) Posterior commissure, (E) Left thalamus

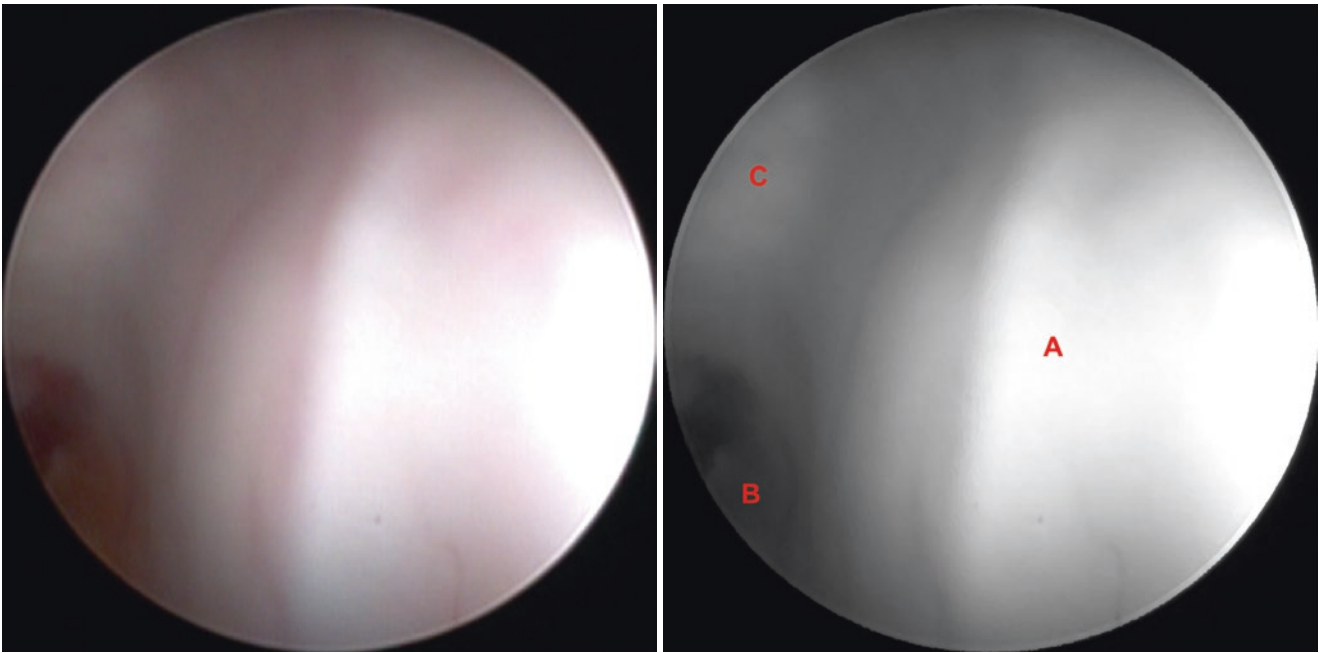


**Fig. 4.119** Normal anatomy. (A) Right thalamus, (B) Clot at the cerebral aqueduct entrance, (C) Left thalamus

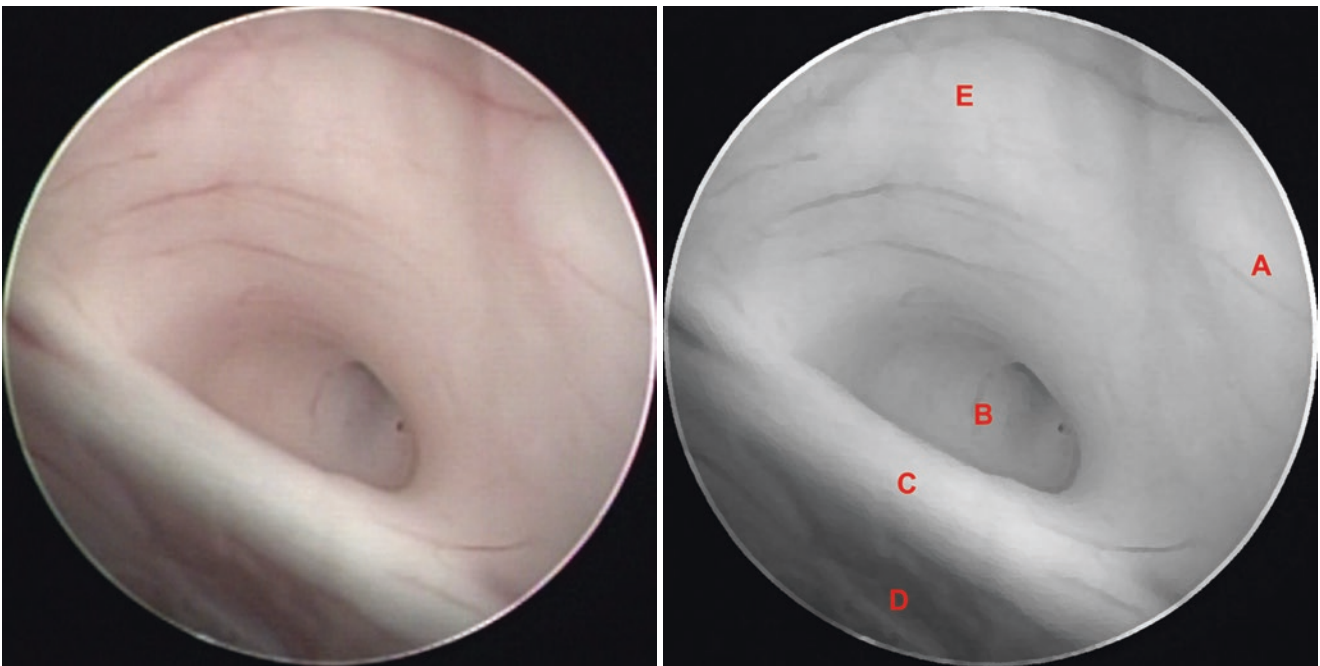


**Fig. 4.120** Normal anatomy. (A) Right thalamus, (B) Cerebral aqueduct entrance, (C) Posterior commissure, (D) Pineal recess, (E) Left thalamus

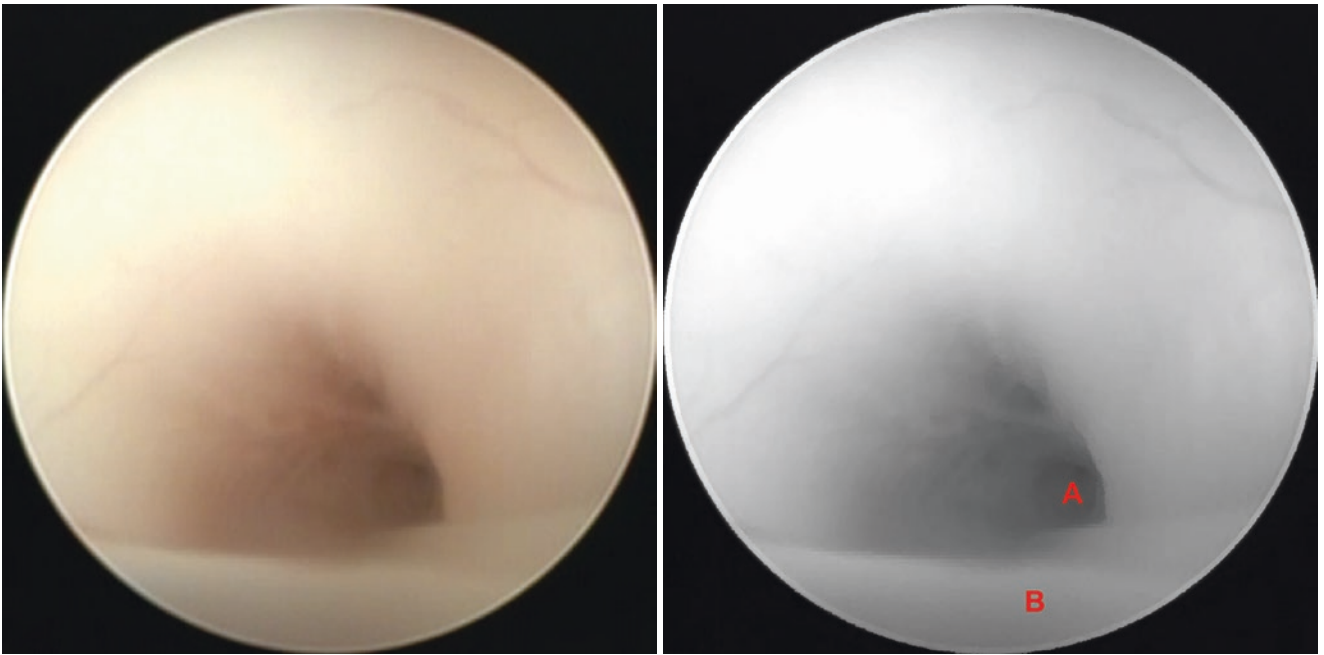


**Fig. 4.121** Normal anatomy. (A) Cerebral aqueduct entrance, (B) Posterior commissure

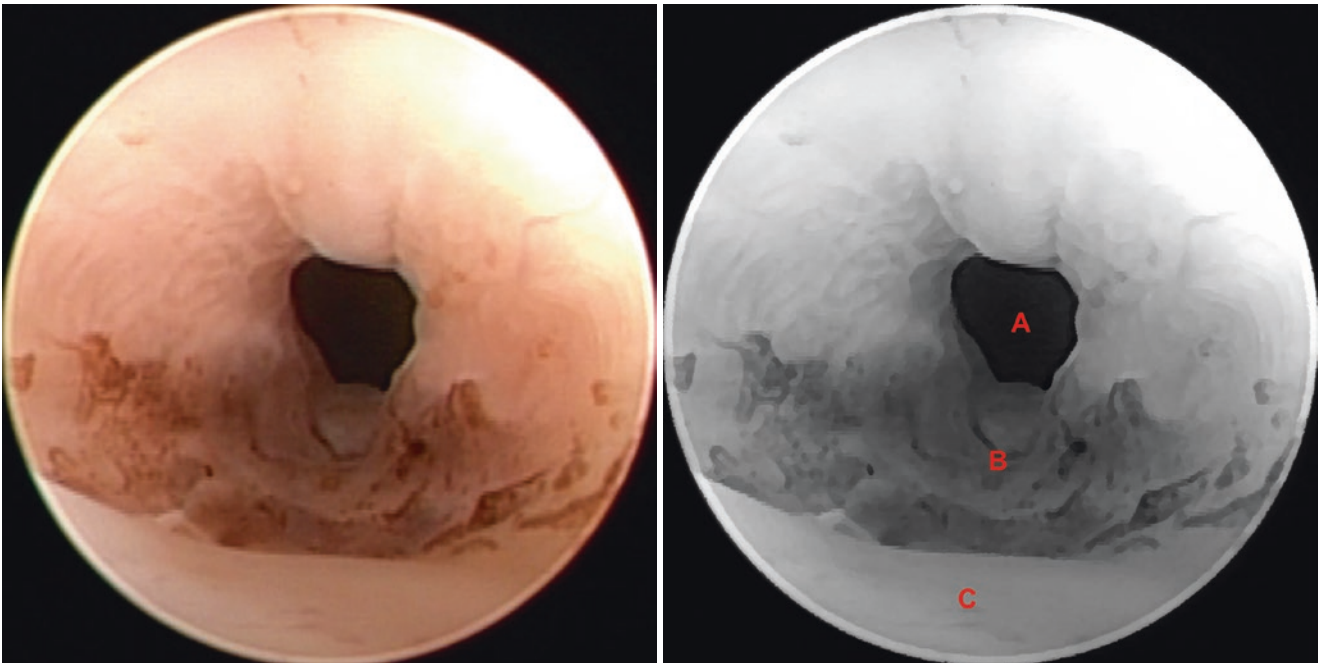


**Fig. 4.122** Normal anatomy. (A) Cerebral aqueduct entrance, (B) Clots, (C) Posterior commissure

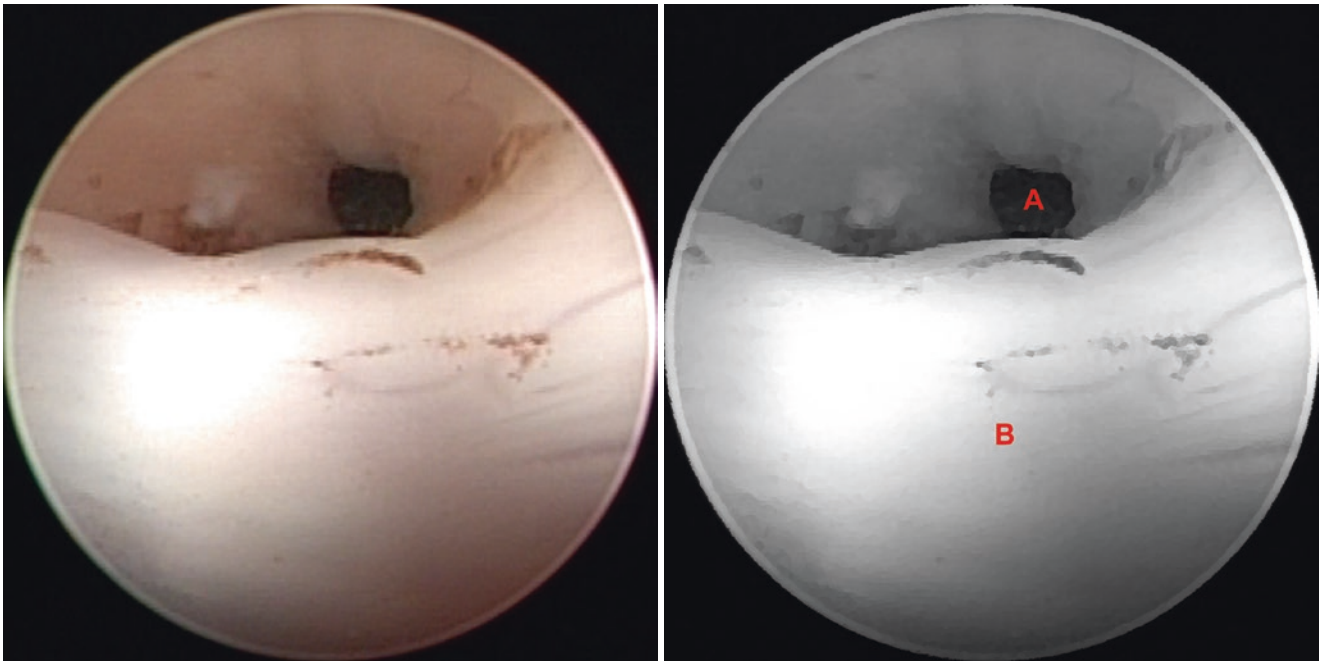


**Fig. 4.123** Normal anatomy. (A) Cerebral aqueduct entrance, (B) Posterior commissure

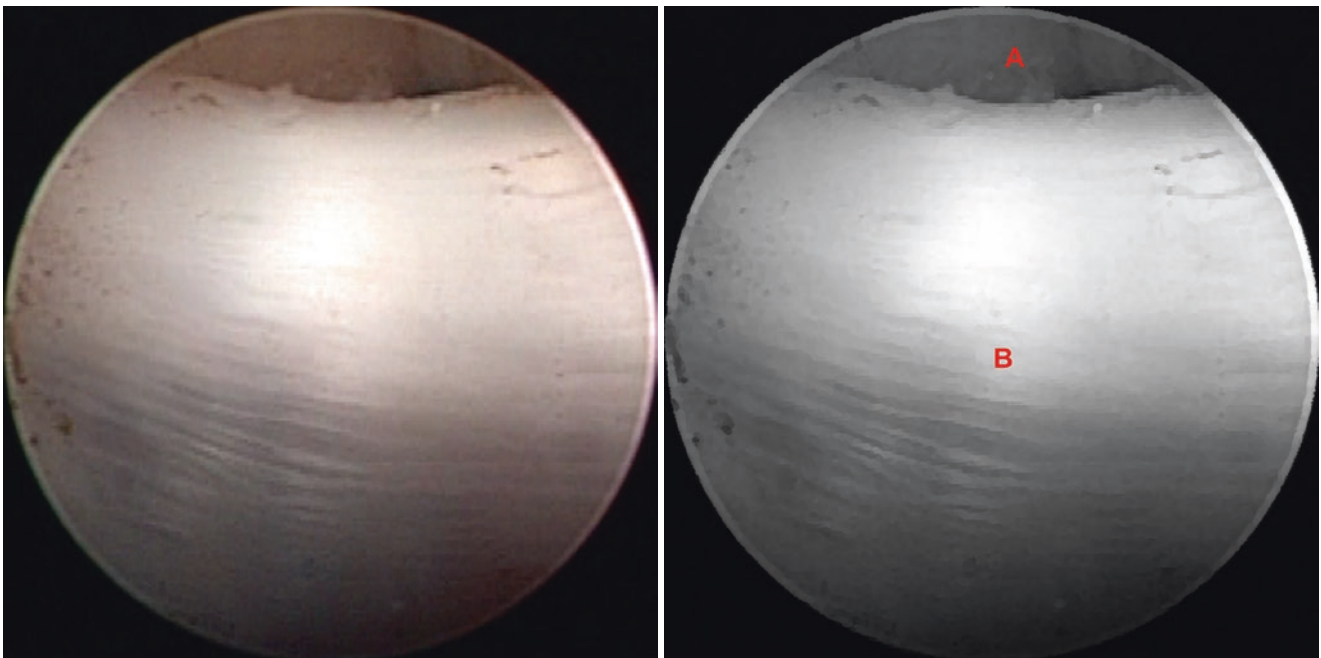


**Fig. 4.124** Normal anatomy. (A) Cerebral aqueduct entrance, (B) Posterior commissure

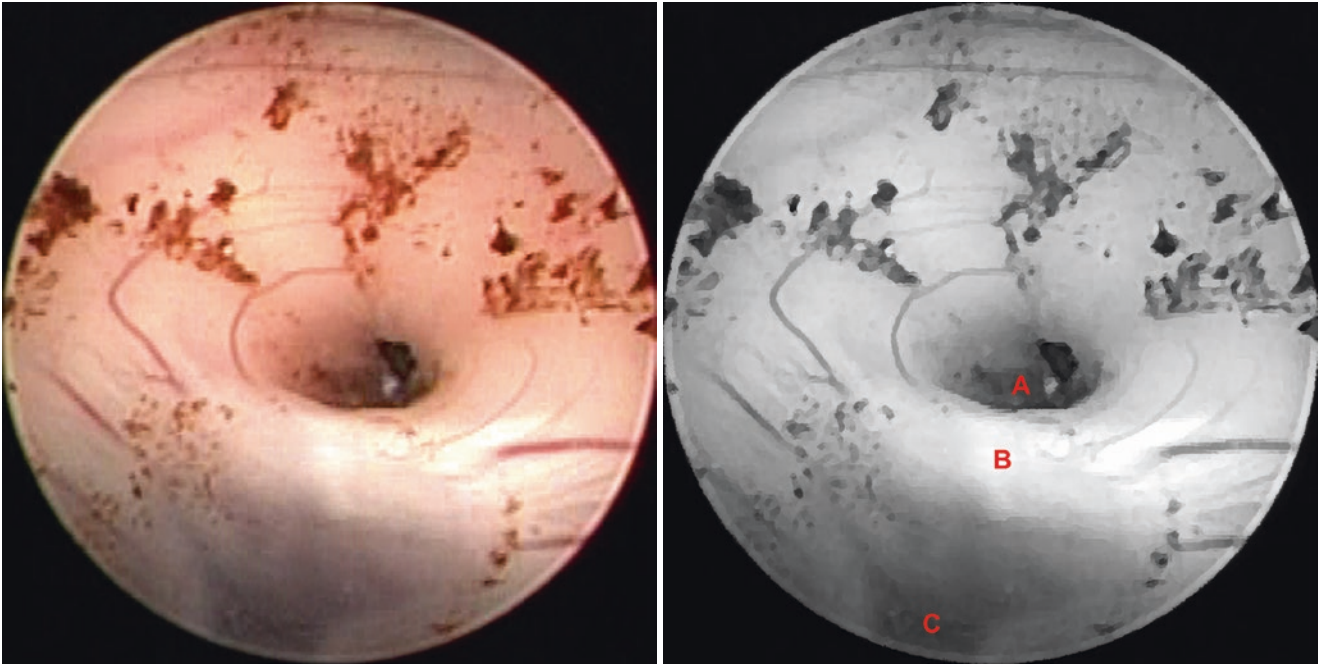


**Fig. 4.125** Normal anatomy. (A) Cerebral aqueduct entrance, (B) Posterior commissure, (C) Pineal recess

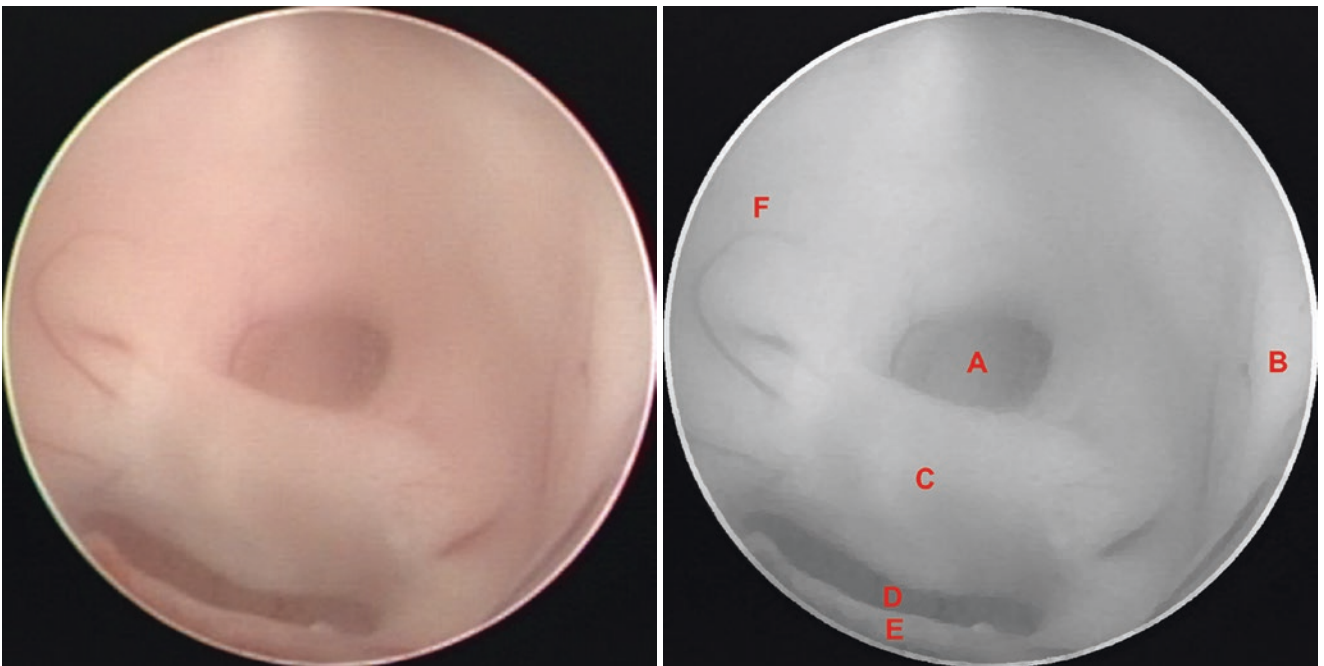


**Fig. 4.126** Normal anatomy. (A) Cerebral aqueduct entrance, (B) Right thalamus, (C) Posterior commissure, (D) Pineal recess, (E) Habenular commissure, (F) Left thalamus



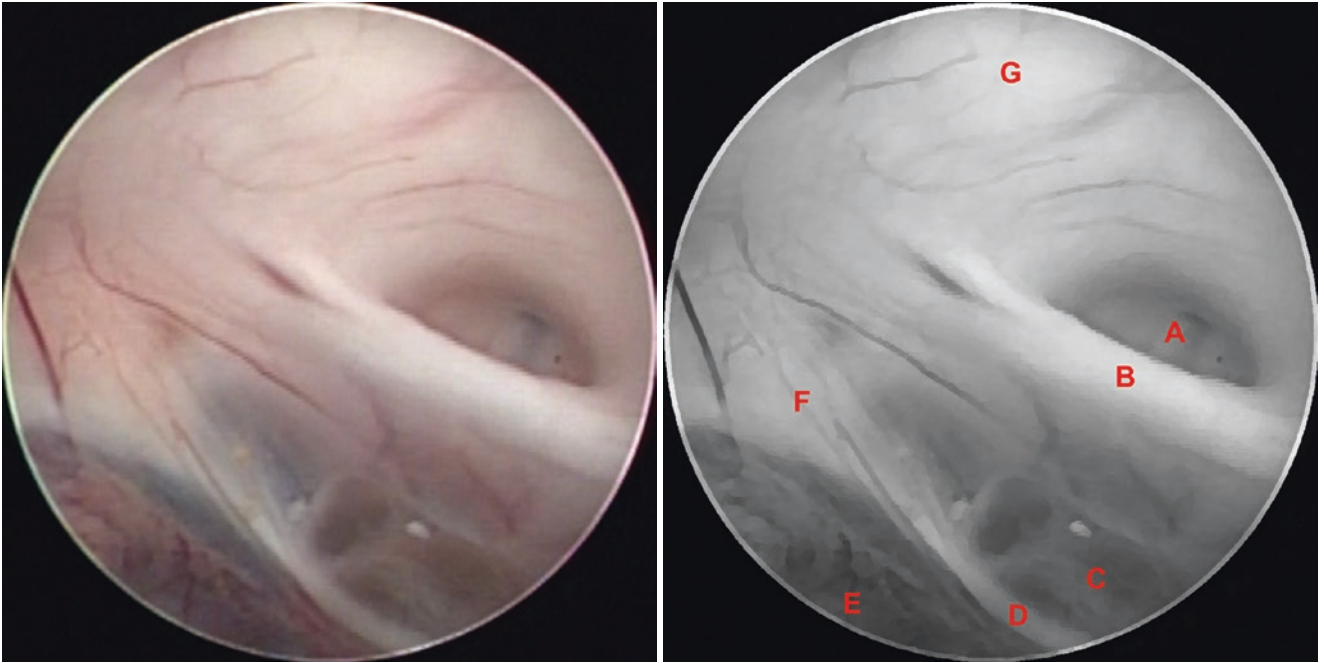


**Fig. 4.127** Normal anatomy. (A) Cerebral aqueduct entrance, (B) Posterior commissure, (C) Pineal recess and pineal gland, (D) Habenular commissure, (E) Suprapineal recess, (F) Habenular trigone, (G) Left thalamus

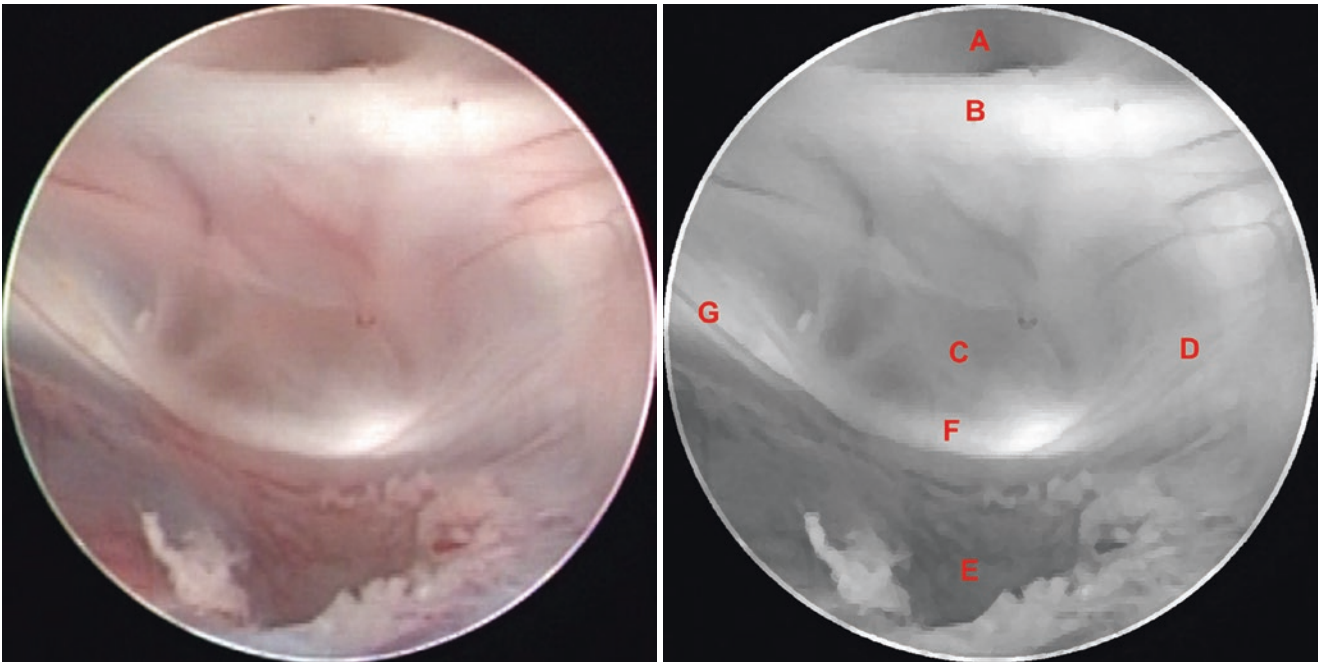


**Fig. 4.128** Normal anatomy. (A) Cerebral aqueduct entrance, (B) Posterior commissure, (C) Pineal recess and pineal gland, (D) Right habenular trigone, (E) Suprapineal recess, (F) Habenular commissure, (G) Left habenular trigone

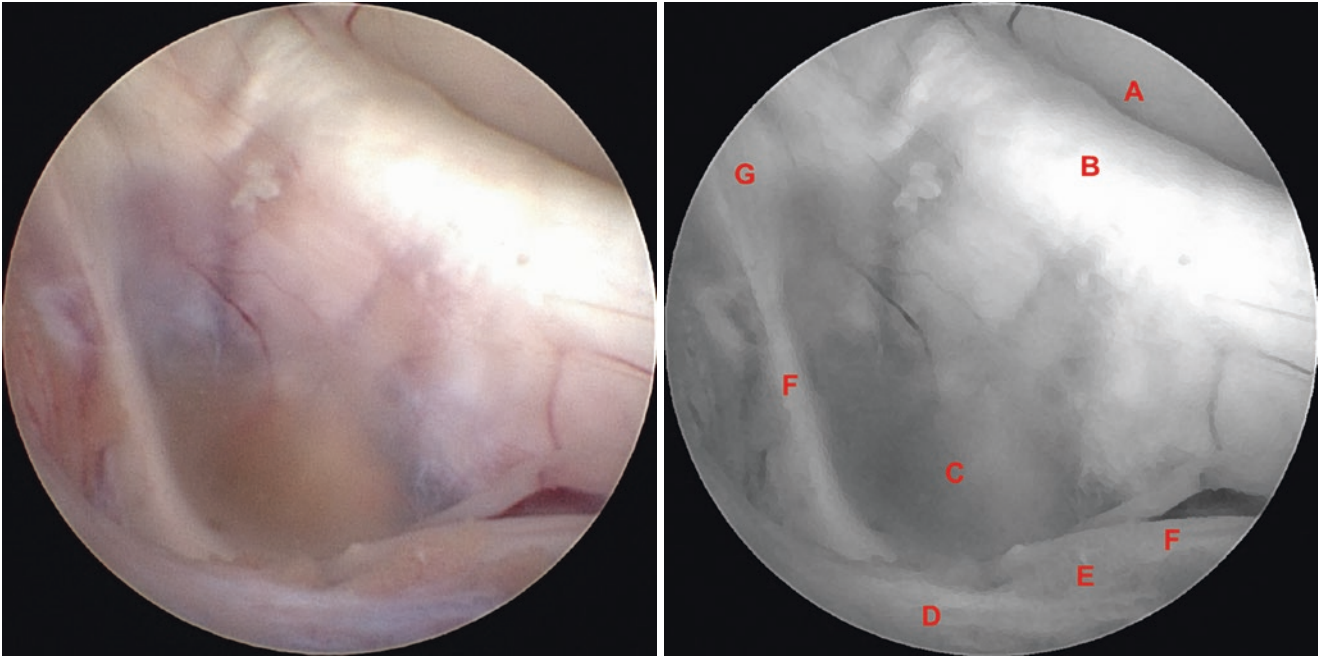


**Fig. 4.129** Normal anatomy. (A) Cerebral aqueduct entrance, (B) Posterior commissure, (C) Pineal recess and pineal gland, (D) Roof of the third ventricle, (E) Choroid plexus, (F) Habenular commissure, (G) Left habenular trigone

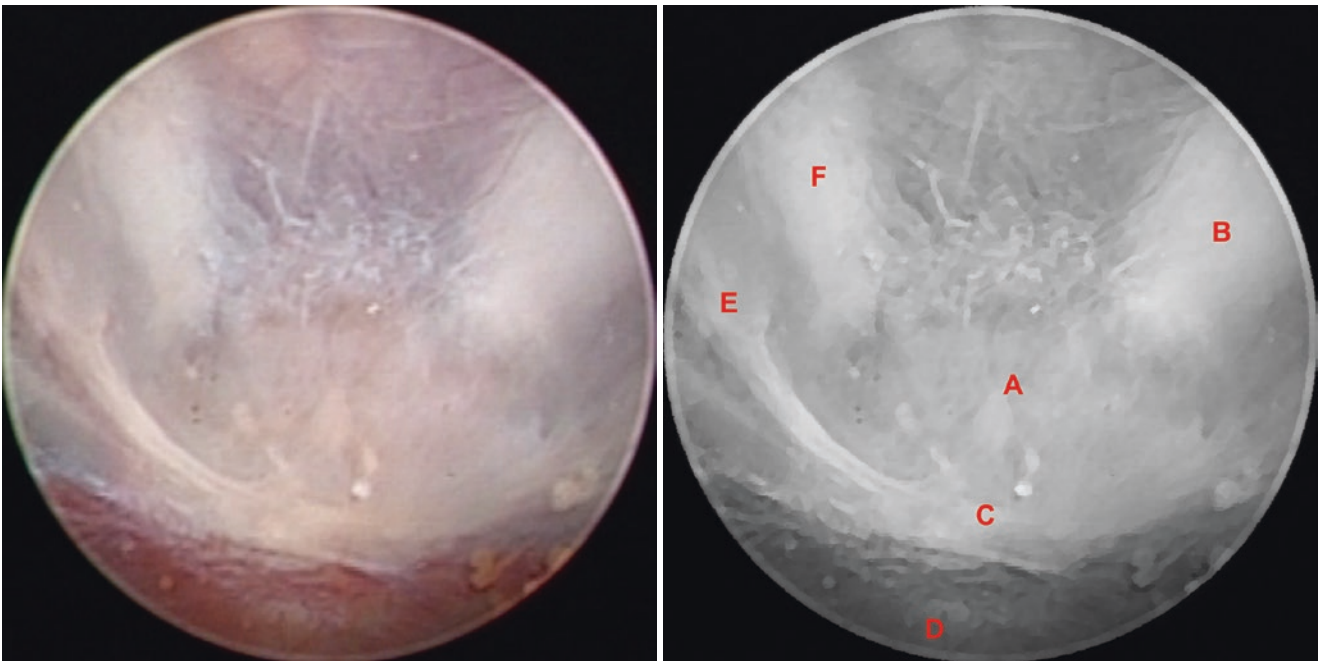


**Fig. 4.130** Normal anatomy. (A) Pineal recess and pineal gland, (B) Right pineal stalk, (C) Habenular commissure, (D) Suprapineal recess, (E) Left habenular trigone, (F) Left pineal stalk

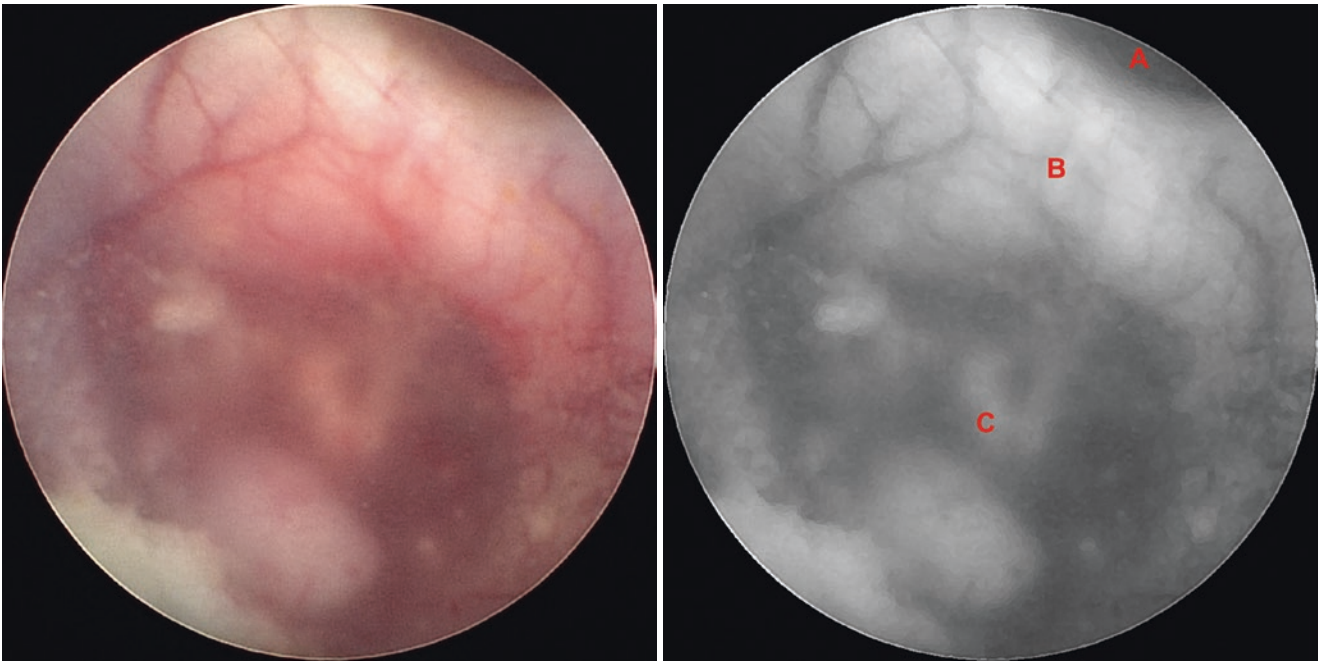


**Fig. 4.131** Normal anatomy. (A) Cerebral aqueduct entrance, (B) Posterior commissure, (C) Pineal recess and pineal gland

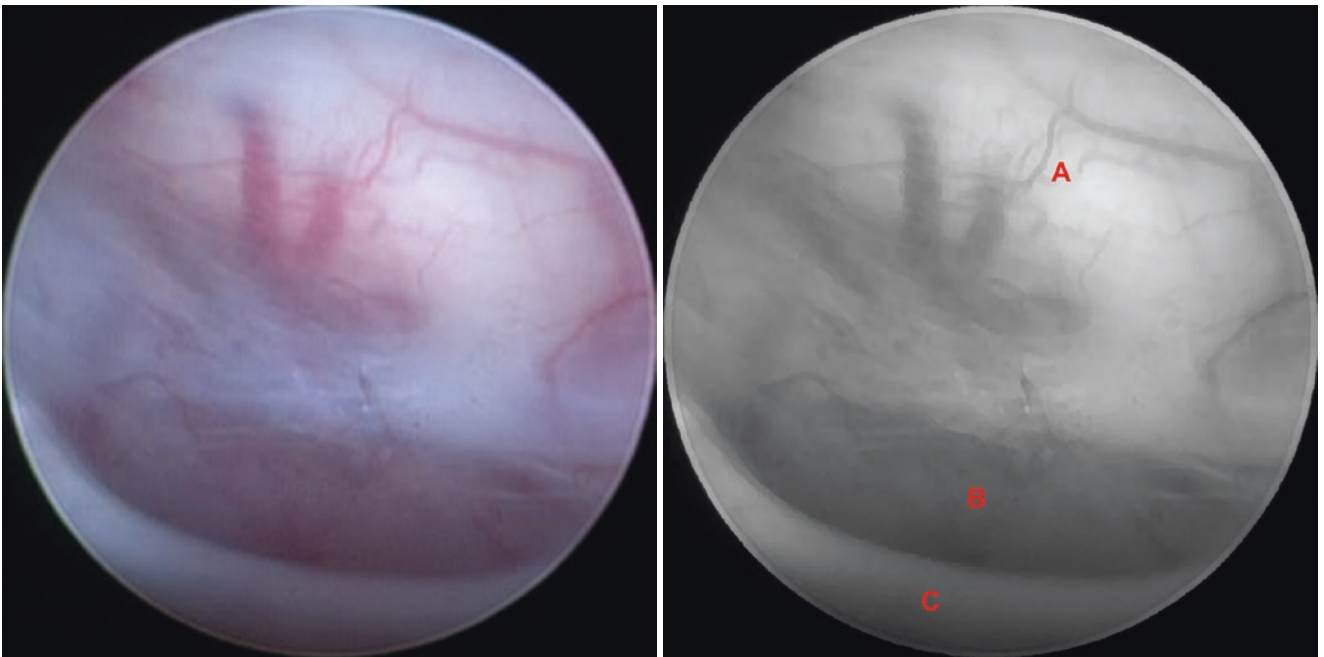


**Fig. 4.132** Normal anatomy. (A) Posterior commissure, (B) Pineal recess and pineal gland, (C) Habenular commissure

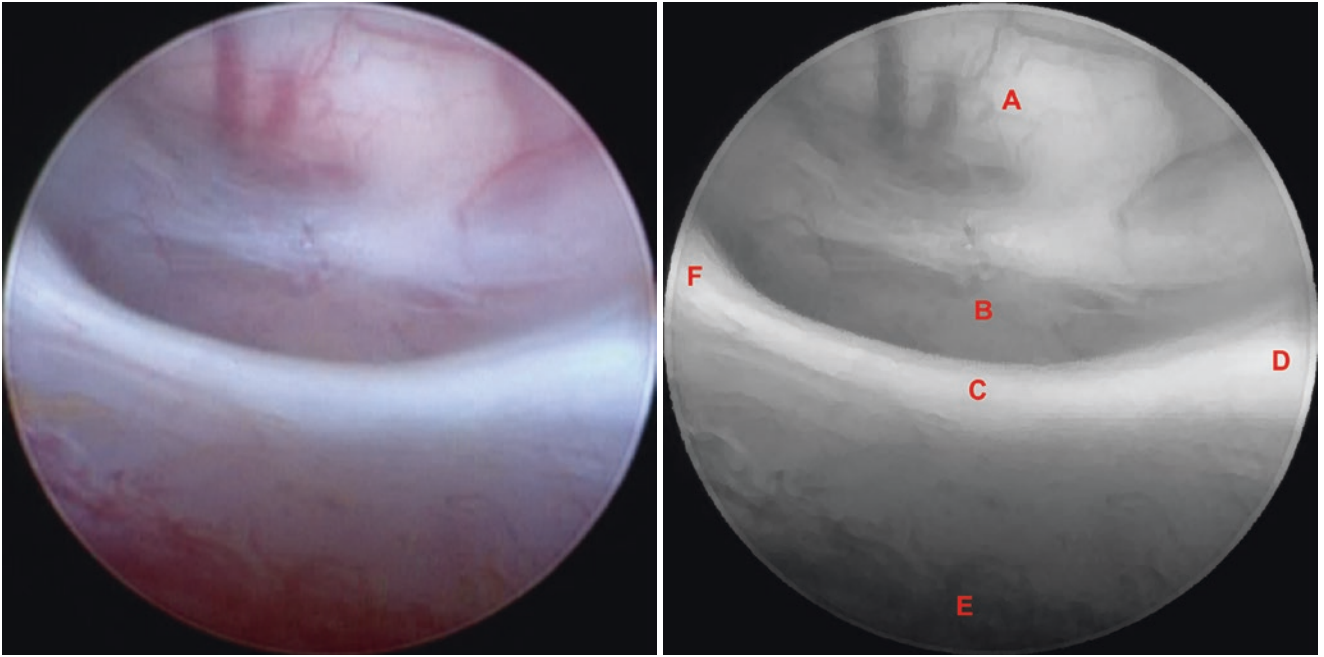


**Fig. 4.133** Normal anatomy. (A) Posterior commissure, (B) Pineal recess and pineal gland, (C) Habenular commissure, (D) Right habenular trigone, (E) Suprapineal recess, (F) Left habenular trigone

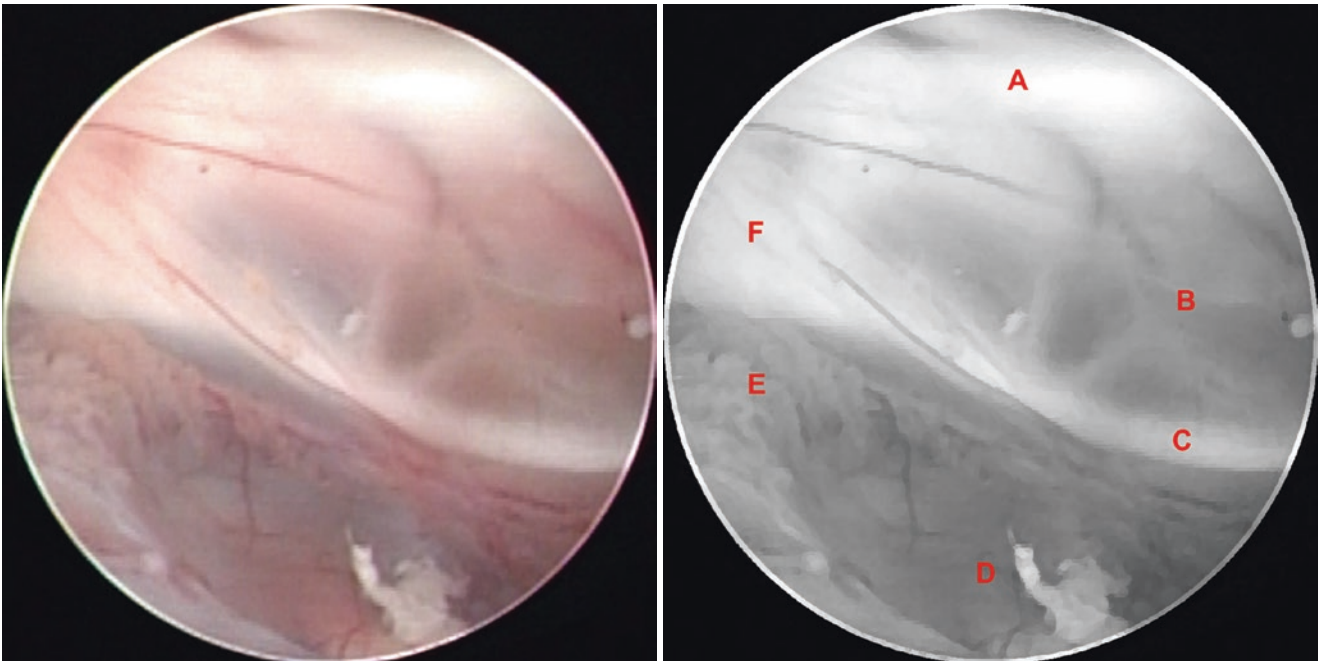


**Fig. 4.134** Normal anatomy. (A) Posterior commissure, (B) Pineal recess and pineal gland, (C) Habenular commissure, (D) Suprapineal recess, (E) Choroid plexus, (F) Left habenular trigone

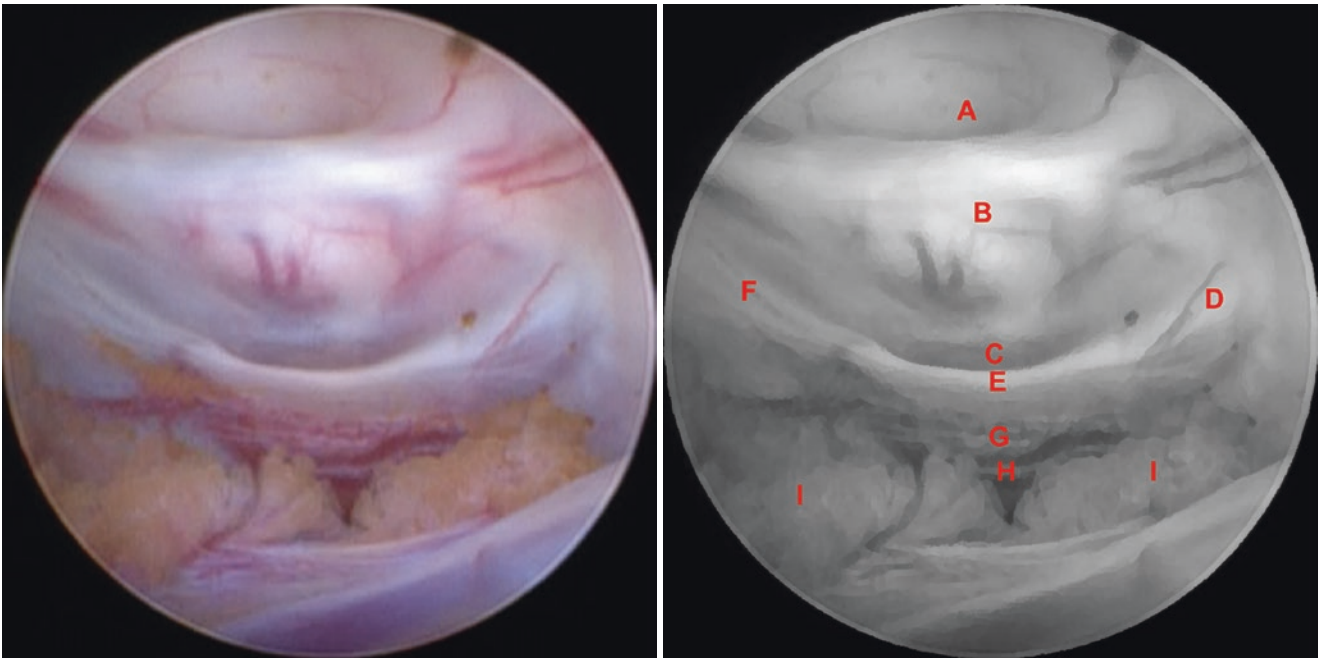


**Fig. 4.135** Normal anatomy. (A) Cerebral aqueduct entrance, (B) Posterior commissure, (C) Pineal recess and pineal gland, (D) Right habenular trigone, (E) Habenular commissure, (F) Left habenular tri-

gone, (G) Suprapineal recess, (H) Venous drainage to great cerebral vein, (I) Choroid plexus of the roof of the third ventricle

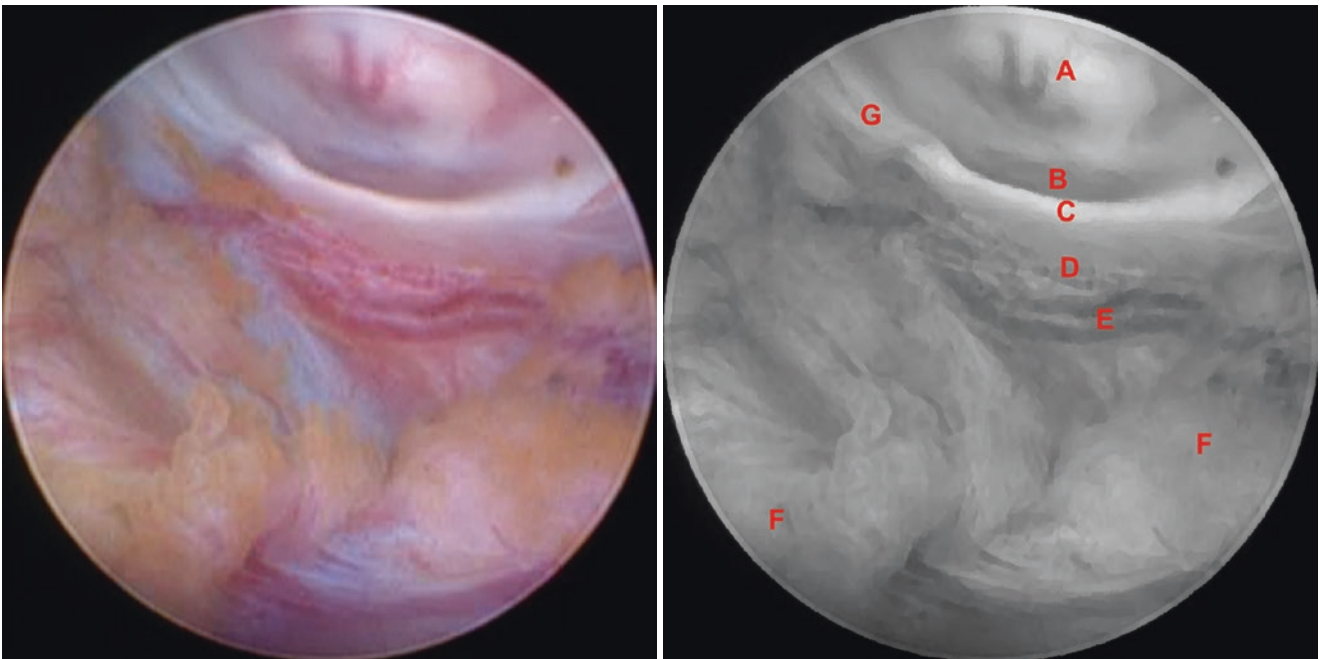


**Fig. 4.136** Normal anatomy. (A) Posterior commissure, (B) Pineal recess and pineal gland, (C) Habenular commissure, (D) Suprapineal recess, (E) Venous drainage to great cerebral vein, (F) Choroid plexus of the roof of the third ventricle, (G) Left habenular trigone

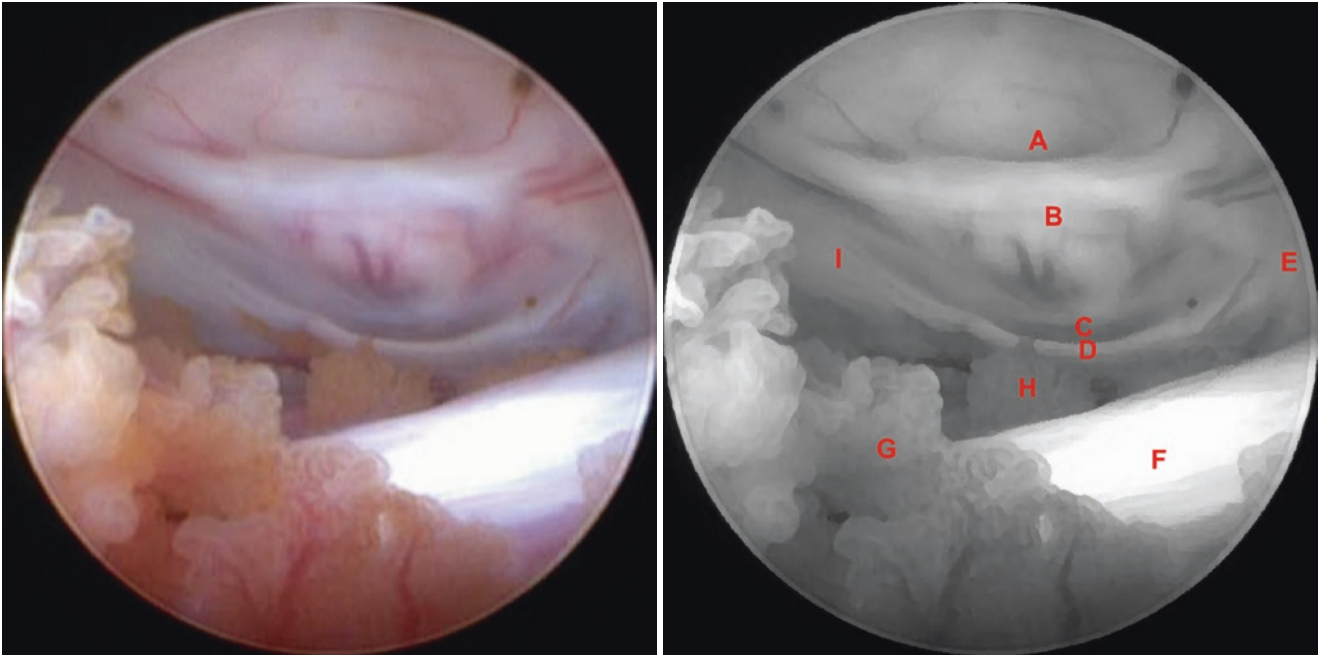


**Fig. 4.137** Normal anatomy. (A) Cerebral aqueduct entrance, (B) Posterior commissure, (C) Pineal recess and pineal gland, (D) Habenular commissure, (E) Right habenular trigone, (F) Superior thalamostriate

vein, (G) Choroid plexus at the foramen of Monro, (H) Choroid plexus at the roof of the third ventricle, (I) Left habenular trigone

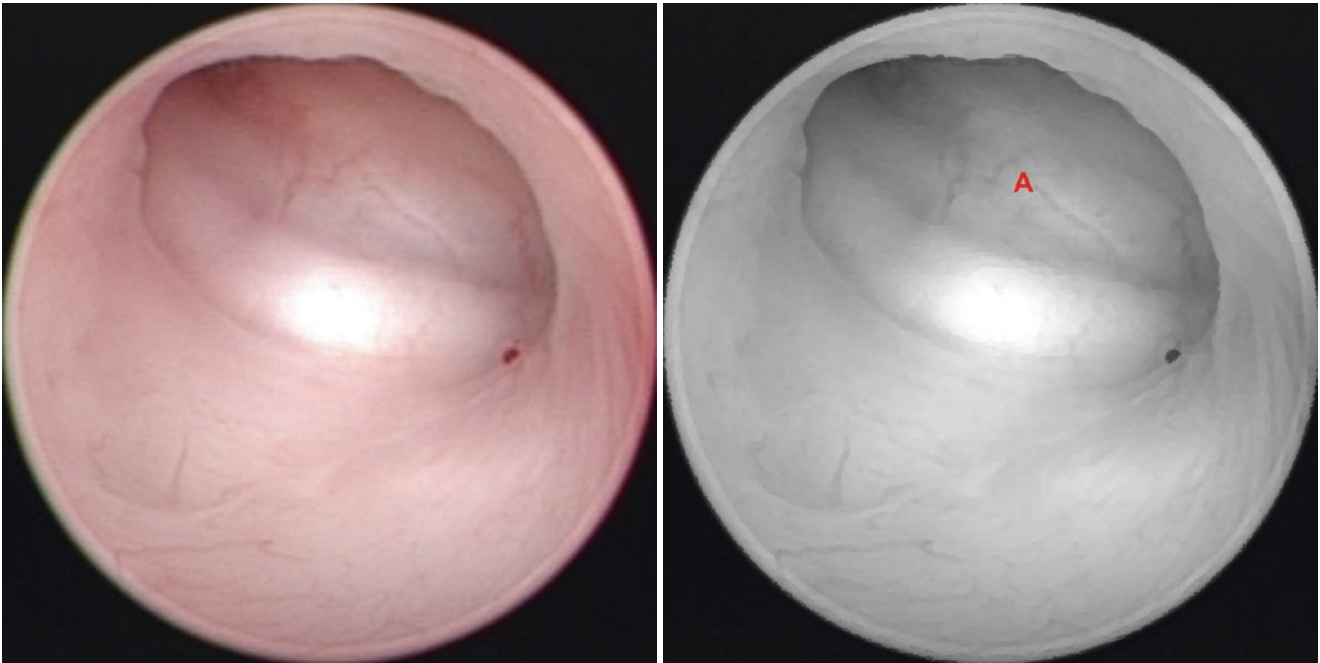


**Fig. 4.138** Abnormal anatomy. (A) Cerebral aqueduct entrance obstructed by a tumor

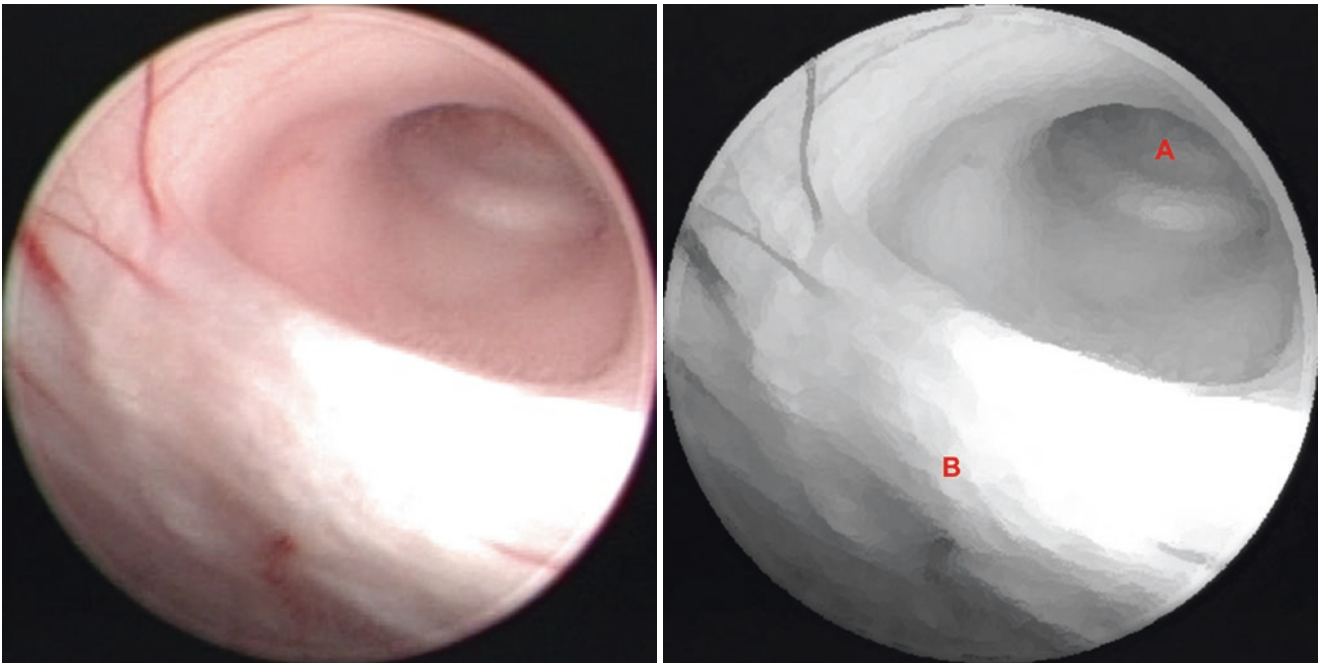


**Fig. 4.139** Abnormal anatomy. (A) Cerebral aqueduct entrance obstructed by a tumor, (B) Posterior commissure

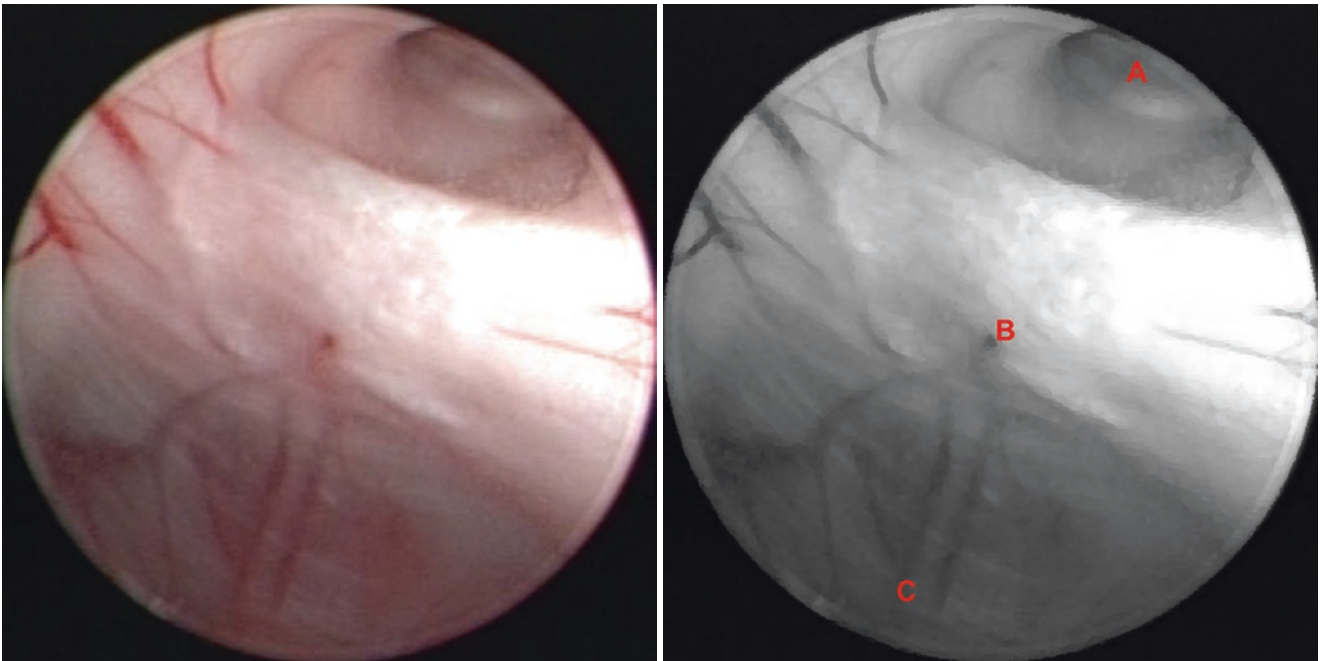


**Fig. 4.140** Abnormal anatomy. (A) Cerebral aqueduct entrance obstructed by a tumor, (B) Posterior commissure, (C) Pineal recess

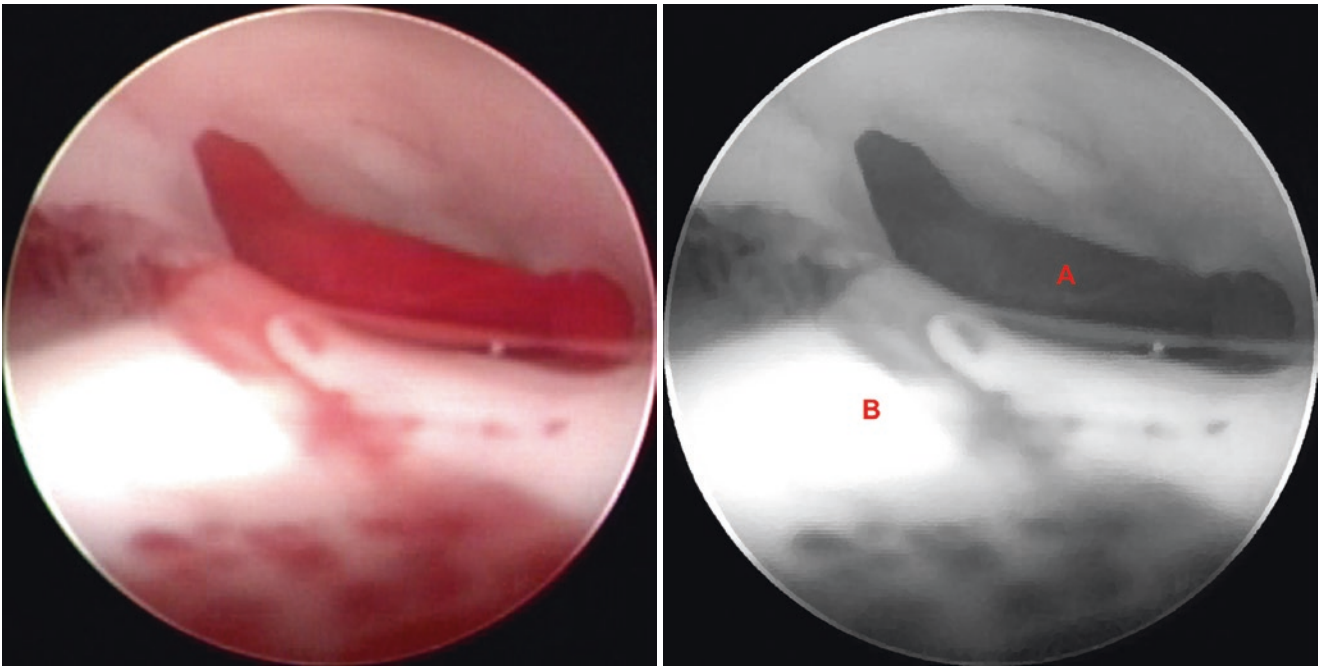


**Fig. 4.141** Surgical procedure – removal of cerebral aqueduct obstruction. (A) Cerebral aqueduct entrance obstructed by a clot, (B) Posterior commissure

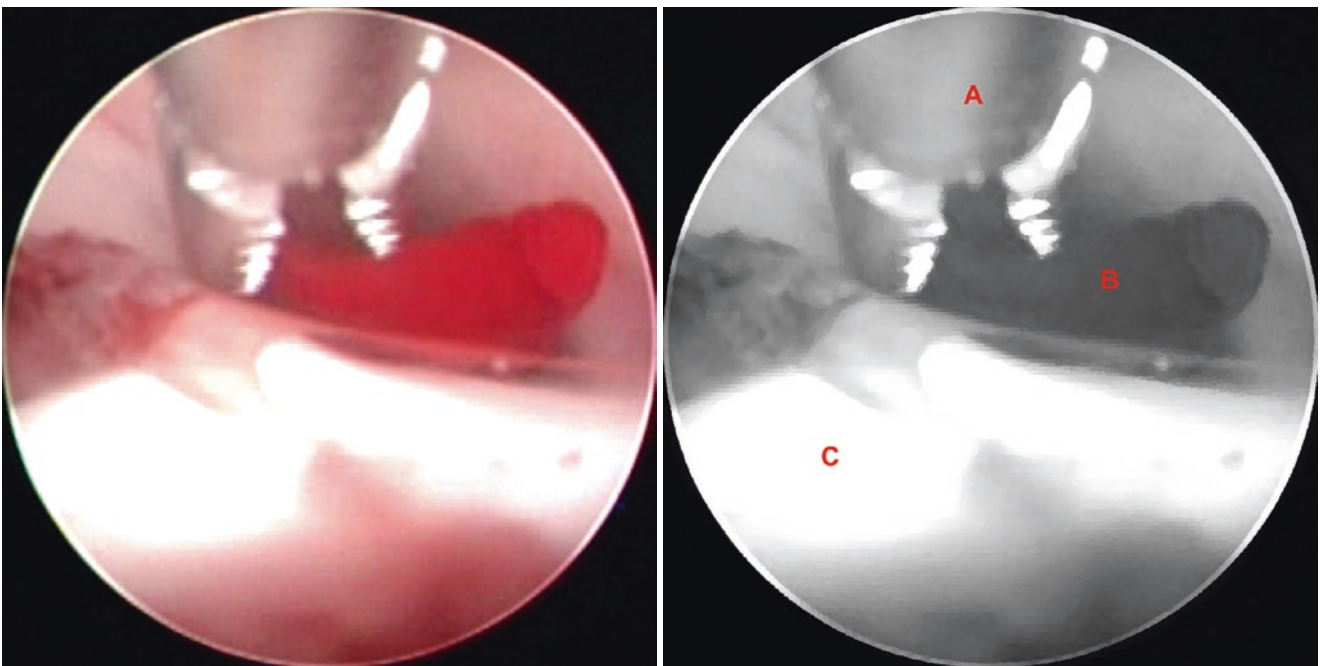


**Fig. 4.142** Surgical procedure – removal of cerebral aqueduct obstruction. (A) Removal of the clot with grasping forceps, (B) Cerebral aqueduct entrance obstructed by a clot, (C) Posterior commissure



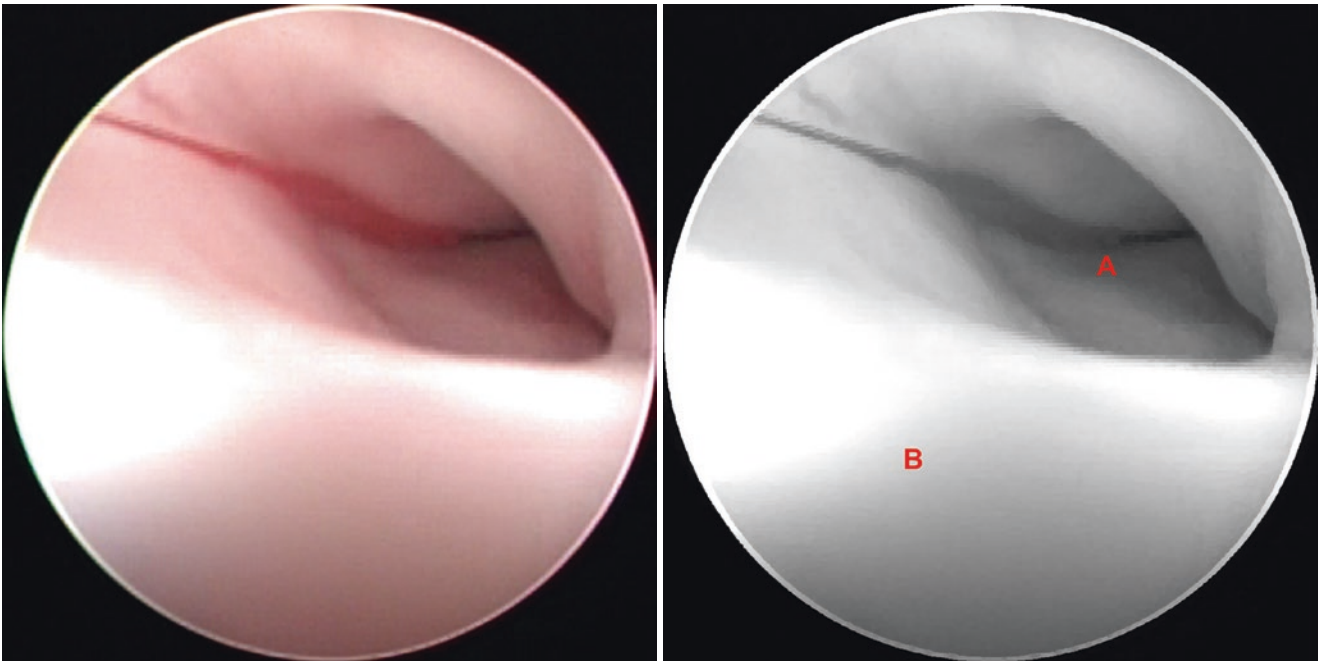


**Fig. 4.143** Surgical procedure – removal of cerebral aqueduct obstruction. (A) Unobstructed cerebral aqueduct, (B) Posterior commissure

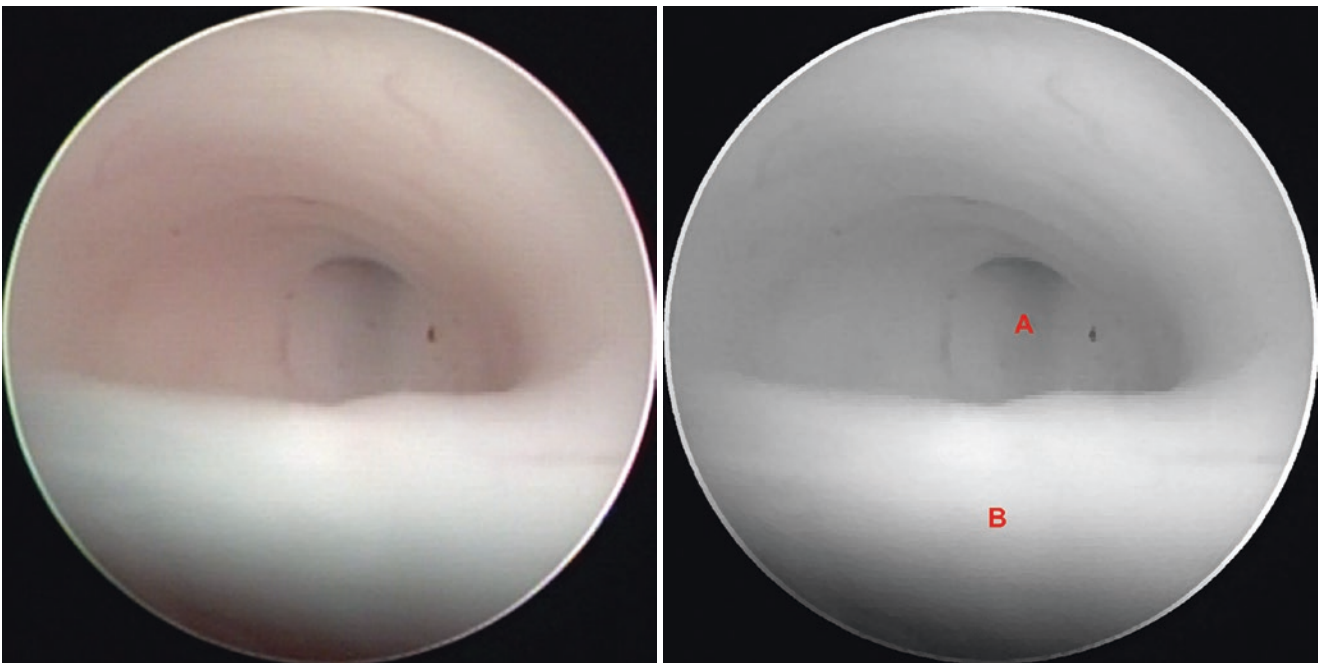


**Fig. 4.144** Surgical procedure – aqueductoplasty without Fogarty balloon catheter insufflation. (A) Cerebral aqueduct entrance obstructed by an adhesion, (B) Posterior commissure

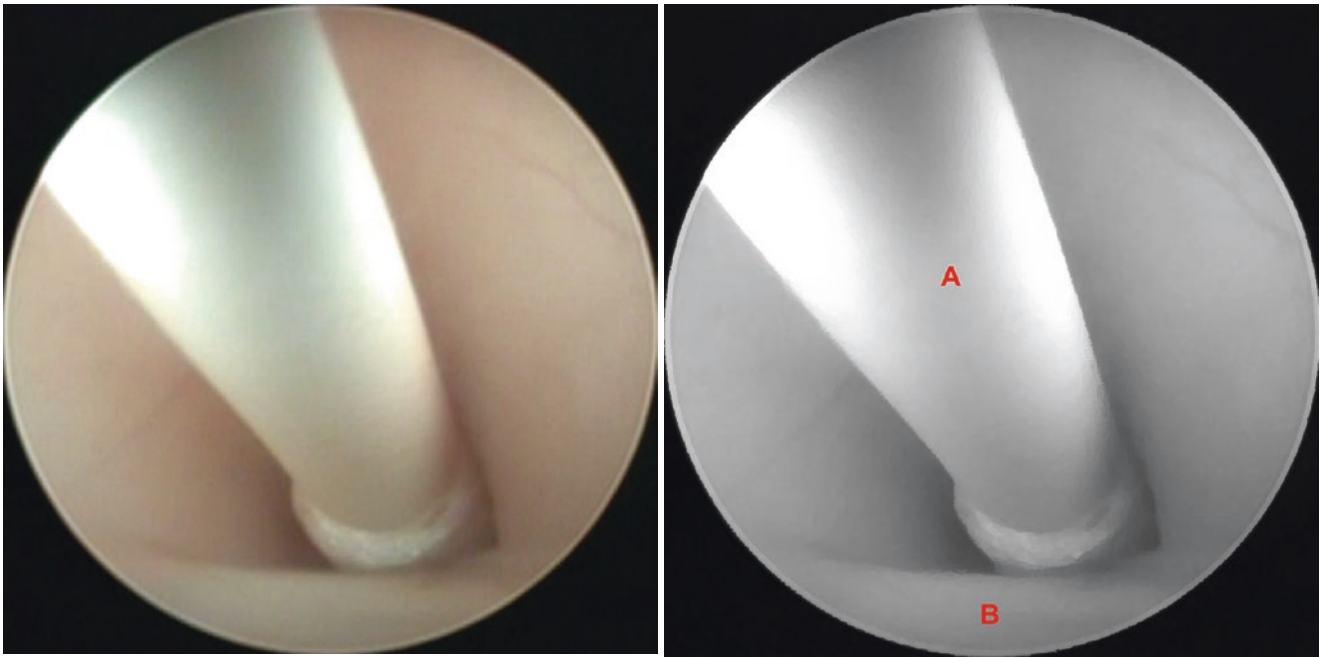


**Fig. 4.145** Surgical procedure – aqueductoplasty without Fogarty balloon catheter insufflation. (A) Fogarty balloon catheter, (B) Posterior commissure

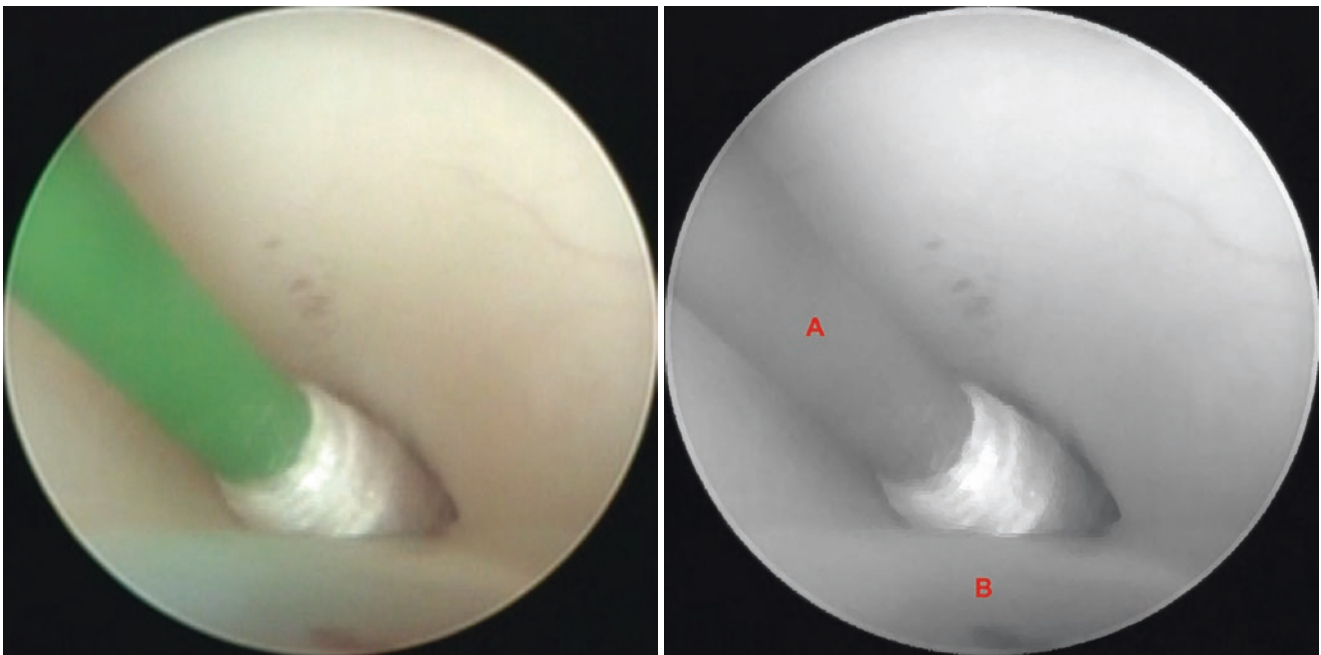


**Fig. 4.146** Surgical procedure – aqueductoplasty without Fogarty balloon catheter insufflation. (A) Fogarty balloon catheter, (B) Posterior commissure

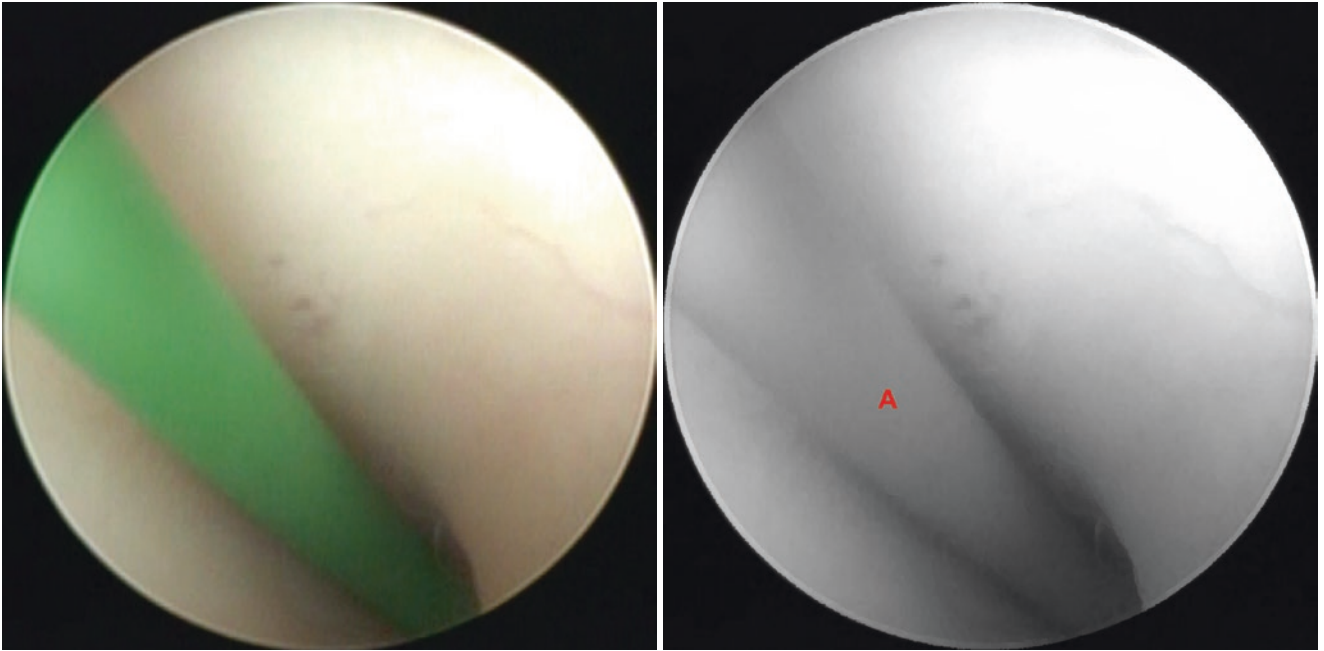


**Fig. 4.147** Surgical procedure – aqueductoplasty without Fogarty balloon catheter insufflation. (A) Fogarty balloon catheter

Illustrative case 5 – aqueductoplasty with Fogarty balloon catheter insufflation after ETV.

Clinical data: 1-year-old child, downward ocular deviation.

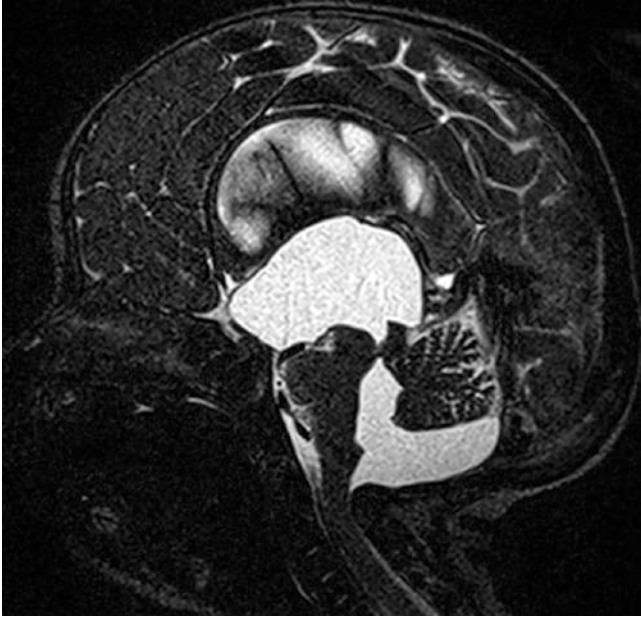


**Fig. 4.148** Sagittal T2-weighted MRI showing cerebral aqueduct obstruction and hydrocephalus in a Dandy-Walker complex case

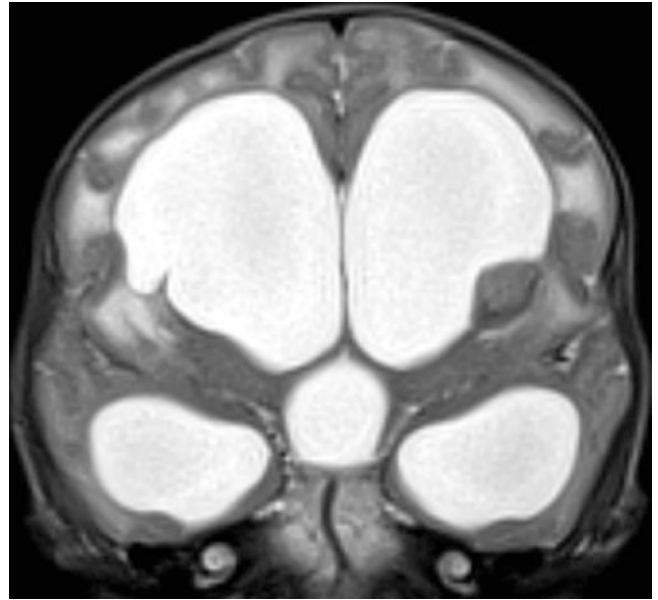


**Fig. 4.149** Coronal T2-weighted MRI showing hydrocephalus

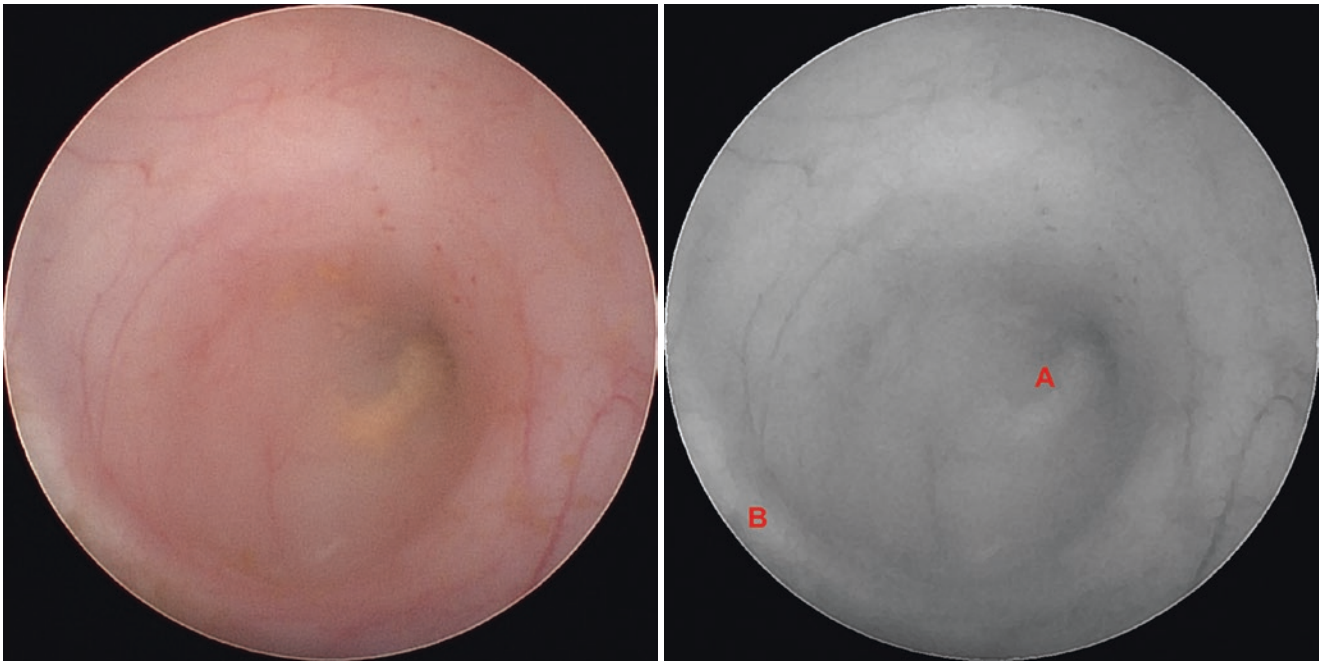


**Fig. 4.150** Illustrative case 5 – aqueductoplasty with Fogarty balloon catheter insufflation after ETV. (A) Cerebral aqueduct entrance obstructed by an adhesion, (B) Posterior commissure

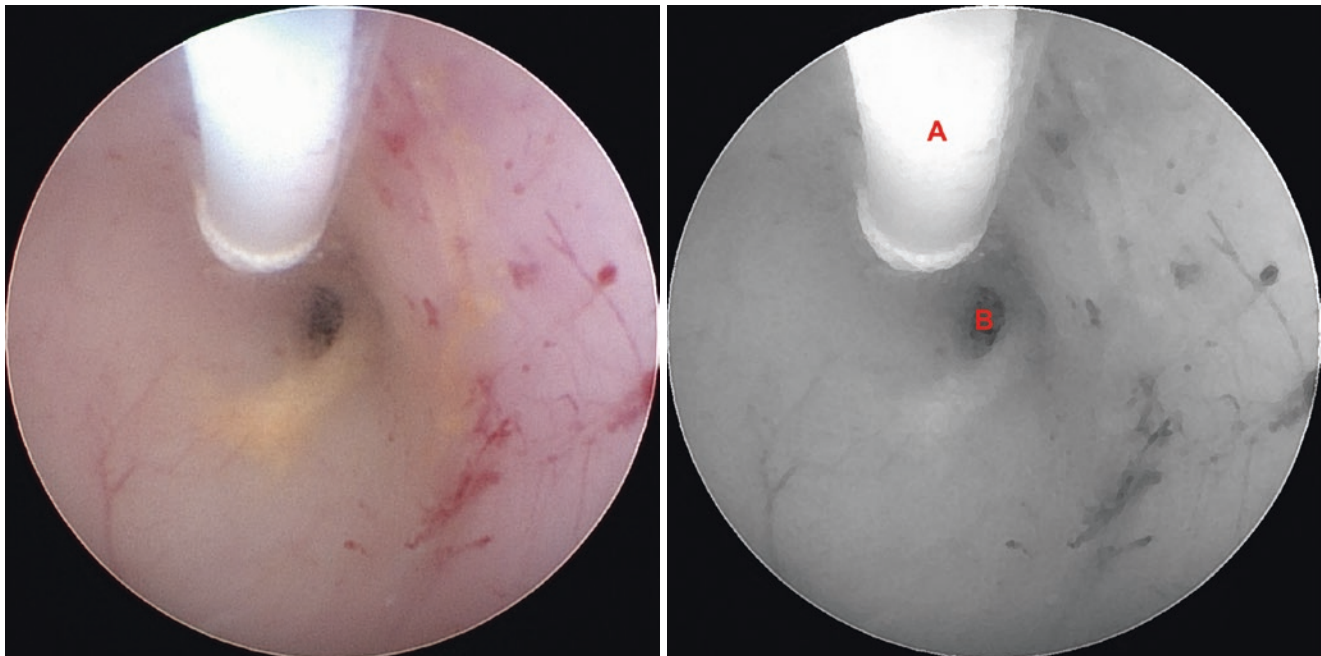


**Fig. 4.151** Illustrative case 5 – aqueductoplasty with Fogarty balloon catheter insufflation after ETV. (A) Fenestration by Fogarty balloon catheter, (B) Cerebral aqueduct entrance fenestration

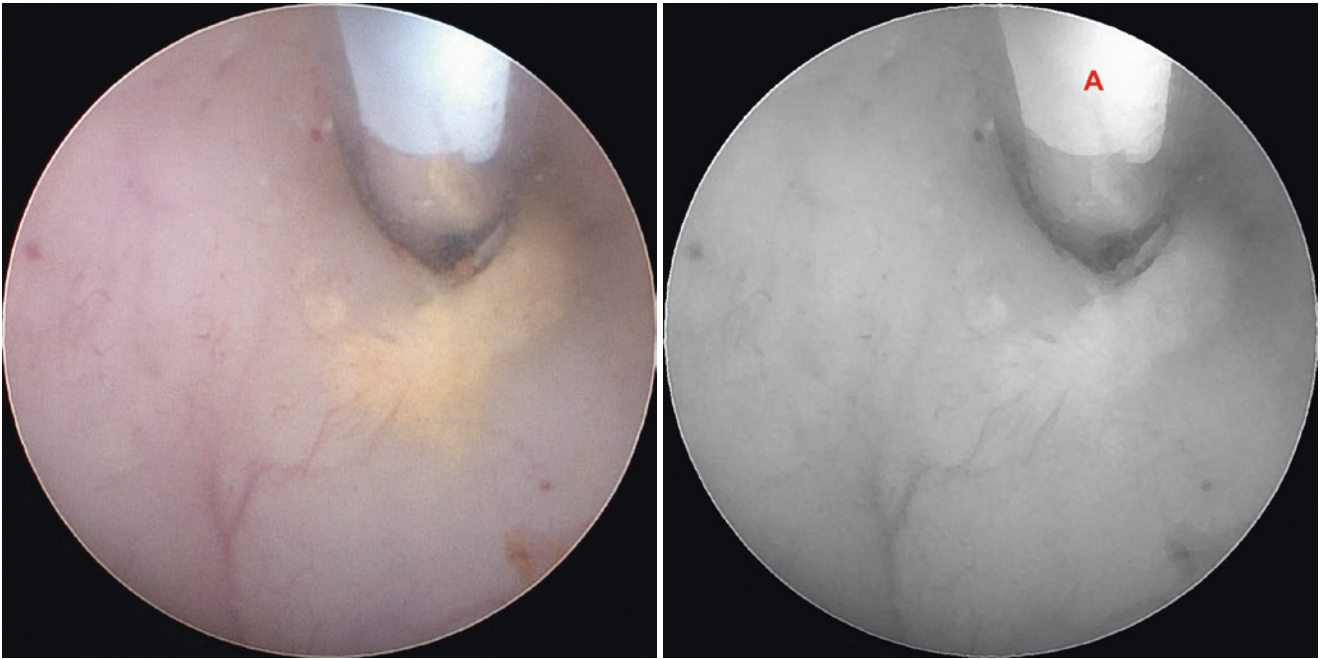


**Fig. 4.152** Illustrative case 5 – aqueductoplasty with Fogarty balloon catheter insufflation after ETV. (A) Fogarty balloon catheter

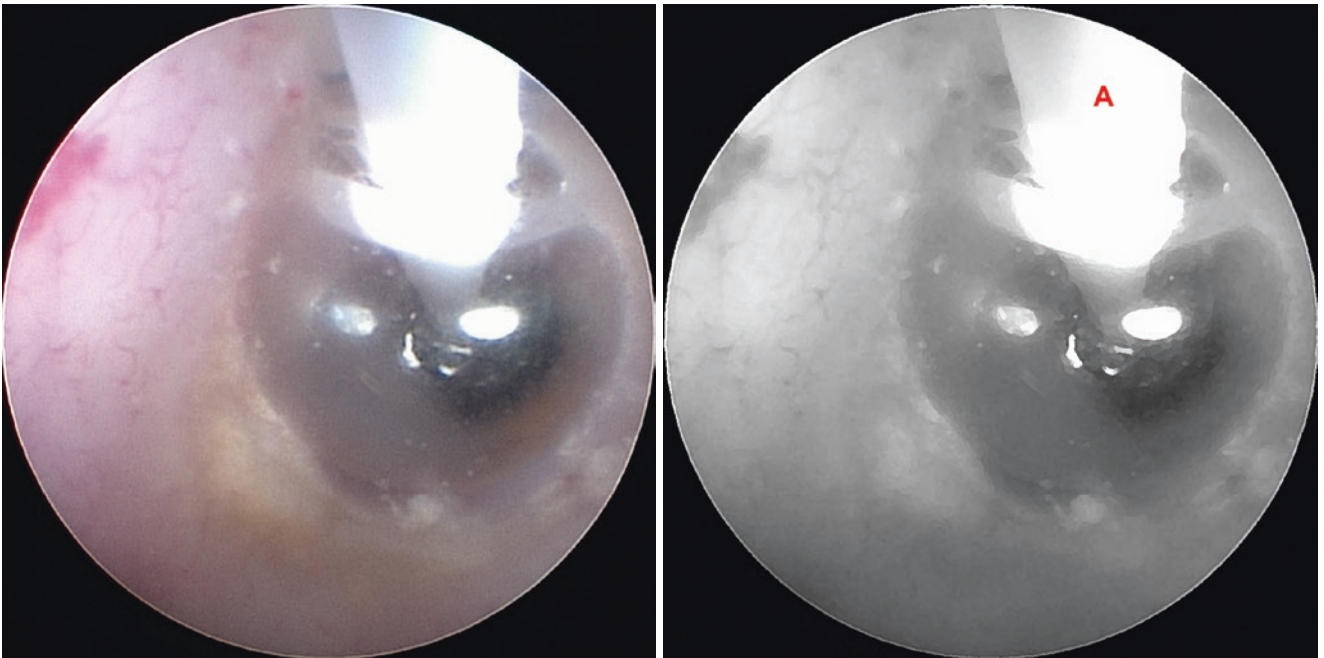


**Fig. 4.153** Illustrative case 5 – aqueductoplasty with Fogarty balloon catheter insufflation after ETV. (A) Insufflated Fogarty balloon catheter

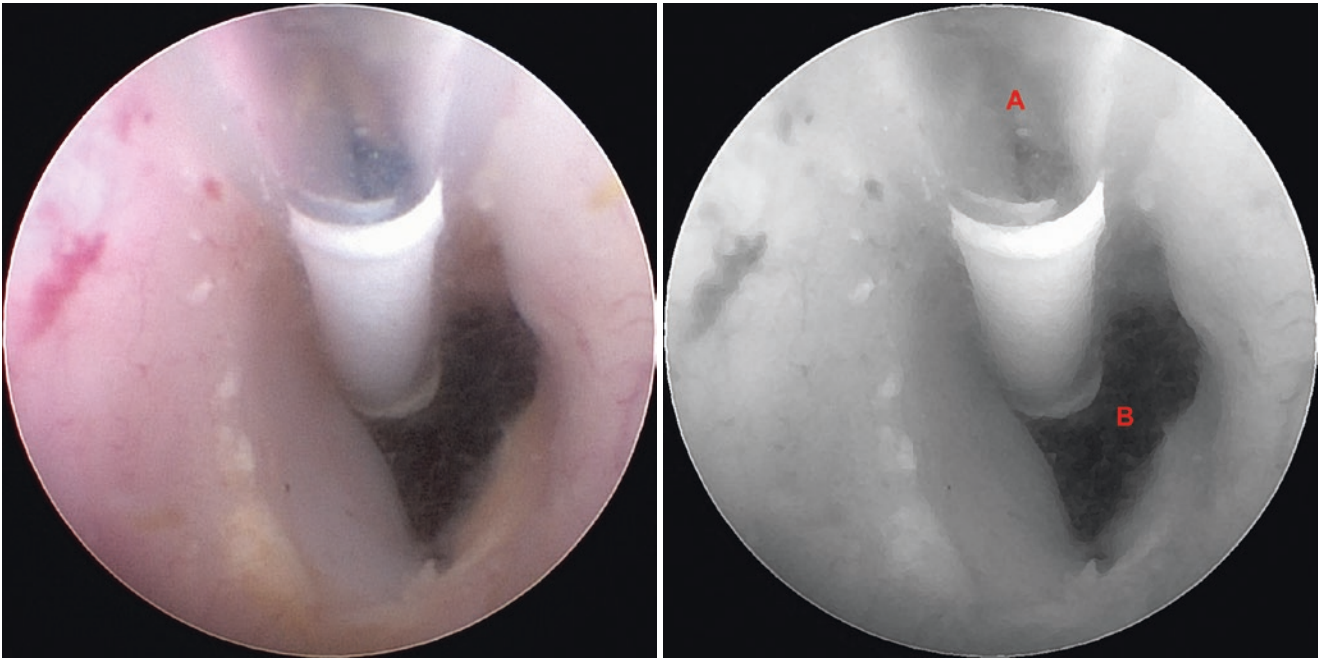


**Fig. 4.154** Illustrative case 5 – aqueductoplasty with Fogarty balloon catheter insufflation after ETV. (A) De-insufflated Fogarty balloon catheter, (B) Fenestrated cerebral aqueduct entrance

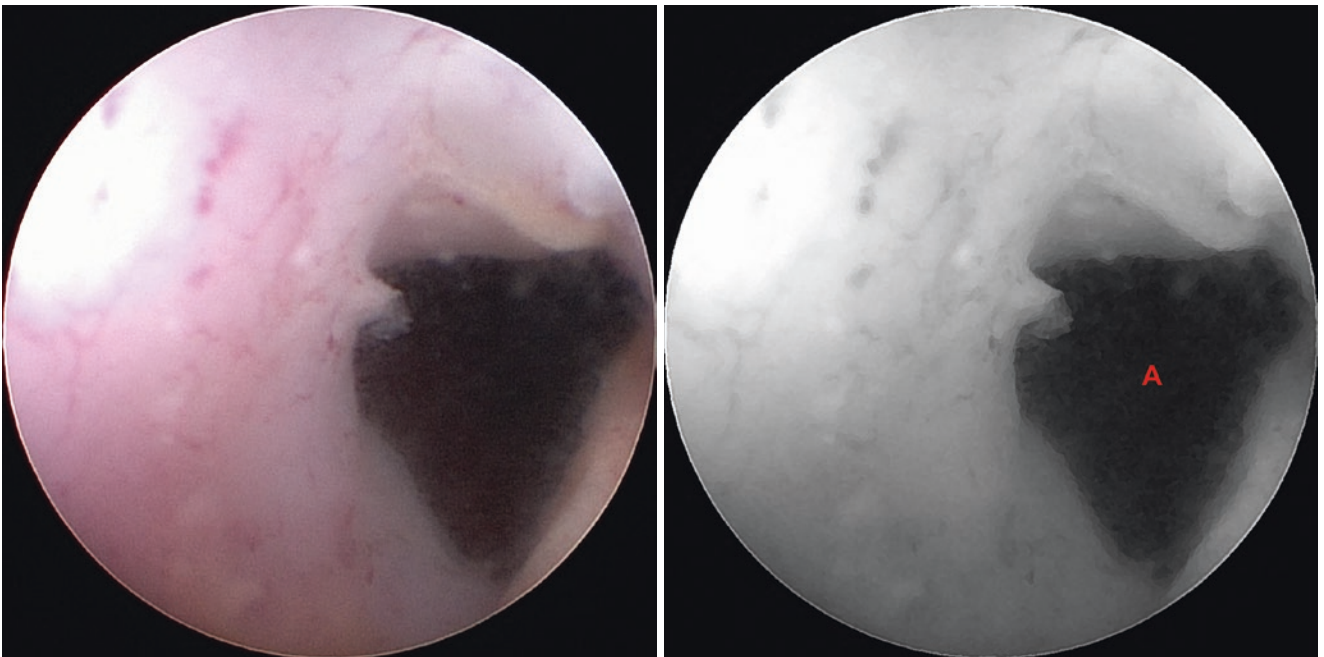


**Fig. 4.155** Illustrative case 5 – aqueductoplasty with Fogarty balloon catheter insufflation after ETV. (A) Final aspect of the cerebral aqueduct entrance

Illustrative case 6 – tumor biopsy after ETV.  
Clinical data: 54-year-old; headache.



**Fig. 4.156** Gadolinium-enhanced sagittal T1-weighted MRI showing a tumor in the pineal region

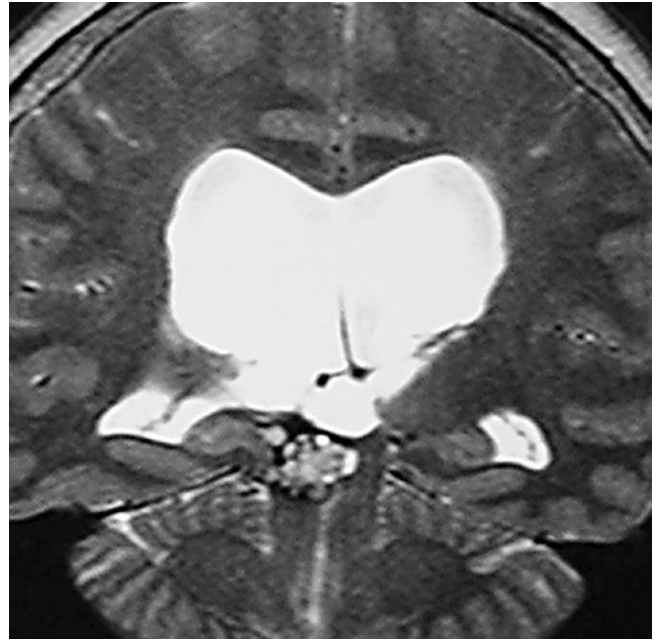


**Fig. 4.157** Coronal T2-weighted MRI showing a tumor in the pineal region



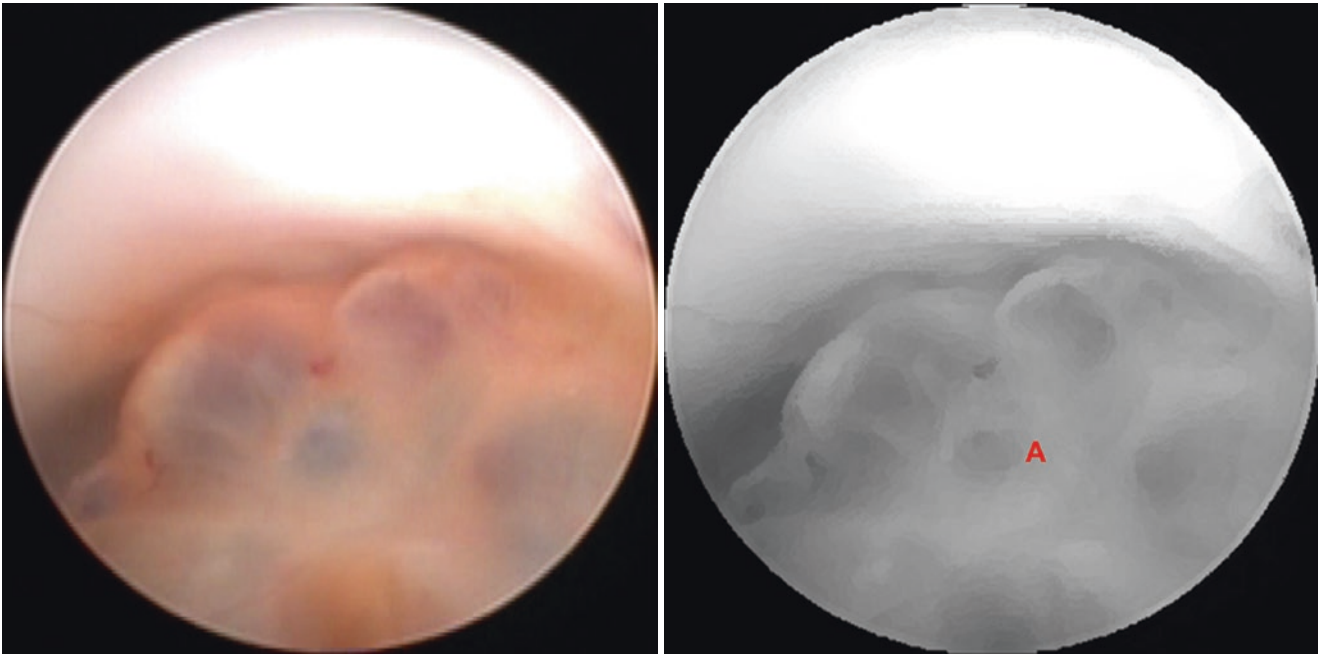


**Fig. 4.158** Illustrative case 6 – tumor biopsy after ETV. (A) Cerebral aqueduct entrance obstructed by a tumor

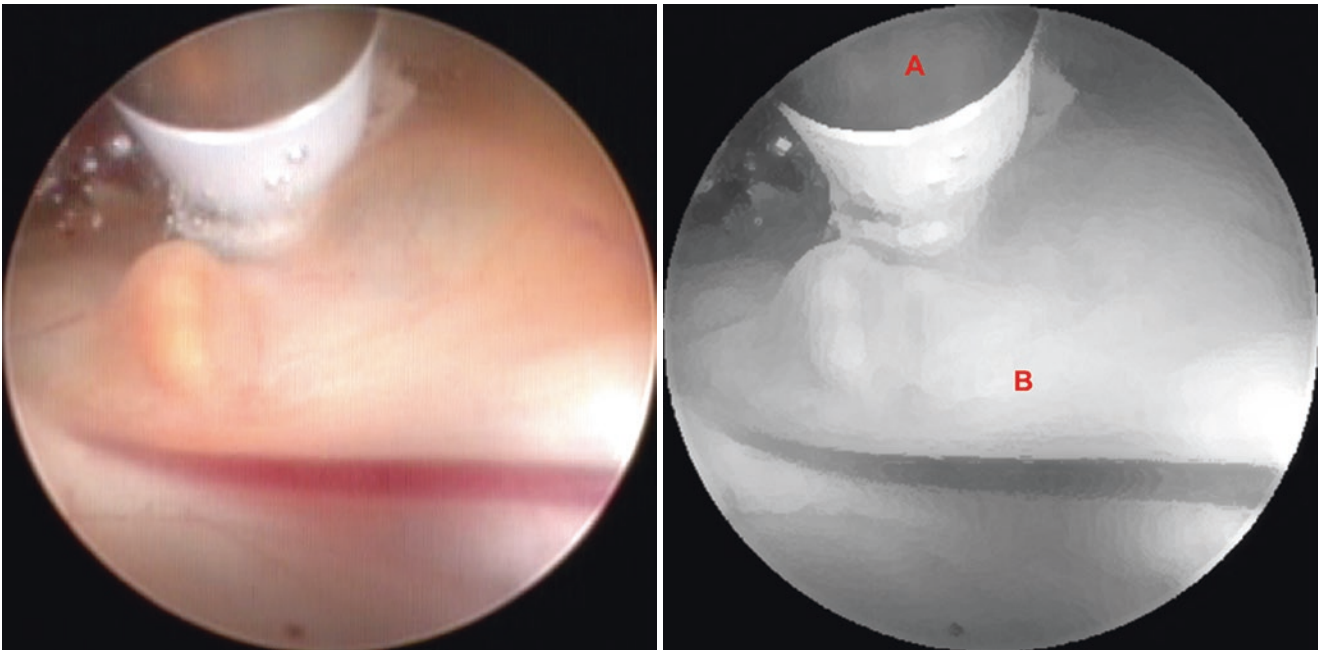


**Fig. 4.159** Illustrative case 6 – tumor biopsy after ETV. (A) Bipolar coagulation electrode, (B) Tumor wall

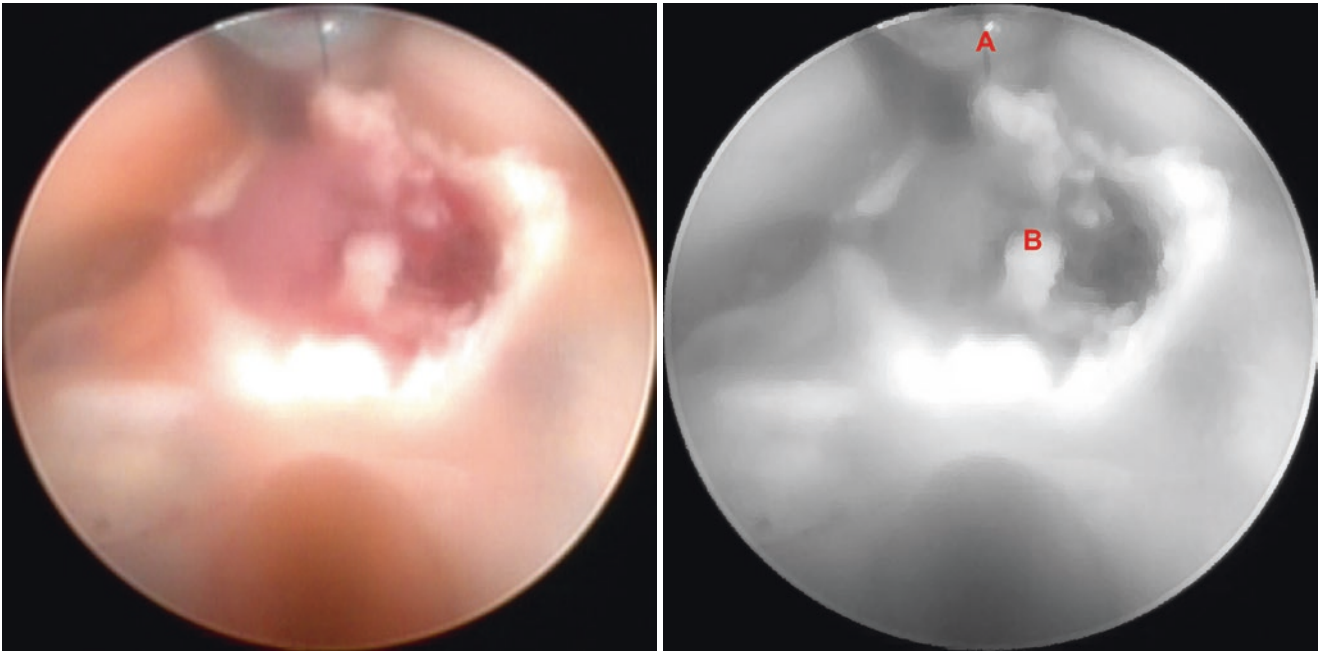


**Fig. 4.160** Illustrative case 6 – tumor biopsy after ETV. (A) Biopsy forceps, (B) Tumor

Illustrative case 7 – fenestration of a giant posterior fossa arachnoid cyst.

Clinical data: 2-year-old child; headache, increased head circumference.



**Fig. 4.161** Axial T2-weighted MRI showing a huge posterior fossa arachnoid cyst

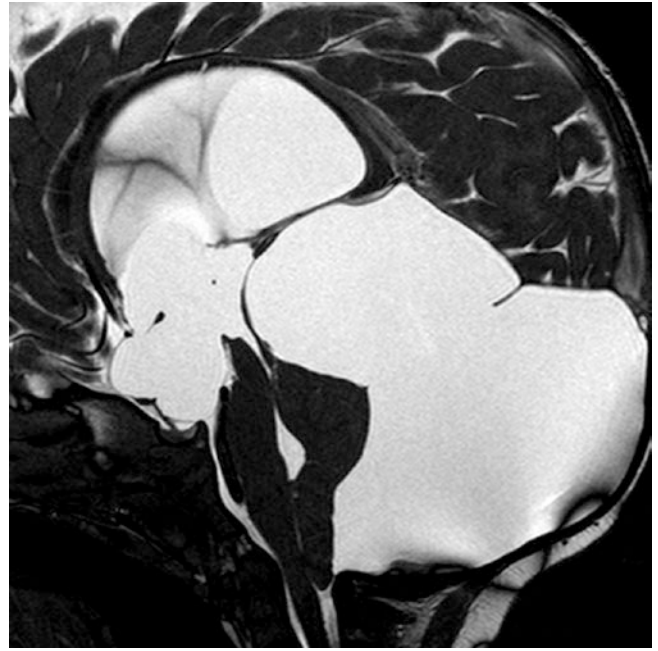


**Fig. 4.162** Sagittal T2-weighted MRI showing a huge posterior fossa arachnoid cyst with supratentorial extension and hydrocephalus

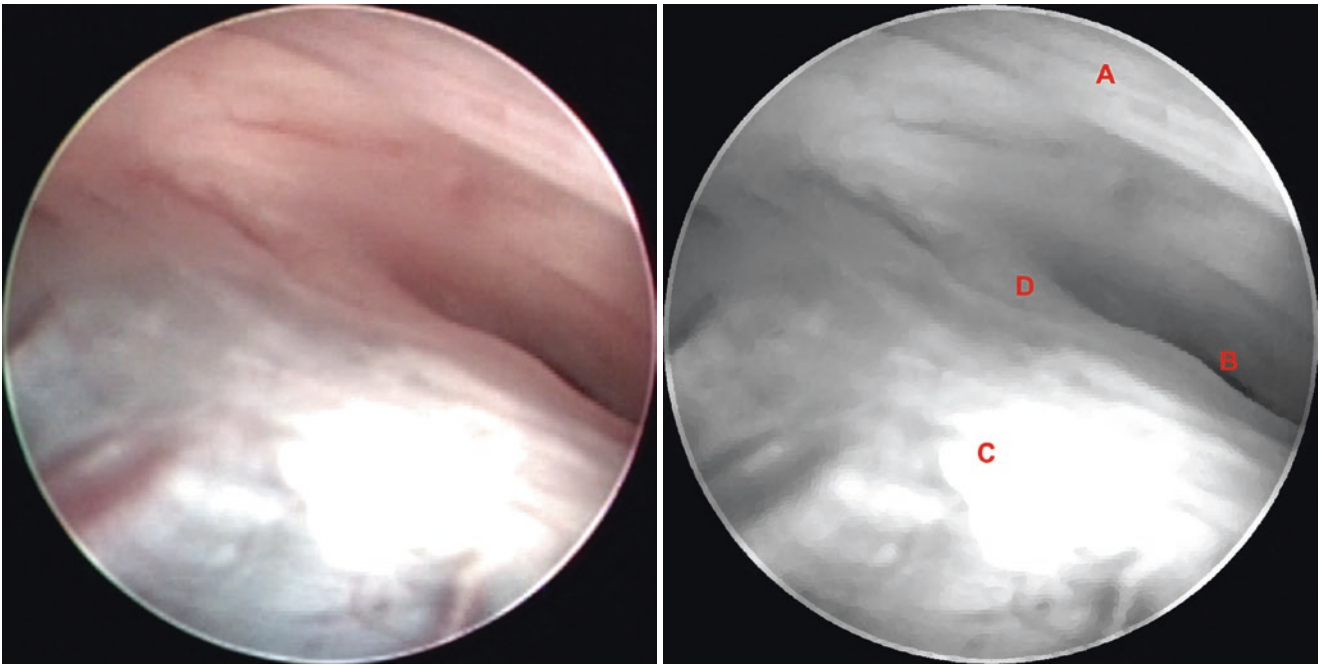


**Fig. 4.163** Illustrative case 7 – fenestration of a giant posterior fossa arachnoid cyst. (A) Interthalamic adhesion, (B) Cerebral aqueduct entrance, (C) Cyst wall, (D) Posterior commissure

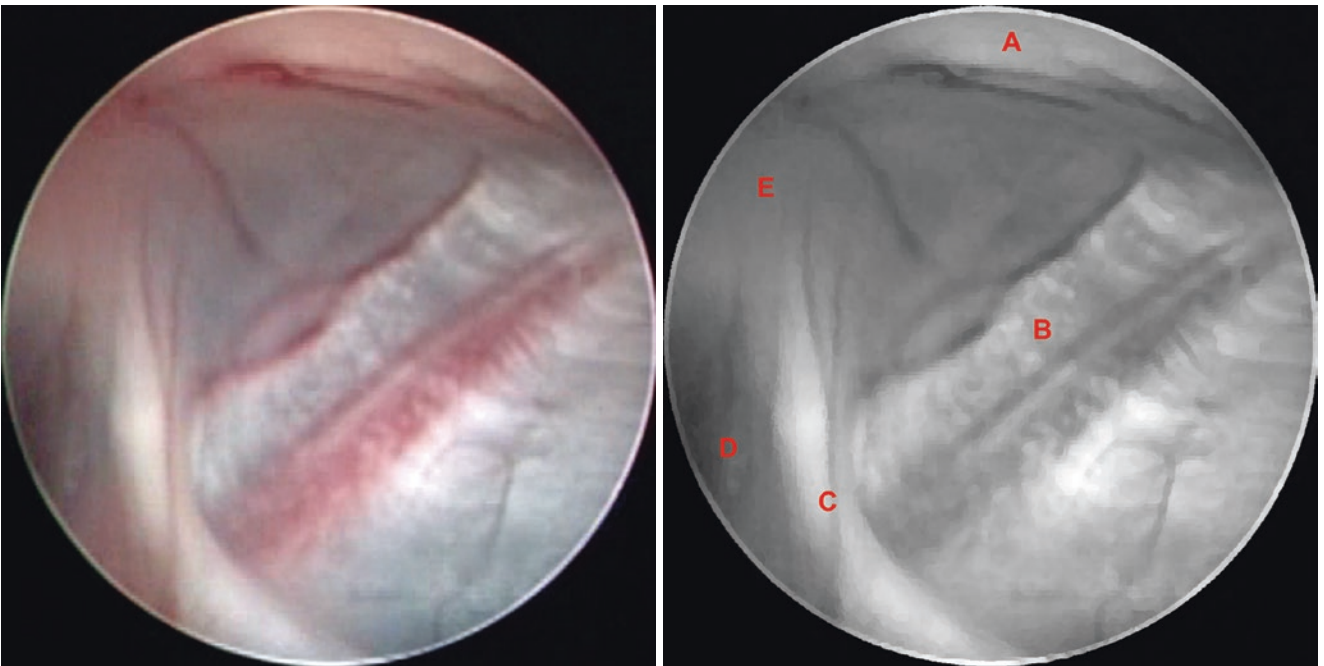


**Fig. 4.164** Illustrative case 7 – fenestration of a giant posterior fossa arachnoid cyst. (A) Posterior commissure, (B) Cyst wall, (C) Habenular commissure, (D) Suprapineal recess, (E) Left habenular trigone

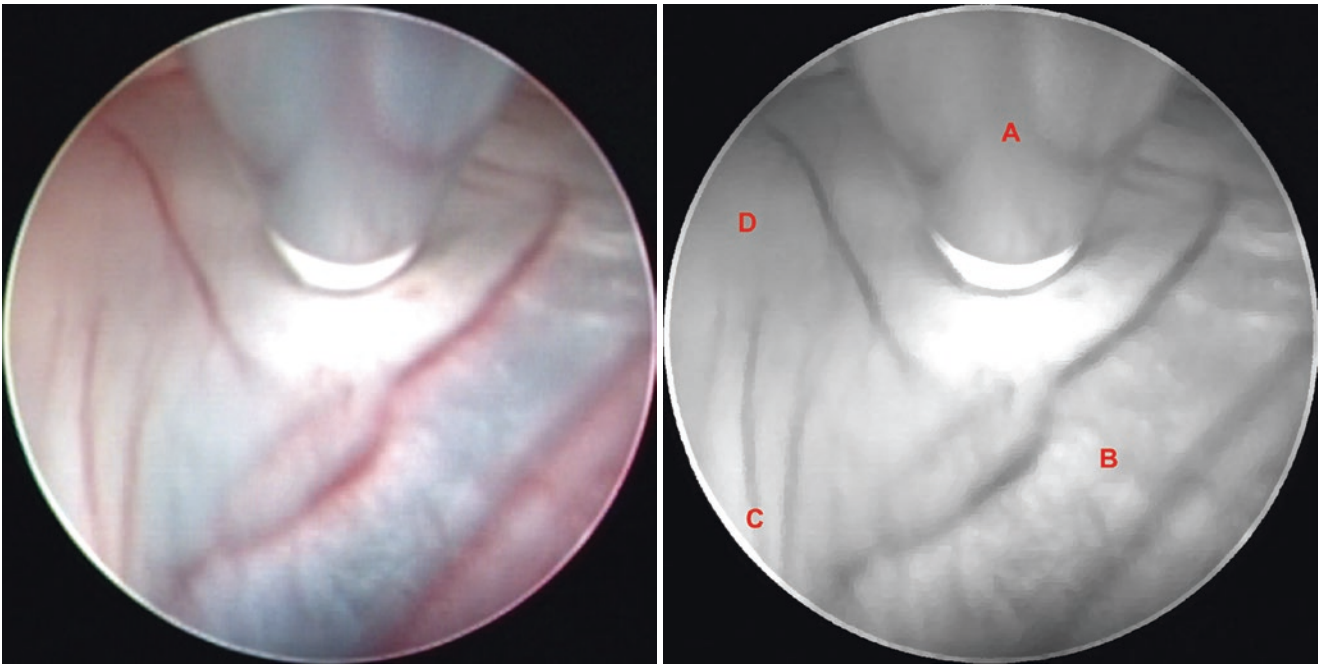


**Fig. 4.165** Illustrative case 7 – fenestration of a giant posterior fossa arachnoid cyst. (A) Bipolar coagulation electrode, (B) Cyst wall, (C) Habenular commissure, (D) Left habenular trigone

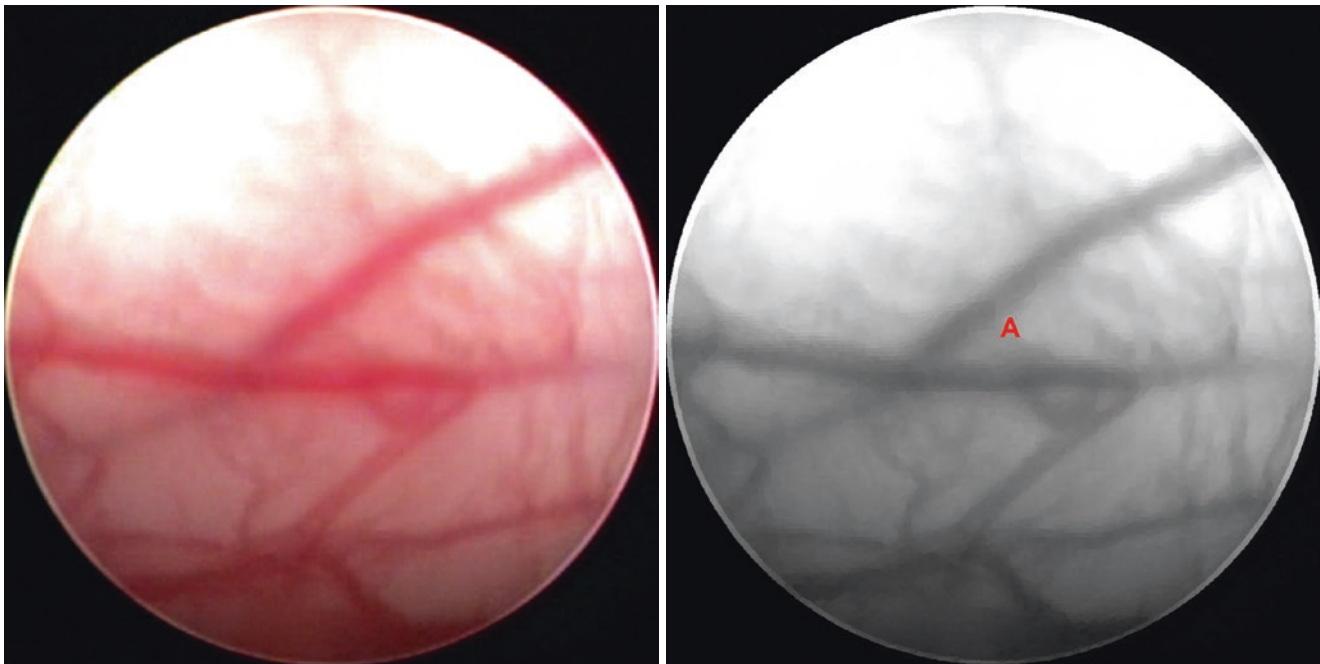


**Fig. 4.166** Illustrative case 7 – fenestration of a giant posterior fossa arachnoid cyst. (A) View of the cerebellum after fenestration

## References

1. Seeger W. Endoscopic anatomy of the third ventricle. Microsurgical and endoscopic approaches. Wien: Springer; 2006. doi:[10.1007/3-211-31178-5](https://doi.org/10.1007/3-211-31178-5).
2. Enchev YP, Oi S. The application of neuroendoscopic techniques in improving altered CSF physiology. In: Sgouros S, editor. Neuroendoscopy. Berlin/Heidelberg: Springer; 2014. p. 11–30. doi:[10.1007/978-3-642-39085-2\\_2](https://doi.org/10.1007/978-3-642-39085-2_2).
3. Baydin S, Gungor A, Baran O, Tanriover N, Rhoton AL. The double massa intermedia. *Surg Neurol Int.* 2016;7:30. doi:[10.4103/2152-7806.179383](https://doi.org/10.4103/2152-7806.179383).
4. Riegel T, Hellwig D, Bauer BL, Mennel HD. Endoscopic anatomy of the third ventricle. *Acta Neurochir Suppl.* 1994;61:54–6.
5. Segal S. Endoscopic anatomy of the ventricular system. In: King WA, Frazee JG, De Salles AAF, editors. Endoscopy of the central and peripheral nervous system. Stuttgart: Thieme; 1998. p. 37–57.
6. Decq P. Endoscopic anatomy of the ventricles. In: Cinalli G, Sainte-Rose C, Maixner WJ, editors. Pediatric hydrocephalus. Milan: Springer; 2005. p. 351–9. doi:[10.1007/978-88-470-2121-1\\_24](https://doi.org/10.1007/978-88-470-2121-1_24).
7. Fallah A, Wang AC, Weil AG, Ibrahim GM, Mansouri A, Bhatia S. Predictors of outcome following cerebral aqueductoplasty: an individual participant data meta-analysis. *Neurosurgery.* 2016;78:285–96. doi:[10.1227/NEU.0000000000001024](https://doi.org/10.1227/NEU.0000000000001024).

## 5.1 Introduction

The subarachnoid space below the third ventricle is reached after opening the ependymal layer just ahead of the mammillary bodies (tuber cinereum) when an endoscopic third ventriculostomy (ETV) is performed [1]. The structure in this region that divides the space into individual cisterns is the membrane of Liliequist [2, 3]. This membrane presents a sellar portion, which is inserted in the dorsum sellae, and this sellar portion is subdivided into a posterior projection, a diencephalic portion, and a mesencephalic portion. The diencephalic portion is in close contact with the ependymal layer and extends to the mammillary bodies, and the mesencephalic portion has a posterior inferior projection, surrounding the mesencephalon [4, 5, 6]. The membrane of Liliequist limits the interpeduncular cistern. This cistern has a pars profunda, adjacent to the ependymal layer, and a pars superficialis, just below the pars profunda. The diencephalic portion of the membrane of Liliequist divides the two segments [6]. The pars profunda contains the anterior group of thalamoperforating arteries. Located in the pars superficialis is the bifurcation of the basilar artery with its two main branches, the posterior cerebral arteries (P1) and the superior cerebellar arteries (located immediately before the bifurcation of the basilar artery), and the oculomotor

nerves (CN III) [6]. The lower limit of the pars superficialis is the mesencephalic portion of the membrane of Liliequist. The recess below the latter is the prepontine cistern [6] (Fig. 5.1). In most ventricular procedures it is difficult to identify this anatomy. On sagittal T2-weighted magnetic resonance imaging (MRI) it is sometimes possible to visualize these structures (Fig. 5.2). But regardless of whether or not they are in clear view, the key to the success of an ETV is the opening of the membrane of Liliequist, at least of its diencephalic portion (Fig. 5.3). In certain cases progression of the endoscope inside the prepontine cistern is possible, enabling visualization of the trajectory of the basilar artery, and the nerves that emerge from the anterior side of the brainstem, such as the abducens nerve (CN VI), in the transition between the pons and the medulla oblongata, and the hypoglossal nerve (CN XII), at the medulla oblongata (Fig. 5.4). The endoscopic viewing angle for the interpeduncular and prepontine cisterns is shown in Fig. 5.5, and the structures of this region are shown in Figs. 5.6, 5.7, 5.8, 5.9, 5.10, 5.11, 5.12, 5.13, 5.14, 5.15, 5.16, 5.17, 5.18, 5.19, 5.20, 5.21, 5.22, 5.23, 5.24, 5.25, 5.26, 5.27, 5.28, 5.29, 5.30, 5.31, 5.32, 5.33, 5.34, 5.35, 5.36, 5.37, 5.38, 5.39, 5.40, 5.41, 5.42, 5.43, 5.44, 5.45, 5.46, 5.47, 5.48, 5.49, and 5.50.

An illustrative case is presented.

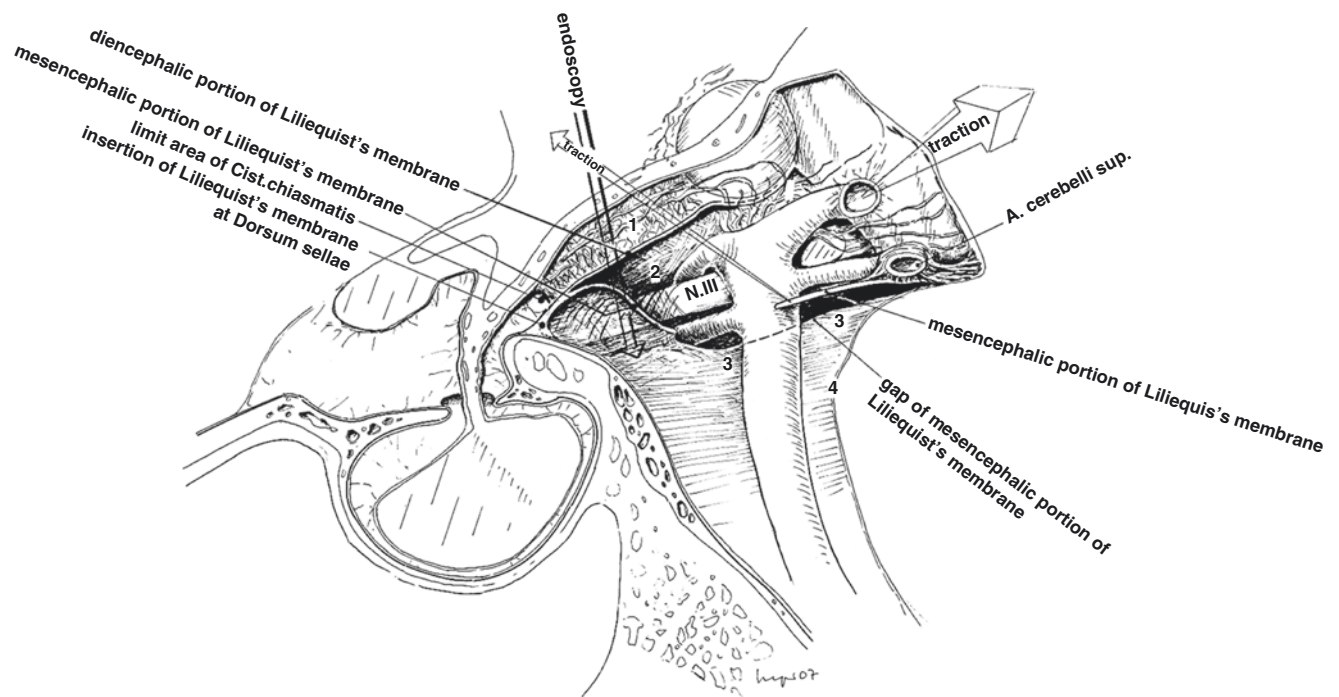


**Fig. 5.1** Detail of the membrane of Lilliequist just below the third ventricle. Pars profunda of the interpeduncular cistern (1), pars superficialis of the interpeduncular cistern (2), prepontine cistern (3), and pia mater (4) (Reprinted from Seeger [6], with permission)



**Fig. 5.2** Sagittal T2-weighted magnetic resonance imaging (MRI) depicting the membrane of Lilliequist and cisterns below the third ventricle. Ependymal layer (A), pars profunda of the interpeduncular cistern (B), diencephalic portion of the membrane of Lilliequist (C), pars superficialis of the interpeduncular cistern (D), mesencephalic portion of the membrane of Lilliequist (E), prepontine cistern (F), insertion of the membrane of Lilliequist at the dorsum sellae (G)



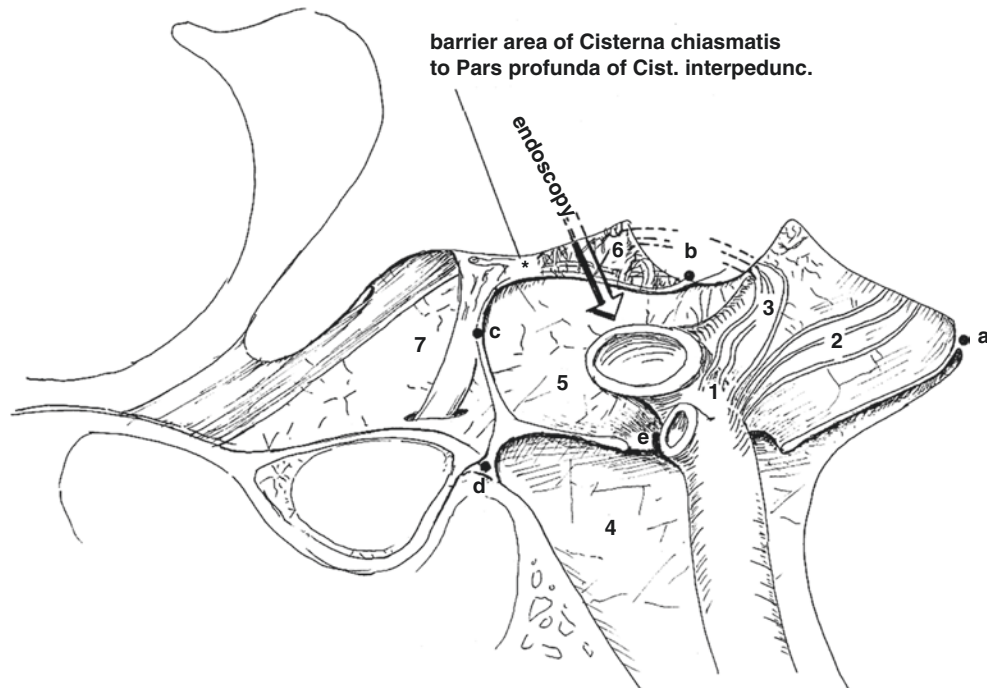


**Fig. 5.3** Trajectory of the neuroendoscope through the pars profunda of the interpeduncular cistern. This step is mandatory for ETV success. Insertion of the mesencephalic portion of the membrane of Liliequist at the pontomesencephalic rim (*a*), insertion of the diencephalic portion of the membrane of Liliequist at mammillary body (*b*), bulging of this segment against the chiasmatic cistern (*c*), insertion of the membrane of Liliequist at the dorsum sellae (*d*), gap of the mesencephalic segment

(*e*). Bifurcation of the basilar artery (*1*), posterior bundle of the thalamoperforating arteries, penetrating the posterior perforated substance (*2*), anterior bundle of the thalamoperforating arteries, crossing pars superficialis of the interpeduncular cistern (*3*), prepontine cistern (*4*), pars superficialis of the interpeduncular cistern (*5*), pars profunda of the interpeduncular cistern (*6*), chiasmatic cistern (*7*) (Reprinted from Seeger [6], with permission)

**Fig.5.4** Figure depicting sellar and clivus regions, viewed from behind. It is possible to see cranial nerves II to XII and other structures. Endoscopic view is possible of the III, VI, and XII cranial nerves. Anterior intercavernous sinus (1), internal carotid artery (2), projection of the anterior clinoid process (3), posterior intercavernous sinus (4), vascularization of the dorsum sellae and the posterior clinoid process (5), projection of the internal opening carotid channel of the petrous bone (6), oval foramen (7), basilar venous plexus (8), foramen magnum (9) (Reprinted from Seeger [6], with permission)

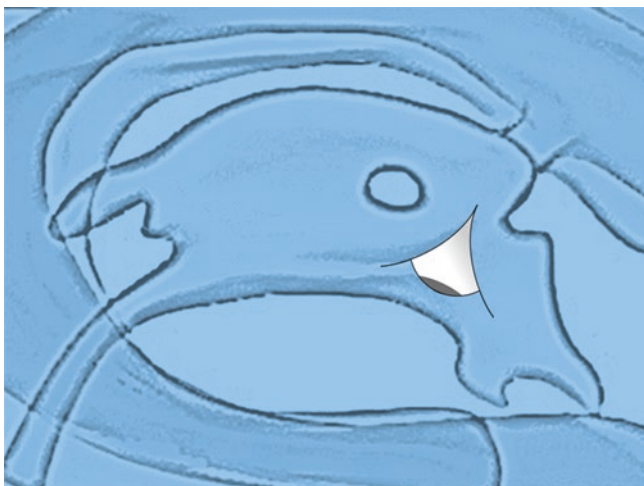
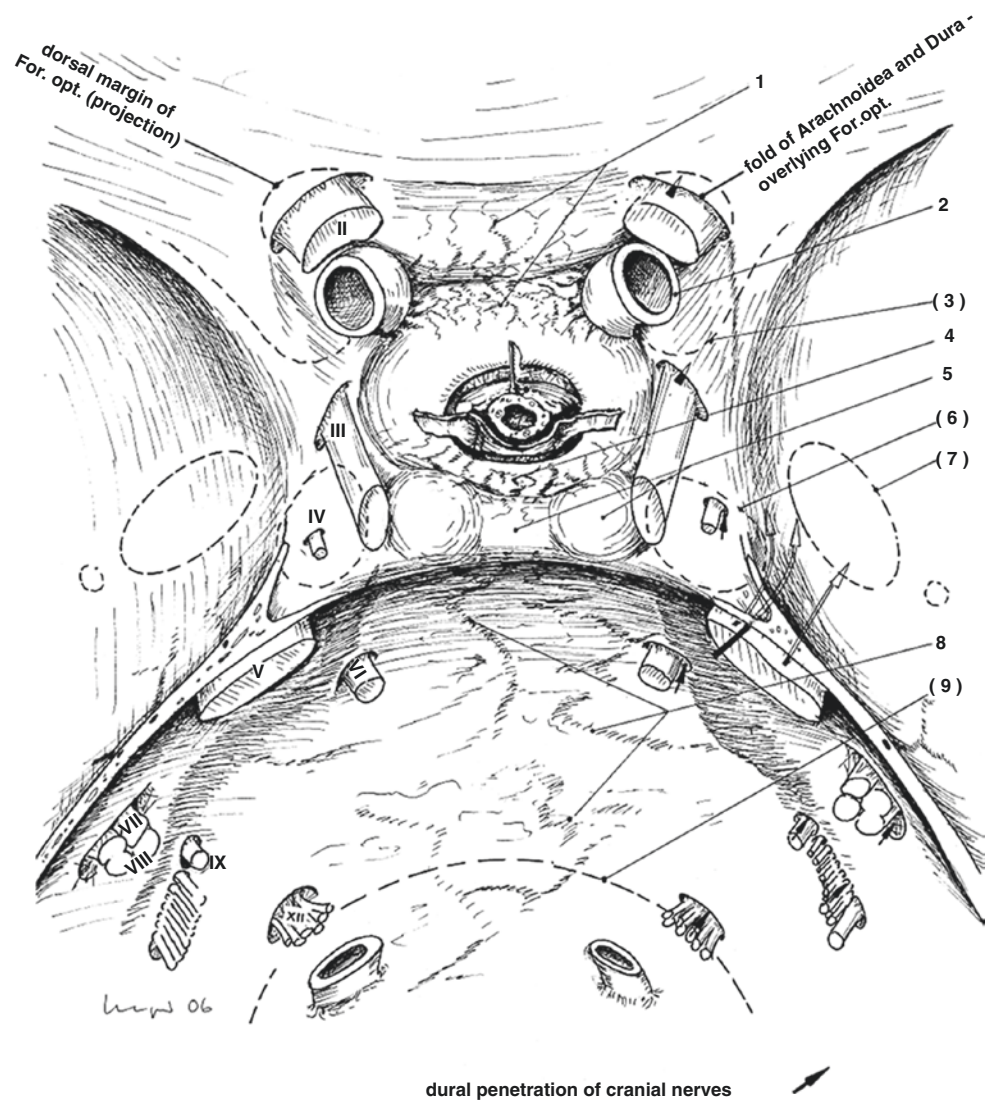


**Fig.5.5** Direction of the endoscopic vision for interpeduncular and prepontine cisterns

## 5.2 Interpeduncular and Prepontine Cisterns

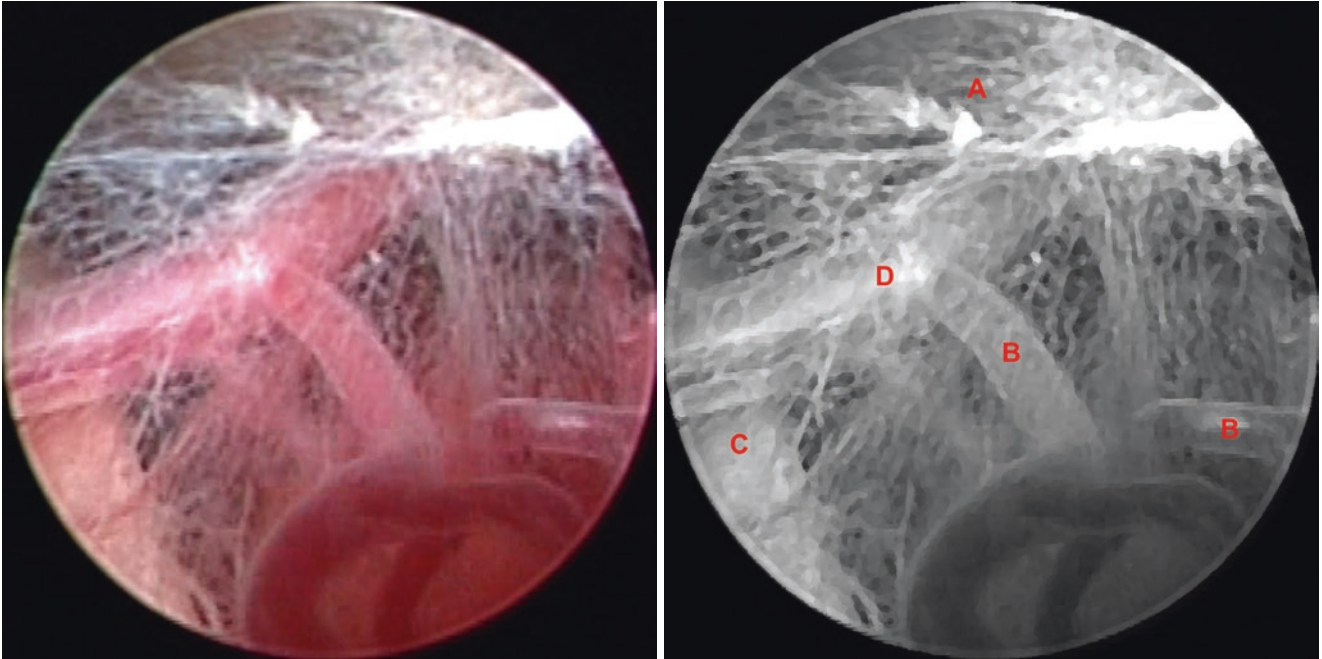


**Fig.5.6** Normal anatomy. (A) Membrane of Liliequist – diencephalic portion, (B) thalamoperforating arteries, (C) left oculomotor nerve (CN III), (D) left posterior cerebral artery (P1)

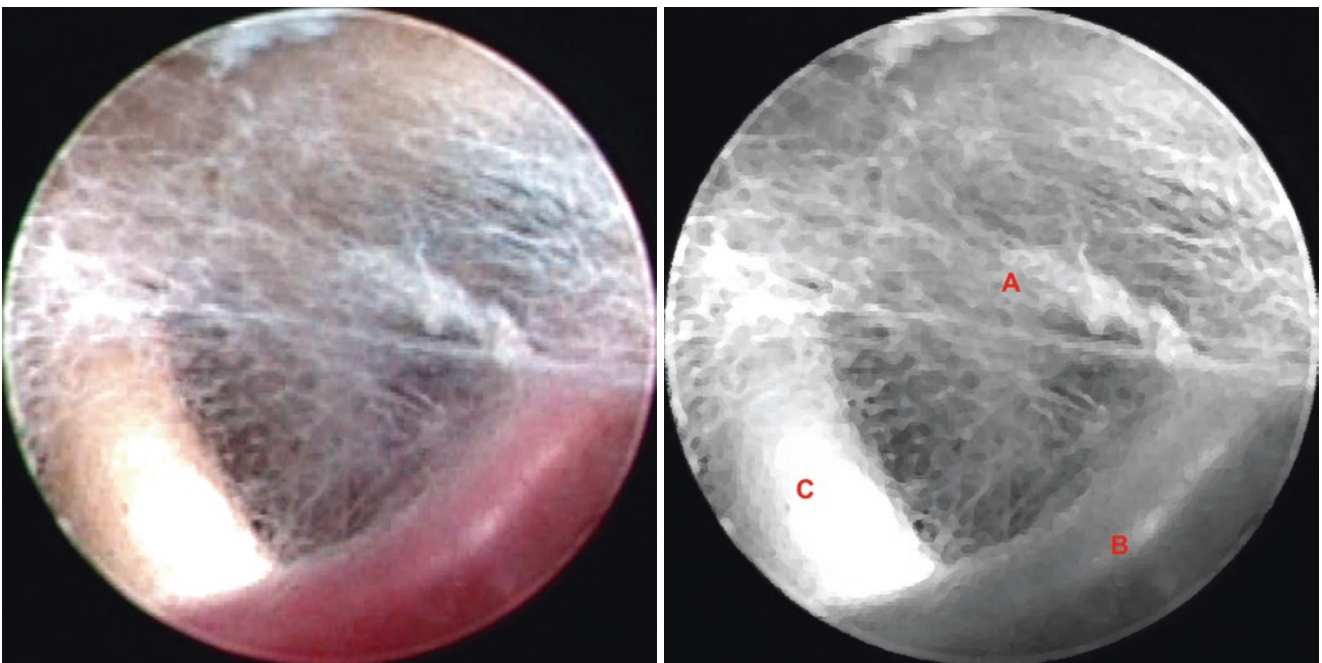


**Fig.5.7** Normal anatomy. (A) Membrane of Liliequist – diencephalic portion, (B) Left posterior cerebral artery (P1), (C) Left oculomotor nerve (CN III)

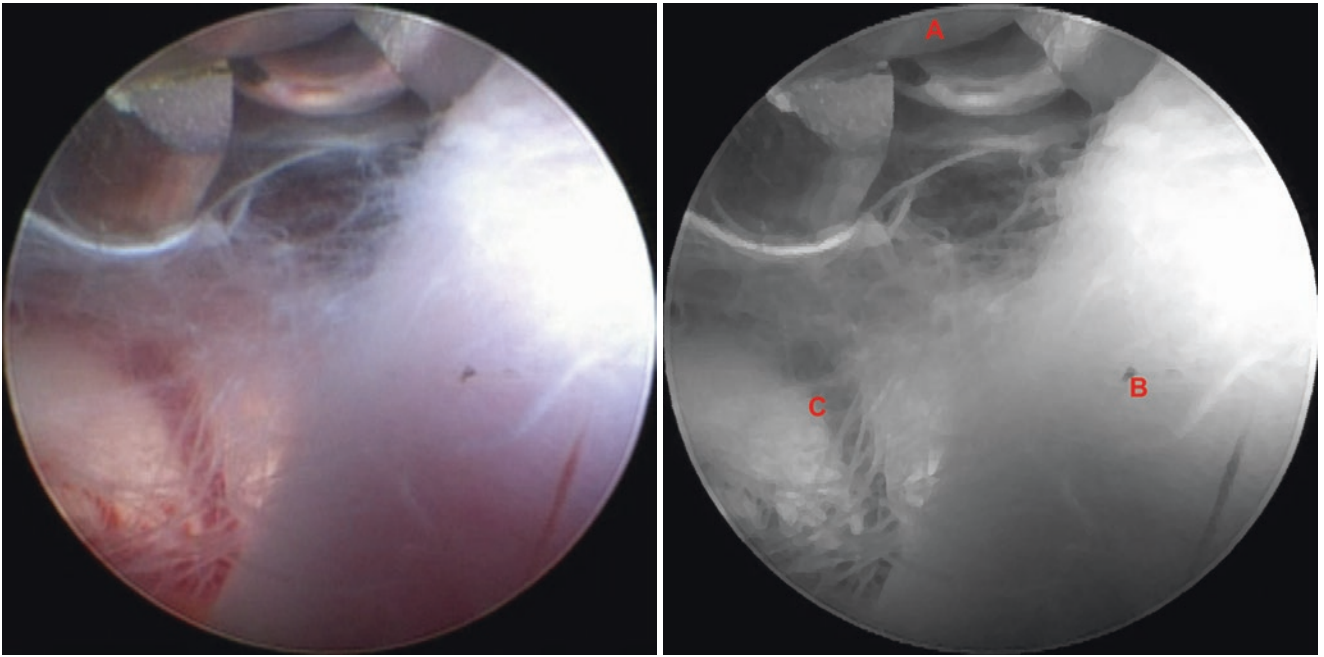


**Fig.5.8** Normal anatomy. (A) Membrane of Liliequist – diencephalic portion, fenestration by biopsy forceps, (B) Basilar artery, (C) Pons

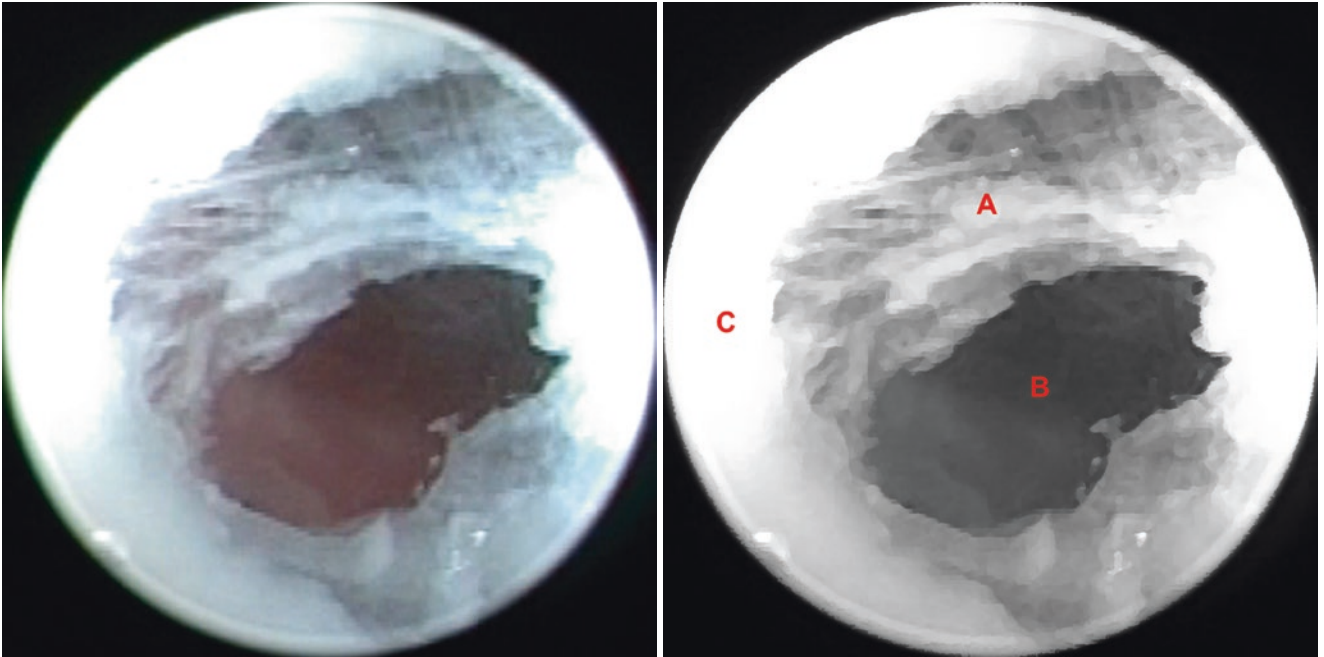


**Fig. 5.9** Normal anatomy. (A) Membrane of Liliequist – diencephalic portion, (B) Interpeduncular cistern, (C) Ependymal layer

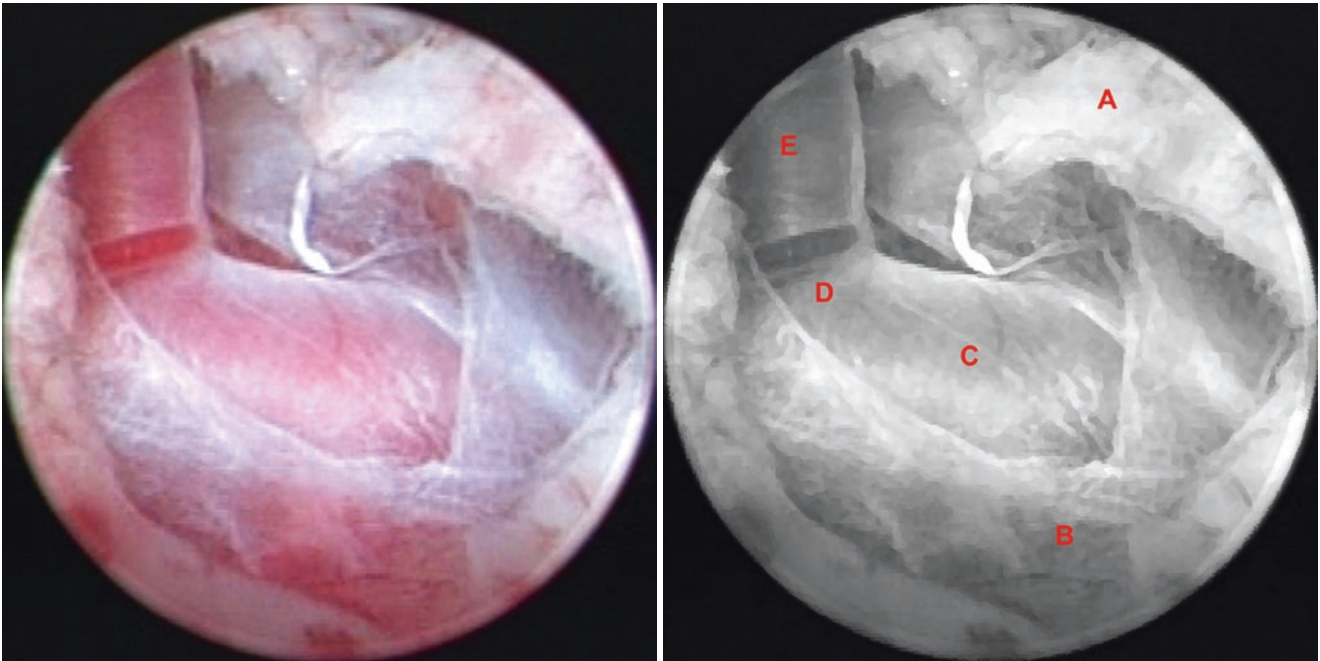


**Fig. 5.10** Normal anatomy. (A) Ependymal layer, (B) Membrane of Lilliequist – diencephalic portion, (C) Right posterior cerebral artery (P1), (D) Bifurcation of the basilar artery, (E) Left posterior cerebral artery (P1)

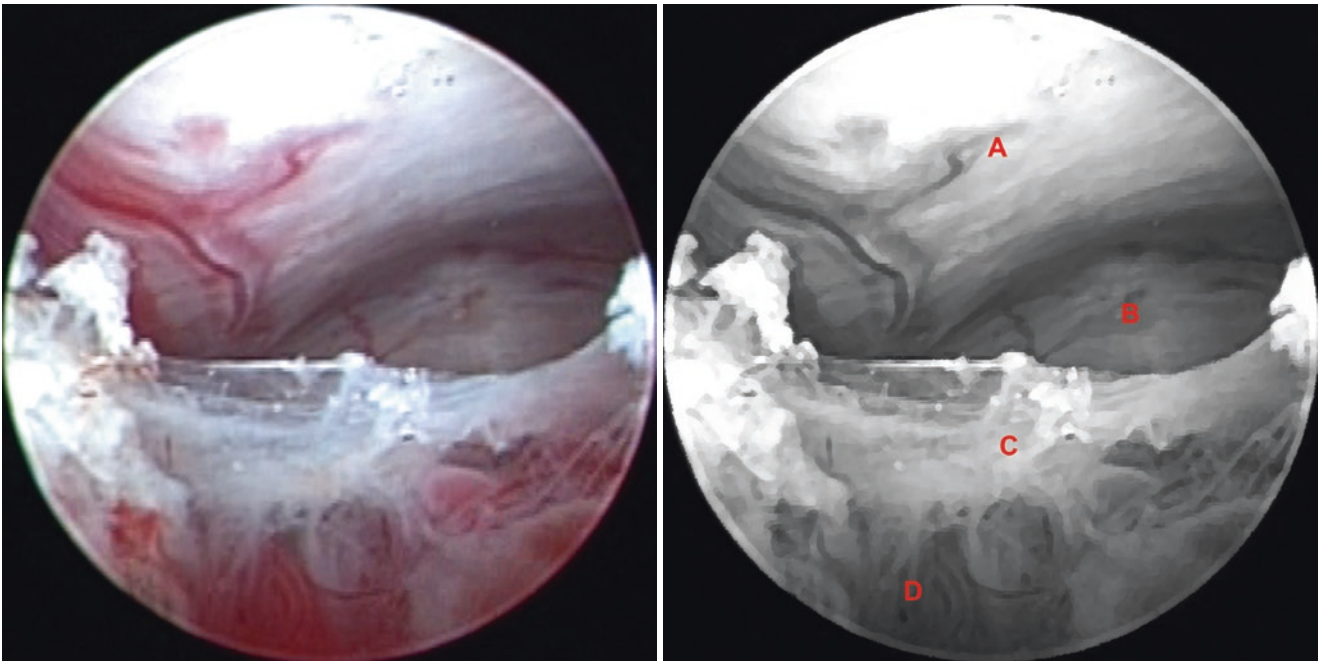


**Fig. 5.11** Normal anatomy. (A) Dorsum sellae, (B) Clivus, (C) Membrane of Lilliequist – diencephalic portion, (D) Thalamoperforating arteries

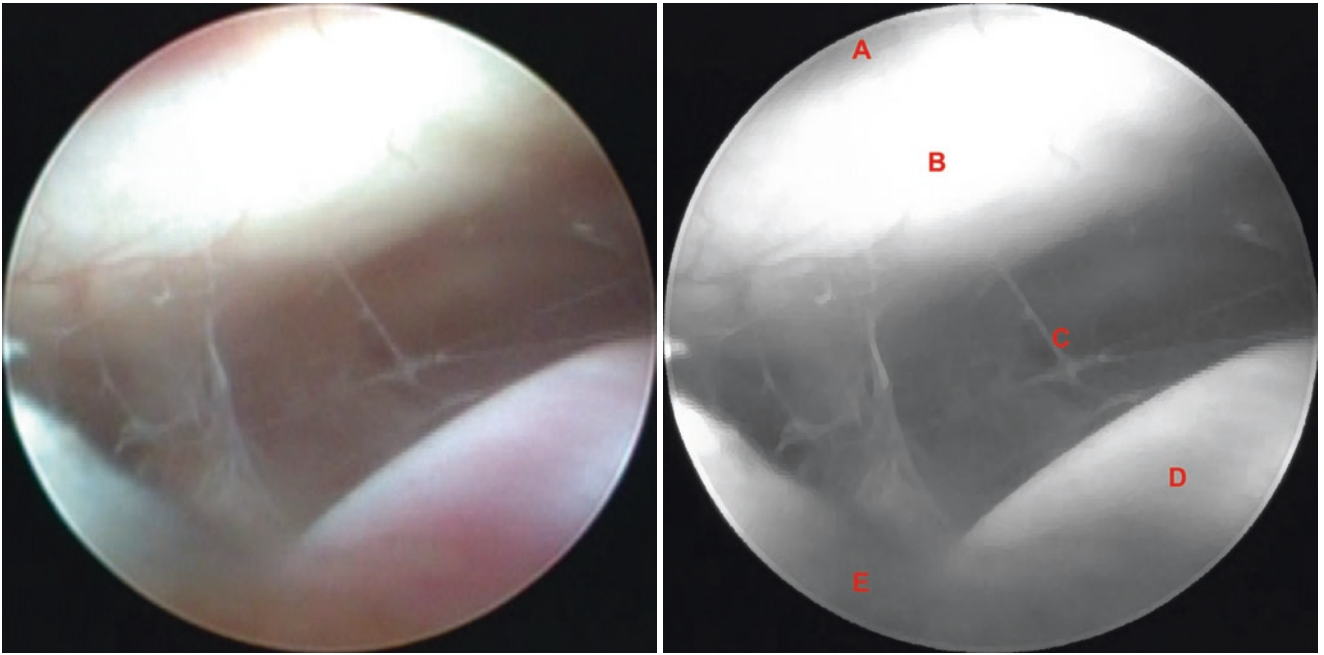


**Fig. 5.12** Normal anatomy. (A) Pituitary gland, (B) Dorsum sellae, (C) Prepontine cistern, (D) Basilar artery, (E) Membrane of Liliequist – diencephalic portion

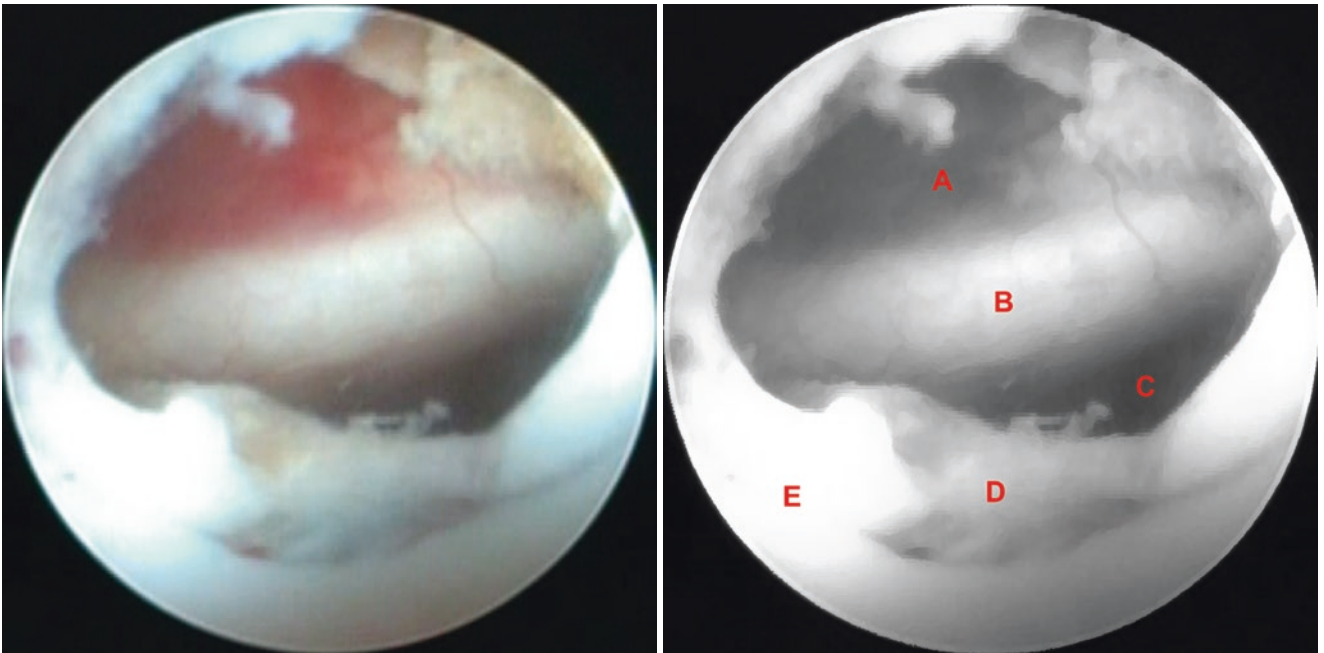


**Fig. 5.13** Normal anatomy. (A) Pituitary gland, (B) Dorsum sellae, (C) Prepontine cistern, (D) Membrane of Liliequist – diencephalic portion, (E) Ependymal layer

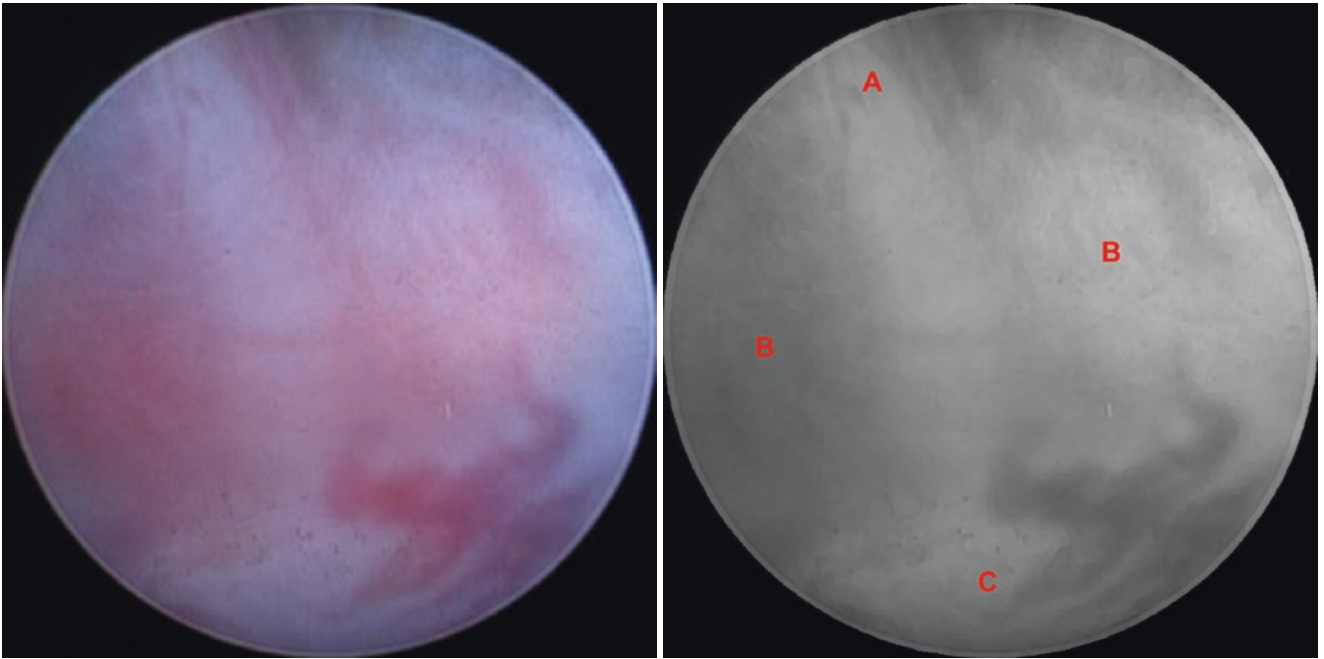


**Fig. 5.14** Normal anatomy. (A) Pituitary stalk, (B) Pituitary gland, (C) Dorsum sellae

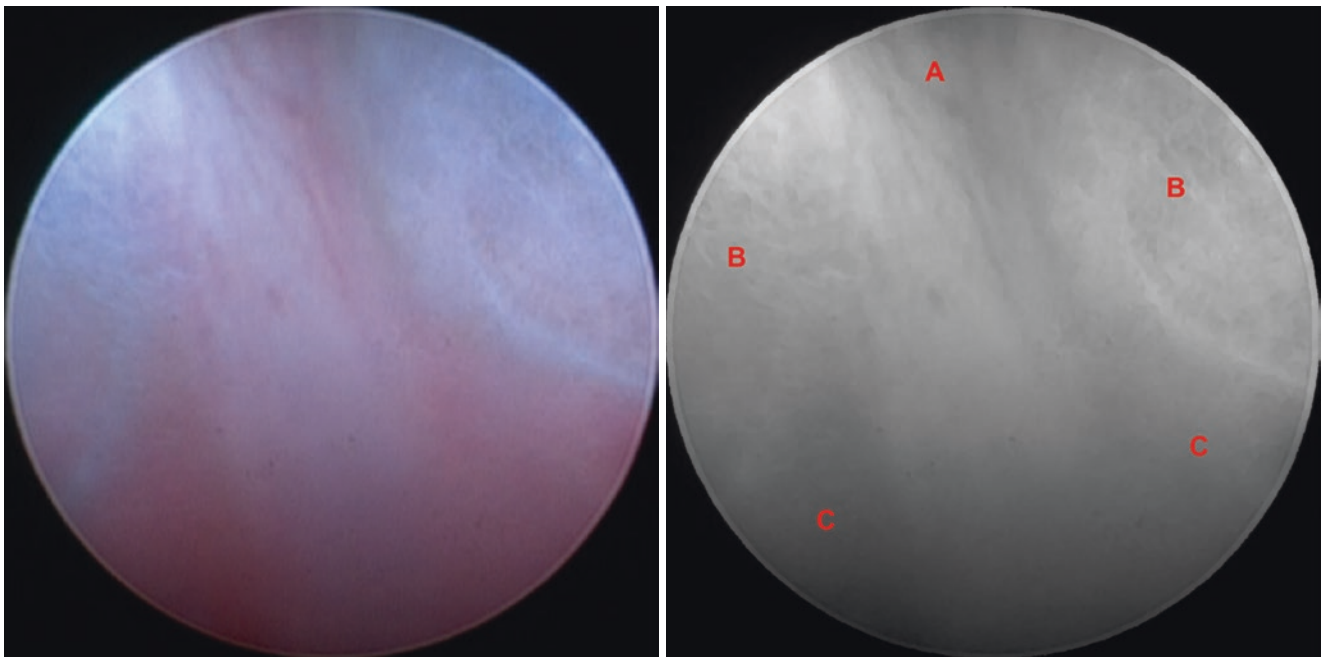


**Fig. 5.15** Normal anatomy. (A) Pituitary stalk, (B) Sellar diaphragm, (C) Pituitary gland

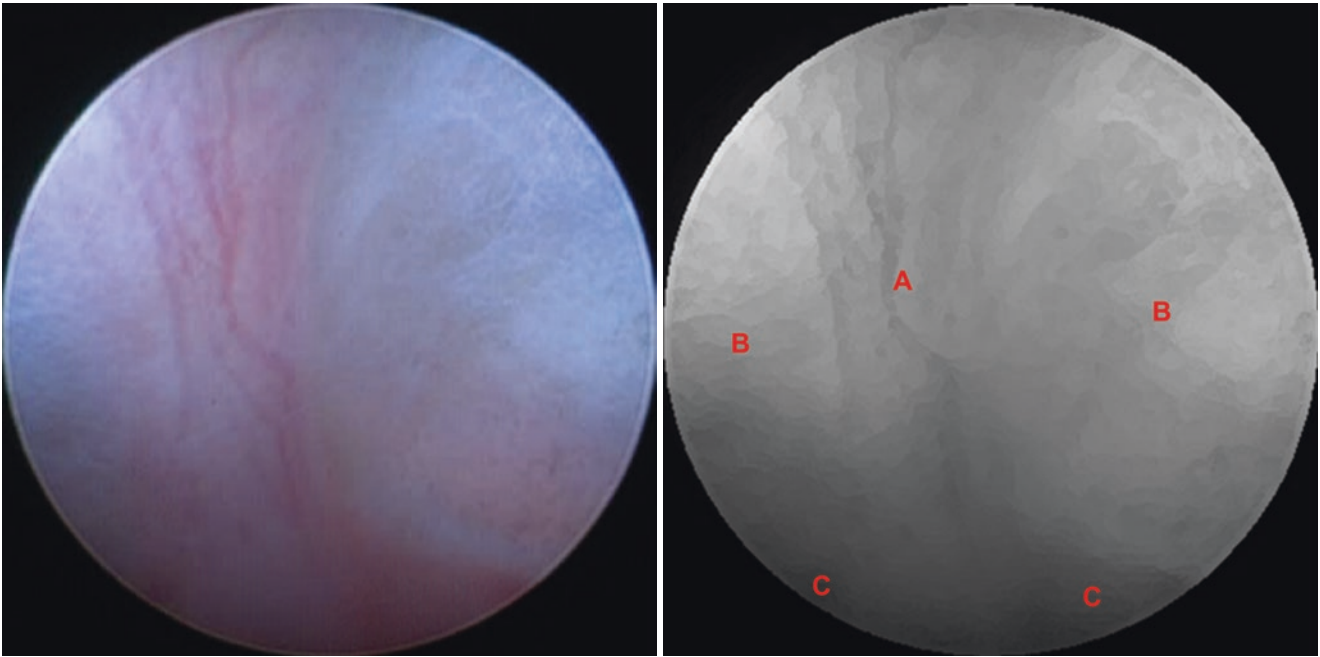


**Fig. 5.16** Normal anatomy. (A) Pituitary stalk, (B) Sellar diaphragm, (C) Pituitary gland

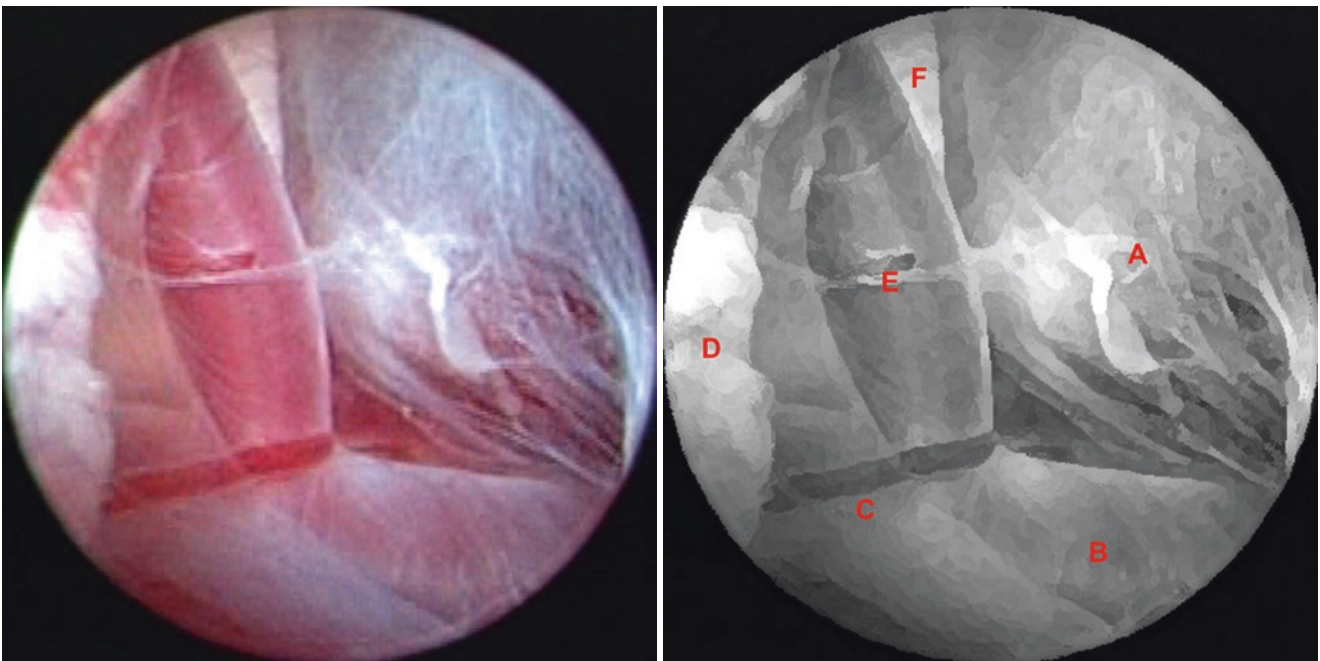


**Fig. 5.17** Normal anatomy. (A) Membrane of Liliequist – mesencephalic portion, (B) Right posterior cerebral artery (P1), (C) Bifurcation of the basilar artery under membrane of Liliequist – diencephalic portion, (D) Ependymal layer, (E) Left posterior cerebral artery (P1), (F) Left oculomotor nerve (CN III)

tion, (D) Ependymal layer, (E) Left posterior cerebral artery (P1), (F) Left oculomotor nerve (CN III)



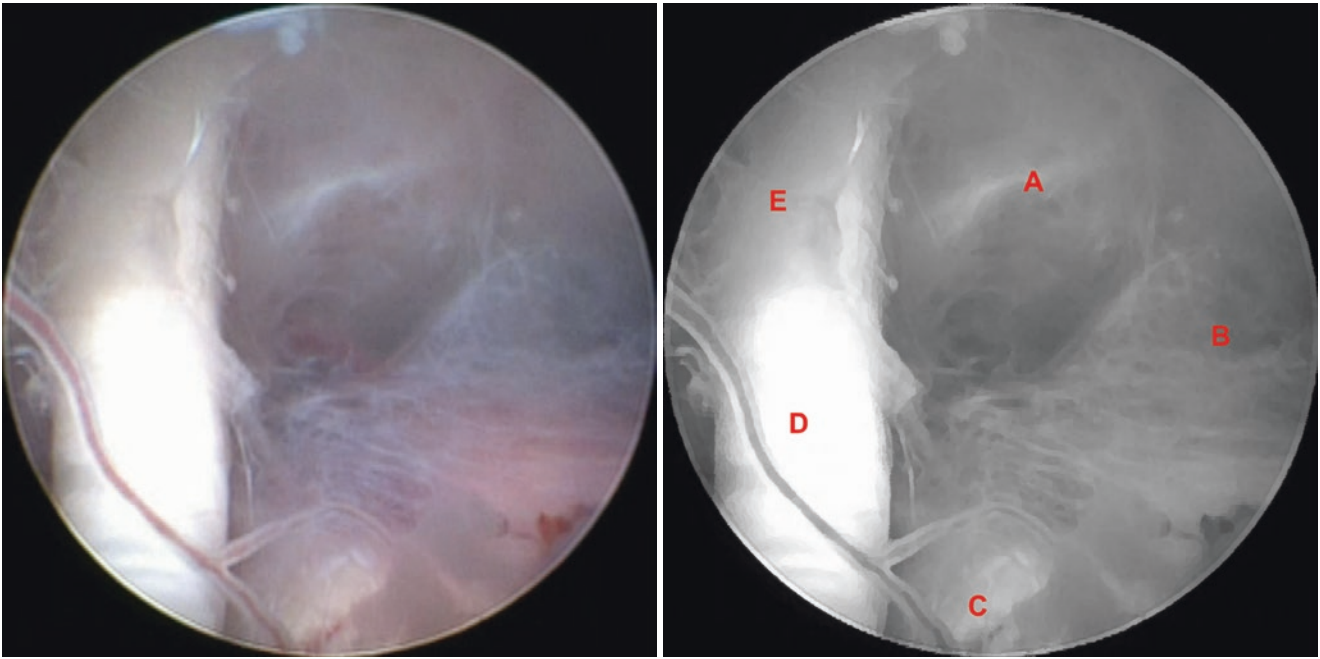


**Fig. 5.18** Normal anatomy. (A) Clivus under membrane of Liliequist, (B) Membrane of Liliequist – mesencephalic portion, (C) Pons, (D) Left oculomotor nerve (CN III), (E) Membrane of Liliequist – diencephalic portion

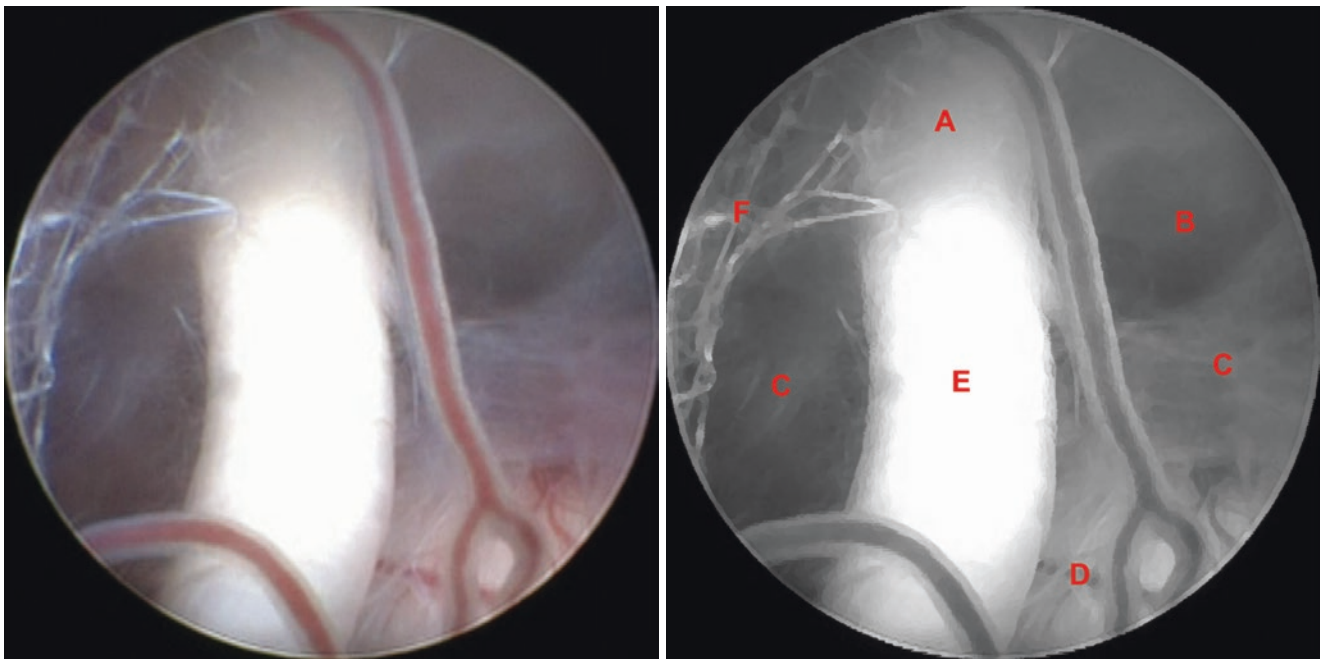


**Fig. 5.19** Normal anatomy. (A) Membrane of Liliequist – diencephalic portion, (B) Prepontine cistern, (C) Membrane of Liliequist – mesencephalic portion, (D) Pons, (E) Left oculomotor nerve (CN III), (F) Arachnoid trabeculae

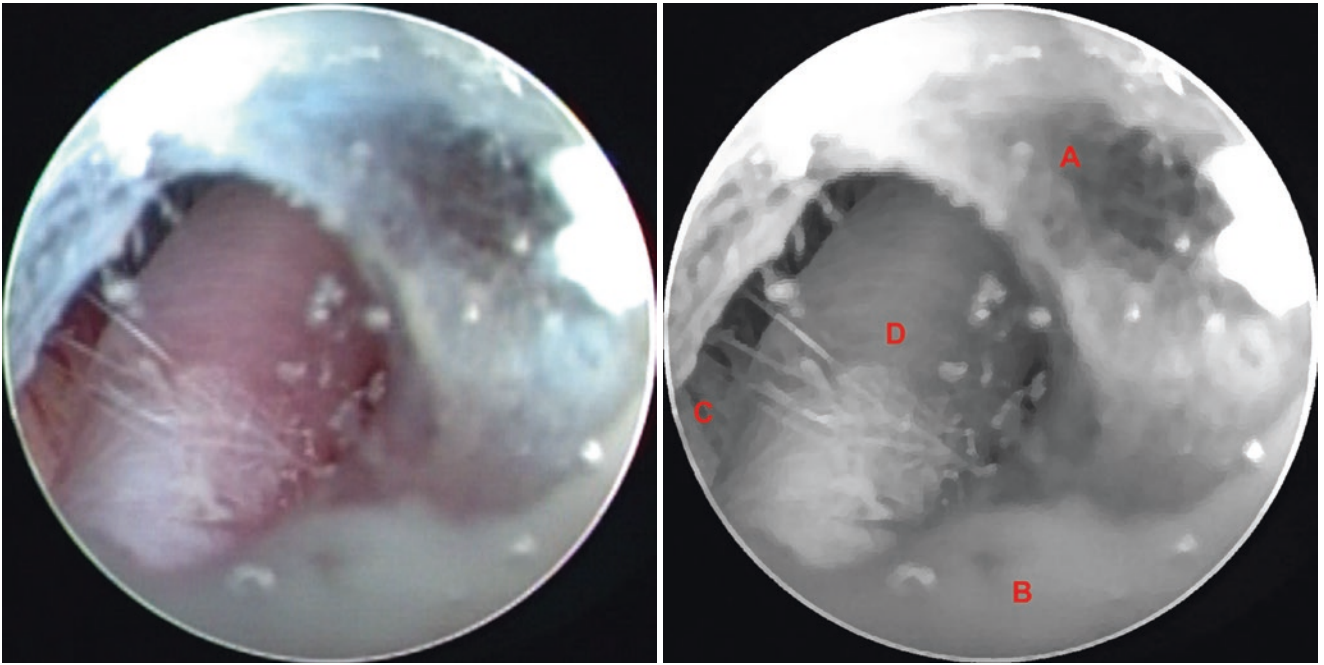


**Fig. 5.20** Normal anatomy. (A) Membrane of Liliequist – diencephalic portion, (B) Ependymal layer, (C) Pons, (D) Basilar artery

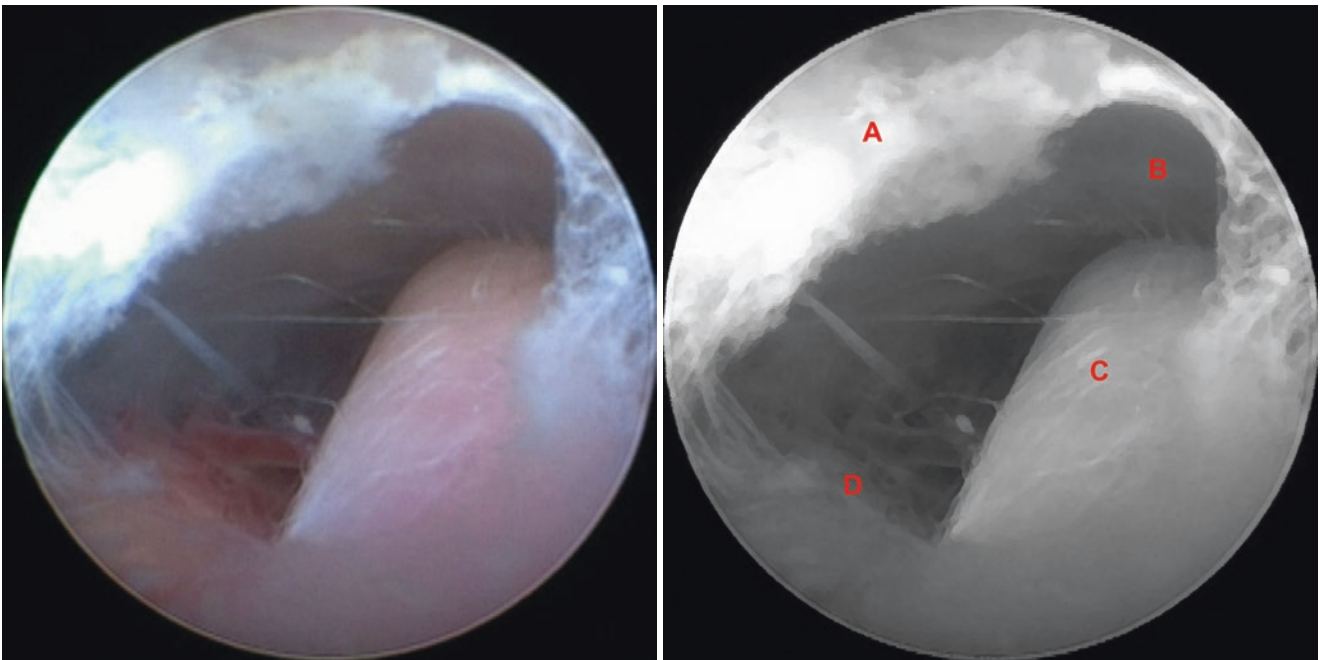


**Fig. 5.21** Normal anatomy. (A) Membrane of Liliequist – diencephalic portion, (B) Clivus, (C) Basilar artery, (D) Pons

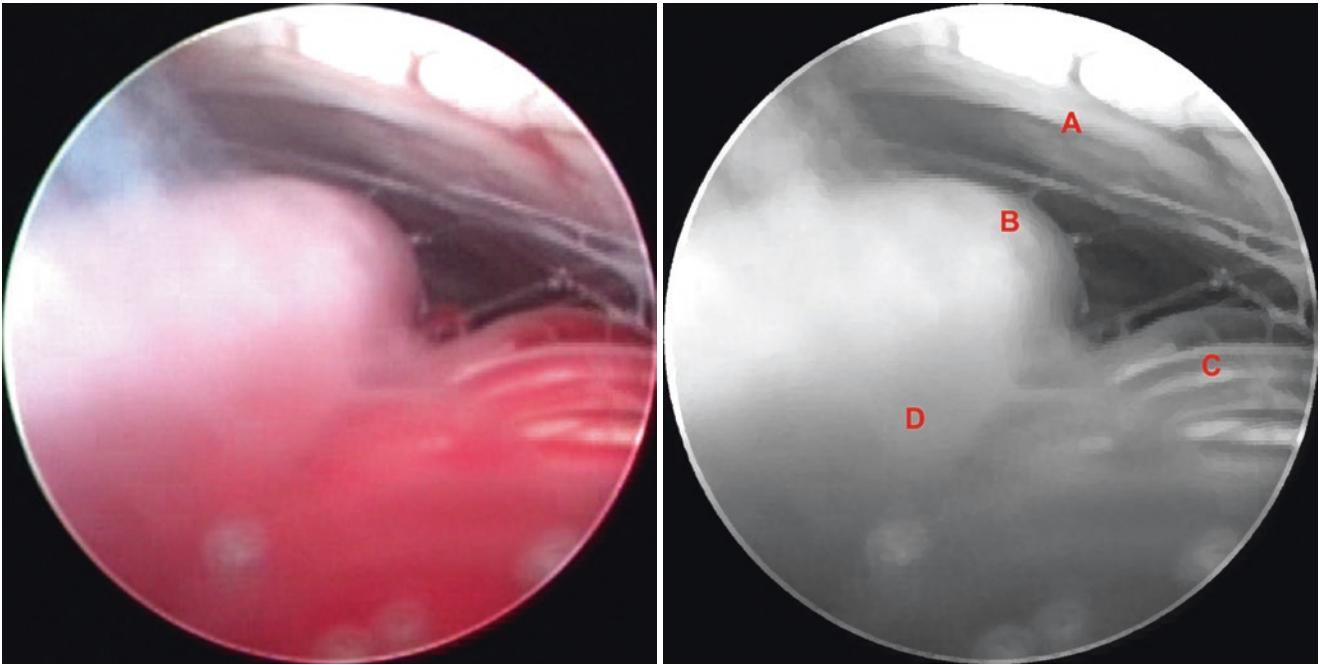


**Fig. 5.22** Normal anatomy. (A) Clivus, (B) Basilar artery, (C) Pontine arterial branches, (D) Membrane of Liliequist – diencephalic portion

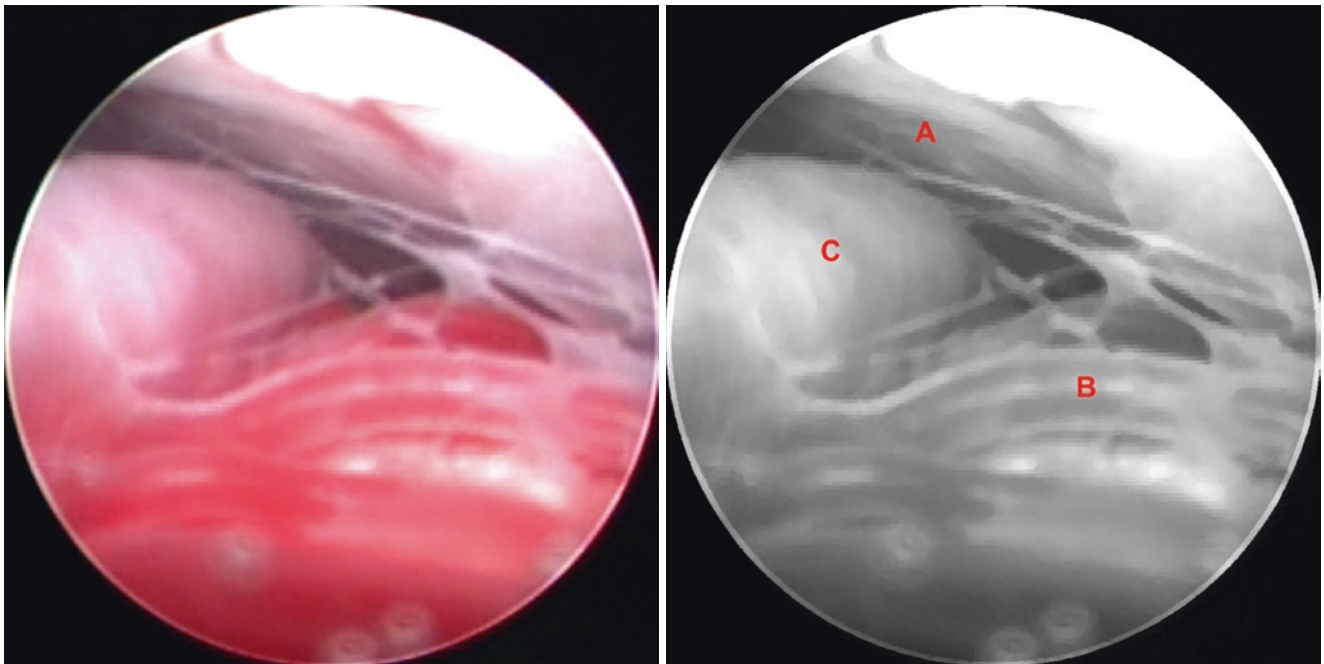


**Fig. 5.23** Normal anatomy. (A) Clivus, (B) Pontine arterial branches, (C) Basilar artery

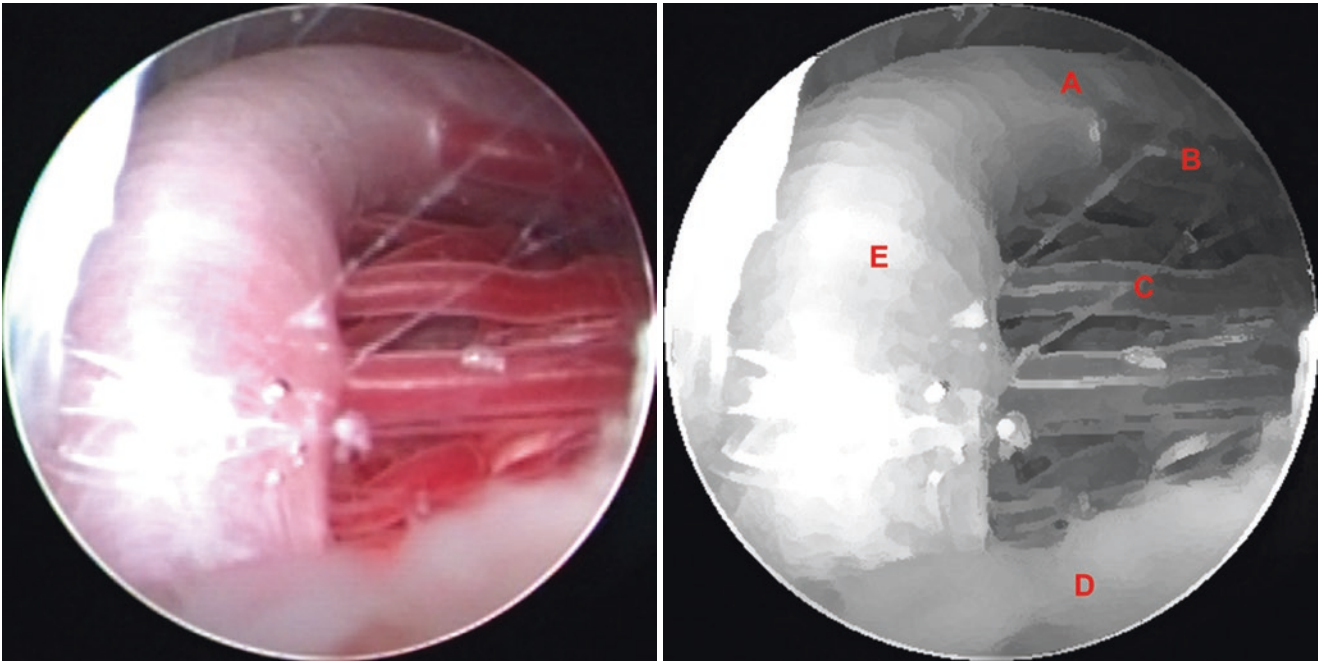


**Fig. 5.24** Normal anatomy. (A) Right vertebral artery, (B) Right posterior inferior cerebellar artery (PICA), (C) Pontine arterial branches, (D) Ependymal layer, (E) Basilar artery

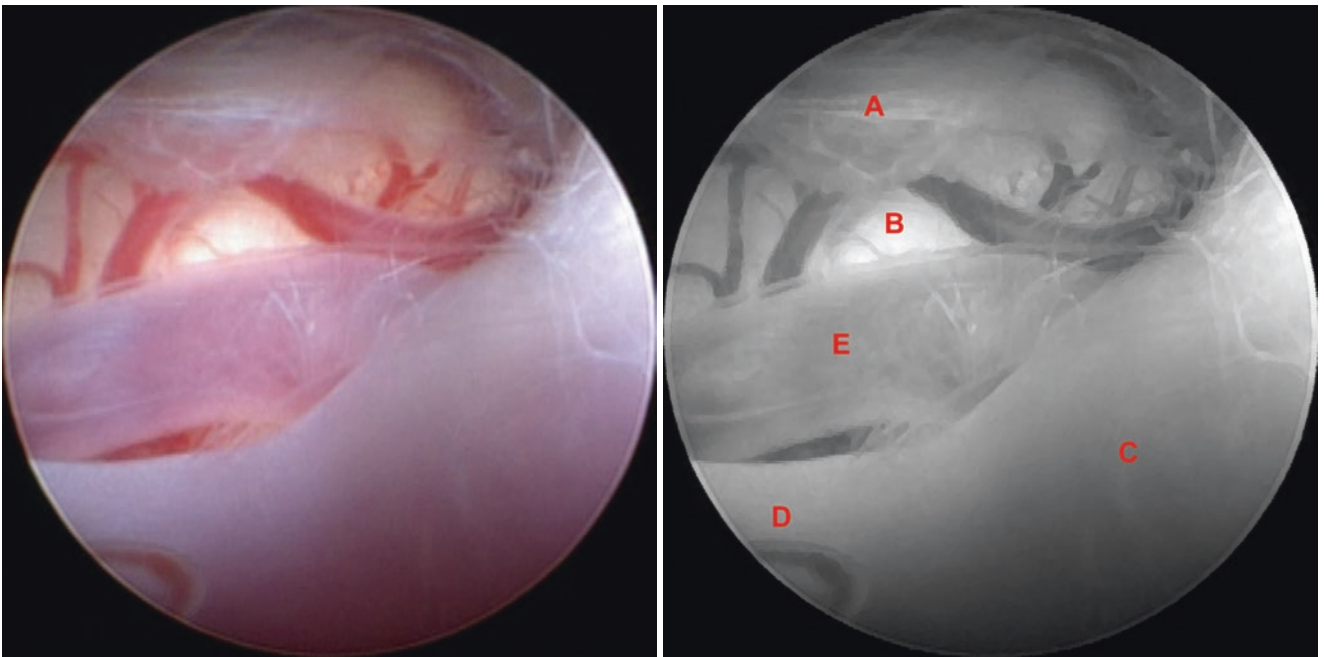


**Fig. 5.25** Normal anatomy. (A) Membrane of Lilliequist – mesencephalic portion, (B) Pons, (C) Basilar artery, (D) Left posterior cerebral artery (P1), (E) Left superior cerebellar artery

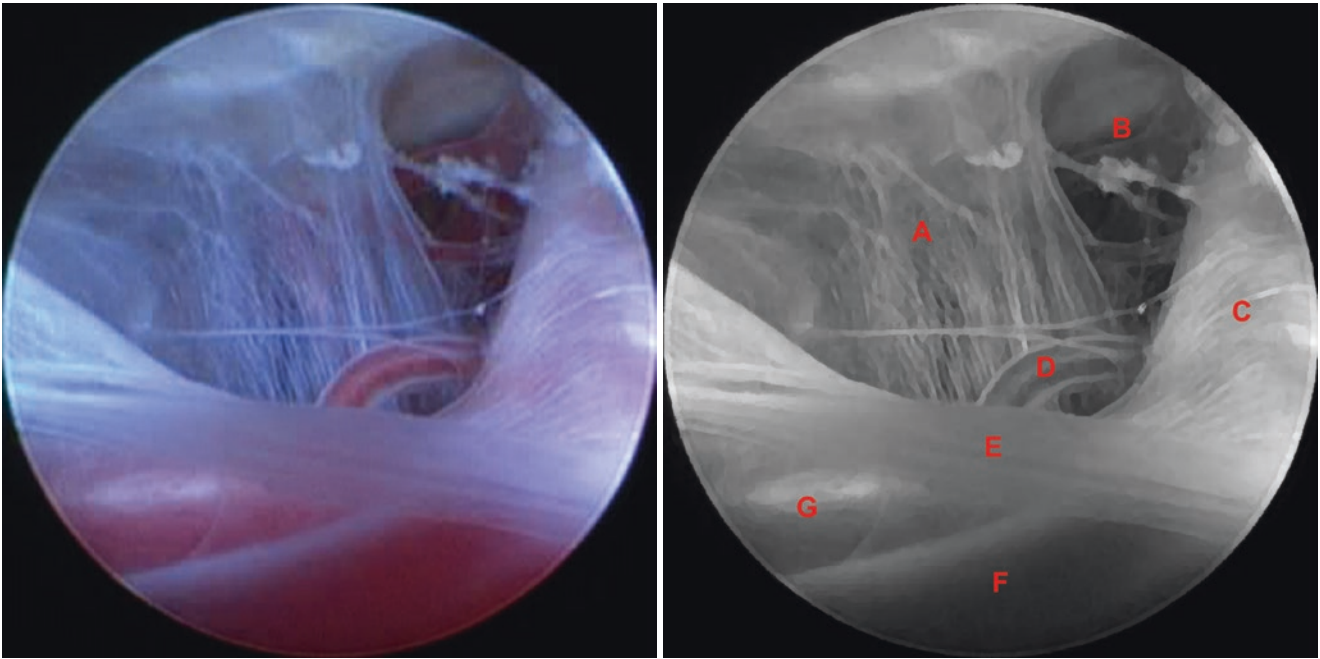


**Fig. 5.26** Normal anatomy. (A) Membrane of Liliequist – mesencephalic portion, (B) Prepontine cistern, (C) Basilar artery, (D) Pontine arterial branch, (E) Membrane of Liliequist – diencephalic portion, (F) Left posterior cerebral artery (P1), (G) Left superior cerebellar artery

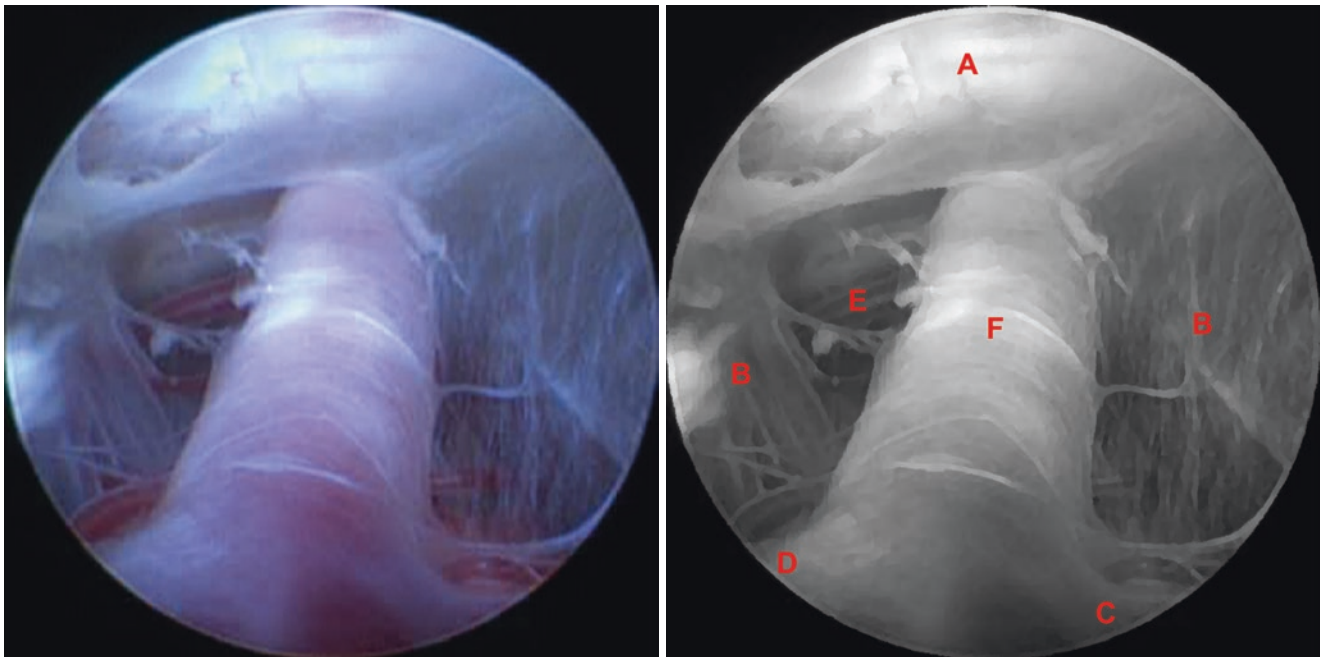


**Fig. 5.27** Normal anatomy. (A) Clivus, (B) Membrane of Liliequist – mesencephalic portion, (C) Right superior cerebellar artery, (D) Left superior cerebellar artery, (E) Left labyrinthine artery, (F) Basilar artery

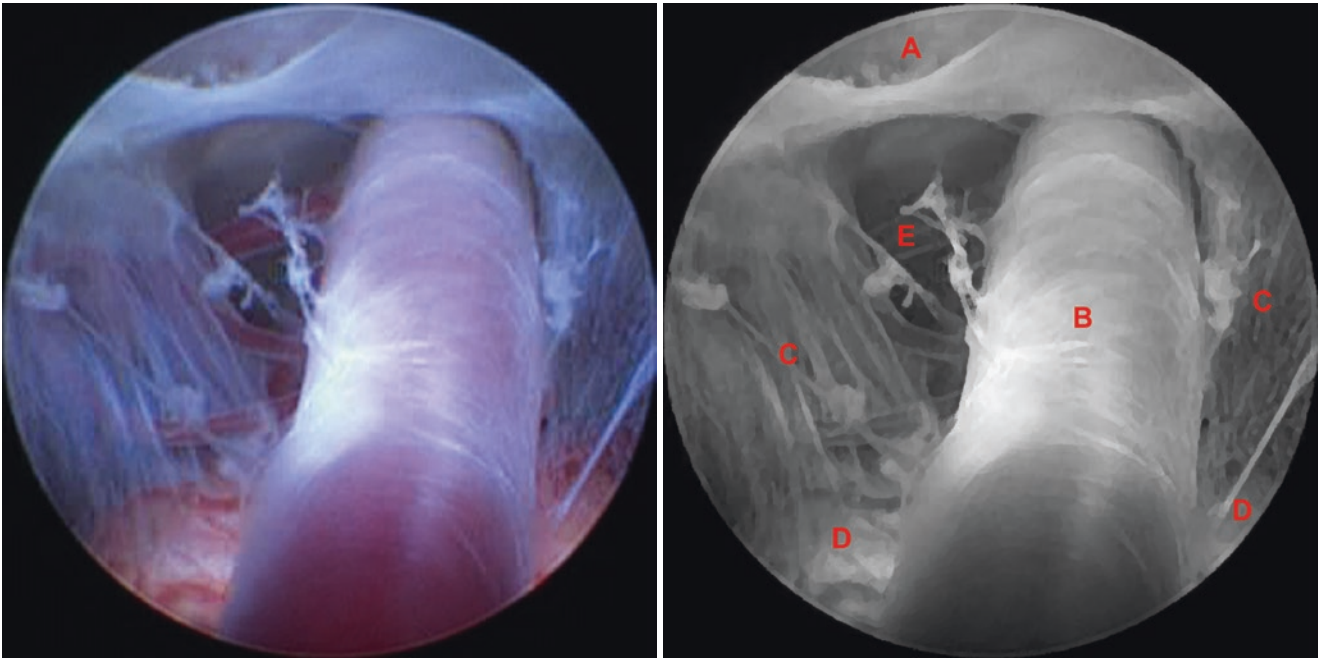


**Fig. 5.28** Normal anatomy. (A) Clivus, (B) Basilar artery, (C) Membrane of Lilliequist – mesencephalic portion, (D) Pons, (E) Left labyrinthine artery

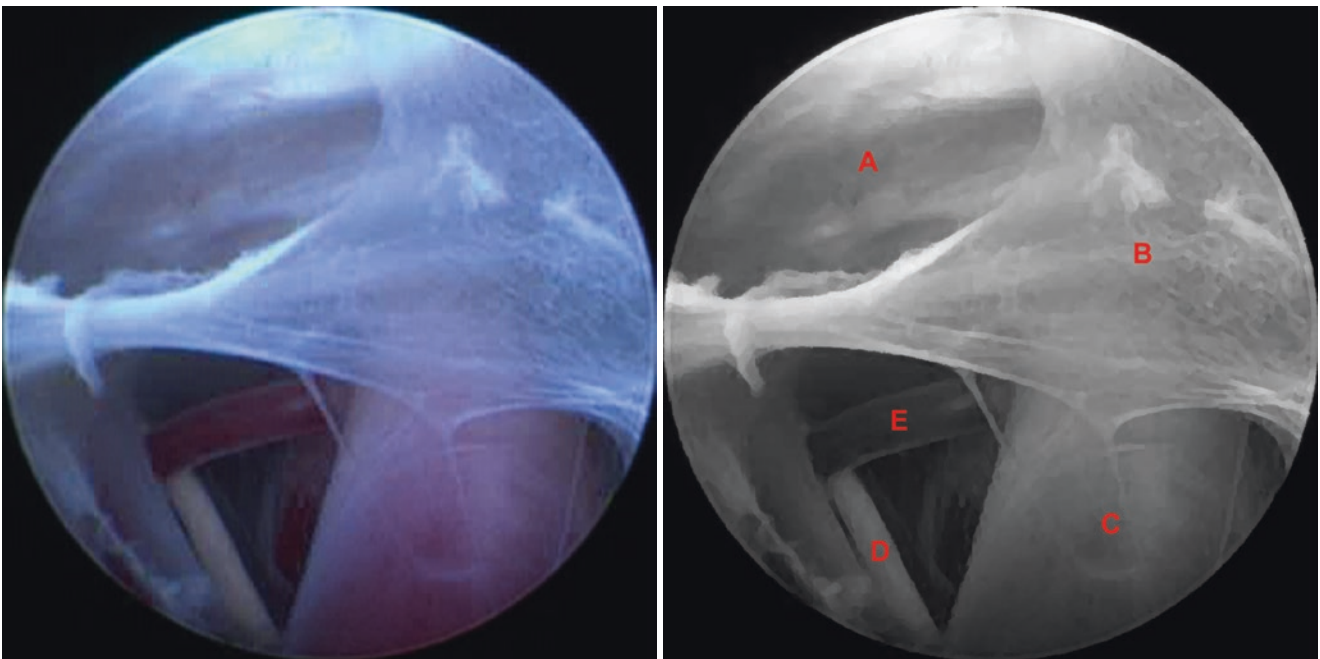


**Fig. 5.29** Normal anatomy. (A) Clivus, (B) Membrane of Lilliequist – mesencephalic portion, (C) Basilar artery, (D) Left abducens nerve (CN VI), (E) Left anterior inferior cerebellar artery (AICA)

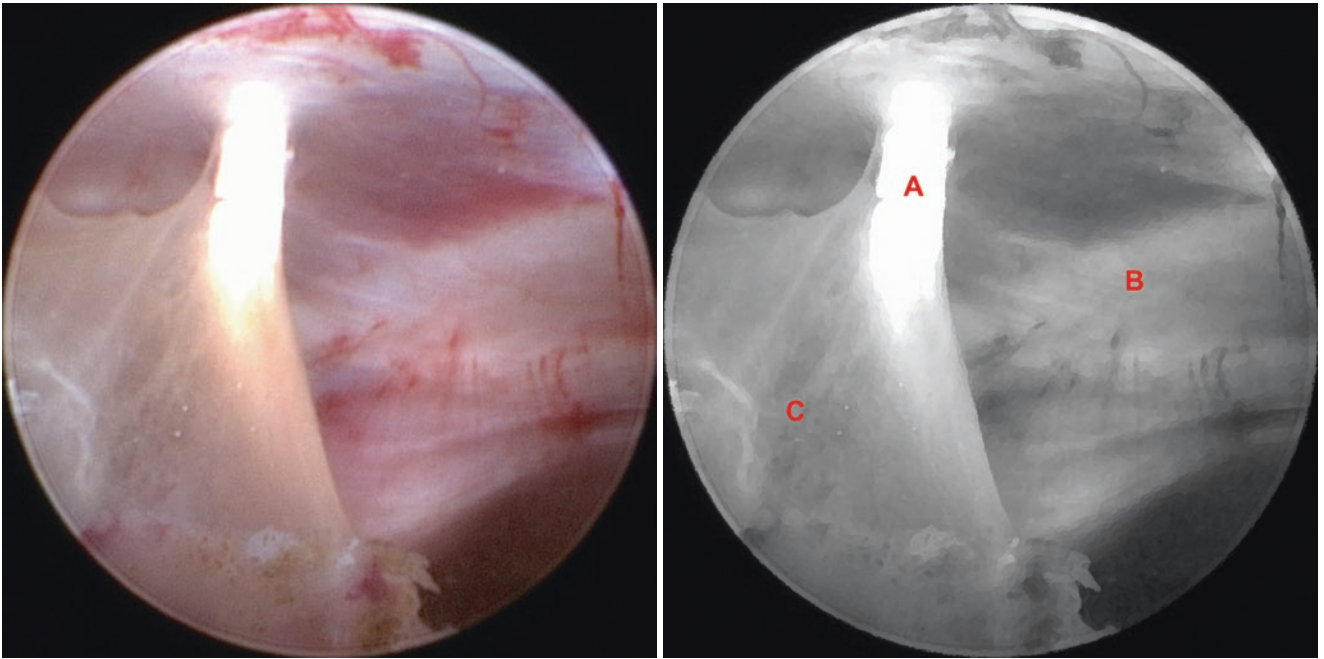


**Fig. 5.30** Normal anatomy. (A) Left abducens nerve (CN VI), (B) Clivus, (C) Membrane of Liliequist – mesencephalic portion

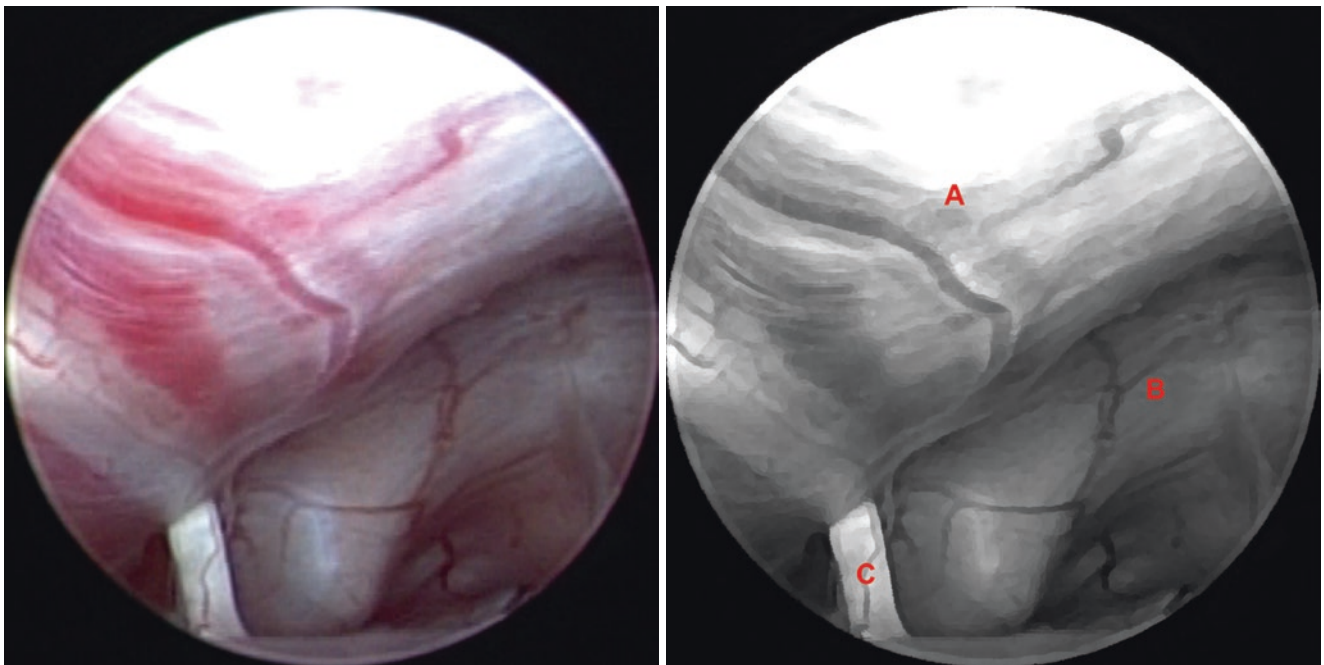


**Fig. 5.31** Normal anatomy. (A) Dorsum sellae, (B) Clivus, (C) Left abducens nerve (CN VI) entering the Dorello canal

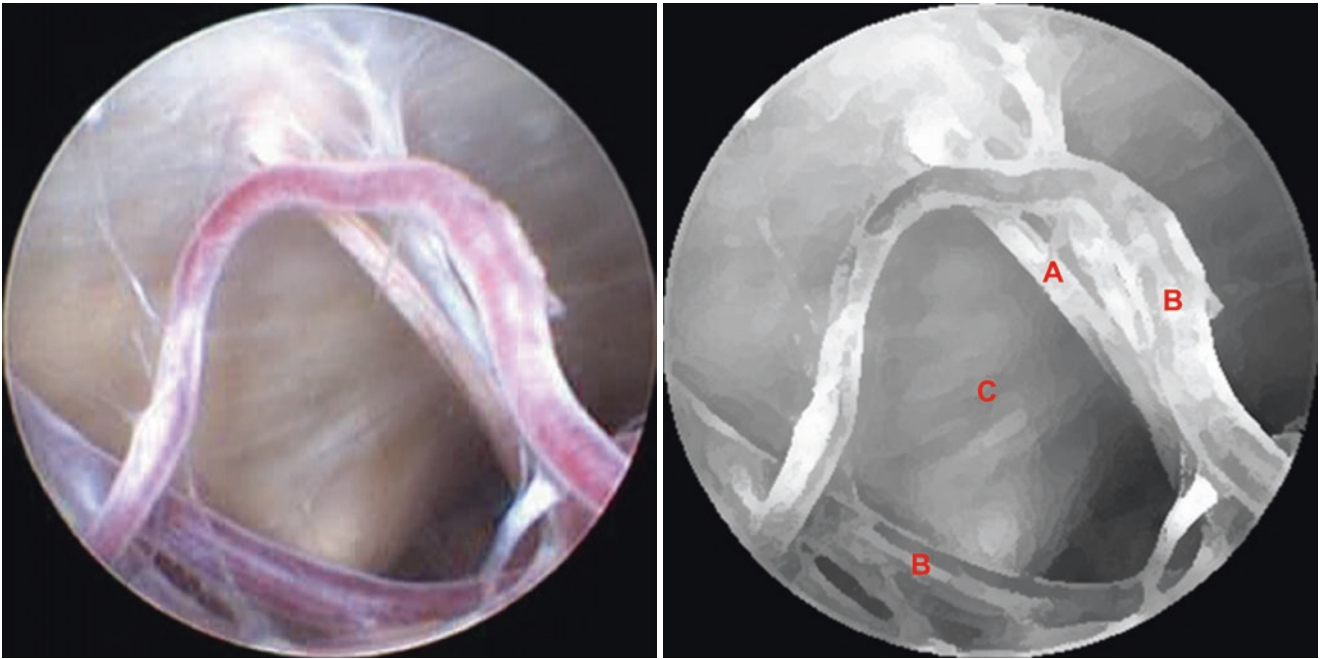


**Fig. 5.32** Normal anatomy. (A) Left abducens nerve (CN VI), (B) Pontine veins, (C) Clivus

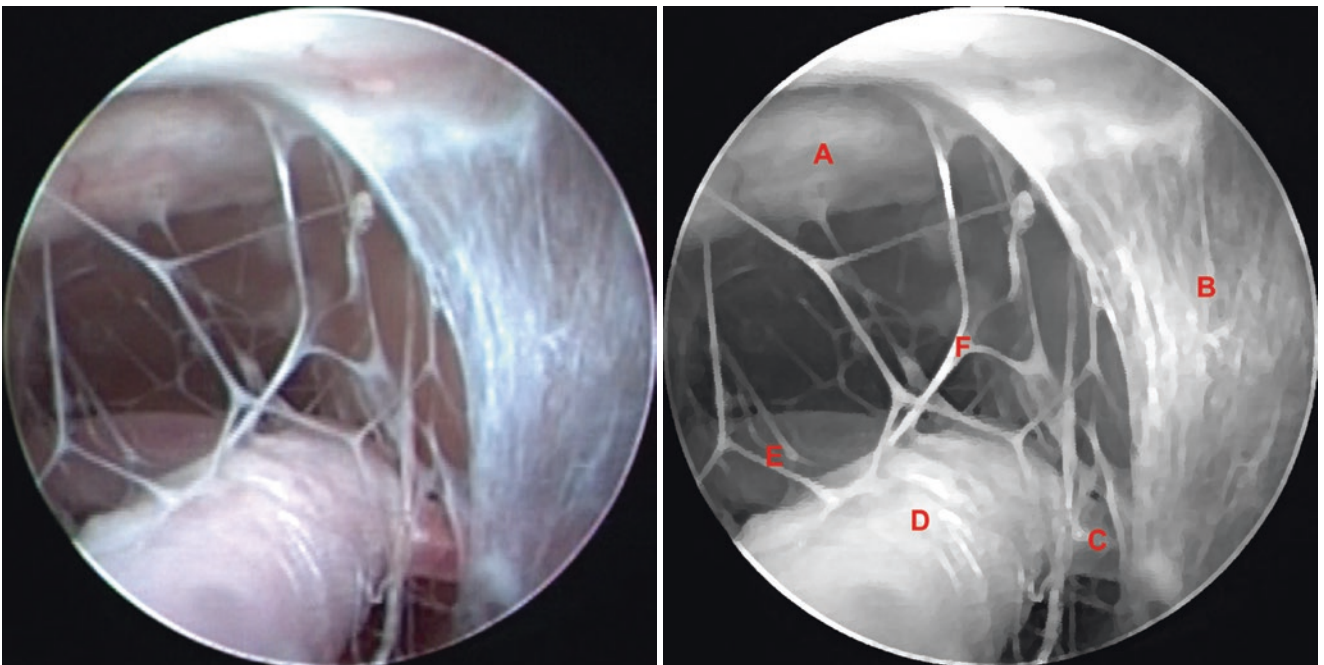


**Fig. 5.33** Normal anatomy. (A) Clivus, (B) Membrane of Liliequist – mesencephalic portion, (C) Right vertebral artery, (D) Basilar artery, (E) Left vertebral artery, (F) Arachnoid trabeculae



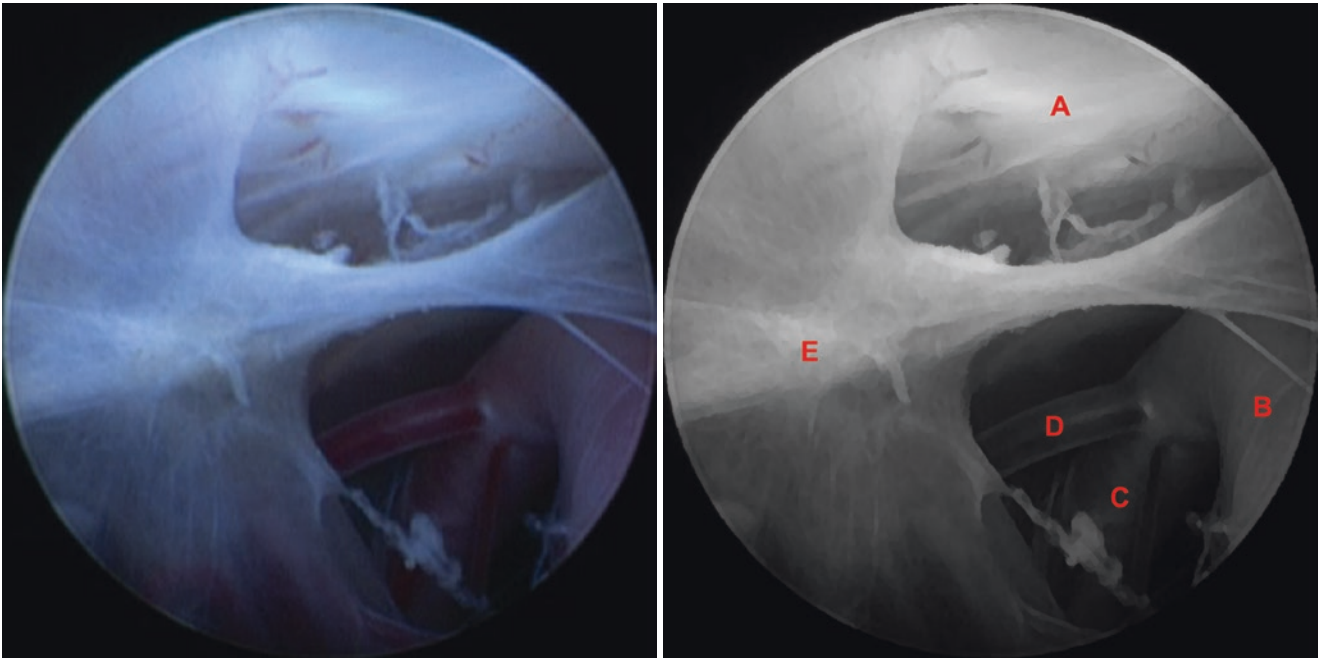


**Fig. 5.34** Normal anatomy. (A) Clivus, (B) Basilar artery, (C) Left vertebral artery, (D) Left posterior inferior cerebellar artery (PICA), (E) Membrane of Liliequist – mesencephalic portion

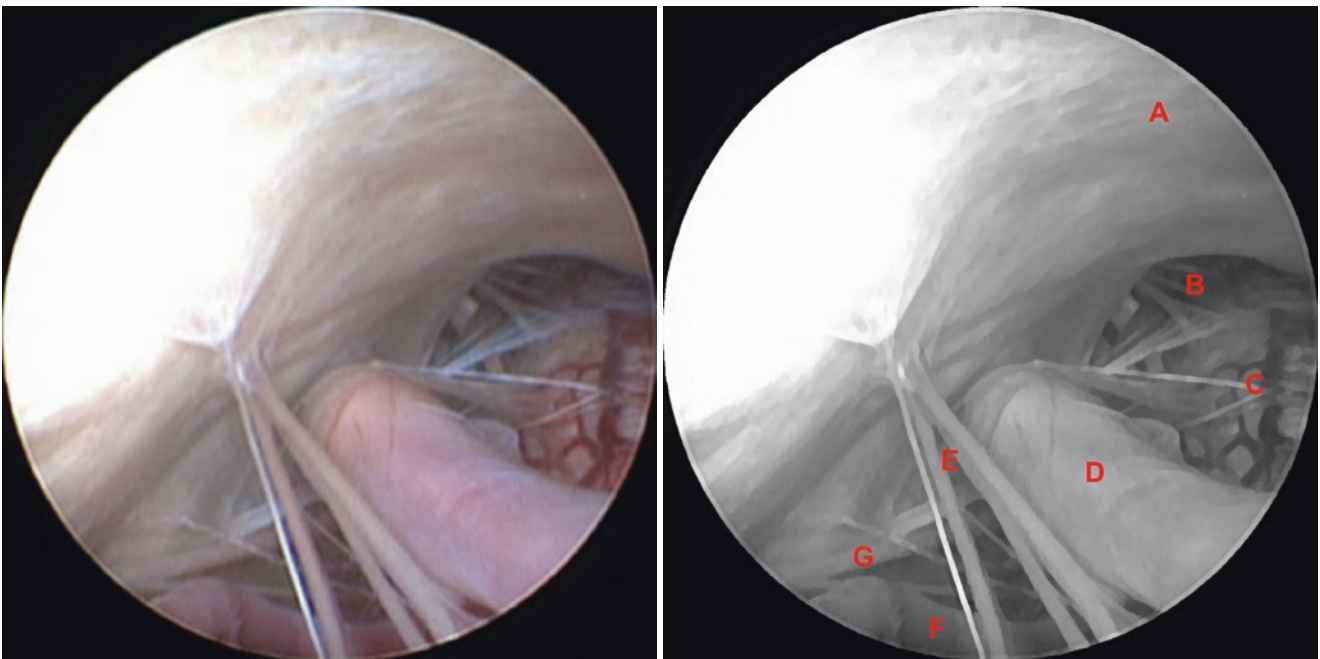


**Fig. 5.35** Normal anatomy. (A) Clivus, (B) Foramen magnum, (C) Medulla oblongata, (D) Left vertebral artery, (E) Left hypoglossal nerve (CN XII), (F) Left posterior inferior cerebellar artery (PICA), (G) Left accessory nerve (CN XI)

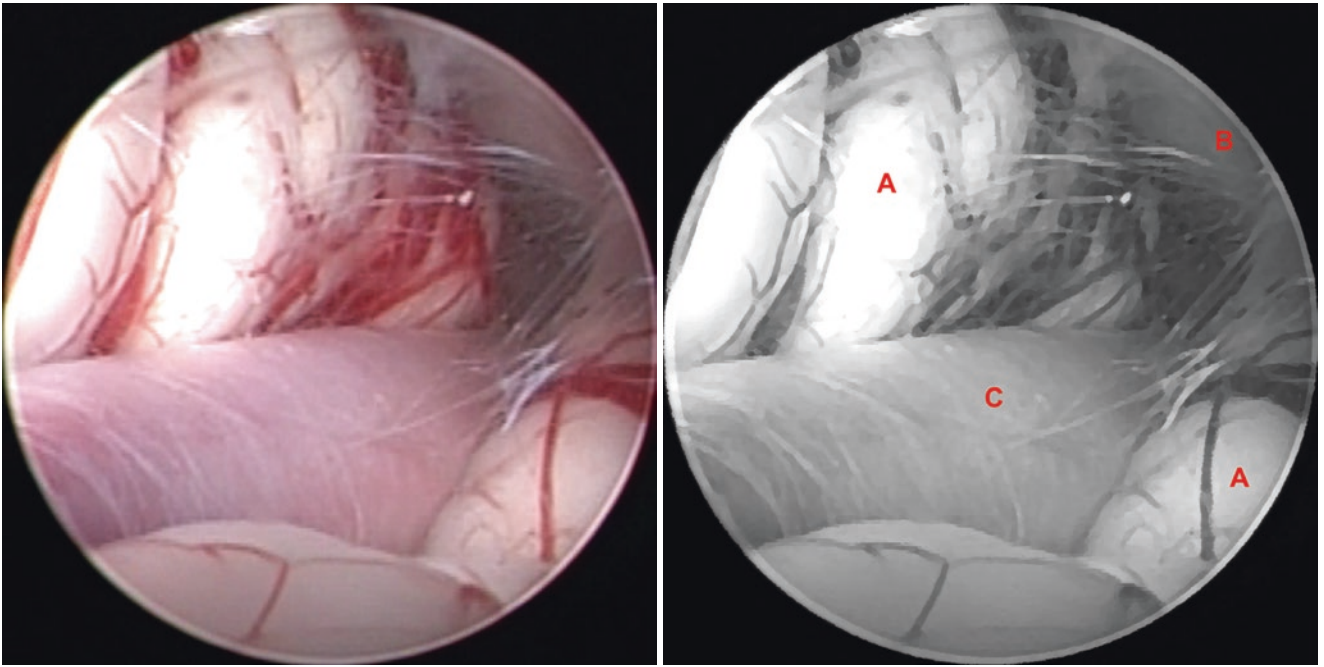


**Fig. 5.36** Abnormal anatomy – intrinsic brainstem tumor (A), pons, (B) clivus, (C) basilar artery

### 5.3 Illustrative Case: Racemose Neurocysticercosis

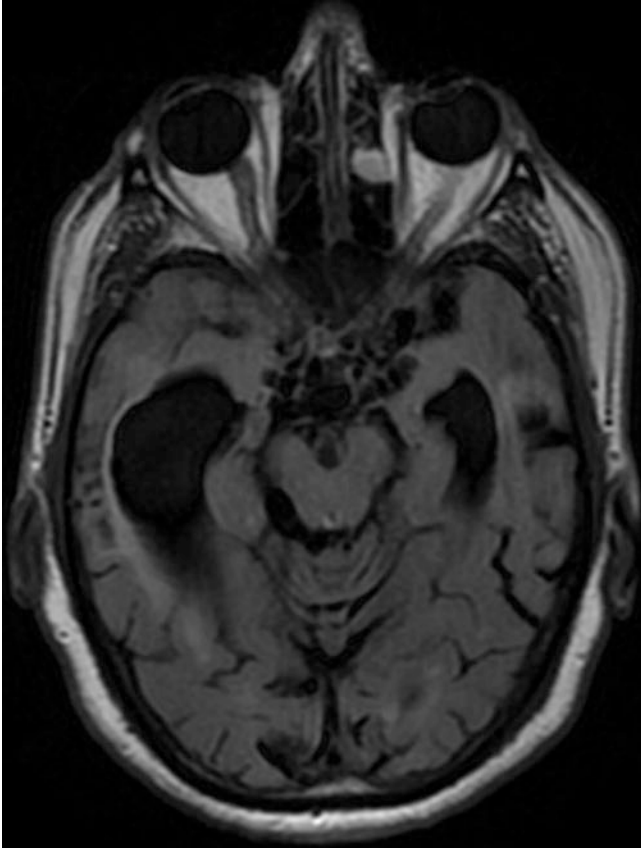


**Fig. 5.37** Axial T1-weighted magnetic resonance imaging (MRI) showing racemose cysts anterior to mesencephalon

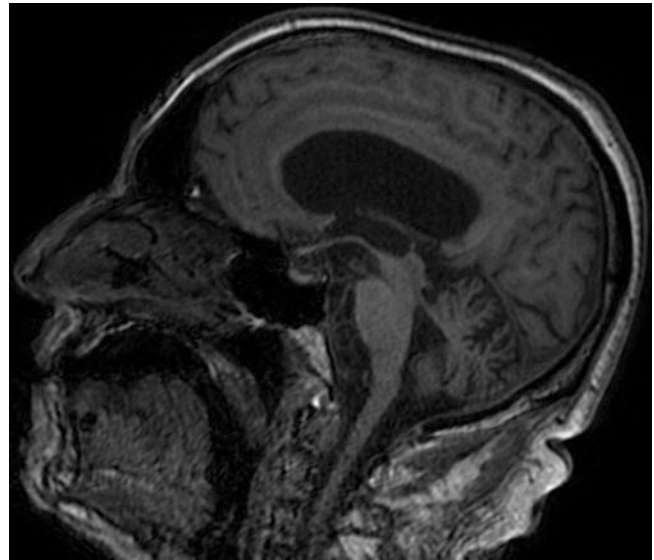


**Fig. 5.38** Sagittal T1-weighted MRI showing racemose cysts anterior to brainstem

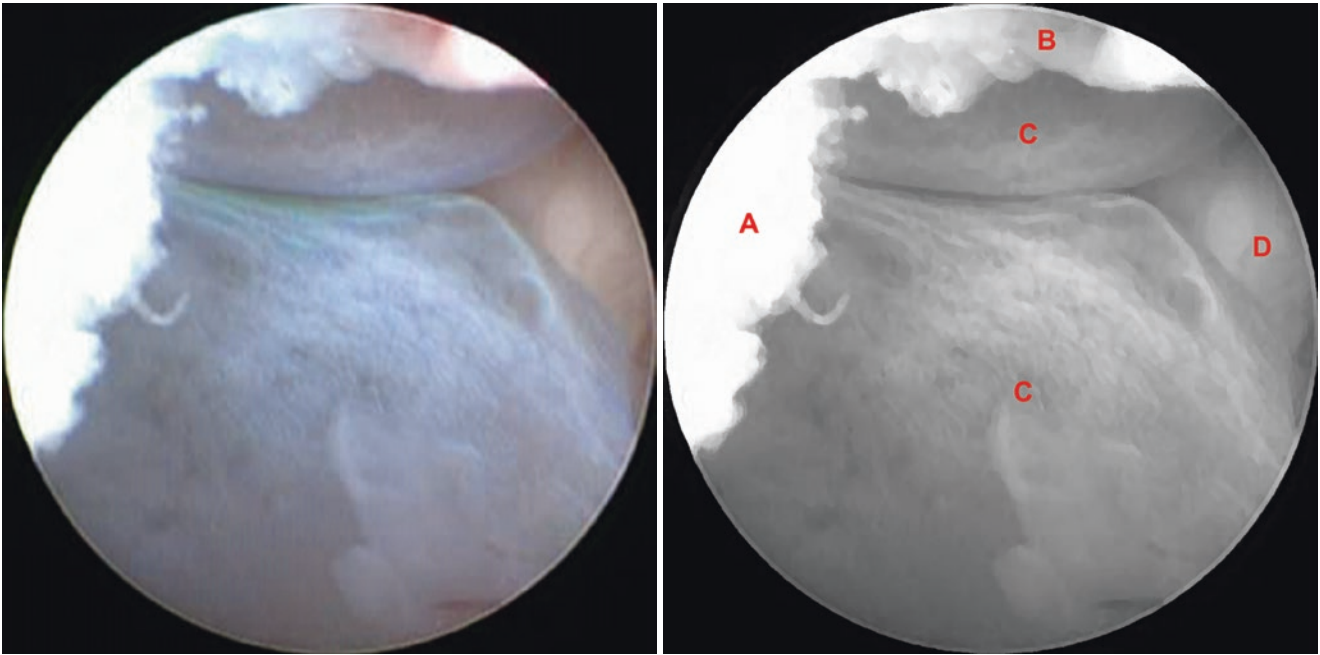


**Fig. 5.39** Illustrative case – racemose neurocysticercosis. (A) Ependymal layer, (B) Membrane of Lilliequist – diencephalic portion, (C) Racemose cysts, (D) Adhesion due to inflammatory process

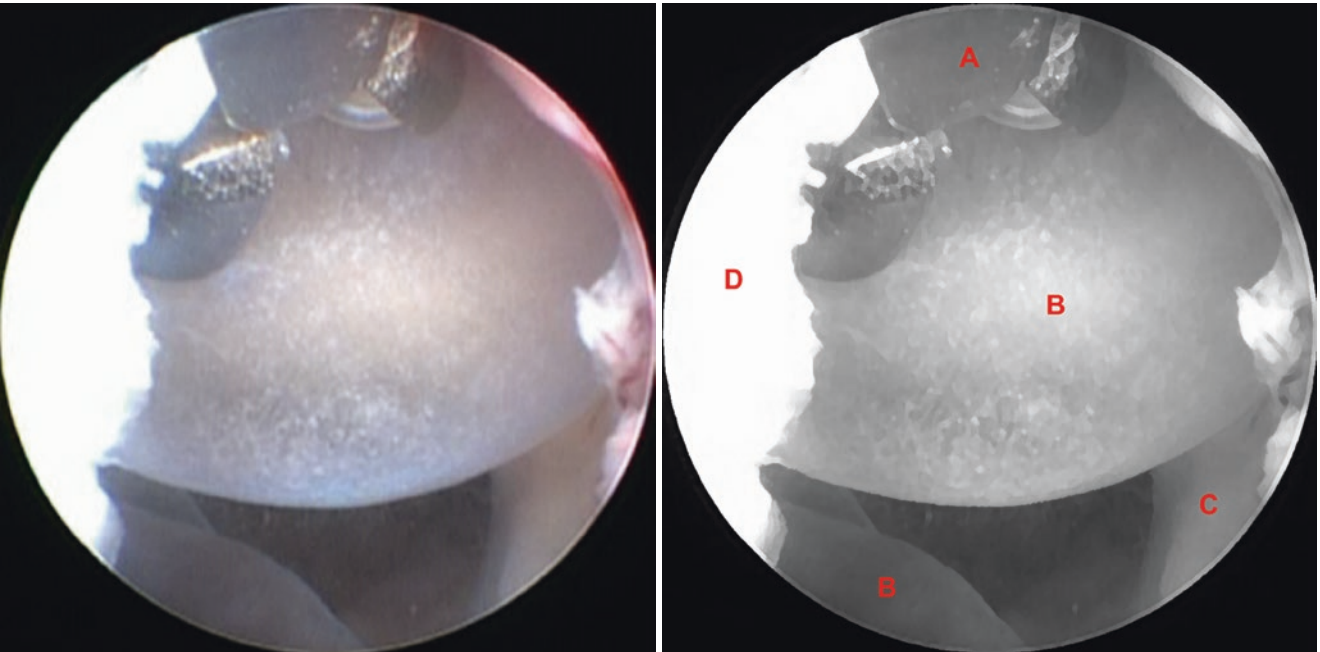


**Fig. 5.40** Illustrative case – racemose neurocysticercosis. (A) Biopsy forceps, (B) Racemose cyst, (C) Right oculomotor nerve (CN III), (D) Ependymal layer

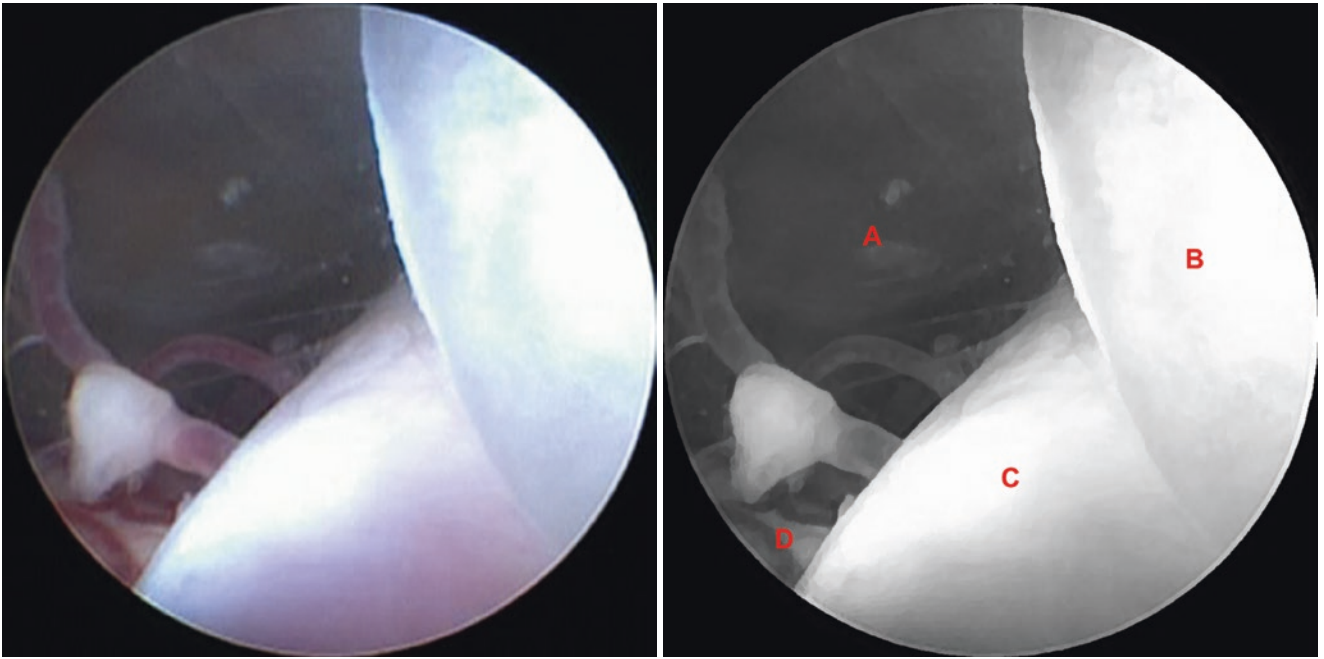


**Fig. 5.41** Illustrative case – racemose neurocysticercosis. (A) Preoptine cistern, (B) Racemose cyst (C) Basilar artery, (D) Pons

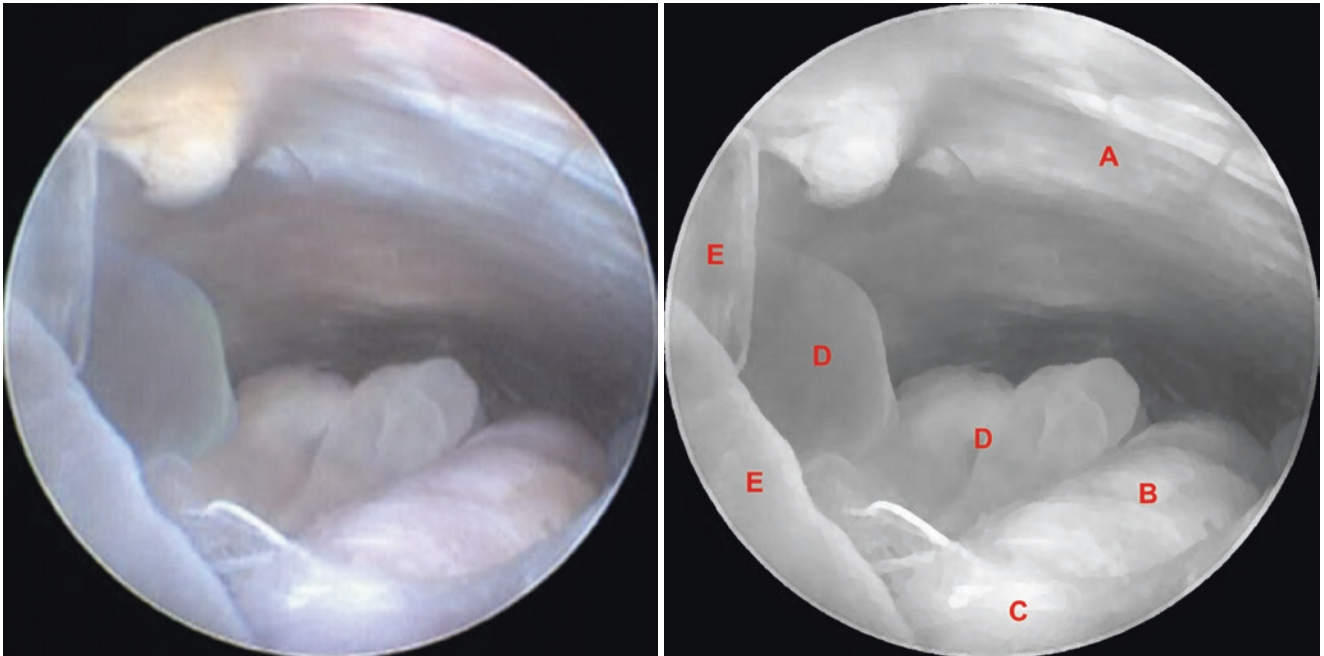


**Fig. 5.42** Illustrative case – racemose neurocysticercosis. (A) Clivus, (B) Basilar artery, (C) Membrane of Liliequist – mesencephalic portion, (D) Racemose cysts inside preoptine cistern, (E) Racemose cysts inside interpeduncular cistern

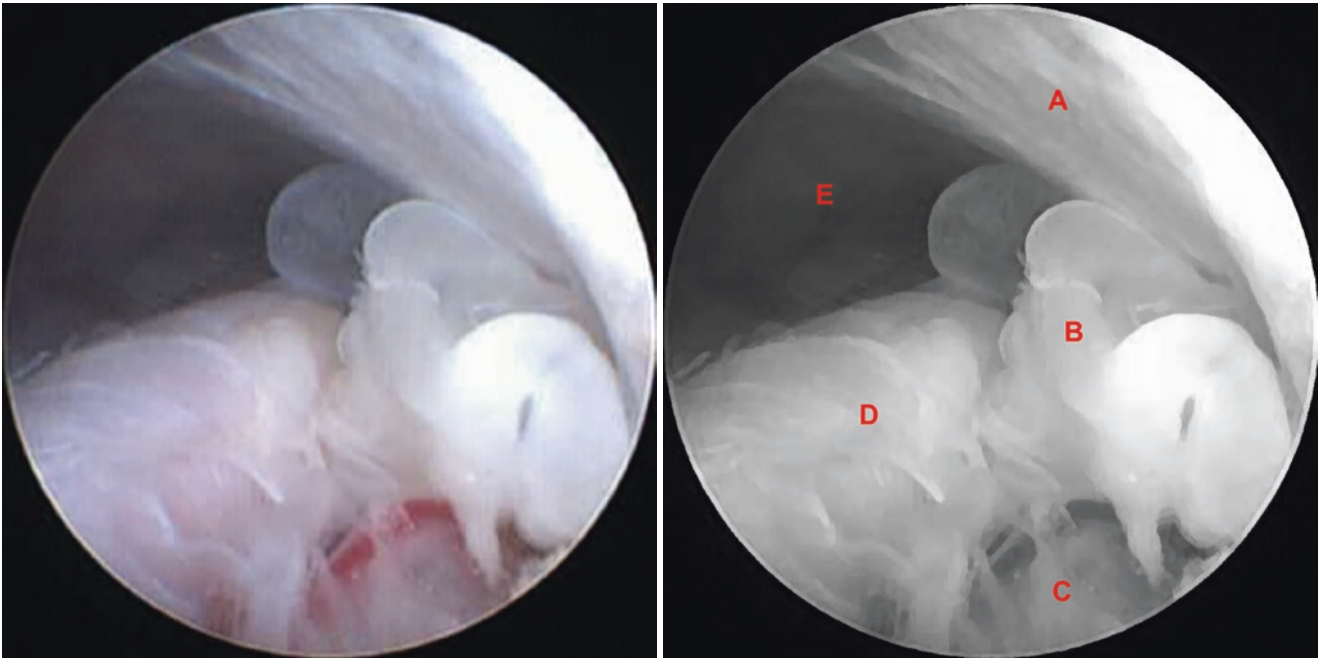


**Fig. 5.43** Illustrative case – racemose neurocysticercosis. (A) Clivus, (B) Racemose cysts, (C) Adhesion due to inflammatory process, (D) Basilar artery, (E) Preponine cistern

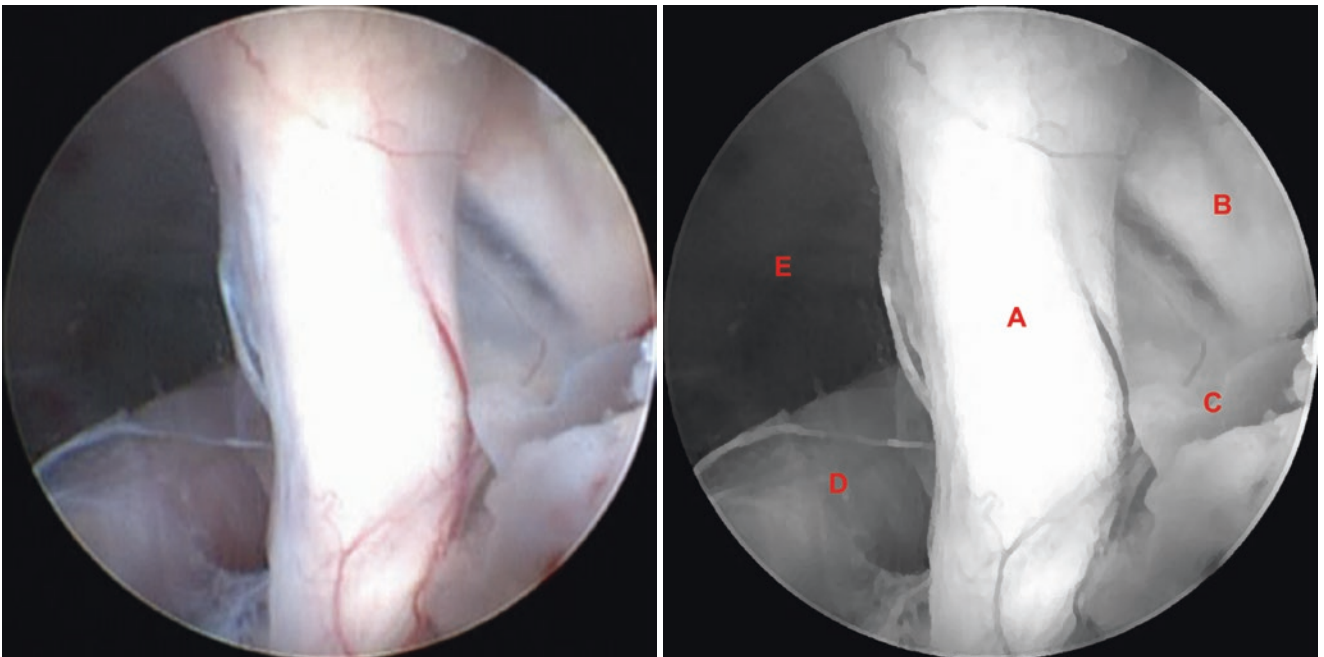


**Fig. 5.44** Illustrative case – racemose neurocysticercosis. (A) Right oculomotor nerve (CN III), (B) Right trigeminal nerve (CN V), (C) Racemose cysts, (D) Basilar artery, (E) Preponine cistern

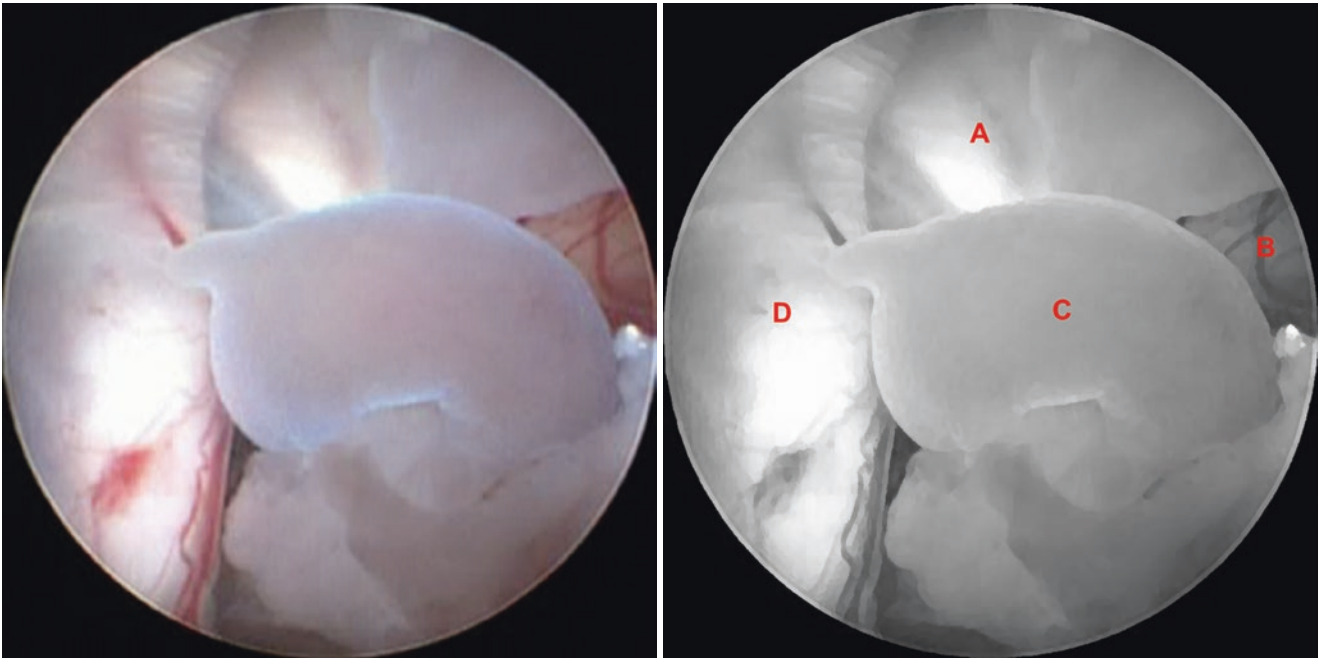


**Fig. 5.45** Illustrative case – racemose neurocysticercosis. (A) Right trigeminal nerve (CN V), (B) Right temporal lobe, (C) Racemose cyst, (D) Right oculomotor nerve (CN III)

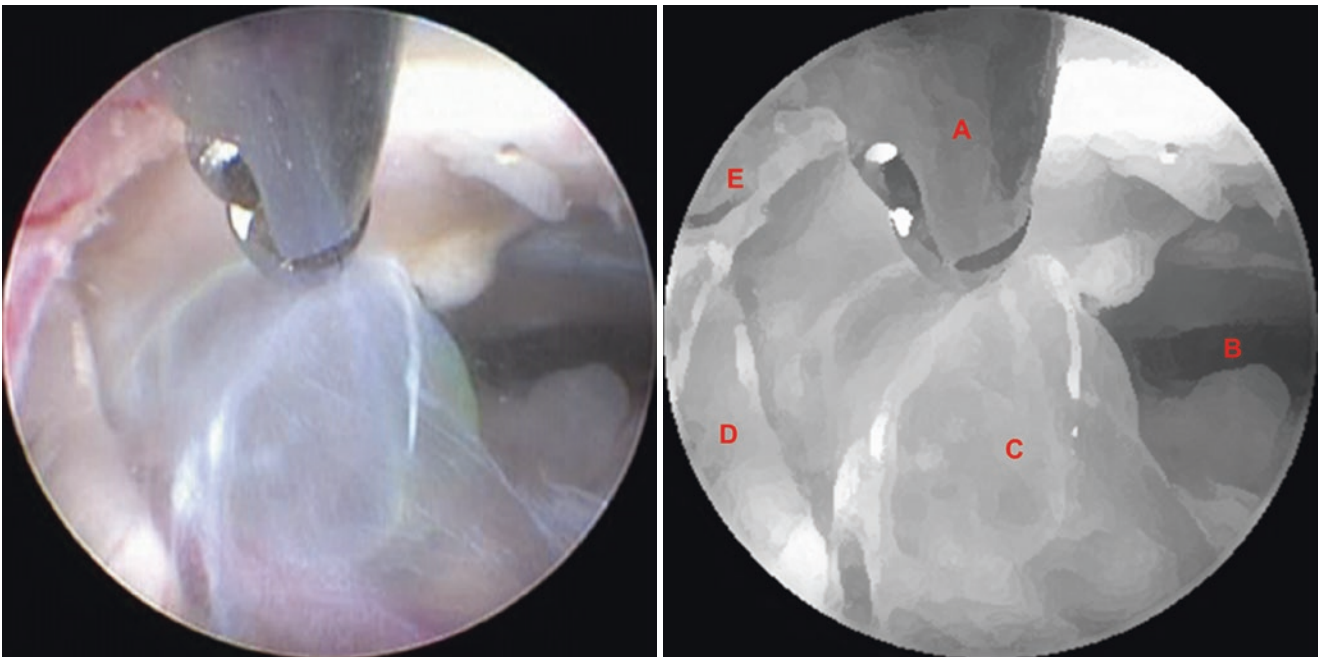


**Fig. 5.46** Illustrative case – racemose neurocysticercosis. (A) Biopsy forceps, (B) Prepontine cistern, (C) Racemose cyst, (D) Left oculomotor nerve (CN III), (E) Ependymal layer

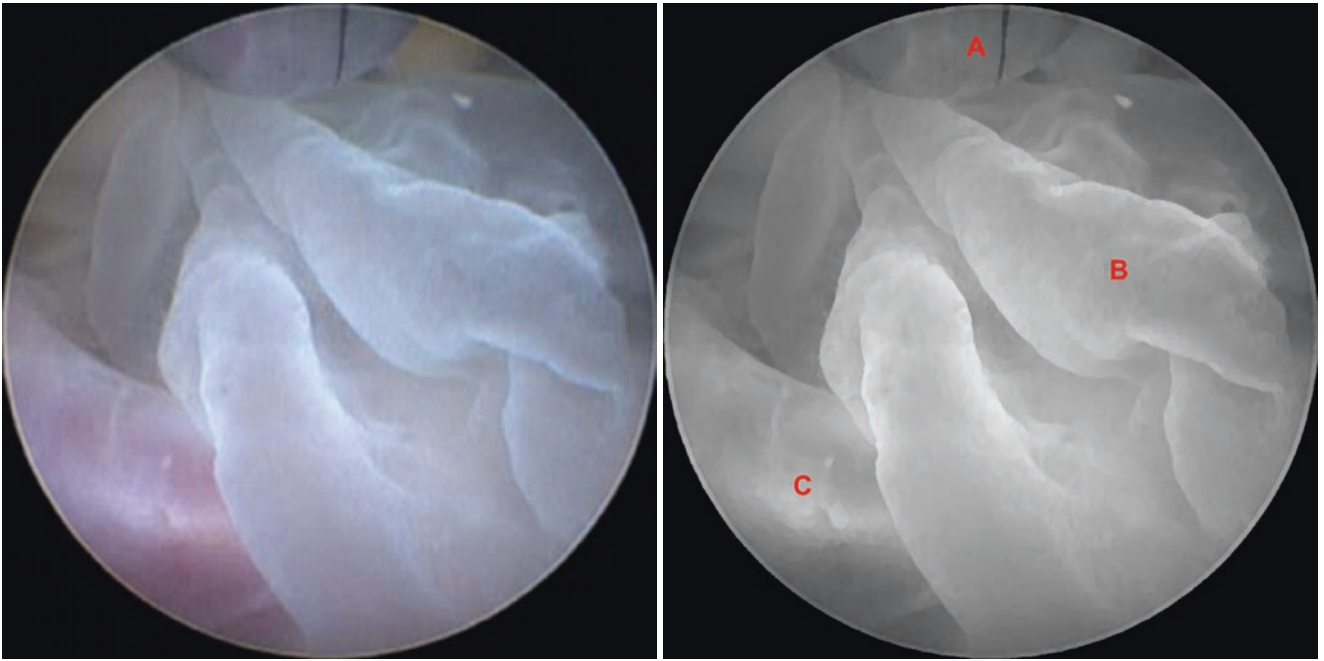


**Fig. 5.47** Illustrative case – racemose neurocysticercosis. (A) Biopsy forceps, (B) Racemose cyst, (C) Left posterior cerebral artery (P1)

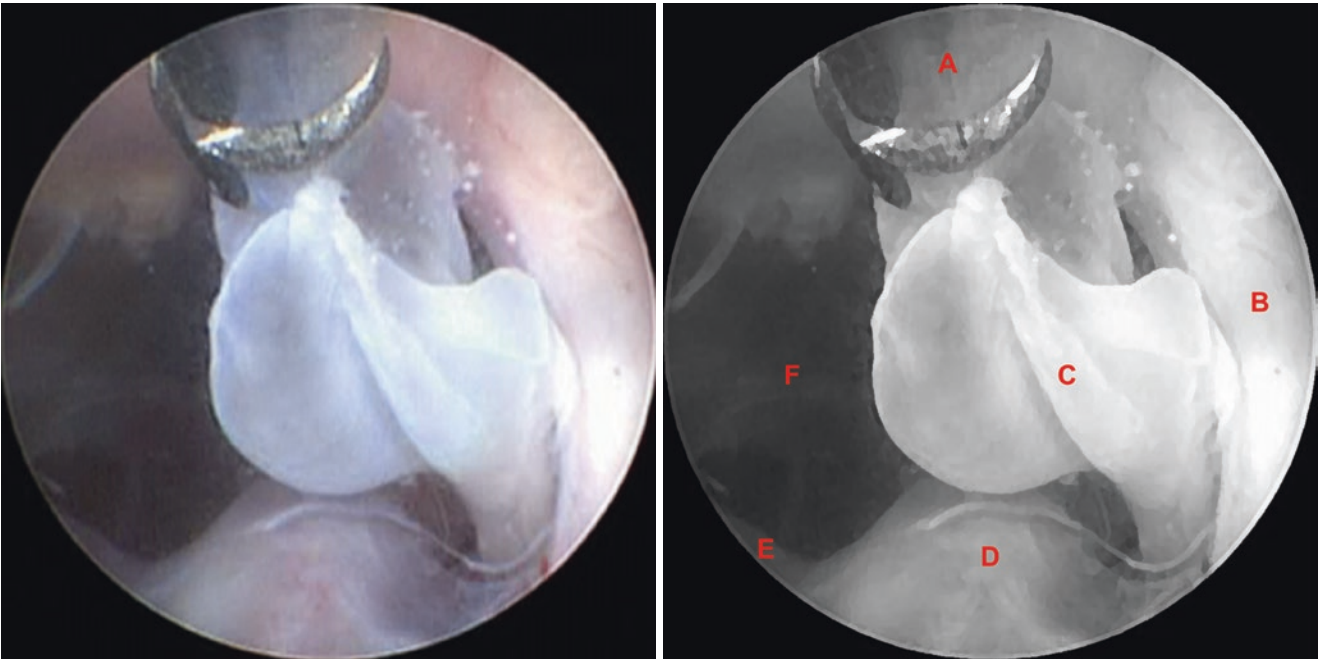


**Fig. 5.48** Illustrative case – racemose neurocysticercosis. (A) Biopsy forceps, (B) Right oculomotor nerve (CN III), (C) Racemose cyst, (D) Basilar artery, (E) Left superior cerebellar artery, (F) Preponine cistern



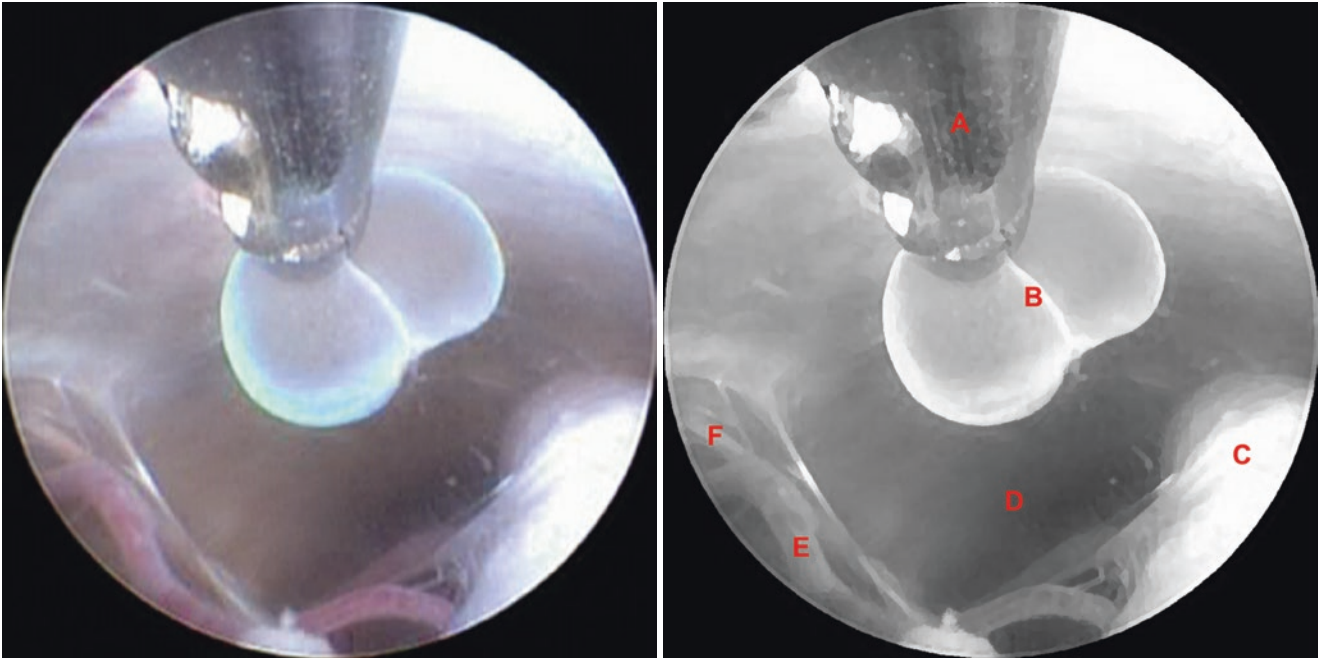


**Fig. 5.49** Illustrative case – racemose neurocysticercosis. (A) Biopsy forceps, (B) Racemose cyst, (C) Basilar artery, (D) Prepontine cistern, (E) Pontine vein, (F) Left abducens nerve (CN VI)

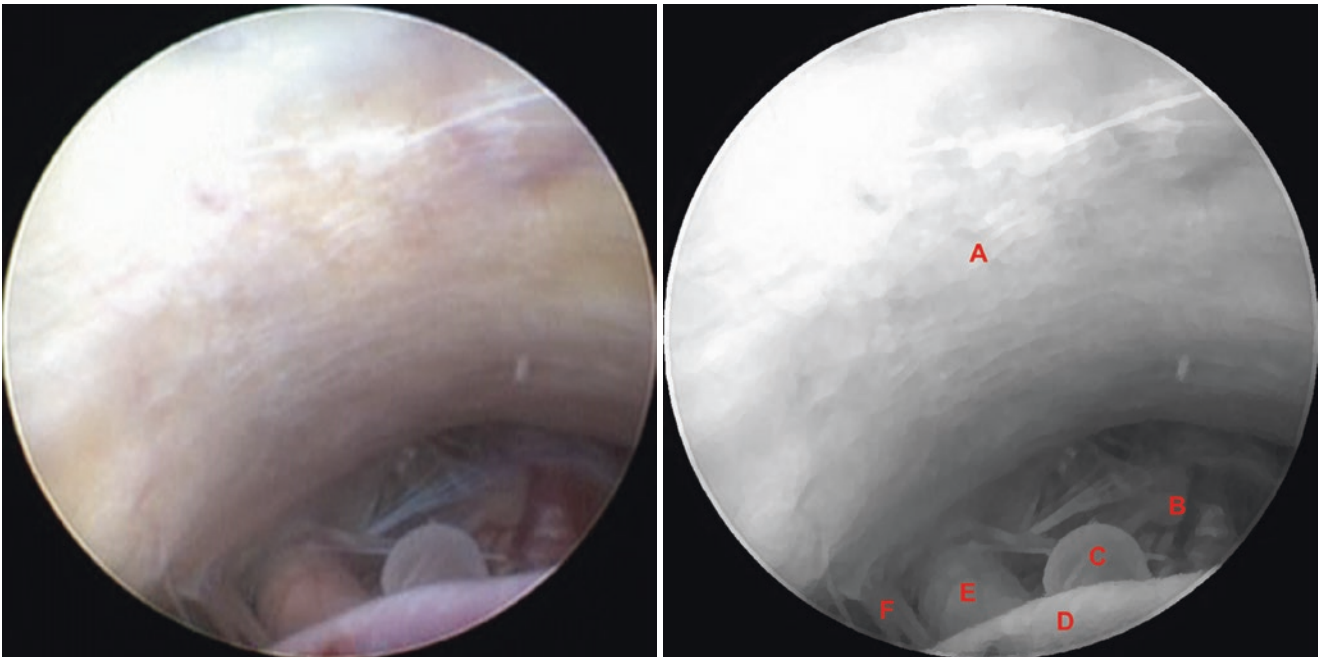


**Fig. 5.50** Illustrative case – racemose neurocysticercosis. (A) Clivus, (B) Medulla oblongata, (C) Racemose cyst, (D) Basilar artery, (E) Left vertebral artery, (F) Left hypoglossal nerve (CN XII)

## References

1. Enchev YP, Oi S. The application of neuroendoscopic techniques in improving altered CSF physiology. In: Sgouros S, editor. *Neuroendoscopy*. Berlin Heidelberg: Springer; 2014. p. 11–30. doi:[10.1007/978-3-642-39085-2\\_2](https://doi.org/10.1007/978-3-642-39085-2_2).
2. Decq P. Endoscopic anatomy of the ventricles. In: Cinalli G, Sainte-Rose C, Maixner WJ, editors. *Pediatric hydrocephalus*. Milan: Springer; 2005. p. 351–9. doi:[10.1007/978-88-470-2121-1\\_24](https://doi.org/10.1007/978-88-470-2121-1_24).
3. Seeger W. Endoscopic anatomy of the third ventricle. *Microsurgical and endoscopic approaches*. Wien: Springer; 2006. doi:[10.1007/3-211-31178-5](https://doi.org/10.1007/3-211-31178-5).
4. Fushimi Y, Miki Y, Ueba T, Kanagaki M, Takahashi T, Yamamoto A, et al. Liliequist membrane: Three-dimensional constructive interference in steady state MR imaging. *Radiology*. 2003;229:360–5. doi:[10.1148/radiol.2292021507](https://doi.org/10.1148/radiol.2292021507).
5. Wang SS, Zheng HP, Zhang FH, Wang RM. Microsurgical anatomy of Liliequist's membrane demonstrating three-dimensional configuration. *ActaNeurochir (Wien)*. 2011;153:191–200. doi:[10.1007/s00701-010-0823-2](https://doi.org/10.1007/s00701-010-0823-2).
6. Seeger W. Endoscopic and microsurgical anatomy of the upper basal cisterns. Wien: Springer; 2008. doi:[10.1007/978-3-211-77035-1](https://doi.org/10.1007/978-3-211-77035-1).

## 6.1 Introduction

Suprasellar arachnoid cysts (SACs) are benign congenital collections of cerebrospinal fluid (CSF), accounting for approximately 9% of all arachnoid cysts [1–4]. These cysts progressively enlarge from an abnormality in the interpeduncular cistern or in the membrane of Liliequist. They can be classified as communicating cysts; that is, cystic dilatations of the interpeduncular cistern, and as non-communicating intra-arachnoid cysts of the diencephalic portion of the membrane of Liliequist [5]. In communicating cysts, the basilar artery bifurcation is located inside the cyst with no overlying membrane, whereas in a non-communicating cyst, the basilar artery and its branches are pushed posteriorly against the brainstem, and the cyst can be observed through a transparent membrane (diencephalic portion of the membrane of Liliequist). A new recent classification divides SACs into three types: SAC-1, SAC-2, and SAC-3. SAC-1 may arise from an expansion of the diencephalic portion of the membrane of Liliequist. SAC-2 shows a dilatation of the interpeduncular cistern and corresponds to a defect of the mesencephalic portion of the membrane of Liliequist. SAC-3 is an asymmetrical form that expands to other subarachnoid spaces [6]. However, even on a high-definition intraoperative view it can be difficult to distinguish these types of SACs, because the diencephalic portion of the membrane of Liliequist is very thin and transparent. Due to this difficulty this classification is not applied to the intraoperative images shown here.

Endoscopic neurosurgery is the best surgical approach for SACs [7], being performed mainly in patients with associated hydrocephalus. At present, there are two main types of endoscopic surgical procedures: ventriculocystostomy (VC), in which the goal is to establish communication between the cyst cavity and the ventricles, and ventriculocystocisternostomy (VCC), in which the goal is to open the cyst into both the ventricles and cisterns. There are other reports concerning different endoscopic approaches [8, 9]. Currently, the main controversy is about whether VCC is preferable to VC

alone. The two procedures, VC and VCC, have proven to be almost equally effective both clinically and radiologically. Nevertheless, because of the statistically significant difference between the incidences of recurrence after VC and VCC during long-term follow-up, it has been concluded that VCC should be considered as the procedure of choice in the treatment of SACs [10]. Crimmins et al. reported on seven patients treated with VC and 13 patients treated with VCC. They found that VCC had a higher success rate, although the difference was not statistically significant, but they also found that the failure rate of VC was higher than that of VCC [11]. VCC is an effective and durable treatment for symptomatic SACs in most cases [12]. In a metareview of 23 series reported after 1980, of 176 patients with SACs treated by different surgical procedures, the endoscopic procedure was VC in 49 patients and VCC in 53. The rate of clinical-radiological improvement was higher after VCC (94.3%) than after VC (85.7%) [13]. In another review, VCC was also more frequently effective (48 of 50) than VC (18 of 21) [14]. There are two explanations for this result: First, the superior fenestration tends to close, regardless of whether a single or dual fenestration is performed, because stretching of the third ventricle creates excess tissue that can overlap and seal the fenestration after the operation. The persistence of the basal opening, even in the face of secondary closure of the apical fenestration, allows adequate cyst decompression into the basal cisterns, thus decreasing the risk of recurrence [15]. Second, chronic mesencephalon compression by the cyst may lead to secondary aqueductal occlusion. In this scenario, apical membrane fenestration alone, although allowing for adequate cyst decompression, may not result in extraventricular CSF flow [14]. In a recent study it was concluded that VCC was superior and that the postoperative radiological examinations must reveal the adequacy of fenestrations and flow through fenestration sites, reduction of the cyst and ventricle size, and reorientation of the chiasm and mammillary bodies to an acceptable anatomical position [16]. Therefore, endoscopic VCC should be performed as the first surgical procedure in all patients with SAC and

hydrocephalus. Patients who do not improve after the VCC procedure may be treated with a shunt [14]. In SAC patients without hydrocephalus, endoscopic VCC can be performed as an effective, safe, and simple treatment option by using intraoperative image-based neuronavigation. The image-guided neuroendoscopic procedure improved the accuracy of the endoscopic approach and minimized brain trauma [17].

Also, virtual endoscopy could be an interesting option for surgical planning [18]. Figures 6.1 and 6.2 depict typical aspects of SAC on magnetic resonance imaging (MRI). Intraoperative images are shown in Figs. 6.3, 6.4, 6.5, 6.6, 6.7, 6.8, 6.9, 6.10, 6.11, 6.12, 6.13, 6.14, 6.15, 6.16, 6.17, 6.18, 6.19, 6.20, 6.21, 6.22, 6.23, 6.24, 6.25, 6.26, 6.27, 6.28, 6.29, 6.30, 6.31, 6.32, 6.33, 6.34, and 6.35.

## 6.2 Suprasellar Arachnoid Cyst

### 6.2.1 Typical MRI Aspect



**Fig. 6.1** Axial T1-weighted magnetic resonance imaging (MRI) showing a typical suprasellar arachnoid cyst

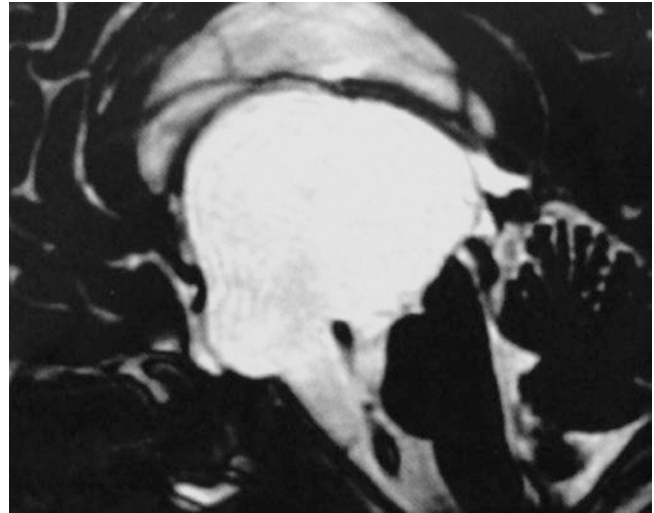


**Fig. 6.2** Sagittal T2-weighted MRI showing a communicating suprasellar arachnoid cyst

### 6.2.2 Intraoperative Images

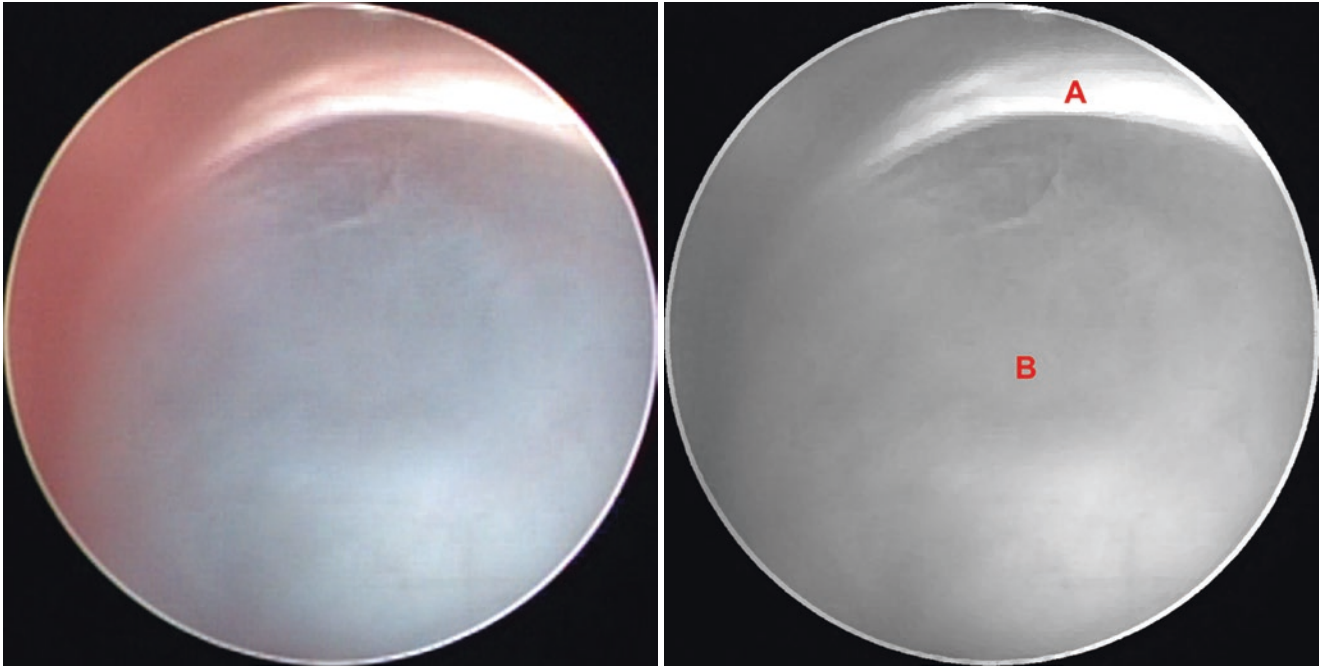


**Fig. 6.3** (A) Column of the fornix, (B) Suprasellar arachnoid cyst through foramen of Monro

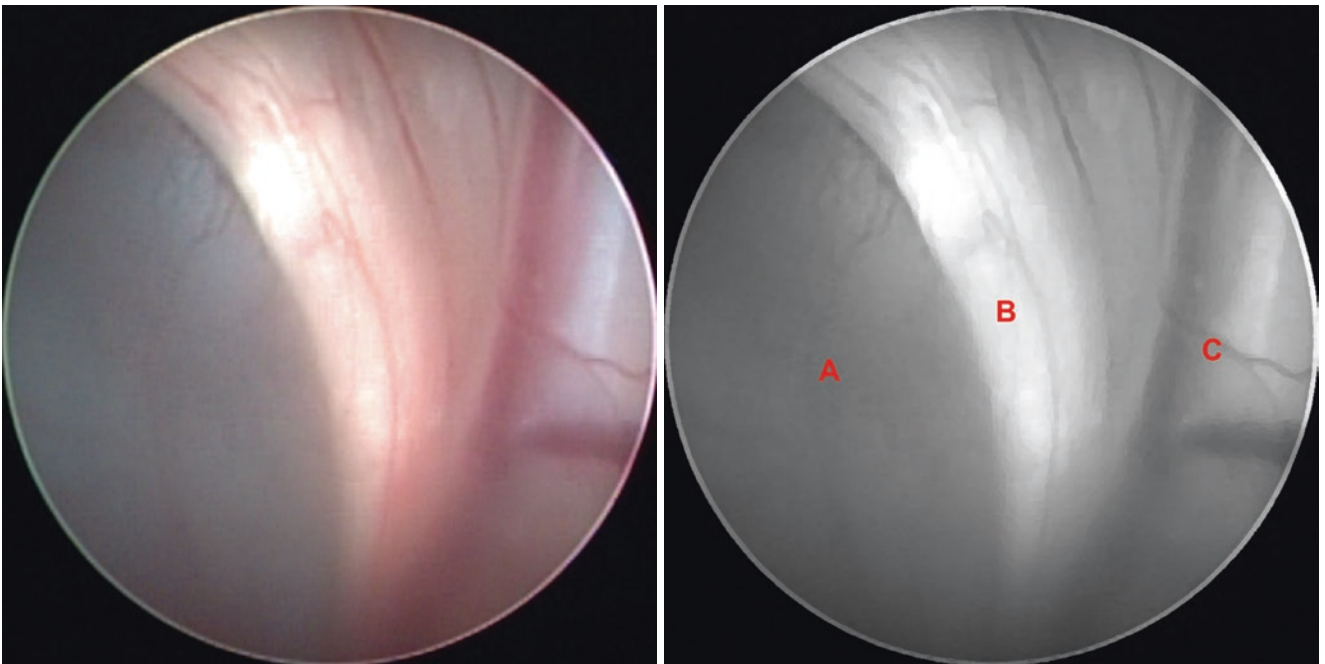


**Fig. 6.4** (A) Suprasellar arachnoid cyst through foramen of Monro, (B) Column of the fornix (C), Superior thalamostriate vein

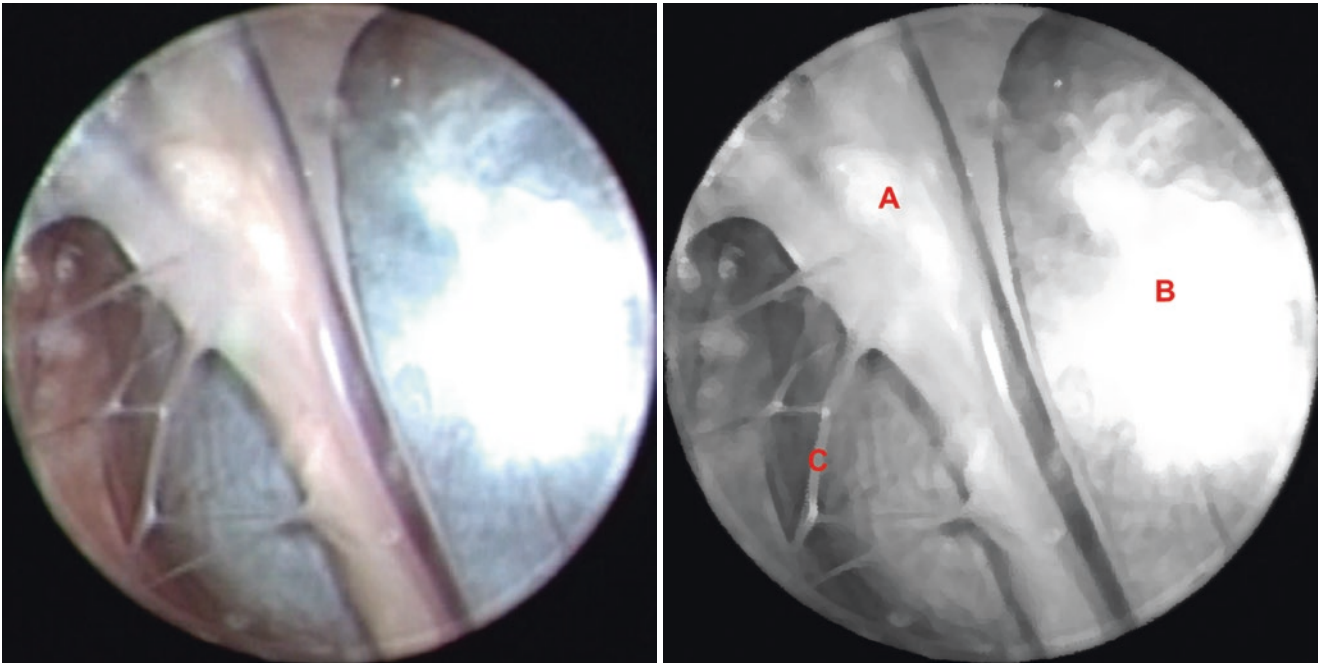


**Fig. 6.5** (A) Septum pellucidum, (B) Suprasellar arachnoid cyst through foramen of Monro, (C) Septum pellucidum spontaneous fenestration due to chronic hydrocephalus

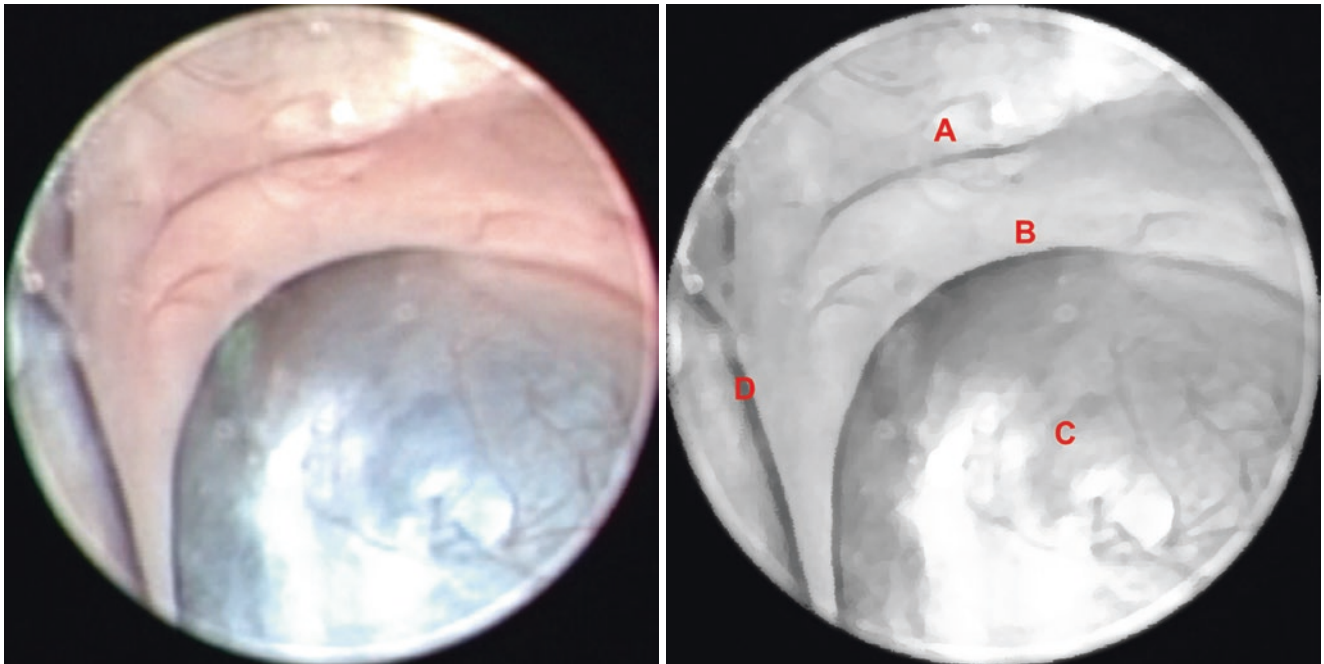


**Fig. 6.6** (A) Septum pellucidum, (B) Column of the fornix, (C) Suprasellar arachnoid cyst through foramen of Monro, (D) Anterior septal vein

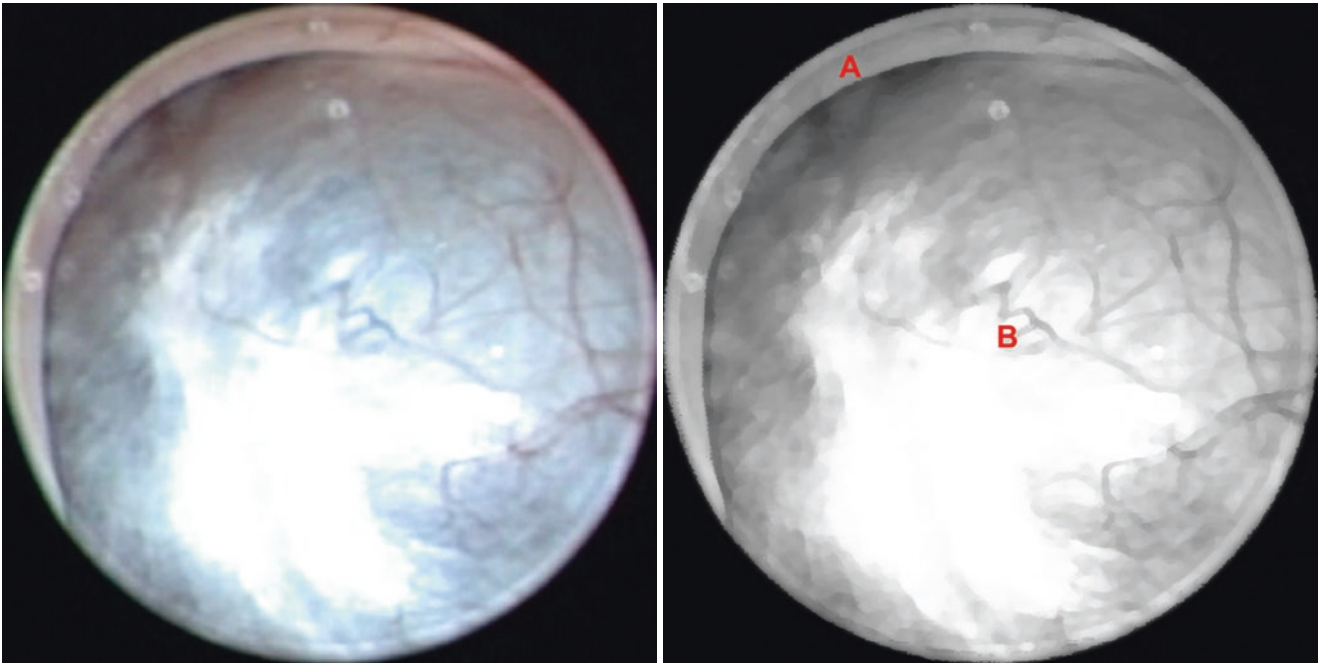


**Fig. 6.7** (A) Column of the fornix, (B) Suprasellar arachnoid cyst through foramen of Monro

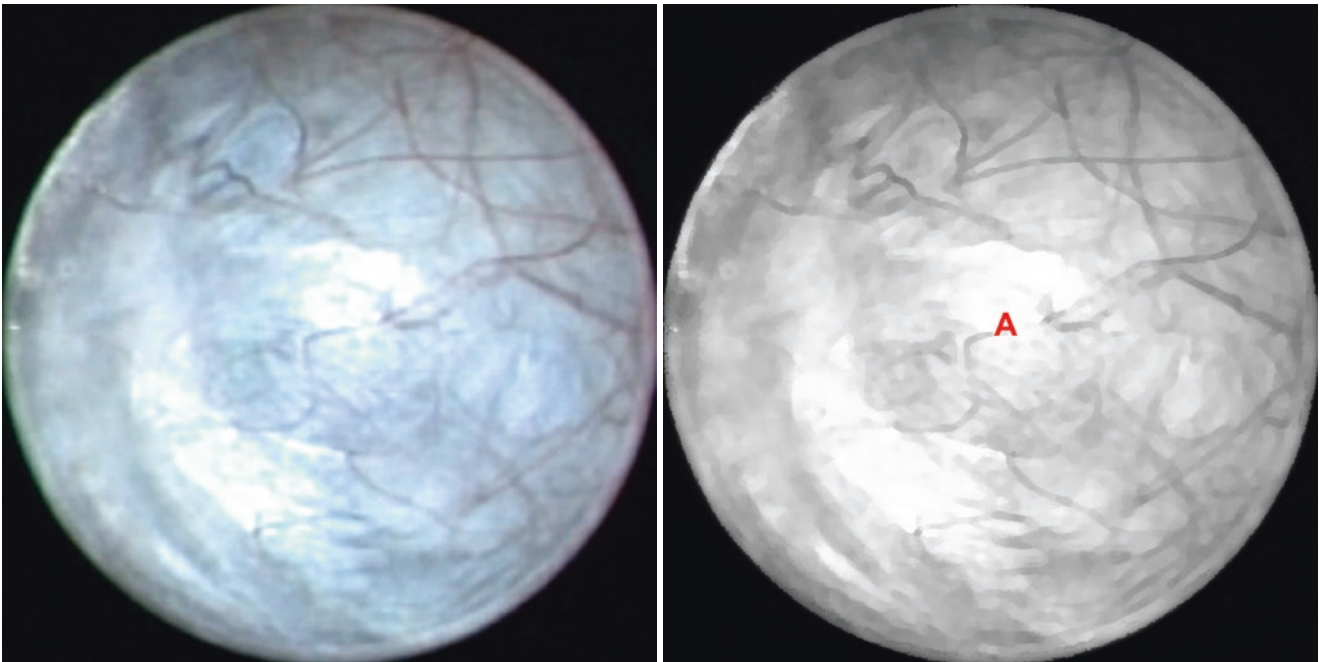


**Fig. 6.8** (A) Cyst wall



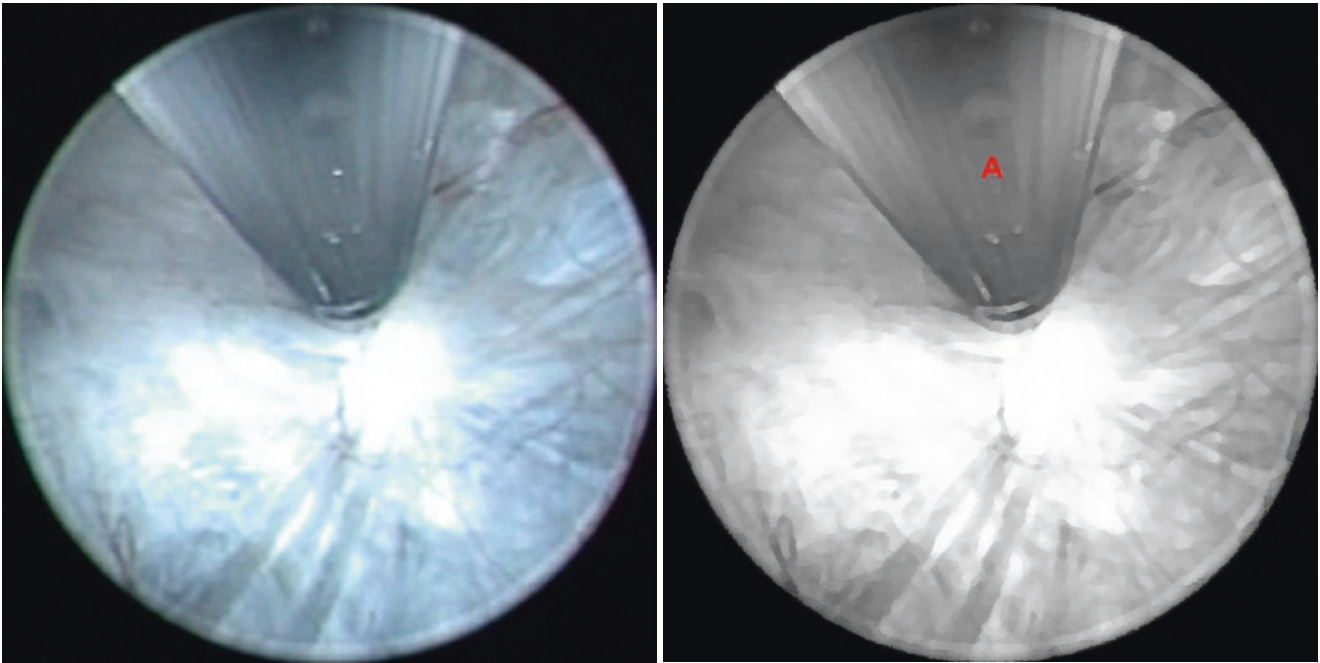


**Fig. 6.9** (A) Monopolar coagulation electrode at the cyst wall

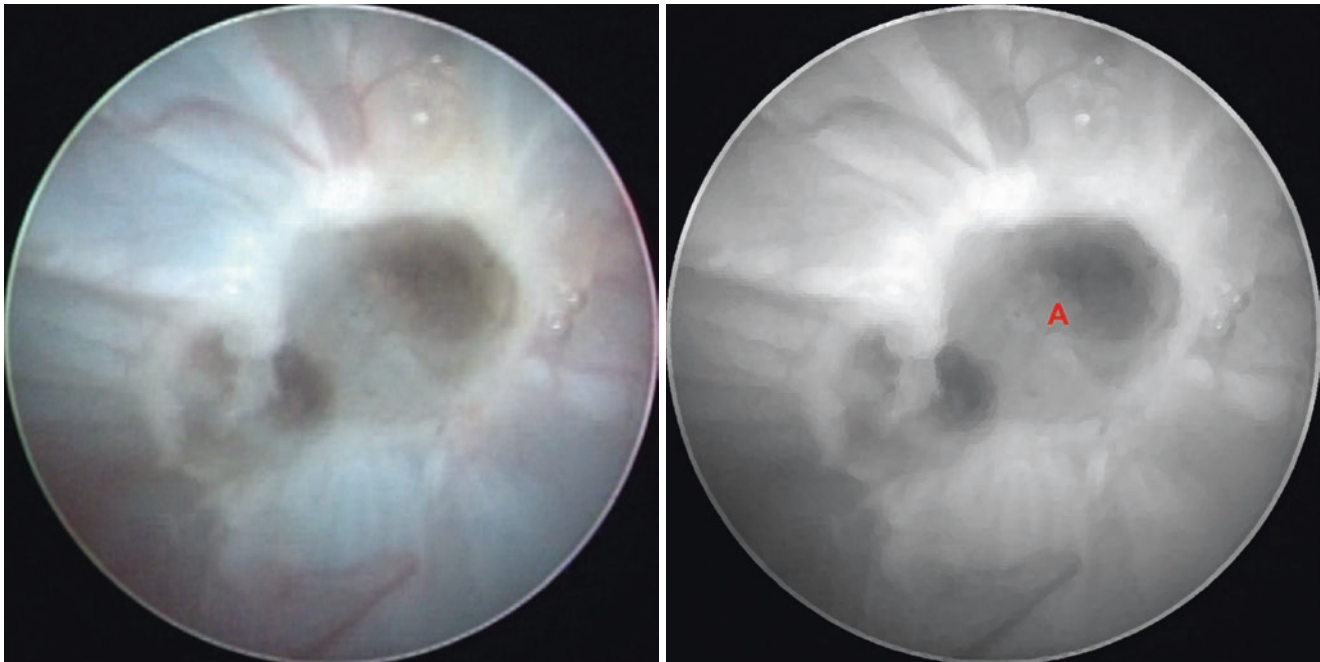


**Fig. 6.10** (A) Coagulated cyst wall

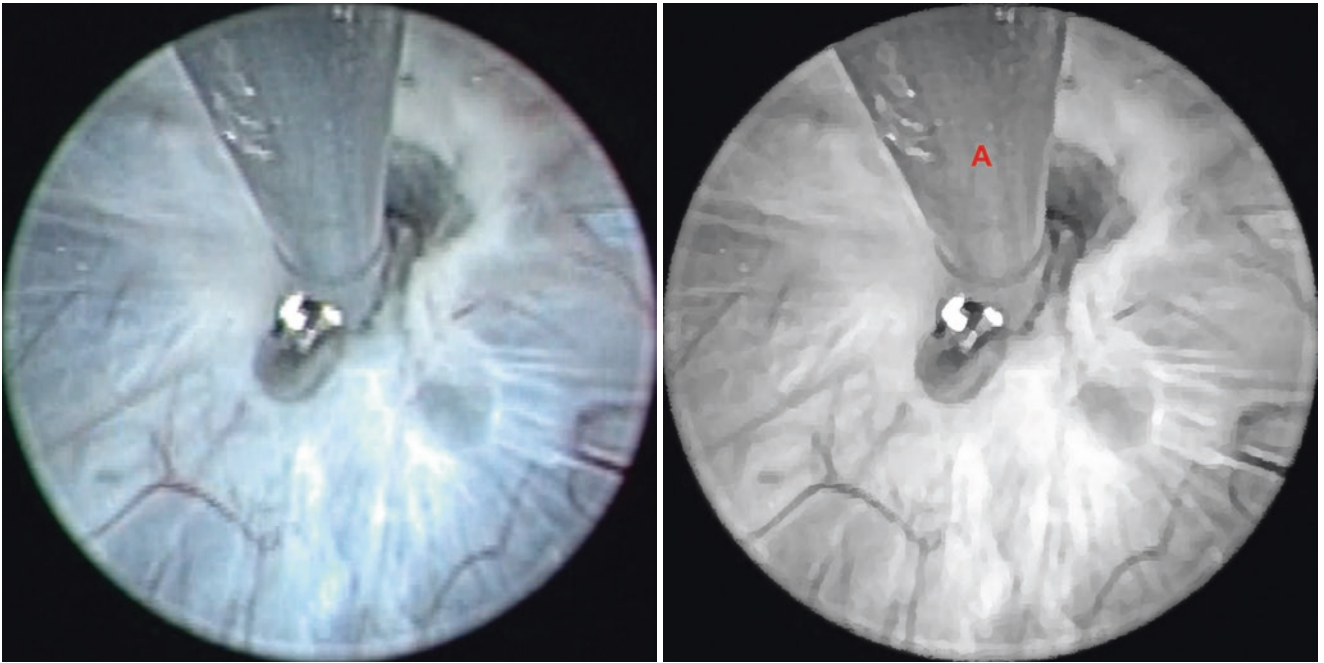


**Fig. 6.11** (A) Biopsy forceps fenestrating the cyst wall

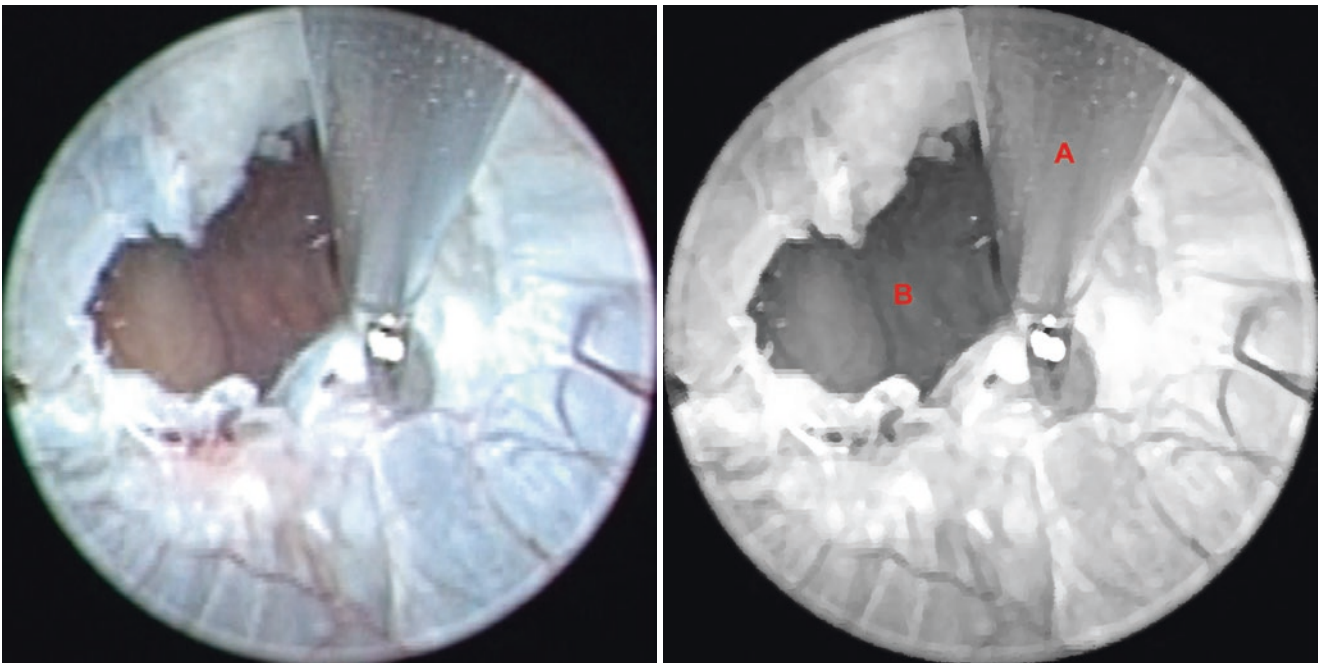


**Fig. 6.12** (A) Biopsy forceps fenestrating the cyst wall, (B) Fenestration

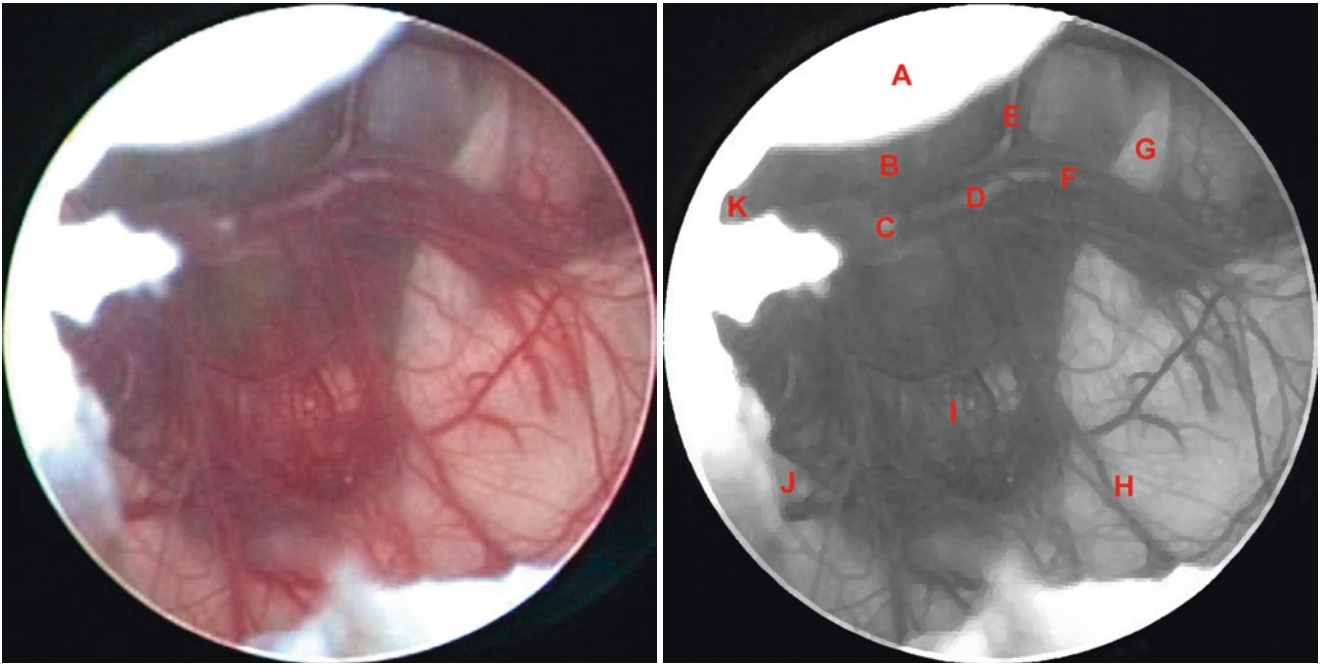


**Fig. 6.13** (A) Cyst wall, (B) Membrane of Lilliequist – mesencephalic portion, (C) Bifurcation of the basilar artery, (D) Right posterior cerebral artery (P1), (E) Right posterior communicating artery, (F) Right

posterior cerebral artery (P2), (G) Right oculomotor nerve (CN III), (H) Mesencephalon, (I) Thalamoperforating arteries, (J) Left oculomotor nerve (CN III), (K) Left posterior communicating artery

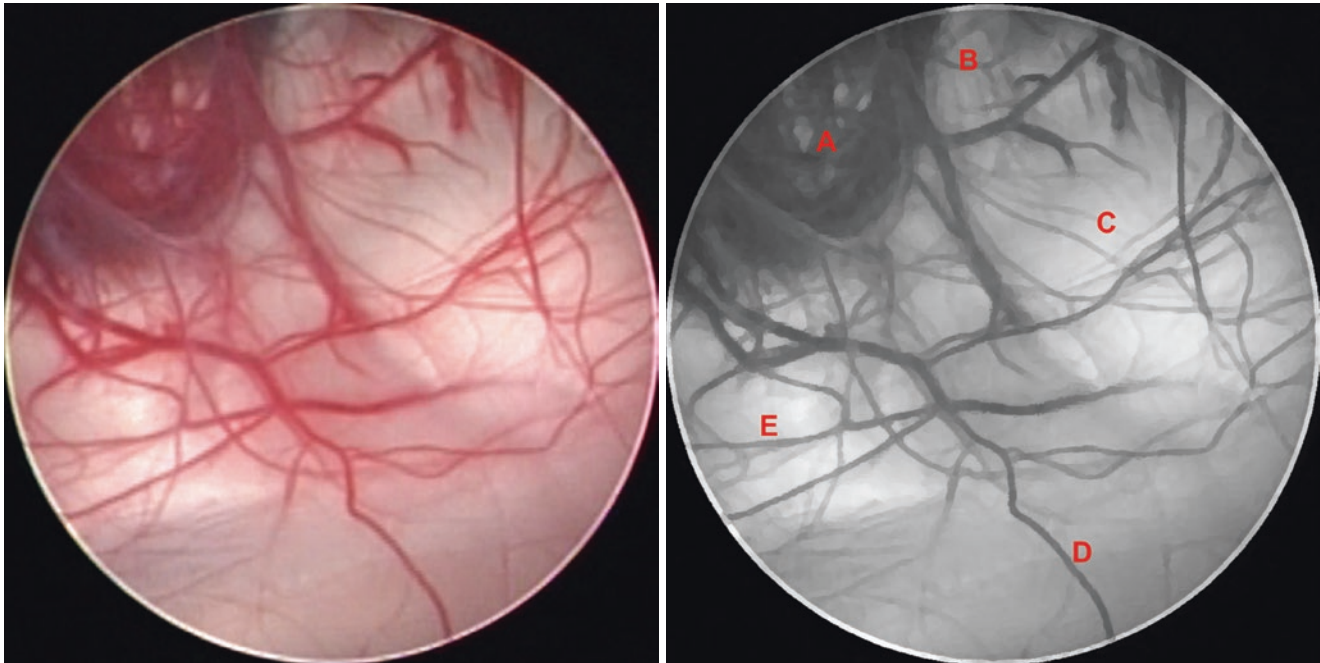


**Fig. 6.14** (A) Thalamoperforating arteries, (B) Right oculomotor nerve (CN III), (C) Right cerebral peduncle, (D) Tegmentum of mesencephalon, (E) Left cerebral peduncle

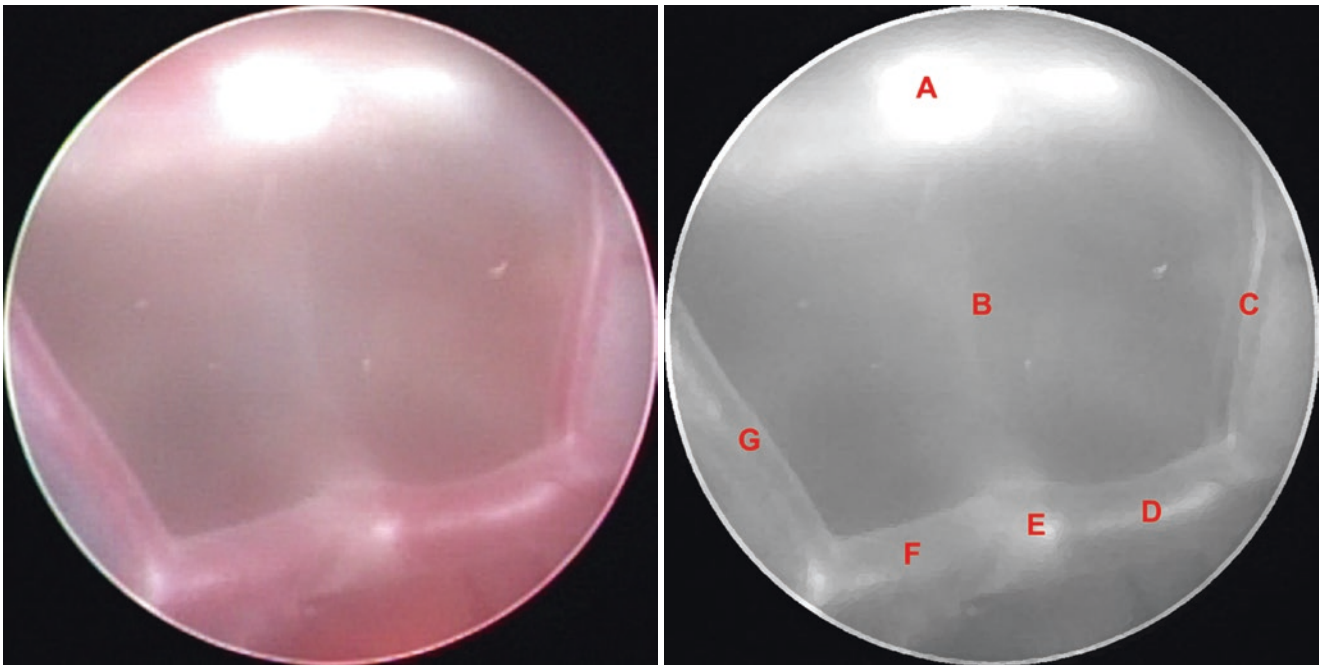


**Fig. 6.15** (A) Dorsum sellae, (B) Membrane of Liliequist–mesencephalic portion, (C) Right posterior communicating artery, (D) Right posterior cerebral artery (P1), (E) Bifurcation of the basilar artery, (F) Left posterior cerebral artery (P1), (G) Left posterior communicating artery

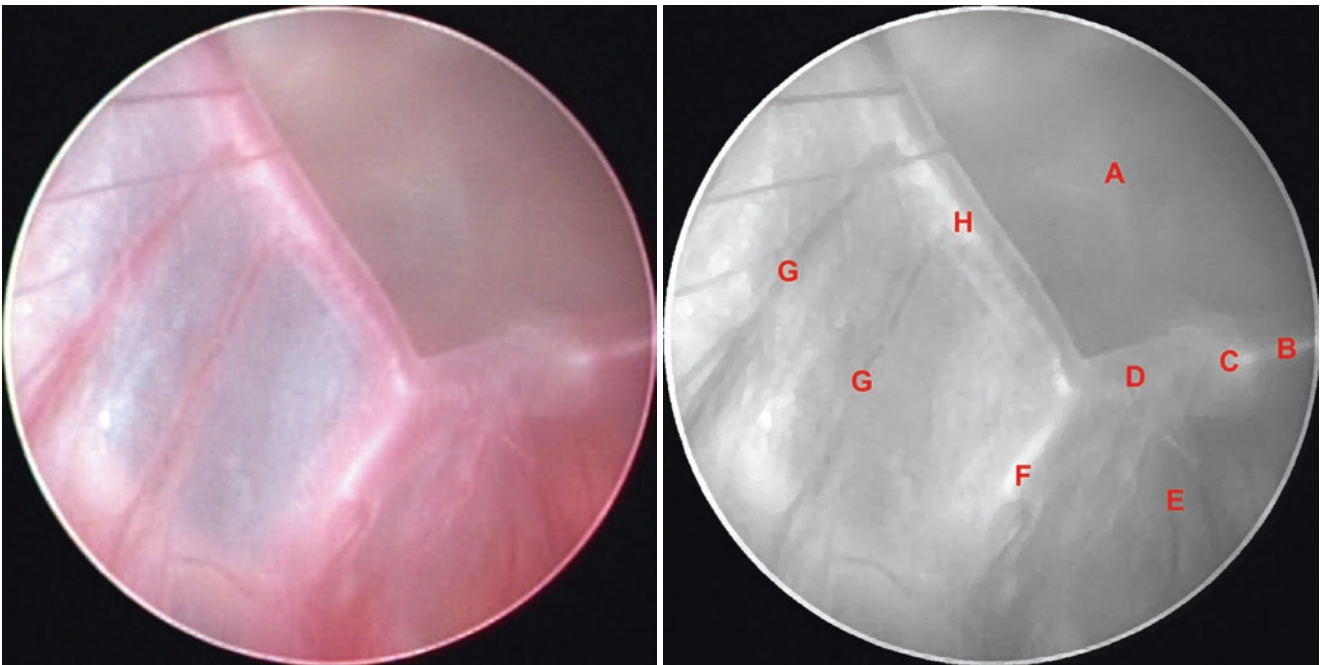


**Fig. 6.16** (A) Membrane of Liliequist – mesencephalic portion, (B) Right posterior cerebral artery (P1), (C) Bifurcation of the basilar artery, (D) Left posterior cerebral artery (P1), (E) Thalamoperforating arteries, (F) Left posterior cerebral artery (P2), (G) Left anterior thalamoperforating or premammillary arteries, (H) Left posterior communicating artery

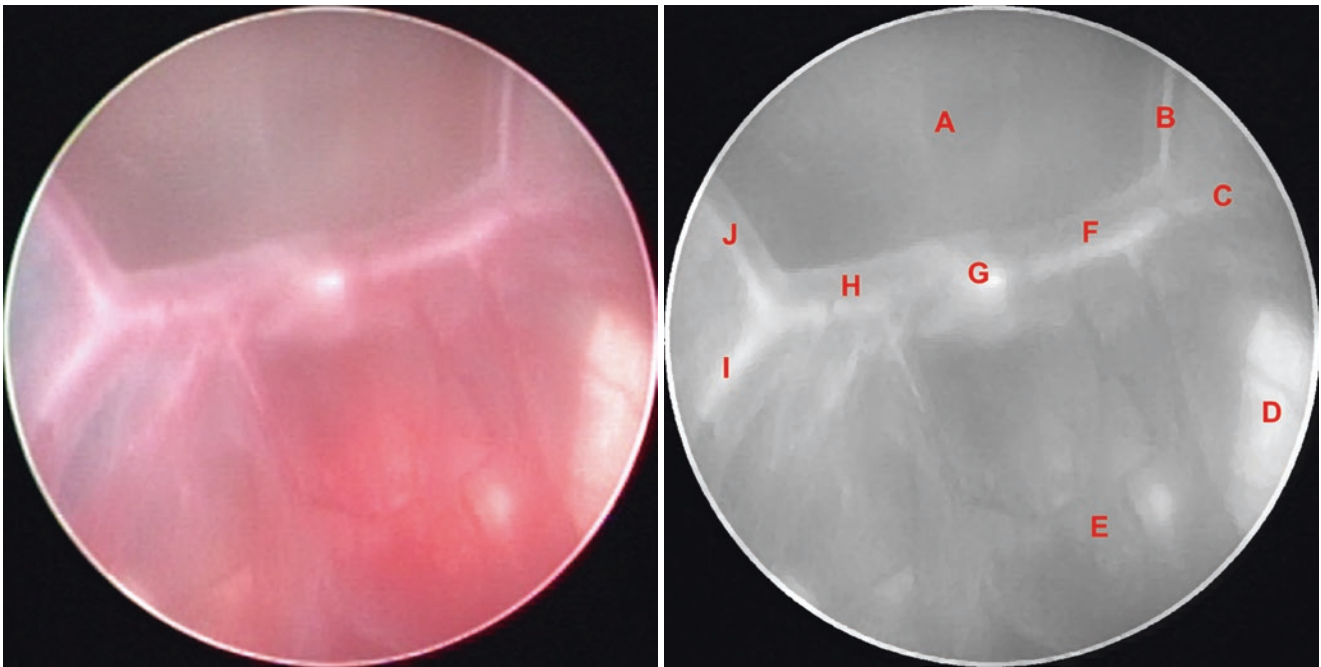


**Fig. 6.17** (A) Membrane of Liliequist – mesencephalic portion, (B) Right posterior communicating artery, (C) Right posterior cerebral artery (P2), (D) Right oculomotor nerve (CN III), (E) Thalamoperforating

arteries, (F) Right posterior cerebral artery (P1), (G) Bifurcation of the basilar artery, (H) Left posterior cerebral artery (P1), (I) Left posterior cerebral artery (P2), (J) Left posterior communicating artery

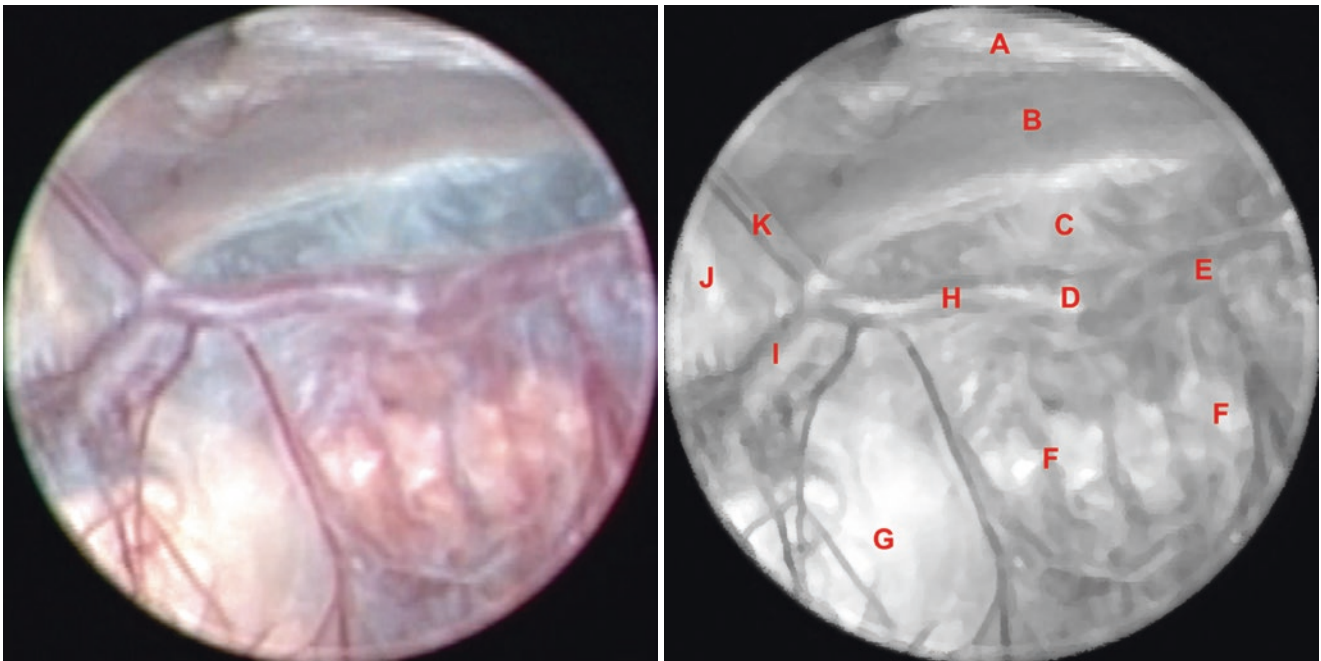


**Fig. 6.18** (A) Dorsum sellae, (B) Clivus, (C) Membrane of Liliequist – mesencephalic portion, (D) Bifurcation of the basilar artery, (E) Right posterior cerebral artery (P1), (F) Thalamoperforating arteries, (G) Left

cerebral peduncle, (H) Left posterior cerebral artery (P1), (I) Left posterior cerebral artery (P2), (J) Left oculomotor nerve (CN III), (K) Left posterior communicating artery

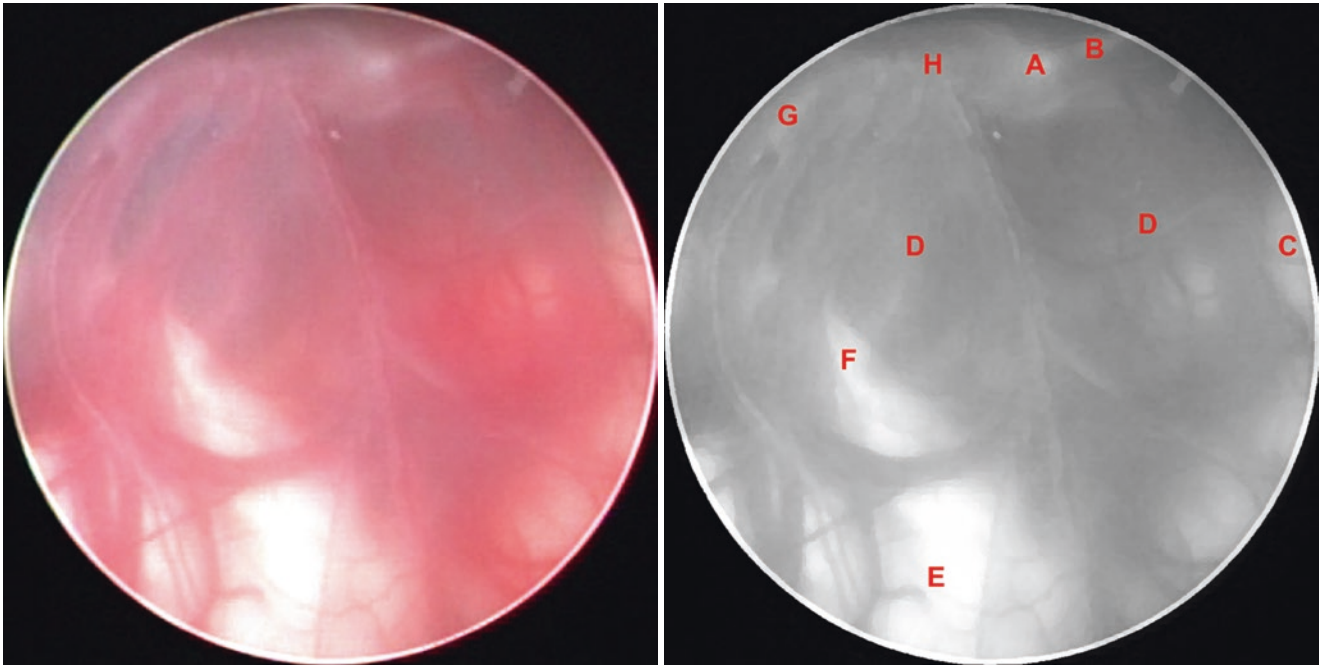


**Fig. 6.19** (A) Bifurcation of the basilar artery, (B) Right posterior cerebral artery (P1), (C) Right oculomotor nerve (CN III), (D) Thalamoperforating arteries, (E) Left cerebral peduncle, (F) Left oculo-

motor nerve (CN III), (G) Left posterior cerebral artery (P2), (H) Left posterior cerebral artery (P1)

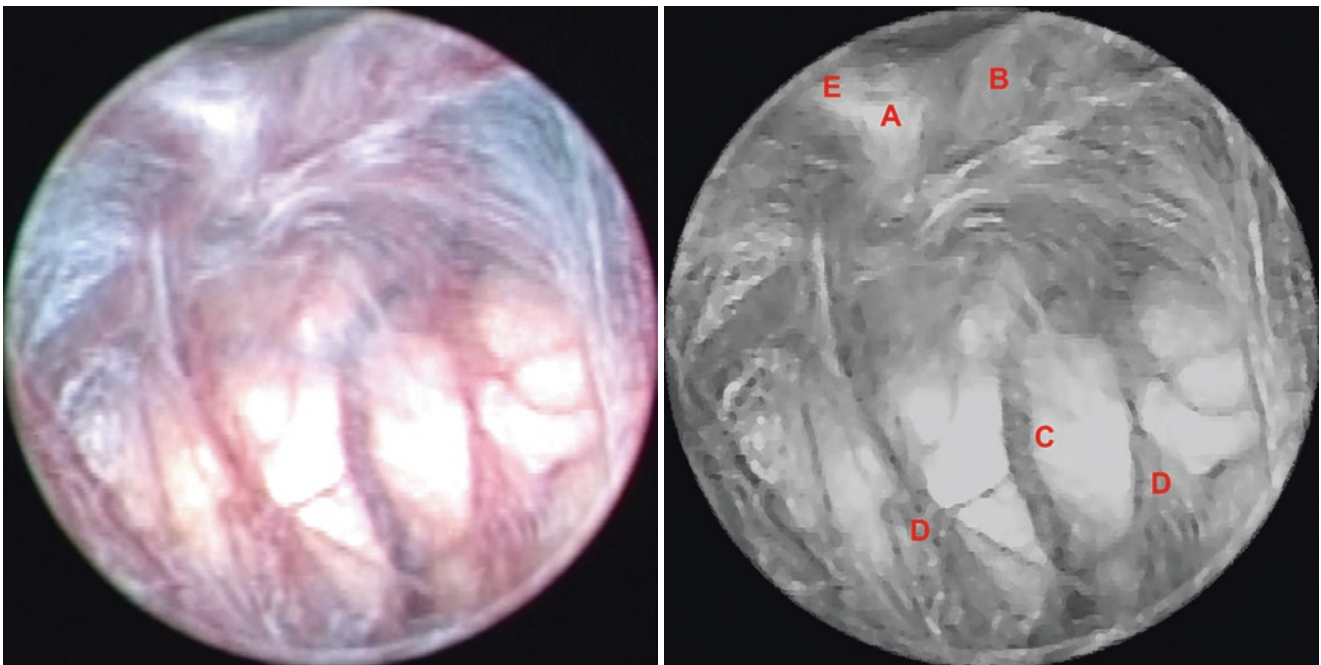


**Fig. 6.20** (A) Bifurcation of the basilar artery, (B) Right posterior cerebral artery (P1), (C) Mesencephalon, (D) Thalamoperforating arteries, (E) Left posterior cerebral artery (P1)

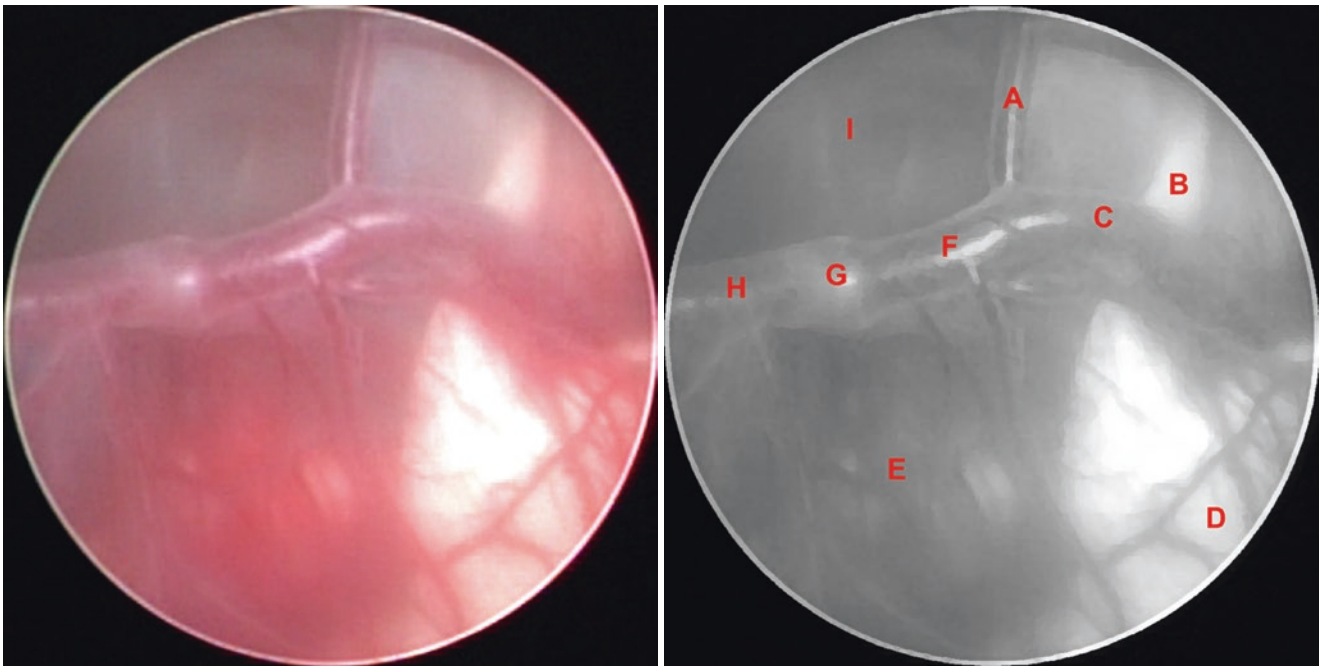


**Fig. 6.21** (A) Right posterior communicating artery, (B) Right oculomotor nerve (CN III), (C) Right posterior cerebral artery (P2), (D) Right cerebral peduncle, (E) Thalamoperforating arteries, (F) Right posterior

cerebral artery (P1), (G) Bifurcation of the basilar artery, (H) Left posterior cerebral artery (P1), (I) Membrane of Lilliequist – mesencephalic portion

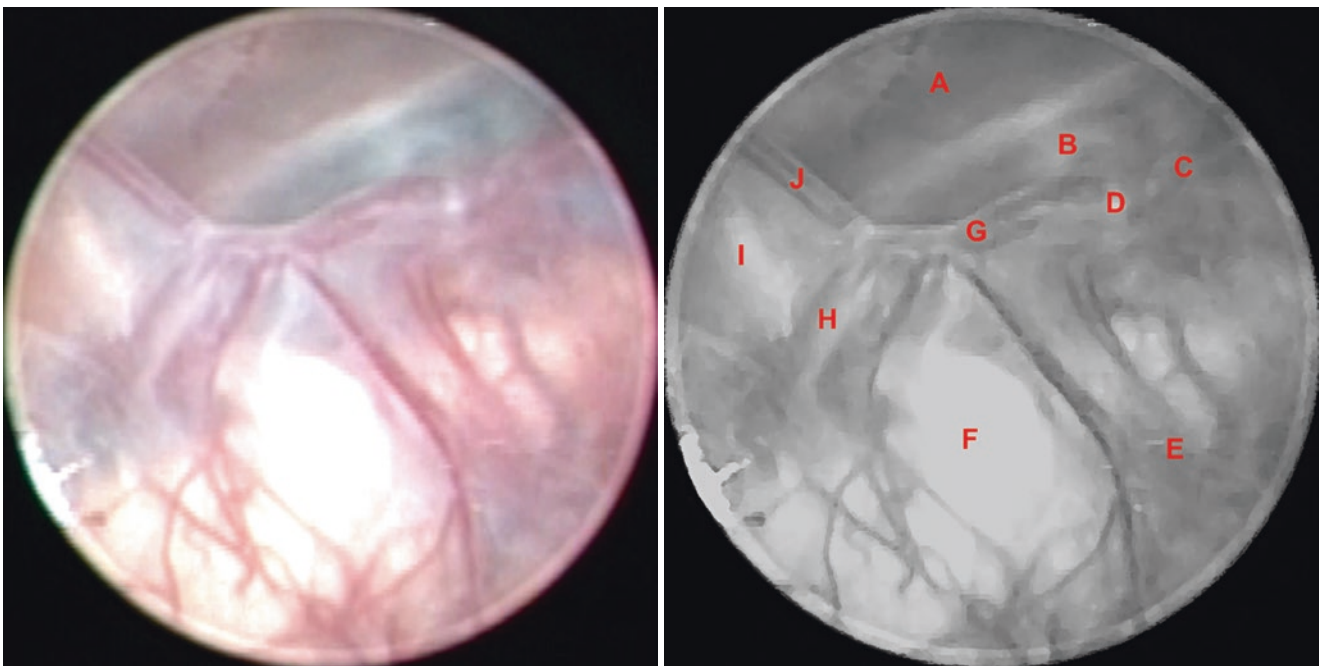


**Fig. 6.22** (A) Clivus, (B) Membrane of Lilliequist – mesencephalic portion, (C) Right posterior cerebral artery (P1), (D) Bifurcation of the basilar artery, (E) Thalamoperforating arteries, (F) Right cerebral

peduncle, (G) Left posterior cerebral artery (P1), (H) Left posterior cerebral artery (P2), (I) Left oculomotor nerve (CN III), (J) Left posterior communicating artery

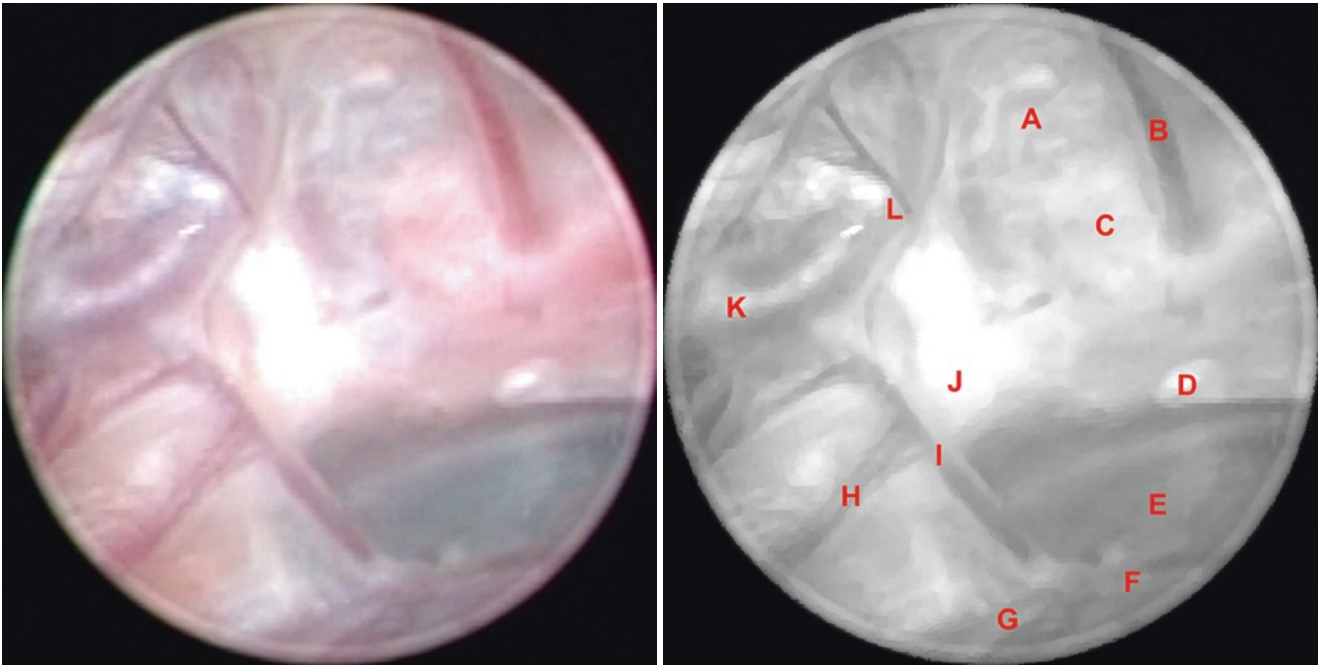


**Fig. 6.23** (A) Sellar diaphragm, (B) Pituitary stalk, (C) Pituitary gland, (D) Dorsum sellae, (E) Membrane of Lilliequist – mesencephalic portion, (F) Left posterior cerebral artery (P1), (G) Left posterior cerebral

artery (P2), (H) Left anterior thalamoperforating or pre-mammillary arteries, (I) Left posterior communicating artery, (J) Posterior clinoid process, (K) Middle cerebral artery (M1), (L) Internal carotid artery

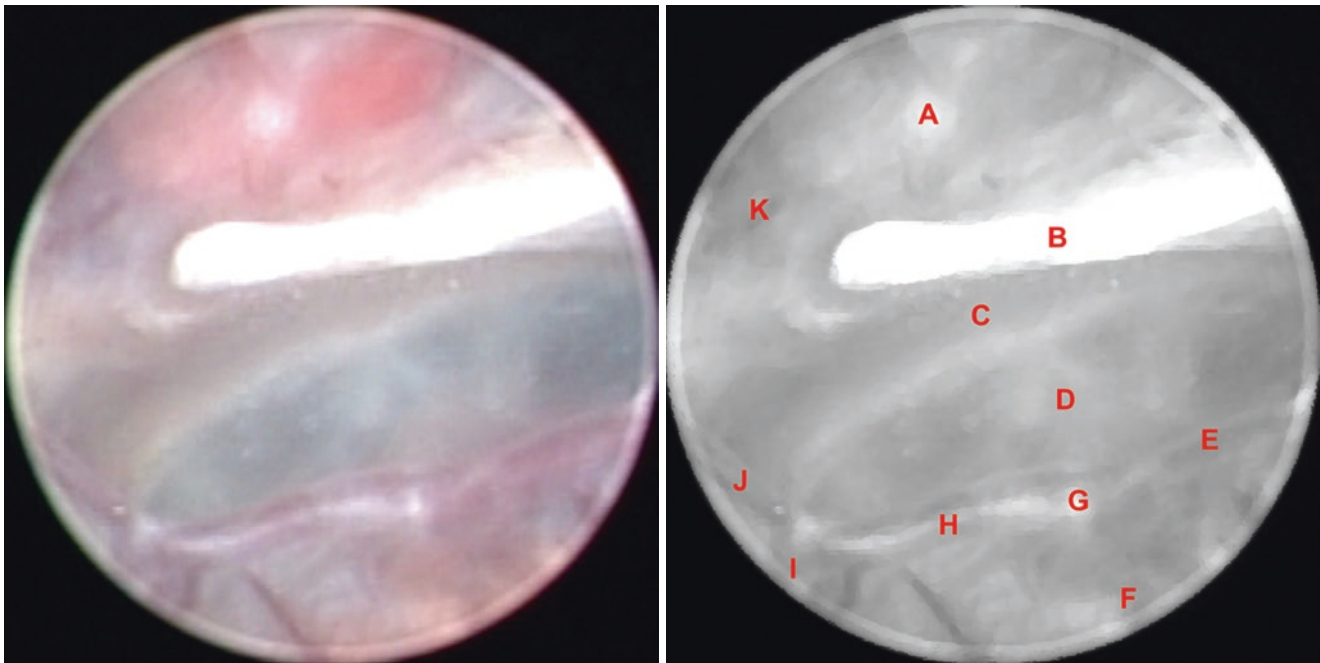


**Fig. 6.24** (A) Pituitary gland and stalk, (B) Dorsum sellae, (C) Clivus, (D) Membrane of Lilliequist – mesencephalic portion, (E) Right posterior cerebral artery (P1), (F) Thalamoperforating arteries, (G)

Bifurcation of the basilar artery, (H) Left posterior cerebral artery (P1), (I) Left posterior cerebral artery (P2), (J) Left posterior communicating artery, (K) Sellar diaphragm



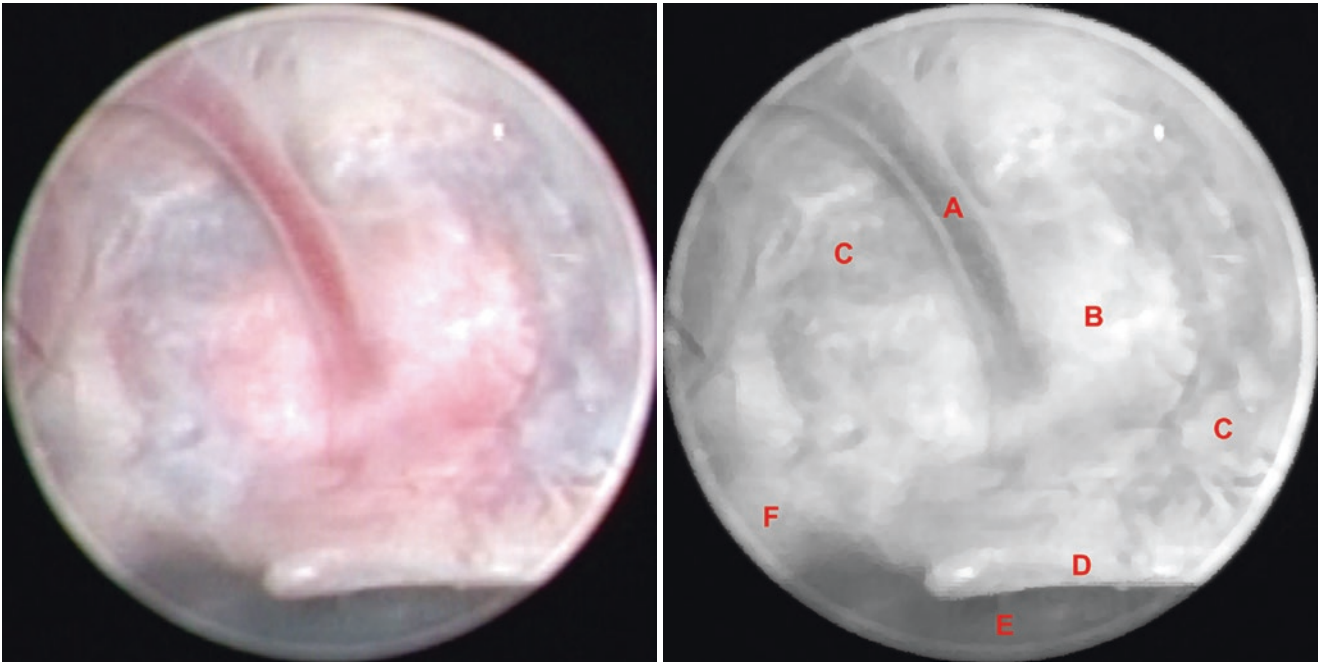


**Fig. 6.25** (A) Pituitary stalk, (B) Pituitary gland, (C) Sellar diaphragm, (D) Dorsum sellae, (E) Membrane of Liliequist – mesencephalic portion, (F) Posterior clinoid process

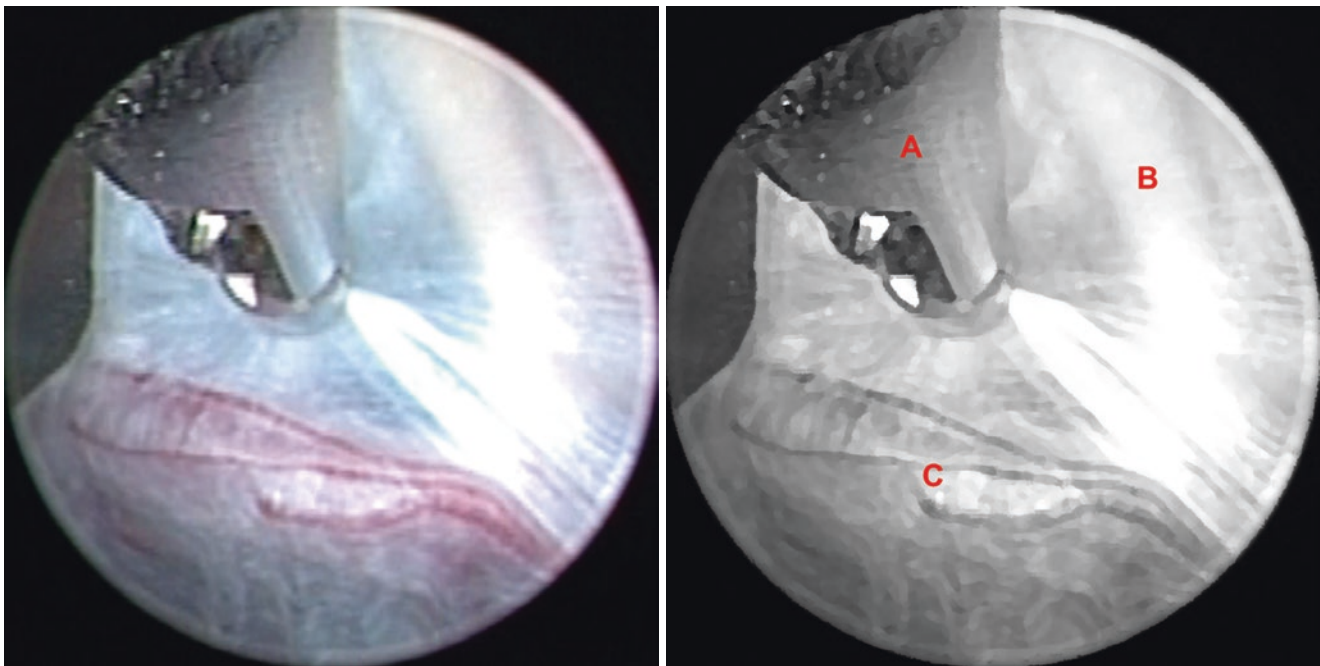


**Fig. 6.26** (A) Biopsy forceps fenestrating the membrane of Liliequist – diencephalic portion, (B) Right oculomotor nerve (CN III), (C) Right posterior cerebral artery (P2)

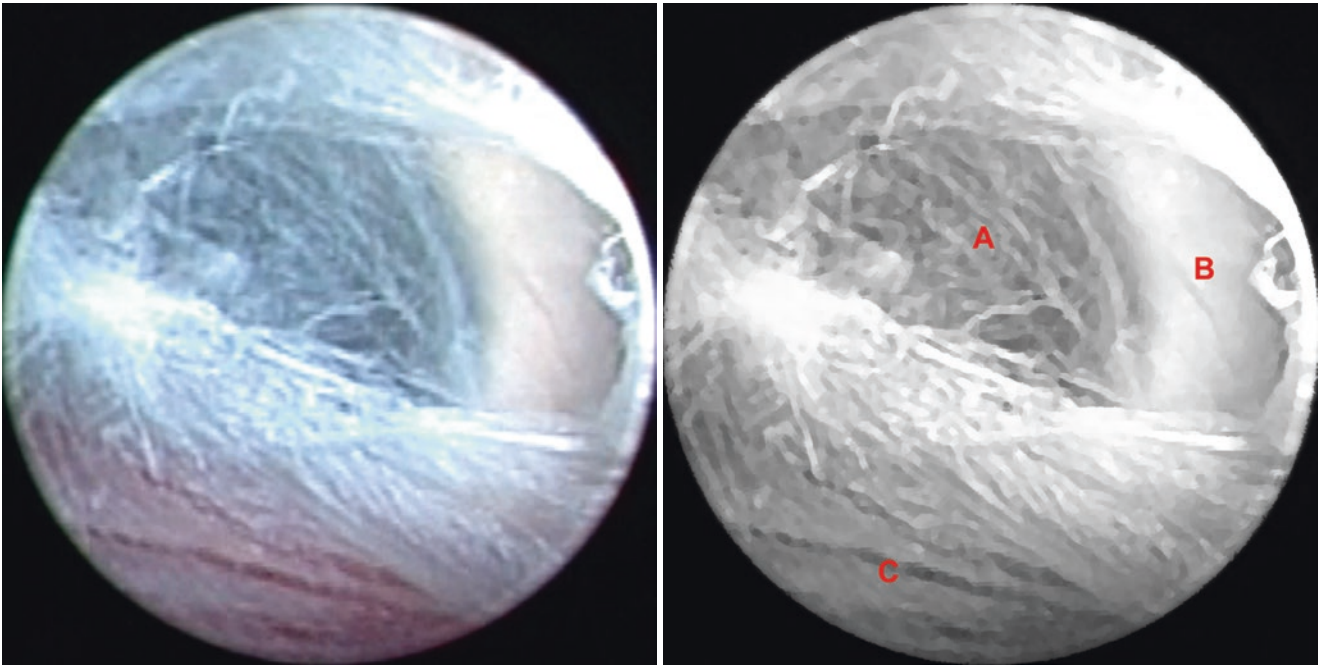


**Fig. 6.27** (A) Membrane of Liliequist– diencephalic portion, (B) Right oculomotor nerve (CN III), (C) Right posterior cerebral artery (P2)

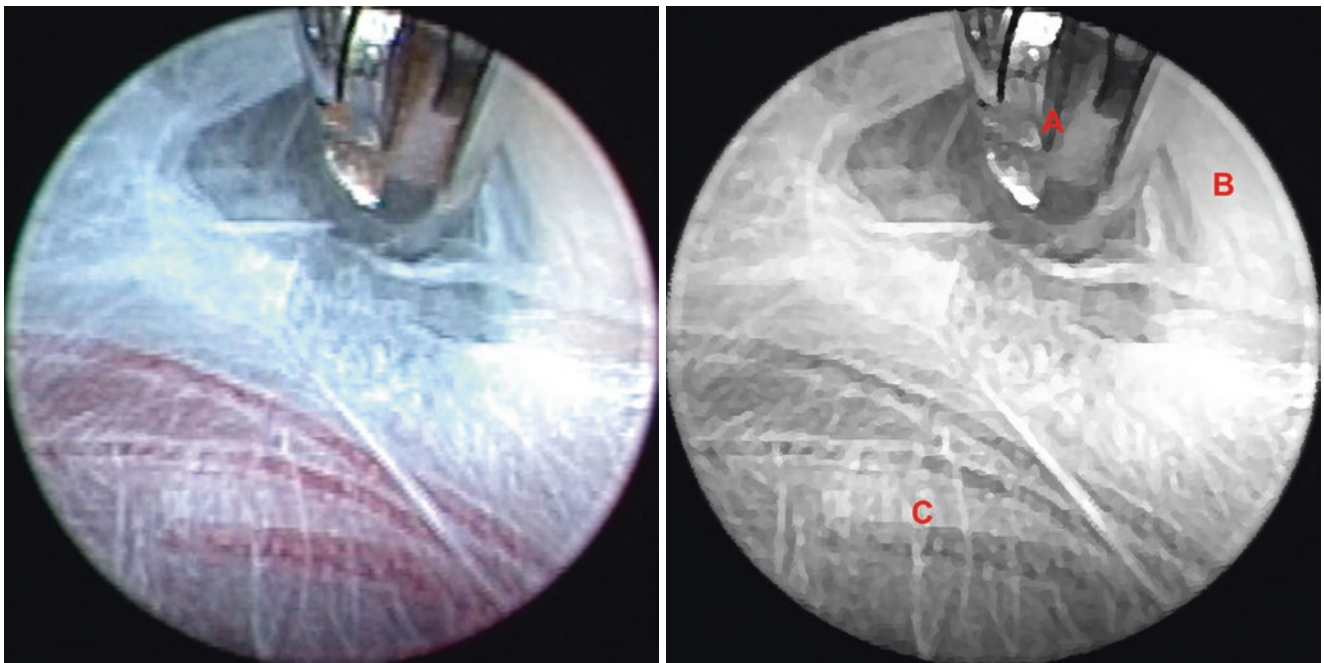


**Fig. 6.28** (A) Biopsy forceps fenestrating the membrane of Liliequist – diencephalic portion, (B) Right oculomotor nerve (CN III), (C) Right posterior cerebral artery (P2)

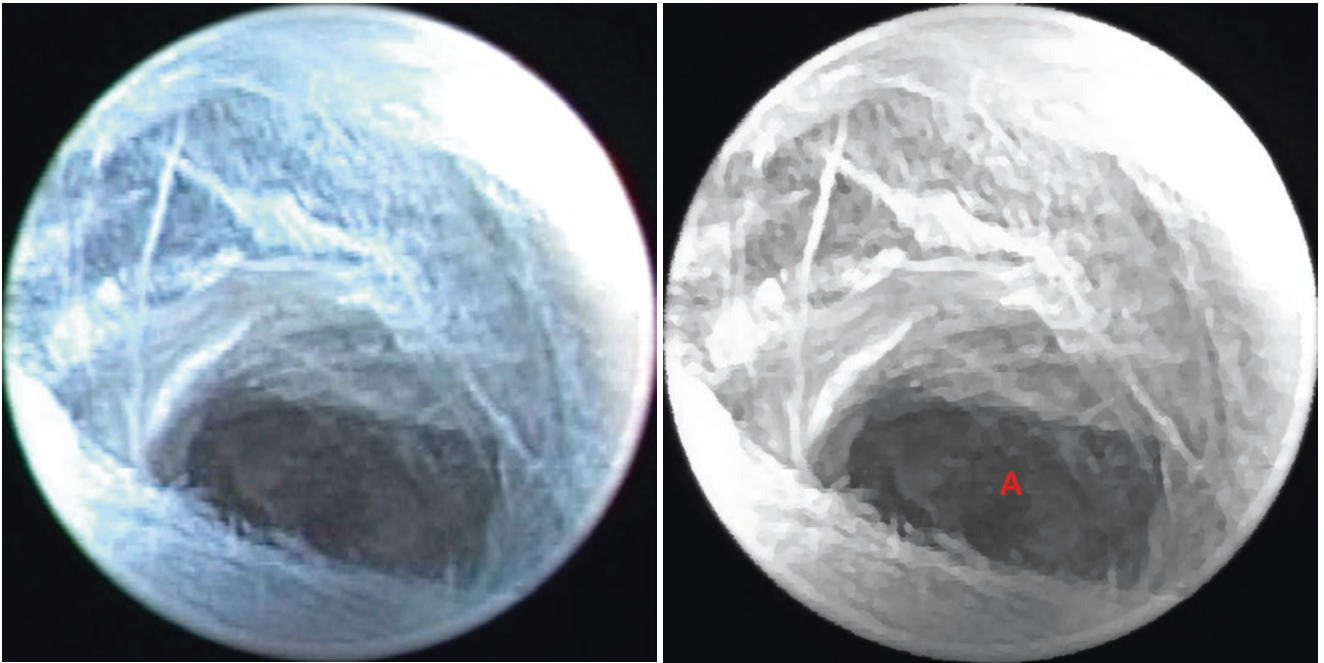


**Fig. 6.29** (A) Fenestration at the membrane of Liliequist – diencephalic portion

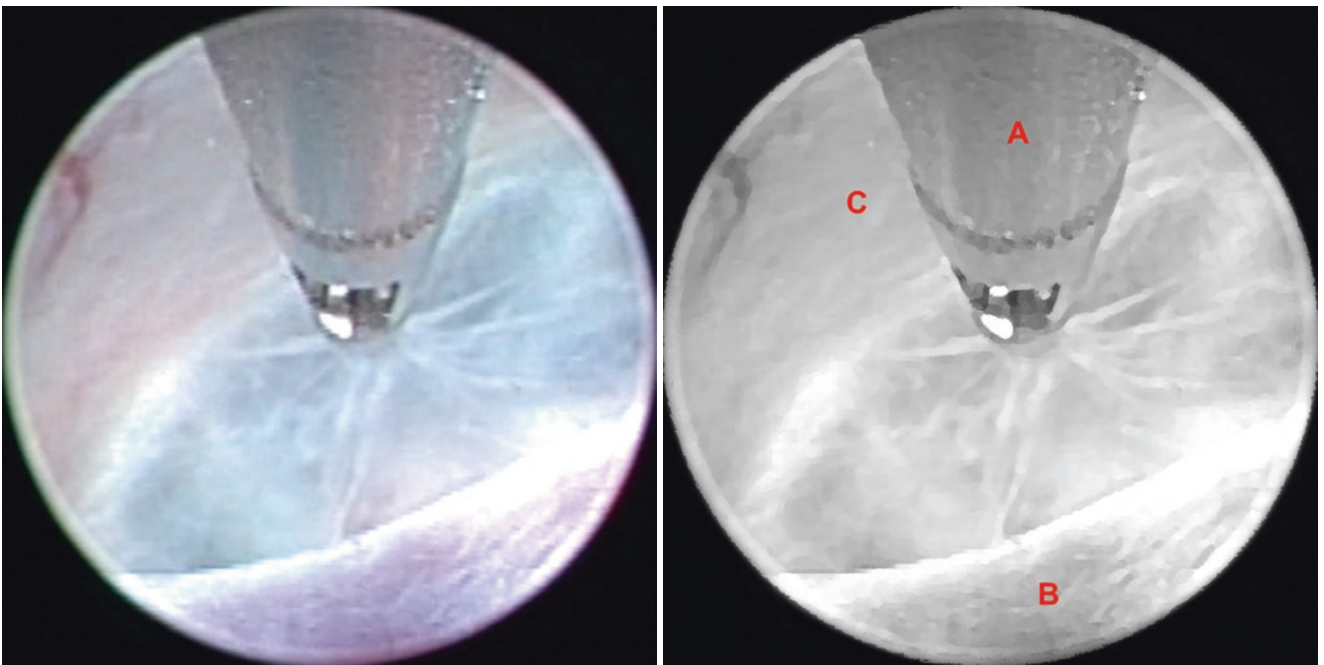


**Fig. 6.30** (A) Biopsy forceps fenestrating the membrane of Liliequist – mesencephalic portion, (B) Left posterior cerebral artery (P1), (C) Clivus

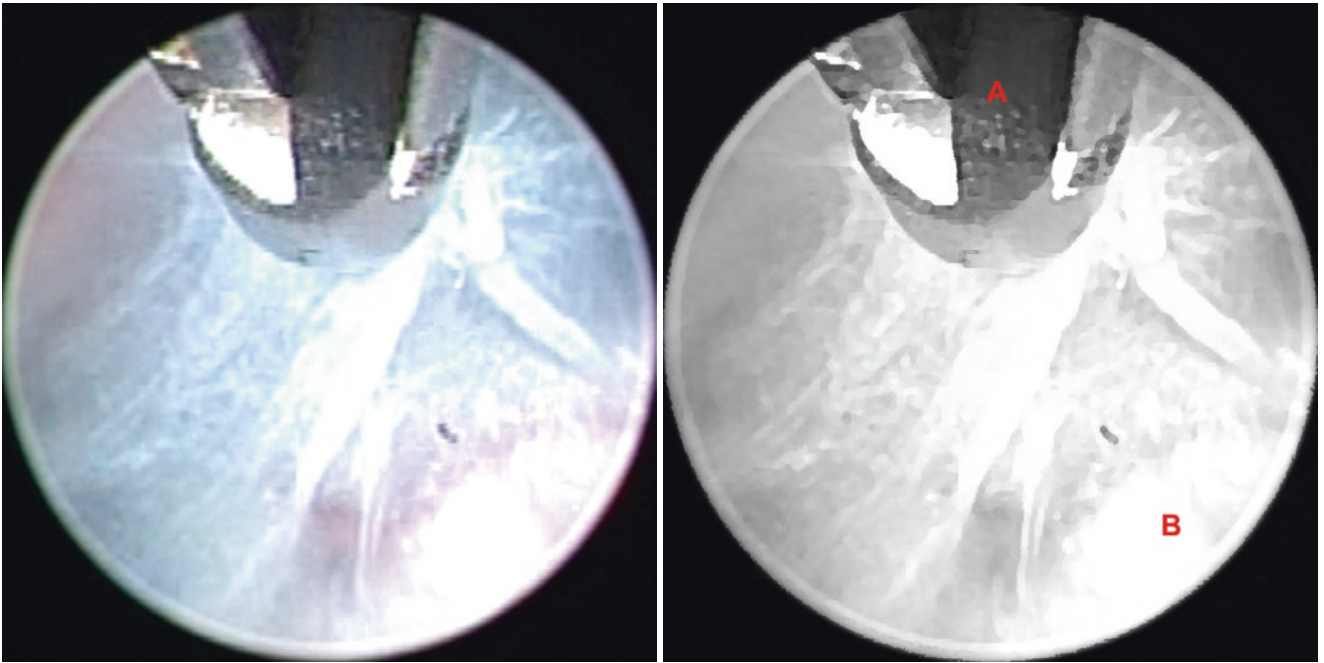


**Fig. 6.31** (A) Biopsy forceps fenestrating the membrane of Liliequist – mesencephalic portion, (B) Left posterior cerebral artery (P1)

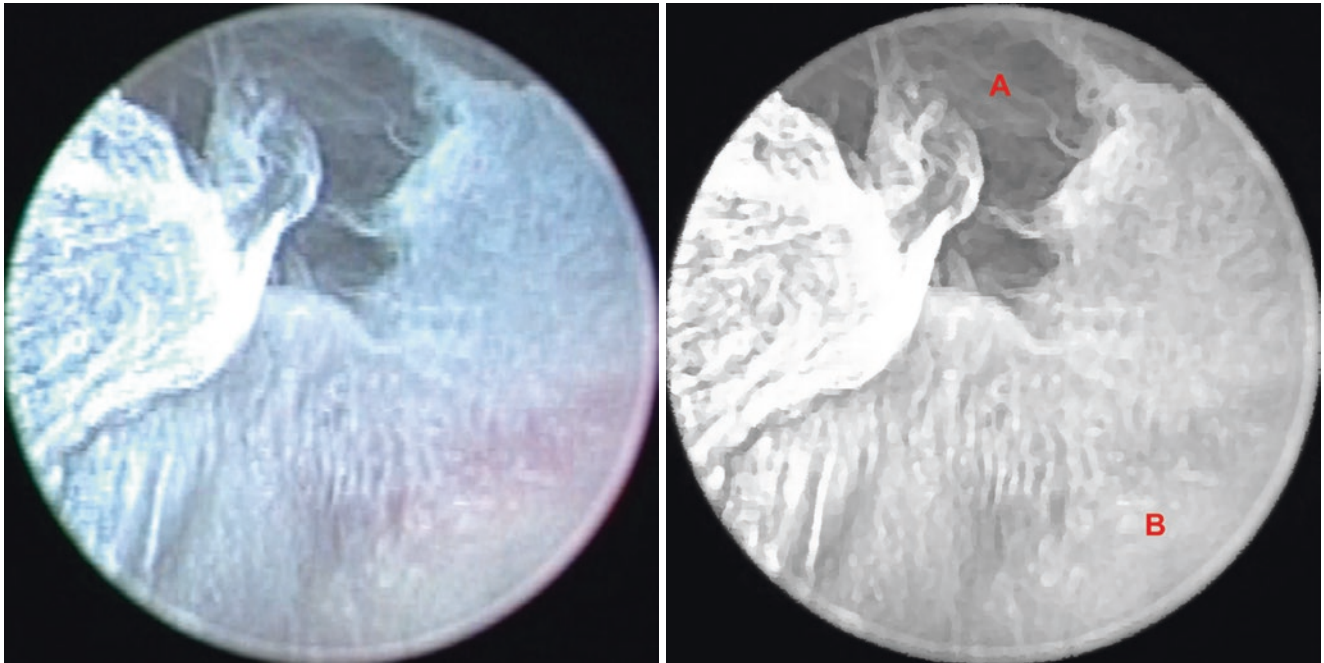


**Fig. 6.32** (A) Fenestration at the membrane of Liliequist – mesencephalic portion, (B) Left posterior cerebral artery (P1)

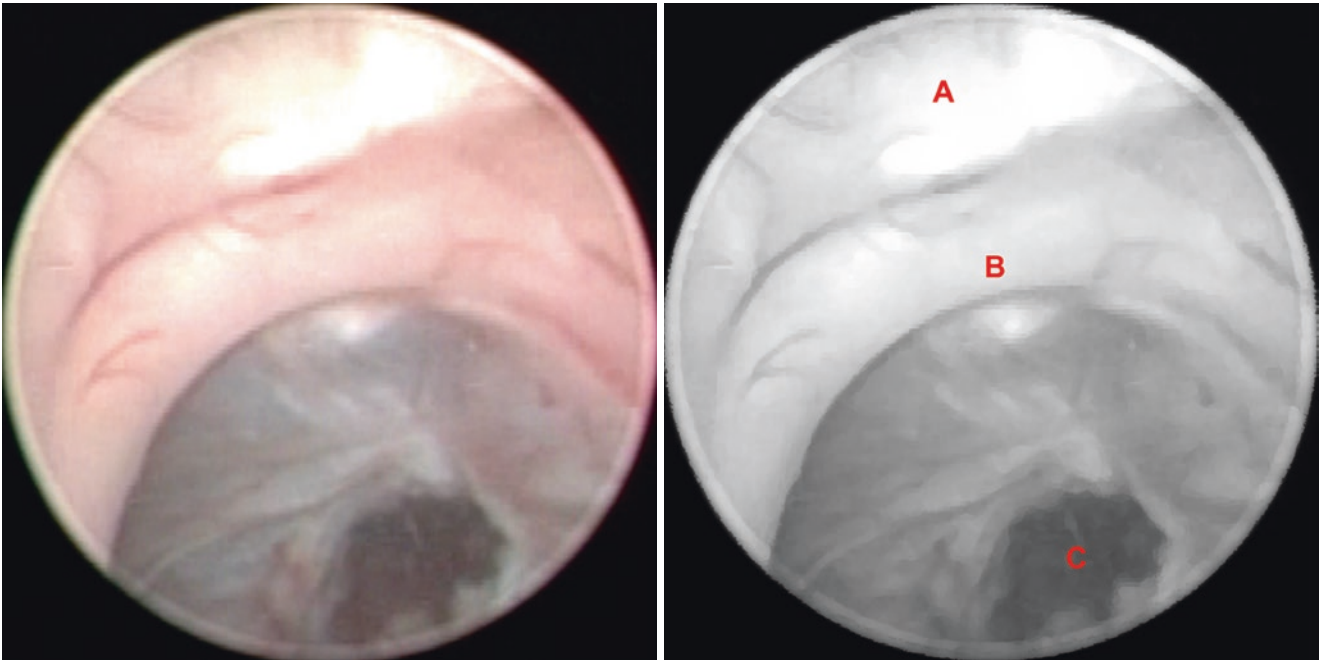


**Fig. 6.33** (A) Septum pellucidum, (B) Column of the fornix, (C) Cyst wall fenestration at the end of the procedure

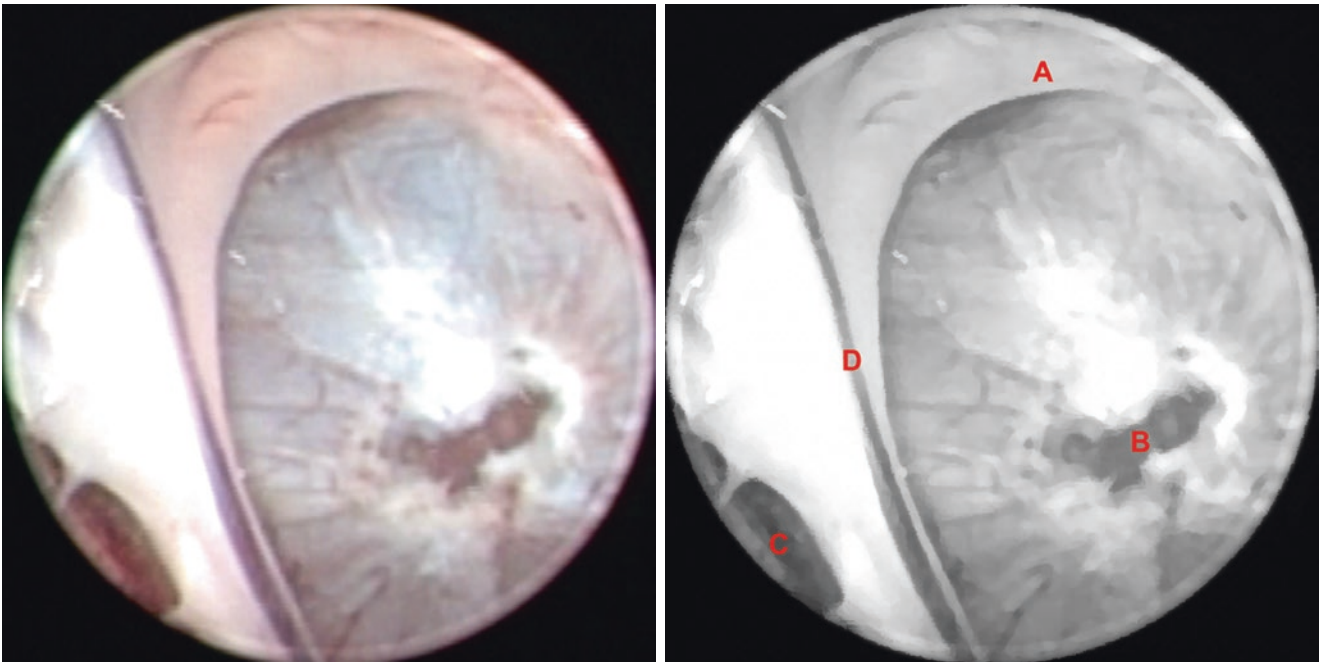


**Fig. 6.34** (A) Column of the fornix, (B) Cyst wall fenestration at the end of the procedure, (C) Septum pellucidum spontaneous fenestration due to chronic hydrocephalus, (D) Anterior septal vein

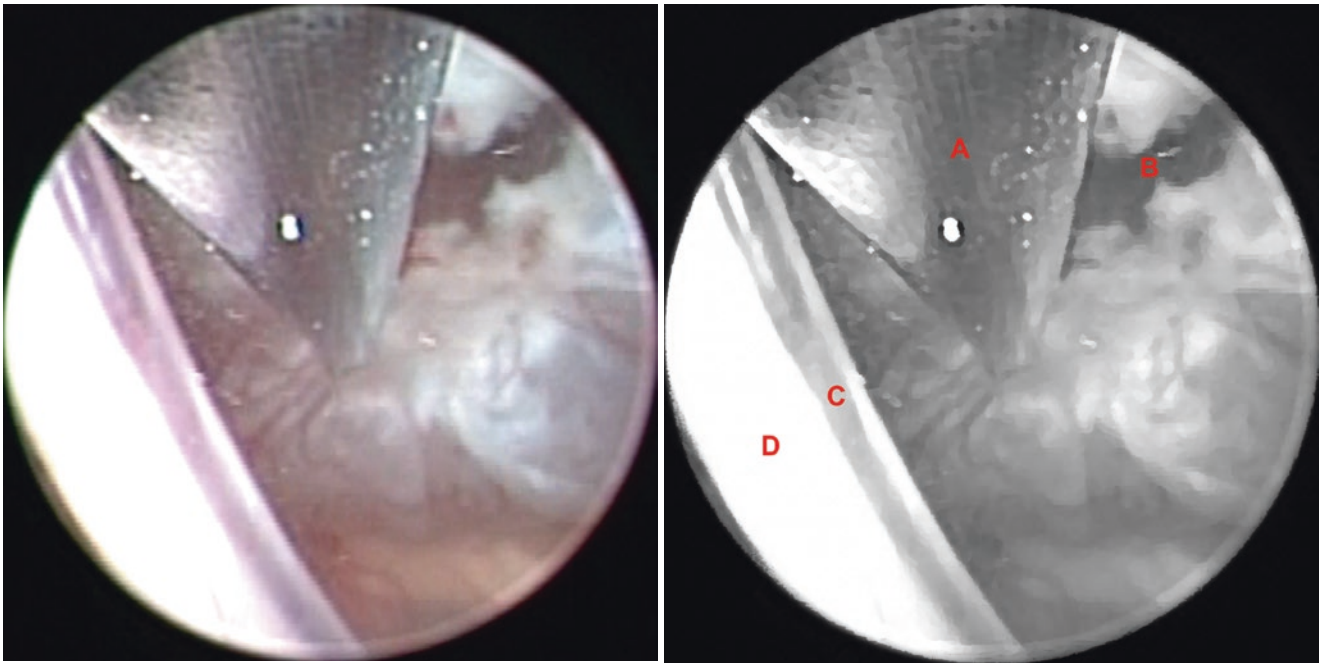


**Fig. 6.35** (A) Bipolar coagulation electrode, (B) Cyst wall fenestration at the end of the procedure, (C) Anterior septal vein, (D) Septum pellucidum

## References

- Golash A, Mitchell G, Mallucci C, May P, Pilling D. Prenatal diagnosis of suprasellar arachnoid cyst and postnatal endoscopic treatment. *Childs Nerv Syst.* 2001;17:739–42. doi:[10.1007/s003810100467](https://doi.org/10.1007/s003810100467).
- Pierre-Kahn A, Hanlo P, Sonigo P, Parisot D, McConnell RS. The contribution of prenatal diagnosis to the understanding of malformative intracranial cysts: state of the art. *Childs Nerv Syst.* 2000;16:619–26.
- Raffel C, McComb JG. To shunt or to fenestrate: which is the best surgical treatment for arachnoid cysts in pediatric patients? *Neurosurgery.* 1988;23:338–42.
- Rengachary SS, Watanabe I. Ultrastructure and pathogenesis of intracranial arachnoid cysts. *J Neuropathol Exp Neurol.* 1981;40:61–83.
- Miyajima M, Arai H, Okuda O, Hishii M, Nakanishi H, Sato K. Possible origin of suprasellar arachnoid cysts: neuroimaging and neurosurgical observations in nine cases. *J Neurosurg.* 2000;93:62–7. doi:[10.3171/jns.2000.93.1.0062](https://doi.org/10.3171/jns.2000.93.1.0062).
- André A, Zerah M, Roujeau T, Brunelle F, Blauwblomme T, Puget S, et al. Suprasellar arachnoid cysts: toward a new simple classification based on prognosis and treatment modality. *Neurosurgery.* 2016;78:370–9. doi:[10.1227/NEU.0000000000001049](https://doi.org/10.1227/NEU.0000000000001049).
- Shim KW, Lee YH, Park EK, Park YS, Choi JU, Kim DS. Treatment option for arachnoid cysts. *Childs Nerv Syst.* 2009;25:1459–66. doi:[10.1007/s00381-009-0930-7](https://doi.org/10.1007/s00381-009-0930-7).
- Sood S, Schuhmann MU, Cakan N, Ham SD. Endoscopic fenestration and coagulation shrinkage of suprasellar arachnoid cysts. Technical note. *J Neurosurg.* 2005;102:127–33. doi:[10.3171/ped.2005.102.1.0127](https://doi.org/10.3171/ped.2005.102.1.0127).
- Fujio S, Bunyamin J, Hirano H, Oyoshi T, Sadamura Y, Bohara M, et al. A novel bilateral approach for suprasellar arachnoid cysts: a case report. *PediatrNeurosurg.* 2016;51:30–4. doi:[10.1159/000440811](https://doi.org/10.1159/000440811).
- El-Ghandour NM. Endoscopic treatment of suprasellar arachnoid cysts in children. *J NeurosurgPediatr.* 2011;8:6–14. doi:[10.3171/2011.4.PEDS1184](https://doi.org/10.3171/2011.4.PEDS1184).
- Crimmins DW, Pierre-Kahn A, Sainte-Rose C, Zerah M. Treatment of suprasellar cysts and patient outcome. *J Neurosurg.* 2006;105:107–14. doi:[10.3171/ped.2006.105.2.107](https://doi.org/10.3171/ped.2006.105.2.107).
- Maher CO, Goumnerova L. The effectiveness of ventriculocystocisternostomy for suprasellar arachnoid cysts. *J NeurosurgPediatr.* 2011;7:64–72. doi:[10.3171/2010.10.PEDS10356](https://doi.org/10.3171/2010.10.PEDS10356).
- Gangemi M, Colella G, Magro F, Maiuri F. Suprasellar arachnoid cysts: endoscopy versus microsurgical cyst excision and shunting. *BrJNeurosurg.* 2007;21:276–80. doi:[10.1080/02688690701339197](https://doi.org/10.1080/02688690701339197).
- Gui SB, Wang XS, Zong XY, Zhang YZ, Li CZ. Suprasellar cysts: clinical presentation, surgical indications, and optimal surgical treatment. *BMC Neurol.* 2011;11:52. doi:[10.1186/1471-2377-11-52](https://doi.org/10.1186/1471-2377-11-52).
- Decq P, Brugieres P, Le Guerin C, Djindjian M, Keravel Y, Nguyen JP. Percutaneous endoscopic treatment of suprasellar arachnoid cysts: ventriculocystostomy or ventriculocystocisternostomy? Technical note. *J Neurosurg.* 1996;84:696–701. doi:[10.3171/jns.1996.84.4.0696](https://doi.org/10.3171/jns.1996.84.4.0696).
- Ozek MM, Urgan K. Neuroendoscopic management of suprasellar arachnoid cysts. *World Neurosurg.* 2013;79:S19.e13–8. doi:[10.1016/j.wneu.2012.02.011](https://doi.org/10.1016/j.wneu.2012.02.011).
- Gui SB, Yu SY, Cao L, Bai JW, Wang XS, Li CZ, et al. Endoscopic treatment of suprasellar cysts without hydrocephalus. *J Neurosurg Pediatr.* 2016;17:1–8. doi:[10.3171/2016.4.PEDS15695](https://doi.org/10.3171/2016.4.PEDS15695).
- Li Y, Zhao Y, Zhang J, Zhang Z, Dong G, Wang Q, et al. Low-cost interactive image-based virtual endoscopy for the diagnosis and surgical planning of suprasellar arachnoid cysts. *World Neurosurg.* 2016;88:76–82. doi:[10.1016/j.wneu.2015.12.038](https://doi.org/10.1016/j.wneu.2015.12.038).

## 7.1 Introduction

Hydranencephaly (HE) is a rare, mostly isolated abnormality, which is reported to affect about 1 of 5000 continuing pregnancies [1, 2]. It is one of the most severe forms of bilateral cerebral cortical anomalies. In this condition, the cerebral hemispheres are completely or almost completely missing. In their place, there is a membranous sac filled with cerebrospinal fluid (CSF), glial tissue, and ependyma. There is, however, preservation of the skull. There is variable and partial involvement of the frontal, parietal, temporal, and occipital lobes. The mesencephalon, cerebellum, thalami, basal nuclei, and choroid plexus are usually not involved [3–5]. The etiopathogenesis of HE is still unknown; however, most researchers support the hypothesis that the brain damage in HE is related to early internal carotid artery involvement [6–8]. Unlike the unilateral form, the prognosis of HE is usually quite poor. Affected patients mostly die in utero. In the survivors, death usually occurs in the first year of life. Developmental delay, drug-resistant seizures, spastic diplegia, severe growth failure, and respiratory infections are features that burden the life of these patients and are frequent causes of their death. However, patients with survivals of 20 [9], 22 [10], and 32 [7] years have been reported in the literature. The survival of the patient is related to the integrity of the brainstem, which regulates vital aspects, such as temper-

ature, blood pressure, and cardiorespiratory function [6]. For the child with HE who survives, there is debate as to whether or not to perform any surgical treatment, considering the severe brain impairment [11]. Classical surgical treatment consists of a shunt, which drains the CSF, reducing the cerebral tension and the progressive increase of the cerebral volume. Recently, an optional treatment has been proposed, consisting of choroid plexus coagulation (CPC) [12]. CPC stabilizes macrocephaly in approximately 40% of infants with severe congenital hydrocephalus and hydranencephaly and can be considered as an alternative to shunt placement [13]. In particular, in cases of hydranencephaly with an excellent view of the choroid plexus, the procedure had good indications for avoiding the complications associated with a shunt. Because hydranencephaly is very rare and the follow-up period is typically short due to the disease characteristics, a large number of patients and long-term follow-up are needed to determine the real effectiveness of the CPC procedure in this patient group [14]. Arachnoid collapse is a previously unreported complication of CPC treatment of hydranencephaly [15]. Figures 7.1 and 7.2 depict typical aspects of hydranencephaly on computed tomography (CT) scan and magnetic resonance imaging (MRI), and Figs. 7.3 and 7.4 show neuroendoscopic techniques. Intraoperative images are shown in Figs. 7.5, 7.6, 7.7, 7.8, 7.9, 7.10, 7.11, 7.12, 7.13, and 7.14.

## 7.2 Hydranencephaly

### 7.2.1 Typical Aspect on Imaging Examinations



**Fig. 7.1** Typical aspect of hydranencephaly on CT scan, with presence of posterior fossa



**Fig. 7.2** Typical aspect of hydranencephaly on axial T2-weighted MRI, with presence of thalami, brainstem, superior part of cerebellar vermis, and occipital lobe (Image courtesy of Dr. Ian Bickle, [Radiopaedia.org](http://Radiopaedia.org), rID 25,150)



### 7.2.2 Intraoperative Images



**Fig. 7.3** Gaab system (Karl Storz, Tuttlingen, Germany) inspection showing aspect of the skull similar to that on transillumination examination



**Fig. 7.4** Free-hand technique with Gaab system (Karl Storz, Tuttlingen, Germany), performing choroid plexus coagulation (aspect of the skull similar to that on transillumination examination)

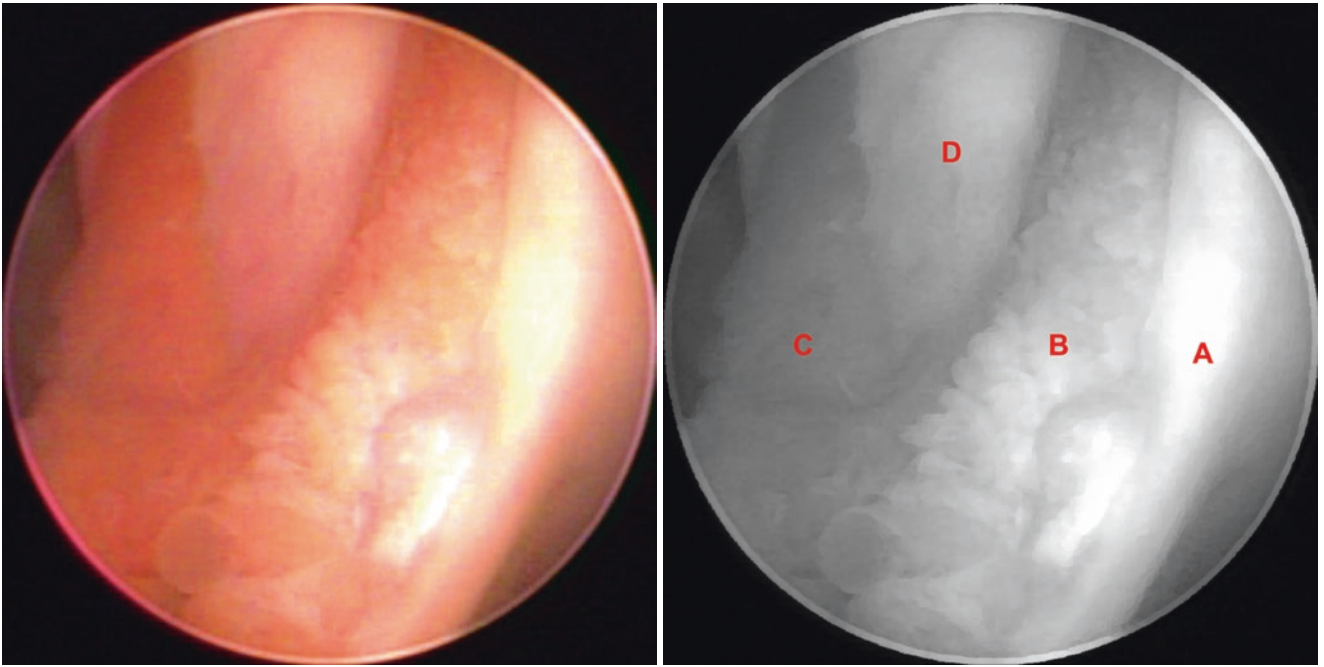


**Fig. 7.5** (A) Right thalamus, (B) right choroid plexus, (C) left choroid plexus, (D) left thalamus

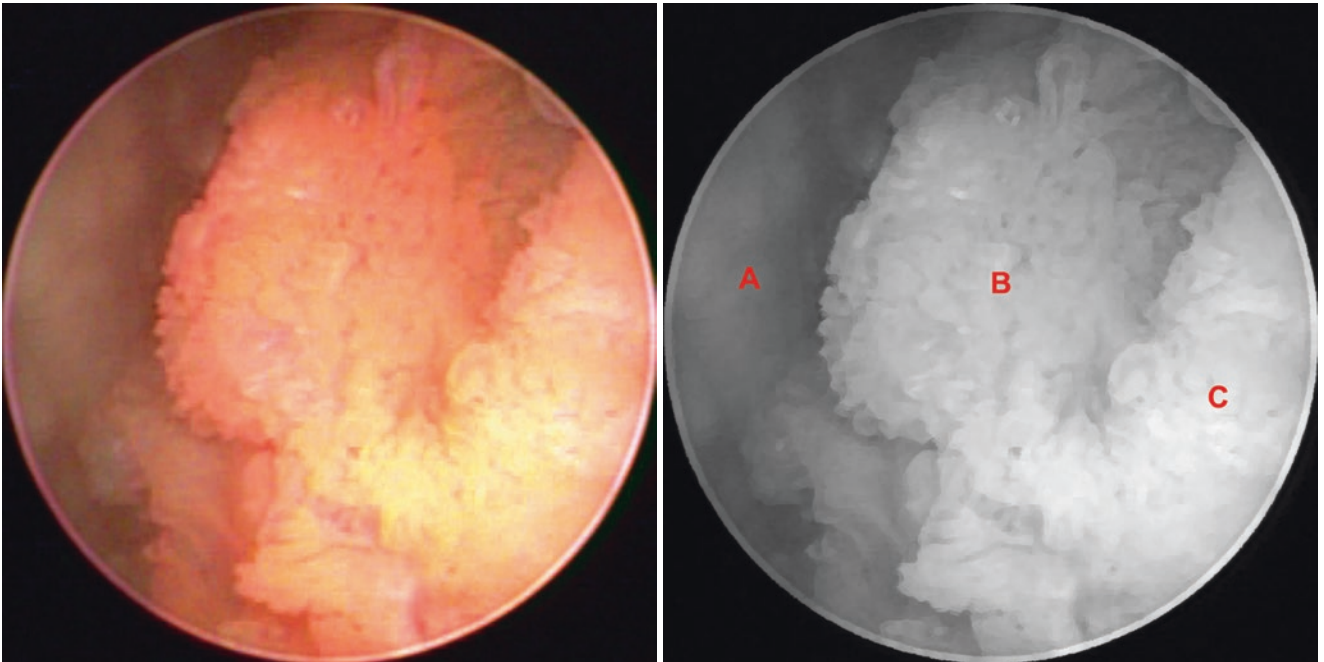


**Fig. 7.6** (A) Intracranial space (no ventricle!), (B) Left choroid plexus, (C) Right choroid plexus

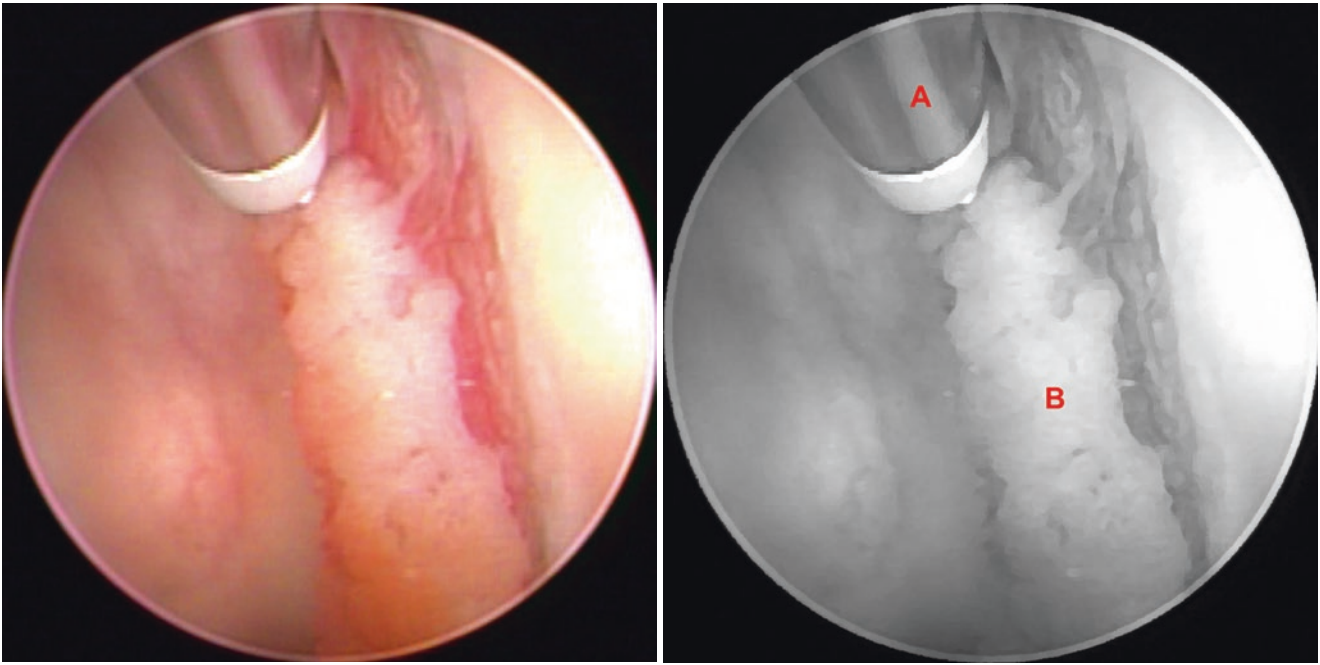


**Fig. 7.7** (A) Bipolar coagulation electrode, (B) Right choroid plexus and its basal vessels

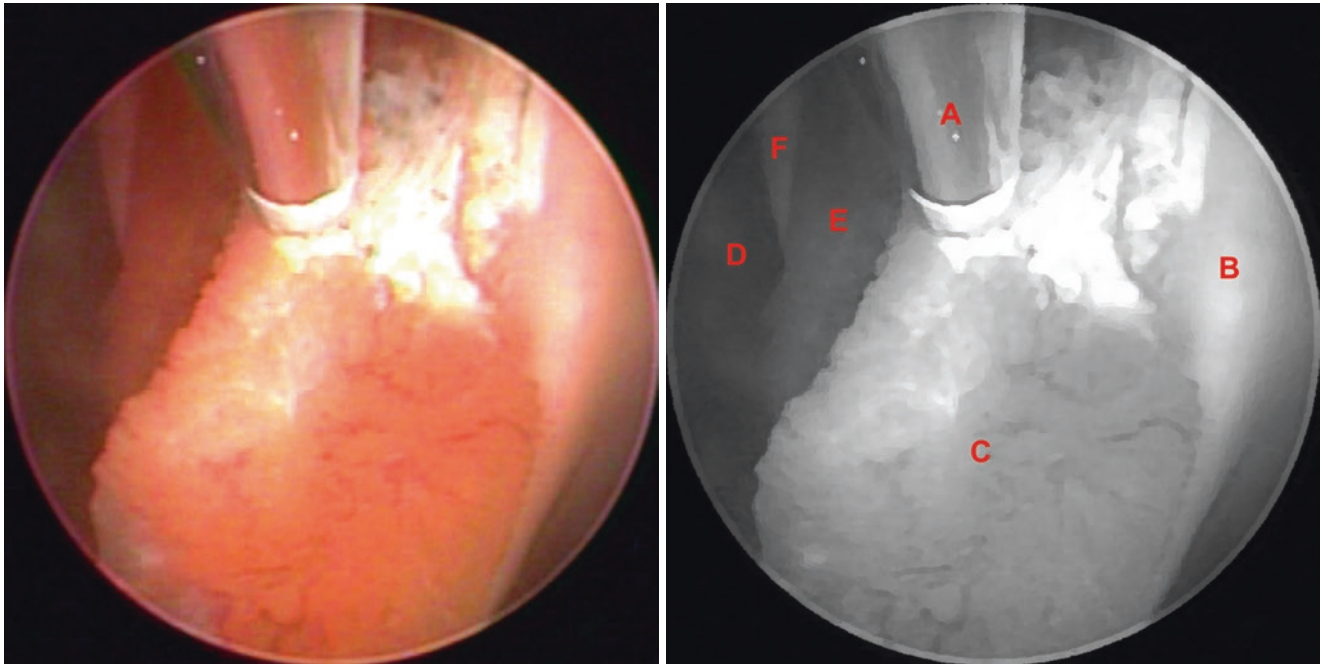


**Fig. 7.8** (A) Bipolar coagulation electrode, (B) Right thalamus, (C) Right choroid plexus, (D) Intracranial space (no ventricle!), (E) Left choroid plexus, (F) Left thalamus

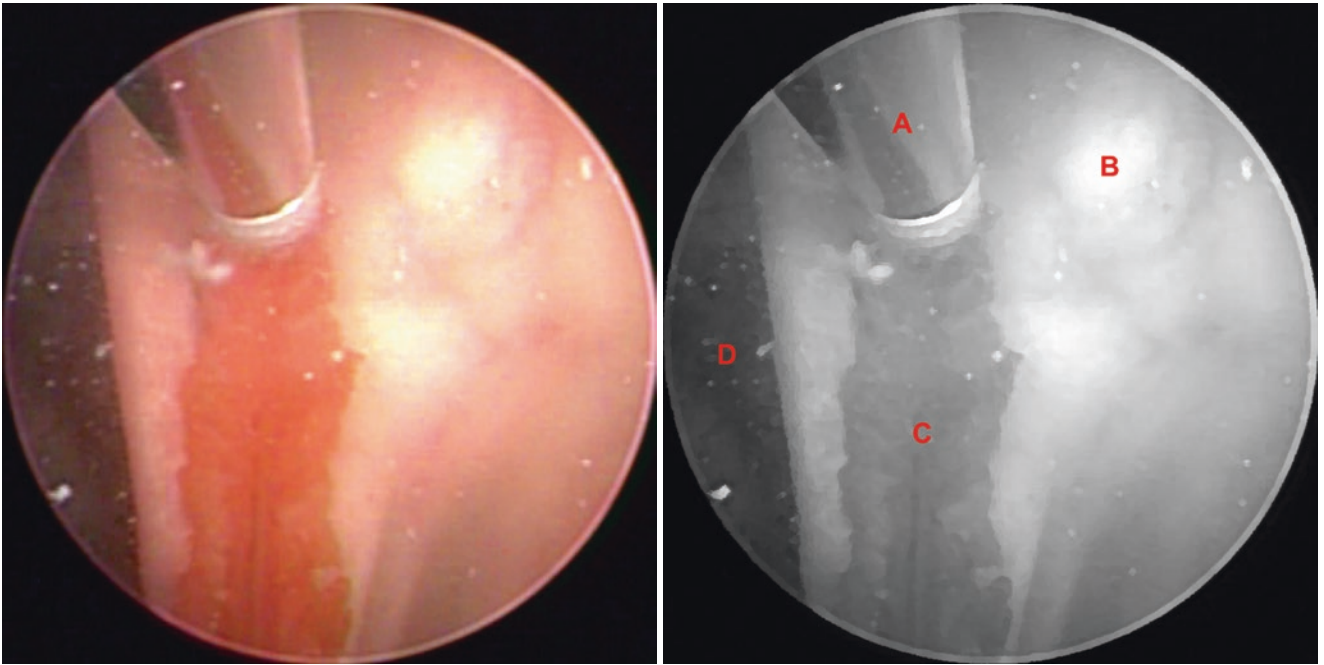


**Fig. 7.9** (A) Bipolar coagulation electrode, (B) Left thalamus, (C) Left choroid plexus, (D) Intracranial space (no ventricle!)

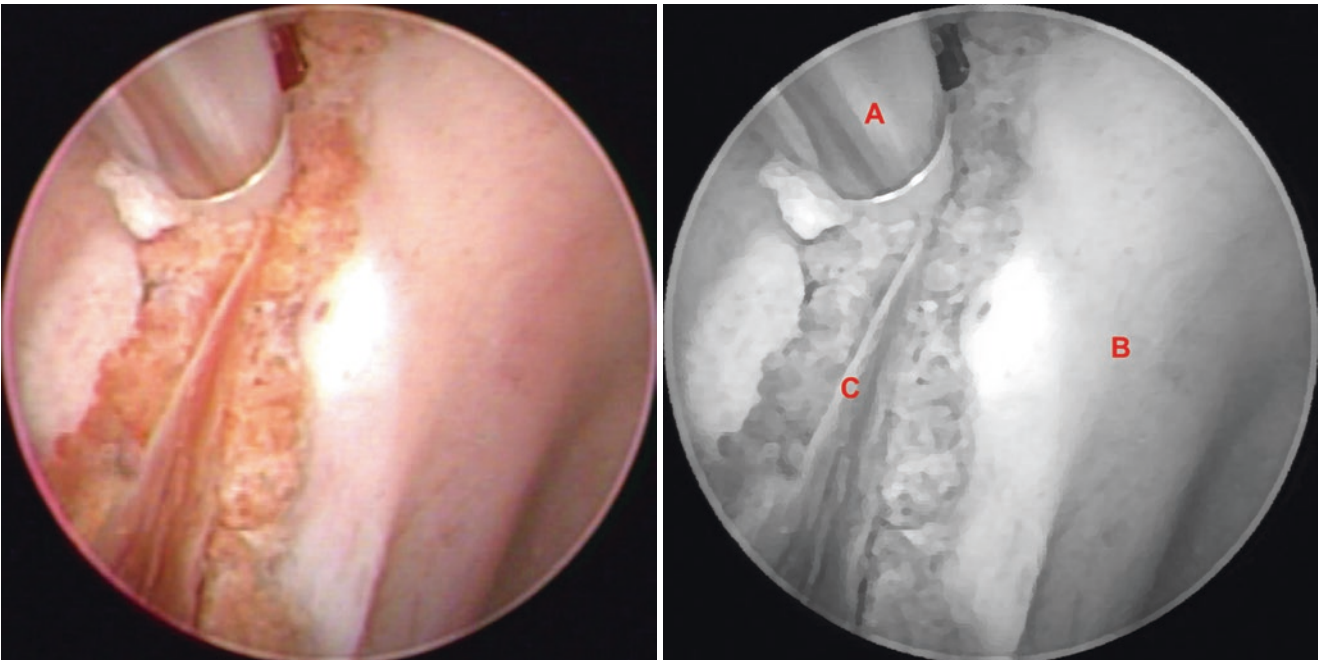


**Fig. 7.10** (A) Bipolar coagulation electrode, (B) Left thalamus, (C) Left choroid plexus

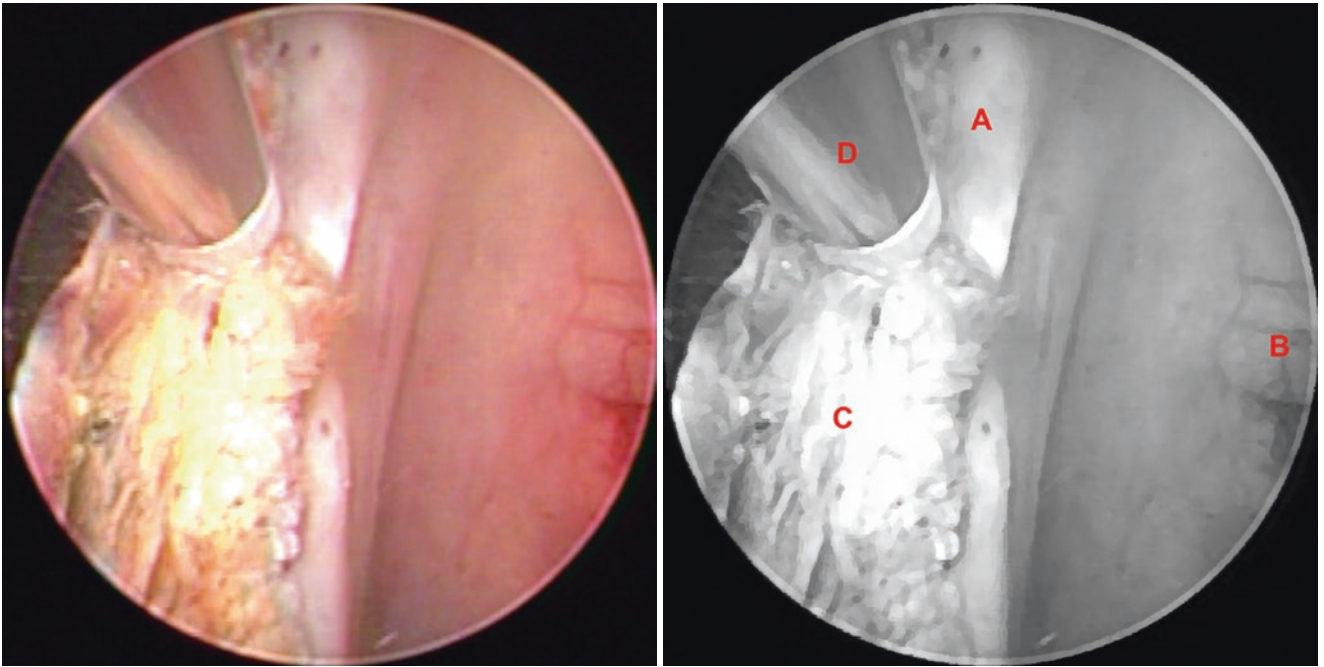


**Fig. 7.11** (A) Left thalamus, (B) Cerebellar culmen, (C) Left choroid plexus, (D) Bipolar coagulation electrode

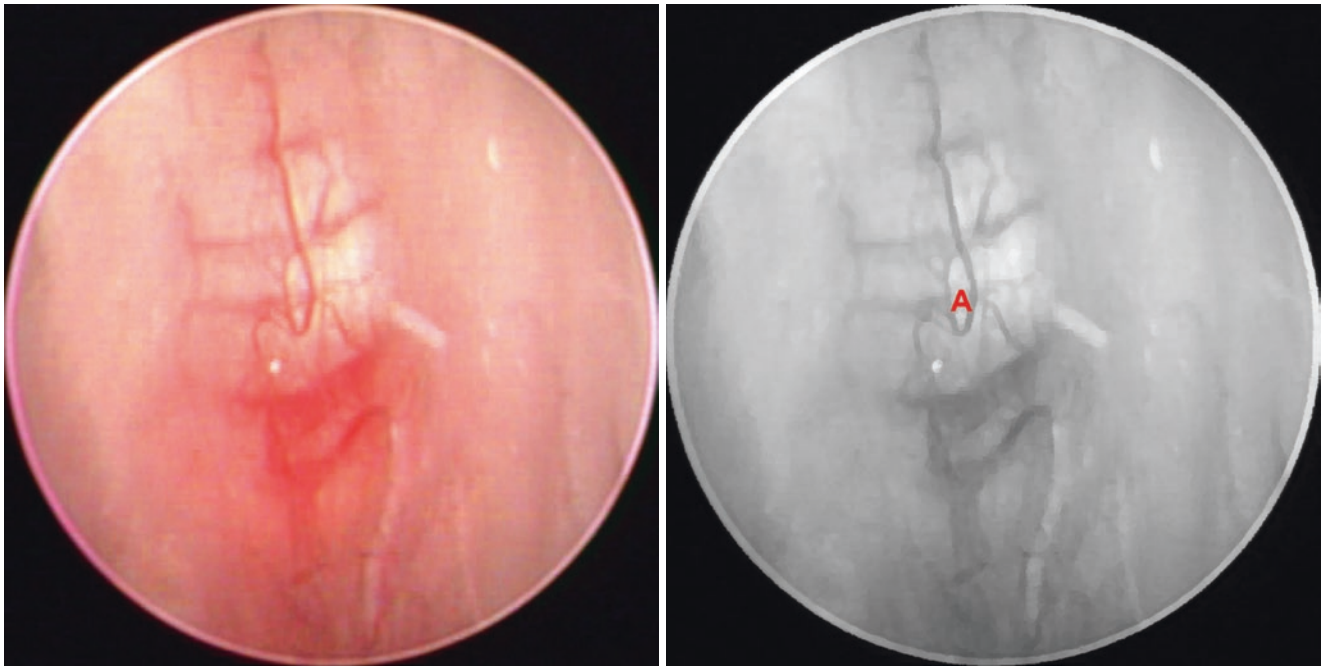


**Fig. 7.12** (A) Cerebellar culmen

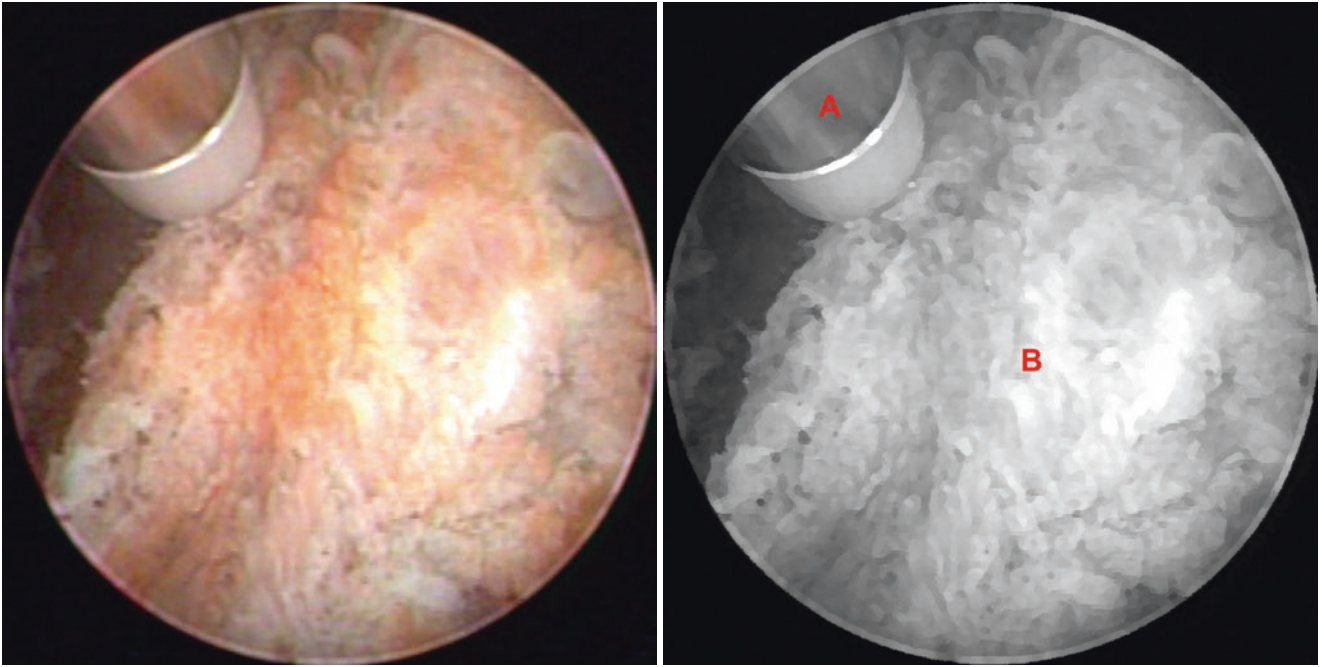


**Fig. 7.13** (A) Bipolar coagulation electrode, (B) Coagulated choroid plexus

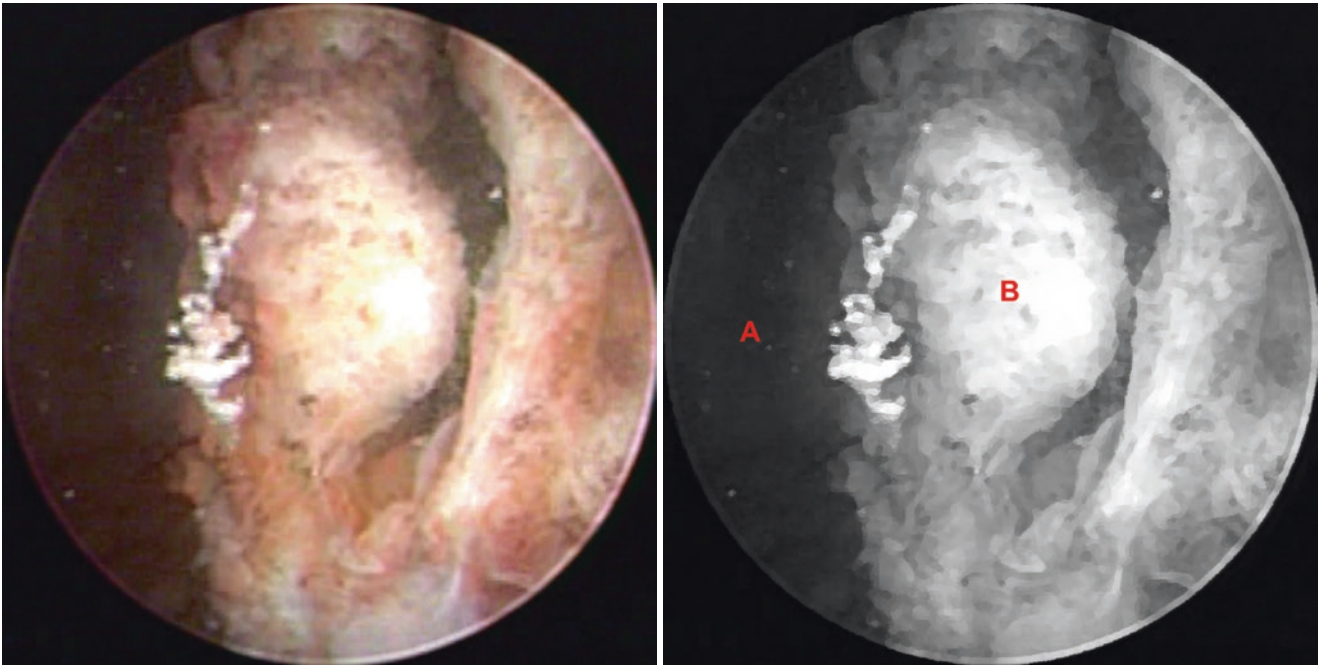


**Fig. 7.14** (A) Intracranial space (no ventricle!), (B) Coagulated choroid plexus (final aspect)

## References

1. Filly RA. Ultrasound evaluation of the fetal neural axis. In: Callen PW, editor. *Ultrasonography in obstetrics and gynecology*. 3rd ed. Philadelphia: WB Saunders; 1994. p. 189–234.
2. Chervenak FA, Isaacson GC, Campbell S. Hydranencephaly. In: Chervenak FA, Isaacson GC, Campbell S, editors. *Ultrasound in obstetrics and gynecology*. Boston/Toronto/London: Little, Brown and Company; 1993. p. 1187–8.
3. Hamby WB, Krauss RF, Beswick WF. Hydranencephaly: clinical diagnosis; presentation of seven cases. *Pediatrics*. 1950;6:371–83.
4. Kurtz AB, Johnson PT. Diagnosis please. Case 7: hydranencephaly. *Radiology*. 1999;210:419–22. doi:10.1148/radiology.210.2.r99fe50419.
5. Potter EL. *Pathology of the fetus and the newborn*. 1st ed. Chicago: Year Book Publishers; 1952.
6. McAbee GN, Chan A, Erde EL. Prolonged survival with hydranencephaly: report of two patients and literature review. *Pediatr Neurol*. 2000;23:80–4.
7. Cecchetto G, Milanese L, Giordano R, Viero A, Suma V, Manara R. Looking at the missing brain: hydranencephaly case series and literature review. *Pediatr Neurol*. 2013;48:152–8. doi:10.1016/j.pediatrneurol.2012.10.009.
8. Quek YW, Su PH, Tsao TF, Chen JY, Ng YY, Hu JM, et al. Hydranencephaly associated with interruption of bilateral internal carotid arteries. *PediatrNeonatal*. 2008;49:43–7. doi:10.1016/S1875-9572(08)60011-X.
9. Covington C, Taylor H, Gill C, Padaliya B, Newman W, Smart 3rd JR, et al. Prolonged survival in hydranencephaly: a case report. *Tenn Med*. 2003;96:423–4.
10. Bae JS, Jang MU, Park SS. Prolonged survival to adulthood of an individual with hydranencephaly. *Clin Neurol Neurosurg*. 2008;110:307–9. doi:10.1016/j.clineuro.2007.12.003.
11. Pavone P, Praticò AD, Vitaliti G, Ruggieri M, Rizzo R, Parano E, et al. Hydranencephaly: cerebral spinal fluid instead of cerebral mantles. *Ital J Pediatr*. 2014;40:79. doi:10.1186/s13052-014-0079-1.
12. Zhu X, Di Rocco C. Choroid plexus coagulation for hydrocephalus not due to CSF overproduction: a review. *Childs Nerv Syst*. 2013;29:35–42. doi:10.1007/s00381-012-1960-0.
13. Shitsama S, Wittayanakorn N, Okechi H, Albright AL. Choroid plexus coagulation in infants with extreme hydrocephalus or hydranencephaly. *J Neurosurg Pediatr*. 2014;14:55–7. doi:10.3171/2014.3.PEDS13488.
14. Kim SY, Cho JH, Kim KH. Endoscopic coagulation of choroid plexus in hydranencephaly. *J Korean Neurosurg Soc*. 2014;55:375–8. doi:10.3340/jkns.2014.55.6.375.
15. Ray C, Mobley J, Thompson M, Nagy L. Hydranencephaly: considering prolonged survival and treatment by endoscopic choroid plexus coagulation. *Turk Neurosurg*. 2015;25:788–92. doi:10.5137/1019-5149.JTN.10453-14.1.

# Index

- A**  
Abducens nerve (CN VI), 207, 233  
Adhesion between mammillary bodies, 161  
Adhesion due to inflammatory process, 228, 230  
*Aestimativa*, 5  
AIDA system, 43, 52  
Alexander Monro secundus, 17, 18  
*Anathomia*, 10, 11  
*Anathomia Mundini*, 6–10, 14  
Andrea del Verrocchio, 10  
Andreas Vesalius, 14  
Anterior  
    caudate veins, 74, 76, 77, 80, 89, 111  
    commissure, 21, 22, 122, 125, 135, 138, 139  
    segment, 72, 121, 123, 125–167  
    septal vein, 69, 74–78, 84, 86, 87, 89, 93, 95, 96, 99, 103, 112, 239, 253, 254  
Antiochus I Soter, 3  
Aquaporin 4 (AQP4), 33  
Aqueduct of Sylvius, 15, 20, 35  
Aqueductoplasty, 41, 43, 60, 121  
Aqueductoplasty with Fogarty balloon catheter insufflation after ETV, 196–199  
Aqueductoplasty without Fogarty balloon catheter insufflation, 194, 195  
Arachnoid cysts, 61, 69, 96, 100–102, 235  
Arachnoid granulations, 18, 19, 25, 27, 28, 30, 53, 60  
Arachnoid trabeculae, 217, 224  
Atrium, 20–22, 69, 75, 77, 79, 81–83, 102, 113–118  
Axel Key, 18  
Axial CT scan, 55, 59  
Axial T1-weighted MRI, 106  
Axial T2-weighted MRI, 97, 203
- B**  
Balloon catheter, 53  
Basal nuclei, 255  
Basilar artery  
    under premammillary membrane, 154  
    under premammillary recess, 133, 135, 143, 144, 147–149, 152, 153  
Benjamin Warf, 57  
Bifurcation of the basilar artery, 53, 127, 131–135, 140, 142–144, 155, 160, 207, 209, 213, 216, 243–248  
Bifurcation of the basilar artery  
    under membrane of Lilliequist–diencephalic portion, 216  
    under premammillary recess, 133, 135, 143, 144  
Biological glue, 43, 52  
Biopsies and tumor resections, 61  
Biopsy forceps  
    dilatation, 148  
    fenestrating the cyst wall, 242  
Biopsy forceps fenestrating the membrane of Lilliequist  
    diencephalic portion, 249, 250  
    mesencephalic portion, 251, 252  
Bipolar coagulation electrode  
    over premammillary recess, 141  
    over the tuber cinereum, 165  
Bipolar coagulation of the tuber cinereum, 165  
Body  
    of the caudate nucleus, 20, 21, 79–81  
    of the fornix, 21, 74, 75, 79, 84, 96, 103  
    of the right caudate nucleus, 109  
Brain hemispheres, 20  
Brainstem, 20, 207, 227, 235, 255, 256  
Bulb of the occipital horn, 114–116, 118
- C**  
Cadaverous fixation techniques, 11  
*Calamus Herophili*, 3  
*Calamus scriptorius*, 3  
Calcar avis, 21, 114–116, 118  
Carotid artery, 210, 248, 255  
Caudate branches to superior thalamostriate vein, 80, 109  
Caudate nucleus, 20, 21, 60, 74, 79–81, 102, 109, 111, 112  
CCDs. *See* Charged-couple devices (CCDs)  
CCHU ETV Success Score, 58  
Cell doctrine, 4–6, 11, 13–15  
Cells, 3–6, 11, 13–15, 25, 28, 32, 33  
Cerebellar culmen, 116, 117, 261  
Cerebellar vermis, 256  
Cerebellum, 20, 205, 255  
Cerebellum after fenestration, 205  
Cerebral aqueduct, 15, 20–22, 24, 25, 29, 30, 60, 121, 124, 193  
Cerebral aqueduct entrance, 122, 168, 171, 180–187, 189–194, 197, 199, 201, 204  
    obstructed by adhesion, 194, 197  
    obstructed by clot, 192, 193  
    obstructed by tumor, 191, 192, 201  
Cerebral hemispheres, 20, 255  
Cerebral peduncles, 22, 243, 245–247  
Cerebral trajectory, 71  
Cerebrospinal fluid (CSF), 15, 18, 25, 27–33, 37, 43, 53, 54, 56–61, 235, 255  
    circulation, 25, 28, 32, 43, 53, 54, 60, 61  
    flow, 25, 28, 29, 56, 235  
    flow artifact, 56  
    shunt, 57–60  
    third circulation, 25, 27, 28  
Charged-couple devices (CCDs), 40, 42  
Charles V, 14  
Choroidal fissure, 21



- Choroid plexus  
 at the Foramen of Monro, 190  
 at the left foramen of Monro, 170  
 at the right foramen of Monro, 169, 171  
 at the roof of the third ventricle, 190
- Choroid plexus coagulation (CPC), 35, 39, 54, 57–59, 69, 91, 92, 104, 105, 118, 255, 257
- Choroid plexus of the roof of the third ventricle, 189, 190
- Choroid plexus over colloid cyst, 97
- Chronic hydrocephalus, 84, 100–104, 139, 140, 239, 253
- Chronic inflammatory process, 86
- Chronic intraventricular adhesion, 95
- Ciliary beat, 28
- Claudius Galenus, 3, 4
- Clivus, 53, 54, 162–164, 210, 213, 217–219, 221–226, 229, 230, 233, 245, 247, 248, 251
- Clivus under membrane of Liliequist, 217
- Clot at the cerebral aqueduct entrance, 181
- Clots, 159, 160, 181, 183, 192, 193
- Coagulated choroid plexus (final aspect), 92, 104, 118, 262
- Coagulated cyst wall, 241
- Coagulated lateral posterior choroidal artery, 92, 118
- Coagulated left choroid plexus, including lateral posterior choroidal artery, 105
- Coagulated right choroid plexus, including lateral posterior choroidal artery, 105
- Coagulated tuber cinereum, 142, 146, 149, 159, 160
- Cogitativa, 5
- Cognatio, 5
- Cognitive, 4, 5
- Collateral eminence, 21, 114–116, 118
- Collateral sulcus, 21
- Collateral trigone, 21
- Colloid cyst, 61, 69, 97, 98, 172
- Column of the fornix, 72, 74–77, 84, 87, 93, 95, 111, 112, 125, 238–240, 253
- Communicating cyst, 235
- Communicating hydrocephalus, 39, 57, 58
- Complex hydrocephalus, 45, 59, 60, 106
- Computerized tomography (CT) scan, 22, 23, 44, 45, 55, 57, 59, 173, 255, 256
- Congenital membrane, 85
- Coronal CT scan, 55
- Coronal T2-weighted MRI, 106, 196, 200
- Corpus callosum, 15, 20, 21, 111, 112
- CPC. *See* Choroid plexus coagulation (CPC)
- Crus of the fornix, 21, 22
- CSF. *See* Cerebrospinal fluid (CSF)
- CT scan. *See* Computerized tomography (CT) scan
- Cushing, 28, 57
- Cyst fenestrations, 43
- Cystocisternostomy, 61
- Cyst of racemose neurocysticercosis, 93
- Cystoventriculostomy, 61
- Cyst wall, 61, 204, 205, 240–243
- Cyst wall fenestration at the end of the procedure, 253, 254
- D**
- Dandy-Walker malformation, 58
- Dandy-Walker variant, 58
- Dark Ages, 5, 6
- De humani corporis fabrica*, 14, 16
- De humani corporis fabrica libri septem*, 14
- De Natura Hominis*, 5
- Developmental delay, 255
- Diencephalic portion and a mesencephalic portion, 207
- Diencephalic portion of the membrane of Liliequist, 207–209, 235
- Diencephalon, 20
- Dilatation by grasping forceps, 61
- Disputationes, 15
- Dissections, 3, 4, 6, 7, 10–12, 14, 15, 43
- Domenico Felice Antonio Cotugno, 15
- Dominant hand, 43, 50
- Dorsum sellae, 61, 140, 141, 145, 153–155, 162–164, 207–210, 213–215, 245, 248, 249, 223, 244
- Dryander, 11, 14, 15
- Dural opening, 43, 47, 51, 70
- Dural watertight closure, 43
- E**
- Endoscope-assisted microneurosurgery, 42, 43
- Endoscope-controlled microneurosurgery, 42
- Endoscopic biopsy, 61, 173–178
- Endoscopic neurosurgery, 35–61, 235
- Endoscopic third ventriculostomy (ETV), 38, 43, 53–58, 61, 121, 173–178, 196–202, 207, 209
- Endoscopic vision, 73, 98, 110, 113, 125, 167, 179, 210
- Enzephaloskopie, 37, 39
- Ependyma, 25, 27, 33, 255
- Ependymal layer, 28, 71, 72, 207, 208, 212–214, 216, 218, 220, 228, 231
- Ependymocytes, 25, 28
- Erasistratus, 3, 4
- Erwin Payr, 37
- ETV. *See* Endoscopic third ventriculostomy (ETV)
- ETV/CPC, 57–59
- ETV Success Score (ETVSS), 54, 58, 209
- Eugene Spitz, 40
- F**
- Fabrica, 10, 11, 14, 16, 17
- Fantasia, 5
- Fay and Grant, 38
- Fenestrated cyst, 95
- Fenestrated membrane of Liliequist, 149
- Fenestrated septum pellucidum, 104, 105, 109
- Fenestration, 43, 53, 58–61, 69, 77, 84, 94–96, 100, 101, 103, 143, 153, 197, 203–205, 212, 235, 239, 242, 251–254
- Fenestration at the membrane of Liliequist–diencephalic portion, 251
- Fenestration at the membrane of Liliequist–mesencephalic portion, 252
- Fenestration at the tuber cinereum and the membrane of Liliequist after coagulation, 143
- Fenestration at tuber cinereum after coagulation, 143
- Fenestration of the membrane of Liliequist by biopsy forceps, 153
- Filippo Brunelleschi, 10
- Fimbria of the fornix, 21
- Floor, 20–22, 40, 41, 53, 123–125, 176–178
- Fogarty, 53, 60, 61, 69, 87, 89, 108, 144–146, 152, 154, 164, 194–199
- Fogarty balloon catheter, 53, 60, 61, 69, 87, 89, 144–146, 152, 154, 164, 194–199
- Fogarty balloon catheter dilatation, 144, 145, 152
- Fontanelle, 43, 45, 53, 57, 70
- Foramen of Luschka, 18, 29
- Foramen of Magendie, 17, 18, 60
- Foramen of Monro, 17, 20–22, 29, 35, 36, 53, 57, 59–61, 69, 72, 74–80, 84–98, 111, 112, 121, 122
- Foraminoplasty, 43, 59, 69, 87–90

- Fornix, 20–22, 60, 72, 74, 76, 77, 79, 84, 87, 93, 95, 96, 103, 111, 112, 125, 238–240, 253  
 Fourth ventricle, 3–5, 15, 17, 18, 20, 22, 24, 25, 27, 29, 30, 35, 53, 57, 60  
 Frameless, 43, 50  
 Frameless free-hand system, 50  
 Franciscus Sylvius, 15, 17  
 François Jean Magendie, 17, 18  
 Frank Nulsen, 40  
 Franz de le Boë, 15, 17  
 Free-hand technique, 43, 50, 257  
 Frontal  
   horn, 20–24, 53, 69, 74, 110–113  
   skull base, 140
- G**
- Gaab system, 43, 49, 50, 69, 70, 257  
 Gadolinium-enhanced sagittal T1-weighted MRI, 200  
 Genu of the corpus callosum, 21, 111, 112  
 Gerard Guiot, 41  
 Giant arachnoid cyst, 95  
 Giant infra/supratentorial, 94–96  
 Giant posterior fossa arachnoid cyst, 203–205  
 Gladiators, 4  
 Glial tissue, 255  
 Glomus of the choroid plexus, 114  
 Grasping forceps, 48–50, 53, 61, 93, 150, 151, 156, 157, 160  
 Guido da Vigevano, 10, 11
- H**
- Habenular commissure, 22, 185–190, 204, 205  
 Habenular trigone, 185–190, 204, 205  
 Harold Horace Hopkins, 40  
 Head of the caudate nucleus, 21, 74, 111, 112  
 Hemorrhage over collateral eminence, 118  
 Herophilus, 3  
 High rotation drill, 43, 47  
 Hippocrates, 3  
 Holy Trinity, 5  
 Hopkins rod-lens system, 40, 42  
 Hubert von Luschka, 18, 19  
 Human, 3, 6, 9, 12, 14, 16, 25, 28, 30, 31, 42  
 Hydranencephaly, 59, 255–262  
 Hydrocephalus, 28, 35, 39–41, 45, 53, 54, 57–61, 84, 100–104, 106, 121, 139, 140, 173, 176, 196, 203, 235, 236, 239, 253, 255  
 Hypoglossal nerve, 207, 225
- I**
- Imagination, 4, 5  
 Imaginativa, 5  
 Infra/supratentorial arachnoid cyst, 94–96, 103, 104  
 Infundibular recess, 22, 53, 72, 122, 125–127, 130, 131, 133, 135, 137–139, 143, 151, 154, 155, 159, 161  
 Internal carotid artery, 210, 248, 255  
 Internal cerebral vein, 21, 22  
 Interpeduncular cistern, 23, 24, 53, 56, 149, 154, 155, 207–209, 212, 229, 235  
 Interthalamic adhesion, 22, 29, 84, 121, 168–172, 180, 204  
 Interthalamic adhesion through spontaneous fenestration at the septum pellucidum, 84  
 Interventricular foramen, 17, 20, 24  
 Intracranial arachnoid cysts, 61  
 Intracranial space, 258–260, 262
- Intracranial space (no ventricle!), 258–260, 262  
 Intraventricular arachnoid cyst, 100–102  
 Intraventricular hemorrhage, 53, 58, 60, 84  
 Intraventricular racemose neurocysticercosis, 93  
 Intrinsic brainstem tumor, 176–178, 226  
 Isagoge, 15
- J**
- Jacobus Sylvius, 15  
 Jacopo Berengario da Carpi, 11  
 Jacques Dubois, 15  
 Jan Stephen van Calcar, 14  
 Johannes Dryander, 11  
 Johannes Eichmann, 11  
 Johannes Gutenberg, 6  
 Johannes Oporinus, 14, 16  
 John Edwin Scarff, 39  
 Judgment, 5
- K**
- Karl Storz, 40, 42, 43, 48, 49, 52, 69  
 Karolinska Institute, 18  
 Key and Retzius, 18, 19, 28
- L**
- Lamina terminalis, 21, 22, 136–140, 153, 154, 172  
 Late intraventricular hemorrhage, 84  
 Lateral apertures of the fourth ventricle, 18  
 Lateral posterior choroidal artery, 76, 80–83, 91, 92, 104, 105, 114, 118  
   and vasa vasorum, 82  
 Lateral ventricles, 5, 10, 17, 20, 21, 27, 28, 35, 37, 57, 59, 69  
 Lateral walls, 20–22  
 Left abducens nerve (CN VI), 222–224  
   entering in the channel of Dorello, 223  
 Left accessory nerve (CN XI), 225  
 Left anterior inferior cerebellar artery (AICA), 222  
 Left anterior thalamoperforating/mamillary arteries, 244, 248  
 Left atrium, 23, 24, 104, 105  
 Left body, 105  
 Left cerebral peduncle, 126–128, 133–135, 140, 141, 143, 144, 146–148, 150–154, 159–161, 165, 166, 172  
 Left choroid plexus, 104, 105, 258–261  
 Left habenular trigone, 186–190, 204, 205  
 Left hypoglossal nerve (CN XII), 225  
 Left hypothalamus, 126–128, 133–135, 140, 141, 143, 144, 146–148, 150–154, 159–161, 165, 166, 172  
 Left infratentorial portion of the cyst, 104  
 Left labyrinthine artery, 221, 222  
 Left lateral posterior choroidal artery, 104  
 Left mamillary body, 125–135, 140, 142–144, 146–155, 159, 160, 165–167, 169, 172, 174  
 Left mamillary body under clots, 159, 160  
 Left oculomotor nerve (CN III), 127, 135, 142–144, 162, 163, 211, 216, 217, 231, 243, 245, 247  
 Left optic tract, 135–138, 154  
 Left pineal stalk, 187  
 Left pontine branch of the basilar artery, 162, 163  
 Left portion of the arachnoid cyst, 101, 102  
 Left posterior cerebral artery (P2), 127, 129, 131, 132, 134, 140, 142–144, 149, 162, 163, 211, 213, 216, 220, 221, 232, 244–248, 251, 252  
 Left posterior communicating artery, 243–245, 247, 248  
 Left posterior inferior cerebellar artery (PICA), 220, 225

Left pulvinar of the thalamus, 104, 105  
 Left superior cerebellar artery, 162, 163, 220, 221, 232  
 Left thalamus, 104, 171, 172, 180–182, 185, 258–261  
 Left vertebral artery, 224, 225, 233  
 Leonardo da Vinci, 10  
 Looking around the corner, 42

## M

Magnetic resonance imaging (MRI), 22, 24, 29, 53, 54, 56, 58, 94, 97, 106, 121, 122, 162–167, 176, 196, 200, 203, 207, 208, 227, 236, 237, 255, 256  
 Magnum foramen, 210, 225  
 Magnus, Albertus, 5, 6  
 Magnus Gustaf Retzius, 18  
 Mammillary bodies, 22, 53, 121, 124, 161, 207, 235  
 Medial atrial vein, 115, 118  
 Medial posterior choroidal artery, 21, 22  
 Median aperture of the fourth ventricle, 17  
 Medulla oblongata, 20, 207, 225, 233  
 Mega cisterna magna, 58  
 Membrane of Lilliequist, 53, 142, 143, 149, 151, 153, 157, 158, 160, 207–209, 211–214, 216–229, 235, 243–245, 247–252  
 Membrane of Lilliequist–diencephalic portion, 211–214, 216–219, 221, 228, 249–251  
 Membrane of Lilliequist–diencephalic portion fenestration by biopsy forceps, 212  
 Membrane of Lilliequist–mesencephalic portion, 216, 217, 220–225, 229, 243–245, 247–249, 251, 252  
 Memorativa, 5  
 Memoria, 5  
 Memory, 4, 5, 69  
 Mental functions, 5  
 Mesencephalic portion of the membrane of Lilliequist, 207–209, 235  
 Mesencephalon, 20, 22, 207, 227, 235, 243, 246, 255  
 Middle, 5, 6, 25, 53, 121, 123, 124, 167–169, 171, 173, 175, 177, 179, 248  
 Middle ages, 5, 6, 25  
 Middle cerebral artery (M1), 248  
 Middle segment, 121, 123, 124, 167–179  
 Minicraniotomy, 43, 46, 52  
 Mondino de'Liucci, 14  
 Monopolar coagulation electrode at the cyst wall, 241  
 Monro foraminoplasty, 87–90  
 Multiloculated hydrocephalus, 58, 60  
 Myelomeningocele, 57

## O

Obstructive hydrocephalus, 41, 53, 54, 57, 58  
 Occipital, 14, 20–22, 58, 60, 114–116, 118, 255, 256  
   horn, 20–22, 58, 114–116, 118  
 Occluded foramen of Monro, 86  
   by choroid plexus, 86  
 Oculomotor nerves, 127, 135, 142–144, 162, 163, 207, 211, 216, 217, 228, 230–232, 243, 245–247, 249, 250  
 Oi HandyPro system, 43, 48, 50, 69  
 Operating sheath, 48, 49, 70, 71  
 Optic  
   chiasm, 21, 22, 53, 72, 125, 135–140, 146, 149, 153–155, 159, 172  
   recess, 21, 22, 122

## P

Papyrus of Edwin Smith, 25  
 Parietal, 20, 59, 255

## Pars

  profunda, 207–209  
   superficialis, 207–209  
 Perspective, 10, 11  
 Philip II, 14  
 Pineal  
   body, 22  
   gland, 121, 122, 185–190  
   recess, 22, 121, 122, 180, 182, 184–188, 190, 192  
   recess and pineal gland  
 Pituitary gland, 140, 141, 155, 162, 214–216, 248, 249  
   and stalk, 248  
 Pituitary infundibulum, 121  
 Pituitary stalk, 141, 215, 216, 248, 249  
 Pneuma, 3  
*Pneuma psychikon*, 3, 4, 15  
*Pneumazooticon*, 3  
 Pneumoventriculography, 35–37  
 Point of Kocher, 45  
 Pons, 20, 149, 150, 158, 207, 212, 217, 218, 220, 222, 226, 229  
 Pons under membrane of Lilliequist, 158  
 Pons under thinner portion of the premammillary recess  
 Pontine arterial branches, 219–221  
 Pontine branches of the basilar artery, 145  
 Pontine veins, 224, 233  
 Poseidon, 5  
 Posterior cerebral arteries, 127, 129, 131, 132, 134, 140, 142–144, 149, 155, 158, 162, 163, 207, 211, 213, 216, 220, 221, 232, 243–252  
   Posterior clinoid process, 210, 248, 249  
   Posterior commissure, 22, 121, 122, 124, 168, 180–195, 197, 204  
   Posterior perforated substance, 22, 209  
   Posterior segment, 121, 123, 179–205  
   Posterior septal vein, 77, 81, 83, 113  
 Postinfectious occlusion of the foramen of Monro, 86  
 Postmammillary recess, 128, 129, 132, 153, 155–157, 159–161, 167–172, 174, 180, 181  
 Postmeningitis hydrocephalus, 60  
 Premammillary recess, 126–128, 130–135, 140, 141, 143, 147–150, 152, 153, 157, 165, 169, 172  
 Prepontine cistern, 24, 53, 58, 207–233  
 Processes, 5, 32  
 Prosencephalon, 20

## R

Racemose cysts, 165–167, 227–233  
   inside interpeduncular cistern, 229  
   inside prepontine cistern  
 Racemose neurocysticercosis, 93, 227–233  
 Ratio, 5, 58  
 Reason, 4, 5, 40, 42  
 Reduced arachnoid cyst, 96  
 Removal of the clot by a grasping forceps, 193  
 Renaissance, 5, 10, 11, 14, 15, 25  
 Right atrium, 23, 105, 113  
 Right cerebral peduncle, 243, 247  
 Right choroid plexus, 105, 258, 259  
   and its basal vessels, 259  
 Right coagulated choroid plexus, 104  
 Right habenular trigone, 186, 188–190  
 Right hypothalamus, 126–128, 133, 135, 141, 143, 146–148, 150, 152–154, 159, 161, 165–167  
 Right lateral posterior choroidal artery, 104  
 Right mammillary body, 72, 126–135, 140–142, 144, 146–157, 159, 160, 165–167, 172

- Right mammillary body under clots, 159, 160  
 Right oculomotor nerve (CN III), 228, 230–232, 243, 245–247, 249, 250  
 Right optic nerve (CN II), 140  
 Right pineal stalk, 187  
 Right pontine branch of the basilar artery, 162  
 Right portion of the arachnoid cyst, 101  
 Right posterior cerebral artery (P1), 127, 140, 142–144, 149, 155, 158, 213, 216, 244, 246–248  
 Right posterior cerebral artery (P2), 243, 245, 248  
 Right posterior communicating artery, 243–245, 247  
 Right posterior inferior cerebellar artery (PICA), 220, 225  
 Right pulvinar of the thalamus, 104  
 Right superior cerebellar artery, 162, 221  
 Right superior thalamostriate vein, 109  
 Right temporal lobe, 231  
 Right thalamus, 109, 171, 180–182, 185, 258, 259  
 Right trigeminal nerve (CNV), 230, 231  
 Right vertebral artery, 220, 224  
 Rigid endoscopy, 42, 43, 69  
 Rod-lens system, 40, 42  
 Romboencephalus, 20  
 Roof, 20–22, 121, 180, 186, 189, 190  
 Roof of the third ventricle, 21, 121, 180, 186, 189, 190  
 Rostrum of the corpus callosum, 21
- S**  
 SAC-1, 235  
 SAC-2, 235  
 SAC-3, 235  
 Sagittal CT scan, 55  
 Sagittal T1-weighted MRI, 97, 200, 227  
 Sagittal T2-weighted MRI, 24, 53, 54, 56, 94, 121, 122, 196, 203, 207, 208, 237  
 St. Augustine, 5  
 Sellar diaphragm, 215, 216, 248, 249  
 Sensus communis, 5  
 Septal vein, 69, 74, 76–78, 81, 83, 84, 86, 87, 89, 93, 95, 96, 99, 103, 107, 112, 113, 239, 253, 254  
 Septostomy, 43, 59–60, 69, 106–110  
 Septum pellucidum, 20, 21, 24, 35, 59, 60, 69, 74, 76, 77, 81, 82, 84, 86, 87, 89, 93, 95–114, 118, 239, 253, 254  
 Septum pellucidum spontaneous fenestration due to chronic hydrocephalus, 239, 253  
 Shunt, 40, 53, 54, 57–61, 236, 255  
 Sitting position, 51  
 Sonic Hedgehog (Shh), 20  
 Spontaneous fenestration at the septum pellucidum, 77, 84, 100, 101, 103  
 Spontaneously fenestrated lamina terminalis, 14  
 Spontaneously fenestrated septum pellucidum, 104, 105  
 Spontaneous opening at the lamina terminalis, 139  
 Standing position, 43, 51  
 Stents, 43, 60  
 Stratonice, 3, 4  
 Stria terminalis, 20, 72, 125  
 Striothalamic sulcus, 20, 21  
 Subarachnoid space, 17–19, 25, 27, 28, 31–33, 53, 54, 207, 235  
 Substitute superior thalamostriate vein [12], 76–78, 80, 111  
 Superior cerebellar artery, 140, 162, 163, 207, 220, 221, 232  
 Superior choroidal vein, 75, 77, 102, 113  
 Superior portion of the right optic foramen, 140  
 Superior thalamostriate vein, 20, 69, 74–81, 84, 86, 87, 89, 93, 95–97, 102, 109, 111, 171, 190, 238
- Suprapineal recess, 21, 22, 121, 122, 185–190, 204  
 Suprasellar arachnoid cysts (SACs), 61, 235–254  
 Suprasellar arachnoid cyst through foramen of Monro, 238–240  
 Systems, 3–33, 35, 37, 40–43, 48–50, 52–54, 57, 60, 61, 69, 70, 73, 121, 257
- T**  
 Tabulae Sex, 14  
 Tail of the caudate nucleus, 21, 102  
 Takanori Fukushima, 41  
 Tegmentum of mesencephalon, 243  
 Tegmentum of the mesencephalon, 22  
 Telencephalon, 20  
 Temporal lobe, 20, 21, 231, 255  
 Temporal horn, 20–23  
 Thalami, 255, 256  
 Thalamic tumor, 173–176  
 Thalamoperforating arteries, 128–131, 134, 140, 155–158, 207, 209, 211, 213, 243–248  
   under membrane of Liliequist, 157  
   under premammillary recess, 128, 130, 131, 134  
 Thalamus, 20–22, 60, 72, 75, 76, 79–82, 102, 104, 105, 109, 125, 171, 172, 180–182, 185, 258–261  
 Third ventricle, 5, 17, 20–24, 27–30, 35, 36, 40, 41, 53, 56, 61, 69–118, 121–205, 207–233, 235–262  
 Third ventricle floor, 41, 53, 176–178  
 Thought, 3–5, 18  
 Tiziano Vecelli, 14  
 Tracy Jackson Putnam, 39  
 Transfontanelle approach, 45, 70  
 Tuber cinereum, 22, 53, 121, 124, 126–128, 130, 131, 133–136, 141–143, 146, 148–150, 155, 158–163, 165, 172, 207
- Tumor**  
   biopsy after ETV  
   vessels, 97  
   wall, 97, 98, 201  
 T2-weighted MRI, 54, 94, 97, 106, 196, 200, 203, 237
- U**  
 University of Tübingen, 18
- V**  
 Venous drainage to great cerebral vein, 189, 190  
 Ventricular endoscopy, 20  
 Ventricular system, 3–33, 35, 37, 43, 53, 54, 57, 60, 61, 70–73, 121  
 Ventricular wax injection, 11  
 Ventriculocystocisternostomy, 61, 235  
 Ventriculocystostomy, 61, 235  
 Ventriculography, 35–37, 61  
 Ventriculoperitoneal shunts (VPS), 57–59  
 Ventriculoscopy, 35, 37  
 Ventriculostomy, 35, 37  
 Vesalius, 5, 10, 11, 14  
 Victor Darwin Lespinasse, 35  
 Vincent Alexander Bochdalek, 18  
 Virchow-Robin space, 28, 31, 32  
 Virtual endoscopy, 236
- W**  
 Walter Edward Dandy, 35  
 William Jason Mixer, 37